Cambrian Granite-Related Hydrothermal Alteration and Cu-Au Mineralisation in the Southern Mt Read Volcanics, Western Tasmania, Australia

William F. Wyman (MSc, BSc)

Submitted in [redacted] fulfillment of the requirements

for the degree of

Doctor of Philosophy (Geology)

University of Tasmania

February 2001

UNIVERSITY OF TASMANIA

THESIS STATEMENT

This thesis contains the results of five years research undertaken at the Centre for Ore Deposit research, University of Tasmania, between April, 1995 and July, 2000. The author states that this thesis contains no material that has been accepted for the award of any other higher degree or graduate diploma in any tertiary institution, and to the best of the author's knowledge and belief, it does not contain any material previously published or written by another person except where due reference is made in the context of the thesis. This thesis may be made available for loan and limited copying in accordance with the Copyright Act (1968).

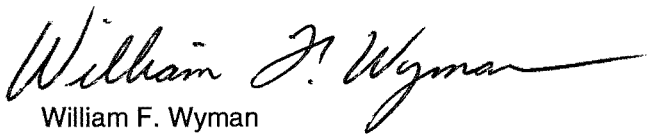

William F. Wyman

Dated: 15/02/01

Distribution List

1. University Copy
2. University Copy
3. Prof. Ross Large
4. Dr. Dave Cooke
5. AMIRA
6. Bill Wyman
7. Bill Wyman
8. Spare unbound copy

ABSTRACT

The Darwin Granite is located in the south central portion of the Cambrian Mt. Read Volcanic Belt in western Tasmania. It has been dated at 510 +64, -21 Ma by Adams et al. (1985) and is of particular interest because of it's association with several nearby Cu-Au prospects and its apparent contemporaneous timing with respect to ore formation at the Mt. Lyell mining field. The main aims of this research are to determine the nature and origin of the Darwin Granite, its relationship to the various volcanic suites in the Mt. Read Volcanics, and its relationship to the hydrothermal alteration and copper-gold mineralisation in the district.

The Darwin Granite is a highly fractionated phanerocrystalline I-Type magnetite series equigranular granite with Suite I characteristics as defined by Crawford et al. (1992). The main pink granite phase is intruded by smaller white leucocratic, phanerocrystalline, equigranular to porphyritic, medium to coarse-grained granodiorite and microgranite phases. GENMIX modeling of major elements and REE data supports a model that the granodiorite and microgranite formed from fractionation of the pink granite phase. Negative $\varepsilon Nd_{(500Ma)}$ values indicate the Darwin Granite was derived from partial melting of a crustal source. REE patterns and abundances in host Central Volcanic Complex (CVC) rocks have virtually identical Suite I characteristics, but REE and trace element data suggest the Darwin Granite was not comagmatic with the volcanic units and they were sourced from a magma with REE and trace element characteristics similar to the Murchison Granite. A Murchison-like parental granite has not been identified in the study area, although geochemical evidence suggests that such a granite occurs beneath the study area.

Numerous small tonnage, relatively high grade copper-gold prospects are located along exposed flanks and subsurface projections of the Darwin Granite. With increasing distance from the granite, ore styles are variable from iron-oxide veins and stockworks containing pyrite and chalcopyrite ± specular-hematite ± magnetite ± tourmaline and quartz-pyrite-chalcopyrite veins, to disseminated pyrite-chalcopyrite ± covellite, to veins containing quartz, bornite, neodigenite, chalcopyrite and hematite. At the Jukes Prospect, alteration and ore related assemblages are hosted in coherent dacitic volcanics of the CVC. Mineralisation occurs as disseminated pyrite and chalcopyrite, magnetite-pyrite ± tourmaline ± scheelite veins, chalcopyrite-pyrite-magnetite veins, magnetite ± chlorite hydrothermal breccias, and quartz-chalcopyrite stringers.

Hydrothermal sericite, chlorite and K-feldspar alteration styles occur throughout a 15 km X 3 km zone that extends northward from the Darwin Granite to the Jukes Prospect and regional aeromagnetic data suggests that the Darwin Granite underlies the entire northerly trending belt (Leaman and Richardson, 1989; Payne, 1991; Large et al., 1996). Hydrothermal alteration zones around the Darwin Granite and Jukes Prospect represent different parts of the same hydrothermal system. Hydrofracturing and phreatic brecciation of the cupola region released magmatic-hydrothermal fluids which reacted with country rocks and resulted in a complex zoned alteration system. The inner zone is composed of intense secondary K-feldspar assemblages associated with copper mineralisation and grades outward to zones of chlorite and sericite assemblages. Accessory minerals in the K-feldspar zone include sericite, chlorite, pyrite, magnetite, and chalcopyrite. In the chlorite zone accessory sericite, pyrite, magnetite occur as well as chalcopyrite veins. Initial sericite ± chlorite alteration styles were associated with microfracture and vein formation around and above the granite.

Total mass changes at the Jukes Prospect were minor and typically involved replacement of one mineral with another without significant nett mass changes. In sericite altered rocks, K_2O gains effectively balanced $\Delta(Na_2O + CaO)$ depletions (from plagioclase destruction) and total mass changes were small. In K-feldspar altered rocks, K_2O gains were larger and were accompanied by minor SiO_2 and Fe_2O_3 gains, although the total mass changes were still small (av. 6.1 gms/100gms). Total mass changes in chlorite altered rocks effectively balance $\Delta(K_2O + MgO + Fe_2O_3)$ gains with $\Delta(Na_2O + CaO + SiO_2)$ losses. In contrast to the minor mass change at the Jukes Prospect, large mass changes occurred near the Darwin Granite. In the dacites, large gains in SiO_2 (+80 gms/100gms) accompanied smaller mass gains in Al_2O_3, K_2O, Ba and Sr, while depletions of SiO_2 and Al_2O_3 occurred in adjacent andesites. The mass changes observed are explained by invoking a magmatic hydrothermal model in which magmatic fluids exsolved from the Darwin Granite. These fluids mixed with modified seawater in reaction zones around the hotter portions of the upflow or discharge zones and K_2O, and Fe_2O_3 rich alteration assemblages resulted.

Monomineralic vein phases suggest that close to the center of the hydrothermal system fluids were buffered by water (high volume, water/rock ratio). Farther from the systems centre, poly-mineralic veins and alteration styles suggest rock buffering due to lower water/rock ratios. The widespread occurrence of tourmaline throughout the Jukes-Darwin area suggests significant B in the mineralising fluids. Boron, in addition to H_2O, may have depressed the solidus temperature of the Darwin Granite allowing the ascending granite additional time for cooling and intrusion to a higher crustal level (and a lower lithostatic pressure regime) than otherwise may have occurred. The higher level of intrusion allowed the granite to reach a level at which second boiling occurred releasing enough mechanical energy to fracture host rocks at depths of 4-5 km (Burnham and Ohmoto, 1980; Burnham, 1985) consistent with estimated depths of emplacement at Mt. Darwin.

Whole rock $\delta^{18}O$ data for the Darwin Granite is consistent with crystallisation from a magma with $\delta^{18}O$ values between 9‰ and 10.5‰. Magmatic fluids in equilibrium with the granite had $\delta^{18}O$ values around 9 ± 1‰. Limited quartz and K-feldspar data suggest that they formed from the same fluid at 485 +90°C, -60°C and $\delta^{18}O_{fluid}$ value of ~6 ± 1‰. Magnetite $\delta^{18}O$ values are 6 to 7.5 ± 1‰ at temperatures of 460-550°C. Quartz, K-feldspar and magnetite probably formed from nearly pure magmatic fluids, the likely source of which was the Darwin Granite.

Sulfur isotopes in the Jukes-Darwin system suggests that the initial sulfur budget was dominated by magmatic sulfur ($\delta^{34}S$ = 6‰) and volcanic rock sulfur ($\delta^{34}S$ = 10-15‰) and the seawater contribution was small (<25%). As the hydrothermal system developed, the contribution of rock sulfur and magmatic sulfur decreased and the contribution of reduced seawater sulfate increased, consistent with the arguments of Solomon et al. (1988). $\delta^{34}S$ values (average 7‰) from the Prince Lyell Cu-Au deposit at Mt. Lyell are interpreted to represent magmatic values but are not uniquely definitive of a genetic source of sulfur. Based on $\delta^{34}S$ values, either Suite II andesites (Crawford et al., 1992) or Cambrian granites could have provided the magmatic sulfur in the Mt. Lyell pyrite-chalcopyrite ores.

REE patterns for the Prince Lyell Suite II andesites and Suite I Murchison diorite and granodiorite are nearly identical to REE patterns in apatite at Prince Lyell and the Garfield Cu-Au Prospect.

However, apatite $\varepsilon Nd_{(500ma)}$ values from the two prospects are different and are strong evidence that the Prince Lyell and Garfield apatites were derived from different source rocks. The Prince Lyell apatite $\varepsilon Nd_{(500ma)}$ values suggest that the apatites were derived from a primitive Suite I diorite or granodiorite precursor with a crustal signature similar to the Darwin and Murchison Granites. This evidence, combined with similar REE patterns, support the interpretation that magmatic fluids derived from a Suite I granite were directly responsible for apatite-magnetite ores at Prince Lyell. Although the magnetite-apatite was almost certainly derived from a Suite I granite precursor, the source granite is either too deep to be geophysically detectable or the fluids migrated from the east, probably along the Great Lyell Fault.

ACKNOWLEDGMENTS

First and foremost my most sincere thanks to my wife Tina and my sons, Daniel and Joe. They have survived five years of my moodiness, absence and 'personal growth', while providing me with unwavering love and support. To them I am profoundly grateful. Secondly, I thank my parents Dick and Anne, without whose encouragement and financial support, this thesis would not have been possible. I am greatly indebted to my supervisors, Ross Large and Dave Cooke for their encouragement, patience and direction over the course of this project. In addition, thank you to Mike Solomon for reviews of Chapters 5-7, Gary Davidson for reviewing Chapters 8 and 9, Rick Varne for his unselfish and most welcome review of Chapter 3, Tony Crawford for reviewing my REE interpretations and to Ron Berry, Bruce Gemmell and Clive Burrett for discussions and suggestions that have helped to guide this research. Thank you to Peter McGoldrick for taking me under his wing early in my stay and introducing me to volleyball. I would also like to extend my thanks to the support staff at the Centre for Ore Deposit Research and the Geology Department for their assistance and advice, especially to Peter Cornish, Simon Stephens, Christine Higgens, Marilyn Feast, Nilar Hlaing, Katie McGoldrick, Di Steffens, Jessica Tyler, Lyn Starr, Nathan Duhig and Andrew Jones. Thank you to Dave Steele for his guidance and assistance concerning the Electron Microprobe. A special thanks to June Pongratz for helping me with my computer frustrations and to Mike Blake and Wally Herrmann for stepping out of the mold and talking about more stimulating subjects in the tea room than footy.

This research was supported by the Australian Mineral Industries Research Association Limited (AMIRA) Project P439 (Studies of VHMS related alteration: geochemical and mineralogical vectors to mineralisation). P439 was sponsored by: Aberfoyle Resources Limited, Copper Mines of Tasmania, Denehurst Limited, Mineral Resources Tasmania, Normandy Exploration, Pasminco Exploration, Queensland Metals Corporation Limited, RGC Exploration and Rio Tinto Exploration. Additional logistic support and helicopter access to the more remote areas was received from RGC Exploration and I would specifically like to thank Scott Halley, Kim Denwar, Mike Vicary, Bruce and Chopper for their help. I am also grateful to the Kevin Wills and Will Godsall from Copper Mines of Tasmania, who gave me several surface tours of the Mt. Lyell lease and underground tours of the Prince Lyell mine as well as unrestricted access to their data base and core.

And finally, thank you to my office mates and fellow students, Ali Raos, Catherine Reid, Steve Hunns, Russell Fulton, Cathryn Gifkins, Andrew Rae and Bruce Anderson. You have made it all bearable and I wish you all the best.

Cheers

TABLE OF CONTENTS

LIST OF FIGURES

LIST OF TABLES

LIST OF PLATES

CHAPTER 1

1.0 INTRODUCTION

1.1 PREAMBLE

This PhD research formed part of a larger AMIRA program entitled; Studies of VHMS-Related Alteration: Geochemical and Mineralogical Vectors to Mineralisation. The role of granitic magmas in volcanic-hosted massive sulfide (VHMS) genesis has been widely debated in the literature, most recently by Large et al. (1996), and earlier by Solomon (1976), Sawkins (1981), Stanton (1985; 1990) and Stolz and Large (1992), among others. Two primary schools of thought exist: I) The granites act as heat engines, driving circulation systems which leach the metals and other components from the overlying volcanic piles by sea-water convection; 2) In addition to heat transfer, the granites supply magmatic components, primarily metals, directly to the ore forming solutions. Magmatic components possibly supplied by the granites include Cu, Au, Mo, Sn, Pb, Zn and W. Circulating seawater or magmatic fluids are expected to leave behind textural and/or geochemical signatures in the rocks that may be identifiable. The search for such signatures is the focus of this PhD research project. The study area is located in the Darwin Granite and surrounding volcanics in the Cambrian Mt. Read Volcanic Belt (MRV) of western Tasmania (Figure 1.1).

1.2 AIMS

The Darwin Granite is spatially associated with several small Cu-Au prospects, that occur within a 15 km long and 3 km wide belt of hydrothermal alteration and mineralisation known as the Jukes-Darwin mineral field (Figure 1.2). This spatial association has been interpreted by large et al. (1996) to indicate that plutonism was active in the late Cambrian, simultaneous with formation of the major VHMS deposits at Mt. Lyell and Rosebery. Therefore, this research project has four major goals: 1) evaluate the evidence for a magmatic link between the Cambrian granites and their host volcanic rocks within the Central Volcanic Complex (CVC) in the southern MRV, 2) document the regional extent of hydrothermal alteration associated with the Cambrian granites and evaluate the genetic link between the hydrothermal alteration in and around the granites and the hydrothermal alteration around the Prince Lyell Cu-Au deposit at Mt. Lyell, 3) evaluate the relationship of hornblende-phyric andesites to the VHMS deposits and the hydrothermal alteration within the CVC, and 4) establish the source of ore forming fluids involved in the generation of Cambrian Cu-Au mineralisation in western Tasmania and determine the extent of mixing between various fluid types.

1.3 LOCATION AND ACCESS

The study area is located in the southern MRV and extends from the Jukes Proprietary Prospect (Jukes Prospect) south to the Darwin Granite and Mt. Darwin, approximately 20 km south of Queenstown (Figure 1.1). To the south, the study area is bounded by the southern end of the Darwin Granite. It is also bounded by the King River (north), Mt Sorell (Mt. Sorell) and by a large N-S fault with younger rocks to the east.

Access to the area is gained via the Jukes Road south from Queenstown, and several four wheel drive tracks. Access to the Darwin Granite on the Darwin Plateau was provided by helicopter and four wheel drive vehicles.

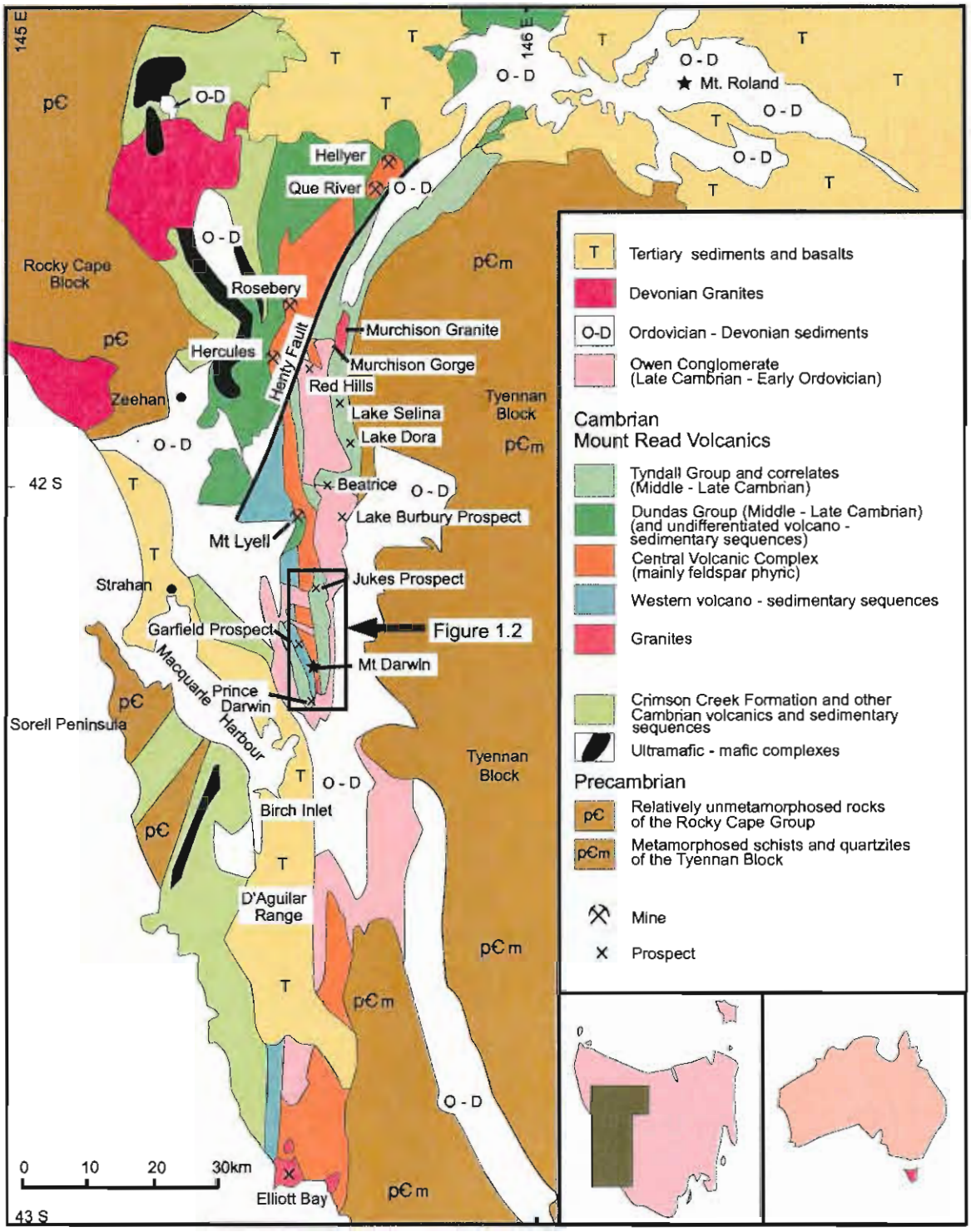

Figure 1.1. Location map of the study area and general geology of the Mt. Read Volcanics. Modified from Corbett and McNeil, 1988 and Corbett and Solomon, 1989.

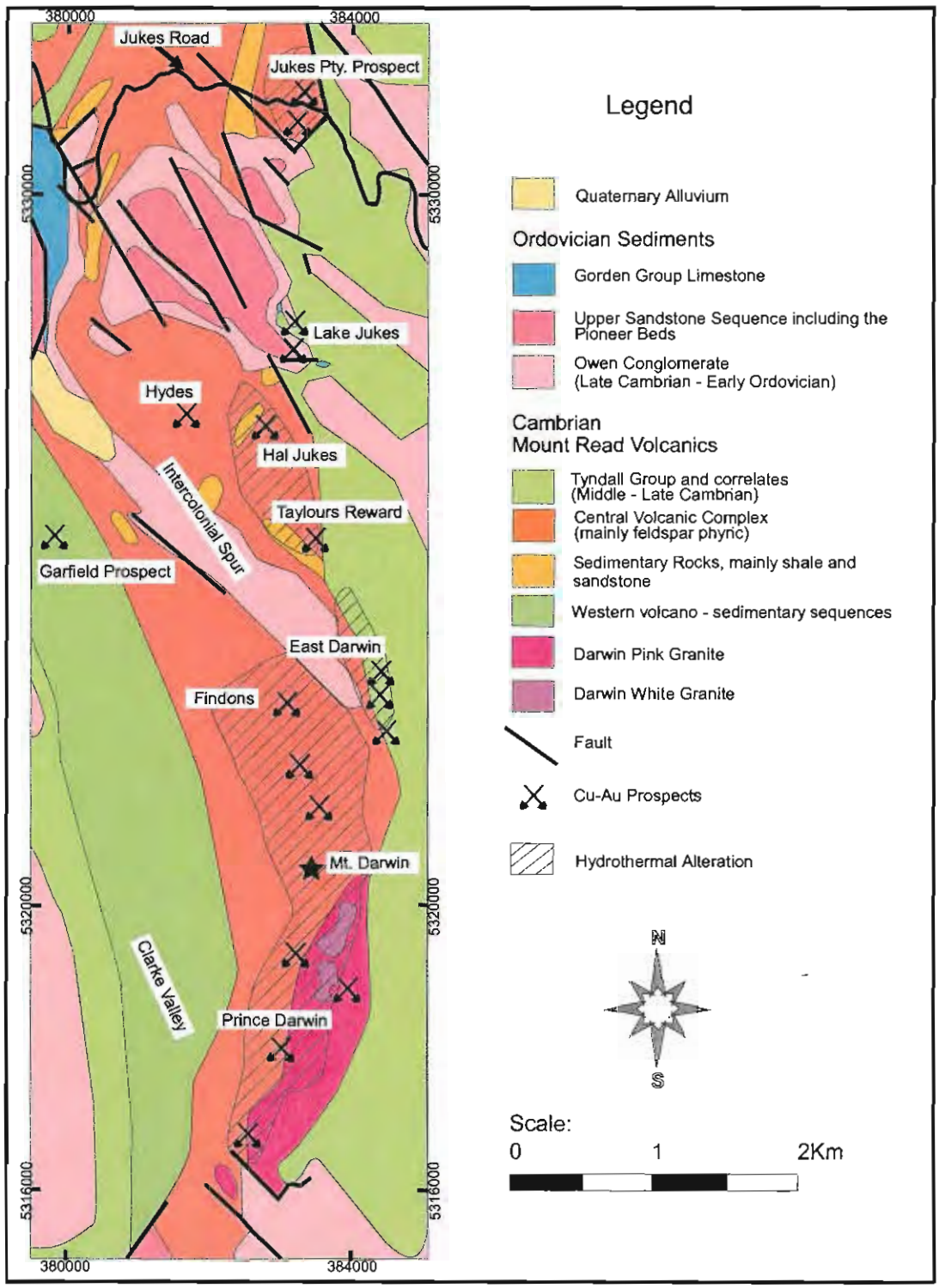

Figure 1.2. Study area showing the local geology, location of significant Cu-Au prospects and the extent of granite-related hydrothermal alteration. Data from this study and Corbett et al., 1993.

1.4 PREVIOUS WORK

The Darwin Granite and surrounding volcanic rocks have been studied by Hills (1914), Corbett and Cuffley (1970), White (1975), Corbett et al. (1993) and Jones (1993). These studies have focused on lithologic and structural relationships between units, but have mostly ignored the hydrothermal alteration and mineralisation around the granite and in the surrounding volcanics.

Cu-Au occurrences at the Jukes Prospect were studied by Doyle (1990) and Halley et al. (1996). The East Darwin Prospect and the Intercolonial Spur area were studied by Gadaloff (1996) and the Garfield Prospect was documented by Halley et al. (1996) and Duncan (1997). Leaman and Richardson (1989) and Large et al. (1996) included the study area in regional geophysical studies of gravity and magnetic data designed to define Cambrian granite morphology. Solomon et al. (1988) included the Jukes-Darwin area in a regional sulfur isotope study of the entire MRV. Large et al (1996) compared hydrothermal alteration and mineralisation styles in the Jukes-Darwin area to hydrothermal alteration and mineralisation in the Mt. Lyell mining field, and proposed a genetic model linking the two mineralisation styles. Part of this research is directed to test that model.

1.5 WORK PLAN

The proposed research has two primary components, field mapping and geochemistry. The field program involved detailed geologic mapping of volcanic rocks in the Clark Valley, west of the Darwin Granite, inward toward the granite contact with CVC rocks The objectives were to map and identify the effects of hydrothermal alteration related to the Darwin Granite, and to determine if the hydrothermal alteration formed identifiable zones. In addition, rock samples were collected for petrographic examination and geochemical analysis. Geologic mapping within the Darwin Granite was undertaken to detail the composition and characteristics of the various phases of itself. Significant effort was track geochemical changes in both whole rock compositions and hydrothermal alteration mineral assemblages in relation to distance from the granite. The following geochemical techniques were applied.

- Whole rock geochemistry (major, minor, trace elements, and REE) was conducted on samples of the Darwin Granite and unaltered and altered volcanics. Analytical results from the least-altered rocks were used to classify the granite and the surrounding volcanic rocks. Mass changes to the volcanic rocks as a result of hydrothermal alteration were calculated in comparison to least-altered equivalents.
- Sulfur isotope ($\delta^{34}S$) analysis of pyrite within the granites and through cross-sections of various hydrothermal alteration styles near the Darwin Granite and along the Jukes Road at the Jukes Prospect. Samples were collected to determine the sources of sulfur in the hydrothermal system and the extent of mixing with other fluids.
- Oxygen isotope analysis ($\delta^{18}O$) of K-feldspar, quartz, magnetite and chlorite were conducted to identify fluid sources and possible crystallisation temperatures.

1.5.1 Sampling and Sample Numbers

Along the Jukes Road, 115 ten metre long chip samples were collected along a 5.7Km long traverse. Rock chip and whole rock samples were collected at 500 metre intervals outside the Jukes Prospect and at 10 metre intervals within the prospect. Samples collected along this traverse are numbered with respect to distance from the Tyndall Group contact with the overlying Owen Conglomerate, arbitrarily given the metreage of 800. In other words, 10330 refers to the sample collected at the metreage 10330 along the road, 530 metres along the road from the

Tyndall Group contact with the Owen Conglomerate. For reference, the main mineralisation at the Jukes Prospect occurs at approximately 10100 to 10200 metres. All other rock samples were numbered using a numbering system starting with B1000. From the Jukes Road, 87 selected chip-samples and 47 selected hand specimens were collected, analysed, and 80 thin-sections were prepared and examined. 60 rock samples from the Darwin Granite and Clark Valley-Slate Spur area were analysed and compared to the samples from the Jukes Road and Intercolonial Spur. A cross-reference to the University of Tasmania catalog system is provided in Appendix A.

1.6 ORGANISATION OF THESIS

The general geology and regional geologic setting of the southern MRV is summarised in Chapter 2. In Chapters 3 and 4, petrographic descriptions of least-altered granites and volcanic rocks are presented and geochemical characteristics discussed. These two chapters provide detailed descriptions of the multiple phases of the Darwin Granite, and of a number of volcanic facies within the three main volcanic sequences intruded by the Darwin Granite. Petrographic descriptions of hydrothermally altered volcanic rocks are presented in Chapter 5, together with documentation of mapped hydrothermal alteration zones, mineral assemblages and styles. Chapter 6 discusses calculated mass changes in relation to the various hydrothermal alteration assemblages, and proposes likely alteration reactions. Mineral chemistry is also discussed. Vein styles, ore mineral assemblages, hydrothermal breccias and mineralisation paragenesis are documented in Chapter 7. Oxygen-deuterium and sulfur isotope results are presented in Chapters 8 and 9 respectively. Chapter 10 includes: 1) comparisons between hydrothermal alteration and mineralisation in the Jukes-Darwin area and Prince Lyell and a new genetic interpretation for Prince Lyell, 2) a discussion of the Large et al. (1996) Cambrian granite-related model for formation of the Mt. Lyell field, 3) conclusions of this research, and 4) a genetic model for the Jukes-Darwin area.

CHAPTER 2

2.0 REGIONAL GEOLOGY, STRUCTURAL SETTING AND MINERALISATION OF THE SOUTHERN MT. READ VOLCANIC BELT

2.1 INTRODUCTION

The Cambrian Mt. Read Volcanic Belt (MRV) occur as a continuous belt of calc-alkaline rhyolitic and dacitic rocks with minor basalts, andesites and granites (Figure 1.1). The MRV is 10 to 20 km wide by 200 km long and fills the eastern margin of a Mid-Cambrian extensional basin known as the Dundas Trough. The Dundas Trough lies between quartzites and schists of the Tyennan Precambrian nucleus to the east and poly-deformed but weakly metamorphosed Late Proterozoic quartzite-quartz wacke-slate sequences of the Rocky Cape Group to the west (Corbett, 1981; Corbett, 1992). The MRV is overlain by late Cambrian to early Ordovician conglomerates and sandstones of the Owen Conglomerate. Comprehensive summaries of the regional geologic setting of the MRV and the various lithostratigraphic units are provided in Seymour (1980); White and Chappell (1983); Corbett and McNeil (1988); Corbett (1989); Corbett (1994); Berry (1994); and White and McPhie (1996).

The MRV comprise seven major lithostratigraphic units: the Sticht Range Beds, the Eastern Quartz-Phyric Sequence (EQPS), the Central Volcanic Complex (CVC), the Tyndall Group, the Western Volcano-Sedimentary Sequences (Yolande River Sequence, Dundas Group, and Mt. Charter Group), andesitic to basaltic volcanics, and tholeiitic mafic rocks (Corbett, 1992). The general geology of the southern Mt. Read Volcanics is shown on Figures 1.1 and 1.2. Figure 2.1 is a comparative stratigraphic column, and Figure 2.2 is a generalised cross-section through the Garfield Valley north of Mt Darwin. The Sticht Range beds are a thin clastic unit that contains Precambrian detritus and lies directly over the Tyennan basement along the eastern margin of the Dundas Trough. The EQPS is composed of quartz-feldspar-porphyritic lavas (rhyolites, dacites, and minor andesites) and volcaniclastic rocks, with abundant quartz-feldspar (± biotite) porphyry intrusions and some related granitoids (Corbett, 1992). The CVC consists of a sequence of feldspar-porphyritic lavas and associated volcaniclastics extending from Macquarie Harbour in the south to Red Hills in the north. The CVC lies adjacent to and may interfinger with the EQPS making a strict stratigraphic definition impossible (Corbett, 1992; Halley and Roberts, 1997). Western Volcano-Sedimentary Sequence rocks interfinger with the CVC and thus, together with fault disruption and lateral variations, makes definition of a strict stratigraphic sequence difficult. The Western Sequence south of the Henty Fault is called the Yolande River Sequence. North of the Henty Fault, it is called the Dundas Group. In the Hellyer area, this sequence is known as the Mt. Charter Group (Corbett, 1992).

Andesitic to basaltic volcanics occur as discrete lenses throughout the upper portions of the CVC and within the Yolande River Sequence (Corbett, 1992; Crawford et al., 1992). Crawford et al. (1992) described the geochemistry and petrogenesis of the andesites in the Mt. Read Volcanics.

Tholeiitic mafic rocks, including basalts, gabbros and dolerites, together with minor ultramafic rocks, occur along the western part of the Mt. Read belt, particularly south of Queenstown. These rocks are geochemically unique from the typical calc-alkaline Mt. Read rocks and are discussed in detail by Corbett (1992) and Crawford et al. (1992).

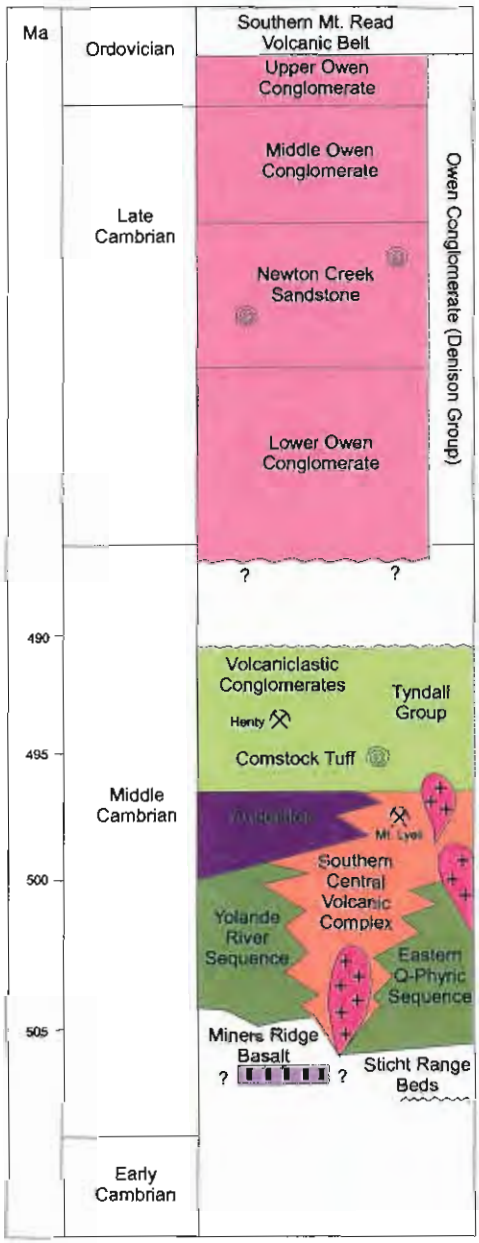

Figure 2.1. Comparative stratigraphic column of the Mt. Read Volcanic Belt in the study area. Modified from Corbett (1992), dates from Perkins et al. (1993).

The Tyndall Group is a sequence of distinctive mass-flow breccias, sandstones and volcanolithic conglomerates that extend from Mt. Darwin to Red Hills. The Tyndall Group and its correlates overlie the CVC and have been described by numerous authors Corbett (1974), McNeil and Corbett (1988), Corbett (1992), Corbett et al. (1993), Jones (1993) and White and McPhie (1996). The top of the Tyndall Group is a conformable to unconformable contact with the siliciclastic Owen Conglomerate. The Tyndall Group consists of mainly crystal-rich (quartz, feldspar, and lesser pyroxene) tuffaceous mass-flow breccias and sandstones. The basal unit in the Tyndall

group has been defined as the Comstock Tuff (Corbett et al., 1974) and contains an unusual fossiliferous limestone with late Middle Cambrian trilobites (Jago et al., 1972). This unit was deposited in a shallow marine, near-shore, shallow bank environment. Welded tuffs occur in the volcaniclastic mass-flow units in the upper Comstock Tuff suggesting a shallow-marine environment (Corbett, 1992).

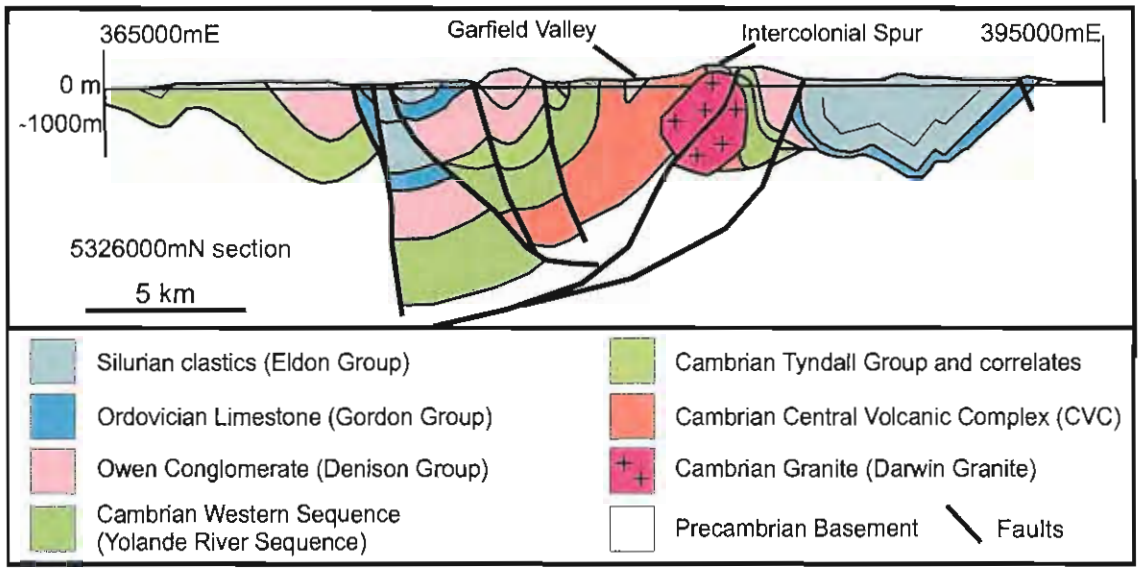

Figure 2.2. Generalised cross-section through the Garfield Valley and Intercolonial Spur, north of the Darwin Granite. Modified from Berry and Keele (1993).

Metamorphism and deformation of the Cambrian and Ordovician sequences occurred during the Tabberabbereran Orogeny in the mid-Devonian. Widespread intrusion of post-tectonic granitoids followed in the Late Devonian and Early Carboniferous.

2.2 REGIONAL SETTING

Volcanic sequences of the MRV are interpreted to have been deposited in a series of complex basins or troughs separated by areas of Proterozoic basement rocks (Corbett, 1981; Corbett and Lees, 1987; Corbett, 1992; Crawford and Berry, 1992). The volcanic sequences interfinger to the west with sedimentary sequences of the Dundas Trough, the largest of these basins (Corbett, 1981). Sedimentary sequences in the Dundas Trough are of two main types. (1) Early shallow marine clastics and carbonates (Success Creek Group) are overlain by deeper marine graywacke-mudstone-chert sequences with associated tholeiitic basalts (Crimson Creek Formation). (2) Fossiliferous Middle to Late Cambrian flysch-type sequences (Dundas Group and correlates) that interfinger with and are partly derived from the MRV (Corbett, 1992; Crawford et al., 1992). Recent detailed descriptions of Dundas Group sedimentary rocks were provided by Selley (1997). Cambrian age ultramafic-mafic complexes occur throughout the trough and include High Mg and low Ti lavas and associated cumulates of boninitic affinities (Corbett, 1992; Crawford et al., 1992). Ultramafic-mafic detritus derived from these complexes occurs in the lower Dundas Group conglomerates.

Cambrian volcanism occurred during Dundas Group time (Middle to Late Cambrian) but the age of the earliest eruptions is not certain. There may have been a peak of volcanism during the late Middle Cambrian, with declining activity in the early Late Cambrian (Corbett, 1981).

During the Late Cambrian to Early Ordovician, the CVC was buried under fluvial and shallow marine siliciclastic conglomerates and sandstones (the Owen Conglomerate and correlates), derived from unroofing of the Precambrian Tyennan nucleus. The Owen Conglomerate reaches a thickness of over 1200 m in graben structures parallel to the margins of the Precambrian nucleus. The Owen Conglomerate is overlain by a sequence of regionally transgressive shallow marine carbonates (Gordon Group) and Siluro-Devonian clastic shelf sequences (Eldon Group).

The stratigraphy of the MRV is divided on a geographical basis into rocks north and west of the Henty Fault and rocks south and east of the Henty Fault (Figure 1.1). This research is primarily concerned with those rocks within the MRV that are south and east of the Henty Fault, and in particular south of Mt. Lyell. The stratigraphy north and west of the Henty Fault is defined differently from that south of the fault. In the Northwest of the belt the Western Sequence consists of the Mt. Charter Group (north, around Hellyer) and part of the Dundas Group (south, around Rosebery, Corbett, 1992). The Mt. Charter Group hosts the Hellyer and Que River VHMS deposits. At Rosebery, Corbett and Lees (1987) proposed that the west-facing White Spur Formation at the base of the Dundas group unconformably overlies lavas and volcaniclastic rocks of the CVC. However, recent work in the Hall Rivulet canal suggests the opposite (Nunn, 1995). The Rosebery and Hercules massive sulfide deposits are thought to be hosted within the CVC (Corbett, 1986).

2.2.1 Regional Geology of the Southern Mt. Read Volcanics in the Mt. Darwin-Mt. Lyell Area

2.2.1.1 THE WESTERN VOLCANO-SEDIMENTARY SEQUENCE

The Western Volcano-Sedimentary Sequence is the oldest sequence of volcanic rocks in the MRV. In the southern MRV, the sequence contains marine fossils. It typically consists of interbedded tuffaceous mass-flow deposits (typically quartz-feldspar phyric), turbiditic sandstones (of volcanic or mixed volcano-metamorphic provenance), shard-rich tuffaceous mudstone, micaceous siltstones, and graphitic black shales (Corbett, 1992). Locally, andesitic lavas and breccias occur within the sequence in some areas such as the Garfield Valley. Intrusive porphyries and felsic lavas are common.

The portion of the Western Sequence exposed in the southern MRV is known as the Yolande River Sequence (YRS). The YRS typically dips west in the study area. A major lens of andesitic-basaltic rocks (mainly lavas and breccias with some intrusions), referred to as the Lynch Creek basalts, occurs within, or at the top of the sequence at Lynchford. Similar bodies of rocks occur northwest of Queenstown in the Howard's Plains area (Calver et al., 1987).

The YRS is well exposed in the north-south Clark Valley and Slate Spur area immediately to the west of Mt. Darwin and the south Darwin plateau. Rocks of the CVC are exposed along the eastern part of the Clark Valley, where they interfinger with rocks of the upper YRS. YRS rocks are unconformably overlain by Tyndall Group correlates (Corbett et al., 1993).

The YRS in the Mt. Darwin area is a mixed sequence of quartz-phyric lavas and volcaniclastic rocks, with minor mudstones, sandstones and graphitic black shales. Quartz-feldspar porphyries and feldspar-phyric units are subordinate. The rocks are easily identified by their clear glassy quartz crystals. Typically they have a pale green, sericitic, foliated groundmass. Volcaniclastic rocks are medium to fine-grained and, because of the well-developed cleavage, are not easily distinguishable from coherent lavas.

2.2.1.2 CENTRAL VOLCANIC COMPLEX (CVC)

The Central Volcanic Complex (CVC) consists of a sequence of feldspar-phyric volcanics, including abundant rhyolitic-dacitic lavas and pumice-bearing volcaniclastic rocks and minor volcano-sedimentary horizons. The CVC forms the main central portion of the MRV from Macquarie Harbour to Red Hills (Figure 1.1). In the southern Mt. Read Volcanics, the CVC is intruded by the Cambrian Elliott Bay and Darwin Granites. The CVC lies between and interfingers with the EQPS and the Western Sequence. The CVC is characterised by pink-weathering K-rich lavas with albite phenocrysts and rare quartz phenocrysts in a spherulitic felsic groundmass. This lack of quartz phenocrysts is characteristic of the CVC, and serves to separate it from other sequences in the Mt. Read belt. Flow-banding and autobrecciation are common and columnar jointing is locally well developed, particularly along the Jukes Road (Figure 1.2). In the study area, the CVC is in fault contact with the EQPS and interfingers with the YRS (this study).

Bedded sedimentary rocks are rare in the CVC in all areas, and together with the abundance of lavas and pumaceous units originally led Corbett (1981); Cox (1981); and Green et al. (1981) to interpret the CVC as subaerial in origin. Studies by Allen and Cas (1990) at Rosebery-Hercules suggest that the massive pumaceous mass-flow units are submarine with false welded textures produced by compaction and metamorphism. Current thinking has most of the CVC forming in a submarine environment of variable depth (Corbett, 1992; Crawford et al., 1992; McPhie and Allen, 1992; McPhie and Gemmell, 1992; Large et al., 1996).

2.2.1.3 EASTERN QUARTZ-PHYRIC SEQUENCE

The EQPS is composed of quartz-feldspar-porphyritic lavas (rhyolites, dacites, and minor andesites) and volcaniclastic rocks, with abundant quartz-feldspar (± biotite) porphyry intrusions. The EQPS is characterised by the large (2-3 mm) quartz phenocrysts that occur throughout the volcanic facies within the sequence. Near Red Hills, quartz porphyries intruded the Precambrian basement adjacent to the Cambrian contact indicating that the volcanics were erupted through the continental basement (Corbett, 1992). Several units of bedded sandstone, siltstone and shard-rich mudstone occur within the sequence, indicating a subaqueous environment of deposition. No evidence of subaerial conditions (eg., welded tuffs, cross-bedding) has been reported (Corbett, 1992).

The EQPS is exposed along Jukes Road for over 1 km in the study area. Two primary lithologies are present: (1) Coherent quartz-feldspar-phyric dacite is exposed, in an area between the CVC and Tyndall Group rocks. Quartz-feldspar-phyric dacites have well-developed tectonic cleavage and contain up to 30% feldspar and quartz phenocrysts (average crystal size 0.5 to 1 mm) in a groundmass with a sandy texture. The dacites are sericite-altered with minor K-feldspar, chlorite, pyrite, and carbonate. 2) Quartz-phyric rhyolitic volcaniclastics containing up to 20% feldspar and quartz crystals (average crystal size 1 mm) in a matrix of quartz and feldspar. Lithic clasts of quartz-feldspar-phyric volcanic rocks are common.

2.2.1.4 TYNDALL GROUP AND CORRELATES

Tyndall Group rocks occur in a linear belt extending from eastern Mt. Lyell through Mt. Owen to Mt. Jukes and Mt. Darwin. Correlates of the Tyndall group overlap and interfinger with the EQPS and the YRS in the study area (Corbett, 1992). Within the study area, Tyndall Group rocks are exposed to the east of the Darwin Granite where an erosional unconformity between Tyndall Group volcanolithic conglomerate and the Darwin Granite occurs (Figure 1.2). Facies identified in the study area include: basal conglomerate, volcaniclastic lithic conglomerate, polymictic lithic volcaniclastic sandstone, and feldspar-phyric dacites (Jones, 1993). The basal conglomerate of the Tyndall Group rests unconformably on the Darwin Granite (White, 1975), and grading in the basal conglomerate suggests younging to the east (Jones, 1993). Tyndall Group rocks in contact with the Darwin Granite are medium to coarse-grained polymictic conglomerates containing rounded clasts of sericite-altered coarse-grained pink Darwin Granite and other volcanic clasts derived from the CVC. This is taken as unequivocal evidence of late Cambrian uplift and erosion of the Darwin Granite (Jones, 1993).

2.2.1.5 DARWIN GRANITE

The Darwin Granite and its associated hydrothermal alteration and mineralisation are the primary focus of this research. As such, it is thoroughly described in Chapter 3 and other sections of this thesis. The Darwin Granite crops out at two separate locations between Mt. Darwin and South Darwin Peak. The main body is approximately 5 km long by 1 km wide and forms the Darwin Plateau. The second body is smaller (120 m x 50 m) and crops out west of South Darwin Peak. Jones (1993) conducted a detailed geological and geochemical investigation of the Darwin Granite. Additional studies of the Darwin Granite and surrounding volcanic rocks were conducted by Hills (1914); Solomon (1960); White (1975); Corbett (1976), and others. The Darwin Granite contains two major phases and two minor phases as mapped in the field. The four phases are pink granite, white granite, microgranite and quartz porphyry. All previous workers have recognised the two dominant phases of granite. White (1975), named them the 'Pink' and 'White' phases, based on their distinctive mineralogy. The pink granite phase is volumetrically the most common phase, making up about 80% of the mapped granite outcrop. The white granite comprises approximately 15% with the remainder consisting of microgranite and quartz porphyry phases.

In the west, the Darwin Granite has intruded volcanic rocks of the CVC along a sharp and well-defined boundary. The eastern contact between the Darwin Granite and the Tyndall Group is an

erosional unconformity. The erosional contact means that the Darwin Granite was emplaced in CVC volcanics, cooled, uplifted and eroded before the deposition of Tyndall Group rocks.

The granite contains several large elongate bodies of altered and hornfelsed volcanic rocks trending NE-SW, parallel to the long axis of the granite (Solomon, 1960; White, 1975; Jones, 1993). These bodies were interpreted to be large xenoliths or roof pendants of host volcanic rocks (Solomon, 1960; Jones, 1993). White (1975), concluded that the volcanic bodies are underlying volcanics caught up in the core of a tight anticline trending roughly parallel to the length of the granite.

2.2.1.6 ANDESITIC-BASALTIC VOLCANICS

Andesitic and basaltic volcanics occur within all of the sequences within the Mt. Read belt. The andesitic rocks are calc-alkaline and tholeiitic. The geochemistry of the andesites is discussed in Chapter 4. The andesites typically consist of interbedded flows and breccias, associated with shallow intrusive bodies (Corbett, 1992). Some of the andesites are entirely intrusive. The andesites are either plagioclase-pyroxene-phyric or plagioclase-hornblende-phyric. Large plagioclase-hornblende-phyric bodies occur along the Anthony Road, the Queenstown area and in the Garfield Valley. A 500 m thick sequence of andesites occurs at Mt. Lyell and hosts the Comstock orebody. Pyroxene-phyric andesites such as the Reservoir Andesite and the Little Owen Andesite crop out near Queenstown. The pyroxene-phyric Lynch Creek Basalts and a series of minor intrusions of similar composition crop out south and northwest of Queenstown respectively (Corbett, 1992).

The andesite bodies typically contain breccias and quench-fragmented textures, including pillows and pillow breccias. These textures are consistent with a submarine extrusive origin for the andesites.

2.2.1.7 CAMBRIAN AND ORDOVICIAN RELATIONSHIPS

The Ordovician Owen Conglomerate consists of red to purple stained (hematite stained) quartz pebble conglomerates, sandstones and siltstones that contain abundant Precambrian detritus. This detritus was eroded from the Tyennan Nucleus following regional uplift associated with the Late Cambrian Jukesian (Dalamerian) Orogeny (Corbett and Solomon, 1989; Corbett and Turner, 1989). Siliceous sandstone and quartz-pebble conglomerates of the Owen Conglomerate unconformably overlie Late Cambrian Tyndall Group rocks in the South Darwin Peak area and rest unconformably but directly on CVC rocks to the west of the peak (Corbett, 1976). On Mt. Sorell, the Owen Conglomerate is 1200 m thick and overlies a major volcaniclastic conglomerate of the Tyndall Group. At Mt. Lyell, an unconformity of similar age has been named the Haulage Unconformity and the overlying unit within the Owen Conglomerate has been named the Pioneer Beds (Reid, 1975; Cox, 1981).

2.2.2 Structure of the Southern Mt. Read Volcanics

2.2.2.1 STRUCTURAL SETTING

The structural history of western Tasmania is complex and has been the subject of numerous studies (Solomon and Griffiths, 1974; Corbett, 1976; Seymour, 1980; Corbett and Lees, 1987; Berry and Keele, 1992; Crawford and Berry, 1992; Keele, 1992; Berry and Keele, 1993; Jones, 1993). The structural history is dominated by non-cylindrical folding, and there is strong evidence of multiple reactivation of early fold and fault structures (Berry, 1994). The result of the complex deformation history is an abundance of local unconformities, disconformities and contradictory structural relationships. An example of a contradictory relationship is Devonian cleavage orientations that are not parallel to the axial plane of the folds with which they are associated. Many of the fold trends considered to be Devonian structures are open Cambrian folds that were tightened in the Devonian (Berry, 1994). Berry and Keele (1993) and Berry (1994) and have outlined nine major geological events that have affected western Tasmania between the Late Precambrian and the Devonian. They are summarised below.

Event 1: Neo Proterozoic shallow water sedimentation on the eastern margin of the East Antarctic shield.

Event 2: Penguin Orogeny, the oldest demonstrated event in Tasmania

Event 3: Passive margin formation (600 Ma to early Cambrian); A two-stage rift phase is recognised in most of western Tasmania. An early shallow water sequence followed by tholeiitic volcanism (Crawford and Berry, 1992).

Event 4: Arc collision and thrusting (525-510 Ma); The passive margin of eastern Australia collided with an oceanic arc, and major slices were thrust over Tasmania. Allochthonous elements include mafic/ultramafic complexes.

Event 5: Delamerian Orogeny (510-490 Ma), 3 phases.

Part 1. Middle-Middle Cambrian extension, characterised by rapid subsidence, complex extensional fault geometry, active syn-orogenic deposition, major post-collisional felsic-dominated volcanism (MRV) and VHMS mineralisation.

Part 2. Late-Middle to early Late Cambrian north-south compression followed extension. Intrusion of the Darwin, Elliott Bay and Murchison granites. Tyndall Group deposition.

Part 3. Late Cambrian reactivation of earlier extensional faults as reverse faults (Henty Fault) and development of upright north-trending open folds. Uplift of the Tyennan block and development of the Owen Conglomerate. This event corresponds to the Jukesian Orogeny of previous authors.

Event 6: Ordovician-Silurian sag phase; shallow water platform sedimentation.

Event 7: Silurian Deformation recognised in eastern Victoria and farther north; is represented as a hiatus in deposition in Tasmania.

Event 8: Early Devonian cycle of deposition including renewal of shelf sedimentation.

Event 9: Middle Devonian orogenesis (Tabberabberan Orogeny): characterised by complexity of fold orientations probably controlled, in part, by pre-existing Cambrian fold trends. The Sn-W related western Tasmania Devonian granites were intruded during and after the orogenic event.

2.2.2.2 STRUCTURE OF THE MT. DARWIN-MT LYELL AREA

The study area contains evidence for the fifth and ninth events listed above. Shortly after, or coeval with, the deposition of the southern MRV the Darwin Granite intruded the CVC. Solomon (1960); Solomon (1981); and Jones (1993) have argued that the Darwin Granite is a high level (2-3 km), subvolcanic intrusion genetically related to the CVC volcanic sequence. This argument is based, in part, on strong evidence that the Darwin Granite was emplaced, cooled, uplifted and eroded, all after the deposition of the CVC and before, or simultaneous with, the beginning of Tyndall Group deposition. Evidence includes clasts of all rock types in the basal conglomerate of the Tyndall Group. In some of the volcanic clasts, a well-developed penetrative cleavage is found. This cleavage development is taken as evidence of folding and uplift prior to the deposition of the Tyndall Group. A second unconformity occurs between the Owen Conglomerate and Tyndall Group rocks on South Darwin Peak and the Owen Conglomerate rests directly on CVC volcanics in places. This unconformity may be due to either a continuation or resurgence of the uplift event that exposed the Darwin Granite during late Tyndall Group time.

The structure of the volcanics is difficult to determine because of the massive nature of the rocks and the lack of evidence of primary facing. Primary banding and bedding in the YRS rocks in the Clark Valley (Figure 1.2) typically strike roughly N-S and are sub-vertical or have steep westerly dips. The rocks are cut by a prominent sub-vertical foliation striking N to NNW. CVC rocks along the western margin of the Darwin Granite strike roughly N-S, have steep westerly dips, and well-developed N to NNW cleavage. Bedding in the Tyndall Group rocks around South Darwin Peak strikes NE-NNE and has moderate dips to the south-east (Corbett, 1976). The Tyndall Group rocks are cut by the dominant N to NNW cleavage.

Tabberabberan-related deformation structures are well defined in the area around the Darwin Granite. Features associated with the event have created a strongly-developed N-S trending cleavage in many of the altered volcanic rocks, obscuring original textural relationships. A strong NNW-N cleavage developed in the Owen Conglomerate overlying the Tyndall Group, is interpreted to be of Tabberabberan age (Corbett, 1976). Numerous quartz-chlorite veins presumably of Devonian age cut earlier fabrics. Locally, sulfides were concentrated along these structures.

2.2.3 Geochronology

There is good biostratigraphic control for the Mt. Read belt, firmly establishing the sedimentary lithologies as Middle to Late Cambrian in age. However, the exact boundary between the Late Cambrian and the Early Ordovician is unclear. Because of the lack of marker horizons and the interfingering and overlapping nature of large volcanic piles, detailed volcanic stratigraphy of the MRV remains poorly understood. The results of K-Ar radiometric age dating have been imprecise, due in part to the effects of alteration, deformation and metamorphism (McDougall and Leggo, 1965; Adams et al., 1985). However, K-Ar dating has identified the major periods of deformation and metamorphism (clusters of data are around 475-455 Ma and around 400 Ma) in the Ordovician and the Devonian (McDougall and Leggo, 1965; Adams et al., 1985). Some of the original U-Pb zircon ages determined were complicated by inherited zircon populations (Adams et al., 1985).

More recently, Perkins and Walshe (1993) and Turner et al. (1998) have dated a number of geologic events in the Mt. Read Volcanics. They utilized the SHRIMP ion microprobe to obtain U-Pb on zircons and conventional $^{40}Ar/^{39}Ar$ dating on hornblende separates. Their results are summarised in Table 2.1. The Darwin Granite (510 +64 -21 Ma, Adams et al., 1985) has intruded feldspar and quartz-feldspar phyric rocks of the Central Volcanic Complex. The CVC has a mean age of 502.6 ± 3.5 Ma (Perkins and Walshe, 1993), and recent analyses of a Jukes Road feldspar-phyric rhyolite within the CVC gave an age of 499.7 ± 4.4 Ma (Turner et al., 1998). Tyndall Group rocks are dated from 505.6 ± 2.8 to 494.4 ± 3.8 Ma (Table 2.1).

Radiometric dates of Perkins and Walshe (1993) and Turner et al. (1998) agree closely with the biostratigraphic evidence (Jago et al., 1972) and place the formation of the Central Volcanic Belt at 502.6 ± 3.5 (Perkins and Walshe, 1993). The Comstock Tuff in the Tyndall Group and the Mt. Black Dacite in the northern CVC gave younger ages of 494.4 ± 3.8 Ma and 494.9 ± 4.3 Ma respectively. This indicates that the entire MRV must have formed somewhere between 508-490 Ma.

Table 2.1. Geochronology of the Southern Mt. Read Volcanic Belt.

LITHOLOGY	DATING METHOD	MATERIAL	AGE	REFERENCE
Owen Conglomerate				
Newton Creek Sandstone	Biostratigraphic	Fossils	Late Cambrian	Jago et al. (1972)
Tyndall Group				
Comstock Tuff	U-Pb	Magmatic zircons	494.4 ± 3.8	Perkins and Walshe (1993)
Comstock Limestone	Biostratigraphic	Fossils	Late Middle Cambrian	Jago et al. (1972)
Volcaniclastic	U-Pb	Igneous zircons	502.5 ± 3.3	Perkins and Walshe (1993)
Ignimbrite	U-Pb	Igneous zircons	505.6 ± 2.8	Turner et al. (1998)
Central Volcanic Complex (CVC)				
Concordant Age	U-Pb	Magmatic zircons	502.6 ± 3.5	Perkins and Walshe (1993)
Mount Black Dacite	U-Pb	Igneous zircons	494.9 ± 4.3	Perkins and Walshe (1993)
Jukes Road Lava	U-Pb	Igneous zircons	499.7± 4.4	Turner et al. (1998)
Darwin Granite	U-Pb	Magmatic zircons	510 +64, -21	Adams et al. (1985)
Murchison Granite	$^{40}Ar/^{39}Ar$	Hornblende	501.0 ± 5.7	Perkins and Walshe (1993)

2.3 TECTONIC MODELS FOR THE MT. READ VOLCANICS

The Late Cambrian MRV are composed of submarine felsic and intermediate lavas, volcaniclastics and volcano-sedimentary sequences. The MRV are important tectonically as they represent a Cambrian sequence that is extensive in western Tasmania but poorly exposed on the mainland of southern Australia. The MRV formed as a result of three distinctive tectonic events: 1) Middle-Middle Cambrian compression and subsequent relaxation and extension associated with massive felsic to intermediate volcanism. This event produced the major Cambrian VHMS mineralisation of the belt. 2) The reversal from extension to compression during the Delamerian Orogeny (510-490 Ma) formed E-W upright folds. 3) Subsequently a N-trending upright fold event occurred along the Dundas Trough and the Owen Conglomerate was deposited. The major problem with interpreting these events has been the strong Devonian overprint resulting from the Tabberabberan Orogeny. The entire MRV was deposited, uplifted at least twice and eroded twice in a maximum time period of 20 million years.

Previously two major models for the tectonic evolution of the Cambrian rocks in the Dundas trough were proposed. Corbett and Lees (1987) suggest that the Middle to Late Cambrian portion of the Dundas Trough developed as a forearc-arc sequence above an easterly dipping subduction zone between the Rocky Cape region to the west and the Tyennan region to the east. However, a reinterpretation of the stratigraphy and geochemistry during the late 1980's and early 1990's (Berry and Crawford, 1988; Corbett and Turner, 1989; Corbett, 1992; Crawford and Berry, 1992) has discounted the 'arc' model based on a lack of arc-type stratigraphy and the demonstrable post-collisional nature of the MRV. Currently, the most widely accepted model is the 'allochthon model' of Berry and Crawford (1988) and Crawford et al. (1992), shown in Figure 2.3. A variation of the 'allochthon model' has the Tyennan region itself being an allochthon (Lees and Wright, 1994).

In summary, the MRV are post-collisional volcanics formed after arc-continent collision (Berry and Crawford, 1988; Crawford and Berry, 1992). The volcanics are a compositionally and texturally diverse sequence of lavas and volcaniclastic rocks that were affected by regional deformation and greenschist facies metamorphism. Distribution and lithofacies characteristics suggest that deposits from intrabasinal submarine and extrabasinal subaerial and/or shallow-marine centres are common (McPhie and Allen, 1992).

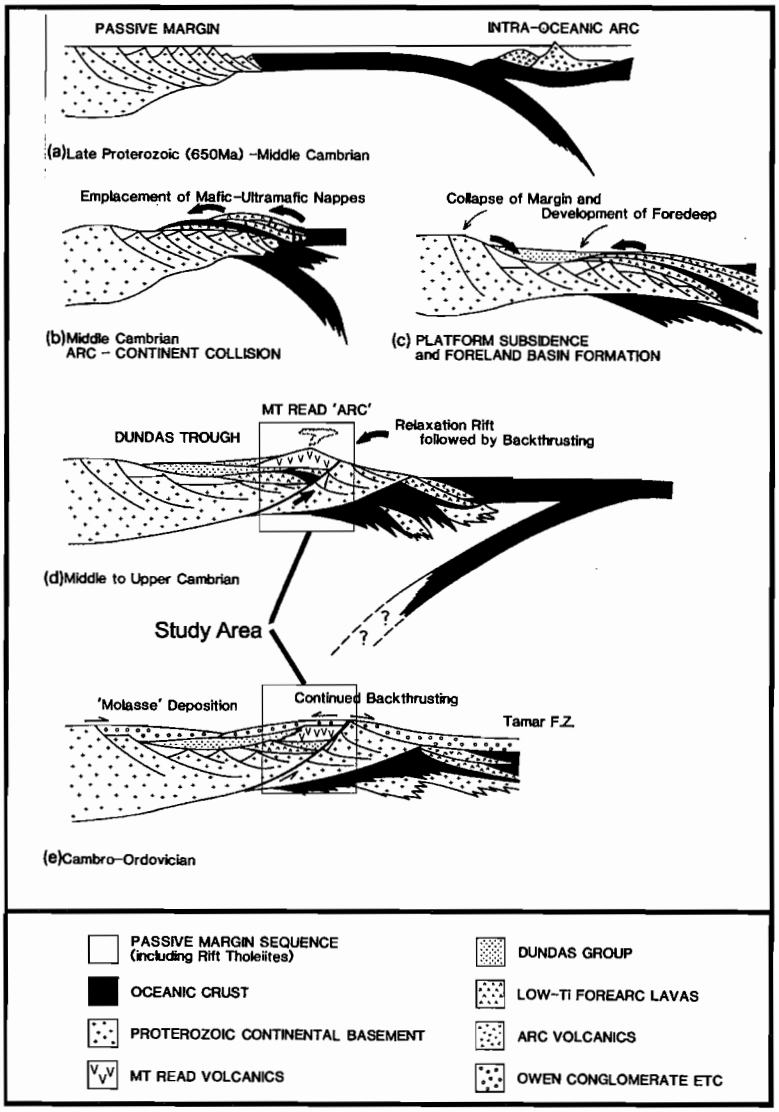

Figure 2.3. Hypothetical tectonic scenario for the Late Proterozoic and Early Palaeozoic evolution of Tasmania. (a) late Proterozoic evolution of a thinned, east-facing passive margin, and subsequent growth of oceanic arc farther east; (b and c) collision of attenuated passive margin with forearc of an intra-oceanic arc led to large-scale overthrusting of the forearc crust on to the passive margin. In (d) possible continued compression at the suture initiated a brief period of west-dipping subduction and development of a narrow tensional rift zone astride the MUC (mafic-ultramafic complexes) allochthon, in which the CVC lavas of the MRV were erupted. Extension related to relaxation and subsidence of the thickened crust in the collision zone may have resulted in generation (from subcontinental mantle of the underthrust passive margin) of the K_2O, P_2O_5 and LREE-enriched shoshonitic basalts in the upper MRV, and eventually, of the tholeiitic basaltic dyke swarm which intruded the CVC late in the history of the belt. Buoyant extrusion of the Proterozoic basement along major backthrusts provided for exposure and erosion of the Tyennan Block, and deposition of the Dennison Group (Owen Conglomerate) along the margins of the upthrust block (d and e). Figure and explanation from Crawford and Berry (1992). The tectonic setting of the study area is shown.

2.4 GEOLOGY AND MINERALISATION IN THE MT. LYELL FIELD

One of the major goals of this research is to document the regional extent of hydrothermal alteration associated with the Cambrian granites and evaluate the genetic link between the hydrothermal alteration in and around the granites and the hydrothermal alteration around the

Prince Lyell Cu-Au deposit at Mt. Lyell. This section summarises the geology, geochemistry and current theories on the genesis of hydrothermal alteration and ore styles in the Mt. Lyell field.

2.4.1 Geology of the Mt. Lyell Field

The Mt. Lyell mining field contains 22 known mineral deposits that span a spectrum of ore types, 17 of which are shown on Figure 2.4. More than 114 Mt of ore grading approximately 1.2% Cu, 6.7 g/t Ag and 0.4 g/t Au (Godsall, 1997a) were mined from the field to 1997 and mining continues.

The Mt. Lyell field is hosted in a package of interbedded coherent and volcaniclastic rhyolites and dacites with interbedded Suite I and Suite II andesites (Crawford et al. 1992) of the CVC. The regional geology (Figure 2.4) has been described by numerous authors (Loftus-Hills, 1927; Wade and Solomon, 1958; Solomon, 1960; Corbett, 1976; Corbett, 1981; Cox, 1981; Solomon, 1981; Walshe and Solomon, 1981; Corbett et al., 1989; Berry, 1992a; Crawford et al., 1992; Raymond, 1992). In the Mt. Lyell field, the CVC is subdivided into six conformable units known as the Mine Sequence (Cox, 1981) or Lyell schists by earlier workers (Gregory, 1905; Loftus-Hills, 1927). A summary is presented in stratigraphic order in Table 2.2. This sequence, with various localised modifications, has been used by all workers within the mine lease.

Table 2.2. Mine sequence stratigraphy at Mt. Lyell. Modified after Cox (1981).

Unit	Description
Unit F	0-350 m of dominantly dacitic to intermediate volcaniclastics and lavas
Unit E	0-800 m of silicic volcaniclastics
Unit D	250-800 m of volcaniclastics, lavas, open framework volcanic breccias and minor intermediate volcaniclastics and intrusives
Unit C	0-600 m of dominantly coarse-grained silicic volcaniclastics and pumice-bearing submarine breccias
Unit B	0-200 m of feldspar-phyric silicic lavas
Unit A	800 m of plagioclase-amphibole-phyric andesites and minor felsic volcaniclastics and siltstones

The structural history of the Mt. Lyell area is dominated by three major episodes. The earliest of these, the 'Haulage Deformation' occurred during the early Ordovician, prior to the deposition of the Pioneer beds above the Haulage Unconformity and was a local event (Cox, 1981). The main result of this event was the development of the Great Lyell Fault, which juxtaposes CVC volcanics against the Owen Conglomerate (Figure 2.5). In addition, minor thrusting and recumbent folding occurred. The 'Haulage Deformation' is significant because it describes the sequence of events that led to the current orientation of the Mt. Lyell ore bodies. Two subsequent deformations occurred during the Devonian Tabberabberan Orogeny (Cox, 1981; Arnold and Carswell, 1990; Berry, 1992a; Berry and Keele, 1993a). Formation of N-S trending folds and cleavage (D1) were followed by the development of N-W trending cleavage common in volcanics throughout the CVC (D2).

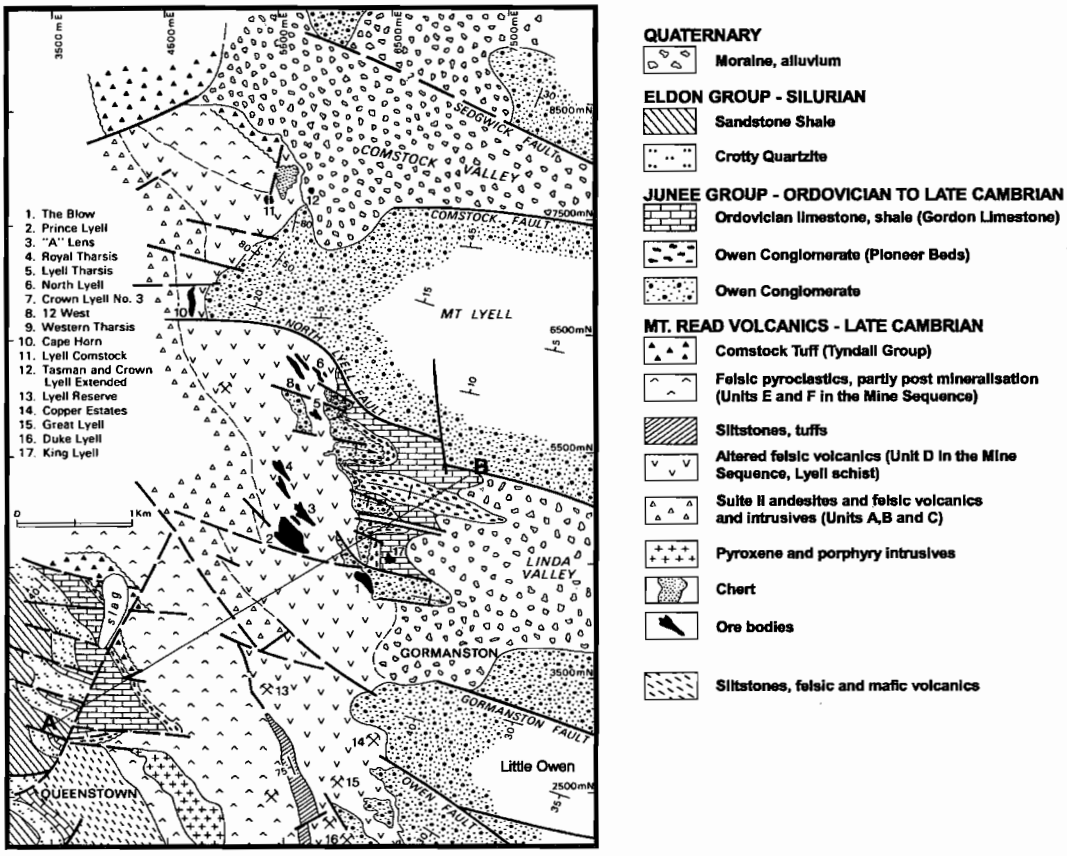

Figure 2.4. Geologic map of the Mt. Lyell mine area with orebody and prospect locations. Modified from Walshe and Solomon, (1981).

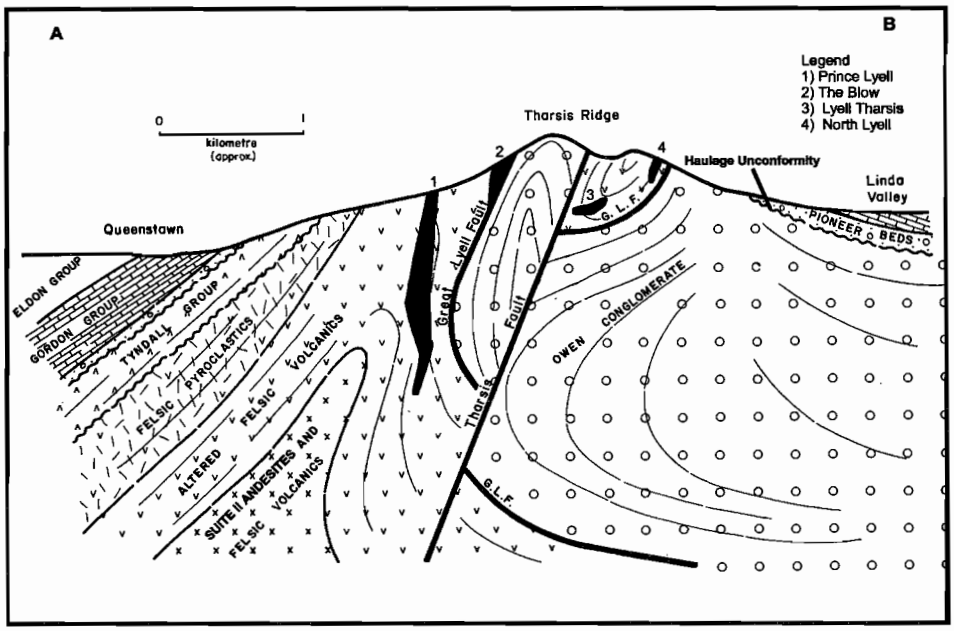

Figure 2.5. Schematic cross-section through Mt Lyell looking northwest. The section approximates line A-B in Figure 2.4. Ore bodies are projected onto the section and attitudes are shown with respect to the Great Lyell Fault (GLF). Modified after Hills (1990).

2.4.2 Hydrothermal Alteration

Within the Mt. Lyell field, hydrothermal alteration studies have typically focused on individual deposits (Green, 1971; Bryant, 1975; Walshe, 1977; Henley and Thornley, 1979; Hendry, 1981; Walshe and Solomon, 1981; Braithwaite, 1985; Sheppard, 1987; Arnold and Carswell, 1990; Manning, 1990; Raymond, 1992; Hart, 1993; Godsall, 1997b; Huston and Kamprad, in press). Only a few papers (Reid, 1975; Eastoe et al., 1987a; Arnold and Carswell, 1990) have summarised the general hydrothermal alteration styles in the Mt. Lyell field. The entire Mine Sequence at Mt. Lyell, stretching for over 10 km from the Little Owen to the Comstock Valley (Figure 2.4), has undergone pervasive feldspar-destructive quartz + sericite, quartz + sericite + chlorite + pyrite ± carbonate, and sericite ± albite alteration. While variations in hydrothermal alteration assemblages reflect differences in original rock compositions, alteration assemblages formed contemporaneous with mineralisation (Reid, 1975; Eastoe et al., 1987a; Arnold and Carswell, 1990).

2.4.3 Ore Styles

Five primary ore styles in the Mt. Lyell field have been documented by previous workers (Loftus-Hills, 1927; Solomon and Elms, 1965; Reid, 1975; Walshe and Solomon, 1981; Calver et al., 1987; Arnold and Carswell, 1990; Raymond, 1992; Godsall, 1997b) and others. The five are: 1) massive pyrite-chalcopyrite (the Blow and South Lyell), 2) chalcopyrite-bornite (North Lyell, Twelve West), 3) disseminated pyrite-chalcopyrite (Prince Lyell, Western Tharsis), 4) banded galena-pyrite-sphalerite (Tasman, Comstock and Crown Lyell Extended) and 5) native copper or 'copper clays' (Lyell Consols and King Lyell). The first three were all significant producers at Mt. Lyell and, including the fourth, are hosted within the mine sequence. The consensus of opinion is that the banded galena-pyrite-sphalerite ores are typical exhalative VHMS ores (Markam, 1968; Solomon et al., 1969; Green, 1971; Reid, 1975; Arnold and Carswell, 1990; MacDonald, 1991) and the 'copper clays' are considered to be a result of Late Cenozoic supergene processes (Solomon and Carswell, 1989). Neither of these two styles will be further discussed here.

At the Blow, massive pyrite-chalcopyrite ores occurred in a silicified pyritic lens with quartz-barite-sericite gangue containing minor chalcopyrite, tetrahedrite, tennantite, and enargite, and lesser stromeyerite (CuAgS), molybdenite, arsenopyrite and gold (Reid, 1975). A bonanza shoot discovered in 1893 yielded 850 t of ore grading 21.3% copper and 31,310 g/t silver as stromeyerite with tetrahedrite, chalcopyrite, bornite and chalcocite (Solomon and Elms, 1965). The nearby South Lyell deposit was also enriched in tetrahedrite toward the footwall (Reid, 1975).

Chalcopyrite-bornite orebodies were the richest in the field (Hills, 1990). The ores consisted of coarse-grained masses of bornite within bodies of pyritic chert adjacent to overhanging or steeply dipping parts of the 'schist'-conglomerate contact. Bornite occurs in three assemblages, bornite-chalcopyrite, bornite-pyrite and bornite-chalcocite with accessory tennantite, galena, digenite, covellite, mawsonite, enargite, molybdenite, sphalerite and rutile (Markam, 1968). The ores are associated with hematite-barite-quartz assemblages. Due to the stratigraphic location of the bornite rich deposits and their apparent association with a faulted contact against the Owen

Conglomerate, the bornite rich orebodies are interpreted to be either primary ores (Arnold and Carswell, 1990), or ores remobilised during the Devonian (Solomon et al., 1987a; Arnold and Carswell, 1990; Hart, 1993). At Lyell Tharsis and Western Tharsis, bornite-chalcopyrite occur in association with disseminated pyrite-chalcopyrite ores. The Western Tharsis deposit may be transitional between the two types (Huston and Kamprad, in press).

Disseminated pyrite-chalcopyrite ore bodies were the largest producers at Mt. Lyell. The Prince Lyell deposit is by far the largest (>100 Mt). The ores are hosted in quartz-chlorite and quartz-sericite-altered volcaniclastic rocks. Disseminated pyrite-chalcopyrite comprises 10-20% of the rock with lesser amounts of galena, sphalerite, bornite, molybdenite, stromeyerite, mawsonite, tetrahedrite, tennanite, and gold (Markam, 1968; Reid, 1975; Raymond, 1992). A Cu:Au ratio of 3 to 1 (wt.% : ppm) is consistent throughout the deposit (Raymond, 1992; Halley et al., 1996). Massive and semi-massive sulfide lenses 15-20 cm thick containing banded sphalerite and galena similar to the exhalative ores at Lyell Comstock have been reported (Solomon and Groves, 1994). At Prince Lyell, magnetite-apatite veins have cross-cut and replaced hypogene pyrite (Pyrite I) and chalcopyrite ores (Raymond, 1992; Raymond, 1996). Similar disseminated pyrite-chalcopyrite and magnetite-apatite ores occur at the Garfield Prospect (Figure 1.1) northwest of the Darwin Granite (Halley et al., 1996; Duncan, 1997).

2.4.4 Genesis of the Mt. Lyell Ore Deposits

Historically there has been a tendency to propose a common genetic model for all of the Mt. Lyell deposits, but the detailed studies of individual deposits resulted in numerous genetic interpretations. The earliest geological studies centred on high-grade banded massive Cu ores at the Blow. Various origins were proposed including: syngenetic deposition in association with geysers and sinters (Thureau, 1886), an epigenetic replacement model involving fault controlled deposition along the Great Lyell Fault (Gregory, 1905) and an epigenetic replacement model involving fault controlled deposition with magmatic-hydrothermal fluids from either a Cambrian granite (Loftus-Hills, 1927; Nye et al., 1934) or Devonian granite (Wade and Solomon, 1958). It was not until the 1960s, after discovery and analysis of other deposits in the mining field, that the idea that the mineralisation could be syngenetic/synvolcanic and associated with Cambrian volcanism was proposed as an idea to encompass the whole field (Hall and Solomon, 1962; Solomon and Elms, 1965). The syngenetic/synvolcanic model for Mt. Lyell gained momentum as the seafloor exhalative VHMS (Kuroko) model became accepted world wide in the late 1960s (Markam, 1968; Solomon et al., 1969). Work on the Cape Horn-Lyell Comstock deposits (Green, 1971), Corridor area (Bryant, 1975) and Tasman and Crown Lyell Extended fit well with this model. With further development of the VHMS model, disseminated deposits such as Prince Lyell, Western Tharsis and Royal Tharsis were interpreted to be either subseafloor disseminated VHMS deposits or cogenetic subsurface replacement ores associated with seafloor style mineralisation (Reid, 1975; Hendry, 1981; Walshe and Solomon, 1981; Braithwaite, 1985; Sheppard, 1987). Mineralising fluids that leached metals from the volcanic pile were thought to be circulating seawater localised at the junction of the proto Great Lyell Fault and Cambrian growth faults (Raymond, 1996). The recognition of secondary hematite and barite in the Owen

Conglomerate adjacent to the Great Lyell Fault revived the earlier post-Cambrian (Devonian) metamorphic replacement model (Sillitoe, 1985; Berry, 1990; Hart, 1993; Raymond, 1996). The Mt. Lyell deposits were deformed by post emplacement events during the 'Haulage Deformation' and the later Tabberabberan events. As a result, some bornite-chalcopyrite ores were remobilised and re-deposited in the Devonian (Solomon et al., 1987a; Arnold and Carswell, 1990; Hart, 1993).

Based on εNd values in apatite at the Garfield Prospect, together with $\delta^{34}S$ values, hydrothermal alteration assemblages, the association of magnetite-apatite with Cu-Au ore and an association to Suite II andesites, Halley et al., (1996) suggested that fluids responsible for the Prince Lyell ores exsolved from the Suite II andesites (Mine Sequence Unit A). The Prince Lyell system was still a seawater-dominated hydrothermal system (as indicated by sulfur isotopes), but was a VHMS-porphyry copper hybrid with mineralisation occurring at a mixing interface between a magmatic fluid and seawater. The key features are the apatite-magnetite association and the association with Suite II andesites as a source of magmatic fluid (Halley et al., 1996). Ores and hydrothermal alteration styles at Prince Lyell are similar to those at the Garfield Prospect (Duncan, 1997) in the southern MRV, where the model originated.

The newest contribution to the plethora of genetic models for Mt. Lyell come from Huston (in press) and Huston and Kamprad (in press) who studied the Western Tharsis deposit. Their work describes zoned hydrothermal alteration assemblages starting with a core of quartz-chlorite ± sericite surrounded by: quartz-pyrophyllite ± topaz ± fluorite ± zunyite ± woodhousite, pyritic quartz-sericite and quartz-chlorite-carbonate-sericite ± albite. The association of woodhousite, zunyite, topaz and fluorite with pyrophyllite-bearing advanced argillic alteration assemblages and a re-interpretation of Prince Lyell Pb isotope data (Figure 2.6, Gulson and Porritt, 1987) and geochemical dispersion patterns led them to propose a hybrid high sulfidation acid-sulfate Cu-Au model, again with similarities to porphyry copper deposits. However, there are problems with this model. The heat source for their model is an Ordovician granite of which no examples are currently known in Tasmania. Although sulfur isotope data from Mt. Lyell sulfates (barite) cluster around two nodes (23‰ and 38‰) both were interpreted to represent different fractionation models involving circulating Cambrian seawater (Solomon et al., 1969; Solomon et al., 1988; Manning, 1990). Huston and Kamprad (in press), however, suggest that the node of values at 23‰ (representing vein barites) could reflect precipitation from the postulated Ordovician event. Sulfide $\delta^{34}S$ values are tightly constrained at 5-6‰ (Manning, 1990). Another problem with their model is that hematite clasts in the lower Owen Conglomerate suggest a significant pre-Owen mineralising event (Hart, 1993). However, the hematite clasts could have been selectively replaced after deposition.

In summary, three possible magmatic origins for the Mt. Lyell field have been proposed: 1) Cambrian granites (Large et al., 1996) and this thesis, 2) Suite II andesite magmas, (Halley et al., 1996) and 3) an as yet unidentified Ordovician granite (Huston, in press; Huston and Kamprad, in press), in addition to the VHMS seawater convection models of Markam (1968), Solomon et al. (1969), Green (1971), Bryant (1975), Reid, (1975), Hendry, (1981), Walshe and Solomon (1981), Braithwaite (1985) and Sheppard (1987).

2.4.5 Lead Isotopes at Mt. Lyell

Ores at Mt. Lyell have not been dated directly, however constraints on the sources of lead and the timing of mineralisation can be inferred from Pb isotope ratios reported by Gulson and Porritt (1987). Pb isotope ratios (Figure 2.6) indicate two populations: 1) a cluster of values from the Comstock sphalerite-galena-pyrite ore body with ratios similar to the Rosebery VHMS deposit, and 2) a second cluster of more radiogenic values from the Prince Lyell and Crown Lyell deposits. The dispersion in the second array results from high U/Pb values in the sampling medium (Gulson and Porritt, 1987). The two populations are interpreted by Gulson and Porritt (1987) to be mostly Cambrian lead with additional lead derived from the Precambrian basement. Inherited zircons in CVC volcanics (Adams et al., 1985), and Sr isotope data from barites (Whitford et al., 1992) further support a model involving crustal contamination. Huston and Kamprad (in press), however, interpret the Pb isotope values from Prince Lyell differently. The Prince Lyell values form a cluster with $^{206}Pb/^{204}Pb$ values between the Comstock values and the Devonian Renison Sn deposits (Figure 2.6). Huston and Kamprad (in press) interpret these values as primary Prince Lyell values and suggest an Ordovician age (about 460 Ma) for the Prince Lyell and Western Tharsis ores.

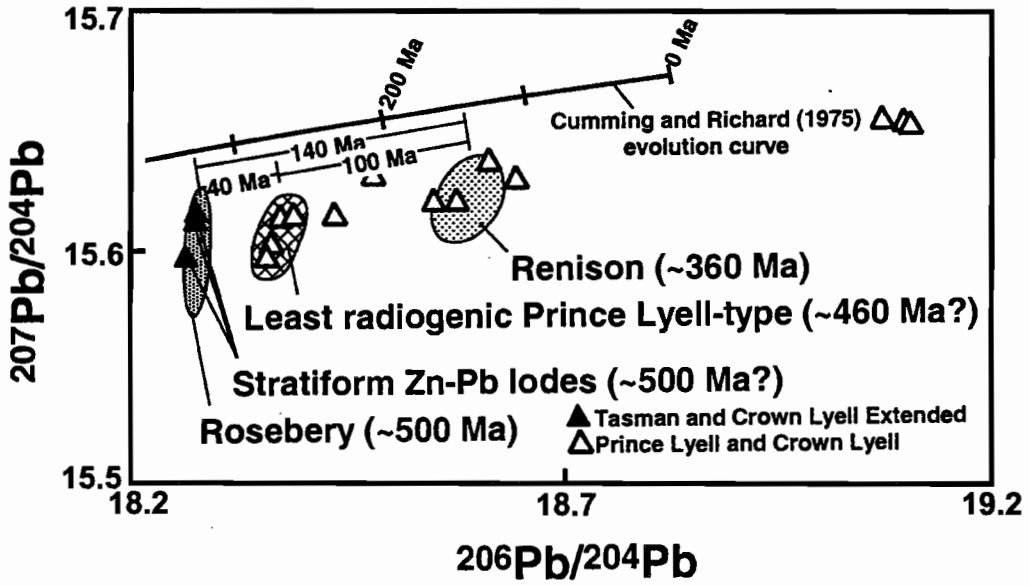

Figure 2.6. Lead isotope systematics of the Mt. Lyell deposits in comparison with the Rosebery VHMS and Renison Sn deposits. Figure from Huston and Kamprad, in press, modified after Gulson and Porritt (1987) and Cumming and Richard (1975)

2.5 OTHER CAMBRIAN GRANITE-RELATED Cu-Au PROSPECTS IN THE MRV

Cambrian granite-related mineralisation occurs at Murchison Gorge, Lake Selina, Red Hills, Lake Dora, Beatrice, the Lake Burbury prospect, the Garfield Prospect and at Elliott Bay (Figure 1.1). This section summarises the hydrothermal alteration and mineralisation styles and theories of genesis for these smaller prospects. Simplified schematic cross-sections of each of the prospects are shown in Figure 2.7 and more detailed descriptions are provided in Appendix B.

Hydrothermal K-feldspar and chlorite alteration styles occur in association with magnetite veins and minor pyrite and chalcopyrite at all of the prospects but apatite-magnetite has only been identified at Lake Selina. Arguments by Polya et al. (1986) suggest that the Murchison Gorge, Lake Selina, and Red Hills sections are all part of a continuum through a Cambrian massive sulfide system and that the Murchison Granite acted as the heat engine and also provided some of the metal budget. Similar $\delta^{34}S$ values characterise all sections (Eastoe et al., 1987b; Solomon et al., 1988) and indicate that mineralisation occurred within a zone dominated by reduced Cambrian seawater sulfate (Solomon et al., 1988). No evidence has been documented to connect the deep hydrothermal alteration and mineralisation styles to a seafloor position at any of these prospects although stratiform sulfides occur at Lake Selina and Elliott Bay.

The Murchison Gorge (Figure 2.7) exposes the contact between the Murchison Granite (Figure 1.1) and the EQPS volcanics that closely resemble the volcanic rocks below the ore horizon at Red Hills (Polya et al., 1986; Corbett and Lees, 1987; Corbett, 1992). The volcanic rocks are overlain by the steeply dipping Farrell Slates (Polya, 1981; Corbett and Lees, 1987), similar to the ore horizons at Rosebery and Hercules. Polya (1981) and Polya et al. (1986) described the hydrothermal alteration zones as: 1) a potassic zone, 2) an epidote zone, 3) a chlorite zone and 4) two sericite zones. Intense potassic, chlorite and sericite-altered zones and late veins are occur throughout the granite (Polya, 1981; Polya et al., 1986; Corbett and Lees, 1987; Abbott, 1992; Davidson, 1998). Ore styles include disseminated, vein and replacement style pyrite and chalcopyrite.

Volcanic rocks in the Lake Selina area (Figures 1.1, 2.7) were intruded by Cambrian granites similar to the Murchison Granite. K-feldspar, chlorite and sericite/quartz/carbonate assemblages occur in discrete overlapping zones (Hunns, 1987). Mineralisation consist of disseminations and cross-cutting veins of magnetite, pyrite, chalcopyrite and sphalerite. Lake Selina is interpreted to be a small-scale massive sulfide system (Solomon et al., 1987b) or a stockwork feeder system to a larger (yet undiscovered) massive sulfide system (Cartwright, 1984). However, the shape of the hydrothermal alteration zones closely follows the shape of the underlying Murchison Granite, and the alteration zones have closer affinities to porphyry-copper or granite-related hydrothermal alteration systems than to VHMS systems (Large, 1988; Hunns, 1997).

Figure 2.7. Simplified schematic cross-sections of other Cambrian granite-related Cu-Au prospects in the MRV. Figures are not to scale and are diagrammatic only. Figures are modified from various authors as referenced. Other cross-sections are interpretations made by the author.

A) Murchison Gorge (modified from Polya, 1981)

B) Lake Selina

C) Red Hills

D) Lake Dora

E) Beatrice (modified from Hope, 1999)

F) Lake Burbury Prospect

G) Garfield Prospect

H) Elliott Bay (modified from Large et al., 1987)

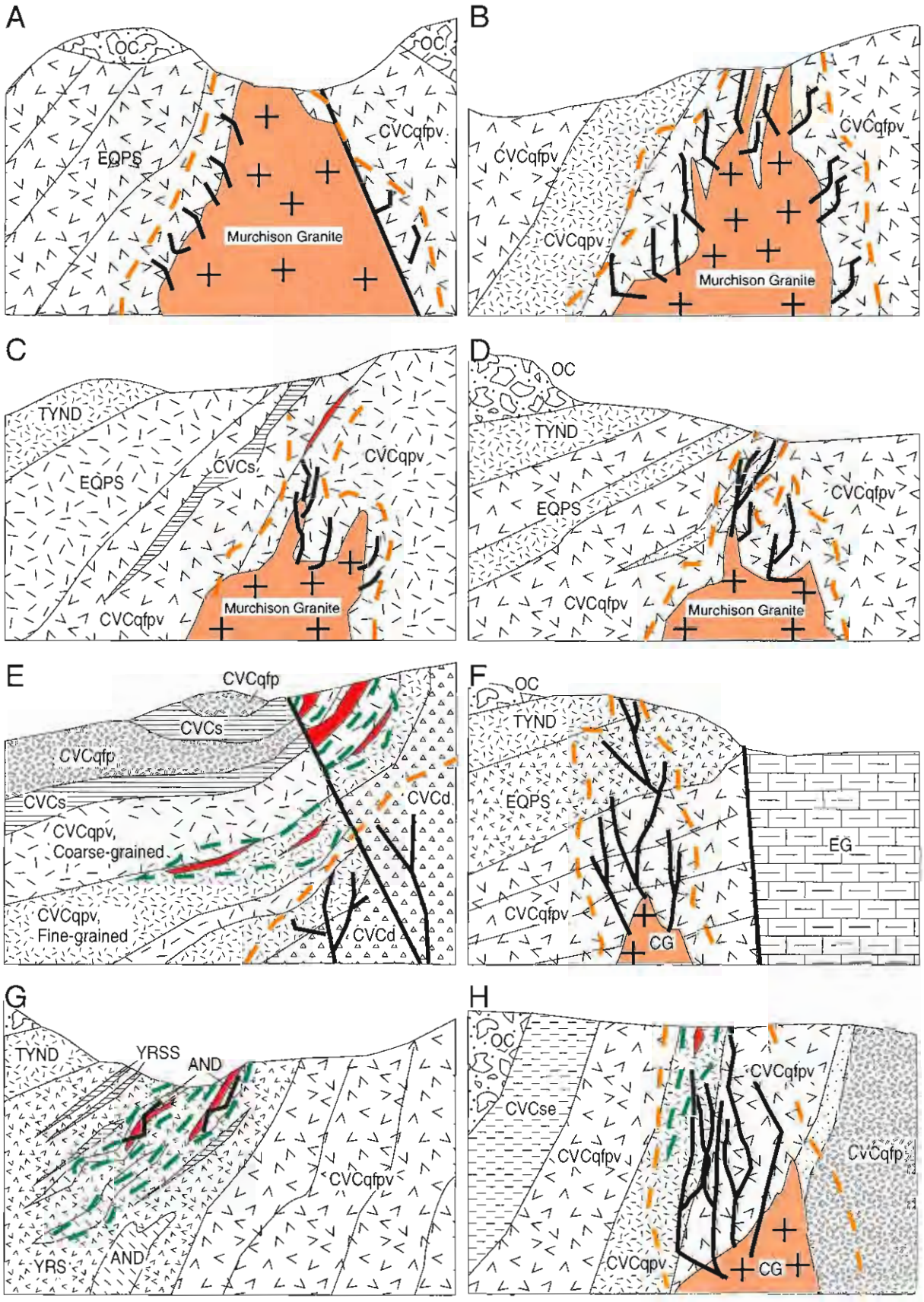

OC = Owen Conglomerate
EG = Devonian-Silurian Eldon Group
CG = Cambrian Granite
AND = Cambrian Suite II Andesite
TYND = Tyndall Group
EQPS = Quartz-Phyric Lavas and Volcaniclastics
CVCqfpv = Quartz and Feldspar-Phyric Lavas and Volcaniclastics
CVCqpv = Quartz-Phyric Volcaniclastics
CVCqfp= Quartz-Feldspar Porphyry
CVCs = Shales
CVCd = Dacite Lava
YRS = Quartz-Phyric Lavas and Volcaniclastics
YRSS = YRS Shale and Thinly Bedded Sandstones

Mineralisation as discribed in text.

Magnetite vein systems with gold and copper.

Granite style K-feldspar, chlorite and sericite bearing alteration system.

Sericite-chlorite-pyrite-magnetite bearing alteration system.

At the Red Hills Prospect (Figures 1.1, 2.7), two ore styles occur; a narrow (3 metre thick) massive sulfide lens containing banded sphalerite, galena and minor chalcopyrite (44% combined lead-zinc) and stockwork veins of pyrite, chalcopyrite and magnetite. The sulfides occur within a sequence of interbedded black shales and clastic and coherent felsic volcanics of the CVC (Eastoe et al., 1987a; Jenkins, 1991). Hydrothermal alteration assemblages are not conformable to lithological facies and occur in discrete zones (Eastoe et al., 1987a). Chlorite alteration is confined to a pipe-like zone that widens and increases in K-feldspar content with depth. Ore styles at Red Hills have been interpreted to be of two genetic origins: 1) syngenetic gold-rich massive sulfide pods and, 2) stockwork veins similar to other granite-related mineral occurrences in the MRV (Large, 1988; Jenkins, 1991). The Red Hills Prospect is believed to directly overlie a buried Cambrian granite (Payne, 1991; Large et al., 1996).

At Lake Dora (Figures 1.1, 2.7), disseminations and veinlets of pyrite, chalcopyrite, galena and sphalerite are associated with magnetite and hematite veins (Corbett, 1981; Solomon et al., 1988; Corbett, 1992).

A section similar to the Red Hills section occurs at the Beatrice Prospect northeast of Mt. Lyell (Figures 1.1, 2.7). Hydrothermal alteration assemblages contain K-feldspar, chlorite and sericite (Hope, 1999): Magnetite and hematite occur at depth beneath the prospect in association with K-feldspar assemblages. Mineralisation styles include veinlets and small (<3 cm) lens-like replacements of pyrite, sphalerite, galena and minor chalcopyrite within a volcaniclastic and shale sequence (Hope, 1999). Chalcopyrite is intergrown with pyrite in veins within K-feldspar-chlorite-magnetite-altered volcanics. The two genetic interpretations for the Beatrice Prospect are: 1) epigenetic veins and selective replacements (Wilde and Kerr, 1990; Hope, 1999), and 2) bedded syn-sedimentary sulfides (Boyd, 1994). The occurrence of hydrothermal K-feldspar + magnetite suggest a relationship to the Cambrian granites, however the nearest granite is at least 2 km to the east.

At the Lake Burbury Prospect (Figures 1.1 and 2.7), hydrothermal sericite-chlorite-K-feldspar alteration assemblages occurs in association with a series of magnetite ± tourmaline ± pyrite veins and magnetite-hematite breccias (Jaeger, 1996). Overall, the mineralisation and alteration styles are identical to those observed along Jukes Road in the current study and were concluded to be related to buried Cambrian granite (Jaeger, 1996).

One of the goals of this research is to evaluate the relationship of hornblende-phyric andesites to the VHMS deposits and the hydrothermal alteration within the CVC. The Garfield Prospect (Figures 1.1, 1.2 and 2.7) formed in several of these andesites and is described in detail in Sections 4.3.1.6 and 4.4.5. The andesites are comprised of two hornblende-phyric phases that intruded rhyolitic volcanics of the YRS (Crawford et al., 1992; Halley et al., 1996). Hydrothermal alteration assemblages include chlorite and sericite. Pyrite and chalcopyrite are principally hosted in the main Garfield andesite (Halley et al., 1996; Duncan, 1997). They occur in veins and as disseminations. Magnetite and apatite occur in veins and as disseminated grains.

In the Elliott Bay region (Figures 1.1, 2.7), CVC volcanics were intruded by the Cambrian Elliott Bay Granite. Ore styles include several small (3-6 metres wide and 10-20 metres long) but high-

grade (up to 36 % combined lead-zinc) stratiform massive sulfide lenses, disseminated domains of galena, sphalerite and pyrite and disseminated and quartz vein gold. The massive sulfide lenses lack footwall stringer alteration styles suggesting that they were deposited distal to the hydrothermal vents (Large et al., 1987). Several breccia styles occur including volcaniclastics, hematite breccias with chlorite-altered clasts, and tourmaline breccias and breccia veins (Garrett, 1989). South of the massive sulfide lenses, a laterally extensive zone of hydrothermal chlorite and sericite alteration assemblages occurs that is underlain by extensive disseminations and stock-works of magnetite. The chlorite-sericite alteration assemblages and associated magnetite veins were reported to be similar to hydrothermal alteration assemblages at Mt. Darwin and the Murchison Granite (Large et al., 1987). The genetic model for the Elliott Bay massive sulfides and associated Cu-Au ores involves a typical VHMS model for the stratiform ores and intrusion of high-level granites and quartz porphyries to form the hydrothermal chlorite-magnetite alteration styles and associated gold (Gulson et al., 1987; Large et al., 1987

CHAPTER 3

3.0 PETROGRAPHY OF CAMBRIAN GRANITES IN WESTERN TASMANIA

3.1 INTRODUCTION

Five Cambrian granites have been mapped in western Tasmania: the Murchison, Darwin, Elliott Bay, Timbertop and the Dove Granites (Leaman and Richardson, 1989). Cambrian granites in western Tasmania are small, pipe-like or sheet-like bodies that have intruded Cambrian lavas and volcaniclastic rocks of the Western, Central and Eastern volcanic sequences. The Cambrian granites were interpreted by Solomon (1976; 1981) to be subvolcanic intrusions genetically related to the surrounding volcanic piles that were emplaced in a volcanic arc that was accreted onto continental crust. However, recently the granites were interpreted to be post-collisional granites emplaced after the arc-continent collision (Crawford and Berry, 1992; Crawford et al., 1992).

The Cambrian granites of Tasmania are of particular interest because they are spatially and temporally associated with Cu-Au prospects and VHMS mineral deposits. Large et al. (1996) have proposed that the granites were a source of heat and magmatic-hydrothermal fluids responsible for Cu-Au and VHMS ores in the MRV. Small Cu-Au prospects are spatially located along the margins of the granites and occur in continuous linear belt from the Elliott Bay Granite in the south to the Murchison Granite in the north (Figure 1.2). Little information was available for the poorly exposed Timbertop and Dove Granites, and they will not be discussed further. The focus of the current study will be on the Murchison, Darwin and Elliott Bay Granites, with particular emphasis on the Darwin Granite. The current study reviews and re-evaluates the existing geological data for the Murchison, Darwin and Elliott Bay Granites.

3.2 MORPHOLOGY AND PETROLOGY OF THE DARWIN, MURCHISON AND ELLIOTT BAY GRANITES

This section will focus on the physical characteristics of the granites, including their morphology and petrology.

3.2.1 Cambrian Granite Field Relationships, Residual Gravity and Aeromagnetic Data

The morphology of the Cambrian granites in western Tasmania can be best defined by combining known geological field relationships with residual gravity and aeromagnetic data. The general Cambrian granite morphology has been interpreted from regional gravity and magnetic data (Leaman and Richardson, 1989; Payne, 1991; Large et al., 1996). From just south of the Darwin Granite, a continuous belt of magnetic anomalies extends northward for over 60 km, joining with a complex magnetic anomaly around the Murchison Granite (Figure 3.1). Computer modeling of

gravity and magnetic data along this trend has enabled the subsurface position of the granite to be approximated at depths of <8 km (Leaman and Richardson, 1989; Payne, 1991; Large et al., 1996). A series of E-W geophysical models along the belt indicate that the narrow granite is semi-continuous along the eastern side of the Central Volcanic Complex, from the Darwin Granite to the Murchison Gorge (Payne, 1991; Large et al., 1996).

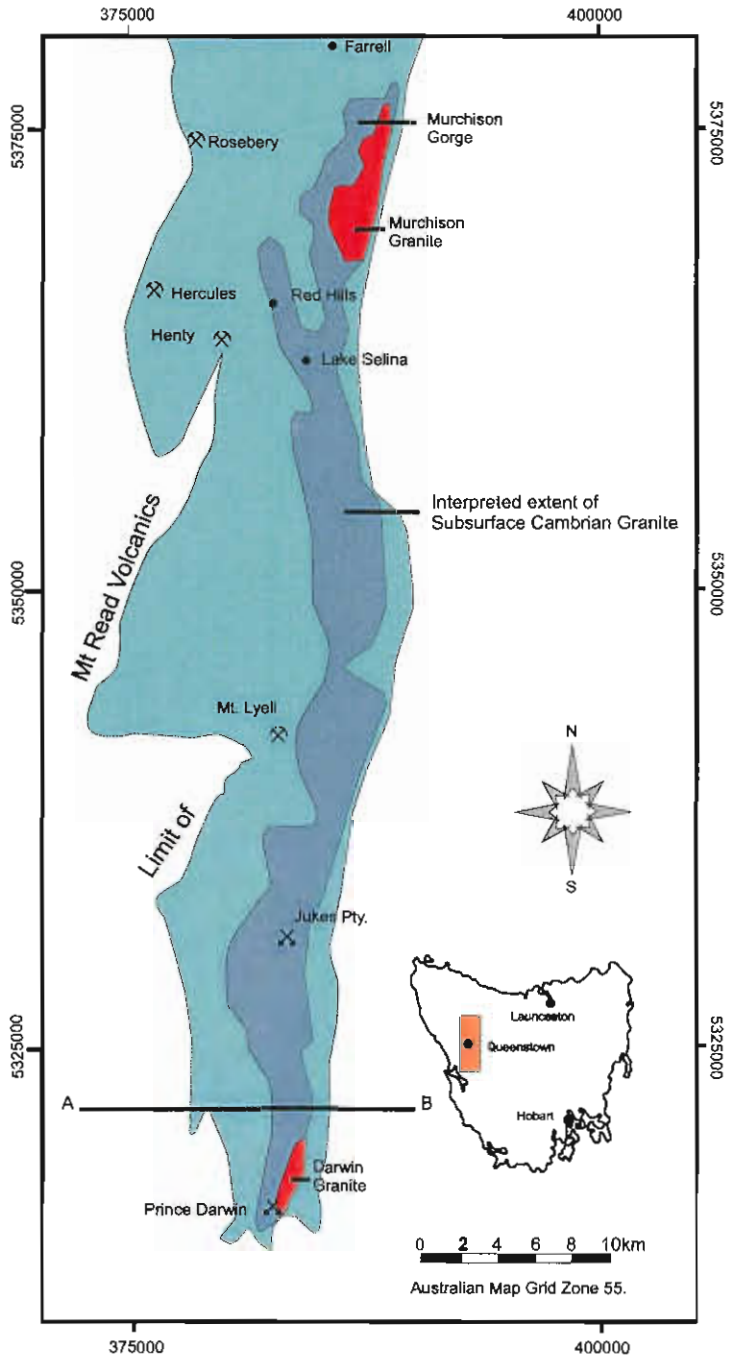

Figure 3.1. Interpreted sub-surface position of Cambrian granites based on modeling of gravity and magnetic data. Compiled from Leaman and Richardson (1989), Payne (1991) and Large et al. (1996).

3.2.1.2 SURFACE AND SUBSURFACE FEATURES OF THE MURCHISON GRANITE

The main body of the Murchison Granite forms an irregular sill-like body about 0.5 km wide that extends for over 12 km along strike and its surface expression has been described by several researchers (Polya, 1981; Polya et al., 1986; Eastoe et al., 1987; Hunns, 1987; Davidson, 1998). The overall subsurface morphology of the Murchison Granite has been developed from geophysical studies (Leaman, 1986; Leaman and Richardson, 1989; Payne, 1991). Their interpretation indicates that the Murchison Granite is 3 km wide and 14 km long in the rough shape of an elongate pipe-like plug. The granite has a density similar to the host acid volcanics, but a strong magnetic contrast (Leaman and Richardson, 1989).

The Murchison Granite disappears beneath volcanic cover toward the south and is apparent only as a magnetic anomaly until it resurfaces in the Lake Selina area. Geophysical modeling of the Murchison Granite by Payne (1991) indicated that the Murchison Granite was near the surface in the Red Hills area. Hunns (1987) reported and described altered and unaltered granite from several drill intersections in the Lake Selina area. Payne (1991) concluded that the Murchison Granite was the principle source of the north-south trending zone of high magnetic intensity along the western margin of the Tyennan Region.

3.2.1.3 DARWIN GRANITE SURFACE AND SUBSURFACE MORPHOLOGY

Numerous authors have examined the Darwin Granite as part of their broader regional studies (Hills, 1914; Corbett and Cuffley, 1970; Corbett, 1976; Corbett, 1979; Corbett and McNeil, 1988; Solomon et al., 1988; Corbett et al., 1993; Gadaloff, 1996; Large et al., 1996). Detailed studies of the granite were carried out by White (1975), Leaman and Richardson (1989) and Jones (1993). The Darwin Granite is approximately 2Km wide and 5Km long. White (1975) described the Darwin Granite as a sheet-like intrusion approximately 800 metres thick that was broadly concordant with the intruded rocks although the western margin was locally discordant and contains xenoliths of the country rocks. Contact relationships along the western margin, as observed in this study, were sharp and locally discordant to the strike of the enclosing CVC rocks. The eastern contact was an erosional unconformity overlain by Tyndall Group volcaniclastic rocks.

Because roof pendants of CVC feldspar-phyric volcanics occur on the Darwin plateau, the current top of the Darwin Granite body is interpreted to be one side of the granite that was recently exposed. The original top of the granite was exposed by erosion prior to deposition of the Tyndall Group, and has subsequently been tilted to the east.

As with the Murchison Granite, the most reliable guide to the subsurface morphology of the Darwin Granite comes from geophysical data. Leaman and Richardson (1989) reviewed gravity, aeromagnetic and ground magnetic data and concluded that the total volume of the Darwin Granite was not large enough to be easily separated from the signature of the surrounding volcanics based on gravity data alone. Leaman and Richardson (1989) concluded that the Darwin Granite must be a narrow plug-like body and that a large granite body of substantial thickness was not possible or consistent with the current outcrop pattern.

A strong elongate magnetic anomaly is shown extending from the Darwin Granite, north to the Murchison Granite on Figure 3.1. The magnetic anomaly over the outcrop area of the Darwin Granite is related to magnetite veining and hydrothermal alteration within and around the margins of the granite and to disseminated magnetite within the granite itself. An E-W cross-section has been constructed north of the Darwin Granite on the basis of geophysical data (Figure 3.2) and shows a vertical sheet of granite about 2 km wide with a depth to the top of approximately 1 km (Large et al., 1996). This sheetlike granite body extends at least as far north as the Jukes Prospect near the King River (Figure 2.1). Current outcrop patterns combined with the geophysical data support the theory that the Darwin Granite is a thin, nearly vertical, sheet-like body that has been tilted to the east. It was interpreted to have intruded into the CVC as a subvolcanic sill (Jones, 1993).

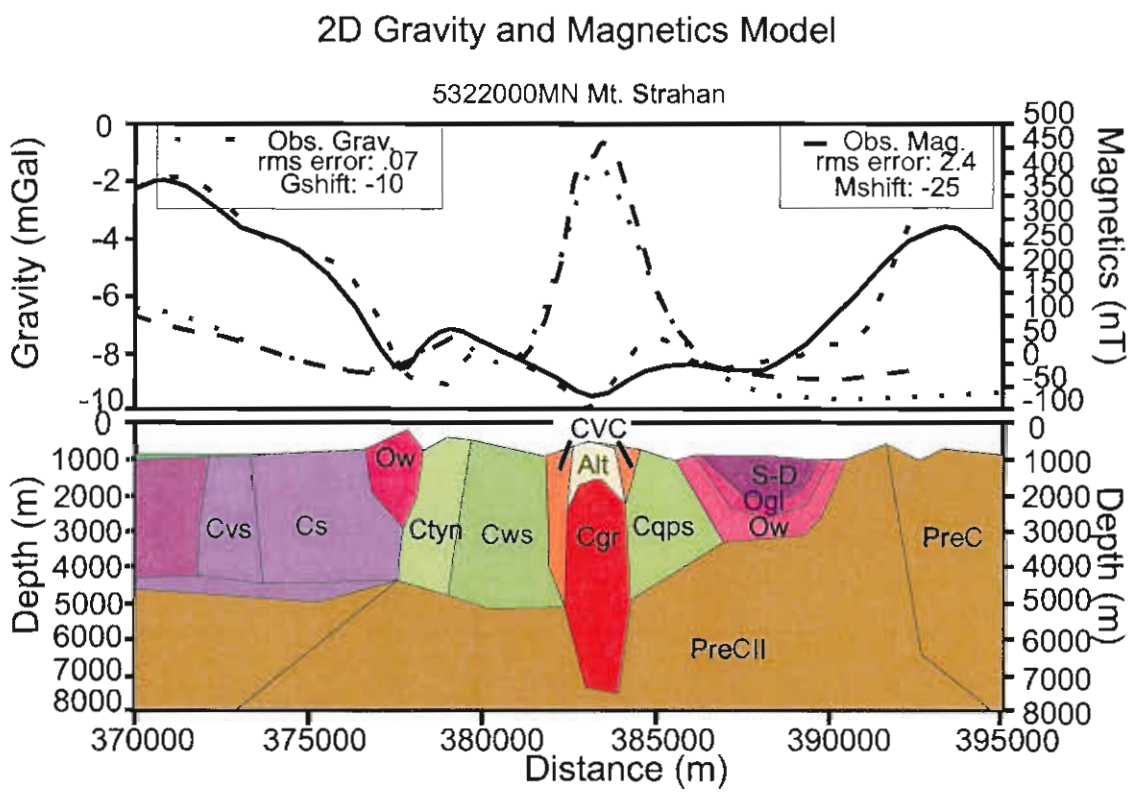

Figure 3.2 E-W geophysical cross-section just north of the Darwin Granite. S-D = Siluro-Devonian Eldon Group; Ogl = Ordovician Gordon Group; Ow = Ordovician Owen Conglomerate; Cqps = Cambrian Eastern Quartz-Phyric Sequence, CVC = Cambrian Central Volcanic Complex, Alt = granite-related hydrothermal alteration; Cws = Cambrian Western Sequence; Ctyn = Cambrian Tyndall Group Volcanics; Cs and Cvs = Dundas Group; Cgr = Cambrian Darwin Granite; PreC and PreCll = Precambrian rocks. Units are described in Corbett, (1989, 1992). Modified from Large et al. (1996).

3.2.1.4 ELLIOTT BAY GRANITE SURFACE AND SUBSURFACE INTERPRETATIONS

The Elliott Bay Granite is composed of at least three composite granitoid bodies that are exposed over an area covering approximately three square kilometres. These granitic bodies intrude volcanic rocks of either the Tyndall Group or the CVC (Large et al. 1987) and Precambrian schists of the Tyennan nucleus (White, 1975). The Little Rocky River Pluton of the Elliott Bay Granite is the largest of the bodies, and contains blocks of Precambrian schist up to tens of

metres in size enclosed within a quartz-feldspar porphyry phase. Sharp intrusive contacts were observed between the granite and the Precambrian schists and volcanics rocks (White, 1975).

Leaman and Richardson (1989) and (Leaman, 1986) modeled magnetic and gravity data from the Elliott Bay region. Based on the weak magnetic expression, they concluded that the granite is of limited extent, is a volumetrically minor set of intrusions, has minor compositional variations and was emplaced as sheet-like or tapering carrot-like bodies.

3.2.2 Petrography of the Murchison, Darwin and Elliott Bay Granites

3.2.2.1 PETROLOGY OF THE MURCHISON GRANITE

The petrology of the Murchison Granite has been described by various workers (Polya, 1981; Polya et al., 1986; Hunns, 1987; Davidson, 1998). Polya (1981) described the unaltered Murchison Granite as having a modal composition of 25-35 percent orthoclase, 20-30 percent quartz, 25-30 percent sodic plagioclase and accessory hornblende, biotite, zircon, apatite, magnetite, ilmenite, and pyrite. Plagioclase was euhedral to subhedral, zoned with sericitised and saussuritised cores and albitised rims. Plagioclase core compositions are typically An_{20} with little variation. Hornblende occurs as anhedral to euhedral, simply-twinned crystals, typically with corroded margins. Hornblende euhedra are common as inclusions in biotite. Hornblende, Ti-poor magnetite, ilmenite and euhedral biotite commonly occur together in 1-2 millimetre sized clots. Euhedral zircons occur in biotite and hornblende. Orthoclase crystals are clear and subhedral to anhedral. Quartz was interstitial to the plagioclase, had ragged boundaries and undulose extinction. Apatite euhedra occur as inclusions in biotite and orthoclase (Polya, 1981).

Hunns (1987) describes the petrology of the Murchison Granite from the Lake Selina area as fine to medium-grained pink, green granite to porphyritic granite. In the altered granite, feldspar phenocrysts were extensively altered to sericite, although compositional zoning was still evident. Quartz grains have strong undulose extinction and deformation lamellae. Quartz grain margins were corroded by sericite, and the grains were cross-cut by sericite veinlets. Larger grains have overgrowths of recrystallised quartz. Hornblende was altered to chlorite.

3.2.2.2 PETROLOGY OF THE DARWIN GRANITE, FOUR PHASES

Understanding the petrology of the Darwin Granite was important in interpreting the effects of hydrothermal alteration and the geochemical changes that occur within and around it. The following petrographic descriptions were made as part of this study. Reference was made to the work of others, including Hills (1914), White (1975) and Jones (1993).

Heavy mineral separates were made from all four phases of the Darwin Granite. The heavy mineral separates were examined under the Scanning Electron Microscope (SEM) and analysed for REE using the Laser Microprobe at the Central Science Laboratory (CSL) at the University of Tasmania.

Petrographic Description of the Pink Granite

The dominant phase of the Darwin Granite is a phanerocrystalline pink-green granite previously described by Hills (1914), White (1975) and Jones (1993). The texture is predominantly equigranular. The appearance of the pink granite phase is illustrated in Plate 3.1A-B. Light to dark pink/red K-feldspar and light to dark green sericite/chlorite-altered plagioclase give the rock its distinctive pink-green color. Primary biotite occurs in fresh granite only. Estimated modal compositions as determined in the current study and by Jones (1993), were K-feldspar (45-50%), quartz (25-30%), plagioclase (20-25%), biotite (0-1%), and accessory hornblende, pyrite, magnetite, and zircon (<0.01%). Heavy accessory minerals identified on the SEM include rutile, sphene, monazite and leucoxene. The accessories are modally < 0.001 wt.%. Zircons were broken and widely scattered. Apatite occurs as rare, small (0.1 - 0.2 mm) crystals.

Quartz is anhedral with straight, interdigitating or sutured grain boundaries. Extinction was commonly undulose, indicating considerable dynamic strain. Domains of 0.01-0.02 mm interlocking crystals of recrystallised quartz occur as aggregates up to 1 mm in size. Plagioclase and K-feldspar occur as subhedral to anhedral crystals. Microperthitic inclusions of plagioclase in K-feldspar and granophyric textures are common.

Petrographic Description of the White Granite

Jones (1993), classified the Darwin white granite as a granodiorite using modal classification. However, for the purposes of this thesis, and to stay remain consistent with previously used terminology, the term 'white granite' will be used. The Darwin white granite, as shown in Plate 3.2A and Plate 3.2B, is a leucocratic, phanerocrystalline, equigranular, medium to coarse-grained (2-7 mm) rock. Compositionally the rock is 25-30% quartz, 40-50% plagioclase, 25% K-feldspar, < 1% mafic and accessory minerals. Heavy minerals separated from the white granite include rutile, magnetite, zircon and thorite ($ThSiO_4$). Zircons are rare and euhedral. Grainsize variations within the white granite were observed in weathered blocky outcrops. The white granite intruded the pink granite in the northern part of the Darwin Plateau, and has produced a sharp contact. No evidence of a chilled margin or development of thermal changes to the pink granite was observed other than minor chlorite development. These observations contradict Jones (1993), who interpreted the contact to be gradational.

Euhedral to subhedral plagioclase crystals are characterised by albite and carlsbad twinning. Plagioclase was moderately to intensely replaced by secondary sericite. K-feldspar commonly had relict micrographic intergrowths with quartz (Plate 3.2B). Quartz crystals are subhedral to anhedral, unaltered and had undulose extinction. The non-uniform or shadowy extinction is indicative of the rock having undergone considerable dynamic strain. Quartz grain boundaries are ragged and interdigitated with surrounding feldspars. Most of the quartz grains were recrystallised and have sutured grain boundaries with adjacent quartz and feldspar crystals.

Plate 3.1. Hand specimen and photomicrographs of the pink equigranular phase of the Darwin Granite.

A. Photograph of a slab of equigranular pink Darwin Granite. Feldspars are of two types, light to dark pink/red K-feldspar, and light to dark green sericite ± chlorite replaced plagioclase giving the rock its pink-green color. Sample B2053

B. Photomicrograph of the equigranular pink granite. Notice the sutured and interdigitating grain boundaries with quartz (Q) and K-feldspar (K). Relict twinning occurs in plagioclase (P) and undulose extinction (U) was visible in quartz. Crossed polars, field of view width = 3.4 mm. Sample B2053.

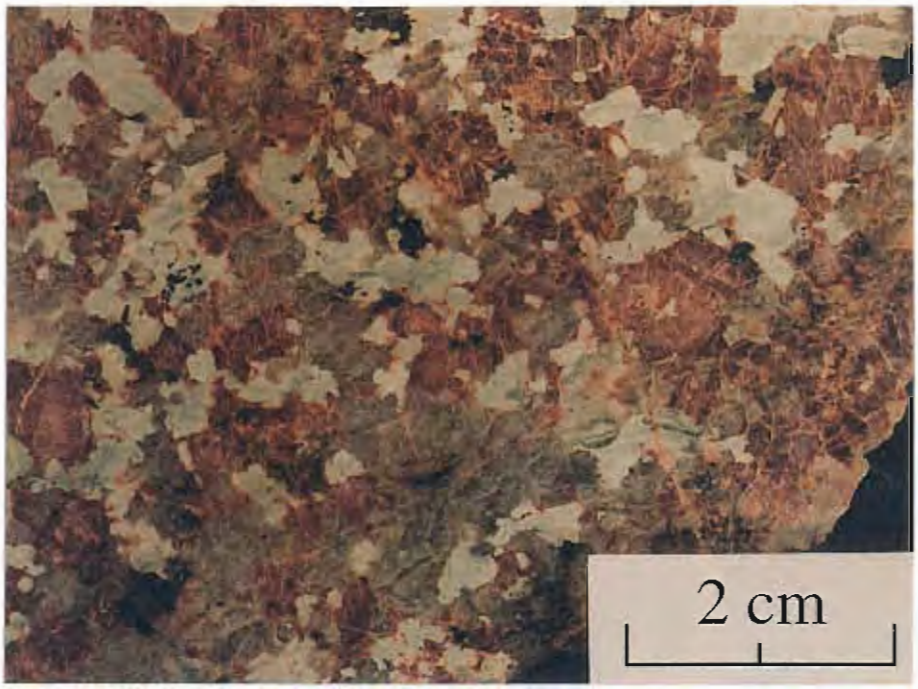

A

B

Plate 3.2. Hand specimen and photomicrograph of the white equigranular phase of the Darwin Granite.

A. Photograph of a slab of the Darwin white granite. The rock is a leucocratic, phanerocrystalline, medium to coarse-grained (2-7 mm) granodiorite. Plagioclase (P) is a faint pale-green color and occurs as discrete crystals. K-feldspar (K) is white and typically intergrown with quartz in irregularly shaped crystals. Sample B2043.

B. Photomicrograph of the white granite. Note that the plagioclase (P) crystals were altered to masses of fine-grained sericite but relict twinning was preserved in some crystals. K-feldspar (K) commonly has relict micrographic intergrowths with quartz. Quartz has undulose extinction and sutured grain boundaries. Crossed polars, field of view width = 3.4 mm. Sample B2043.

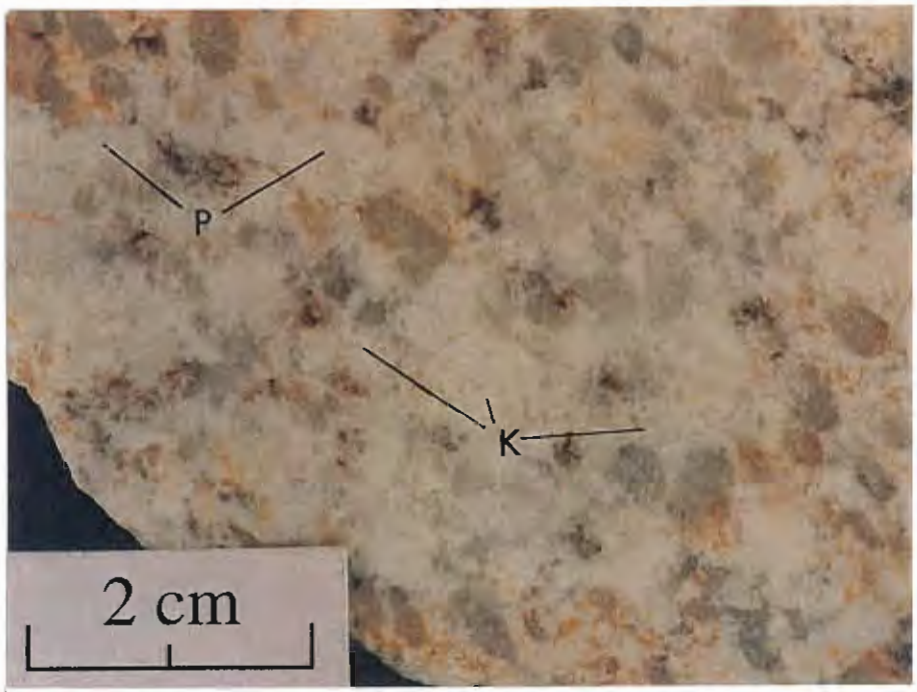

A

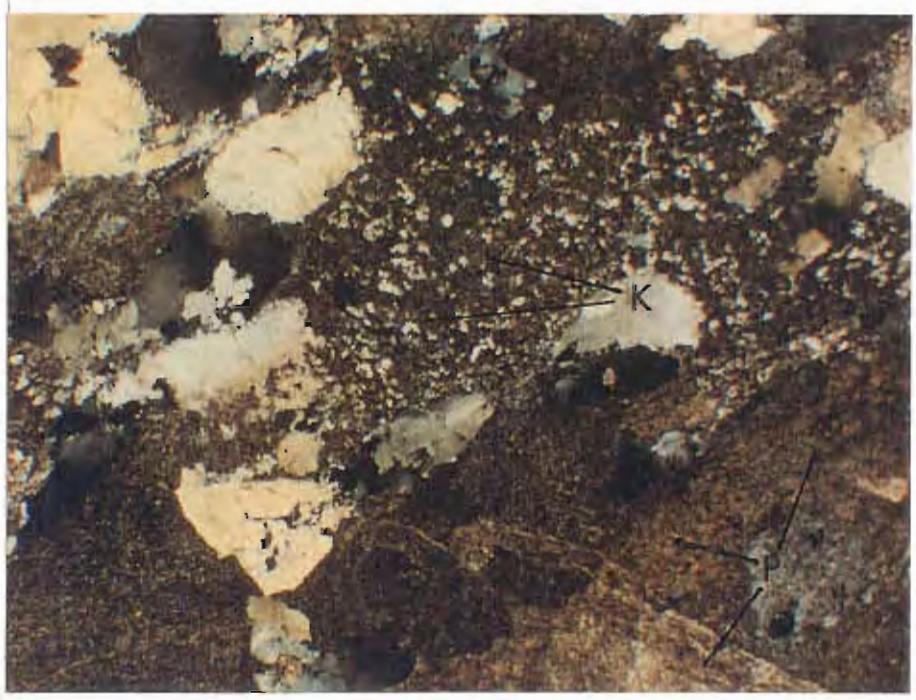

B

Petrographic Description of the Quartz-Feldspar Porphyry

Intrusive into the pink and white granite is a volumetrically minor phase of granite, here called the quartz-feldspar porphyry. Jones (1993), included this phase of granite as part of the white granite or granodiorite. Although in hand specimen the texture of the quartz-feldspar porphyry and the white granite appeared similar (compare Plate 3.2A to Plate 3.3A), in thin-section they are distinctly different (compare Plate 3.2B to Plate 3.3B). The quartz-feldspar porphyry was classified as a separate phase due to its unique texture and clear intrusive relationships with the pink and white granite phases. Tourmaline veins are common within several metres of the contact with intruded phases. The porphyry postdates the white granite, and was common near tourmaline veining. The texture of the quartz-feldspar porphyry was similar to the texture of the quartz-feldspar porphyry dykes that intrude the feldspar phyric rhyolite along the Jukes Road (Chapter 5).

Euhedral to subhedral quartz phenocrysts, up to 1 x 0.5 cm, are set in a fine-grained equigranular groundmass (Plate 3.3B). The groundmass is an interlocking mosaic of quartz and feldspar. Quartz phenocrysts were partially recrystallised into interlocking mosiacs of fine-grained quartz, and have undulose extinction. Relict euhedral to subhedral crystal shapes are preserved, and boundaries with the fine-grained groundmass are sharp. K-feldspar and plagioclase occur as phenocrysts up to 5 mm in diameter that were weakly to moderately sericitised with relict twinning preserved. Heavy minerals identified on the SEM include sphene, euhedral zircon and magnetite.

Petrographic Description of the Microgranite Dykes

Previous researchers have described microgranite dykes (Jones, 1993) and aplite veins (White, 1975) from the western half of the Darwin Granite. The microgranite and aplite dykes intrude the pink granite. The dykes were observed near the contact of the pink granite and the CVC. Jones (1993), proposed that these dykes formed part of a chilled margin to the main pink granite phase. This interpretation was incorrect because cross-cutting relationships exist (Plate 3.4C). The dykes observed in the current study occur perpendicular to the granite/CVC contact. However, some may be intrusive along the contact zone which lead to the conclusions of Jones (1993). During the current study, the coarse-grained pink granite was observed in contact with CVC volcanics at several locations, with no evidence of chilled margins in the granite. This observation was supported by observations made by Hills (1914), who dug trenches across the contact in several places.

Microgranite and aplite dykes consist of a granular mixture of fine-grained equigranular holocrystalline quartz and feldspar as shown on Plate 3.4A-B. The primary texture is subhedral to anhedral granular with scattered euhedral granular domains. Most grain boundaries are interdigitating (consertal texture). Compositionally, the rock consists of K-feldspar, plagioclase and quartz (Plate 3.4B) with accessory biotite. Heavy minerals separated from a microgranite dyke include rutile, titano-magnetite, magnetite, sphene, zircon and thorite ($ThSiO_4$). Albite twinning was commonly well-preserved. Perthitic texture in K-feldspar and micrographic texture in quartz is common. Quartz is subhedral to anhedral and has ragged and interdigitating grain boundaries with adjacent feldspar and quartz grains. Quartz has undulose or non-uniform extinction. The microgranite modal composition is 48% K-feldspar, 27% plagioclase, and 25%

Plate 3.3. Hand specimen and photomicrograph of the quartz-feldspar porphyry phase of the Darwin Granite.

A. Photograph of a slab of the Darwin quartz-feldspar porphyritic granite. Quartz (Q) and feldspar (F) phenocrysts are set in a very fine quartz and feldspar matrix (M). Sample B2061.

B. Photomicrograph (crossed polars) of the Darwin quartz-feldspar porphyritic granite. Quartz phenocrysts (Q), up to 1 x 0.5 cm, are euhedral to subhedral and set in a finer-grained equigranular groundmass of quartz, and feldspar. Relict euhedral to subhedral quartz phenocrysts were typically recrystallised into interlocking mosiacs of fine-grained quartz. K-feldspar and plagioclase (F) occur as phenocrysts up to 5 mm in size. K-feldspar and plagioclase phenocrysts were weakly to moderately sericitised with relict twinning. Although in hand specimen, the texture of the quartz-feldspar porphyry and the Darwin white granite appeared similar (compare Plate 3.2A to Plate 3.3A), in thin-section they are distinctly different as shown by comparing with Plate 3.2B. Crossed polars, field of view width = 3.4 mm. Sample B2061.

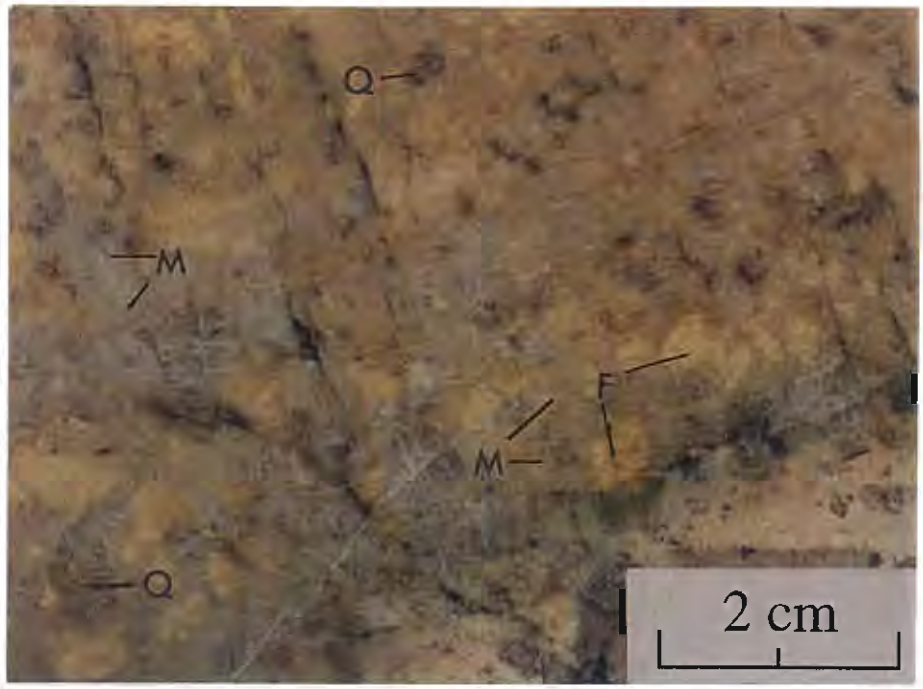

A

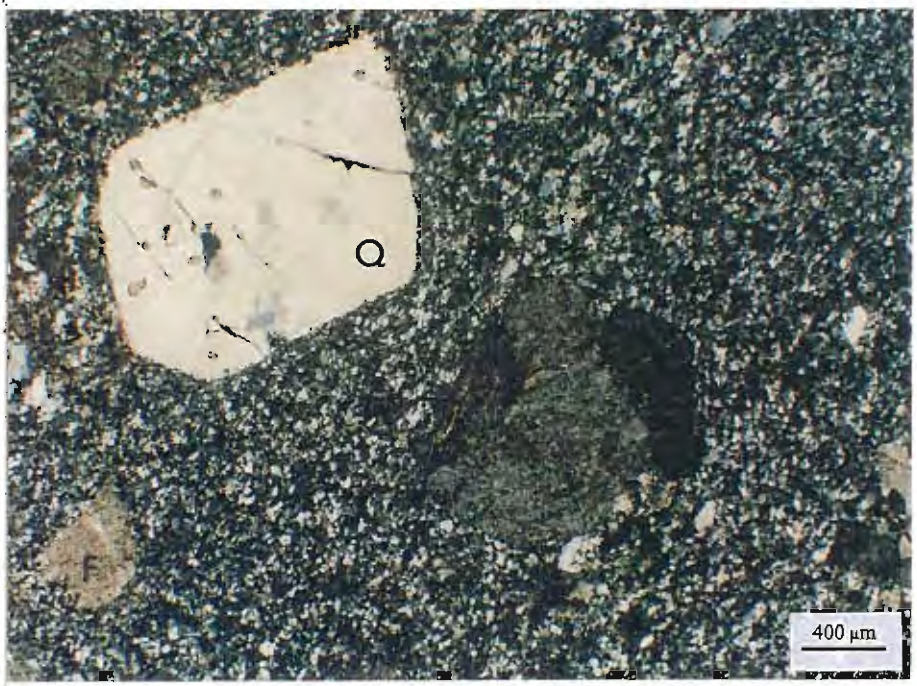

B

Plate 3.4. Hand specimen and photomicrograph of the microgranite phase of the Darwin Granite.

A. Photograph of a slab of the Darwin microgranite. Microgranite consists of a granular mixture of fine-grained equigranular quartz (Q), white plagioclase (P) and pink K-feldspar (K). Magnetite is scattered throughout. Sample B2033.

B. Photomicrograph of the Darwin microgranite. Subhedral to anhedral granular texture. Grain boundaries are interdigitating (consertal texture). K-feldspar (K), plagioclase (P) and quartz (Q) are the primary minerals, with accessory biotite and magnetite. Crossed polars, field of view width = 3.75 mm. Sample B2033.

C. Microgranite dyke intruded the Darwin pink granite perpendicular to the granite contact with the CVC.

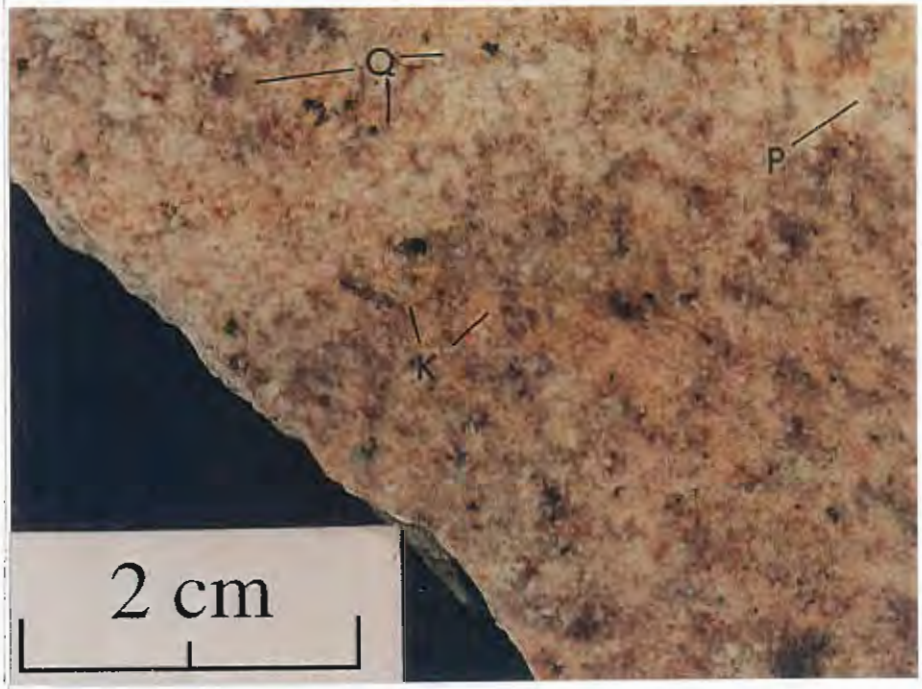

A

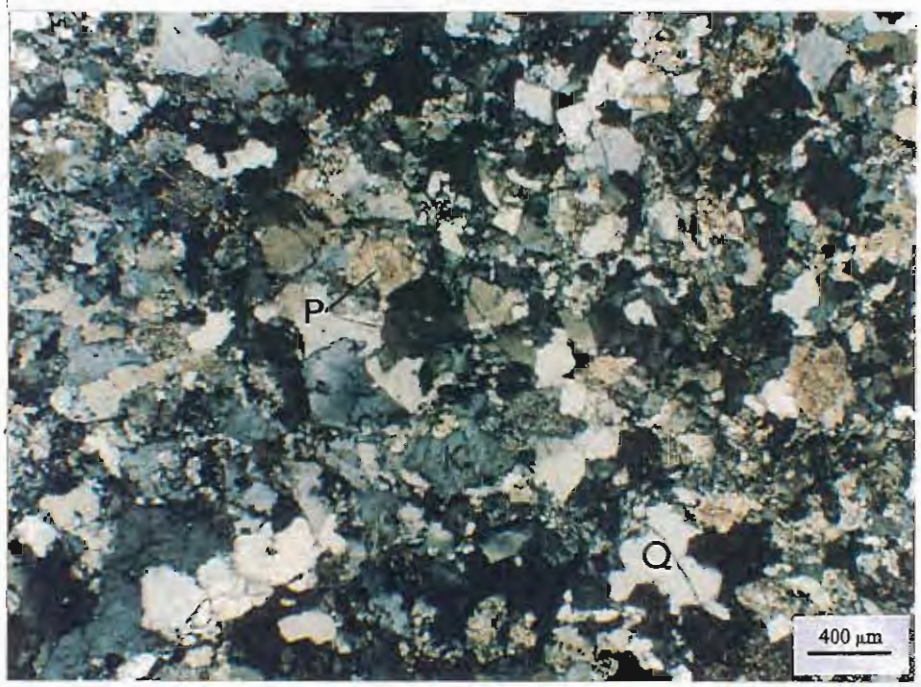

B

C

quartz (Jones, 1993). Scattered throughout the rock are well-rounded quartz and feldspar crystals and small sub-centimetre size granite lithic clasts interpreted to have been derived from the pink granite. The rounded quartz grains were totally recrystallised into fine-grained interlocking mosiacs.

3.2.3 Classification of Granites by Modal Mineralogy

The current study has attempted to classify the Murchison and Darwin Granites using the modal classification system developed by Streckeisen (1976).. Data used in the classifications are from the literature and this study. In Streckeisen's standard QAP diagram (Figure 3.3), Q is modal quartz, A is modal alkali-feldspar and P is plagioclase feldspar. Overlain on this figure are various calc-alkaline trends defined by Lameyre and Bowden (1982). The Murchison and Darwin Granite series plot within the granite and granodiorite fields of Streckeisen (1976) and near the calc-alkaline-granodiorite (medium K) trend (line B) of Lameyre and Bowden (1982).

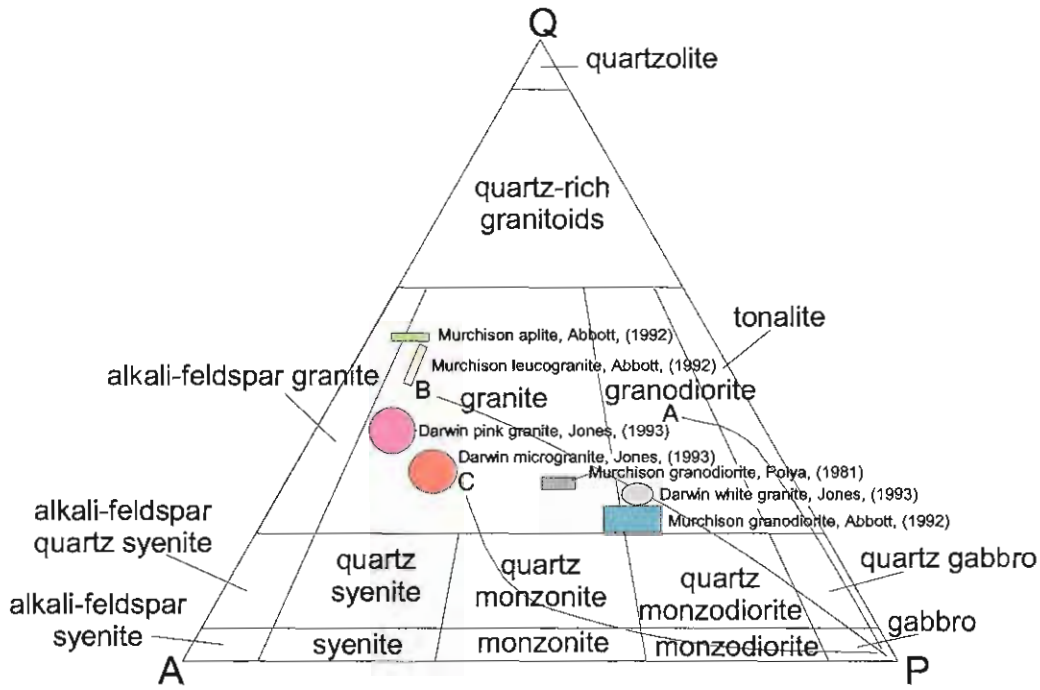

Figure 3.3. QAP diagram showing the modal classification of both the Darwin and Murchison Granites. Darwin Granite data is from Jones (1993) and the Murchison Granite data is from Polya (1981), and Abbott (1992). QAP classification from Streckeisen (1974). A, B and C trends from Lameyre and Bowen (1982). A = Calc-alkaline - Trondhjemitic (Low K); B = Calc-alkaline - Granodiorite (Medium K); C = Calc-alkaline - Monzonitic (High K).

3.2.4 Summary

Although no completely unaltered samples of the Darwin Granite were described (based on the presence of minor sericite), the four phases are still easily distinguished from each other on the basis of petrology (Plates 3.1-3.4). Since the presence of sericite indicates at least minor alteration, the geochemical discussion and classification of the Darwin Granite are deferred to Chapter 6. However, based on modal mineralogy, the Murchison and Darwin Granite series plot within the granite and granodiorite fields of Streckeisen (1976).

CHAPTER 4

4.0 PETROGRAPHY AND GEOCHEMISTRY OF CAMBRIAN VOLCANIC ROCKS IN THE JUKES-DARWIN AREA

4.1 INTRODUCTION

Cambrian volcanic rocks are well-exposed throughout the southern MRV. The volcanic rocks examined for this research were mapped at two primary locations, the Mt. Darwin area and along the Jukes Road (Figure 4.1). Volcanic facies in the southern MRV were the subject of several studies (Halley, 1996; Duncan, 1997). The examination of volcanic rocks in the Mt. Darwin area included a detailed examination of the YRS and the CVC. Jukes Road (Figure 4.1) cuts through well-exposed sections of YRS, CVC, EQPS and Tyndall Group rocks.

Two major volcanic facies of the CVC are exposed along Jukes Road; a thick columnar-jointed feldspar-phyric dacite and a thick sequence of volcaniclastic and mass-flow deposits. Sedimentary facies are minor. The columnar-jointed dacite is the host rock for the Jukes Prospect and its associated hydrothermal alteration and mineralisation. Rocks of the CVC interfinger with the YRS along Jukes Road and in the eastern Clark River Valley. YRS rocks have a gradational contact with the Tyndall Group rocks in the western Clark valley.

The EQPS lies between Tyndall Group volcaniclastic rocks, to the East, and CVC rocks, to the West. Two facies exposed are a quartz-feldspar-phyric volcaniclastic facies and subordinate quartz-feldspar-phyric lavas. The contact between the EQPS and the Tyndall Group is gradational. The contact between the EQPS and the CVC was faulted

4.2 PHYSICAL CHARACTERISTICS (NATURE) OF THE CAMBRIAN VOLCANIC ROCKS

This section will focus on the physical characteristics of the volcanic rocks, including facies, structural relationships and petrology. A later section of the chapter will cover geochemistry.

4.2.1 Yolande River Sequence

The YRS rocks in the Clark Valley and Slate Spur area (Figure 4.1) were investigated for two reasons: 1) A continuous uninterrupted stratigraphic sequence occurs between the YRS rocks in the western Clark Valley, through an interfingering contact and into CVC rocks to the east. The CVC rocks were intruded by the Darwin Granite along the eastern ridge of the Clark Valley. YRS rocks are well-exposed on Slate Spur, an east-west saddle that defines the north end of the Clark Valley, south end of the Garfield Valley and runs directly west from Mt. Darwin. Distal hydrothermal alteration effects, related to intrusion of the Darwin Granite, occur in the YRS. 2) Cu-Au mineralisation occurs around several andesitic bodies (collectively known as the Garfield

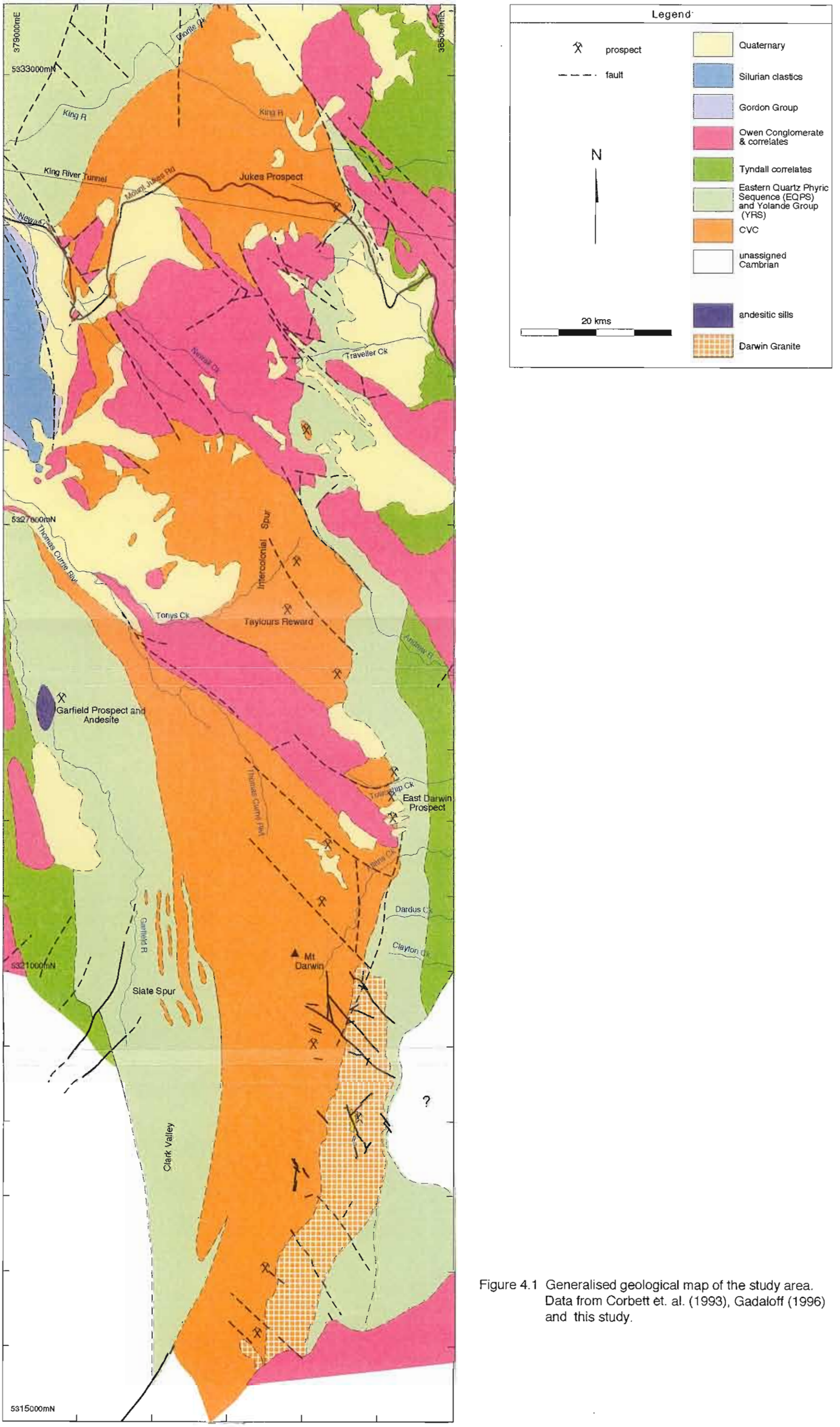

Figure 4.1 Generalised geological map of the study area. Data from Corbett et. al. (1993), Gadaloff (1996) and this study.

andesites) that intruded the YRS. This Cu-Au occurrence is known as the Garfield Prospect and has many similarities to Cu-Au mineralisation in the Prince Lyell deposit, at Mt. Lyell (Corbett, 1992).

The YRS contains interbedded tuffaceous mass-flow deposits, turbiditic sandstones, shard-rich tuffaceous mudstones, micaceous siltstones, and black graphitic shales (Corbett, 1992). Complex lateral facies variations, numerous fault disruptions and interfingering relationship with the CVC have complicated geologic interpretations. Corbett (1992) subdivided the Western Sequence into four main groups; the Mt. Charter Group (Hellyer area), the Dundas Group (north of the Henty Fault Zone), the Henty fault wedge sequence, and the YRS (the South of the Henty Fault Zone).

The YRS was previously considered to be the oldest sequence of volcanic rocks recognised in the southern MRV (Corbett, 1992). The oldest units of the sequence, exposed in the core of the Miners Ridge anticline south of Queenstown, include siliciclastic sandstone facies of the Miners Ridge Sandstone, underlain by the tholeiitic Miners Ridge basalt (Corbett, 1992). The Miners Ridge sandstone was overlain by an extensive volcano-sedimentary sequence containing a mixed sequence of quartz-phyric lavas and volcaniclastic rocks, with minor sedimentary facies, including mudstones, sandstones and shales. At or near the top of the sequence in the Lynchford area, is the andesitic-basaltic sequence of the Lynch Creek Basalt. A subordinate series of plug-like and sheet-like quartz-feldspar (± biotite) porphyries intruded the sequence to the North and south of Queenstown (Corbett, 1992). Although the YRS was known to have an interfingering relationship with the CVC (Corbett, 1992), it was considered to underlie the CVC in the area. Detailed geological mapping, in the Garfield Prospect area and the Clark and Garfield Valleys, defined an interfingering relationship between the YRS rocks, the CVC and Tyndall Group correlates (Halley, 1996). These outcrops were visited as part of the current study and the interfingering relationships confirmed. In the Clark and Garfield Valleys the rocks dip west, face west and the YRS rocks are younger than the CVC. This research, suggests that, in the study area, YRS and EQPS rocks are at the same structural position, relative to the CVC, and were sourced from the same magma. The Garfield andesites were emplaced in the lower YRS, after the last eruption of feldspar-phyric rocks of the CVC.

The YRS is dominated by medium to coarse-grained quartz-feldspar-phyric volcaniclastics and lavas. The volcaniclastics and lavas are interbedded with intrusives, juvenile volcaniclastics, siltstones, sandstones and mudstones and black graphitic shales (Corbett, 1992; White, 1996). Black shales, like the siltstones and mudstones, occur as a minor portion of YRS rocks and a proportionally smaller portion of rocks in the study area. Their occurrence suggests that the YRS formed in a deeper water environment than the other volcanic units.

4.2.2 Central Volcanic Complex

The CVC consists predominantly of feldspar-phyric rhyolitic-dacitic lavas and volcaniclastic rocks and minor sedimentary facies throughout its entire length (Corbett et al., 1974; Corbett, 1981; Corbett, 1992; McPhie and Gemmell, 1992). Basaltic and intermediate rocks are common north of the Henty Fault, but are infrequent south of Queenstown (Corbett, 1989; Corbett and Solomon,

1989). Coherent feldspar-phyric rhyolitic lavas, quartz-feldspar-phyric volcaniclastics, subordinate volcaniclastic sandstones and mudstones, and pumice breccias characterise the CVC within the study area. Sedimentary facies are minor but volcaniclastic sandstones and mudstones do occur on Intercolonial Spur (Gadaloff, 1996) and along the Jukes Road.

Flow-banding, autobrecciation, and columnar jointing are common (Doyle, 1990; Corbett et al., 1993). A variety of breccia types were identified, including, hyaloclastite breccias, polymictic lithic volcaniclastic breccias, and monomictic and polymictic hydrothermal breccias. The hyaloclastite breccia on the Allan's Creek plateau was interpreted to be the top of a single lava flow (Gadaloff, 1996). The presence of the hyaloclastite breccia along with volcaniclastic sandstones and mudstones, suggests a submarine environment of deposition, consistent with other interpretations (Berry and Crawford, 1988; Allen and Cas, 1990; Crawford and Berry, 1992; McPhie and Allen, 1992).

4.2.3 Eastern Quartz-Phyric Sequence

The EQPS occurs from the East Darwin area (Figure 4.1) to the Jukes Road but is absent on the Darwin Plateau. At the East Darwin prospect the EQPS is in faulted contact with the CVC to the West and with the Tyndall Group to the East (Gadaloff, 1996). The least deformed and altered samples of the EQPS were identified as quartz-feldspar-phyric rhyolite and volcaniclastic sandstone (Gadaloff, 1996). Along the eastern Jukes Road, near the contact of the Owen Conglomerate, a Tyndall Group feldspar-phyric dacite interfingers with a polymict volcaniclastic of the upper EQPS. This conformable relationship is important given the conformable relationship between the YRS and Tyndall Group rocks mentioned previously. This conformable relationship, combined with lithologic similarities, facies similarities, and geochemical similarities (later in this chapter) support the hypothesis that the EQPS and YRS, in the study area, are from the same magmatic source.

4.2.4 Tyndall Group

Tyndall Group rocks were briefly examined since granite-related hydrothermal alteration of Tyndall Group rocks did not occur in the study area. However, granite-related hydrothermal alteration and mineralisation do occur in the Tyndall Group farther north in the MRV (Hunns, 1987; Halley and Roberts, 1997; Jaeger, 1996). Facies identified in the Jukes-Darwin area include: basal conglomerate, volcaniclastic lithic conglomerate, polymictic lithic volcaniclastic sandstone, and feldspar-phyric dacites (Doyle, 1990; Jones, 1993; Gadaloff, 1996). The basal conglomerate of the Tyndall Group rests unconformably on the Darwin Granite, and graded bedding suggests younging to the East (Jones, 1993). Tyndall Group rocks in contact with the Darwin Granite are medium to coarse-grained polymictic conglomerates containing rounded clasts of sericite-altered coarse-grained pink Darwin Granite and other volcanic clasts derived from the CVC. This is taken as unequivocal evidence of a localised Late Cambrian uplift and erosion of the Darwin Granite. Elsewhere in the MRV, Tyndall Group rocks are conformable with the CVC. In the East Darwin area a polymictic crystal-lithic volcaniclastic breccia grades into a crystal-rich volcaniclastic sandstone. This facies was correlated with the polymictic lithic

volcaniclastic sandstone of Jones (1993) and the Mt Julia Member, a normally graded volcaniclastic breccia/sandstone of the Comstock Formation (Gadaloff, 1996). On Intercolonial Spur, this facies is in faulted contact with the EQPS (Gadaloff, 1996).

Tyndall Group volcaniclastics are interpreted to have been sourced from subaerial pyroclastic flows and lavas (White and McPhie, 1996). The presence of sub-angular lithic clasts in the volcaniclastic breccias suggests that the lavas and pyroclastic materials were transported to a near-by depositional basin where they were deposited as mass flows in a subaqueous environment. White and McPhie (1996), suggested that these facies were emplaced in a below-storm-wave-base depositional setting. Such an environment is consistent with the textures noted from the Tyndall Group in the study area.

4.3 PETROLOGY OF THE CAMBRIAN VOLCANIC ROCKS

The following descriptions of volcanic and volcano-sedimentary textures for the Cambrian volcanic rocks are based on the descriptive classification of McPhie et al. (1993). Grain size nomenclature is from Chough and Sohn (1990).

4.3.1 Yolande River Sequence

Fine to coarse-grained quartz-feldspar-phyric felsic volcaniclastics and lavas are interbedded with siltstones, sandstones and mudstones in the region west of Mt. Darwin. The rocks interfinger with feldspar-phyric rocks of the CVC along the eastern side of the Clark Valley. In areas of well-developed cleavage, volcaniclastics and lavas are not easily distinguished from each other. Distinguishing features are the grain size of the matrix and the percentage and types of lithic clasts.

4.3.1.1 FINE TO MEDIUM-GRAINED QUARTZ-FELDSPAR-PHYRIC LAVA

In the western part of the mapped area a fine to medium-grained quartz-feldspar-phyric lava or shallow sill occurs. The rock contains rare lithic clasts set in a uniformly fine-grained matrix (Plate 4.1A). In the western part of the Slate Spur area, this facies is massive, weakly foliated and is interpreted to be coherent. Contacts with other facies were not observed.

The groundmass is composed of an interlocking fine-grained mosaic of quartz, plagioclase, K-feldspar, biotite, sericite and minor chlorite, magnetite and hematite (Plates 4.1B-C). The groundmass grain-size is between 0.02-0.1 mm. Phenocrysts of quartz and feldspar comprise 10-20 % of the rock, biotite 1-2 % and opaques are 1-2 %. Lithic clasts are rare (< 0.5 %), and are confined to rounded medium to coarse-grained masses of quartz and feldspar. These clasts are interpreted to represent wall-rock fragments caught up in the magma during its eruption.

The phenocryst population is dominated by quartz crystals (60-70 %) up to 3 mm in diameter (Plates 4.1B-G). Quartz crystals occur as unaltered to embayed euhedral crystals, euhedral crystals with rounded corners, subhedral crystals or broken and angular crystals (Plate 4.1B-C). Most have uniform extinction but deformation related undulose extinction was observed. 2 mm

crystals of K-feldspar dominate the feldspar phenocryst population (30 to 40 % of the total crystals in the rock) but rare plagioclase phenocrysts were observed. Feldspar crystals are broken and rounded to sub-rounded, although occasional euhedral to subhedral crystals were observed. K-feldspar was preserved in the matrix of weakly altered rocks and carlsbad twinning was observed.

The rocks in this facies strike NNW. Cleavage was well-developed parallel or subparallel to bedding and flow banding.

4.3.1.2 FINE TO MEDIUM-GRAINED QUARTZ-FELDSPAR-PHYRIC VOLCANICLASTIC

This facies is a matrix-supported volcaniclastic rock with scattered lithic clasts set in a uniformly fine-grained matrix (Plate 4.2A-C). Lithic clasts of variable size were observed and their occurrence separates this facies from the quartz-feldspar-phyric lava previously described. Contacts with other facies were not observed due to scarce outcrops and can be gradational.

The matrix consists of mixed domains of very fine-grained (< 0.01-0.05 mm) and fine-grained (0.05-0.1 mm) interlocking mosaics of quartz, plagioclase, K-feldspar, sericite, and chlorite. Magnetite, hematite (after magnetite) and zircons occur as accessory minerals.

The crystal population is dominated by quartz crystals (50-60 %) up to 2 mm in diameter. Quartz crystals vary from subhedral crystals with rounded corners, to broken and angular crystals and are typically embayed. Many of the broken quartz crystals were pulled apart by later shearing and have preserved jigsaw-fit textures. Most have uniform extinction but undulose extinction was observed. The edges of quartz and feldspar crystals are typically corroded and ragged but sharp edges were observed. The maximum feldspar crystal size observed is 2 mm, and most are broken and rounded to sub-rounded. Of the total crystal population, K-feldspar crystals are approximately 30% and plagioclase crystals 20 %.

Lithic clasts average 5 % of the rock. Two primary lithic clast types were observed. Clasts of fine to coarse-grained quartz-feldspar-phyric rocks similar to the facies described previously and irregularly shaped vesicular and tube pumice up to 2 cm in length and 0.2 to 0.5 cm wide. Pumice clasts typically have well-preserved vesicular textures.

In two locations, the rock is dominated by lithic clasts (70-80 %), averaging 5-10 cm long, with some clasts up to 70 cm in length. Most lithics are partially rounded to sub-rounded, but the larger ones tend to be angular. Lithics are monomictic and are composed of flow-banded quartz-feldspar-phyric lava in a matrix of aphanitic rhyolite. The bodies are tens of metres in size and were not mappable along strike. These rocks are interpreted to be autobreccias or hyaloclastites.

Cleavage was well-developed parallel or subparallel to bedding and flow banding. The facies has well-developed light-green sericite on cleavage surfaces. Foliation developed as a result of shearing along cleavage surfaces.

Plate 4.1. Yolande River Sequence fine to medium-grained quartz-feldspar-phyric lava.

A. The fine to medium-grained quartz-feldspar-phyric lava is illustrated. Sample B2003, scale in centimetres.

B and C. Typical K-feldspar phenocrysts (K) weakly replaced by secondary sericite. Note that twinning was preserved. Plate 4.1B is plane polarized light and Plate 4.1C is crossed polars. Field of view width = 6 mm, Sample B2007.

A

B

C

Plate 4.2. Yolande River Sequence fine to medium-grained quartz-feldspar-phyric volcaniclastics.

A. The variety of appearances of the fine to medium-grained quartz-feldspar-phyric volcaniclastic is illustrated. Cleavage is parallel or subparallel to bedding, and flow banding and shearing along cleavage surfaces resulted in a distinctive foliation. From left to right the rocks shown are B1086, B1087, B2013, and B1094.

B and C. Feldspar crystal (A) and fine grained lithic clast (B) in fine-grained quartz-sericite-feldspar matrix. The foliation, enhanced by sericite, is parallel to the NNW structural trend in the rocks. Quartz crystals are subrounded and broken and were disjointed by stretching related to the foliation. Plate 4.2B is plane polarized light and Plate 4.2C is crossed polars. Field of view width = 6 mm. Sample B1094.

A

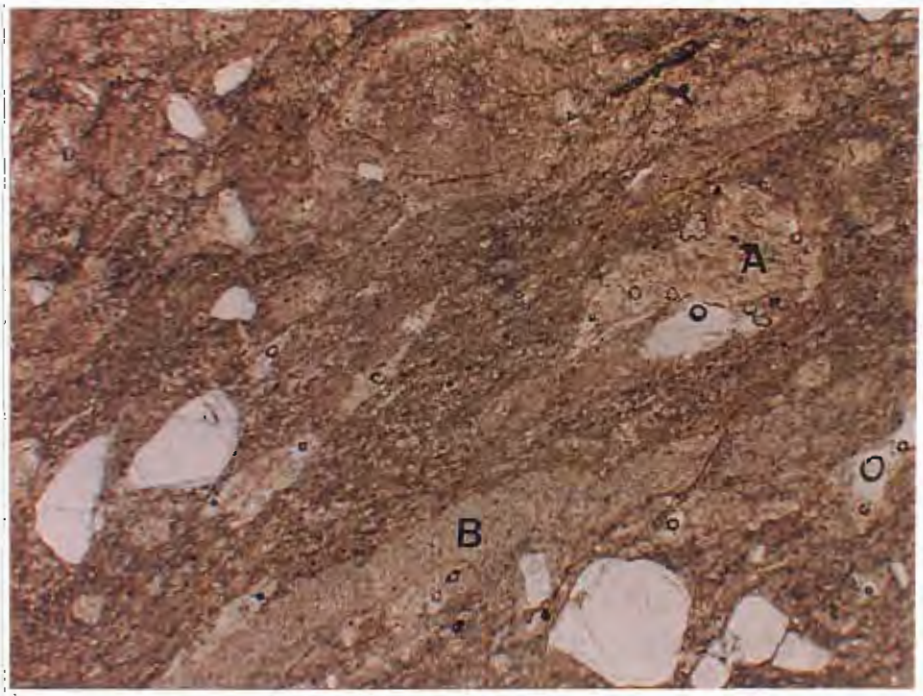

B

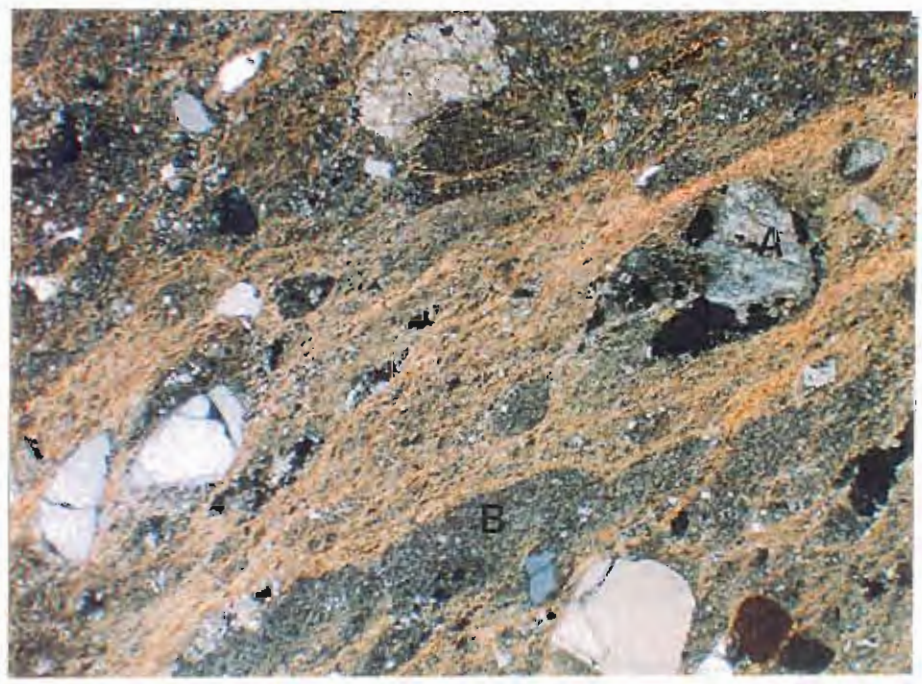

C

4.3.1.3 SANDSTONE

The most continuous sedimentary deposits in the YRS are sandstones but they occur as less than 1% of the total outcrop and float observed. Individual horizons were traceable by float fragments for up to a kilometre along the western side of the Clark Valley-Slate Spur area. Sandstone occurs as thin lenses in the fine to medium-grained quartz-feldspar-phyric lava sequence. Sandstone horizons are up to fifty metres thick but are typically thinner. Grading, crossbedding, and other features useful in determining facing direction, were not observed, due to poor exposure.

Sandstones are medium to coarse-grained graywackes. The fine-grained matrix consists of subangular to subrounded quartz and feldspar with grains sizes from <0.1 to 0.2 mm. Compositionally, quartz is 40% and feldspar 60%. Crystals of subrounded quartz and K-feldspar (to 0.5 mm) and lithic clasts are less than 2%.

This facies occurs interbedded with the fine to medium-grained quartz-feldspar-phyric lava and is interpreted to be an immature volcaniclastic sandstone.

4.3.1.4 SILTSTONES AND MUDSTONES

Siltstones and mudstones occur as less than 0.1% of the total outcrop and float observed. Thin individual horizons were traceable along strike for several hundred metres. Siltstones and mudstones occur as thin lenses within the sandstone facies, with maximum thickness of a few metres. The sandstone and mudstone were not studied in detail.

4.3.1.5 SHALE

Several black shale horizons occur within the sedimentary rocks along the western part of the Clark Valley. The black shale was recognised by the occurrence of minor float amongst the other siltstone and mudstone float. Black shales appear to transition along strike into siltstones and mudstones. The black shales are fine-grained, black to dark green, with well-developed slaty cleavage. Disseminated pyrite is a common accessory mineral.

Black shales are a very minor portion of the YRS rocks. Due to their small overall volume, they were not studied in detail. However, there occurrence supports the interpretation that the YRS formed in a deep water environment.

4.3.1.6 ANDESITES

The Garfield Prospect was briefly examined because of similarities between the style of Cu-Au and apatite-magnetite mineralisation in the Garfield Prospect and the style of Cu-Au and apatite-magnetite mineralisation in the Prince Lyell deposit at Mt. Lyell. The Garfield andesites are hornblende-phyric andesites texturally and compositionally similar to the Crown Hill and Anthony Road andesites (Halley, 1996). Two phases of andesite occur that are conformable with the enclosing rhyolitic volcanics of the YRS. Sharp contacts with the enclosing rocks, support an interpretation of intrusive emplacement in contrast to the brecciated, quench-fragmented tops

expected in submarine lavas. In the volcanic sequence above the andesites, a feldspar-phyric lava occurs that is interpreted to be the last (highest) appearance of CVC rocks in the stratigraphy. This CVC lava was intruded by a number of similar andesitic dykes separate from the main Garfield andesites. Intrusion of the andesites into the CVC constrains the timing of the andesite emplacement to post CVC volcanism. The andesites are characterised by a high content of feldspar and chloritised ferro-mag phenocrysts (Halley, 1996).

Hand specimen photographs of the two phases of andesite observed are shown in Plate 4.3A. The first phase is feldspar-hornblende-phyric. The groundmass consists of quartz, sericite, chlorite and traces of carbonate. Euhedral to subhedral feldspar phenocrysts, up to 1 mm long and 0.8 mm wide, comprise up to 25% of the rock (Plate 4.3B-C). Other phenocrysts include relict hornblende (1-2%) and small subangular quartz crystals (0.02-1 mm, up to 5%). A complete gradation in crystal fragment size was observed. Accessory minerals include apatite (to 1 cm), euhedral pyrite grains (cubes to 0.8 cm), and carbonate. Rare felsic lithic clasts several cm in size were observed. Well-developed pressure shadows have formed around many quartz, apatite and sulfide grains.

The second phase of andesite (Plate 4.3F-G) is feldspar hornblende-phyric, but unlike the first, contains less than 0.1% fine-grained quartz crystal fragments. The groundmass is uniformly microcrystalline sericite and chlorite with a trace of carbonate. Relict feldspar phenocrysts, comprise up to 15% of the rock and relict hornblendes, 1-2%. Typically, the two phases are intensely sheared with a well-developed cleavage.

4.3.2 Central Volcanic Complex

Feldspar-phyric and quartz-feldspar-phyric volcanics host the mineralisation at Mt. Darwin and a columnar-jointed feldspar-phyric dacitic sill is the primary host facies to the Jukes Cu-Au prospect. In the study area, feldspar-phyric and quartz-feldspar-phyric rocks are exposed from the eastern side of Clark Valley, up to and along the ridge separating the Darwin plateau from the Clark Valley, and northward through Intercolonial Spur and the Jukes Road.

4.3.2.1 FELDSPAR-PHYRIC LAVAS AND SILLS

Due to the intensity and extent of hydrothermal alteration in the Darwin area, the following description of the feldspar-phyric facies comes from the least-altered rocks observed along the Jukes Road. The assumption that Jukes Road rocks are similar to Darwin area rocks is valid as feldspar-phyric rocks from the Darwin Granite area and Intercolonial Spur (Gadaloff, 1996), are of similar texture and mineralogy.

The best exposed and least-altered feldspar-phyric facies is exposed along Jukes Road for over a kilometre. The feldspar-phyric facies contains well-developed columnar joints (Plate 4.4A) and is interpreted to be a single sill or flow, although actual tops and bottoms were not observed. Plate 4.4B is a photograph of a cut slabs from a typical feldspar-phyric rock. At the Jukes Prospect, this facies has been named the Jukes Road columnar-jointed dacite. Due to the massive nature of the weakly altered feldspar-phyric facies, regional cleavage was poorly developed.

Plate 4.3. Yolande River Sequence andesites.

A Hand specimen photographs of the various andesitic styles observed. From left to right the rocks are: least-altered feldspar hornblende-phyric andesite (B1064) with quartz, sheared chlorite-altered feldspar hornblende-phyric andesite (B1046) with quartz, and feldspar hornblende-phyric andesite without quartz (B1053).

B and C. Euhedral plagioclase phenocrysts (P) were altered to carbonate and sericite. The groundmass consists of quartz, sericite, chlorite and traces of carbonate. Sample B1064. Plate 4.3B is plane polarized light and Plate 4.3C is crossed polars. Field of view width = 6 mm.

D and E. Feldspar hornblende-phyric andesite. Note the uniformly microcrystalline groundmass of sericite, chlorite and a trace of carbonate. Relict feldspar (F) and hornblende (H) phenocrysts were intensely sheared and the texture is dominated by a well-developed cleavage. Sample B1053. Plate 4.3D is plane polarized light and Plate 4.3E is crossed polars. Field of view width = 6 mm.

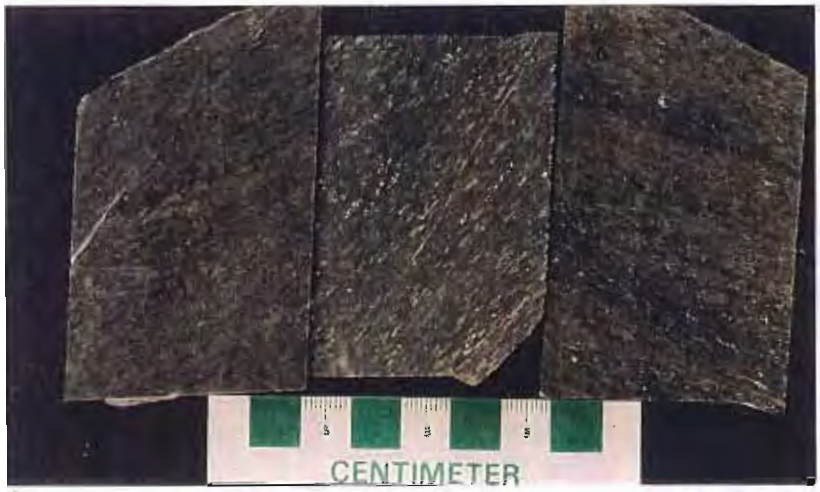

A

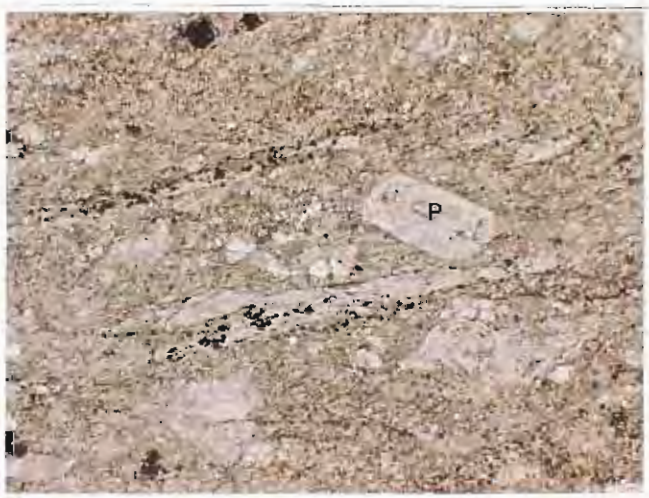

B

C

D

E

Plate 4.4. Feldspar-phyric lavas and sills.

A. Well-developed columnar joints in the Jukes Road columnar jointed feldspar-phyric dacite. Although the top and bottom were not observed, this facies is interpreted to be a sill or flow.

B. Cut slab from a typical hand sample of the feldspar-phyric dacite. The fine-grain groundmass (G) and small (1 to 5 mm) feldspar phenocrysts (F) are characteristic. Sample B2057.

C. Euhedral to subhedral phenocrysts of albite and orthoclase (F) in the micropoikilitic groundmass (G). Sample 10270. Polarized light, field of view width = 1.9 mm.

A

B

C

The least-altered feldspar-phyric dacite consists of quartz, albite, orthoclase, sericite, and chlorite with accessory magnetite, rutile, pyrite and zircon. The groundmass has a granular texture because of the presence of micropoikilitic quartz grains (micropoikilitic quartz is described in detail in Chapter 5). Albite and orthoclase, in the groundmass, occur as 0.1-0.2 mm size subhedral to anhedral lath-like crystals. However, euhedral laths with carlsbad twinning were observed. In the least-altered samples, small (<1 mm) K-feldspar is enclosed in the micropoikilitic quartz. Electron microprobe analysis of feldspar in the columnar-jointed feldspar-phyric dacite along Jukes Road indicate that the average composition of K-feldspar is 93% orthoclase and plagioclase is 98% albite (Appendix I).

Albite and orthoclase phenocrysts are euhedral to subhedral and vary from 1 to 5 mm in size. Orthoclase phenocrysts are less abundant than albite phenocrysts and typically smaller in size.

4.3.2.2 QUARTZ-FELDSPAR-PHYRIC VOLCANICLASTICS AND MASS-FLOW DEPOSITS

Typical volcanic breccias (volcaniclastics) occur throughout the Jukes-Darwin area and include mass-flow deposits and hydrothermal breccias. Doyle (1990) and Gadaloff (1996) identified volcaniclastic rocks such as hyaloclastites in their respective research areas at the Jukes Prospect and Intercolonial Spur. In addition, one volcanic breccia, described by Doyle (1990), was examined as part of the current study and is reinterpreted to be a hydrothermal breccia. The "hyaloclastite" described by Gadaloff (1996) was not visited, but a brief description was included below.

In the Mt Darwin area, the Clark Valley and throughout the western part of the CVC, quartz-feldspar-phyric volcaniclastics are abundant, although subordinate to feldspar-phyric lavas and sills. They are interbedded with, and interfingered with, feldspar-phyric lavas throughout the mapped area, although actual contact relationships were obscured due to alteration effects. Several varieties of quartz-feldspar-phyric volcaniclastics were recognised, including tube pumice breccias, pumiceous mass-flow deposits, polymictic crystal-rich volcaniclastic breccias and finer-grained rhyolitic volcaniclastic rocks. Most volcaniclastic rocks observed, underlie the fine-grained sedimentary facies of the CVC. In addition to the feldspar-phyric lavas, quartz-feldspar-phyric volcaniclastics have a conformable and gradational contact with the poorly exposed overlying YRS.

Quartz-feldspar-phyric volcaniclastic varieties were grouped together, as they have similar mineralogies, compositions and lithic clast sizes. Two exceptions deserve mention. The first exception is a pumice breccia along the Jukes Road that has been locally named the 'Jukes Road Pumice Breccia.' This facies contains outstandingly preserved diagenetic alteration textures and is described in detail in Section 5.2.2. The second exception is a coarse volcaniclastic mass-flow deposit illustrated by a photograph in Plate 4.5A. This facies occurs for several hundred metres along Jukes Road and is a clast supported breccia with angular and subrounded clasts of variable size from 0.5 cm up to boulders. A variety of lithic clast types were observed including; coherent feldspar-phyric lavas, crystal-rich volcaniclastic sandstones, mudstones, and pumiceous volcaniclastics.

A typical example of a polymictic crystal rich pumiceous volcaniclastic deposit occurs at the summit of Mt. Darwin and is shown in a photograph in Plate 4.5B. Photomicrographs of the common microscopic textures and features are shown in Plates 4.5C-D. Typical volcaniclastic rocks contain 10 to 20% quartz and feldspar crystals (up to 5 mm in length) set in a fine to medium-grained matrix of < 0.1 to 0.5 mm interlocking quartz and feldspar crystals. The rocks are comprised of quartz, plagioclase, K-feldspar, sericite, with minor chlorite, pyrite and epidote.

Subhedral prismatic plagioclase crystals (up to 3.5 mm) are abundant and occur in glomocrysts. Glomocrysts of plagioclase are either a primary texture or indicate little transport. K-feldspar crystals are less abundant and typically smaller in size. Small angular quartz fragments (up to 2 mm) were observed throughout some rocks. Quartz and feldspar crystals are broken and jigsaw fits were observed in weakly deformed rocks. Average quartz crystal size is 2 mm but subhedral crystals to 5 mm were observed.

Polymictic crystal-rich volcaniclastic breccias occur in the Mt. Darwin area and at Intercolonial Spur (Gadaloff, 1996). Photomicrographs of two varieties of volcaniclastic breccias are shown in Plates 4.5C-D. Coarse volcanic breccias are clast-supported, with clasts size variable from 0.5-10 cm. Three clast types observed are: coherent feldspar-phyric lava, crystal-rich volcaniclastic sediments, and crystal-poor volcaniclastic sediments. Coherent feldspar-phyric lava clasts have feldspar phenocrysts replaced with chlorite and a micropoikilitic groundmass with interstitial chlorite between the micropoikilitic quartz grains. Crystal-rich volcaniclastic sediments have quartz crystals, and chlorite-altered glass shards (up to 35%) in a quartz-sericite matrix (Gadaloff, 1996). Quartz crystals range in size from 0.5-1 mm, while the altered glass shards are up to 5 mm long. The crystal-poor volcaniclastic sediment clasts have similar matrix characteristics to the crystal-rich rocks, but do not contain the large quartz crystals or relict glass shards. The matrix of the breccias is fine-grained quartz and feldspar.

The term 'hyaloclastite' is used to describe clastic aggregates formed by non-explosive fracturing and disintegration of quenched lavas and intrusions (McPhie, 1993). The following description of a hyaloclastite on the Intercolonial Spur comes from Gadaloff (1996).

A breccia facies found in the southern half of the study area, is monomictic and has a gradational contact with the surrounding CVC, based on the lack of any sharp contact being observed in outcrop, and on the variable degree of brecciation between outcrops around the interpreted contact. Clast sizes range from 0.1-6 cm, and typically have a jigsaw-fit texture. Clasts have the same micropoikilitic groundmass as the coherent lavas of the CVC, and have been affected by hydrothermal alteration to the same extent, with K-feldspar being the dominant hydrothermal alteration style in this area. The feldspar crystal content in breccia clasts (approx. 2%) is lower than that found in the coherent lavas (approx. 5%). This can be caused by a number of processes; (i) magma fractionation, (ii) complete destruction of feldspars by alteration, (iii) resorption, etc. All vein types observed in this unit cross-cut the brecciation, and this fact, combined with the jigsaw-fit texture, monomictic clast type, interpreted graded bedding and identical alteration assemblages supports a syn-depositional timing for brecciation characteristic of a hyaloclastite breccia.

Plate 4.5, Feldspar-phyric volcaniclastics and mass-flow deposits.

A. CVC Mass-Flow Deposit. Large boulder amongst smaller boulders in a dacitic/rhyolitic volcaniclastic mass-flow deposit along the western Jukes Road.

B. Relict feldspar-phyric pumice clasts occur as well-developed fiamme in a volcaniclastic facies near the summit of Mt. Darwin.

C. Crystal-rich volcaniclastic breccia. This rock has a fine-grained quartz and feldspar rich matrix, small scattered quartz and feldspar crystals and scattered relict glass shards (S). The crystal-poor volcaniclastics have similar matrix characteristics to the crystal-rich rocks, but do not contain the large quartz crystals. Sample 13800. Polarized light, field of view width = 6 mm.

D. Polymict, crystal-rich coarse volcanic breccia. The large lithic clast (L) is a coherent feldspar-phyric lava with a micropoikilitic groundmass with interstitial chlorite between the micropoikilitic quartz grains. Note the angular quartz and feldspar crystals occur as a crystal rich matrix that supports the lithics. Sample B1079. Polarized light, field of view width = 6 mm.

A

B

C

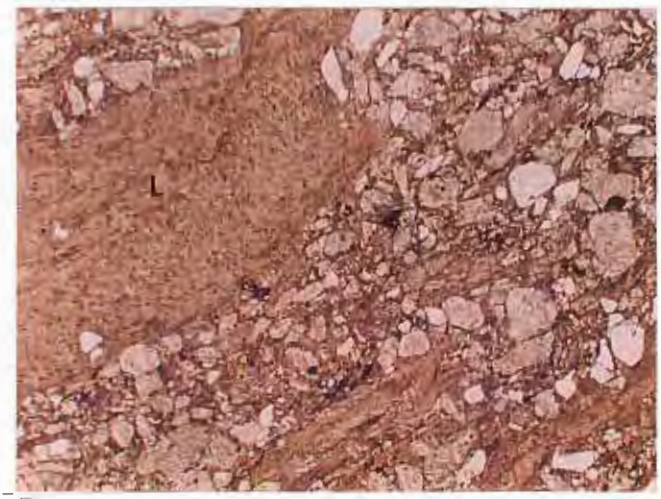

D

Plate 4.6. Tuffaceous-ash/sandstone facies.

A. Photograph of slabs cut from hand samples of the thin tuffaceous-sandstone facies from the Jukes Road. Notice the thinly bedded nature of the rocks. The rock on the left (Sample 11400) is coarser-grained and crystal rich compared to the sample on the right (Sample 11900).

B. Thin tuffaceous-ash horizons interbedded with thin tuffaceous-sandstone and pumiceous volcaniclastic horizons. The dashed lines separate the thinly bedded horizons. In the top horizon, a small pumice clast was replaced by secondary chlorite. Sample 11400. Polarized light, field of view width = 6 mm.

A

B

Tuffaceous-Ash/Sandstone Facies

The tuffaceous-ash/sandstone facies includes thin tuffaceous-ash horizons interbedded with thin tuffaceous-sandstones, mudstones and pumiceous volcaniclastic horizons (Plate 4.6A-B). This interbedded relationship has been recognised throughout the study area (White, 1975; Corbett et al., 1993; Gadaloff, 1996). This facies is exposed along the western side of a major north-south fault at the north end of the East Darwin area, and in the northern part of Intercolonial Spur (Gadaloff, 1996). Along Jukes Road, it is exposed for approximately 230 metres. Graded bedding was preserved in some of the thin sandstone horizons and facing directions upward and to the west were interpreted. The volcaniclastic sandstone contains approximately 15% crystals, dominantly quartz (1-3 mm), with subordinate feldspar and altered glass shards (up to 1.5 cm long).

Mudstones are comprised of clasts of fine-grained quartz and mud particles (<0.1 mm) with scattered quartz crystals 1-2 mm in diameter. Clasts of coherent lava (1-2 cm long; 5% of the rock) elongated in the direction of flow were observed.

A 50 metre thick tuffaceous-ash/sandstone horizon, similar to rocks along Jukes Road, is exposed along the ridge just south of the Mt. Darwin summit. The rocks include interbedded thin tuffaceous-ash and tuffaceous-sandstones. Graded bedding was not preserved therefore facing directions were not determined. Regional cleavage subparallel or oblique to bedding is well-developed because of the chlorite content of the rocks.

4.3.2.3 QUARTZ-FELDSPAR ± BIOTITE PORPHYRY DYKES

Seven quartz ± feldspar-biotite porphyry dykes (referred to as Type 1 and Type 2 dykes) intrude the columnar-jointed feldspar-phyric dacite along the Jukes Road and Intercolonial Spur (Gadaloff, 1996) but none were observed in the Mt. Darwin area. Contacts with the feldspar-phyric dacite are sharp and, in several instances, were used as conduits for hydrothermal fluids (Jukes Prospect). One large dyke (Type 1) has well-developed columnar joints oblique to the columnar joints developed in the feldspar-phyric dacite.

Quartz ± Feldspar Biotite Porphyry Dykes: Type 1

The groundmass of the Type 1 dykes consists of very fine-grained (0.005-0.01 mm) quartz and feldspars, and 2-3% uniformly disseminated magnetite (Plate 4.7A-B). However, one dyke has a finer groundmass averaging 0.005 mm. The groundmass varies from unfoliated to moderately well-foliated and has a seriate texture. Zircons to 0.01 mm are common. Subhedral to anhedral quartz and feldspar phenocrysts make up 30-40% of the rock. Quartz phenocrysts are subhedral to subrounded, comprise up to 20% of the rock and are variable in size from 0.2 to 8 mm (Plate 4.7B). Some have resorbed margins while others are rounded to angular with excellent embayed textures. Commonly, quartz phenocrysts have undulose extinction that is interpreted to be evidence of dynamic strain. Euhedral to subhedral feldspar phenocrysts comprise up to 10 to 20% of the rock and are variable in size from 0.1 to 6 mm. Feldspar phenocrysts were embayed, and

in some dykes, a preferred orientation parallel to the walls of the dykes was observed. Quartz and feldspar phenocrysts have a complete gradation in size from microphenocrysts through to their maximum size. Biotite phenocrysts (2 to 3% of the rock) vary in size from 0.1 to 2 mm.

Quartz-Feldspar Biotite-Porphyry Dykes: Type 2

Compositionally Type 2 dykes (Plates 4.7C-D) differ the Type 1 dykes. The groundmass grainsize is coarser than the groundmass of Type 1 dykes, averaging 0.01-0.1 mm. In addition, the quartz phenocryst population is less and the feldspar phenocryst population is more. Quartz phenocrysts are up to 10% of the rock, plagioclase phenocrysts up to 20% and biotite phenocrysts are rare. Feldspar crystals have uniform and shadowy extinction.

4.3.3 Eastern Quartz-Phyric Sequence

4.3.3.1 QUARTZ-FELDSPAR-PHYRIC VOLCANICLASTICS AND MASS-FLOW DEPOSITS

Quartz-Feldspar-Phyric Rhyolite

Quartz-feldspar-phyric rhyolitic volcaniclastics (Plate 4.8A-E) are the dominant lithologies in the EQPS. In the study area these rocks are exposed from the eastern Jukes Road southward to the East Darwin prospects (Figure 4.1). The matrix has a sandy texture composed of fine-grained (<0.2 mm) quartz and feldspar. Crystals of feldspar and quartz make up 20-30% of the rocks. Quartz crystals have a complete gradation in size from 0.5 to 5 mm and plagioclase crystals range from 0.5-2 mm in diameter. Quartz crystals are euhedral, rounded broken or embayed. The rocks contain quartz (60%), mica (25%), kaolinite (10-15%), chlorite (5%), and K-feldspar (5%) as determined by XRD analysis (Appendix G). Zircons were observed. Lithic clasts of quartz-feldspar-phyric volcanic rocks are common (Plate 4.8B-C). This facies is interpreted to be a massive crystal rich volcaniclastic sediments or mass-flow deposits.

Quartz-Feldspar-Phyric Dacite

Quartz-feldspar-phyric dacite is exposed in an area immediately adjacent to the fault between the CVC and EQPS sequence. Compositionally the rocks contain feldspar, quartz, biotite, relict ferromagnesian minerals (now chlorite), sericite and minor magnetite. Lithic clasts are rare. The matrix is fine-grained and foliated. Average matrix grainsize is 0.001-0.002 mm but coarser areas were observed. The rocks contain up to 30% quartz and feldspar crystals. Quartz crystals range from 0.1 to 5 mm, are euhedral to subhedral and embayed and have broken or rounded corners. Plagioclase crystals (from 0.5 to 4 mm) were broken and margins typically corroded. Some were stretched by cleavage development into augens. Quartz commonly occurs as granophyric intergrowths with feldspar. Albite twinning was observed in many of the crystals. This facies is interpreted to be a volcaniclastic rock.

Plate 4.7. Quartz-feldspar ± biotite porphyry dykes.

A. Slab cut from a hand sample of the Type 1 Quartz-Feldspar ± Biotite Porphyry from near the centre of the Jukes Road Cu-Au Prospect. Note the abundant quartz phenocrysts (white). Feldspar phenocrysts in this sample were replaced by secondary chlorite and appear as darker colored crystals against the brown groundmass. Sample MJ-96-8.

B. Photomicrograph of the Type 1 Quartz-Feldspar ± Biotite Porphyry. Notice the rounded and embayed quartz phenocryst (Q). Feldspar phenocrysts (P) are typically stretched and were partially replaced by secondary sericite or chlorite. Polarized light, field of view width = 6 mm. Sample MJ-96-8.

C. Hand sample of the Type 2 Quartz-Feldspar ± Biotite Porphyry from the Jukes Road. Note the scattered quartz (Q) and abundant feldspar phenocrysts (P) compared to the Type 1. Sample MJ-96-9.

D. Photomicrograph of the Type 2 Quartz-Feldspar ± Biotite Porphyry. The grainsize of the groundmass is coarser than Type 1 averaging 0.01-0.1 mm. Quartz phenocrysts (Q) are subrounded and embayed. Polarized light, field of view width = 6 mm. Sample MJ-96-9.

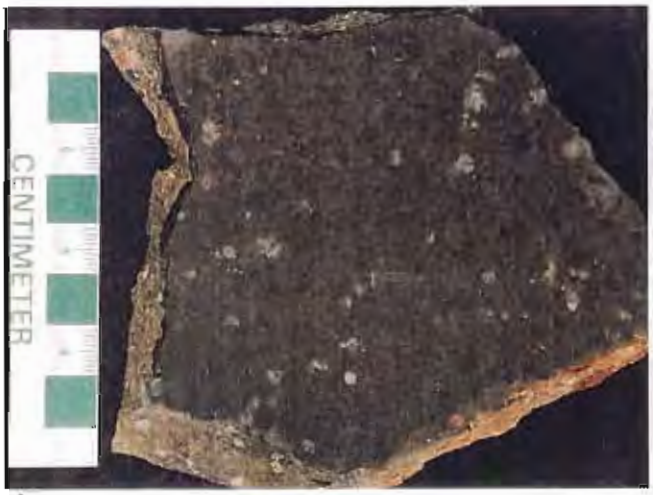

A

B

C

D

Plate 4.8. Eastern Quartz-Phyric Sequence rocks.

A. Cut slabs from hand samples of several types of quartz-feldspar-phyric rhyolitic volcaniclastics and mass-flow deposits from along Jukes Road. Notice the lithic clasts (L), quartz crystals (Q) and feldspar crystals (F). Flow banding, in the right hand rock, is vertical. Samples, left to right, 9550. 9980, 9700.

B-C. A large stretched pumice clast (P), replaced by sericite, occurs in a fine-grained quartz and feldspar matrix. Quartz crystals (Q) all have rounded corners. Sample B1094. Plate 4.8B is plane polarized light and Plate 4.8C is crossed-polars. Field of view width = 6 mm.

D. Cut slabs from hand samples of the quartz-feldspar-phyric dacite porphyry. Notice the even distribution of quartz (Q) and feldspar (F) crystals and the lack of flow banding and foliation. Samples, left to right, 9930, 9940.

E. Photomicrograph of the quartz-feldspar-phyric dacite porphyry. Note the fine-grained groundmass, the well-defined and embayed quartz phenocrysts (Q), and the sericite-altered feldspar phenocryst. (F). Polarized light, field of view width = 6 mm. Sample 9860.

A

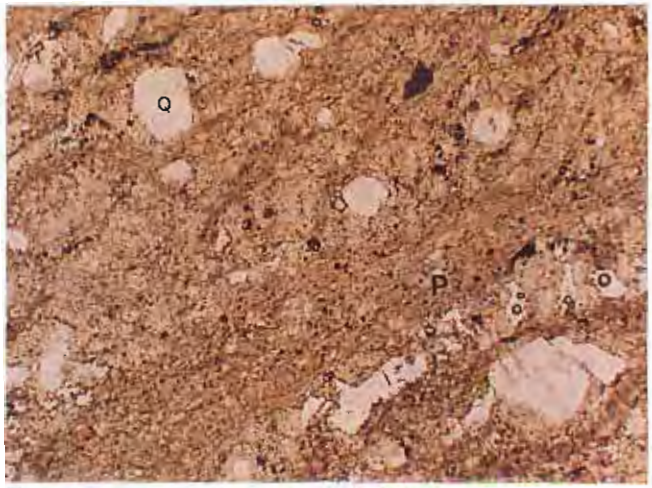

B

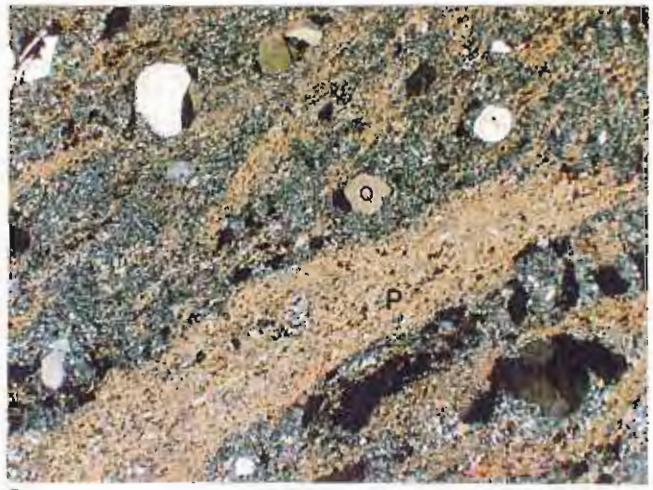

C

D

E

4.3.3.2 QUARTZ-FELDSPAR-PHYRIC DACITE PORPHYRY

Quartz-Feldspar-Phyric Dacite

The quartz-feldspar-phyric dacite porphyry (Plate 4.8C-D) occurs with the quartz-feldspar-phyric volcaniclastic rock described above. The groundmass is a fine-grained (0.03-0.06 mm) pseudo-micropoikilitic mosaic of quartz and feldspar, and is interpreted to be the result of recrystallised volcanic glass. Quartz and feldspar crystals are 1-8 mm in size and comprise up to 30% of the porphyry. Quartz crystals are subrounded to subangular and embayed and broken with jigsaw-fit textures. Feldspar phenocrysts are rarer, range in size from 0.5 to 5 mm, and make up about 5% of the rock. The facies contains a few scattered spherulitic lithic clasts but is interpreted to be a coherent facies.

4.3.3.3 VOLCANICLASTIC SANDSTONE

Sandstones in the EQPS are absent in the Mt. Darwin and Jukes Prospect areas. However, one facies along Intercolonial Spur was interpreted to be volcanic sandstone by Gadaloff (1996). Sandstones within the EQPS are volumetrically minor in the study area and will not be discussed.

4.3.4 Tyndall Group Correlates

Tyndall Group rocks in contact with the Darwin Granite are medium to coarse-grained polymictic conglomerates (basal conglomerates) containing rounded to sub-angular clasts of sericite-altered coarse-grained pink Darwin Granite and other volcanic clasts derived from the CVC (Plate 4.9). Tyndall Group rocks were examined by Jones (1993) who identified a basal conglomerate, unconformable on the Darwin Granite, volcaniclastic lithic conglomerate, polymictic lithic volcaniclastic sandstone, and feldspar-phyric dacites. Since Tyndall Group rocks in the study area were not altered or mineralised and since uplift and erosion put the eruption and emplacement of Tyndall Group rocks after the Darwin Granite intrusion, and hydrothermal event, they will not be discussed.

Plate 4.9. Tyndall Group medium to coarse-grained polymictic conglomerate.

A. This sample is from the basal conglomerate and contains Darwin Granite clasts (G). It was collected from near the erosional contact of the Tyndall Group and the Darwin Granite on the east slope of the Darwin plateau. Sample B2023.

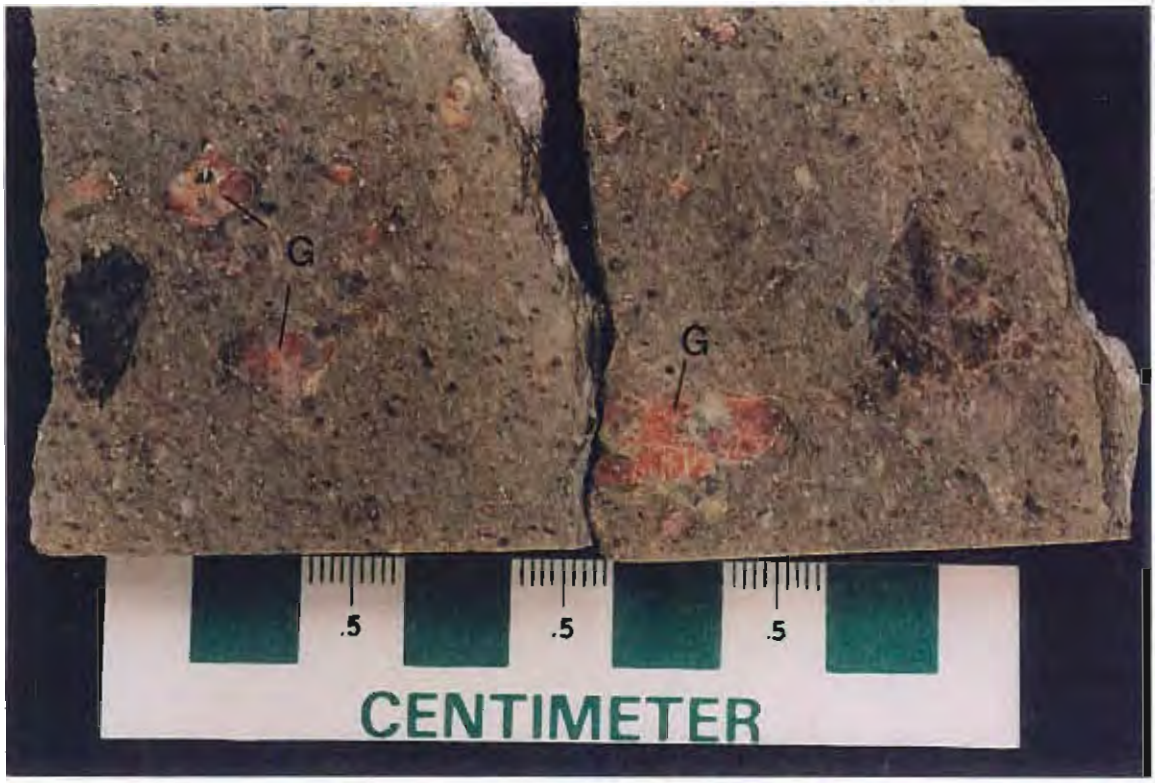

A

4.4 VOLCANIC ROCK GEOCHEMISTRY

The discussion of geochemistry has two goals: first, the classification and characterisation of the tectonic setting of the Cambrian volcanic rocks, and second, attempt to link the Darwin Granite genetically to one or several of the volcanic units. The analytical data in this chapter relate to a suite of least-altered volcanics and intrusive facies selected from traverses in the Mt. Darwin-Slate Spur area and Jukes Road. The authors' data set was supplemented by data from other researchers (White, 1975; Doyle, 1990; Crawford et al., 1992; Jones, 1993; Gadaloff, 1996; Halley, 1996). Geochemical sampling and analytical techniques were discussed in Chapter 3. The entire geochemical data set is listed in Appendix J.

4.4.1 Constraints on the Data

Regionally the MRV have undergone lower greenschist facies metamorphism and have experienced Na and Ca metasomatism as shown by minor calcite alteration of the volcanic groundmass and late veining. Some major and trace elements become mobile under variable degrees of diagenetic, metamorphic and hydrothermal alteration (MacLean and Kranidiotis, 1987; Gemmell and Large, 1992). Therefore, concentrations of the large ion lithophile elements (LILE) such as K, Rb, Ba and Sr are unlikely to provide reliable estimates of pre-eruptive magmatic abundances (Stolz, 1995). Reliable indicators of pre-eruptive abundances and the least mobile elements are the high field strength elements (HFSE) such as Ti, Zr, Y and Nb and the rare earth elements (MacLean and Kranidiotis, 1987; Whitford et al., 1988). It has been shown that Zr, REE, Y, Nb, Hf, Th and U are mobile in F-rich hydrothermal systems related to alkalic, F-rich igneous suites (Baker and De Groot, 1983; Cambell et al., 1984; Lianghat and MacLean, 1995). Under conditions of intense hydrothermal alteration, LREE and the MREE have limited to significant mobility (MacLean and Barrett, 1993). In contrast, the HREE and Zr, Ti and Al are considered immobile under conditions of intense hydrothermal alteration (MacLean and Barrett, 1993). Minor and trace elements including P, Sc, V, Cr, Ni and Th have abundances that approximate their original concentration in the melt (Stolz, 1995).

Tests for element immobility are normally based on the coherence of interelement correlations (Al/Ti, Nb/Zr, Ti/Zr). However, these tests must be confined to rocks within individual rock suites (Stolz, 1995). Small amounts of scatter are normally due to inhomogeneities in the samples and analytical errors. Large amounts of scatter either indicate mobility of one or both elements/ratios or the overlap of data from two or more rock suites. If two or more rock suites are represented, the scatter represents a primary feature rather than element mobilization during metamorphism or hydrothermal alteration (Stolz, 1995).

A data set listing the 'least-altered' rocks is shown in Table 4.1 and rocks are listed according to their unit, facies and reference. The major elements were recalculated to 100% anhydrous to remove variations due to different loss on ignitions. From a total data set of over 400 samples, 22 were selected as 'least-altered' (16 CVC rocks, 5 EQPS rocks and 1 from the YRS). In addition, 3 Tyndall Group rocks from Crawford et al. (1992) are included for comparison. It is important to note that no 'least-altered' CVC volcanics were observed in the Darwin Granite-Mt. Darwin area

and the nearest 'least-altered' CVC rocks are from Intercolonial Spur, several kilometres to the north. The main selection criteria for 'least-altered' rocks included: lavas or coherent rocks only, the presence of relict feldspar phenocrysts (some weakly altered by sericite), lack of cleavage, lack of Na depletion, alteration Index $\leq$76 (Ishikawa et al., 1976), Na_2O/K_2O >0.3 and moderate levels of Al_2O_3 and Zr. In addition, wherever possible, rocks with obvious signs of hydrothermal alteration and excessively high loss on ignition were avoided. Epiclastic and pyroclastic rocks were not included in this list because components from unrelated magmas may have been involved in their petrogenesis, thus complicating the interpretation.

4.4.2 Major Element Geochemistry

The MRV range petrographically from basalts to rhyolites (Corbett, 1976; Corbett, 1979; Corbett, 1981; Corbett and McNeil, 1988; Corbett and Solomon, 1989; Corbett, 1992; Crawford et al., 1992). The geochemistry of the MRV was studied by Crawford et al. (1992) in order to determine the primary magmatic affinities and tectonic setting of eruption for the MRV. Their study identified five suites of volcanic rocks with unique geochemical properties. The five suites are easily separated on the basis of P_2O_5/TiO_2 vs. SiO_2 and Ti/Zr vs. SiO_2 (Figures 4.2A-B).

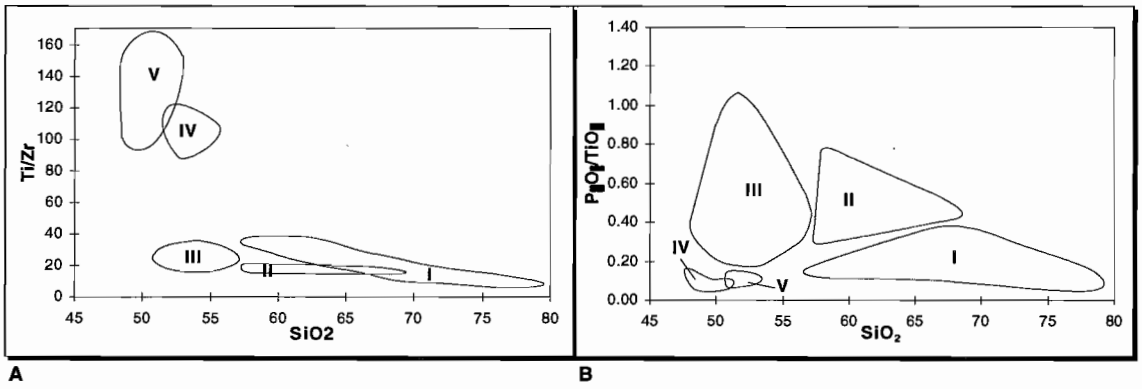

Figure 4.2. Ti/Zr and P_2O_5/TiO_2 vs. SiO_2 diagrams for distinguishing the five volcanic suites in the MRV. Fields from Crawford et al. (1992).

Suite I rocks are calc-alkaline and include all of the felsic rocks of the southern MRV including rhyolites and dacites of the YRS, CVC, EQPS and Tyndall Groups and the Darwin and Murchison Granites. In addition, Suite I rocks include the footwall andesites of the Que-Hellyer VHMS deposits. Suite I rocks have SiO_2 contents >58 wt.%, and smoothly decreasing FeO (Fe_2O_3),TiO_2, and Ti/Zr values with increasing differentation. P_2O_5/TiO_2 values are less than 0.4, REE enrichment is characteristic and $(La/Yb)_n$ values range from 5-8 for andesites to 10-14 for more evolved rhyolites. Suite II rocks occur south of the Henty Fault (Figure 1.1), are high-K calc-alkaline hornblende-phyric andesites and dacites from the upper part of the CVC and include the Garfield and Prince Lyell andesites. Fractionation trends of FeO are typically calc-alkaline and at any SiO_2 content, Suite II rocks are more MgO and P_2O_5 rich and TiO_2 poor than Suite I rocks. Suite I and Suite II are separated on the P_2O_5/TiO_2 vs. SiO_2 diagram (Figure 4.2B). Suite II rocks are more LREE enriched than Suite I rocks at similar SiO_2 levels and have $(La/Yb)_n$ values from 20-26 for the hornblende-porphyritic andesites. Crawford et al. (1992) concluded that Suite II andesites and dacites are high K andesites more K, P and LREE rich than Suite I rocks.

Table 4.1. 'Least-altered' volcanic rocks from the southern Mt. Read Volcanic Belt.

Unit	Central Volcanic Complex																Eastern Quartz-Phyric Sequence					Tyndall Group			
Rock Type	FPV	FPV	FPV	FPV	FPV	FPV	FPV	FPV	FPV	FPV	QFP Dyke	FPV	FPV	FPV	FPV	FPV	QFPV	QFPV	QFPV	QFPV	QFPV	QFPV	QFPV	QFPV	QFPV
Reference	Wyman (1996)											Doyle (1992)	White (1975)		Gadaloff (1996)		Wyman (1996)			White (1975)		Crawford et al. (1992)			Wyman (1996)
Sample Number	**10750**	**10800**	**10900**	**B10750**	**B10800**	**B10850**	**B2014**	**880351**	**880386**	**880418**	**MJ96-9**	**L14**	**41092**	**41134**	**8/4/2**	**15/5/2**	**B9550**	**B9700**	**MJ96-2**	**41379**	**41392**	**AR1**	**1984/6**	**1984/7**	**B1077**
SiO_2	76.23	75.30	74.53	76.17	74.89	75.48	74.18	70.46	73.29	72.98	70.09	75.50	76.01	73.23	73.86	74.60	72.31	73.70	73.84	71.82	72.15	75.80	77.20	75.40	76.80
TiO_2	0.30	0.32	0.33	0.31	0.29	0.29	0.28	0.29	0.29	0.30	0.89	0.32	0.24	0.33	0.31	0.29	0.53	0.41	0.39	0.42	0.47	0.18	0.19	0.17	0.21
Al_2O_3	13.84	13.38	13.89	13.30	13.14	13.09	13.04	12.60	12.97	13.29	14.85	12.96	12.45	13.65	13.30	13.21	15.22	14.61	13.81	15.80	15.26	12.90	11.60	13.00	12.68
Fe_2O_3	3.16	3.37	2.72	3.35	3.87	2.96	3.64	3.95	4.00	4.56	5.91	4.39	2.90	2.79	3.31	3.68	4.64	3.90	3.15	3.70	4.46	3.00	2.09	1.70	1.54
MnO	0.01	0.07	0.10	0.10	0.07	0.13	0.06	0.13	0.05	0.12	0.41	0.05	0.00	0.01	0.02	0.03	0.12	0.25	0.26	0.00	0.09	0.02	0.08	0.02	0.01
MgO	0.74	0.71	0.59	0.67	0.96	0.68	0.48	1.29	0.69	1.21	1.36	0.64	0.36	0.82	0.50	0.64	1.25	1.07	0.82	0.84	1.05	0.81	0.32	0.30	0.35
CaO	0.03	0.15	0.24	0.11	0.54	0.63	0.17	2.84	0.63	0.69	0.50	0.05	0.00	0.52	0.08	0.12	0.05	0.21	0.57	0.02	0.15	0.03	1.23	0.19	0.02
Na_2O	1.48	2.08	2.10	2.29	1.73	2.04	3.63	2.79	1.94	1.54	1.56	1.80	2.62	3.23	2.73	1.89	1.86	2.18	2.71	1.94	1.81	4.47	3.69	3.61	2.46
K_2O	4.17	4.44	5.28	3.66	4.47	4.65	4.32	5.41	5.88	5.12	4.18	4.24	5.25	5.19	5.83	5.48	3.92	3.61	4.19	5.23	4.34	3.08	3.79	5.72	5.77
P_2O_5	0.04	0.05	0.05	0.04	0.05	0.05	0.05	0.05	0.05	0.05	0.21	0.05	0.03	0.05	0.05	0.05	0.09	0.07	0.07	0.06	0.09	0.03	0.03	0.02	0.03
Total Volatile Free	100.00	99.87	99.83	100.00	100.00	100.00	99.86	99.81	99.79	99.86	99.95	100.00	99.86	99.81	100.00	100.00	100.00	100.00	99.81	99.84	99.88	100.32	100.22	100.13	99.87
FeO	2.86	3.05	2.46	3.03	3.50	2.68	3.28	3.58	3.62	4.13	5.35	3.97	2.63	2.53	2.99	3.33	4.18	3.51	2.85	3.35	4.04	2.71	1.90	1.54	1.39
S	<0.01	<0.01	<0.01	<0.01	<0.01	<0.01	<0.01	0.201	0.07	0.08	0.04		0.15	0.01	<0.01	<0.01	<0.01	<0.01	0.01	0	0.17				<0.01
Sc							9.9	7.8	7.7	7.7	20.7		10	7	7	9			10	10	10				6.4
Ti	1786	1893	1955	1830	1715	1709	1708	1764	1719	1785	5318	1818	1455	2000	1886	1768	3160	2465	2337	2498	2803	1079	1139	1019	1278
V							5.4	9.2	9.2	8.9	86.5		20	20	8	8			36.3	58	54	5	<10	<10	7.2
Cr							1.3	4.4	4.9	17	8.4		16	20	3	3			5.1	28	16	<2	50	18	2.1
Co	2			<2	4	<2											6	4							
Ni							1.7	3.6	2.9	61.1	4.6		1	10	2	2			2.6	5	1	<1	9	28	1.9
Cu	6	5	5	4	9	3	2.8	29.8	6.5	9.8	26.1		2	0	20	29	5	4	5.3	15	0				2.7
Zn	57	40	42	39	46	42	49.5	50.1	59.9	38.9	187.4		56	59	53	91	355	428	312.9	33	290				80.5
As	<3			<3	<3	<3	<3	<3	<3	<3	1				<1	<1	<3	<3	<1						<3
Br	<1			<1	<1	<1											<1	<1							
Rb	145	143	159	129	149	148	131	130	171	178	162	149	162	144	143	165	134	139	142	230	202	62	83	128	190
Sr	18	29	45	22	21	33	142	92	80	47	34	17	50	76	55	99	50	106	136	75	95	107	100	109	93
Zr	291	289	298	280	276	268	267	258	268	282	429	276	253	298	282	276	290	258	243	264	298	200	186	189	173
Nb	14			13	13	13	13	12	13	13	18	15		15	13	13	17	17	16	19	20	19			16
Mo	1	1	<1	1	1	1					2				1	0	1	2	1						
Ag											0				<0.1	<0.1			0						
Cd											0				<0.1	<0.1			0						
Sn	5			5	6	4	3	2	2	4							3	3							3
Sb											1				1	1			1						
Cs											2				1	1			5						
Ba	882	1120	1527	822	997	1103	1199	1639	1873	1150	773		1250	1700	1608	1631	1128	1220	1588	1430	1075	1560	1750	1750	1179
La							117	57	44	45	41		82	36	39	54			66	32	24				36
Ce							114	119	91	99	88		100	50	92	103			135	60	50				73
Nd				37	44	38	107	51	35	44	42				39	48	42	44	55						37
Y	38			39	42	36	83	40	35	40	36	38	46	33	29	43	26	30	56	41	43	46	41	54	29
W	4			6	3	4											5	<2							
Tl											1				1	1			1						
Pb	26	8	3	20	2	7	4	7	11	6	7		10	20	7	12	119	10	73	0	35				6
Bi	<1.5	2	<1.5	<1.5	<1.5	<1.5	<2	<2	<2	<2	<2				<2	<2	<1.5	<1.5	<2						<2
Th	22	20	21	21	20	21	19	19	20	21	13		19	20	24	22	17	18	19						25
U	5	5	5	4	5	5	4	6	6	5	3				5	6	4	4	5	20	25				4
AI*	76	70	71	64	71	67	56	54	72	74	73	73	68	62	69	75	73	66	60	76	73	46	46	61	71
CCPI**	39	37	29	38	42	33	32	37	36	44	54	43	28	28	29	35	48	44	35	37	45	32	23	16	17
Ti/Zr	6.1	6.5	6.6	6.5	6.2	6.4	6.4	6.9	6.4	6.3	12.4	6.6	5.7	6.7	6.7	6.4	10.9	9.6	9.6	9.5	9.4	5.4	6.1	5.4	7.4
Zr/Nb	21.4			21.4	20.8	20.6	20.4	21.5	21.1	21.3	23.5	18.4		19.9	21.7	21.2	17.5	15.0	15.6	13.9	14.9	10.5			11.0
Nb/Y	0.4			0.3	0.3	0.4	0.2	0.3	0.4	0.3	0.5	0.4		0.5	0.4	0.3	0.6	0.6	0.3	0.5	0.5	0.4	0.0	0.0	0.5
P_2O5/TiO_2	0.1	0.2	0.2	0.1	0.2	0.2	0.2	0.2	0.2	0.2	0.2	0.2	0.1	0.2	0.2	0.2	0.2	0.2	0.2	0.1	0.2	0.2	0.2	0.1	0.1
Na_2O/K_2O	0.35	0.47	0.40	0.63	0.39	0.44	0.84	0.51	0.33	0.30	0.37	0.42	0.50	0.62	0.47	0.35	0.47	0.60	0.65	0.37	0.42	1.45	0.97	0.63	0.43

* Alteration Index = 100(K2O + MgO) / (K2O + MgO + Na2O + CaO), Ishikawa et al. (1976)

FPV = feldspar-phyric lava, QFPV = quartz-feldspar-phyric lava

** Chlorite-Carbonate-Pyrite Index = 100(MgO + FeO) / (MgO + FeO + Na2O + K2O), Large et al. (in press)

Suites III, IV, and V describe basalts and andesites near Que River-Hellyer and northwest of Queenstown, the Henty Dyke swarm, and Miners Ridge Basalts. Suite III rocks are calc-alkaline basalts to andesites and occur at two locations within the YRS and one location north of the Henty Fault. The Suite III rocks are different from the Suite I and II rocks in that they contain basalts and are dominated by mafic to intermediate lavas and in the Que-Hellyer Hanging wall sequence, have shoshonitic affinities. Suite III rocks vary from low TiO_2 (0.5%) and P_2O_5 (0.1%), flat HREE patterns and $(La/Yb)_n$ values from 8-12, to rocks with low TiO_2 (0.4-0.8%), high P_2O_5 (0.4-1%), LREE enrichment, depleted HREE patterns and $(La/Yb)_n$ values up to 34. Suite IV basalts are tholeiitic and indicate a period of tension and rifting post CVC and pre Tyndall Group in age corresponding to a period of orogenic uplift and erosion of the Darwin Granite (Crawford et al., 1992). Suite IV rocks include dolerite sills, dykes and pillow basalts as well as the Henty dyke swarm which intrudes CVC rocks north of the Henty Fault. Suite IV rocks are high TiO_2, (1.0-1.6%), have increasing FeO, TiO_2 and Zr with increasing fractionation, and have near chondritic Ti/Zr values (88-107, Figure 4.2A). Their low P_2O_5/TiO_2 values distinguish them from Suite III calc-alkaline basalts. Suite IV REE patterns are fairly smooth with slight LREE enrichment and $(La/Yb)_n$ values from 1.4-3.4. Suite V basaltic lavas and basaltic breccias are tholeiitic and are associated with the Crimson Creek formation, part of the pre-MRV basement. Suite V rocks are magnesian, low TiO_2, LREE depleted and are chemically dissimilar to any other basalts in the MRV. They have Ti/Zr values >90 and up to 150 (Figure 4.2A).

The presence of Suite I, II and III rocks occurring in rough stratigraphic order were interpreted by Crawford et al. (1992) to represent a magmatic evolution from transitional medium to high-K rocks through to high-K and shoshonitic rocks. Modern analogs for this evolution occur only in postcollisional regions of arc-continent collisions (Crawford et al., 1992).

Harker diagrams of TiO_2, Al_2O_3, Fe_2O_3, MgO, CaO, Na_2O, K_2O and P_2O_5 vs. SiO_2 are shown on Figures 4.3 to 4.10. These diagrams use the data from the least-altered volcanics in the study area, as shown in Table 4.1. For comparison, data from the Darwin Granite suite is included on Figures 4.3, 4.4, 4.5, 4.6 and 4.10. Darwin Granite samples were not included on Figures 4.7, 4.8, and 4.9 because was established in Chapter 3 that the alkali elements in the granites were mobile (Figures 3.4, 3.6, and 3.8).

Except for Type 1 and Type 2 dykes and the Garfield andesites, SiO_2 values are consistently >70 wt.% making it difficult to observe well-defined trends. In addition to high SiO_2, CVC dacites have <0.05 wt.% P_2O_5. The tight grouping of TiO_2, Al_2O_3 and P_2O_5 data on Figures 4.3, 4.4, and 4.10 is interpreted to be a result of immobility of those elements in the rocks along Jukes Road and Intercolonial Spur.

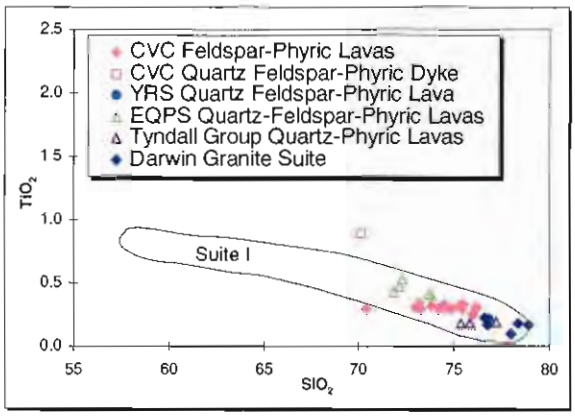

Figure 4.3. Plot of TiO_2 vs. SiO_2 showing a decreasing trend of TiO_2 in relation to increasing SiO_2 for the YRS, CVC, EQPS, Tyndall Group and Darwin Granite. The overlap between the Darwin Granite and CVC suggests they may be comagmatic. Suite 1 boundary from Crawford et al. (1992).

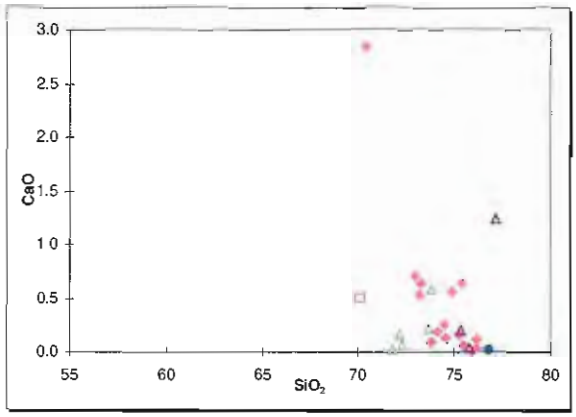

Figure 4.7. CaO vs. SiO_2 plot showing the scatter and addition of CaO within some of the volcanic units. The scatter supports the interpretation that CaO was mobilised by post emplacement processes.

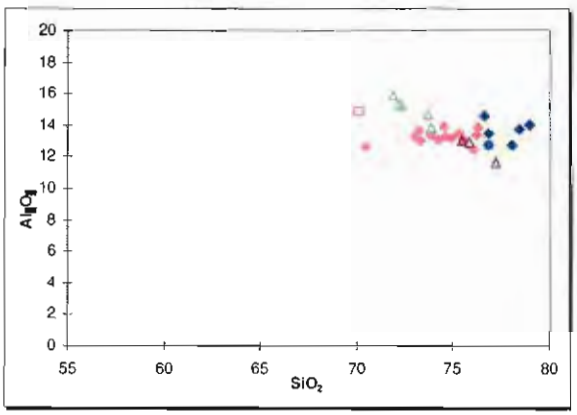

Figure 4.4. Plot of Al_2O_3 vs. SiO_2 showing little scatter within the individual units. This data supports the interpretation that Al_2O_3 behaved in an immobile fashion along Jukes Road.

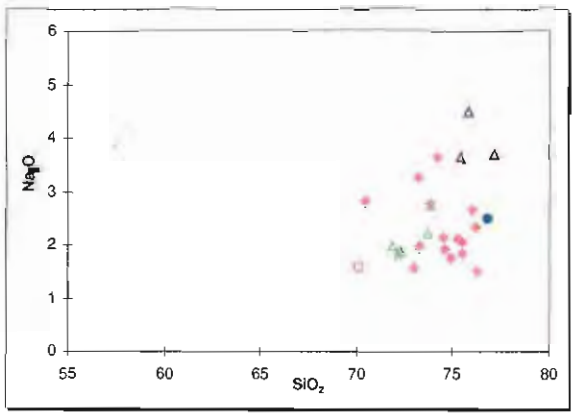

Figure 4.8. Na_2O vs. SiO_2 plot showing scatter in Na_2O values that supports the interpretation that Na_2O was mobilised by post emplacement processes.

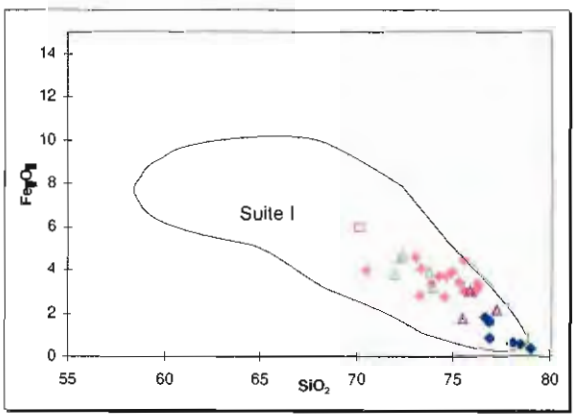

Figure 4.5. Fe_2O_3 vs. SiO_2 plot showing a decrease in iron with increasing SiO_2, typical of magmatic fractionation in high SiO_2 rhyolites and dacites. Suite 1 boundary from Crawford et al. (1992).

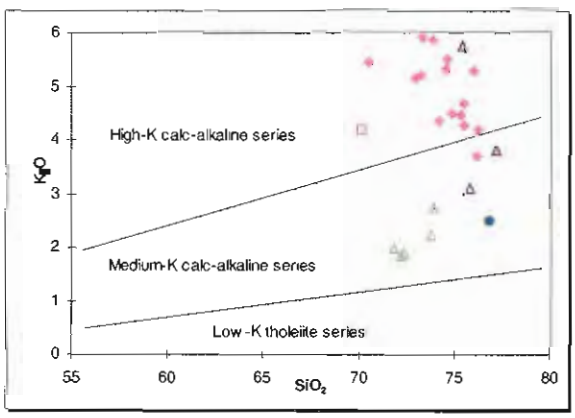

Figure 4.9. K_2O vs. SiO_2 plot that shows high to medium-K affinities of the least-altered rocks in the study area. However, the scatter in K_2O values, may also suggest mobility by post emplacement processes. Field boundaries are from Le Maitre et al. (1989).

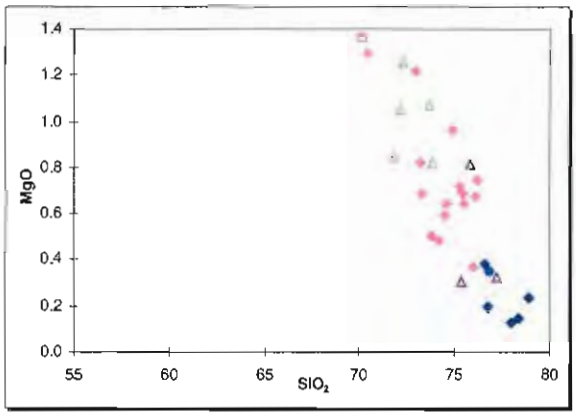

Figure 4.6. MgO vs. SiO_2 plot showing a trend of decreasing MgO with increasing SiO_2, typical of magmatic fractionation trends in high SiO_2 rhyolites and dacites.

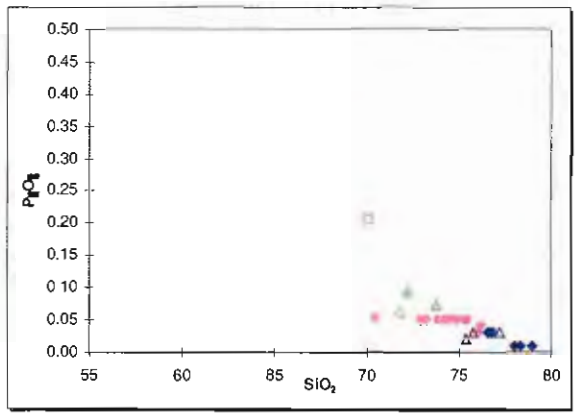

Figure 4.10. Plot of P_2O_5 vs. SiO_2 that shows decreasing P_2O_5 with increasing SiO_2, typical of fractionation trend for high SiO_2 rhyolites and dacites. The horizontal group of CVC data is due to analytical detection limit of 0.05 wt.% P_2O_5 for that group of samples.

The smoothly decreasing Fe_2O_3 and TiO_2 trends (with increasing SiO_2), as shown in Figures 4.3 and 4.5 are characteristically calc-alkaline and represent increasing differentiation (Crawford et al., 1992). Based on TiO_2 and Fe_2O_3 trends (Figures 4.3 and 4.5), felsic rocks within the study area are interpreted to be Suite I rocks as defined by Crawford et al. (1992). Decreasing MgO and P_2O_5 trends (Figures 4.6 and 4.10) are typical magmatic differentiation trends for high SiO_2 rhyolites and dacites (Crawford et al., 1992).

The range of TiO_2 values for the CVC is narrow (0.24-0.33, Figure 4.3). This is interpreted to be a result of a sampling bias introduced to the data by weighting the data set with numerous samples from the Jukes Road columnar-jointed dacite and fewer rocks from Intercolonial Spur and Mt. Darwin. A clear separation between the EQPS and Tyndall Group rocks was made on the basis of TiO_2 values (Figure 4.3). The EQPS rocks have a distribution of TiO_2 values from 0.41 - 0.53 wt.% and Tyndall Group rocks from 0.17 to 0.19 wt.%. The single least-altered YRS rock falls within the range of the Tyndall Group rocks. Polya et al. (1986) compared the Murchison Granite data on a TiO_2 vs. SiO_2 diagram with the Murchison Volcanics (CVC) and concluded that since the trends overlapped, they were comagmatic. The data from the Darwin Granite was compared to the least-altered volcanics on Figure 4.3. The granite data plot at the high silica end of the trend and a similar conclusion is possible. However, the figure is inconclusive because the Darwin Granite may be comagmatic to all of the felsic units observed. This relationship between TiO_2 and SiO_2 is not enough, by itself, to argue this point, as all high SiO_2 rocks in the MRV have a similar TiO_2 range (Crawford et al., 1992).

Typically, fractionating magmatic systems have a well-defined trend of increasing K_2O with increasing SiO_2. This trend is not well-defined in rocks of the study area because of lack of mafic and intermediate members (Figure 4.9). The increasing trend is disrupted due to mobilisation of K_2O as shown by a wide scatter of data points. However, based on the presence of unaltered K-feldspar in the groundmass, combined with weak sericite replacement of K-feldspar phenocrysts in the least-altered rocks, it is interpreted that K_2O values were not originally lower than the minimum values shown on Figure 4.9. Therefore, it is concluded that the least-altered volcanic

rocks were originally medium to high-K calc-alkaline, in agreement with the conclusion of Crawford et al. (1992). The wide scatter of CaO and Na_2O data (Figure 4.7 and 4.8) combined with the scatter in K_2O data (Figure 4.9) confirm that all three alkali elements were mobilised by post emplacement processes.

Summary

The YRS, CVC, EQPS and Tyndall Group rocks span a narrow silica range (70 -78 wt.%, Table 4.1) and are characterised by low P_2O_5, TiO_2, CaO, and MgO contents, consistent with the Suite I classification of Crawford et al. (1992). The broad range in Na_2O and K_2O values suggests alkali contents were modified by post emplacement processes. Tightly grouped TiO_2, Al_2O_3 and P_2O_5 suggests these elements have behaved in an immobile fashion in least-altered rocks along the Jukes Road and can therefore be used for classification purposes. All of the rocks in the study area are medium to high-K calc-alkaline.

4.4.3 Trace Element Geochemistry

This section will identify the important immobile trace elements within the volcanic rocks in the study area. These elements will then be used for classification purposes and later for comparison purposes in the hydrothermal alteration geochemistry chapter (Chapter 6). A lack of consistent data for Hf, Ta and Th in the volcanic rocks of the current study preclude their use as immobile elements. REE data on the volcanics will be discussed later in this chapter.

Figures 4.11 through 4.14 are binary diagrams constructed using Zr, Y, Nb, and TiO_2 data from Table 4.1. Data from the CVC feldspar-phyric lavas plot in tight clusters on Figures 4.11-4.13. These tight clusters suggests immobility of Zr, Nb, Y and TiO_2 (Ti) in the least-altered rocks. The spread in data for the EQPS and Tyndall Group rocks does not necessarily indicate element mobility and is interpreted to represent differences between different lava suites within the same sequence, each with unique Nb/Zr, Y/Zr and TiO_2/Zr values. The magmatic affinities shown on Figure 4.12 are from MacLean and Barrett (1993). These affinities recognise distinctive changes in Zr/Y values with rock affinity and confirm the calc-alkaline affinities of the study area volcanics as shown previously in Figure 4.9.

The separation between volcanic units on Figure 4.13 can be explained in either of two ways: 1) by slight differences in the TiO_2 and Zr concentrations within different magma batches from the same parent magma. or 2) the Type 1 and Type 2 dykes could form a less evolved part of a series that includes the granites as supported by their lower SiO_2 contents compared to the granites (Figure 4.14). The relationship of the granites to the CVC and Tyndall Group volcanic units is unclear, they may not be related to the other rocks or may be different batches of magma from a similar source rather than different batches from the same parent magma. Within the Darwin Granite and Murchison Granite (Phase 1) there is an excellent correlation between Ti and Zr (Chapter 3, Figures 3.12 and 3.15). When compared to the volcanic units, the granite data plot at the low Zr ends of Figures 4.11 to 4.13 and the high silica end of Figure 4.14. From the TiO_2 and Zr data illustrated in Figure 4.13, the granites could be related to any of the volcanic units, including the Type 1 and 2 quartz-feldspar-phyric dykes and no firm discrimination can be made.

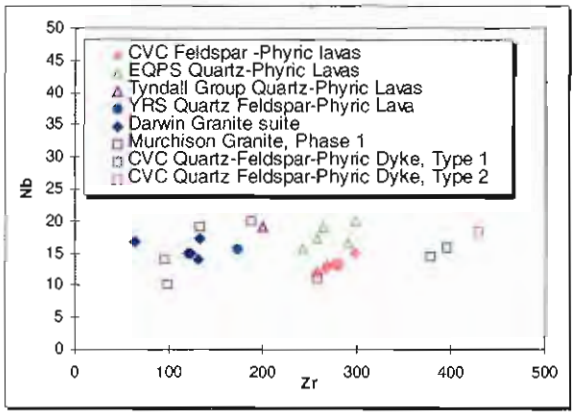

Figure 4.11. Plot of Nb vs. Zr. Data from the CVC feldspar-phyric lavas plot in a tight cluster suggesting immobility of Zr and Nb. The spread in data for the EQPS and Tyndall Group does not represent mobility but is interpreted to represent differences in Nb and Zr contents between lava suites within the same sequence, each with unique Nb/Zr ratios.

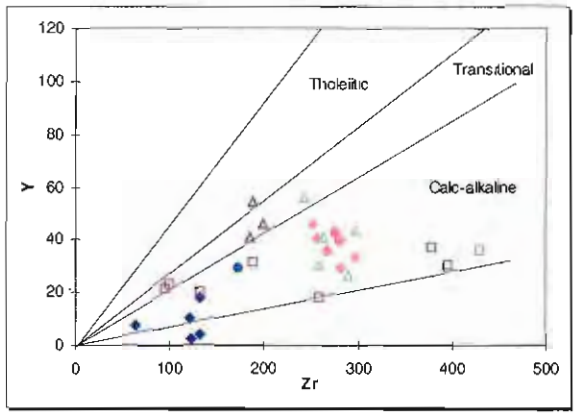

Figure 4.12. Plot of Y vs. Zr. Although the clusters are not as tight as Figure 4.11, immobility of Y is supported in the least-altered rocks. Data for the EQPS and Tyndall Group does not indicate element mobility and is interpreted to represent differences between different lava suites within the same sequence, each with unique Y/Zr ratios. Magmatic affinities from MacLean and Barrett (1995).

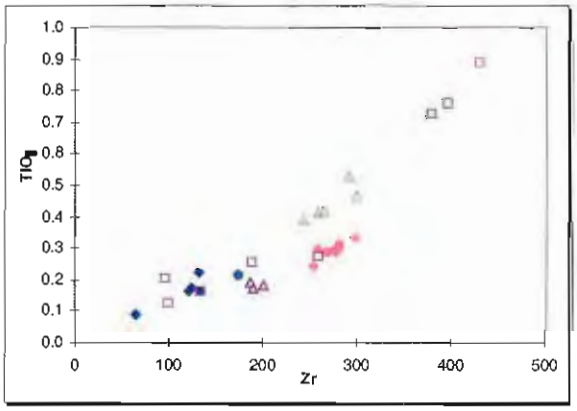

Figure 4.13. TiO_2 vs. Zr plot that separates the four volcanic units. TiO_2 and Zr are interpreted to have been immobile. The relationship of the Darwin and Murchison Granites to the other volcanic units is unclear and either may be related to the volcanic units. Note the location of the CVC quartz-feldspar-phyric dykes relative to the location of the CVC and EQPS.

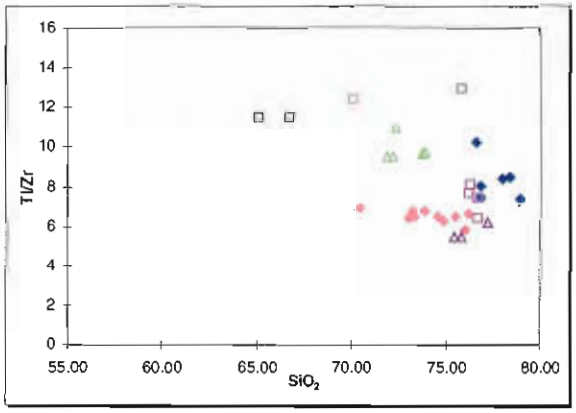

Figure 4.14. Plot of Ti/Zr vs. SiO_2. The Ti/Zr ratio separates the various stratigraphic units in the study area into groups. Note the location of the CVC quartz-feldspar-phyric dykes relative to the location of the CVC and EQPS.

The data shown on Figures 4.11 to 4.14 emphasise the similarities and differences between Type 1 and Type 2 dykes and the major volcanic units. As shown in Table 4.1, Appendix J and Figure 4.14, the range of Ti/Zr values for the Type 1 and Type 2 dykes is 11.5-12.4. This compares to the CVC range of 6-7 and 8-15 for the EQPS rocks along Jukes Road. Differences in Nb/Zr and Y/Zr (Figures 4.11 4.12) are explained by higher Zr levels in the dykes as a result of abundant accessory zircon. Higher TiO_2 and Zr concentrations resulting in higher Ti/Zr values and lower SiO_2 concentrations (Figure 4.14) suggests that, although similarities exist, the Type 1 and Type 2 dykes are not related to a fractionation suite from the Darwin Granite.

Summary

The immobility of Nb, Zr, Y and TiO_2 established in Figures 4.11 through 4.14 are interpreted to represent immobility during diagenesis, metamorphism and weak hydrothermal alteration. Data for the EQPS and Tyndall Group rocks is interpreted to represent differences in Nb/Zr, Y/Zr and TiO_2/Zr values between different lava suites within the same sequence. In the following section these elements and various ratios of these elements will be used in the classification of the volcanic rocks in the study area. Zr/Y values in Figure 4.12 support the calc-alkaline nature of the CVC volcanic rocks as previously identified (Crawford et al., 1992).

4.4.4 Classification of Volcanic Rocks in the Study Area

Volcanic rocks are classified on the basis of $Na_2O + K_2O$ (total alkalis) vs. SiO_2 or $SiO_2 - K_2O$ variations, applying various boundaries for the major volcanic rock types (Peccirillo and Taylor, 1976; Ewart, 1979; Gill, 1981; Le Maitre et al., 1989; Rickwood, 1989). However, these classifications pre-suppose that the volcanic rocks were unaltered. Regional and local alteration episodes in the MRV resulted in mobilisation of major elements. sodium, calcium, and potassium. Since P_2O_5, TiO_2, Nb, Zr, and Y were shown to be immobile (Figures 4.3, 4.10 and 4.11 through 4.14) they will be used in this section to characterise and classify the coherent volcanic rocks from the Jukes-Darwin area. In addition, the Garfield andesites (Duncan, 1997) and Suite II rocks from Crawford et al. (1992) are included for comparison purposes. Tyndall Group rocks are not included since Tyndall Group coherent lava were not observed in the study area.

As the Zr/TiO_2 ratio increases, it reflects the decreasing TiO_2 content of non-basaltic differentiated rocks. It can, therefore, be used as a sensitive differentiation index (Winchester and Floyd, 1977), similar to the standard use of SiO_2. The Nb/Y ratio is used as an alkali index (Pearce and Cann, 1973; Floyd and Winchester, 1975) and therefore a Zr/TiO_2 - Nb/Y diagram becomes the immobile element equivalent of the SiO_2 vs. K_2O or SiO_2 vs. $Na_2O + K_2O$ (total alkalis) described by (Peccirillo and Taylor, 1976; Ewart, 1979; Gill, 1981; Le Maitre et al., 1989; Rickwood, 1989). Zr/TiO_2 and Nb/Y are for the least-altered coherent rocks in the study area are compared on Figure 4.15. All but one of the CVC rocks plot within the rhyodacite-dacite field (the other plots in the rhyolite field). In addition, the one YRS rock and three of the EQPS rocks plot within the rhyodacite-dacite field. The EQPS rock that plots in the trachyandesite field contains 72 wt.% SiO_2 and higher TiO_2 and is interpreted to be an altered dacite. The Type 1 and Type 2 dykes plot in the rhyolite field as a result of their high TiO_2 and Zr contents. The least-altered lavas from the study area all plot within the rhyodacite/dacite field and have SiO_2 contents >70 wt.%. They are therefore interpreted to be high-silica dacites, a field recognised in the 'total alkali' vs. SiO_2 diagram of Le Maitre et al. (1989).

All of the Suite II andesites plot within the rhyodacite/dacite field rather than the andesite field. However, the low TiO_2 and high Zr content of these andesites is a fundamental distinguishing characteristic of the Suite II andesites in western Tasmania and forms the basis of the Suite II designation (Crawford et al., 1992).

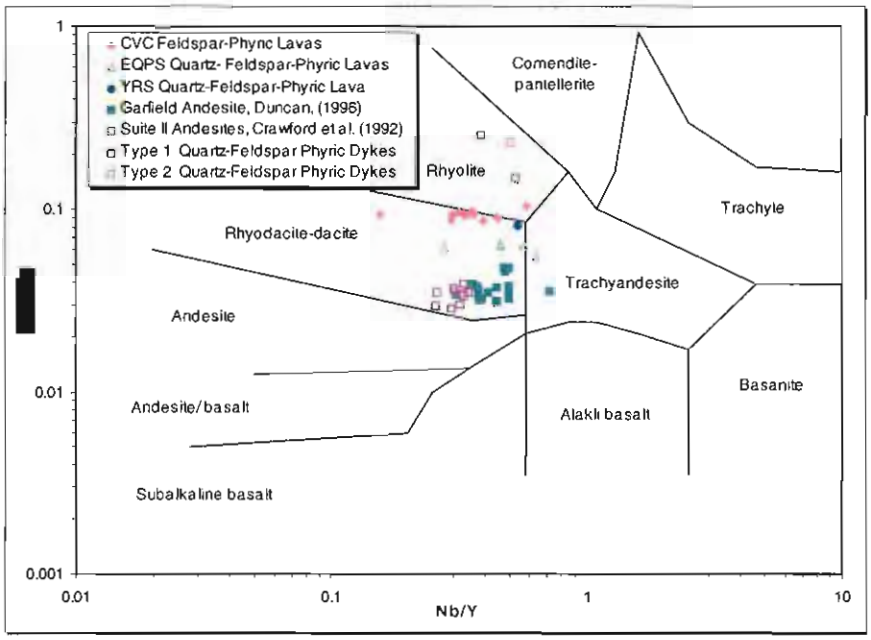

Figure 4.15. Zr/TiO_2 - Nb/Y plot for the least-altered data for the study area. All of the rocks for the CVC plot within the rhyodacite/dacite field as do two of the EQPS rocks. The rock that plots in the trachyandesite field is interpreted to be an altered dacite. Diagram from Winchester and Floyd (1977).

An expanded version of the Ti/Zr vs. SiO_2 diagram (Figures 4.14) is shown in Figure 4.16. The field boundaries shown in this figure were developed for the CVC by Stolz (1989) as part of a comparison between the CVC in the MRV and the Mt. Windsor Volcanics in Queensland. This diagram suggests that the least-altered YRS, CVC and EQPS coherent rocks, in the study area, are all rhyolites. However, Stolz does not have a rhyodacite field on his diagram, nor did he recognise high-silica dacites. The hornblende-phyric andesites are included on the diagram, as are the Suite I-III (part) boundaries of Crawford et al. (1992). The Garfield andesites plot well within the Suite II field, and although a few points plot just below it, they exhibit the typical low TiO_2 and high Zr content characteristic of Suite II rocks.

At the Garfield Prospect, Duncan (1997) described two types of andesites. The two varieties were observed in the current study and are described in Section 4.3.1.1 of this chapter. Duncan (1997) concluded that the two andesites were geochemically unique, based on their compositional fields on P_2O_5/TiO_2 vs. SiO_2 and Ti/Zr vs. SiO_2 diagrams. In Duncan's study, one andesite, the unmineralised "highly feldspar-phyric" unit, plotted in Suite III and the mineralised andesite, the feldspar ± hornblende-phyric unit, plotted in Suite II. However, Duncan (1997) failed to recalculate his major element oxide percentages on a volatile free basis. Recalculating (Appendix J) and replotting, his data (Figures 4.16 and 4.17), shows that there was no geochemical separation between the two andesite types, both plotting almost completely within Suite II. Interestingly, Type 1 quartz ± feldspar-phyric dykes overlap the same range as high silica Suite II andesites.

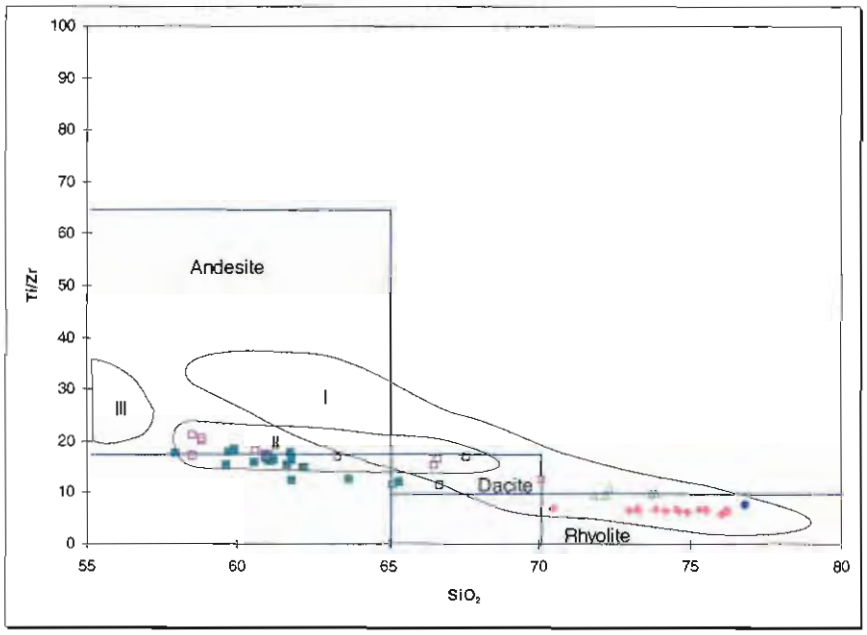

Figure 4.16. Ti/Zr vs. SiO_2 classification diagram for the MRV. All of the least-altered rocks for the YRS, CVC and the EQPS plot within the rhyolite field (blue lines). Garfield andesite data plot in the Suite II field of Crawford et al. (1992), who's Suite I through III (part) boundaries are included for comparison. Interestingly, the Type 1 quartz-feldspar phyric dykes overlap the high silica Suite II andesites. Blue Line classification from Stolz (1989). Legend as Figure 4.15.

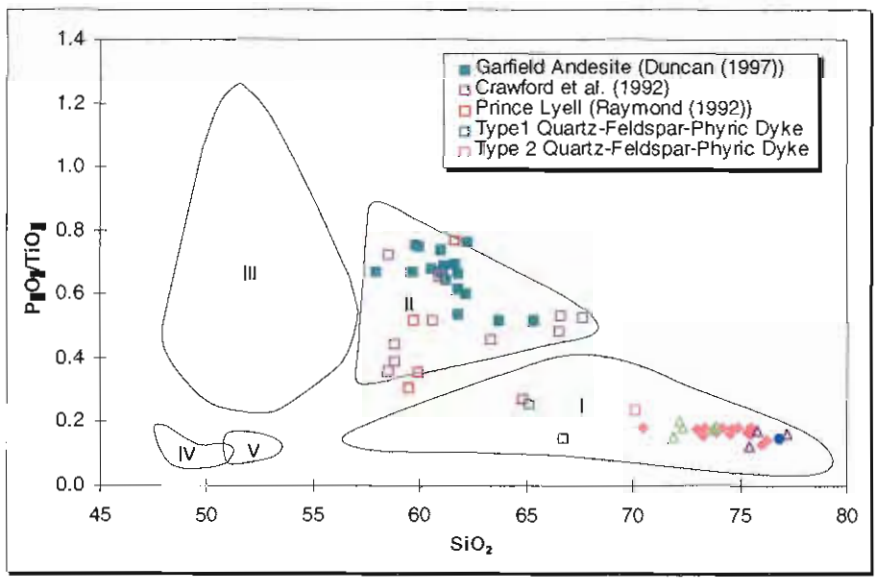

Figure 4.17. P_2O_5/TiO_2 vs. SiO_2 plot showing Suites I - V for the MRV. The Garfield and Prince Lyell andesites are Suite II rocks and the CVC volcanics, Suite I. Fields from Crawford et al. (1992). Legend as Figure 4.15.

Figure 4.17 is a P_2O_5/TiO_2 vs. SiO_2 diagram showing the andesite data and least-altered volcanic data from the Southern MRV. Suite I through Suite V boundaries of Crawford et al. (1992) are included for comparison. The Garfield andesites plot completely within the Suite II field. The least-altered dacitic volcanics from the study area plot completely within Suite I. Andesites from the Prince Lyell Cu-Au deposit are included on this figure for comparison. These rocks are characterised by low SiO_2 due to high sulfide contents (up to 30 %), therefore SiO_2 values were

recalculated for plotting purposes. They plot well within the Suite II field confirming their Suite II association. Type 1 and Type 2 quartz-feldspar-phyric dykes plot within the Suite 1 field, similar to the YRS, EQPS, and CVC volcanics.

4.4.5 Rare Earth Element Geochemistry

REE are immobile in diagenetic, metamorphic and weak hydrothermal alteration (MacLean and Kranidiotis, 1987; Whitford et al., 1988). The REE patterns of least-altered felsic lavas from the YRS, EQPS, and CVC are compared to the Darwin and Murchison Granites and the Suite II andesites. REE data used in constructing the chondrite - normalised REE diagrams (Figures 4.18 through 4.28) is included in Appendix J. The REE data used in these figures was obtained from several sources. The patterns that contain six elements, two LREE (La and Ce), two MREE (Sm and Eu) and two HREE (Yb and Lu) were from a program of INAA analyses called 'Au plus 28' from Becquerel Laboratories, Lucas Heights, NSW, Australia. The more complete data sets were obtained from ICPMS/XRF analyses at the CSL, University of Tasmania, or from ICPMS analyses from ANALABS, Welshpool, Western Australia.

Figure 4.18 shows the REE patterns for the least-altered feldspar-phyric dacites from Jukes Road (Table 4.1). Included on Figure 4.18 is the more complete REE analyses from rock 10620 that includes Gd and, therefore, the weak negative Eu anomaly typical of the CVC volcanics. The overall pattern of 10620 is similar to other least-altered volcanics suggesting that, although Gd was not analysed (in the 'Au plus 28' analysis), other least-altered volcanics have the weak negative Eu anomaly as well. These least-altered rocks are compared to six rocks from the same dacite facies within the intense hydrothermal alteration halo surrounding the Jukes Cu-Au prospect (10220, 10240, 10250, 10280, 10300, 10330). The mobility of REE during hydrothermal alteration is a function of the stability of minerals that host the REE as well as alteration intensity and varies according to the host mineral and the type of alteration. Typically, under conditions of intense hydrothermal alteration, LREE and MREE are mobile while HREE remain immobile (MacLean and Barrett, 1993). There is no variation in light, middle or heavy REE as a result of the intense hydrothermal alteration in the Jukes Road feldspar-phyric dacite (Figure 4.18). The lack of change in LREE and MREE suggests that hydrothermal alteration within the Jukes Prospect may not be as intense as subjective identification of hydrothermal alteration intensities imply.

$(La/Yb)_N$ and $(La/Sm)_N$ values are a measure of the slope of the total REE pattern and LREE end of the spectrum respectively. Higher values indicate steeper slopes or depletions. Comparison of the slopes of the total and partial REE patterns aids in the comparison between different suites. The $(La/Yb)_N$ values of the altered and least-altered rocks from Jukes Road are similar, 8.8-11.8 and 6.4-10.8 respectively. Since REE are immobile in the range of diagenetic, metamorphic and hydrothermal conditions along Jukes Road (Figure 4.18), it was assumed that REE were immobile in other weak alteration styles throughout the study area. REE patterns from altered volcanic units within the Jukes-Darwin area can, therefore, be safely compared to obtain information regarding magmatic affinities.

In Figure 4.19, REE patterns of felsic lavas from the YRS, EQPS (Jukes Road) and CVC (Jukes Road and Mt. Darwin) are compared. Suite I dacitic rocks are characterised by strong REE enrichment (Crawford et al., 1992) and $(La/Yb)_N$ values in the range of 10 to 14. Heavy REE

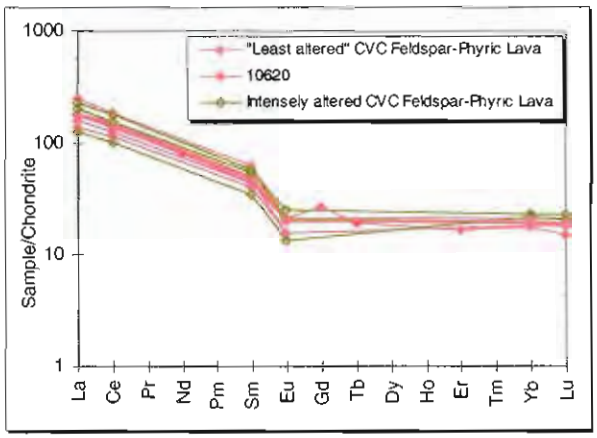

Figure 4.18. Chondrite-normalised REE diagram illustrating patterns for least-altered vs. intensely altered feldspar-phyric rocks from the Jukes Road. least-altered columnar-jointed dacites are compared to altered rocks from within the hydrothermal alteration halo surrounding the Jukes Proprietary Cu-Au prospect. There is no variation in light, middle or heavy REE as a result of hydrothermal alteration. Included is the more complete REE data from rock 10620, from the same facies.

patterns are flat. Within Suite I, rhyolitic rocks can have $(La/Yb)_N$ values that vary from characteristically andesitic values, 5 to 8, to higher values, 10 to 12 (Crawford et al., 1992). The REE concentrations in the YRS, EQPS and CVC are similar and the overall patterns are virtually identical. All three units are characterised by enriched LREE, small negative Eu anomalies and flat HREE patterns. The similarities are emphasised by the overlapping ranges in $(La/Yb)_N$ values, 6.4-11.8 for the CVC, 6.4-11.3 for the EQPS and 8.6-14.6 for the YRS. Crawford et al. (1992) interpreted the REE patterns and $(La/Yb)_N$ values of Suite I rocks to represent variable degrees of crustal assimilation during fractionation of a magma from basalt to rhyolite.

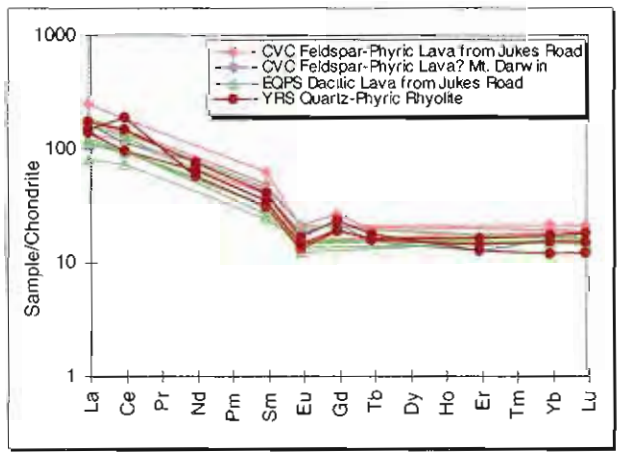

Figure 4.19. Chondrite-normalised REE diagram showing patterns of felsic lavas from the YRS, EQPS and CVC. The REE patterns of the EQPS dacite, YRS rhyolite and CVC dacites are similar suggesting a common magma source or source region with similar conditions of evolution.

Figure 4.20 and 4.21 show the REE relationship between the YRS, EQPS and the Darwin and Murchison Granites. In Figure 4.20, three representative analyses from a YRS rhyolite and EQPS dacite are compared with three phases of the Darwin Granite (Section 3.2.2.2). A similar and overlapping LREE enrichment occurs but the YRS rhyolite and EQPS dacite have pronounced negative Eu anomalies and HREE patterns are flat and at higher abundances than the Darwin Granite. Figure 4.21 compares the Murchison Granite to the YRS rhyolite and EQPS lavas. The overall magnitude of the values and the overall REE patterns are identical between the YRS rhyolite, EQPS and the Murchison Granite. However, one of the YRS rhyolite samples does have a slight depletion in HREE, attributed to zircon fractionation.

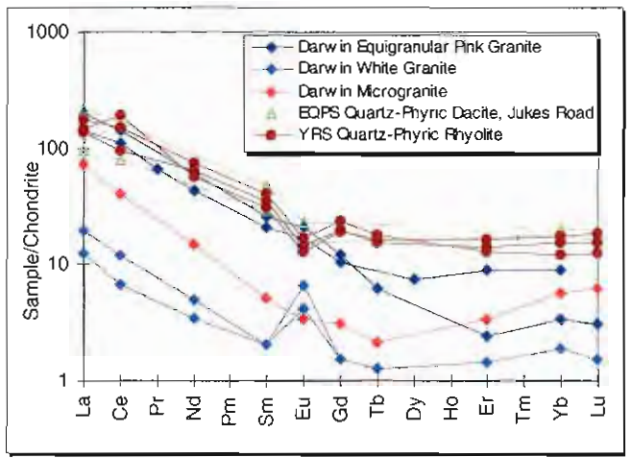

Figure 4.20. Chondrite-normalised REE diagram showing the relationship between the YRS, EQPS and the Darwin Granite. The YRS rhyolite and the EQPS dacite have a pronounced negative Eu anomalies and the HREE pattern is flat and of higher abundances than the Darwin Granite. This data suggests that the Darwin Granite was not comagmatic with the YRS or the EQPS in the study area.

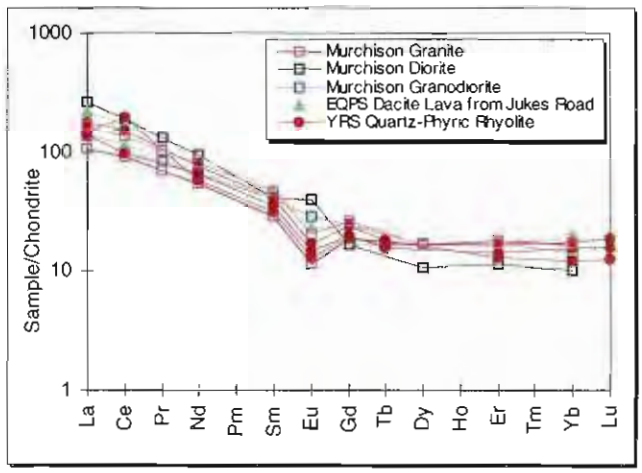

Figure 4.21. Chondrite-normalised REE diagram showing the relationship between the YRS, EQPS and the Murchison Granite. The overall magnitude of the values and the overall REE patterns are virtually identical between the YRS, EQPS and the Murchison Granite. The data suggests that the YRS and EQPS were sourced from a magma with 'Murchison-like' REE characteristics.

$(La/Yb)_N$ and $(La/Sm)_N$ values for the Cambrian granites and study area volcanic rocks are compared on Figure 4.22. Differences between the $(La/Sm)_N$ values for the Darwin Granite phases and the volcanic units are emphasised. $(La/Yb)_N$ values for the Darwin white granite, microgranite and quartz-porphyry overlap the same range as the volcanics. However, the pink granite samples are higher including one pink granite sample with a $(La/Yb)_N$ value of 59 (not plotted) reflecting severe depletion of HREE. Darwin Granite $(La/Sm)_N$ values (5-15) reflect the depletion in LREE (Figure 4.20). Similarities between the EQPS, YRS, CVC and the Murchison Granite are emphasised by the narrow range in $(La/Sm)_N$ values (2.5-5) and similar LREE patterns at similar SiO_2 values.

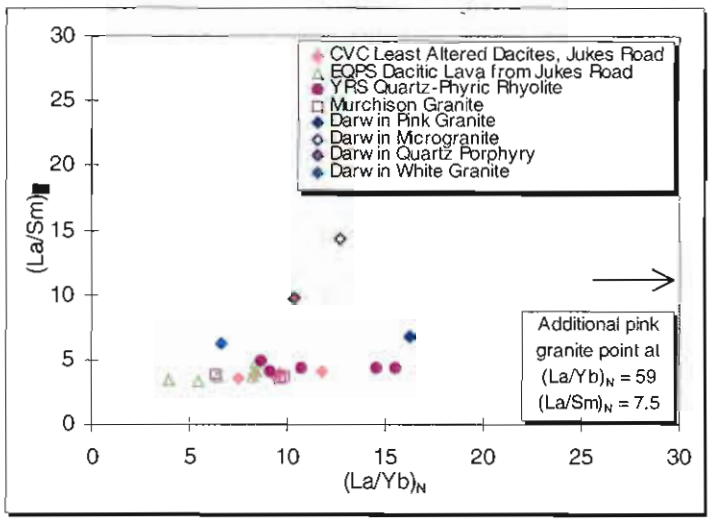

Figure 4.22. $(La/Yb)_N$ vs. $(La/Sm)_N$ diagram comparing study area volcanic rocks to Cambrian granites. The narrow range of $(La/Sm)_N$ values emphasises the similarities between the EQPS, YRS, CVC and the Murchison Granite and differences with the Darwin Granite.

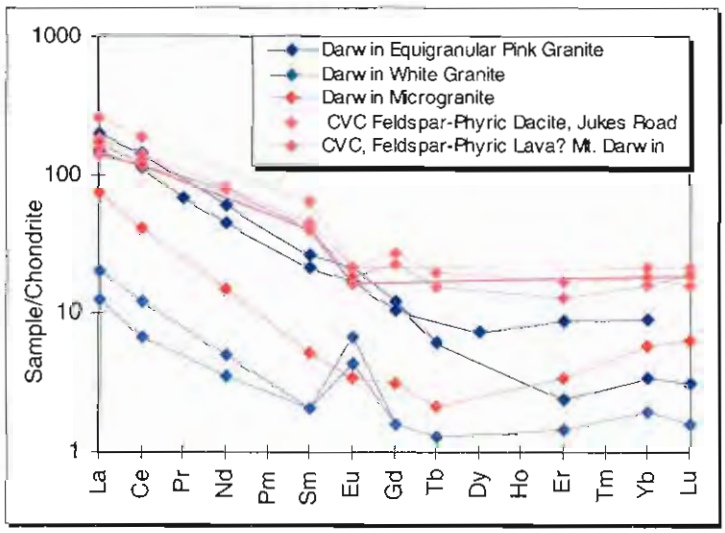

Figure 4.23. Chondrite-normalised REE diagram showing the relationship between the CVC and the Darwin Granite. LREE are similar and overlapping but the CVC dacites have a pronounced negative Eu anomaly and the HREE pattern is flat and of higher abundances than the Darwin Granite.

The relationship between least-altered CVC volcanics, an altered CVC dacite from Mt. Darwin, the three phases of the Darwin Granite and the Murchison Granite are shown on Figures 4.23 and 4.24. The relationships shown are similar to the YRS and EQPS relationships discussed for Figure 4.21. The overall magnitude of the values and the overall REE patterns are identical between the CVC and the Murchison Granite.

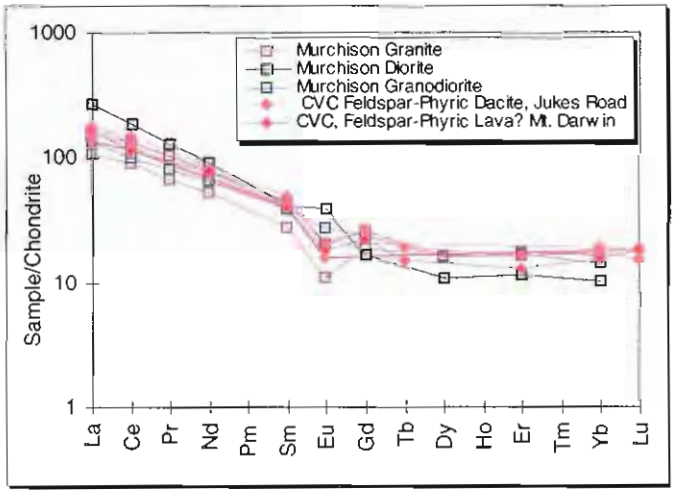

Figure 4.24. Chondrite-normalised REE diagram showing the relationship between the CVC and the Murchison Granite. The overall magnitude of the values and the overall REE patterns are identical between the CVC and the Murchison Granite.

Based on the negative Eu anomalies, flat HREE patterns and dissimilar $(La/Yb)_N$ values it is interpreted that the Darwin Granite was not comagmatic with CVC, EQPS or YRS, and the volcanic rocks were sourced from a magma with 'Murchison Granite-like' REE characteristics. This conclusion is supported by the differences in the Nb/Y (CVC range 0.3 to 0.4 to the Darwin Granite range of 0.5-6) and P_2O_5/TiO_2 (CVC range 0.13 to 0.18 to the Darwin Granite range of 0.06 to 6).

The relationships between the Jukes Road Type 1 and Type 2 quartz-feldspar-biotite porphyry dykes (Section 4.3.2.3) and the Darwin Granite were examined using REE data (Figure 4.25). Type 1 dykes are characterised by LREE enrichment, a more pronounced negative Eu anomaly, flat HREE patterns, higher overall abundances and lower $(La/Yb)_N$ values (5-7), than the Type 2 dykes. Type 1 dykes have lower SiO_2 contents (65-66%) than the Type 2 dykes (70%, Appendix J). Neither the Type 1 nor Type 2 REE pattern is similar to the REE pattern of the Darwin Granite. The slight depletion of HREE in the Type 2 Dyke is attributed to fractionation of zircon.

A significant control on the size of negative Eu anomalies is plagioclase fractionation. Eu has a high K_d for plagioclase and will preferentially partition into plagioclase during fractionation. Type 2 dykes contain higher SiO_2 and more abundant plagioclase phenocrysts (Section 4.3.2.3) than the Type 1 dykes. The comparatively small negative Eu anomaly in the Type 2 dyke is interpreted to

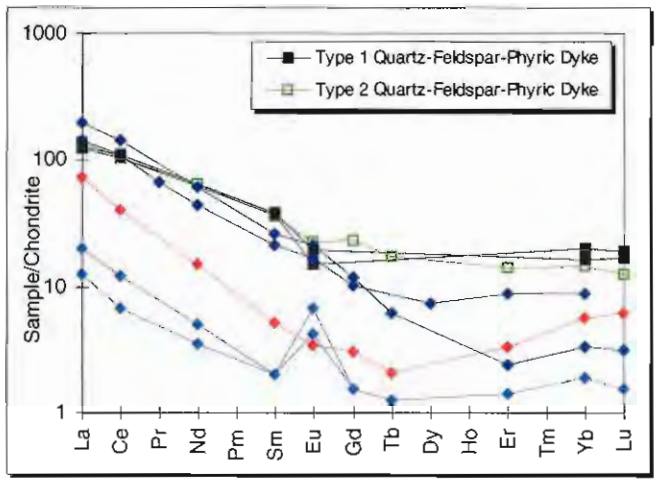

Figure 4.25. Chondrite-normalised REE diagram showing the relationship between Type 1 and Type 2 quartz-feldspar-biotite porphyry dykes and the Darwin Granite. Type 1 dykes are characterised by LREE enrichment, a more pronounced negative Eu anomaly, flat HREE patterns, and higher overall abundances, than the Type 2 dykes. The pattern of neither Type 1 nor Type 2 matches the Darwin Granite except for the enrichment of LREE. Based on the negative Eu anomaly and flat HREE patterns, it is interpreted that neither Type 1 or Type 2 dykes were sourced from the Darwin Granite.

be a result of the increased plagioclase content in the rock. Based on the negative Eu anomaly and flat HREE patterns, it is interpreted that neither Type 1 or Type 2 dykes were comagmatic with the Darwin Granite.

Figure 4.26 compares the Type 1 and Type 2 quartz-feldspar-biotite porphyry dykes to the Murchison Granite. The Murchison Granite is characterised by enriched LREE, a well-defined negative Eu anomaly and flat HREE pattern (the exception in the Murchison Granite suite is the

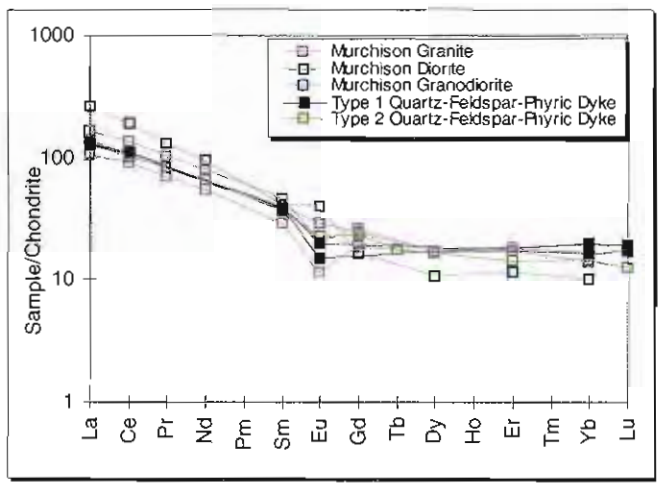

Figure 4.26. Chondrite-normalised REE diagram showing the relationship between Type 1 and Type 2 quartz-feldspar-biotite porphyry dykes and the Murchison Granite. Both dykes have similar overall REE patterns to the granite phase of the Murchison Granite suggesting they formed from a melt of similar origin.

diorite with a positive Eu anomaly and depleted HREE). Both Type 1 and Type 2 dykes have similar overall REE patterns to the granite phase of the Murchison Granite suggesting they formed from a melt of similar origin.

In Figure 4.27 the Garfield andesites, the Lyell-Comstock andesites and the Suite II andesites (Crawford et al., 1992) are shown. Suite II hornblende porphyritic andesites have $(La/Yb)_N$ values of 20 to 26 (Crawford et al., 1992). The Garfield and Lyell-Comstock andesites are characterised by strong LREE enrichment, a pronounced negative Eu anomaly and HREE depletion. The overall REE abundance and patterns are typical of the Suite II andesites. REE analyses for three Garfield andesite samples, the Crown Hill andesite and four Lyell-Comstock andesites were obtained from Halley (written comm.). Note that although two of the Garfield andesites (No's. 22708 and 36816) have overall REE patterns similar to the Suite II andesites, the third andesite sample (No. 22454) is different and has a flat HREE pattern similar to Suite I. The two andesites are also texturally and mineralogically different (Section 4.3.1.1). The $(La/Yb)_N$ and $(La/Sm)_N$ values for two of the Garfield andesites (No's. 22708 and 36816) are similar to the $(La/Yb)_N$ and $(La/Sm)_N$ values for Suite II andesites (Crawford et al., 1992). The third andesite (No. 22454) is closely comparable to either the Queenstown Reservoir andesite, the Suite II andesite with the lowest $(La/Yb)_N$ and $(La/Sm)_N$ values, or Suite I andesites from north of the Henty Fault (Crawford et al., 1992). It is interpreted that two of the Garfield andesites are typical Suite II andesites while the third andesite (No. 22454) is related to a Suite I magma.

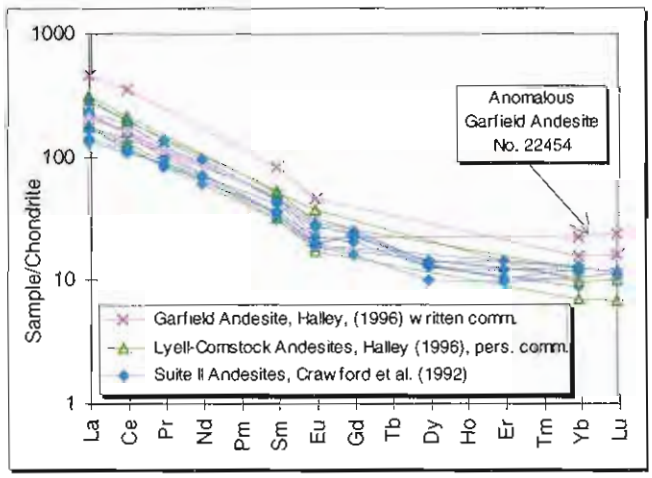

Figure 4.27. Chondrite-normalised REE diagram showing the relationship between the Garfield andesites, the Lyell-Comstock Andesites and Suite II Andesites of Crawford et al. (1992). Two of the Garfield andesites and the Lyell-Comstock andesites are characterised by strong LREE enrichment, a pronounced negative Eu anomaly and HREE depletion, typical of Suite II andesites. The third Garfield andesite sample has a flat HREE pattern and compares closely to the Queenstown Reservoir andesite and other Suite I andesites from north of the Henty Fault.

The Garfield andesites and the Type 1 and Type 2 quartz-feldspar-biotite porphyry dykes along Jukes Road intrude felsic volcanics of similar age, and they occur within 7 km of each other. A relevant question is, therefore, are they somehow related? Figure 4.28 compares the Garfield andesites to the Type 1 and Type 2 dykes. Type 1 dykes have identical LREE enrichment ($(La/Sm)_N$ values), negative Eu anomalies, flat HREE patterns and $(La/Yb)_N$ values as Garfield andesite sample (No. 22454 shown with a bold pink line). The Type 2 dyke, although having a

more depleted HREE pattern, is similar. Neither dyke is similar to the two Suite II Garfield andesite samples (No's. 22708 and 36816) that have more enriched LREE patterns, similar negative Eu anomalies and more depleted HREE patterns.

The Jukes Road Type 1 and 2 dykes and one of the Garfield andesites (22454) are similar to the Suite I granodiorite phase of the Murchison Granite. The REE data, therefore, suggests that a parental magma with more 'Murchison-like' compositions occurs beneath the study area and that the Type 1 and 2 dykes and the Suite I andesite at the Garfield Prospect may be comagmatic or were at least derived from a Suite 1 source. The remainder of the Garfield andesites and the Lyell-Comstock andesites are typical Suite II rocks.

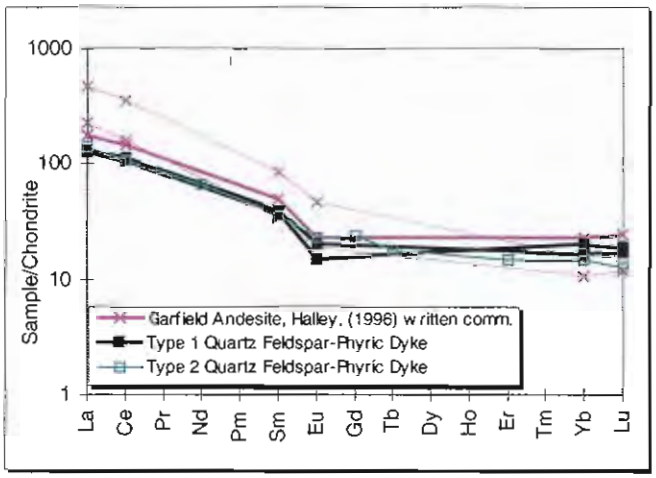

Figure 4.28. Chondrite-normalised REE diagram showing the relationship between the Garfield andesites and the Type 1 and Type 2 quartz-feldspar-biotite porphyry dykes from Jukes Road. Type 1 dykes (bold black lines) have identical LREE enrichment, negative Eu anomalies and flat HREE patterns to the anomalous Garfield andesite (shown with a bold pink line). The Type 2 dyke, while having a more depleted HREE pattern is similar to the same andesite. Neither dyke type is similar to the Suite II Garfield andesites as shown by less enriched LREE (lower $(La/Sm)_N$ values, 3.2 to 3.8 vs. 5.6 to 6.6) and flatter HREE patterns.

4.5 SUMMARY

The YRS, EQPS and CVC sequences cannot be distinguished on the basis of petrography, or mineralogy. All three units contain quartz - or quartz + feldspar-phyric volcaniclastic rocks including pumiceous mass-flow deposits (such as the Jukes Road pumice breccia), sedimentary facies that include reworked volcanic sandstones and siltstones, and coherent dacitic lavas or shallow intrusives (Jukes Road dacite).

The YRS was previously considered to be the oldest sequence of volcanic rocks recognised in the southern MRV. Although the YRS has an interfingering relationship with the CVC (Corbett, 1992), it was considered to underlie the CVC in the study area. Detailed geological mapping in the Garfield Prospect area (Halley, 1996; Duncan, 1997) and the Clark and Garfield Valleys (this study) have shown an interfingering relationship between the YRS, CVC and Tyndall Group correlates. In the Clark and Garfield Valleys the rocks dip west, face west and structural relationships suggests that YRS are younger than, and conformably overlie the CVC. Black shale horizons within the YRS confirm a deep water environment of deposition. Tyndall Group rocks

unconformably overlie the Darwin Granite but otherwise have gradational contacts with the EQPS on the northeast of Mt. Darwin. This relationship supports the interpretation that the EQPS from the eastern part of the study area and the YRS from the western part of the study area, are time equivalent parts of the same volcanic centre. This interpretation is supported by the geochemical and REE evidence presented. Cross-cutting Suite II andesitic dykes (Garfield andesites) were emplaced after the last eruption of feldspar-phyric rocks of the CVC.

The YRS, CVC, EQPS and Tyndall Group rocks within the study area span a narrow silica range (70 -78 wt.%) and are characterised by low P_2O_5, low TiO_2 (Figure 4.2 and 4.9), and low CaO and MgO contents. However, they have a broad range of Na_2O and K_2O values suggesting rocks had their alkali contents modified by post emplacement processes. Tightly grouped TiO_2, Al_2O_3 and P_2O_5 contents suggest these elements were immobile along Jukes Road. YRS, EQPS and CVC rocks in the study area are medium- to high-K calc-alkaline (Figure 4.8) as supported by Zr/Y values (Figure 4.11).

Nb, Y, Zr and TiO_2 were immobile during diagenesis, metamorphism and weak to intense hydrothermal alteration along Jukes Road (Figures 4.11 to 4.14). REE were also immobile in the Jukes Road dacite (Figure 4.18). $(La/Yb)_N$ values of the altered and least-altered rocks are similar and it is interpreted that REE were immobile in other weak alteration styles throughout the study area.

REE abundances and REE patterns in YRS rhyolites, EQPS dacites and CVC dacites are virtually identical. All three units are characterised by enriched LREE, small negative Eu anomalies and flat HREE patterns. Similarities are emphasised by the ranges in $(La/Yb)_N$ values. REE characteristics of the YRS, EQPS and CVC match Suite I characteristics of Crawford et al. (1992).

The negative Eu anomaly, flat HREE patterns and differences in Nb/Y values suggest that the Darwin Granite was not comagmatic with the YRS, EQPS or the CVC. REE data and similarities in Nb, Y, TiO_2 and Ti/Zr values (Figures 4.11-4.14) emphasise the genetic similarities between the YRS, EQPS and CVC and all three units are interpreted to be comagmatic. The YRS, EQPS and the CVC were probably sourced from a magma with REE characteristics similar to Murchison Granite (Phase 1) that is postulated to occur beneath the Jukes-Darwin area. However, an alternative explanation is that multiple batches of magma from a similar source underwent a similar evolutionary process. Multiple eruptive centers could have contributed different magma batches at different times. The YRS, EQPS and the CVC were sourced from a magma with REE characteristics similar to Murchison Granite (Phase 1) that is postulated to occur beneath the Jukes-Darwin area.

Based on differences in Nb/Zr, Y/Zr, TiO_2/Zr, Ti/Zr and REE patterns, Type 1 and Type 2 quartz-feldspar-phyric dykes were not comagmatic with the Darwin Granite. The Type 1 and Type 2 dykes have identical REE patterns, Nb/Y, Ti/Zr and P_2O_5/TiO_2 values to the granodiorite and granite phases of the Murchison Granite, and identical REE patterns and abundances to one of the Garfield andesites (No. 22454). The Type 1 and Type 2 dykes are interpreted to belong to Suite I as defined by Crawford et al. (1992).

Neither of the Garfield hornblende-phyric andesites match the REE patterns of the Darwin Granite. Compared to the Darwin Granite, REE patterns for the Garfield andesites are similar in LREE enrichment (with similar $(La/Sm)_N$ values). However, the andesites have a pronounced negative Eu anomaly, were less depleted in HREE, have high P_2O_5/TiO_2 (and Suite II affinity) as a result of high P_2O_5 were not comagmatic with the Darwin Granite.

Since the Darwin Granite was not comagmatic with the YRS, EQPS, CVC, the Type 1 and Type 2 quartz-feldspar-phyric dykes or the Garfield andesites, a magma with REE characteristics similar the Murchison Granite (Phase 1) is required. At present, such a granite has not been identified in the study area. However the geochemical evidence presented in this chapter suggests that another parental magma of 'Murchison-like' composition occurs beneath the study area and was the source of the volcanics, dykes and at least some of the Suite 1 andesitic intrusive activity in the Jukes-Darwin area.

CHAPTER 5

5.0 ALTERATION STYLES, MINERAL ASSEMBLAGES, TEXTURES AND ZONING IN THE STUDY AREA

5.1 INTRODUCTION

The hydrothermal alteration styles described in this chapter are spatially associated with the Darwin Granite and its northern extension. Similar granite-related hydrothermal alteration has been described associated with the Cambrian age Murchison Granite in the northern MRV (Polya, 1981; Polya et al., 1986; Abbott, 1992; Davidson, 1998) and the Elliott Bay Granite south of Macquarie Harbour (Figure 1.1, Large et al., 1987). The granite-related hydrothermal alteration styles described for the Murchison and Elliott Bay Granites include K-feldspar, chlorite and sericite with accessory magnetite and tourmaline. Small (low tonnage) Cu-Au prospects occur associated with granite-related hydrothermal alteration at Lake Selina (Hunns, 1987), the Jukes Prospect (Doyle, 1990), Intercolonial Spur (Gadaloff, 1996), Prince Darwin and the Darwin Granite (White, 1975; Jones, 1993) and will be discussed in later chapters of this study. In the Mt. Darwin area, studies of the granite (Jones, 1993), regional geology (Corbett and Cuffley, 1970; White, 1975; Corbett et al., 1993), and individual Cu-Au prospects (Doyle, 1990; Gadaloff, 1996; Duncan, 1997), have failed to thoroughly characterise the effects of the granite-related hydrothermal alteration on the host volcanic rocks, or to separate granite-related hydrothermal alteration from regional diagenetic and metamorphic alteration styles. This chapter will focus on the petrographic aspects of that separation.

The rocks in the study area underwent a long evolution that includes: 1) Cambrian diagenesis, 2) low-grade burial metamorphism, 3) hydrothermal alteration, 4) Late Cambrian uplift (Jukesian Orogeny) and 5) metamorphism in the Mid-Devonian Tabberabbereran Orogeny. To discriminate between the products of each of these alteration episodes, it was necessary to unravel the sequence of changes that occurred in the rocks. All four alteration episodes had the potential to form identical mineral assemblages (eg., sericite-chlorite) and each successive stage of alteration potentially modified or destroyed the previous mineral assemblages and related textures. Despite this, by extensive use of the petrographic microscope, hand specimen examination and geologic mapping, it has been possible to recognise relict textures and deduce from the current mineral assemblages the nature of the previous alteration history. Detailed descriptions of the alteration styles are primarily the work of the author. Descriptions of rocks by other workers, from areas not visited, are cited to create a complete picture of the alteration styles and assemblages in the study area.

Definitions of "alteration assemblages" used in the literature are often based on unsupported assumptions regarding timing and equilibrium. Typically the lack of evidence against something is considered "proof" that it is. In other words, if it cannot be proven that minerals were not in

equilibrium when they formed, then that is considered to be proof that they were. Therefore, alteration minerals such as sericite and chlorite are commonly considered to have formed at the same time and under equilibrium conditions because there is no evidence that they didn't. The definition of "alteration mineral assemblage" as used in this thesis is a group (list) of the alteration minerals that occur in a rock. This definition does not require proof of timing, equilibrium conditions or mineral stability and is consistent with the definition of mineral assemblage in the *Glossary of Geology* (Bates and Jackson, 1980) and in common usage in industry. However, an "equilibrium alteration assemblage" as defined in this thesis, does require supportive information about the relative timing of crystallisation although "proof" of equilibrium may still be lacking. Because timing information is required, an "equilibrium alteration assemblage" also allows for the possibility of overprinting relationships to be documented effectively.

In this chapter, the common alteration mineral assemblages and textures observed will be described in 5.2. Interpretation of "equilibrium alteration assemblages" are addressed in 5.4. These interpretations are based on definitive textural criteria and overprinting relationships."

5.2 PETROGRAPHIC DESCRIPTIONS OF ALTERATION FEATURES IN THE STUDY AREA

Detailed petrographic descriptions of the Darwin Granite are presented in Chapter 3 (3.2.2.2) and of the least-altered volcanic rocks in Chapter 4 (s 4.2 and 4.3). This presents the observed alteration mineralogies and textures observed in the rocks and the features are interpreted in 5.4. For the purposes of this , all white to light-green fine-grained mica was classified as sericite.

5.2.1 Alteration Features in the YRS

5.2.1.1 QUARTZ-FELDSPAR-PHYRIC VOLCANICLASTICS AND LAVAS

Alteration in the YRS was typically of weak to moderate intensities and volcanic textures and mineralogies were commonly well-preserved by assemblages of sericite and chlorite. Typical rocks were described in 4.3.1. In most rocks observed, plagioclase and K-feldspar crystals were weakly to moderately replaced by secondary sericite-chlorite, typically in the cores of crystals and along fractures and cleavage surfaces. Preserved spherical to semispherical structures, 1-2 mm in diameter, occur throughout the rocks. Many were stretched, broken and flattened. Some of the rounded structures were lined with secondary quartz, filled with an unknown mineral and subsequently replaced by sericite and minor chlorite. Many of the spherical to semispherical structures consist of cryptocrystalline quartz and feldspar domains that transition into mixed domains of coarser quartz and feldspar (Plates 5.1A-D). Scattered, small (0.5 mm) subrounded radiating quartz aggregrates were also observed.

5.2.1.2 SANDSTONE

Because sandstones, siltstones and mudstones occur as a minor portion of the YRS rocks and a proportionally smaller portion of the total volume of rocks in the study area, they were not studied

in detail. However, sandstones were included in this section because of the intensity of sericite alteration observed in feldspars (60% of the rock). The types of feldspars in the matrix were impossible to distinguish because of the intensity of sericite replacement. Many small subangular to subrounded lithic clasts (up to 2 mm) are 100% altered to fine-grained sericite.

5.2.2 Alteration Features in the CVC

5.2.2.1 QUARTZ-FELDSPAR-PHYRIC VOLCANICLASTICS

Typical volcaniclastic rocks are consist of quartz, plagioclase, K-feldspar, sericite, with minor chlorite, pyrite and epidote. In addition, XRD results indicate the presence of kaolinite (10-15%) in some rocks (Appendix G). Sericite and chlorite typically occur in equal amounts, although intensities vary considerably throughout the study area. Near the Darwin Granite, moderate to intense sericite alteration was pervasive and texturally destructive to the matrix and feldspar crystals. Mafic minerals and quartz were weakly altered. In the Jukes Prospect area, sericite-altered rocks were easily confused with chlorite-altered rocks due to a greenish color imparted to the rock by minor amounts of light green sericite. Silica, K-feldspar and carbonate were also observed in sericite altered rocks, although no textural evidence for timing relationships was observed and it is unclear whether these are part of the sericite equilibrium mineral assemblage. Weak K-feldspar occurs as pinkish colored domains, commonly with sericite and overprints earlier chlorite. Albite replaced feldspar crystals and matrix laths in small (few centimetres) and patchy domains. Like K-feldspar alteration, albite alteration occurs as pink domains due to finely disseminated hematite. However, albite alteration destroyed matrix textures by replacing matrix feldspar and lithic clasts, crystals conformable to bedding, broken crystals between lithic clasts, and as rims around chlorite cores in lithic clasts. Albite replaced matrix consists of fine to medium-grained aggregrates of interlocked albite crystals. Albite alteration was pervasive and conformed to relict bedding. Carbonate occurs as blebs and irregular patches of various sizes within the matrix, in veinlets at high angles to the twinned planes and in broken feldspar crystals. Carbonate and sericite partially replaced feldspar crystals and filled open space in broken plagioclase crystals and coarse pumice shards. Ragged carbonate-plagioclase contacts probably represent plagioclase replaced by carbonate after crystal fracturing. Carbonates identified were calcite, ankerite ($CaFe(CO_3)_2$), and siderite ($FeCO_3$, Appendix G).

Along the western Jukes Road, sericite ± chlorite enhanced textures in feldspar-phyric lithic clasts in some rocks (Plate 5.2A). In addition, clasts with well-developed granophyric textures were observed. Fine-grained quartz-feldspar-sericite mosiacs occur as wispy elongate features (clasts) with the long dimension defined by alignment of chlorite and sericite crystals. In some rocks, they comprise up to 20-30% of the rock. Circular and semicircular structures filled with interlocking aggregates of recrystallised albite and quartz were observed. Chlorite occurs as patches, blebs and as cores in albite-altered clasts. Wispy clasts were weakly to moderately replaced by secondary chlorite + sericite, or chlorite + magnetite (in vesicles). Typically, moderate to intense chlorite replacement of groundmass lithic clasts and feldspar crystals resulted in destruction of

Plate 5.1. Preserved textures showing the sericite ± chlorite-bearing assemblage in the quartz-feldspar-phyric lavas and volcaniclastic rocks of the YRS.

A and B. Spherical to semispherical structures consisting of cryptocrystalline quartz and feldspar form a fine-grained crystalline matrix (fg) that grades across the field of view toward the lower right. Plagioclase (P) and quartz crystals (Q) are subhedral and well-preserved. Plate 5.1A is plane polarized light and Plate 5.1B is crossed polars. Field of view width = 6 mm. Sample B2004.

C and D. Closer view of the semispherical cryptocrystalline quartz and feldspar domains showing cuspate fractures (C), here accentuated by sericite and chlorite. Plate 5.1C is plane polarized light and Plate 5.1D is crossed polars. Field of view width = 3 mm. Sample B2004.

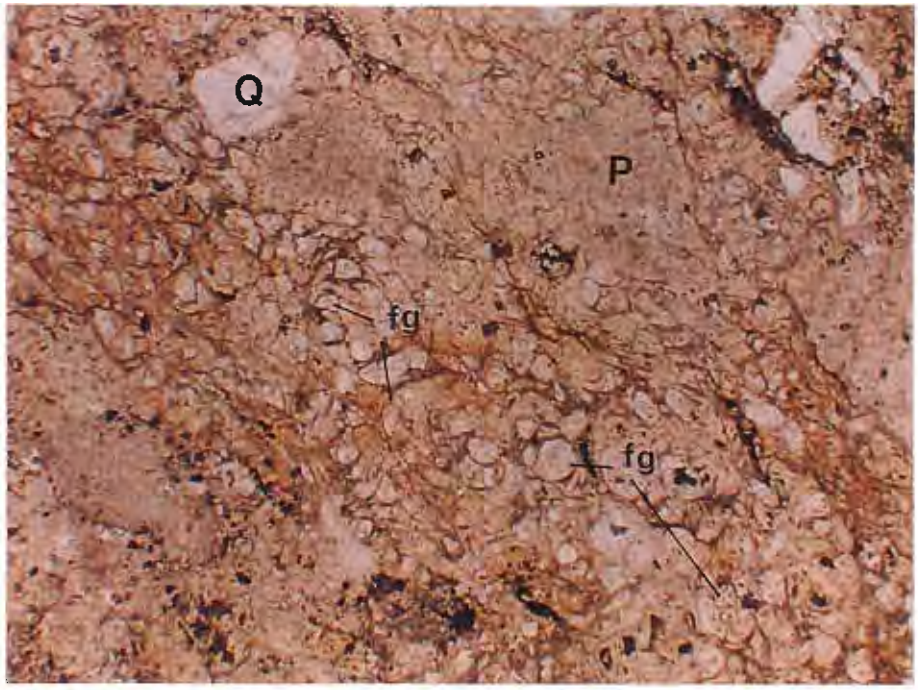

A

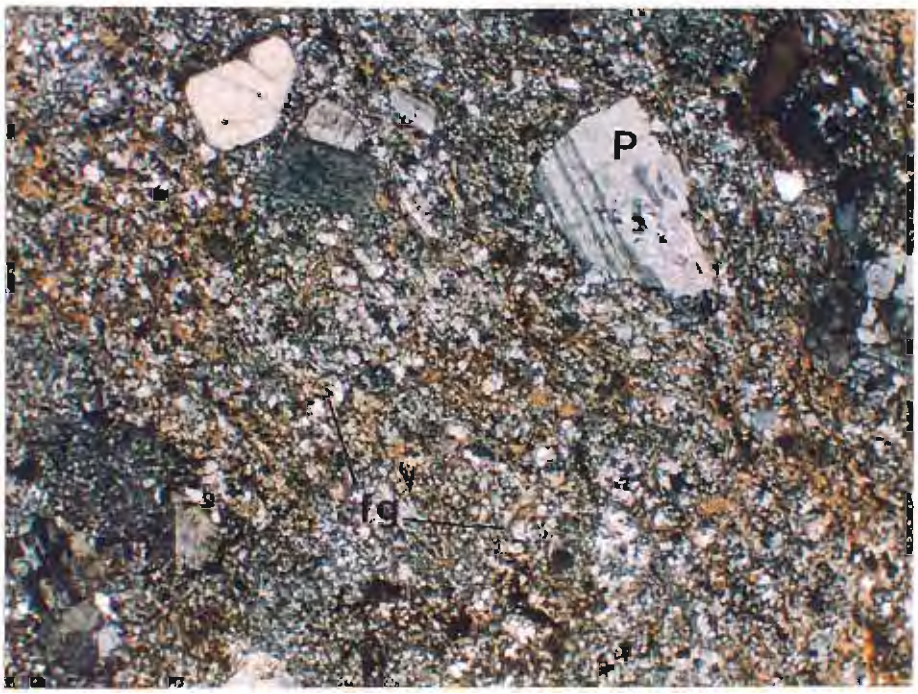

B

C

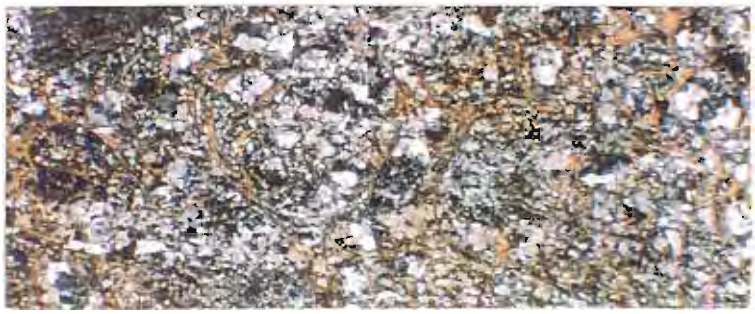

D

Plate 5.2. Lithic clast in a feldspar-phyric volcaniclastic rock of the CVC.

A. Deformed feldspar-phyric lithic clast (P, probably pumice) in a quartz-feldspar-phyric volcaniclastic. The textures were enhanced by minor diagenetic sericite. Polarized light, field of view width = 6 mm. Sample 12450.


P

primary textures. Faint twinned feldspar crystals in the matrix and original clastic textures were preserved.

Scattered euhedral and subhedral pyrite is disseminated throughout as 1-1.5 mm size crystals. Some of the pyrite has altered to magnetite. Wispy coarse chlorite and quartz occur in pressure shadows of pyrite grains.

5.2.3 Tuffaceous-Ash/Sandstone Facies

Rocks in this facies commonly have a distinctive cream to light-green colour, because of the abundance of sericite and subordinate fine-grained quartz in the matrix. Elongate sericite-altered feldspar crystals and sericite grains define a parallel foliation in the rocks Chlorite-altered masses up to 1.5 cm long (Plate 5.3A) were observed. Weak quartz replaced albite or K-feldspar-altered domains and produced light pink or light green cherts in some of the tuffaceous horizons. Carbonate occurs as blebs and irregular patches of various sizes within the matrix.

5.2.3.1 FELDSPAR-PHYRIC DACITE

In the feldspar-phyric dacites along Jukes Road and on Mt. Darwin, feldspar phenocrysts are set in a fine-grained micropoikilitic groundmass (Plate 5.4A-B). Closely spaced micropoikilitic quartz grains are up to 0.4 mm in diametre, and have small irregular quartz cores (0.05-0.2 mm), surrounded by an optically continuous micropoikilitic quartz-rich rim (0.1-0.2 mm, Plate 5.4C-D). The albite laths were replaced by secondary sericite or K-feldspar. Micropoikilitic texture creates a granular texture in hand specimen. The quartz cores were interpreted by McPhie et al. (1993), to represent an initial stage in the formation of granophyric texture or the nucleation point of larger quartz grains. Birdseye texture in the quartz cores of micropoikilitic quartz was caused by embayments of feldspar, later replaced by secondary sericite and/or chlorite. These embayments occur as micrographic and granophyric textures that impart a worm burrow appearance to many of the groundmass quartz and feldspar grains (Plate 5.4C-D). Unaltered quartz cores are optically continuous with the rest of the quartz grain.

Weak to moderate sericite occurs as small aggregates of variable size (<0.02-0.2 mm), replacement of groundmass feldspar and quartz, small individual grains (<0.02-0.2 mm) of irregular orientation along intergrain boundaries and replacement of groundmass feldspar around micropoikilitic quartz. Feldspar crystal shapes were preserved by weak sericite replacement but near the Jukes Prospect and the Darwin Granite, moderate to intense sericite alteration was pervasive and texturally destructive to groundmass and phenocryst textures. Feldspar crystals were typically replaced by light-green sericite ± quartz ± carbonate along cleavages or via fractures but cores and blebs of twinned unaltered relict feldspar crystals were observed in some samples.

Chlorite typically occurs with sericite in the least-altered areas on Mt. Darwin and the Jukes Road. Aligned chlorite ± sericite or sericite ± chlorite crystals in the groundmass formed a weak cleavage. Secondary chlorite ± sericite replaced plagioclase, biotite and other ferromagnesian mineral crystals. Chlorite commonly replaced sericite in the cores of plagioclase crystals, the rims

of which were subsequently replaced by later sericite. Secondary chlorite was observed replacing K-feldspar along fracture margins and behind small centimetre scale diffuse solution fronts around fractures. Irregular domains of moderate to intense chlorite replacement of sericite or sericite-chlorite-altered groundmass were observed near the centre of the Jukes Prospect and near the Darwin Granite contact. Typically, moderate to intense chlorite replacement of groundmass feldspars and feldspar phenocrysts was destruction of primary textures. Pervasive moderate chlorite ± sericite replaced feldspar crystals in weak to moderate K-feldspar-altered groundmasses. Chlorite replaced plagioclase crystals result in a dark-green spotted appearance to the rocks. Complete chlorite replacement of the groundmass was not observed except near the margins of the quartz-feldspar-biotite porphyry dykes. At the Jukes Prospect, mafic minerals were totally replaced by intense secondary chlorite ± sericite ± magnetite/hematite. Magnetite, partially replaced by hematite and irregular masses of chlorite in the cores of magnetite and iron oxide crystals was observed.

Near the centre of the Jukes Prospect and near the Darwin Granite, intense pervasive cryptocrystalline K-feldspar replaced primary quartz and feldspar crystals, feldspar rims of micropoikilitic quartz or other groundmass feldspars and primary rock textures were typically destroyed. In intensely altered rocks, cryptocrystalline K-feldspar occurs without other hydrothermal alteration minerals other than quartz. K-feldspar was also observed in fractures within previously chlorite-altered dacites. Intense textural destruction extends outward from the fractures with decreased intensity. Intensely K-feldspar-altered rocks have a fine-grained pinkish-orange color and a sandy texture and are not magnetic unless chlorite-magnetite domains occur. In some domains, K-feldspar replaced earlier secondary chlorite and magnetite.

Secondary silica (quartz) alteration was only observed near the Darwin Granite and in localised domains near the centre of the Jukes Prospect. Silicification ranges from weak to intense, and localised cryptocrystalline quartz domains were observed. Typically, the groundmass in silica-altered rocks is light-pink to light-green, translucent, dense and hard.

5.2.3.2 QUARTZ FELDSPAR ± BIOTITE PORPHYRY DYKES

Along Jukes Road, well-developed intense texturally destructive secondary alteration assemblages occur within and along the margins of several quartz-feldspar porphyry dykes that intruded the feldspar-phyric dacite. Dyke margins were intensely chloritised, and chlorite alteration graded outward from the dyke margin into the K-feldspar-altered feldspar-phyric dacite. Feldspar phenocrysts were intensely altered to mosiacs of sericite (Plate 5.5A) or sericite ± chlorite (Plate 5.5B). Compositional differences in feldspars are reflected in replacement mineralogies. Calcic plagioclase was replaced by secondary chlorite and sodic varieties by sericite. Chlorite occurs as up to 10% of the rock and typically occurs as irregularly distributed 0.02-0.1 mm patches and blebs throughout the groundmass or replacement of feldspar crystals. Chlorite replacement of the groundmass was moderate to intense and texturally destructive to feldspar phenocrysts and all but the largest quartz phenocrysts. Biotite phenocrysts were partially to completely replaced by secondary chlorite (Plate 5.5C). Magnetite is up to 5% of the rock and pyrite and chalcopyrite are

Plate 5.3. Preserved glass shard in the tuffaceous-ash/sandstone facies, CVC.

A. Thin pumiceous volcaniclastic horizons (Sample 11400). (A) is a chloritised relict glass/pumice shard. The dashed lines outline relict bedding. Polarized light, field of view width = 6 mm.

A

Plate 5.4. Preserved textures in the feldspar-phyric lavas and sills, CVC.

A and B. Micropoikilitic texture in the feldspar-phyric dacite (Sample 10800). Quartz grains (Q) are surrounded by an optically continuous micropoikilitic quartz-rich rim. A detail of the micropoikilitic texture is shown in Plate 5.4C and D. Plate 5.4A is plane polarized light and Plate 5.4B is crossed polars. Field of view width = 3.75 mm.

C and D. Micropoikilitic quartz with irregular quartz cores (Q) surrounded by an optically continuous micropoikilitic quartz-rich rim (R). Groundmass k-feldspars were replaced with an assemblage of sericite + chlorite and magnetite (opaque). Birdseye texture (B) in the quartz cores of micropoikilitic quartz was caused by embayments of k-feldspar, later replaced by secondary sericite or chlorite. Plate 5.4C is plane polarized light. and Plate 5.4D is crossed polars. Field of view width = 1 mm. Sample B1007.

A

B

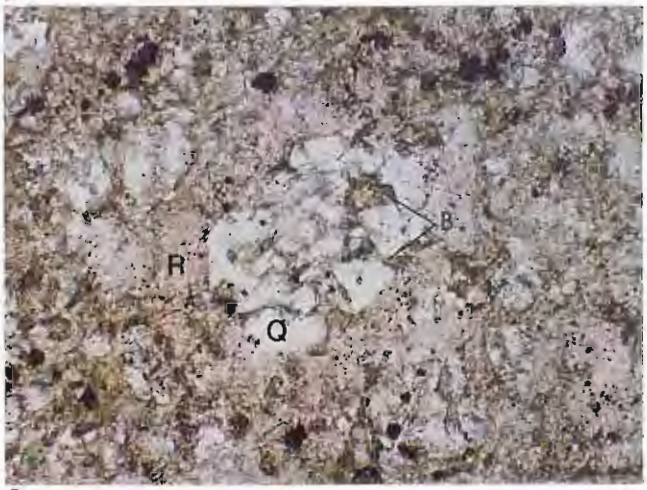

C

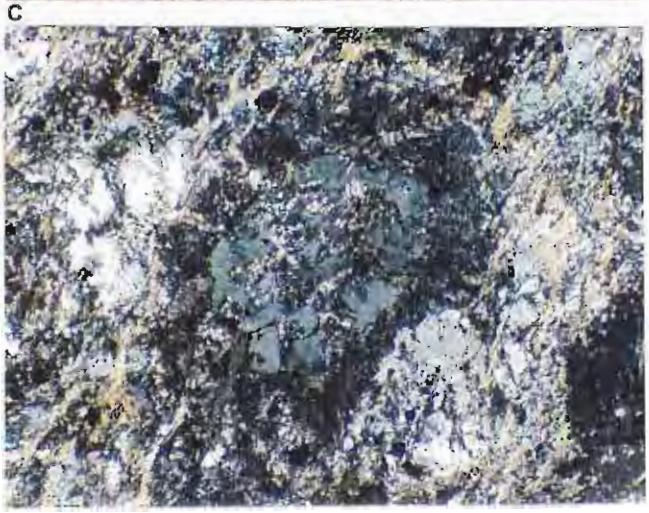

D

Plate 5.5. Typical alteration features in quartz-feldspar ± biotite porphyry dykes of the CVC.

A. Cleavage controlled partial sericite (S) replacement of a plagioclase phenocryst. Some relict feldspar (F) was preserved. Notice the compositionally zoned plagioclase (P) in the upper right with similar sericite replacement of the outer zone. Groundmass was intensely K-feldspar-altered. Crossed polars, field of view width = 3.75 mm. Sample MJ-96-4.

B. Relict plagioclase phenocryst with an intensely sericite-replaced rim (S) and a core replaced by chlorite (C). This replacement is interpreted to represent differential replacement of a compositionally zoned feldspar. Note magnetite occurs in the core with the chlorite. Crossed polars, field of view width = 3.75 mm. Sample MJ-96-8.

C. Biotite phenocryst replaced by secondary chlorite (C) and lesser sericite (S). The opaque minerals are magnetite. Polarized light, field of view width = 3.75 mm. Sample MJ-96-8.

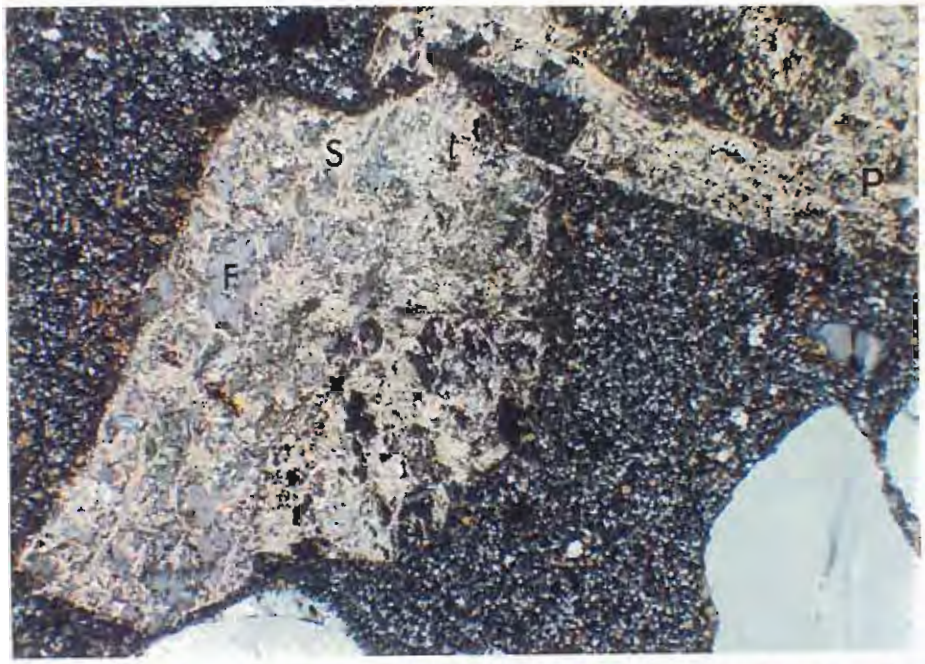

A

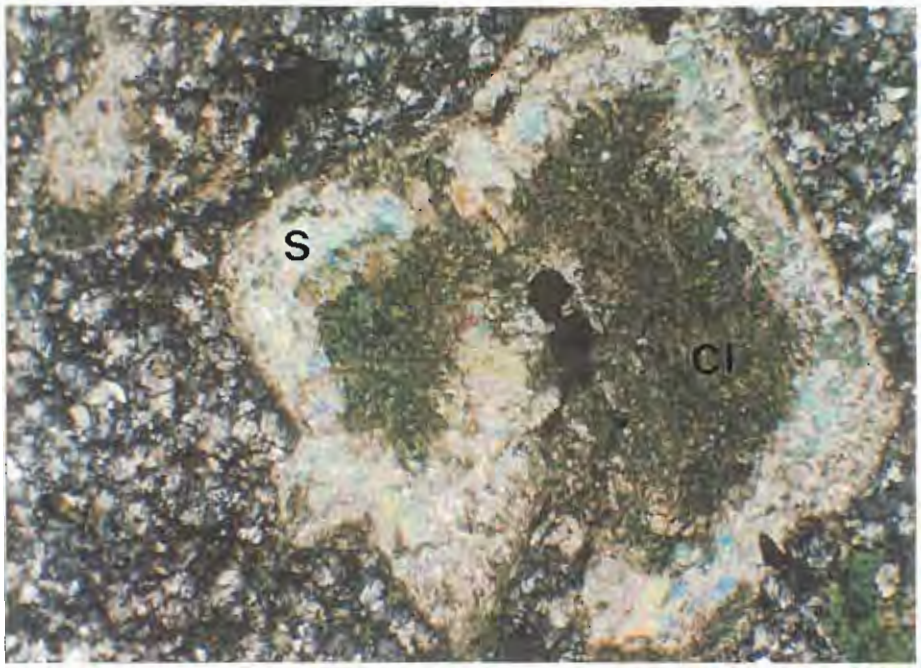

B

C

accessory opaques. Typical secondary chlorite assemblages include; chlorite ± sericite ± quartz and chlorite ± sericite ± magnetite.

5.2.4 Alteration Features in the EQPS

Typical EQPS rocks are described in 4.3.3. Preserved thin, flattened and deformed rod and spine shaped masses are defined by aligned sericite crystals (Plate 5.6A). Plagioclase crystals were replaced by up to 50% sericite and to a lesser, extent chlorite (5-20%). Albite twinning was observed in many crystals. Radial spherical quartz and sericite crystal fibre intergrowths were observed. Some were replaced by secondary sericite and chlorite. Iron oxides occur along cleavage surfaces. A well-defined cleavage was defined by aligned sericite grains (Plate 5.6B-C). Large quartz crystals were typically broken. Commonly, the quartz grains remain in contact and exhibit jigsaw-fit textures. Accessory minerals observed were carbonate and magnetite.

5.2.5 Alteration Features in the Darwin Granite

5.2.5.1 ALTERATION FEATURES IN THE PINK GRANITE

Sericite alteration in the pink granite is most intense near zones with a high fracture density (Plate 5.7A). Cross-cutting fracture sets that occur parallel to major joint sets also contain sericite and sericite is progressively diffuse with increasing distance away from the fractures.

Alteration within the pink granite is expressed as widespread weak to moderate sericite ± chlorite assemblages having a distinctive pink and green color (Plate 3-1A). Weak sericite alteration typically occurs at intergrain boundaries of quartz and K-feldspar crystals (Plate 5.7B). However, sericite also occurs within feldspar crystals, in biotite and in fractures in broken quartz grains. Plagioclase was weakly to intensely altered to sericite ± chlorite. Sericite occurs within individual plagioclase crystals as irregular masses and blebs, cleavage-controlled individual sericite grains, and selective replacements in twinned crystals (Plate 5.7C). Primary micas were altered to sericite (Plate 5.7D), particularly near shrinkage cracks. Chlorite alteration (chlorite + sericite) was weak and irregular in its distribution. However, local areas of moderate to intense secondary chlorite were observed near contacts with the white granite. Hematite staining of individual K-feldspar crystals created a mottled appearance as shown in (Plate 5.7E). This gives the K-feldspar the particularly reddish appearance as shown in Plate 3-1A.

5.2.5.2 ALTERATION IN THE WHITE GRANITE

Weak to moderate secondary sericite ± chlorite occur as replacement rims of plagioclase crystals. Commonly, moderate to intense secondary sericite ± chlorite selectively replaced plagioclase crystals along individual twin planes. In contrast to the plagioclase crystals, K-feldspar crystals were weakly replaced by secondary sericite. Rare biotite was partially to totally replaced by sericite.

Plate 5.6. Preserved textures in rocks of the EQPS.

A. Relict glassy lithic clasts or recrystallised glass shards occur as thin, flattened and deformed rod and spine shaped masses (A). Relict lithic clast and pumiceous textures were preserved by sericite and chlorite replacement and iron oxides were observed along cleavage surfaces. Polarized light, field of view width = 18 mm. Sample 9920.

B and C. Preserved textures within several types of lithic clasts are shown in this crystal-rich volcaniclastic sediment or mass flow deposit (Sample 9550). The large lithic clast (A) is fine-grained feldspar-phyric rhyolite with feldspar crystals (F) replaced by secondary sericite and chlorite. Fine grained mosiacs of quartz and feldspar were formerly volcanic glass (G), now devitrified and recrystallised. Quartz crystals are subrounded, angular, broken and embayed. Note the well defined cleavage created by the alignment of sericite. Plate 5.6B is plane polarized light and Plate 5.6C is crossed polars. Field of view width = 3.75 mm.

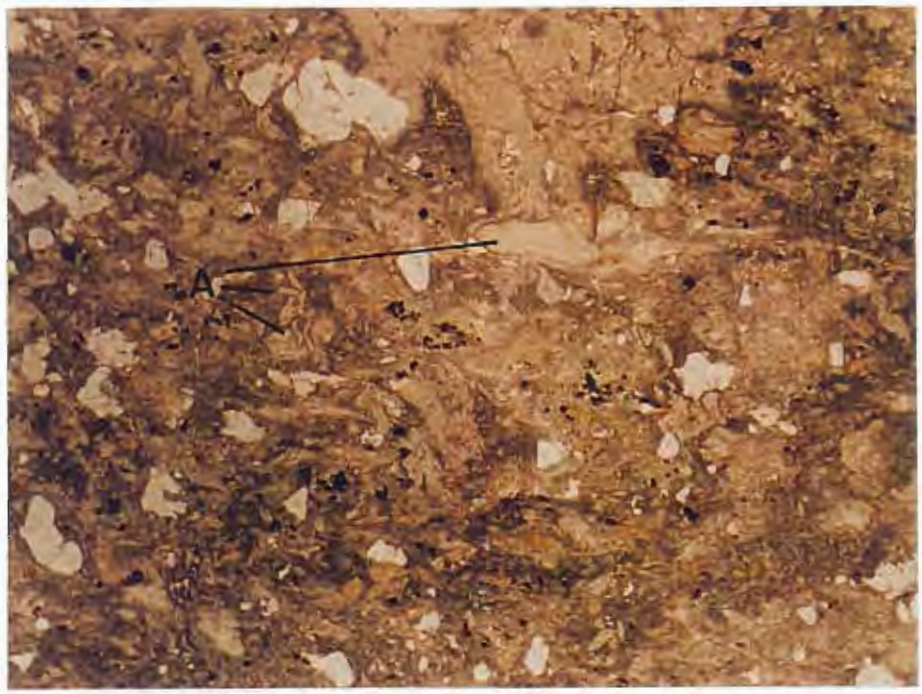

A

B

C

Plate 5.7. Preserved alteration textures in the Darwin Granite.

A. Fracture controlled diffuse sericite alteration in the pink granite phase of the Darwin Granite. Sericite alteration is intense and texturally destructive near the fracture contacts and becomes progressively more diffuse and less intense with increasing distance from the fractures.

B. Hydrothermal sericite alteration in the pink granite was controlled by fracture density, intergrain boundaries and porosity. In this sample, sericite (S) follows the intergrain boundaries between quartz (Q) and plagioclase (P) crystals. Notice that the plagioclase crystals were weakly to moderately replaced but the K-feldspar (K) was unaltered. Crossed polars, field of view width = 3.75 mm. Sample 2053.

C. Sericite within individual plagioclase crystals (P) occurs as irregular masses and blebs, cleavage-controlled individual sericite grains, and selective replacement in twinned crystals. Notice preserved twinning (T). Crossed polars, field of view width = 3.75 mm. Sample 2053.

D. Primary mica (B) altered to sericite. K-feldspar (K) is stained by hematite and Plagioclase (P) is weakly replaced by secondary sericite. Crossed polars, field of view width = 3.75 mm. Sample 2053.

E. Hematite staining in individual K-feldspar crystals (K), created a mottled appearance and gave the K-feldspar the particularly reddish appearance as shown in Plate 3.1A. Plagioclase (P) was sericite-altered and twinning (T) was preserved. Crossed polars, field of view width = 3.75 mm. Sample 2053.

A

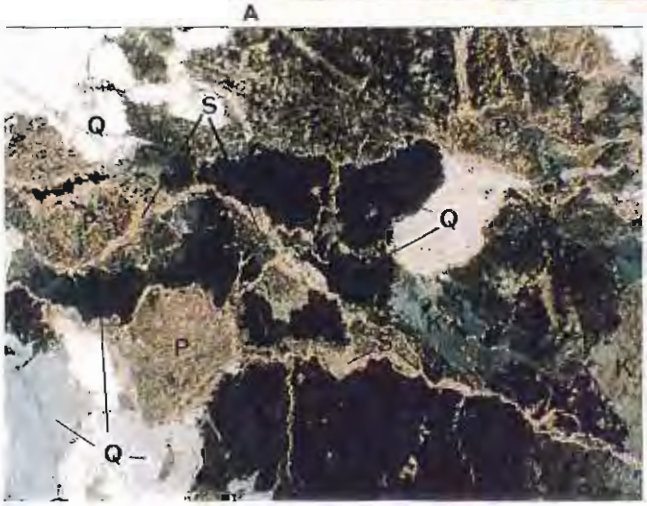

B

C

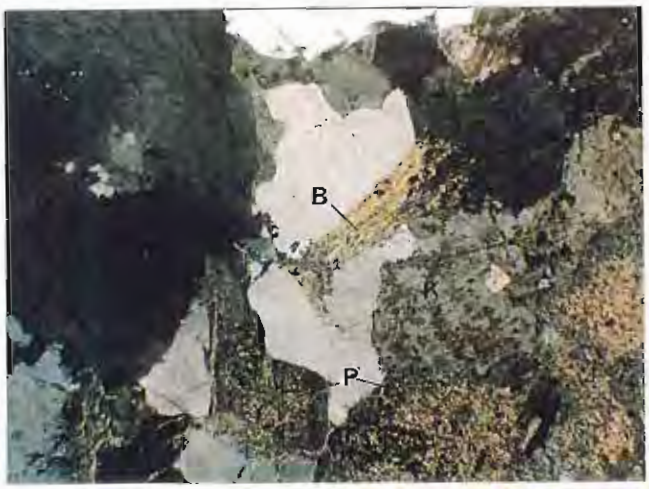

D

E

5.2.5.3 ALTERATION IN THE QUARTZ-FELDSPAR PORPHYRY

K-feldspar and plagioclase phenocrysts were weakly to moderately sericitised and relict twinned zones were preserved. Sericite alteration in the plagioclase crystals was more intense on the rims of crystals than the cores. Rare biotite was partially to totally replaced by sericite.

The quartz-feldspar porphyry was cut by quartz + epidote (zoisite) ± tourmaline veins. These veins are up to 1 mm wide and occur as boxwork-like networks within some outcrops. Some veins contain pyrite and chalcopyrite.

5.2.5.4 ALTERATION IN THE MICROGRANITE

The microgranite dykes were either weak to moderately sericite-altered or intensely K-feldspar-altered (on Mt Darwin). In the weakly altered microgranite dykes, weak to moderate secondary sericite replaced the fine-grained groundmass surrounding quartz and feldspar crystals and weak replacement of individual plagioclase and K-feldspar grain boundaries occurred. Inherited K-feldspar crystals from the pink granite were weakly replaced by sericite and twinning was preserved. Pyrite (0.2 mm) and magnetite (0.02-0.2 mm) occur as fine disseminated crystals, typically with chlorite.

In the intensely K-feldspar-altered microgranite dyke, secondary quartz occurs and plagioclase was replaced by secondary K-feldspar and sericite. The replacement of plagioclase was texturally destructive to twinning. Primary biotite was replaced by sphene (titanite) and secondary biotite developed as scattered patches throughout the rock. Secondary biotite was locally replaced by chlorite.

5.3 TEXTURAL AND PETROGRAPHIC CHARACTERISTICS OF REGIONAL DIAGENESIS AND METAMORPHISM

This section will discuss the ways in which diagenetic, regional metamorphic and hydrothermal alteration styles and mineral assemblages were distinguished from each other.

5.3.1 Diagenesis and Low-Grade Burial Metamorphism

5.3.1.1 DIAGENETIC ALTERATION CHARACTERISTICS OF VOLCANIC ROCKS, A REVIEW

Discussions of submarine diagenesis and diagenetic processes focus on sedimentary rocks in depositional basins and areas of rapid subsidence. This focus on sedimentary rocks resulted in the following definitions of diagenesis:

> "Diagenesis comprises all changes that took place in a sediment between sedimentation and the onset of metamorphism, except those caused by weathering." (Correns, 1950).

Another, recent and broader definition is from Bates and Jackson (1980):

> "All the chemical, physical and biologic changes undergone by a sediment after its initial deposition, and during and after its lithification, exclusive of surficial alteration (weathering) and metamorphism. This definition includes those processes (such as compaction, cementation, reworking, authigenesis, replacement, crystallisation, leaching, hydration, bacterial action, and formation of concretions) that occur under conditions of pressure (up to 1 Kbar) and temperature (maximum range of 100°C to 300°C) that are normal to the surficial or outer part of the earth's crust; and it can include changes occurring after lithification under the same conditions of pressure and temperature."

Many geologists will agree with Correns (1950) definition, but many will find exceptions to the definition of Bates and Jackson (1980) because of their attempt to set some definite P-T limits. That areas of overlap occur between the effects of diagenesis, hydrothermal, and low-grade regional (or burial) metamorphism is indisputable. All three can have temperatures and pressures in the 200-300°C and $\leq$1 kbar range. Temperatures achieved during diagenetic alteration were directly related to the geothermal gradient in the depositional basin and in submarine settings range from 0°C at the seafloor to 250°C at 2-10 km depth (Alt and Honnorez, 1984; Alt, 1995). For low pressure and low temperature (low-P/T) types of metamorphism the geothermal gradient is >35°C/km (Miyashiro, 1994). In geosynclinal areas and areas of rapid subsidence the geothermal gradient may be less, whereas in active belts it can be greater.

One of the earliest diagenetic changes in glassy volcanic rocks is partial or complete devitrification. Volcanic glass is unstable and particularly prone to complete replacement by stable mineral species (Lofgren, 1971b; Bigger and Hansen, 1992; McArthur et al., 1998). Alteration of volcanic glass includes its replacement by clay minerals, zeolites, silica, carbonate, oxidation by oxygen-rich seawater, and the filling of primary porosity (amygdales and vesicles, and interparticle porosity of volcanic and volcaniclastic rocks, Dimroth and Licht Blau, 1979). Although much of the recent work on diagenesis and burial metamorphism of volcanic rocks comes from deep sea drilling and submersible studies of basalts on the Mid-Ocean Ridge (MAR) and Mid-Pacific Rise (MPR), many of the processes and reactions that happen as a result of seawater circulation are similar in other submarine environments.

Seawater alteration of volcanic successions can take place in open, restricted, or closed circulation systems. Open circulation systems are colder (<40°C), seawater-dominated and fluid passes easily through permeable porous rocks or sediments. In restricted circulation systems, seawater-dominated fluids are forced through less permeable rocks by convection, fluids are warmer (100-200°C) and fluid compositions are controlled by reactions with host rocks (von Engelhardt, 1967; Andrews, 1977; Alt and Honnorez, 1984; Alt et al., 1986; Mottl, 1989). In closed systems, fluids are contained in pores within the rocks, permeability is negligible and alteration in in-situ.

In large hydrothermal convection systems, open zones are termed recharge zones (Alt, 1995). The main open system, low temperature processes that affect volcanic rocks are:

1. The hydration of volcanic glass to form perlite (Lofgren, 1970; Lofgren, 1971a; Bigger and Hansen, 1992; McArthur et al., 1998) succeeded by, devitrification to form spherulites, micropoikilitic textures and microlites (Lofgren, 1971b; Bigger and Hansen, 1992; McArthur et al., 1998). However, spherulites can also form above the glass-transition temperature and may not represent devitrification (McArthur et al., 1998). Micropoikilitic texture is a common devitrification texture in volcanic glass (Anderson, 1969; McPhie, 1993).

2. Oxidation can occur by reaction with water. Iron oxides (Fe-oxyhydroxides, goethite and hematite) replace primary sulfide minerals disseminated throughout the groundmass and fill veins and fractures (Alt, 1995).

3. Alkalis (K, Rb, Cs and B) are fixed in ferric mica and smectite or mixtures or intergrowths of the two (Alt, 1995). Alkalis may be lost from the volcanic pile at higher temperatures (250-350°C, Alt and Honnorez, 1984 and Alt, 1995) and this alkali loss at higher temperatures partially compensates for alkali gains at lower temperatures (Thompson, 1983; Seyfried et al., 1984; Alt et al., 1986).

4. Fixation of seawater Mg occurs during the formation of smectite directly from volcanic glass (Noh and Boles, 1989). Mg^{2+} and $(OH)^{-}$ combine to create smectite at low temperatures (<200^{0}C) and diagenetic chlorite at higher temperatures (>200°C) (Alt and Honnorez, 1984; Alt, 1995; Robinson and Santana De Zamora, 1999). Smectites are inherently unstable and can revert to other clay minerals such as illite or chlorite (Post and Noble, 1993; Robinson and Santana De Zamora, 1999).

5. The formation of anhydrite. Heating of seawater as it penetrates the upper crust causes the precipitation of essentially all of the Ca and two thirds of the sulfate as anhydrite when temperatures reach >200^{0}C (Bischoff and Seyfreid, 1978). Anhydrite formation is important because it controls the Ca content of descending fluids, inhibiting the formation of Ca-silicates, and altering Sr isotope concentrations in hydrothermal fluids (Seyfried, 1987; Berndt et al., 1988). Precipitation of anhydrite at lower temperatures controls the amount of sulfate that, at higher temperatures (>250°C) in hydrothermal systems, is available for reduction to sulfide (Alt et al., 1989). Anhydrite created during recharge is subsequently dissolved or replaced by other mineral species at lower temperatures (<200^{0}C) or as the crust ages and undergoes additional alteration (Alt et al., 1986; Alt et al., 1989).

6. Zeolite crystallisation. Zeolites crystallise directly from perlitic glass via a dissolution reaction with smectite (Noh and Boles, 1989) or as replacement of pseudomorphs of glass shards (Walton, 1975).

Although perlite can be created in subaerial conditions through atmospheric absorption of water, perlite development is enhanced and accelerated by access of seawater. Access of seawater to cool the volcanic pile is initially through cracks developed as a result of shrinkage during cooling (Lister, 1982), diffusion or faults (Rona et al., 1993), or corrosion of the surface of glass fragments (Capaccioni and Coniglio, 1995). Access of water can be enhanced by continued development of perlitic cracks (Noh and Boles, 1989).

Early studies of zeolites assumed that zeolite crystallisation was controlled by low P-T conditions and from this view point various zeolites were assigned to various phases of the zeolite facies of metamorphism (Seki et al., 1969). However, Miyashiro and Shido (1970) have shown that composition and pressure of intergranular fluids and the composition of the initial rock are important in zeolite crystallisation. Since zeolites are high in Ca and Na, they are common in volcanic and volcaniclastic rocks where the original material was volcanic glass and plagioclase (Miyashiro and Shido, 1970). Zeolites (for example heulandite) can have compositional variations between adjacent rock units or within different parts of the same rock due to internal variations in composition of the original glass (Boles and Coombs, 1975). In addition, zeolites are subject to Ostwald's Step Rule, i.e., phases driven by kinetics are not necessarily in equilibrium and therefore changes between minerals can occur over time.

Diagenetic smectite (montmorillonite) formed from perlite may be replaced by phyllosylicates (sericite and chlorite) at higher temperatures and pressures (Allen et al., 1998) which enhance and preserve vitroclastic textures (Walton, 1975; Noh and Boles, 1989; Capaccioni and Coniglio, 1995). Sericite-rich and chlorite-rich alteration assemblages are controlled by primary compositional variations in the rock and primary or syn-volcanic textures. Primary feldspars are either well-preserved or pseudomorphed by diagenetic minerals.

5.3.1.2 CHARACTERISTICS OF LOW GRADE BURIAL METAMORPHISM OF VOLCANIC ROCKS, A REVIEW

Diagenetic alteration grades into burial metamorphism and results in broad roughly horizontal alteration zones and low water to rock ratios. Where diagenetic alteration occurs in open and restricted circulation systems, burial-related metamorphic alteration, occurs in closed systems (von Engelhardt, 1967). Thus, according to von Engelhardt (1967), diagenesis and metamorphism are identified by the types of processes that occur in the two alteration styles and it is possible to distinguish between the two on the basis of alteration products. The transition from a diagenetic assemblage to a metamorphic assemblage is the first occurrence of a truly metamorphic mineral paragenesis in the rock, i.e., a paragenesis that occurs only in metamorphic rocks. The problem is, how to define 'metamorphic'. From a sedimentological point of view, the transition from diagenesis to burial metamorphism occurs when interconnected pore space becomes completely blocked. This does not necessarily coincide with the formation of the first metamorphic mineral paragenesis and the role of interstitial fluids on the formation of low-grade zeolite facies mineral assemblages is more important in volcanic rocks (Levi, 1969; Jolly and Smith, 1970). Since diagenesis precedes burial metamorphism, the end of diagenesis occurs and burial metamorphism begins when a mineral assemblage forms that cannot occur in a sedimentary environment (i.e., the crystallisation of the zeolite laumonite + quartz and/or crystallisation of prehnite and pumpellyite). Typically, this is the first occurrence of laumonite (metamorphic zeolite), lawsonite, glaucophane, paragonite (sodic mica), or pyrophyllite and is defined as zeolite-facies metamorphism.

In the Triassic volcaniclastic rocks of New Zealand, a gradation occurs from diagenetic zeolite assemblages to a zone dominated by burial metamorphic alteration assemblages (Coombs,

1954; Coombs et al., 1959; Coombs, 1961). In the upper part of the succession, volcanic glass has been replaced by heulandite and less commonly analcime. The zeolites coexist with newly crystallised quartz and fine-grained smectite. In the lower part of the sequence, analcime and heulandite disappear. Analcime, was replaced by albite, and heulandite was replaced by laumonite plus quartz. The crystallisation of laumonite corresponds to the formation of albite from analcime + quartz in basaltic rocks (Coombs, 1961). Smectite, chlorite, sericite and mixed layer minerals occur and prehnite and pumpellyite appear as accessory minerals. The minerals occur as cements, fine-grained matrix and replacement of detrital minerals and glass shards (Walton, 1975). Two depth stages of the zeolite faces were suggested: A heulandite-analcime stage in the poorly crystallised upper section (diagenesis), and a laumonite (laumonite + quartz + albite) lower stage (burial metamorphism). Three reactions that summarise the processes involved are from Miyashiro and Shido (1970).

heulandite laumonite quartz

Reaction 1: $CaAl_2Si_7O_{18}.6H_2O \Leftrightarrow CaAl_2Si_4O_{12}.4H_2O + 3SiO_2 + 2H_2O$

analcime quartz albite

Reaction 2: $NaAlSi_2O_6.H_2O + SiO_2 \Leftrightarrow NaAlSi_3O_8 + H_2O$

laumonite calcite prehnite quartz

Reaction 3: $Ca(Al_2Si_4O_{12})\ 4H_2O + CaCO_3 \Leftrightarrow Ca_2Al(AlSi_3O_{10})(OH)_2 + SiO_2 + 3H_2O + CO_2$

Hydration of volcanic glass and formation of perlite and zeolites (heulandite and analcime) are considered to be part of the diagenetic process (left hand side of Equations 1 and 2). Burial metamorphism begins with dehydration and decarbonation (loss of CO_2) of the original hydrated zeolites (right hand side of Equations 1 and 2 and Equation 3). However, these minerals do not occur in the same physical conditions or in all types of rocks. Some rocks do not have any changes in mineralogy at the start of metamorphism, while others can have numerous changes. For example, rocks with quartz-chlorite-phengite assemblages can persist unchanged from the diagenetic stage through low grade to medium grade metamorphism. Therefore, rock mineralogies are important if the rock is to be used as an indicator of the onset of metamorphism. In addition, temperature thresholds for the onset of metamorphism can vary for different rock types.

Relict textural evidence of diagenesis (eg., relict perlitic fractures) is important in making a clear distinction between diagenetic and metamorphic alteration. In a comparative study of Archean vs. Cenozoic hyaloclastites (Dimroth and Licht Blau, 1979), textural evidence suggests chlorite, carbonate and silica, formed by load metamorphism, replaced palagonite and zeolites, formed by diagenesis.

As Titley (1982) points out, alteration can enhance primary rock textures under some circumstances. In the study area, differential weathering of the Darwin Granite resulted from sericite-chlorite enhanced fracture patterns. In volcanic rocks, chlorite-epidote enhanced fracture patterns, but intense alteration assemblages destroyed relict pumice and original groundmass or

matrix textures. These mineralogical changes were preserved through subsequent higher grade metamorphism.

5.3.2 Regional Diagenetic and Metamorphic Alteration Styles and Textures in the Study Area

Sericite and chlorite are common alteration minerals throughout all of the volcanic units in the MRV. They are common in greenschist facies metamorphic rocks, diagenetically altered volcanics and in propylitically altered zones in hydrothermal systems. These minerals cannot, therefore be used to uniquely distinguish burial metamorphism, dynamic metamorphism, diagenetic alteration and hydrothermal alteration effects from each other. However, even with recognition of this limitation, an attempt to "draw a line" around the hydrothermal alteration zones in the study area was made. The main criteria used is the widespread occurrence and simultaneous low degree of textural destruction caused by formation of the sericite-chlorite mineral assemblage. Although low water to rock ratios can cause similar hydrothermal alteration assemblages, the widespread occurrence of weak to moderate secondary sericite-chlorite assemblages is interpreted to represent a diagenetic or burial metamorphic origin although a hydrothermal origin cannot be ruled out. In the study area, sericite-chlorite assemblages interpreted to have a hydrothermal origin are confined to a limited zones of moderate to intense texturally destructive alteration of primary mineral textures. Where original glass and devitrification textures were preserved, a diagenetic origin for the sericite-chlorite alteration was interpreted. Burial metamorphic and dynamic metamorphism generally caused moderate to intense development of a sericite chlorite assemblage, but secondary mineral growth was localised in cleavage domains..

5.4 INTERPRETATION OF ALTERATION FEATURES IN THE JUKES-DARWIN AREA

Sericite and chlorite may be diagenetic or burial metamorphic in origin (Alt, 1995). They can replace earlier smectite (Noh and Boles, 1989; Allen et al., 1998), palagonite, zeolites or earlier clays (Dimroth and Licht Blau, 1979) or ferromagnesian minerals. Sericite and chlorite are common in all rocks of rhyolitic to dacitic composition throughout the study area, and throughout the MRV. This widespread occurrence is consistent with a diagenetic and/or metamorphic origin.

5.4.1 Diagenetic and Metamorphic Features in the YRS

Volcaniclastics and lavas were typically weakly to moderately sericite ± chlorite-altered with well-developed light-green sericite on cleavage surfaces. The sericite ± chlorite is interpreted to have crystallised during diagenesis or burial metamorphism. Preserved spherical to semispherical quartz and feldspar domains are interpreted to represent relict perlite (Plate 5.1A-C), lithophysae (Plate 5.8A-B), and spherulites (Plate 5.8C). Lithophysae are interpreted to be a devitrification texture as described by McPhie et al. (1993), and replacement of the original mineralogy probably occurred during late diagenesis or regional burial metamorphism. The typical radiating quartz and

Plate 5.8. Preserved diagenetic and features in the YRS

A and B. Broken and deformed lithophysae (L) and quartz crystals. The lithophysae were rimmed with secondary quartz and subsequently filled (replaced?) with an unknown mineral. The radiating quartz that typically rims lithophysae was recrystallised into optically continuous quartz and later broken. The filling mineral was recrystallised to the present mineralogy of sericite and minor chlorite. Note the embayed subhedral quartz crystal. Plate 5.8A is plane polarized light and Plate 5.8B is crossed polars. Field of view width = 4.5 mm. Sample B2007.

C. Relict spherulite (S) with (from core to centre), a quartz rim, feldspar zone (replaced with sericite and chlorite) and quartz core. The typical radiating quartz and feldspar laths described in the literature (McPhie, 1993) were not observed in the spherulites due to recrystallisation during metamorphism. Polarized light, field of view width = 1.5 mm. Sample B1095.

D. Irregularly shaped vesicular and tube pumice fragments with well-preserved vesicular textures. Tube pumice fragments are thin and flattened (TP) and replaced with sericite and quartz or sericite and magnetite. Blocky vesicular pumice (BP) was replaced with chlorite and magnetite. In this photograph, the two types of pumice are shown. The blocky pumice fragment (BP) is sitting on top of the tube pumice fragment (TP) and has deformed it. Relict vesicles are preserved in the two fragments and illustrate the differences. Polarized light, field of view width = 3 mm. Sample B2010.

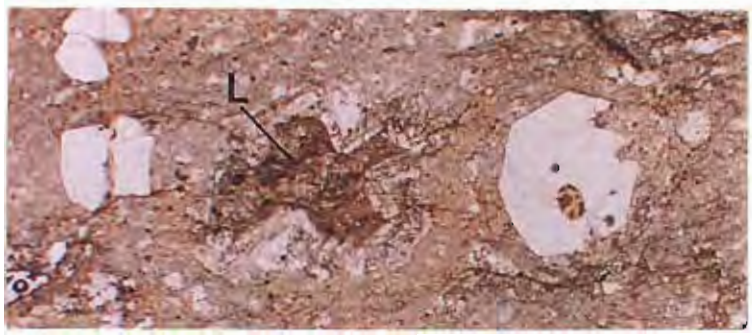

A

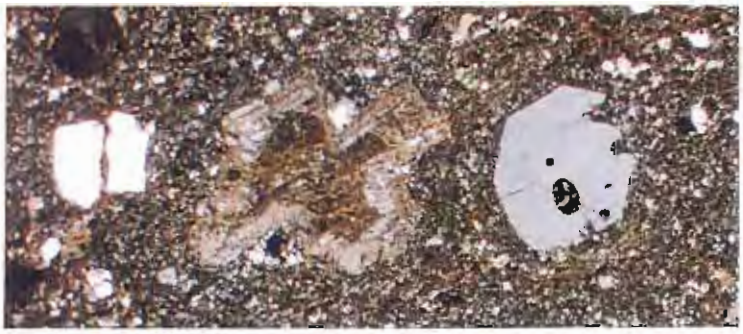

B

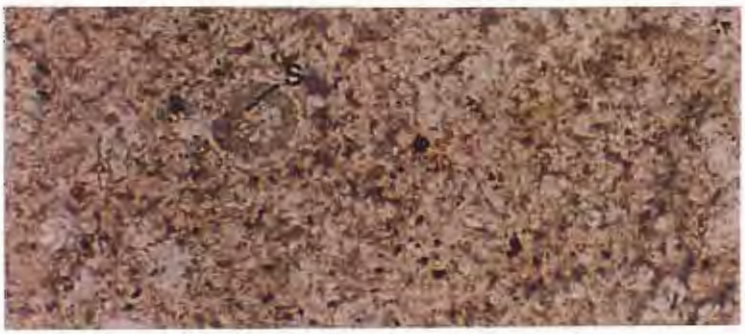

C

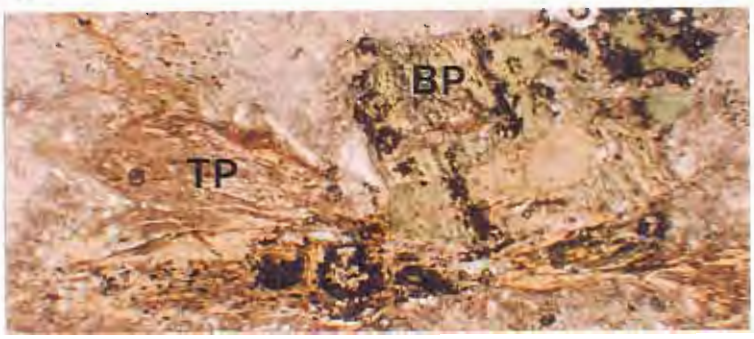

D

feldspar laths described in the literature (McPhie, 1993) were not observed in the spherulites due to recrystallisation during metamorphism. Scattered, small (0.5 mm) subrounded radiating quartz aggregrates and rounded structures lined with secondary quartz were interpreted to represent vesicles.

Vesicular textures were well-preserved in relict pumice clasts. Blocky vesicular pumice clasts were replaced with elongate masses of chlorite, sericite and magnetite (Plate 5.8D). Clasts interpreted to be tube pumice fragments were thin, flattened and replaced with sericite and quartz or sericite and magnetite. Wispy structures in the rocks were interpreted to be relict cuspate glass shards.

5.4.2 Diagenetic and Metamorphic Features in the CVC

Volcaniclastic rocks along Jukes Road have many textures similar to those observed in the Rosebery-Hercules area and elsewhere in the CVC (Allen and Cas, 1990; White and McPhie, 1996), except for the presence of abundant lithic clasts. Structures interpreted to be tube pumice, vesicular pumice and lithic clasts were well-preserved (Plates 5.2A and 5.3A). Preserved tube pumice is wispy, with the long dimension of the tubes defined by alignment of chlorite and sericite crystals. Fine-grained mosiacs of quartz and feldspar were interpreted to be well-preserved relict glass shards. Abundant randomly oriented vesicular and spherulitic pumice shards make up about 30% of the pumiceous shards in the rock. Circular and semicircular relict spherulites or vesicles were filled with interlocking aggregates of recrystallised albite and quartz. Relict perthitic fractures were defined by alignment of sericite-chlorite crystals. Chlorite occurs as patches, blebs and as cores in albite-altered pumice clasts.

Two types of feldspar interpreted to be of diagenetic or burial metamorphic origin occur in the study area; 1) Diagenetic K-feldspar occurs in rhyolitic volcaniclastics in the Clark Valley and along Jukes Road. Secondary K-feldspar development was minor in regional diagenetic processes but was common in magmatic-hydrothermal processes discussed below. This alteration style is common south of the Henty Fault and was first described by Solomon (1960). Diagenetic K-feldspar imparts a distinctive pink-weathered appearance to the rocks and typically contains 5-9 wt.% K_2O in rhyolitic lavas (Solomon, 1960). 2) Diagenetic albite replaced feldspar crystals and matrix laths in patchy domains. Albite alteration was pervasive, destroyed matrix textures and was typically conformable to relict bedding. Albite-rich rocks are distinctly pink and green banded, and occur throughout the Lyell-Darwin area (White, 1975), including Intercolonial Spur (Gadaloff, 1996), Jukes Road and elsewhere in the CVC (Allen and Cas, 1990; White, 1996). Along the Jukes Road, albite is interpreted to have formed after earlier sericite and chlorite because, in feldspar crystals, albite halos occur around fractures and are transitional into sericitic ± chlorite domains.

Coarse-grain carbonate is widespread in the quartz-phyric volcaniclastics. Carbonate occurs as blebs and irregular patches of various sizes within the matrix, in veinlets at high angles to the twinned planes in broken feldspar crystals and in Devonian syn-tectonic quartz ± chlorite veins. Textural relationships and vein associations suggest that the carbonate was post-deformational.

The Jukes Road Pumice Breccia is unique from all other volcaniclastic facies in the southern CVC, due to its pink and green banding (Plate 5.9). The pink and green banding is due to irregular distribution of pink albite and green chlorite-altered domains within the matrix (Plate 5.9B-C). Euhedral to subhedral plagioclase was observed in lithic clasts of tube pumice and vesicular pumice and some larger pumiceous lithic clasts were altered by pink albite. Albite is interpreted to have formed after the chlorite. Textures in the Jukes Road Pumice Breccia are interpreted to represent diagenetic and weak burial metamorphic effects. Weak regional alteration is supported by the occurrence of fine-grained quartz-feldspar-sericite mosiacs that were interpreted to be relict glass shards. Sericite ± chlorite enhanced wispy structures in the rocks were interpreted to represent relict pumice shards and tube pumice and devitrification textures (Plate 5.9D-E). In addition to the pumice and glass lithic clasts, clasts with well-developed granophyric textures were interpreted to be derived from primary lavas. Relict pumice clasts occur as fiamme and undeformed pumice textures are rare. Relict perlitic fractures were observed around large glomocrysts in some lithic clasts.

In the tuffaceous-ash/sandstone facies of the CVC, wispy chlorite-altered masses were interpreted to represent relict glass shards (up to 1.5 cm long, Plate 5.3A).

In the feldspar-phyric dacites of the CVC, micropoikilitic textures, relict perlite, amygdales, spherulites, lithophysae and tuff/ash inclusions are all interpreted to represent relict diagenetic features preserved through subsequent lower greenschist facies metamorphic events. Micropoikilitic texture is a common devitrification texture in volcanic glass (Anderson, 1969; McPhie, 1993). Relict circular structures interpreted to be spherulites are preserved in the micropoikilitic groundmass (Plate 5.10A). Because of the massive nature of the feldspar-phyric facies, regional foliation was poorly developed. Aligned sericite ± chlorite crystals in the groundmass formed a weak cleavage interpreted to have crystallised during burial metamorphism with re-orientation during later dynamic metamorphic events.

5.4.3 Diagenetic and Metamorphic Features in the EQPS

Thin, flattened and deformed rod and spine shaped masses defined by aligned sericite crystals (Plate 5.6A) were interpreted to be relict glassy lithic clasts, recrystallised glassy shards, vesicular clasts and clasts with relict perlitic textures. Radial spherical quartz and sericite crystal fibre intergrowths were interpreted to be relict spherulites. Some of the relict lithic clasts were replaced by secondary sericite and chlorite and were interpreted to have been pumiceous.

Well-developed cleavage, defined by sericite (Plate 5.6B-C), and large broken quartz crystals with jigsaw-fit textures, were interpreted to have formed during deformation. Parallel orientation of elongate sericite-altered feldspar crystals was interpreted to be a result of regional burial metamorphism and created a pervasive tectonic foliation. Regional foliation was variably developed in the sericitic or chloritic facies subparallel or oblique to bedding. Silicification probably predates regional metamorphic sericite-chlorite alteration but specific evidence for timing relationships were not observed.

Plate 5.9. The Jukes Road Pumice Breccia, CVC.

A. Outcrop of the pink and green banded Jukes Road pumice breccia. Pink bands are albite and green bands are chlorite.

B. Pink band in the Jukes Road pumice breccia. Albite (A) has totally replaced and recrystallised the matrix into fine to medium-grained aggregrates of interlocking crystals. Faint twinning in feldspar crystals is common. Chlorite occurs as patches and blebs (C). The albite was post sericite as observed in feldspar crystals where albite occurs around fractures within the feldspar crystal (B). Crossed polars, field of view width = 1 mm. Sample 12600.

C Green band in the Jukes Road pumice breccia. Replacement of matrix feldspars with chlorite (dark greenish-brown) and weak sericite replacement of feldspar crystals (light colored small patches). Crossed polars, field of view width = 3.75 mm. Sample MJ-96-16.

D. Relict pumice shards (A). Randomly oriented tube pumice was preserved as wispy very-fine-grained mosaics of quartz and feldspar. The tube textures were enhanced by alignment of sericite ± chlorite grains. Notice late carbonate (B) interpreted to be metamorphic in origin. Polarized light, field of view width = 3.75 mm. Sample MJ-96-15.

E. Vesicular or spherulitic pumice/glass shard. Circular and semicircular spherulites or vesicles (A) were filled with interlocking aggregates of recrystallised twinned albite and quartz. Textures were enhanced by alignment of sericite grains. Polarized light, field of view width = 3.75 mm. Sample 12450.

A

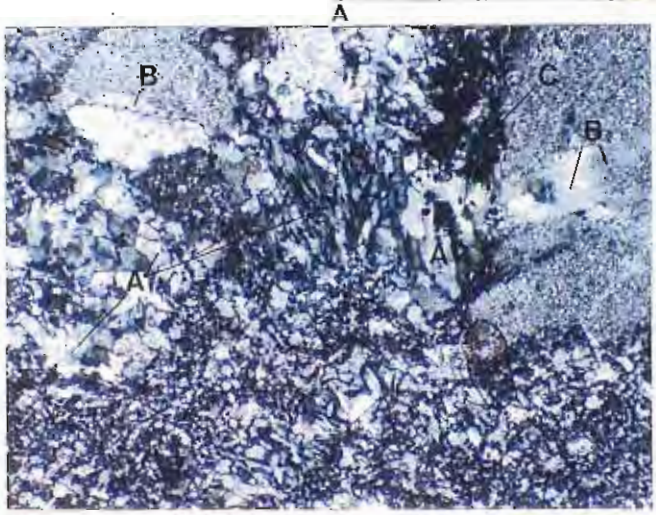

B

C

D

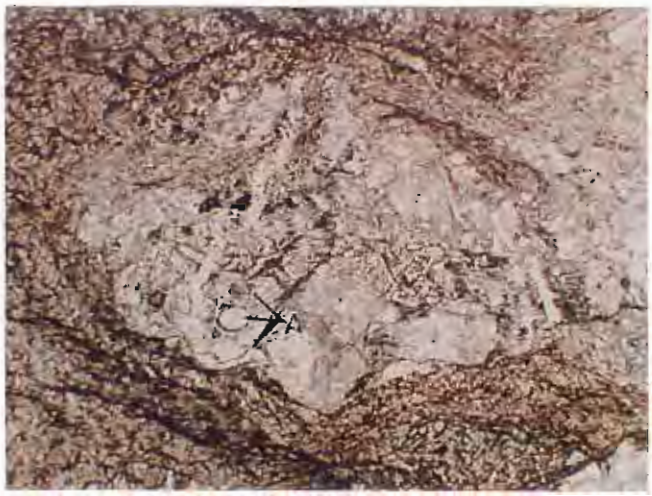

E

Plate 5.10. Preserved spherulite in the feldspar-phyric lavas and sills, CVC.

A. Relict spherulite (S) in the micropoikilitic groundmass. Note the circular shape as defined by sericite and the chlorite-filled core. Polarized light, field of view width = 3.75 mm. Sample 10350.


S

5.4.4 Effects of the NNW Devonian Dynamic Metamorphic Event on Volcanic Rocks of the Study Area

Dynamic metamorphism during the Devonian created planar fabrics (platy and crenulation cleavages) that define a weak NNW foliation in rocks with sericite or chlorite (Corbett and Turner, 1989; Corbett, 1994). Development of this fabric caused dimensional alignment of mineral grains and rock fragments and created wavy extinction in quartz and feldspar grains. Original diagenetic and burial metamorphic volcanic textures were typically destroyed by dynamic metamorphic and intense hydrothermal alteration. Cataclastic fabrics including closely spaced fractures, coarse breccias and brecciation of quartz and feldspar crystals, were observed.

Late post-mineralisation syn-tectonic fractures, faults and veins containing quartz, bright-green or bright blue-green chlorite and well-developed rhombohedral carbonate are interpreted to have formed after the Darwin Granite-related hydrothermal event. Quartz, in late post-mineralisation syn-tectonic fractures, typically occurs as ladder-like structures and the chlorite occurs as interlocked fine-grained (< 0.01 mm) mosiacs between and around quartz grains. Some late veins contain accessory sericite, magnetite and sulfides. Pyrite is the principal sulfide, but chalcopyrite was observed in post-mineralisation faults. The later syn-tectonic fractures are typically flat lying, several centimetres wide and occur as en echelon vein sets filling tectonically created openspace.

5.4.5 Summary

In volcaniclastic rocks with weakly to moderately developed sericite ± chlorite, textural destruction was typically weak, and relict volcanic textures such as glass and pumiceous shards were commonly well-preserved. Relict perlitic textures, in some of the least-altered rocks, were enhanced by alignment of sericite and or chlorite around the rims of relict fractures. In the matrix, sericite ± chlorite replaced fine feldspar crystals, of irregular orientation, and smectite or other clays. Alteration of feldspar crystals (phenocrysts in coherent volcanic rocks) by sericite and chlorite was typically weak to moderate, uniform and pervasive and twinning was preserved. Sericite-chlorite assemblages partially replace ferromagnesian mineral crystals or K-feldspar, and sericite and chlorite are typically spatially associated with carbonate or epidote. Magnetite typically occurs with chlorite in amounts directly proportional to the amount of chlorite. Chlorite formed during regional metamorphism is typically coarse-grained and dull green, brownish or gray-green in plane polarized light, and is particularly well-developed in volcaniclastic and mass-flow deposits.

Devonian metamorphism produced a strong regional foliation and locally intense, fault-related cleavages in rocks with weakly developed sericite-chlorite assemblages. Chlorite formed during the Devonian metamorphism is bright grass-green colored in plane polarised light and commonly confined to syn-tectonic cross-fibre veins, although scattered irregular shaped masses up to several millimetres in diametre were observed.

5.5 TEXTURAL AND PETROGRAPHIC CHARACTERISTICS OF GRANITE-RELATED HYDROTHERMAL ALTERATION

Although the heat engine for mid-ocean ridge recharge, reaction and discharge zones is rising basaltic magma, rising granitic magmas at shallow depths in permeable volcanic host rocks are expected to produce similar zoned hydrothermal alteration systems. Reaction zones are localised and high temperature (>350^{0}C) and it is in these zones that leaching occurs and hydrothermal fluids acquire their chemical signatures (Alt, 1995). Discharge zones occur where the buoyant, high temperature fluids rise rapidly to the surface. Recharge, reaction and discharge zones are shown for the hypothetical hydrothermal circulation system around the Darwin Granite in Figure 5.1. The proximity of intense hydrothermal alteration assemblages to the CVC/Darwin Granite contact and the northward extending cupola region above the buried granite, support an interpretation that the hydrothermal circulation system was driven by heat from the intrusion of the granite. Multiple overprinting relationships between K-feldspar , sericite and chlorite assemblages, support an interpretation that initial high temperature alteration assemblages were overprinted by lower temperature assemblages and that multiple fluid pulses occurred.

The diffuse hydrothermal alteration styles observed in the study area have many similar characteristics to other mineralised granite systems (Lowell and Guilbert, 1970; Sheppard, 1977; Alderton et al., 1980; Beane, 1982; Titley, 1982; Ward et al., 1992; Sillitoe, 1993; Brauhart et al., 1998; Huston and Kamprad, in press). Diagenetic and burial metamorphic alteration styles were replaced by moderate to intense hydrothermal alteration assemblages near the granite. These assemblages were subsequently deformed by Jukesian and Devonian dynamic metamorphic events that resulted in the regional NNW foliation observed throughout the study area. Hydrothermal alteration minerals observed include sericite, chlorite, K-feldspar and quartz with lesser amounts of carbonate, pyrite, magnetite and other minor accessories.

Since weakly developed granite-related hydrothermal alteration assemblages are difficult to distinguished from assemblages resulting from diagenetic and burial metamorphic processes. Therefore, the following criteria were established to identify the effects of granitic alteration:

- Intensity of hydrothermal alteration. Moderate to intense replacement of mafic minerals, feldspars and quartz. Weak hydrothermal alteration assemblages are not distinguishable based solely on intensity.

- Degree of textural destruction. Rocks with moderate or greater degrees of non-tectonic textural destruction were interpreted to have formed from hydrothermal alteration when combined with moderate to intense hydrothermal alteration minerals and proximity to the Jukes Prospect and the Darwin Granite.

- Occurrence of accessory minerals that indicate either mass gain or mass loss. These minerals include pyrite, chalcopyrite, tourmaline or large amounts of magnetite/hematite.

Geochemical techniques (Chapter 6) may help unravel hydrothermal alteration assemblages from diagenetic and burial metamorphic alteration assemblages. Diagenetic alteration shows little

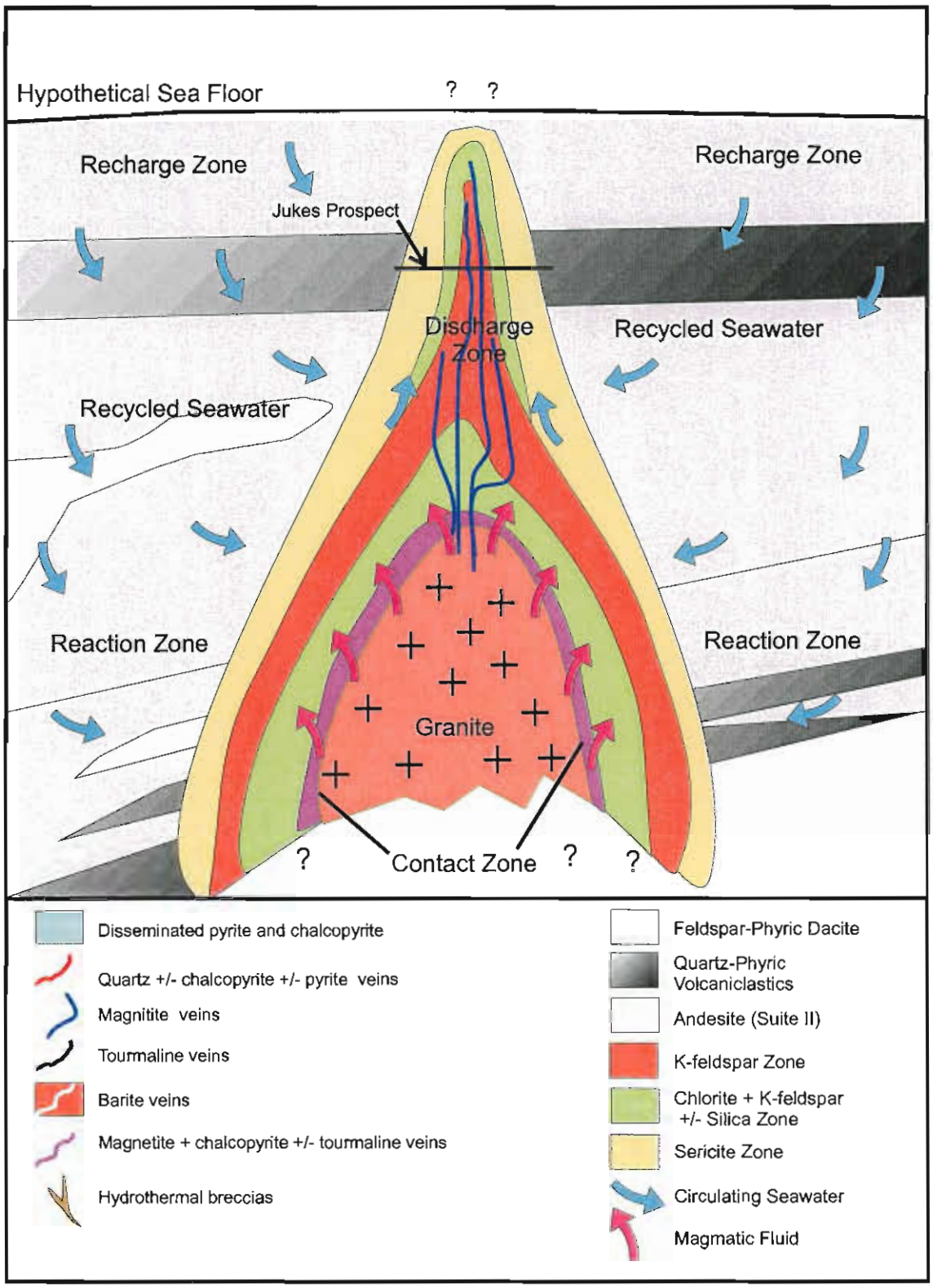

Figure 5.1. Schematic cross-section illustrating hypothetical recharge, reaction and discharge zones around the Darwin Granite. The figure represents pre-deformation, uplift and erosion conditions. The relationship to the broad hydrothermal alteration zones around the Darwin Granite and at the Jukes Prospect is shown (as discussed in 5.6). A large hydrothermal convective system was driven by heat from the Darwin Granite. Initial high temperature alteration zones were probably dominated by magmatic fluids. Mixed magmatic fluids and modified seawater then formed the hydrothermal alteration zones and mineralisation styles in the Jukes-Darwin area. Evidence for discharge of hydrothermal fluids onto the seafloor was not observed in the Jukes-Darwin area. Not to Scale

change in the bulk rock chemistry whereas hydrothermal alteration introduced marked mass changes.

5.5.1 Hydrothermal Alteration Styles in Volcanic Rocks in the Study Area

Hydrothermal sericite, chlorite, K-feldspar and silica alteration styles in the volcanic rocks surrounding the Darwin Granite were weakly to intensely developed and commonly destructive to all rock textures. Magnetite is a common accessory mineral with lesser amounts of pyrite, hematite, goethite, chalcopyrite and leucoxene.

5.5.1.2 SERICITIC-DOMINATED HYDROTHERMAL ALTERATION IN VOLCANIC ROCKS

Based on the petrographic descriptions in Section 5.2, alteration intensity, proximity to the Darwin Granite contact and the main hydrothermal and mineralisation centres in the study area, the amount of textural destruction and the lack of overprinting or cross-cutting relationships, three sericite alteration styles were interpreted to be of hydrothermal origin:

1) *Weak to moderate pervasive alteration of the groundmass, with scattered intensely altered domains and moderate textural destruction.* Small variable sized aggregates (<0.02-0.2 mm) of sericite replaced groundmass feldspar and quartz. Other sericite grains occur along intergrain boundaries and as replacements of groundmass feldspar around micropoikilitic quartz. Chlorite, magnetite and carbonate occur as accessory minerals. Typical secondary sericite assemblages are sericite ± chlorite, or sericite ± chlorite ± magnetite ± carbonate.

2) *Weak to intense, texturally destructive sericite replacement of relict pumice, lithic clasts and feldspar crystals.* The adjacent matrix is typically intensely altered. Light-green sericite ± quartz replaced lithic clasts and feldspar crystals along cleavages or via fractures. Feldspar crystals were later replaced by other alteration minerals.

3) *Veins and veinlets of sericite ± chlorite ± quartz ± carbonate.* Carbonate in hydrothermal veins at the Jukes Prospect was identified as dolomite (Doyle, 1990).

5.5.1.3 CHLORITE-DOMINATED HYDROTHERMAL ALTERATION IN VOLCANIC ROCKS

Six separate texturally destructive chlorite alteration styles were interpreted to be of hydrothermal origin based on the petrographic descriptions in 5.2. Although sericite typically occurs with chlorite and magnetite in many of the alteration assemblages described below, sericite and magnetite have never been observed in textural equilibrium in the study area.

The six styles are:

1) *Chlorite in the groundmass.* Moderate to intense chlorite-altered irregular domains of variable size occur as replacement of the sericite or sericite-chlorite. Complete groundmass replacement was not observed. Wispy pumice fragments were weakly to moderately replaced by secondary chlorite + sericite, or chlorite + magnetite (in vesicles). This alteration style corresponds to an observed increase in fracture density and is interpreted to have formed contemporaneous with

earlier fractures. Typical secondary chlorite groundmass assemblages are chlorite + sericite ± magnetite, or chlorite ± magnetite

2) *Chlorite replacement of phenocrysts and crystals.* Secondary chlorite ± sericite replaced plagioclase, biotite and other ferromagnesian mineral crystals. Chlorite replaced plagioclase crystals result in a dark-green spotted appearance to the rocks. Chlorite is interpreted to have replaced earlier mafic minerals that were the nuclei for magnetite. Typical assemblages in this alteration style are chlorite, chlorite + sericite, or chlorite ± magnetite

3) *Chlorite veins cut sericite ± chlorite-altered dacites.* Diffuse chlorite replaces sericite ± chlorite-altered volcanics on the edges of centimetre scale veins. Typical equilibrium vein assemblages are chlorite + quartz and chlorite + sericite ± quartz.

Styles 4 and 5 are probably not stable mineral assemblages but occur together commonly enough to be noted. However, chlorite-magnetite can occur together in the propylitized zones of porphyry copper deposits but it is a rare assemblage (D. Cooke, 2000 pers. com.). The chlorite may actually be a secondary alteration product of an earlier high temperature alteration phase such as biotite although no definitive evidence was observed to support this interpretation. It is also possible that the assemblages formed from different events, an earlier high-temperature biotite and/or tourmaline event overprinted by a later lower temperature chlorite event.

4) Pervasive diffuse secondary chlorite: This style of chlorite replacement typically occurs as moderate to intense chlorite replacement of groundmass lithic clasts and feldspar crystals and moderate to intense destruction of primary textures. Secondary chlorite replaced K-feldspar around fractures (Plate 5.11) and behind small centimetre scale diffuse solution fronts. Typical diffuse secondary chlorite assemblages include; chlorite ± sericite ± quartz and chlorite ± sericite ± magnetite.

5) *Chlorite ± sericite ± quartz ± tourmaline ± sulfide in veins and breccias.* Sulfides observed include pyrite and chalcopyrite. At Mt. Darwin, this alteration style was confined to veins, but at the Jukes Prospect this stage of chlorite was associated with the hydrothermal and phreatic brecciation. New fracture systems were created and old fracture systems were reopened. Chlorite + quartz + tourmaline ± magnetite occur as the matrix in hydrothermal breccias and fractures. The matrix encloses angular to subrounded, moderate to intensely K-feldspar-altered volcanic clasts and rounded to sub-rounded clasts of chlorite-altered quartz-feldspar porphyry and feldspar-phyric dacite.

6) *Chlorite ± pyrite veins.* In moderate to intensely K-feldspar-altered zones, fractures previously used by hydrothermal fluids were reopened, filled with chlorite ± pyrite, and have diffuse chlorite replaced edges.

5.5.1.4 K-FELDSPAR-DOMINATED HYDROTHERMAL ALTERATION IN VOLCANIC ROCKS

Moderately to intensely developed K-feldspar alteration styles interpreted to be of hydrothermal origin were confined to close proximity (<1 km) to the Jukes Prospect, Intercolonial Spur (Gadaloff, 1996) or the Darwin Granite contact. Overprinting relationships between alteration

Plate 5.11. Secondary chlorite replacement of K-feldspar altered dacite along Jukes Road.

A. Intense chlorite replacement of previously K-feldspar altered dacite. The chlorite alteration is intense and texturally destructive along fractures, but becomes progressively more diffuse with increasing distance away from the fracture. Locally this style of alteration totally replaces the earlier secondary K-feldspar. This outcrop is near the centre of the Jukes hydrothermal system on Jukes Road.

styles are uncommon. Although exact timing relationships were generally difficult to distinguish, it appears that the K-feldspar assemblage was usually overprinted by the sericite-chlorite assemblages. Although mutually overprinting relationships were observed suggesting multiple fluid pulses. In volcanic rocks, the two dominant K-feldspar alteration styles interpreted to be of hydrothermal origin were: 1) Texturally destructive pervasive cryptocrystalline K-feldspar which has replaced primary quartz and feldspar crystals, and feldspar rims of micropoikilitic quartz or other groundmass feldspars. Primary rock textures were destroyed. Intensely K-feldspar-altered rocks have a fine-grained pinkish-orange color and a sandy texture. 2) K-feldspar alteration assemblages replaced and surrounded earlier hydrothermal sericite-chlorite and chlorite-sericite assemblages. K-feldspar occurs in fractures within earlier-chlorite-altered dacites. Intense textural destruction extends outward from the fractures with decreased intensity. Chlorite-replaced phenocrysts were preserved outside of the alteration halo around fractures.

5.5.1.5 HYDROTHERMAL SILICA ALTERATION IN VOLCANIC ROCKS

At the Jukes Prospect and in the rocks near the Darwin Granite, silica alteration interpreted to be of hydrothermal origin occurred as pervasive cryptocrystalline quartz, to a limited extent, in all rock units mapped. The exact timing relationships to other alteration phases is unknown, although secondary cryptocrystalline quartz is typical in the presence of secondary K-feldspar. Intense silica alteration strongest in andesitic dykes on Mt. Darwin.

5.5.2 Hydrothermal Alteration in the Darwin Granite

5.5.2.1 HYDROTHERMAL ALTERATION IN THE PINK GRANITE

Based on the descriptions of the altered pink granite in 5.2.4.1, the alteration of primary micas to sericite (Plate 5.7C) was interpreted to be a result of hydrothermal alteration with fluid access along shrinkage cracks in the cooling granite. Based on jointing patterns and sericite alteration in and around fractures (Plate 5.7A), it is interpreted that the granite had crystallised prior to sericite alteration. Therefore, sericite alteration in the pink granite was controlled by fracture density, intergrain boundaries and porosity (Plate 5.7B). Fracture controlled sericite alteration was most intense near the white granite intrusions and supports the interpretation that the sericite alteration was hydrothermal in origin. Local areas of moderate to intense secondary chlorite occur near the white granite contacts and were also interpreted to be a result of weak hydrothermal alteration related to the white granite intrusion. Late open space fractures were filled with quartz and rimmed with sericite.

5.5.2.2 HYDROTHERMAL ALTERATION IN THE WHITE GRANITE

Hydrothermal alteration is not widespread in the white granite. However, weak to moderate secondary sericite assemblages near the contacts with the pink granite were interpreted to be of hydrothermal origin (Plate 5.12A).

Plate 5.12. Hydrothermal alteration in the Darwin Granite.

A. In the white granite, sericite totally replaced plagioclase (P) but original crystal shapes were preserved. Some of the quartz shows wavy extinction from metamorphic strain. Crossed polars, field of view width = 3.75 mm. Sample 2043.

B. Intense hydrothermal K-feldspar alteration in microgranite. Recrystallised quartz (Q), biotite (B) replacement of the groundmass, pyrite (P), potassic alteration of plagioclase to K-feldspar (K), and later sericite are shown. Sample B2028. Crossed polars, field of view width = 3.75 mm.

A

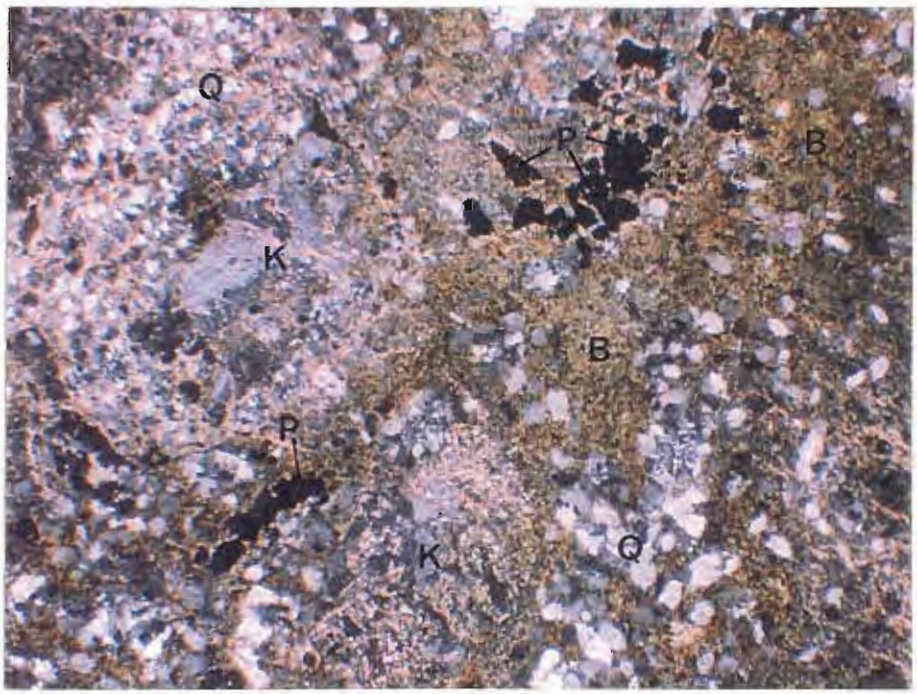

B

5.5.2.3 HYDROTHERMAL ALTERATION IN THE QUARTZ-FELDSPAR PORPHYRY

As in the white granite, hydrothermal alteration is not widespread in the quartz-feldspar porphyry. However, the weak to moderate secondary sericite assemblages and quartz + epidote (zoisite) ± tourmaline veins containing pyrite and chalcopyrite are interpreted to be of hydrothermal origin.

5.5.2.4 HYDROTHERMAL ALTERATION IN THE MICROGRANITE

Although the microgranite dykes are not voluminous in the Darwin Granite suite, those observed were hydrothermally altered. Intensely developed secondary K-feldspar, primary biotite replaced by sphene (titanite), secondary biotite development and the presence of disseminated pyrite and magnetite in the microgranite dyke on Mt Darwin are interpreted to be a result of hydrothermal alteration (Plate 5.12B).

5.5.3 Hydrothermal Alteration in Volcanic Rocks

5.5.3.1 HYDROTHERMAL ALTERATION IN THE YOLANDE RIVER SEQUENCE

The YRS occupies the western side of the Clark and Garfield Valleys (Figure 5.2) and is the farthest from the Darwin Granite of all units in the study area. In localised areas in the quartz-feldspar-phyric volcaniclastics and lavas, moderate sericite replacement is interpreted to be partially hydrothermal in origin. Typical examples are shown in photographs on Plate 5.13A. Hydrothermal sericite styles 1 and 2 and chlorite styles 1 and 2 were observed. K-feldspar phenocrysts were partially replaced by minor secondary sericite ± chlorite, primarily in the cores of crystals and along fractures and cleavage surfaces (Plate 5.13B-C). Secondary sericite and chlorite replacement of K-feldspar phenocrysts was less intense than in plagioclase phenocrysts where complete replacement by sericite ± chlorite was observed.

5.5.3.2 HYDROTHERMAL ALTERATION IN THE CENTRAL VOLCANIC COMPLEX

Feldspar-Phyric Dacite

Along the Jukes Road, a complete transition from weakly diagenetically altered dacite, with good textural preservation (5.4.2), to intense hydrothermally altered K-feldspar-rich rocks with total textural destruction is interpreted. In a general sense, hydrothermal alteration styles in the feldspar-phyric dacite transition from K-feldspar-dominated alteration styles at the centre of the hydrothermal system to chlorite and then sericite dominated assemblages with increasing distance from the centre of the Jukes Prospect. Zoning within this facies is described in 5.5.2. Plates 5.14A-G are photographs and photomicrographs showing typical sericite, chlorite and K-feldspar hydrothermal alteration styles with increasing proximity to the centre of the Jukes hydrothermal system.

Weak to moderate sericite and chlorite hydrothermal alteration styles are widespread in the area between the Jukes Prospect and the Darwin Granite. Weak groundmass sericite assemblages

Plate 5.13. Typical examples of hydrothermal alteration in YRS quartz-feldspar-phyric lavas.

A. A variety of appearances of fine to medium-grained quartz-feldspar-phyric lava. Left to right the rocks shown are B1077, B1098 and B2007. B1077 was K-feldspar-altered. B1098 and B2007 are typical of the weakly sericite and chlorite-altered rocks of this unit.

B and C. Plagioclase phenocryst (F) totally replaced by secondary sericite. Note the embayed and sub-rounded quartz phenocrysts (Q) set in a weakly foliated fine-grained matrix. Plate 5.13B is plane polarized light and Plate 5.13C is crossed polars. Field of view width = 6 mm. Sample B1098.

A

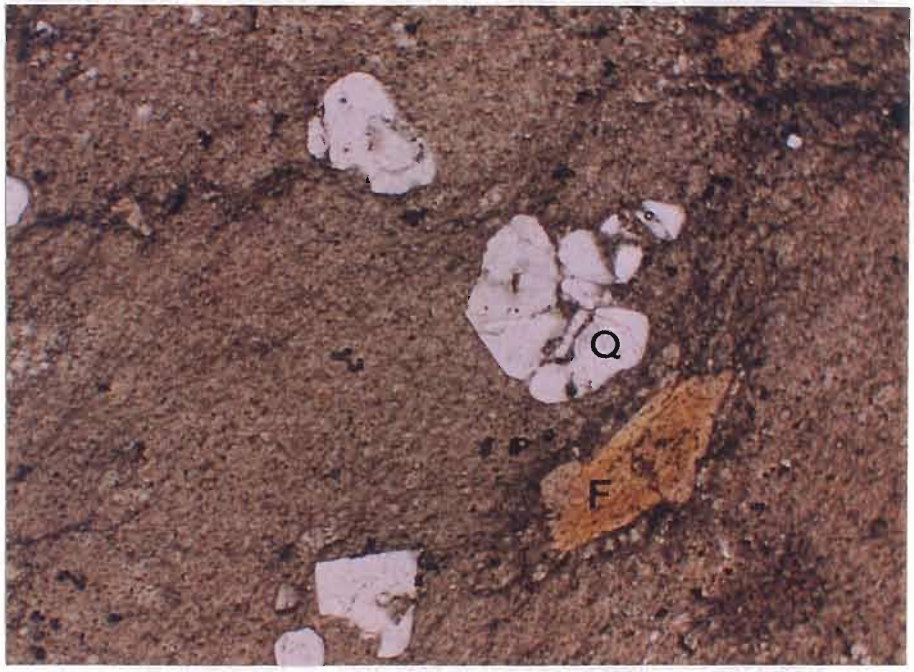

B

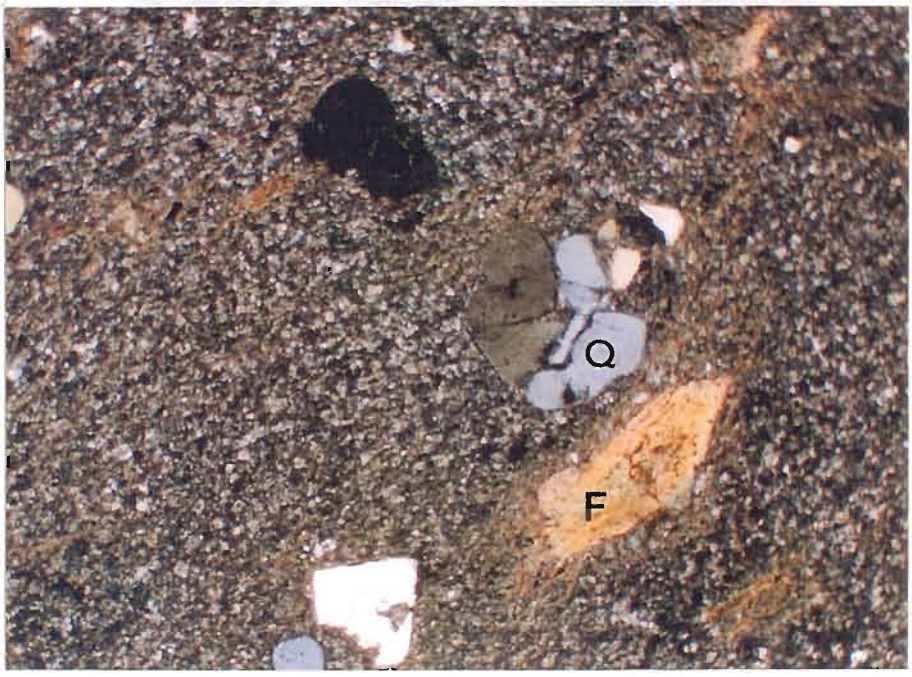

C

grade into chlorite + sericite assemblages as the hydrothermal system is approached, and abrupt localised changes were observed. Groundmass feldspar laths were typically replaced by sericite, sericite and chlorite, or chlorite (Plate 5.14B). However, relict micropoikilitic textures were preserved. Feldspar phenocrysts were weakly replaced by secondary sericite (Plate 5.14C) along fractures and twinned planes. In intensely altered zones, feldspar phenocrysts were 80-90% replaced by fine-grained secondary sericite, sericite + chlorite, or sericite + chlorite + carbonate (Plate 5.14G). Chlorite commonly replaced sericite in the cores of plagioclase crystals, the rims of which were subsequently replaced by later sericite. In addition, moderate to intense secondary sericite assemblages were observed replacing earlier secondary chlorite alteration assemblages (1, 2 and 3). These multiple overprinting relationship supports an interpretation of multiple fluid pulses. Typical chloritic assemblages are dominated by various intensities of chlorite ± sericite replacement of feldspars laths in a chlorite ± K-feldspar-altered micropoikilitic groundmass (Plate 5.14D). Moderately altered rocks are characterised by chlorite ± sericite replaced phenocrysts (Plate 5.14E) and textural destruction varies from weak to intense. Sericite is subordinate in rocks with intense secondary chlorite and weak to moderate secondary K-feldspar alteration assemblages. K-feldspar-altered rocks are characterised by intense secondary K-feldspar domains in the micropoikilitic groundmass (Plate 5.14F), the occurrence of magnetite and chlorite masses and moderate to intense textural destruction of phenocryst shapes. Magnetite ± carbonate ± leucoxene occur as accessory minerals in all of the assemblages observed.

Quartz-Feldspar-Phyric Volcaniclastics

In the Mt. Darwin area, the volcanic pile intruded by the Darwin Granite is dominated by feldspar-phyric dacitic lavas and the quartz-feldspar-phyric volcaniclastics are a minor component. Similarly, at the Jukes Prospect, the host rocks to the hydrothermal alteration and mineralisation is dominated by feldspar-phyric rocks and volcaniclastic rocks occur predominantly outside of the main hydrothermally altered areas. Therefore, hydrothermal alteration in the quartz-feldspar-phyric volcaniclastics of the CVC was not widespread in the rocks observed in this study. However, in the hydrothermally altered quartz-feldspar-phyric volcaniclastics observed, the intensely altered the fine-grained quartz and feldspar matrix is typically dense, silicified and has been replaced by moderate to intense secondary chlorite or K-feldspar alteration assemblages and pyrite has been altered to magnetite.

Quartz Feldspar ± Biotite Porphyry Dykes

Along Jukes Road, well-developed intense texturally destructive secondary chlorite assemblages within and along the margins of several quartz-feldspar porphyry dykes is interpreted to be of hydrothermal origin. Chlorite alteration style 4 was observed in the immediate contact zone of the dykes. Chlorite assemblages in and around the dykes are interpreted to have formed after dyke emplacement chlorite assemblages decrease in intensity with increasing distance from the dyke margins. This is interpreted to be evidence that fluid movement was controlled by the dyke margins. Hydrothermal alteration intensity was typically intense and dominated by chlorite, K-feldspar or chlorite + K-feldspar alteration styles (Plate 5.15). Alteration was typically texturally

Plate 5.14. Hydrothermal alteration styles in the feldspar-phyric dacite.

A. Photograph of three cut slabs representative of the three dominant hydrothermal alteration styles in the feldspar-phyric dacite. From left to right the rocks are, sericite-altered (Sample B2057), K-feldspar-altered (Sample 10220) and chlorite and sericite-altered (Sample B1009).

B. Sericite (S) and patchy chlorite (Cl) altered areas in a micropoikilitic groundmass. Groundmass K-feldspar laths (K) were unaltered but plagioclase laths were replaced with sericite. The opaque minerals are magnetite and leucoxene. Polarized light, field of view width = 2 mm. Sample 10310 (similar to the left hand rock in Plate A).

C. Weak to moderate sericite (S) replacement of the plagioclase feldspar (F) phenocryst occurred along twinning planes and fractures. Relict twinning was preserved. Polarized light, field of view width = 3.5 mm. Sample 10250 (similar to the left hand rock in Plate A).

D. Groundmass and micropoikilitic feldspars were moderately altered by chlorite (CL). Note fractures filled with quartz. Polarized light, field of view width = 2 mm. Sample 10290 (similar to the right hand rock in Plate A).

E. Feldspar phenocrysts were intensely altered to chlorite (Cl) + sericite (S) or sericite + chlorite assemblages. In this sample, two phenocrysts are shown with variable intensities of chlorite replacing earlier sericite. Groundmass feldspar laths were replaced by secondary chlorite. Polarized light, field of view width = 3.5 mm. Sample 10350 (similar to the right hand rock in Plate A).

F. Intense K-feldspar replacement of the groundmass. Destruction of micropoikilitic textures was variable from completely destroyed (C) in the upper left, to moderate (M) in the lower centre right. Chlorite and sericite occur as minor accessories. Polarized light, field of view width = 2 mm. Sample 10420 (similar to the middle rock in Plate A).

G. Intense chlorite + sericite-altered plagioclase phenocryst in an intensely K-feldspar-altered micropoikilitic groundmass. Chlorite replacement is intense along the quartz filled fracture suggesting that the fluids contained iron and magnesium. The groundmass is intensely K-feldspar replaced. Polarized light, field of view width = 3.5 mm. Sample 10220 (similar to the middle rock in Plate A).

A

B

C

D

E

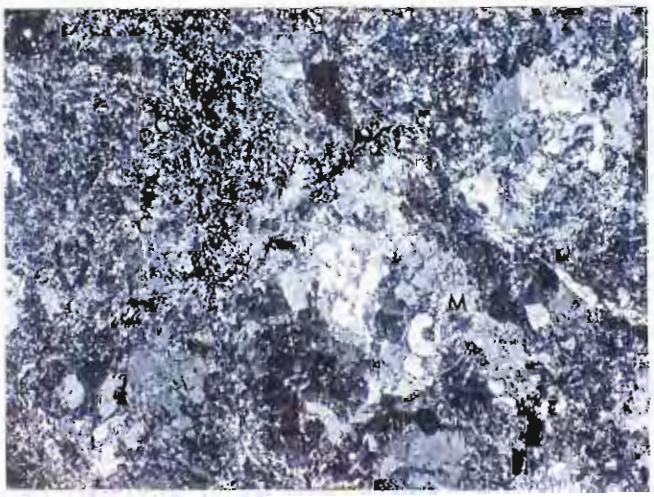

F

G

Plate 5.15. Typical hydrothermal alteration in quartz-feldspar ± biotite porphyry dykes of the CVC.

A. Cut slab of a K-feldspar-altered (reddish-brown) Quartz-Feldspar ± Biotite Porphyry (Sample MJ-96-4) from near the centre of the Jukes Road Cu-Au Prospect. Note the abundant quartz (Q) and feldspar (F) phenocrysts. Feldspar phenocrysts were altered to mosiacs of sericite + chlorite, chlorite ± sericite or sericite ± K-feldspar.


Q
cm

destructive to feldspar phenocrysts and quartz phenocrysts. Pyrite and chalcopyrite occur as accessory sulfides.

5.5.4 Other Alteration Styles

Distal hydrothermal alteration effects interpreted to be related to the Darwin Granite occur in the eastern Clark Valley as sporadic sericite ± chlorite or K-feldspar domains. However, at the Garfield Prospect, andesites intrudes YRS and CVC rocks and hydrothermal alteration assemblages occur that have similarities to Cu-Au mineralisation in the Prince Lyell deposit, at Mt. Lyell (Halley et al., 1996; Duncan, 1997). The principal similarity is a magnetite-apatite association discussed in detail in Chapter 6. The andesites were briefly examined in the current study and described in Sections 4.3.1.1 and 4.4.5. To summarise those sections, one of the Garfield andesites is a Suite I andesite and is interpreted to be comagmatic with a 'Murchison Granite-like' parental magma postulated to exist beneath the study area. The other two Garfield andesites have REE patterns similar to the Lyell-Comstock andesites and are typical Suite II rocks. A positive connection between the hydrothermal alteration around the andesites and the Darwin Granite cannot be made. A description of the altered andesites is included below.

Garfield Andesites

Andesites at the Garfield Prospect occur as two different hornblende-phyric coherent andesitic facies (Section 4.3.1.1.) conformable with the enclosing rhyolitic and dacitic volcanics of the YRS and CVC. Hand specimen photographs of typical altered andesite are shown in Plate 5.16A. The two andesites underwent intense hydrothermal alteration and original mineralogies and textures were destroyed. The rocks were intensely sheared by a post-alteration dynamic event (Jukesian or Devonian ?) and a well-developed cleavage formed. In one andesite, the groundmass is uniformly microcrystalline sericite, minor chlorite, relict feldspar and quartz with a trace of carbonate. Feldspar phenocrysts (up to 25%) were altered to masses of carbonate, carbonate + sericite, carbonate + chlorite, or carbonate + epidote (Plate 5.16B-C). These relict feldspar phenocrysts were later stretched, flattened and aligned with the cleavage in the rocks (Plate 5.16D). Relict hornblende phenocrysts (1-2%) were altered to elongate masses of chlorite with minor carbonate. Accessory minerals include apatite (to 1 cm, Plate 5.16E), euhedral pyrite grains (cubes to 0.8 cm), and chalcopyrite. Well-developed pressure shadows filled with carbonate, chlorite or sericite occur around quartz, apatite and sulfide grains. The second andesite is uniformly altered to microcrystalline chlorite with minor sericite and a trace of carbonate. Feldspar phenocrysts were altered to masses of carbonate + sericite or carbonate + chlorite. Hornblende was altered to elongate masses of chlorite with minor carbonate.

Plate 5.16. Hydrothermal alteration of the Garfield andesites.

A. Typical examples of hydrothermally altered Garfield andesites. In the sample on the left (B1067), feldspars were replaced by secondary sericite and hornblendes by chlorite. The groundmass was intensely replaced by secondary sericite. The right hand sample (B1048) is chlorite-altered with scattered relict sericite domains (white spots). Fine disseminated magnetite occurs throughout the two samples. Scale is in centimetres.

B. Relict feldspar phenocrysts (F) replaced by secondary masses of carbonate ± sericite ± chlorite. Relict hornblende phenocrysts (H) were altered to elongate masses of chlorite with minor carbonate. The entire rock has been sheared and a well-developed cleavage has formed. Polarized light, field of view width = 6 mm. Sample B1046.

C. Stretched apatite crystal (A) dismembered by shearing parallel to cleavage. Chlorite filled the interstices as the grain was pulled apart. Polarized light, field of view width = 1.9 mm. Sample B1064.

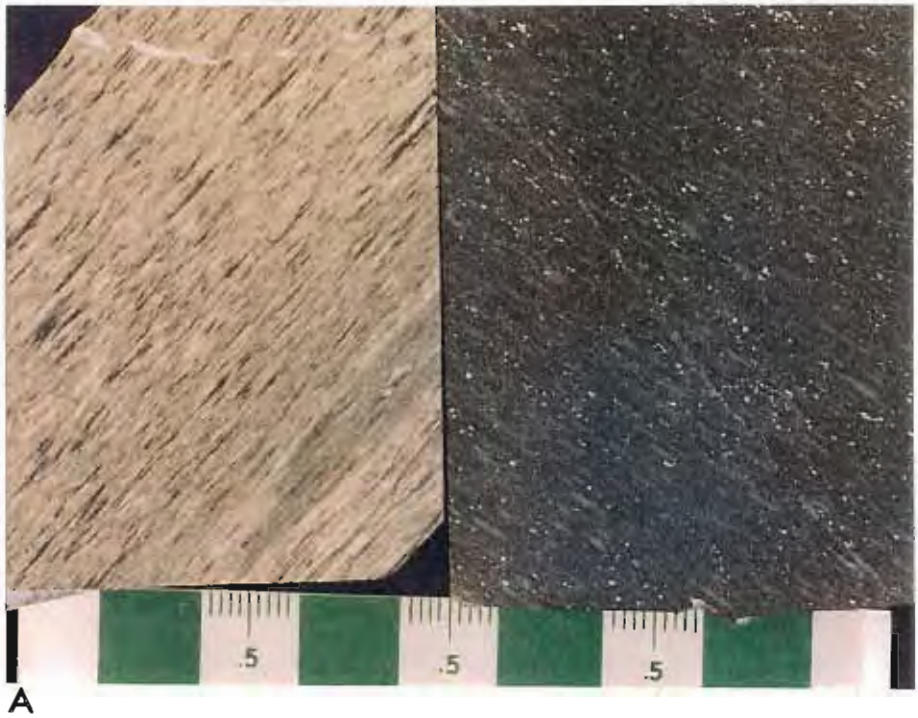

A

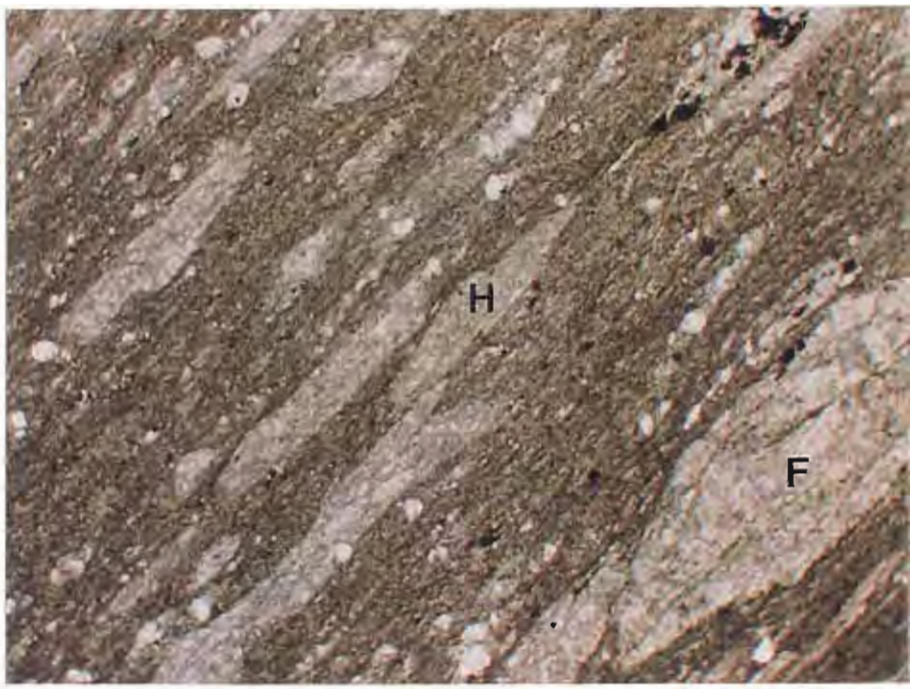

B

C

5.6 ZONATION OF GRANITE-RELATED HYDROTHERMAL ALTERATION STYLES

5.6.1 Zonation Around the Darwin Granite

The hydrothermal alteration styles and mineral assemblages discussed previously occur in zones in and around the Darwin Granite and are particularly well-exposed west of the granite contact on Mt. Darwin. The hydrothermal alteration extends northward through the Intercolonial Spur to the Jukes Prospect (Figure 5.2). The zones are based on field descriptions of the rocks used in compiling the geologic map of Mt. Darwin (Figure 5.3) and the Jukes Prospect (Figure 5.5). The field descriptions were supported by detailed petrographic descriptions of the rocks, summarised in 5.2.

Multiple episodes of replacement resulted in complex mineralogical relationships. Lateral hydrothermal alteration styles were typically pervasive, diffuse and moderate too intense within 1 km of the granite contact and decreased rapidly to 1.5 km. Beyond 1.5 km, weak pervasive hydrothermal alteration styles merged with, and became indistinguishable from, low-grade diagenetic and burial metamorphic alteration styles. Vertically, the hydrothermal alteration styles observed were most intense near the highly fractured zones near the contact with the Darwin Granite and at the Jukes Prospect. The vein paragenesis is discussed in Chapter 7. The vertical limits of the hydrothermal alteration system were destroyed by subsequent erosion. However, the Jukes Prospect is at least 1 km above the north plunging granite (Leaman and Richardson, 1989) and hydrothermal alteration styles similar to those at the Jukes Prospect and Intercolonial Spur were reported 5 km farther north (Corbett et al., 1993). Hydrothermal alteration was variable from weak to intense and was partially to totally destructive to rock textures. The surface expression of the hydrothermal alteration zones discussed below are diagrammatically illustrated in relation to the study area geology on Figure 5.2 and shown in detail near the Darwin Granite on Figure 5.3. Hydrothermal alteration zones along the western side of the Darwin Granite are schematically illustrated in Figure 5.4.

Within the pink phase of the Darwin Granite, pervasive hydrothermal alteration resulted in weak to intense secondary sericite ± chlorite domains. Hydrothermal sericite alteration in the white granite and quartz-feldspar porphyry was intense and tourmaline veins occur near the contact between the two granites. Secondary K-feldspar within the Darwin Granite was observed in the immediate (1 m) contact area with the volcanics and within one microgranite dyke.

Within a narrow zone (10-20 metres) near the granite contact, volcanic rocks were hydrothermally altered by intense secondary K-feldspar ± biotite (now chlorite) ± sulfides and quartz + K-feldspar ± sulfide alteration assemblages. Some of the rocks appear hornfelsed. Locally, coarse breccias occur with a matrix of magnetite ± tourmaline. Small (0.5-5.0 cm wide) magnetite and tourmaline veins with irregular orientation cut the breccias and the volcanics.

Outside of the immediate contact zone, five other zones (Zones 1-5) were recognised, although overlap occurs between the various alteration assemblages (Figure 5.4). In Zone 1 (>20 to 400-500 metres), overlapping moderate to intense secondary chlorite, moderate K-feldspar, weak to moderate silica and weak to moderate sericite alteration styles were observed. Locally, areas of intense chlorite ± quartz or K-feldspar ± quartz replacement occur. Observed alteration intensities vary with lithology with K-feldspar and silica intensities greater in volcaniclastic rocks.

Zone 1 alteration assemblages transition into Zone 2 alteration assemblages over a short distance and moderate to intense chlorite, weak K-feldspar and moderate silica alteration assemblages dominate from 500-700 metres (Figure 5.4). The difference between Zone 1 and Zone 2 is that K-feldspar alteration intensities were weak and in several areas K-feldspar assemblages were absent. Rocks in Zone 2 were cut by large (5 m wide) magnetite veins, and a network of smaller magnetite, magnetite + tourmaline and tourmaline veins.

Zone 3 is a 50-100 metre wide zone of intense silicification and weak to moderate chlorite alteration assemblages that occurs between Zone 2 and Zone 4 (Figure 5.4). In Zone 4, intense K-feldspar and moderate to intense silica alteration assemblages occur from approximately 800 to over 1000 metres above the granite contact. Chlorite and sericite alteration intensities were weak and were overprinted by intense assemblages of silica and K-feldspar. K-feldspar, silica, chlorite and sericite alteration assemblages were observed in this zone, and were probably a result of primary rock permeability. For example, on Mt. Darwin a welded pumiceous volcaniclastic horizon was weakly altered by sericite, with weak textural destruction, while nearby, andesites were totally replaced with K-feldspar and silica. Small (0.5-5.0 cm) magnetite, tourmaline and quartz veins were observed.

Zone 5 varies in width from 500 metres to >1 km and forms the transition zone into least-altered diagenetically and regionally metamorphosed rocks. On the east side of the Darwin Granite, hydrothermal sericite ± chlorite alteration intensities were moderate to intense and, locally, weak K-feldspar domains were observed. In the Clark Valley, west of the Darwin Granite, YRS rocks come to within 1-1.5 km of the granite contact where they interfinger with feldspar-phyric rocks of the CVC. Hydrothermal alteration assemblages occur as pervasive and patchy zones of weak to intense, texturally destructive sericite or sericite + chlorite alteration assemblages. Several minor occurrences of weak K-feldspar ± chlorite were observed.

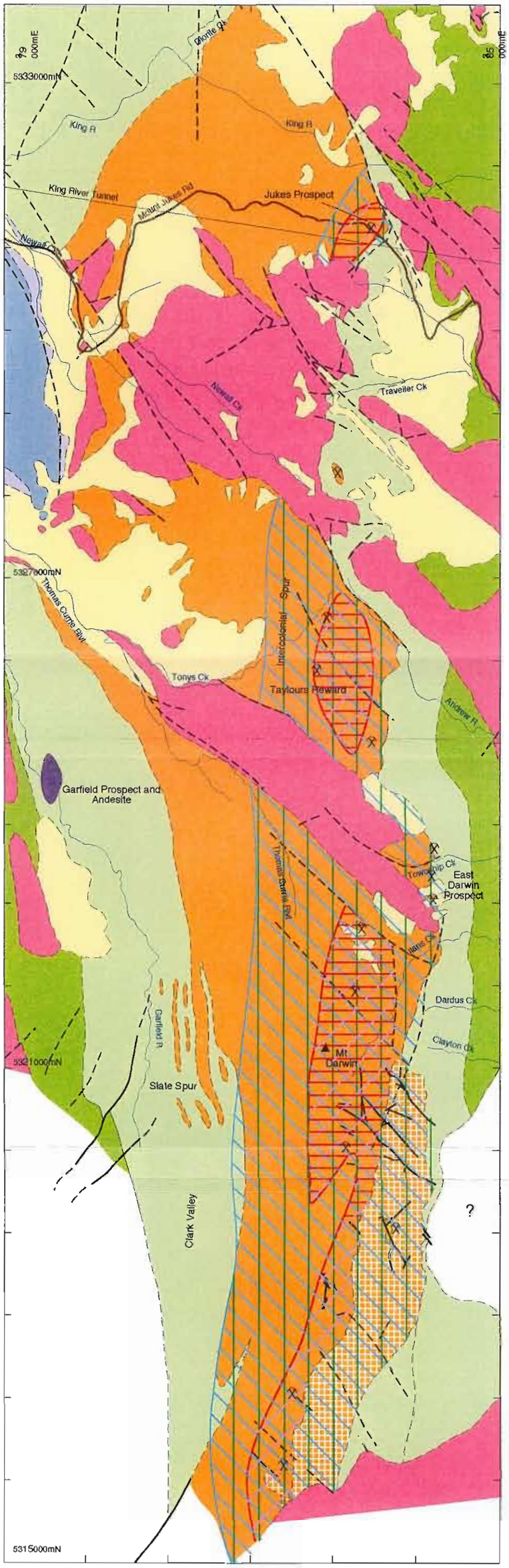

Figure 5.2 Generalised geological map of the study area showing aerial extent of the hydrothermal alteration. Data from Corbett et. al. (1993), Gadaloff (1996) and this study.

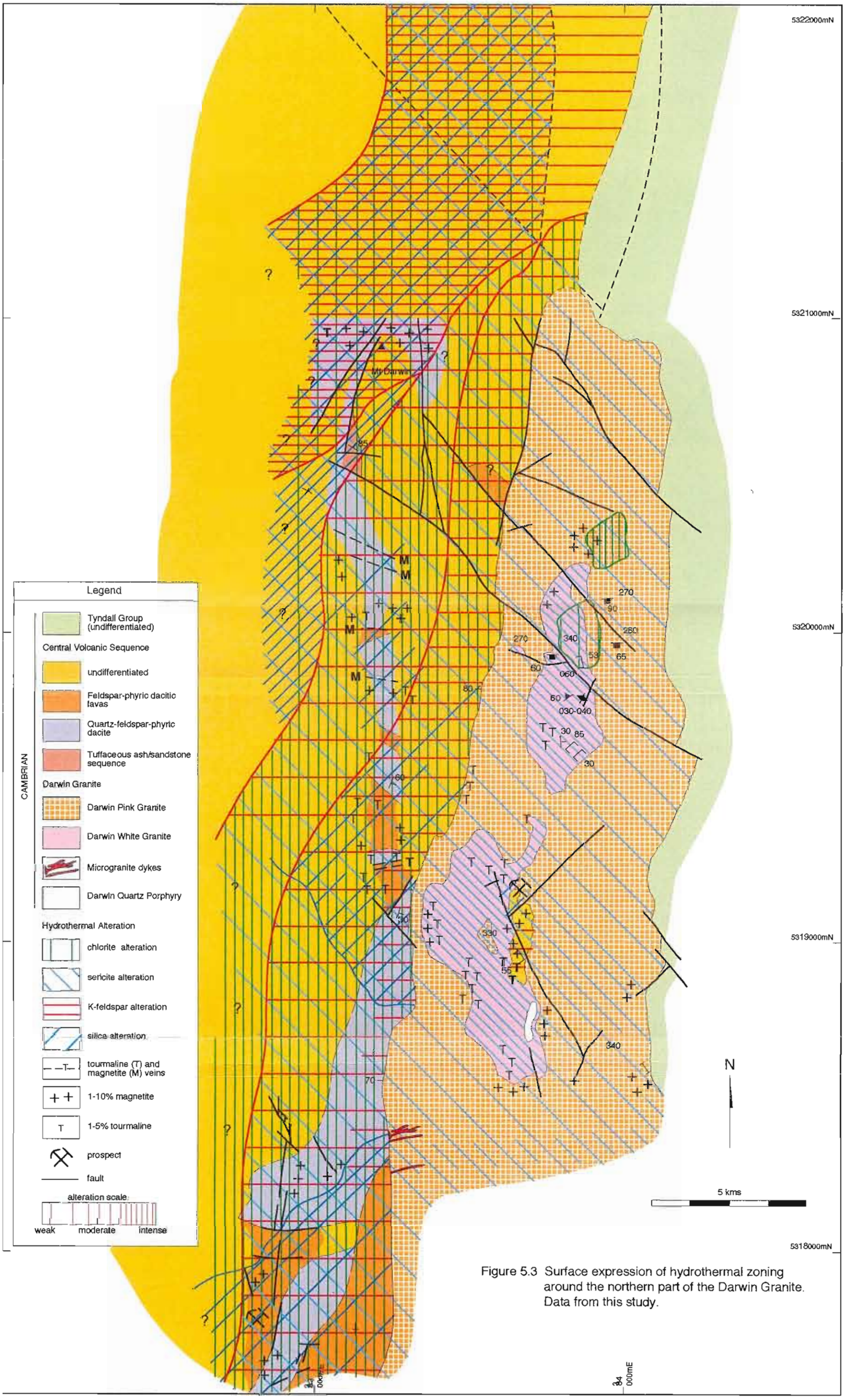

Figure 5.3 Surface expression of hydrothermal zoning around the northern part of the Darwin Granite. Data from this study.

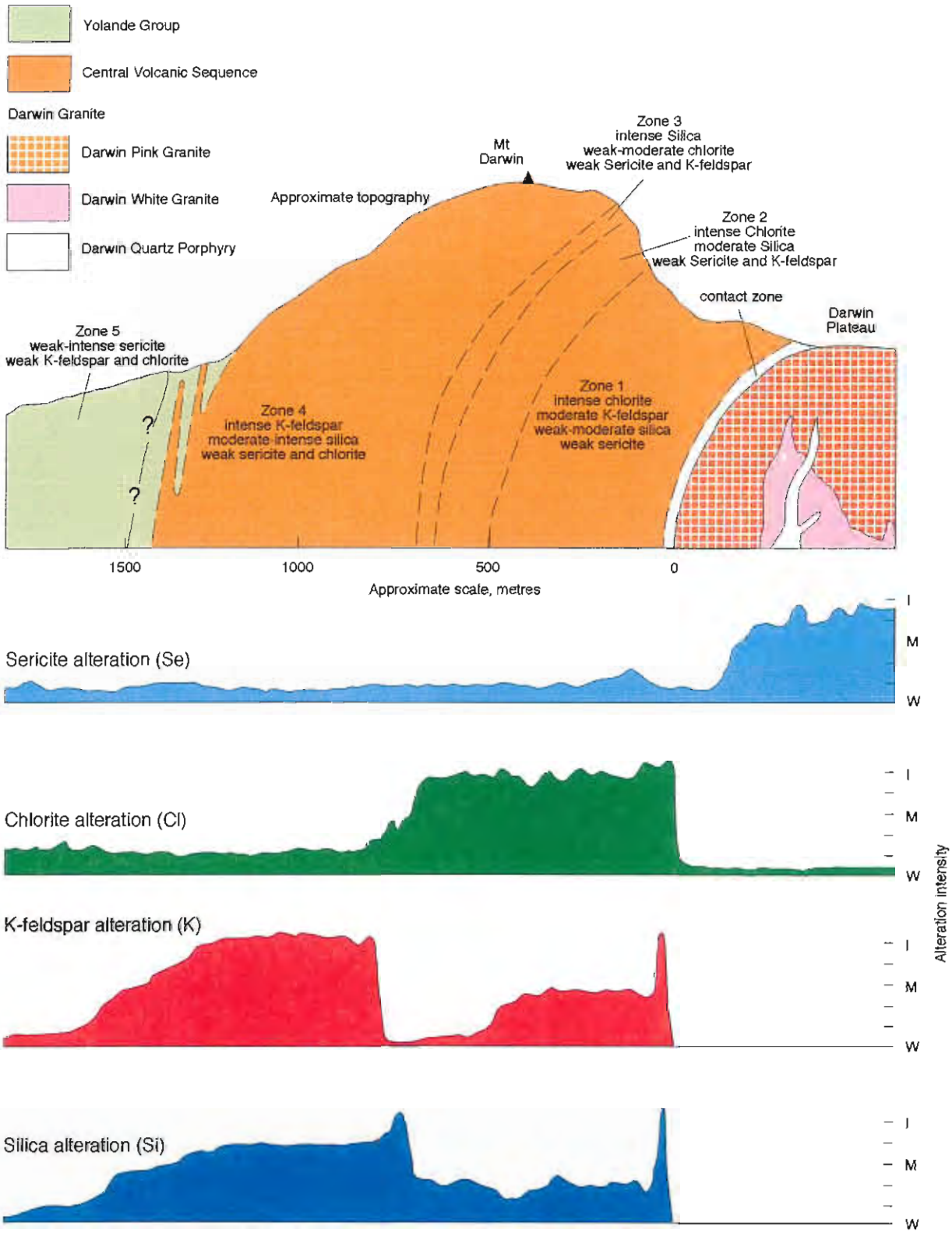

Figure 5.4 Schematic diagram of hydrothermal alteration zones on the western side of the Darwin Granite

(scale: I = intense, M = moderate, W = weak; alteration zones 1-5 discussed in the text)

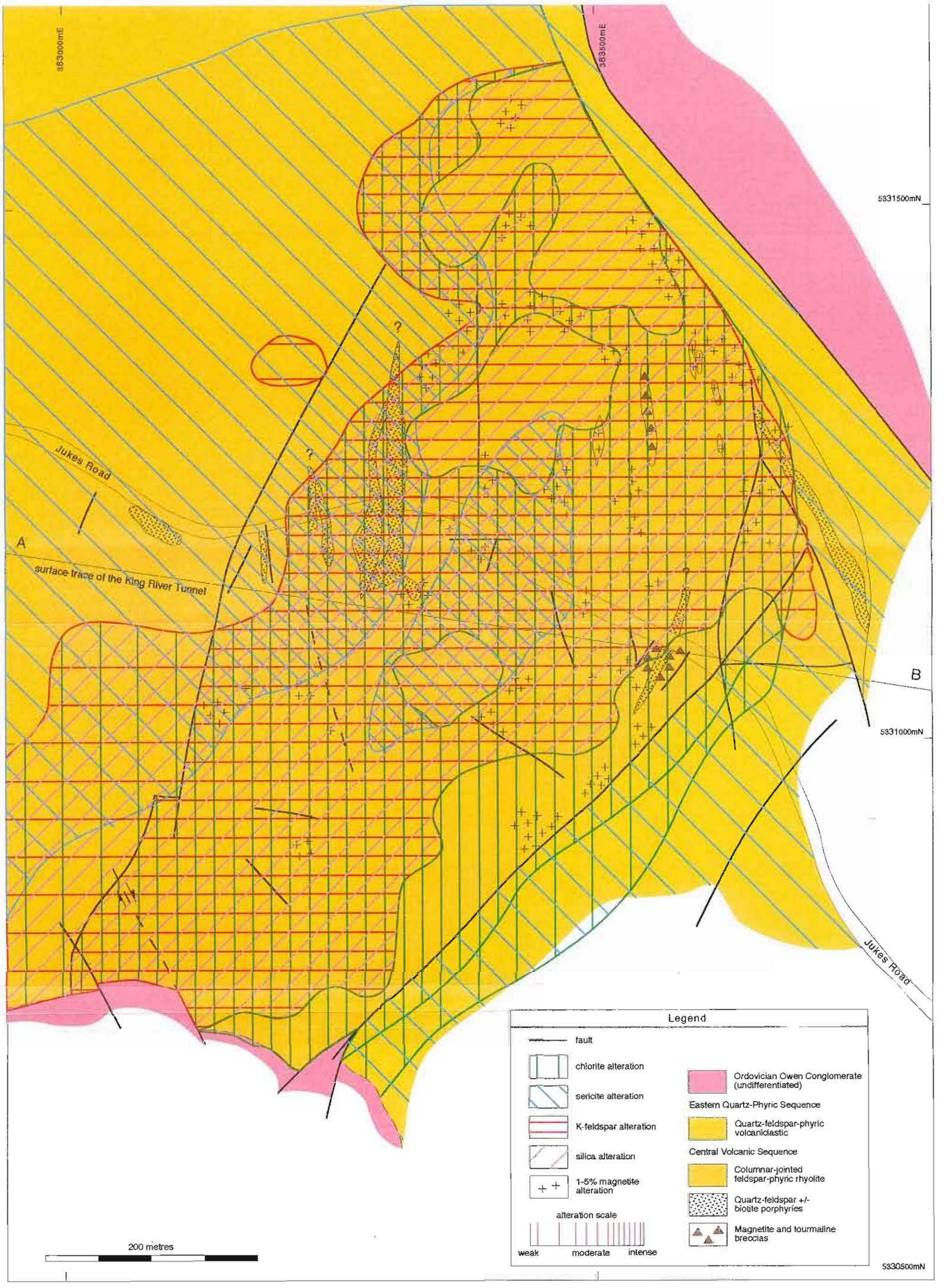

Figure 5.5 Surface expression of hydrothermal alteration zones at the Jukes Prospect.

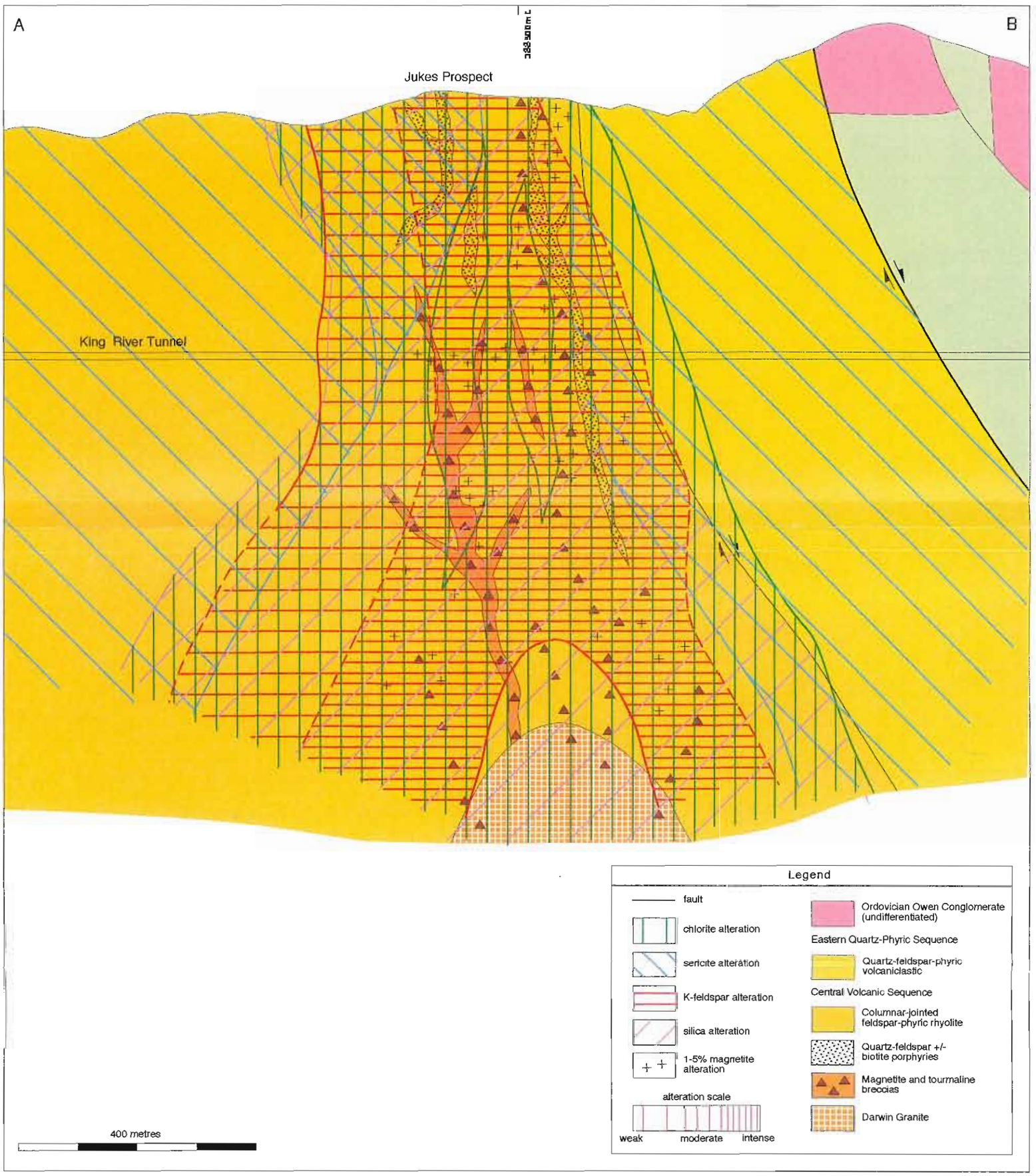

Figure 5.6 Cross-section along the King River Tunnel (KRT) and Jukes Road showing hydrothermal alteration zones. Surface data and data along the KRT are from this study with liberal interpretation below the KRT based on relationships in the Mt. Darwin area. Data modified from Large et. al. (1996).

5.6.2 Alteration Zones along Jukes Road

Along Jukes Road, a transition occurs from diagenetic/metamorphic sericite ± chlorite alteration styles and assemblages in the west into intense hydrothermal alteration styles of K-feldspar, silica, chlorite and sericite at the Jukes Prospect. Hydrothermal alteration styles are zoned with an inner zone of intense K-feldspar and middle and outer zones of chlorite and sericite alteration styles. A large fault on the east side of the prospect offset the eastern portion of the hydrothermal alteration system and juxtaposes weak sericite + chlorite-altered EQPS and Tyndall Group quartz-phyric volcaniclastics rocks against intense chlorite and K-feldspar-altered feldspar-phyric rocks of the CVC. Near the 10-20 metre wide fault zone, hydrothermal alteration effects within the EQPS and Tyndall Group are restricted to distal hydrothermal sericite ± chlorite alteration assemblages and transition into regionally altered and metamorphosed rocks over a short distance. The Jukes Prospect is predominantly hosted within the feldspar-phyric dacite of the CVC. The surface expression of the Jukes hydrothermal system covers an area approximately 1 x 1 km and is shown on Figure 5.5. A cross- showing the vertical hydrothermal alteration zones through the King River Tunnel is shown on Figure 5.6. The widths of the zones described below represents widths as measured along the Jukes Road and in the King River Tunnel.

Hydrothermal alteration styles at the Jukes Prospect are interpreted to represent lateral alteration styles around a hydrothermal vein system. Multiple episodes of replacement resulted in mixed domains of alteration assemblages. The centre (10200 metres along Jukes Road) of the hydrothermal system is a 10-30 metre wide zone of intense K-feldspar and chlorite-altered rocks intruded by hydrothermal breccias and cut by magnetite ± tourmaline ± sulfide veins. The following discussion will describe the zonation as observed from the centre of the hydrothermal system outward.

The hydrothermal K-feldspar zone is approximately 300 metres wide and overprints all earlier chlorite and sericite domains, although small (a few square metres in size) relict domains occur. The K-feldspar zone was subdivided into five separate groundmass mineral assemblages that occur in inner, mid and outer zones. A gross transition from intense inner alteration assemblages to intense, moderate and weak outer transition zone alteration assemblages was observed.

The five groundmass (matrix) alteration assemblages are:

Zone	Intensity	Alteration assemblage
Inner to 50 metres	Intense	K-feldspar
Inner to 50 metres	intense	K-feldspar + quartz
Inner to 100 metres	Intense	K-feldspar + quartz ± chlorite ± sericite
Mid, 50-200 metres	Intense to moderate	K-feldspar + sericite + chlorite ± magnetite
Outer (> 200 metres)	Moderate to weak	K-feldspar + sericite ± chlorite ± magnetite

The inner K-feldspar zone was intensely silicified and most original rock textures were destroyed. The hydrothermal breccia occurs in this zone and clasts within the breccia were intensely K-feldspar and quartz-altered. In the mid-K-feldspar zone, relict feldspar crystals were partially replaced by an assemblage of sericite + chlorite. In the outer zone, feldspar crystals were entirely replaced by secondary sericite + chlorite, and relict zones of sericite and chlorite assemblages were observed.

Chlorite-altered rocks occur throughout the Jukes Prospect. In the centre of the hydrothermal system, intense chlorite assemblages occur in the hydrothermal breccia matrix and in the series of veins and fractures that radiate outward from it. Pervasive secondary chlorite replaces K-feldspar-altered rocks within several centimetres of vein contacts. Intense chloritic-altered rocks occur within the fault zone between the EQPS and the CVC. Rocks outside the fault zone were weakly sericite ± chlorite-altered.

A middle zone of intense to moderate hydrothermal chlorite assemblages overlap the middle K-feldspar zone and a clear separation of the two alteration styles was not possible. In the middle zone, (50 to 200 metres), scattered domains of chlorite ± sericite ± K-feldspar alternately replaced, or were replaced by secondary K-feldspar alteration assemblages. A narrow outer chlorite + sericite zone with scattered K-feldspar and sericite domains separates the outer K-feldspar zone from a wide zone of sericite alteration assemblages. In the outer chlorite zone, scattered K-feldspar domains surrounded and partially replaced by secondary chlorite assemblages are interpreted to represent evidence for multiple hydrothermal alteration episodes. Feldspar crystals within the chlorite zones were 80-100 % replaced by sericite + chlorite. Secondary chlorite alteration assemblages in the middle and outer zones are, chlorite + sericite + magnetite ± K-feldspar ± quartz and chlorite ± sericite ± magnetite.

Hydrothermal sericite alteration styles at the Jukes Prospect occur in three zones: inner, middle and outer. Inner zone sericite assemblages of variable intensities were replaced by secondary K-feldspar and chlorite alteration assemblages within 200 metres of the centre of the system. Inner zone sericite alteration styles were, therefore difficult to separate from either the K-feldspar or chlorite alteration styles, although scattered relict domains were observed. With increased distance from 200 metres, sericite alteration assemblages observed were:

1. Sericite + magnetite (in feldspar phenocrysts)
2. Sericite + chlorite ± K-feldspar
3. Sericite ± chlorite ± magnetite
4. Sericite ± chlorite ± carbonate (in groundmass (matrix) and feldspar crystals)

From 200-300 metres, the outer chlorite zone transitions into a mid-sericite zone of intense secondary sericite + chlorite ± magnetite. This assemblage replaced groundmass feldspar but feldspar crystals were replaced by sericite + magnetite. Relict zones of weak diffuse and fracture controlled K-feldspar were observed and are interpreted to represent an earlier or distal hydrothermal K-feldspar alteration style. In addition, relict diagenetic and later metamorphic

chlorite and sericite alteration styles were observed. An outer, weak sericite halo occurs from approximately 300-700 metres and forms a transition zone from hydrothermal alteration styles into diagenetic and burial metamorphic alteration styles. Hydrothermal alteration assemblages observed in this zone were moderate to intense sericite ± chlorite ± carbonate in the groundmass and sericite + quartz ± carbonate in feldspar crystals. A weak foliation in the groundmass is interpreted to represent a burial metamorphic texture. Moderate to intense hydrothermal alteration assemblages decrease to weak sericite ± chlorite assemblages over approximately 50 metres and by 750 metres from the hydrothermal systems centre are indistinguishable from earlier regional alteration styles.

5.7 DISCUSSION

Hydrothermal alteration zones at Mt. Darwin and the Jukes Prospect are interpreted to represent different parts of the same hydrothermal system. Hydrofracturing of the cupola region above the granite resulted in emplacement of the hydrothermal alteration styles, veins and ore minerals. Initial sericite and chlorite alteration assemblages were associated with the initial fracturing and vein formation around and above the granite. As the fracture system evolved, the Jukes hydrothermal system became part of the discharge zone. Hydrothermal sericite, chlorite and K-feldspar alteration assemblages formed throughout Jukes Darwin area. By the end of the fracture system evolution, widespread hydrothermal fluids had altered rocks at least 1.5 km from the granite margin (reaction zone), as observed in the Clark Valley and vertically in the Intercolonial Spur and Jukes Road area. The vertical extent of the hydrothermal system remains unknown.

The well-defined hydrothermal alteration zones are interpreted to have formed from diffuse circulation of hydrothermal fluids through the rocks. Fluid access was enhanced by hydrothermal brecciation that resulted in a series of barren alteration-related fracture networks and magnetite and tourmaline veins. Multiple hydrothermal episodes occurred, resulting in complex overprinting mineralogical relationships.

Although sericite and chlorite alteration assemblages can occur as a result of regional greenschist facies metamorphism, moderate to intense assemblages that transition outwards from the hydrothermal chlorite and K-feldspar assemblages are interpreted to be hydrothermally related. As the hydrothermal system expanded, weak sericite alteration assemblages were replaced by secondary chlorite and K-feldspar.

Hydrothermal K-feldspar alteration styles are confined to the fractured cupola zone above the granite. Silicification occurred with K-feldspar but chlorite formed after the initial secondary K-feldspar assemblages and continued throughout the duration of the system. Along the Jukes Road, the feldspar-phyric dacite and the quartz-feldspar porphyry were hydrothermally altered. The quartz-feldspar porphyry was altered by chlorite but not by K-feldspar. The hydrothermal breccias contains clasts of quartz-feldspar porphyry and K-feldspar-altered dacite. They therefore intruded after the initial hydrothermal K-feldspar alteration assemblages.

CHAPTER 6

6.0 THE GEOCHEMISTRY OF HYDROTHERMAL ALTERATION IN ROCKS OF THE JUKES-DARWIN AREA

6.1 INTRODUCTION

The Cambrian granites in western Tasmania have been subjected to a long history of evolution that includes: 1) hydrothermal alteration, 2) Late Cambrian uplift (Jukesian Orogeny) and 3) metamorphism in the Mid-Devonian Tabberabbereran Orogeny. As a result, pristine samples of unaltered granite were not obtained for study (Chapter 3) and the geochemistry of the granites reflects this history. This chapter reviews and re-evaluates the existing geochemical data for the Murchison, Darwin and Elliott Bay Granites, and provides new whole rock, trace element, and rare earth element (REE) for the Darwin Granite. The granites are then classified using various classification schemes from the literature.

Electron microprobe analyses of chlorite, sericite and carbonate in altered volcanic rocks were examined in an attempt to quantify their compositions and relate the mineral chemistry to the hydrothermal mass changes in the study area. In addition to microprobe analyses, compositional variations in sericites and chlorites were conducted using PIMA (Portable Infrared Mineral Analyser) on representative rocks from the Jukes Road and Mt. Darwin.

Alteration systems around the Cambrian granitic rocks in the MRV have been discussed previously by several authors (Polya et al., 1986; Eastoe et al., 1987; Jones, 1993; Gadaloff, 1996; Large et al., 1996). They provided mineralogical and textural descriptions of the rocks, However, discussions of hydrothermal alteration geochemistry have typically been based on major element or trace element concentration data normalised to 100% volatile free, data where compositions are described as portions of a whole (percentages and ppm). Correlation analyses produced from those data are potentially flawed because the forced closure can produce results that can be geologically meaningless (Aitchison, 1984; Rollinson and Roberts, 1986; Rollinson, 1992; Aitchison, 1997). Since one of the major goals of the current study is to characterise mass gains and losses in the end members of the hydrothermal alteration styles (Section 5.5), the method of calculating mass changes developed by MacLean and Kranidiotis (1987) and MacLean and Barrett (1993) was applied to the Jukes Prospect and Mt. Darwin data. Mass changes between the alteration end members are then compared for the Jukes Road feldspar-phyric dacite and the Mt. Darwin area. Alteration reactions are presented to support the mass changes observed.

6.2 GEOCHEMISTRY OF THE CAMBRIAN GRANITES IN THE SOUTHERN MT. READ VOLCANICS

6.2.1 Sampling and Analytical Methods

A data base of major element and trace element geochemical analyses of the Darwin, Murchison and Elliott Bay Granites has been compiled from the available literature, from personal communication with various workers and from new analyses conducted during this study. These results are summarised in Table 6.1 and the entire data set is available in Appendix C. The major elements were recalculated to 100% anhydrous to remove variations due to different loss on ignitions. The following discussion focuses on the Darwin Granite with reference to, and comparison with the Murchison and Elliott Bay Granites as necessary.

Representative samples of the Darwin Granite and surrounding volcanic rocks were collected from surface exposures for major and trace element analysis. The largest possible representative rock samples were crushed with a steel jaw-crusher and 1 cm fragments were hand-picked to remove weathered rinds, vein material or unrepresentative fragments that might otherwise contaminate the data. The rock chips were then crushed to powder in a tungsten-carbide disc mill. This powder fraction was used for all whole rock, trace element and isotopic analyses.

Analysis of major, trace and some rare earth elements was carried out in the Geology Department of University of Tasmania by X-ray fluorescence techniques. Major and trace element were analysed on a Phillips XRF spectrometer following the methods of Norrish and Hutton (1969). Analytical precision was monitored by including in-house rock standards, TASGRAN1 (granite), and TASBAS (basalt) and internationally recognised rock standards RGM1 (rhyolite), AWQUARTZ (pure), GSP1 (granodiorite), SDC1 (mica schist), BCR1 (basalt), BIR1 (basalt) and MICAFE (biotite). Loss on ignition (LOI) was measured as the weight percent loss of 1g of powdered sample heated to 1000^{0}C for 12 hours, followed by 5 hours at 400^{0}C. Trace elements were analysed on 6g pressed powder pellets coated with boric acid using the method described by Norrish and Chappell (1969). A few REE analyses were performed by ICP/MS methods at Analabs Laboratory in Perth, Australia. Oxygen isotope analyses were performed in the Geology Department of the University of Tasmania and at the Oxygen Isotope Lab at the University of Arizona (USA) in collaboration with Dr. Mark Barton.

6.2.2 Major, Trace and Rare Earth Elements

The application of major and trace element geochemistry to rock classification is widely used in igneous petrology. Either individually or separately, major element and trace element data is useful in defining the genetic classification of granitic rocks. In addition, trace element data provides information about the tectonic setting and source of the granite magma and information about the crystallization history of the magma itself (Pearce and Cann, 1973; Evans and Hanson, 1993). Major elements as defined in the current study are restricted to the oxides of Si, Al, Fe, Mn, Mg, Ca, Na, and K. Ti and P are treated as major and trace elements even though their analytical results are reported in percent oxides.

Trace element movement during crustal anatexis is dependent upon whether they reside: 1) as trace elements in major minerals (eg. Li, Rb, Cs, Sr, Ba, Eu, Ga, and Ge); 2) as essential structural components in accessory minerals (eg. Zr, Y, Th, U and REE other than Eu); or 3) as trace elements in accessory minerals (eg. Nb, Ta, V, Cr, Cu, Zn, Ni, and Co; Bea, 1995). As shown in Table 6.1, trace element concentrations in the Darwin, Murchison and Elliott Bay Granites are variable. It was difficult to obtain pristine samples from the Cambrian granites in western Tasmania. Most of the samples collected for this and previous studies contain at least some evidence of either hydrothermal or metamorphic alteration, and it was therefore impossible to define a pristine sample from any of the granites. None-the-less, it is feasible that some trace elements were immobile during late stage alteration/metamorphism and can therefore, still yield useful information about the genesis of the granite and its alteration history.

6.2.2.1 Immobile Elements

Immobile Elements within the Granites

Within granitoids, element mobility can occur as a result of metamorphism or hydrothermal activity. Scattered trends on Harker diagrams suggest element mobility, although chemical alteration can sometimes produce systematic changes that mimic other mixing processes such as crystal fractionation. Common immobile elements in hydrothermally altered zones are Al, Ti, Zr, Nb, Y, REE, Hf, Ta, and Th. These elements retain their initial ratios (Al/Ti, Nb/Zr, Ti/Zr) during alteration and produce linear trends that ideally pass through the precursor and the origin of a binary plot (Barrett and MacLean, 1994). Small amounts of scatter are normally due to inhomogeneities in the samples and analytical errors (Barrett and MacLean, 1994). The main criteria for defining an element as immobile is the lack of scatter on variation diagrams, in other words, the variation diagrams have linear trends indicating a consistent ratio between the elements plotted. A lack of consistent data for Hf, Ta and Th in the Cambrian granites of the current study preclude their use as immobile elements.

Binary plots of TiO_2, Al_2O_3, Fe_2O_3, MgO, CaO, Na_2O, K_2O and P_2O_5 vs. SiO_2 are shown for the Darwin, Murchison and Elliott Bay Granites (Figures 6.1 to 6.8). The decreasing linear trends shown in the plots of TiO_2, CaO, Fe_2O_3, MgO and P_2O_5 vs. SiO_2 (Figures 6.1, 6.2, 6.5, 6.7 and 6.8) may be generated through fractional crystallization (Bateman and Chappell, 1979; Cox et al., 1980; Clark, 1992), partial melting or magma mixing (Wall et al., 1987; Chappell, 1996). The wide scatter of CaO, Na_2O and K_2O vs. SiO_2 data (Figures 6.2, 6.4 and 6.6) is interpreted to be the result of post emplacement alteration events. Detailed discussion of the alteration within and around the granites is discussed in Chapters 5. TiO_2, Al_2O_3 and P_2O_5 vs. SiO_2 (Figures 6.1, 6.3 and 6.8) have pronounced linear trends. It was therefore concluded that these elements were immobile in the Darwin, Murchison and Elliott Bay Granites.

Table 6.1 Summary of major and trace element geochemistry for the Cambrian granites. Data summarised from White (1975), Polya (1981), Polya et al. (1986), McNeil and Corbett (1988), Abbott (1992), Crawford et al. (1992), Stolz and Large (1992), Jones (1993) and Hunns (1998, unpublished). The Murchison granite values are based on an average of five granite types, diorite through granite. Major elements in wt.%, trace elements in ppm, N/A = not analysed, Total Vol. Free = Total recalculated on a volatile free basis.

	Darwin Granite		Murchison Granite		Elliott Bay Granite	
	Average		Average		Average	
Element	22 analyses	Range	34 analyses	Range	24 analyses	Range
SiO_2	77.10	69.87 - 80.74	68.38	58.2 - 80.81	74.52	69.25 - 77.86
TiO_2	0.21	0.06 - 0.61	0.57	0.13 - 1.04	0.34	0.11 - 0.55
Al_2O_3	13.41	9.73 - 14.73	14.44	9.98 - 21.76	13.22	12.07 - 14.02
Fe_2O_3	2.08	0.33 - 13.48	4.15	0.41 - 8.25	2.16	0.06 - 7.04
MnO	0.03	0.00 - 0.24	0.17	0.02 - 0.32	0.07	0.01 - 0.75
MgO	0.36	0.08 - 1.16	1.93	0.01 - 3.79	0.86	0.13 - 2.70
CaO	0.21	0.01 - 1.00	2.92	0 - 6.09	1.33	0.11 - 2.38
Na_2O	2.42	0.06 - 4.70	2.52	<0.02 - 6.66	2.65	1.05 - 4.64
K_2O	4.81	1.10 - 9.92	4.86	0.67 - 8.70	4.77	2.87 - 6.14
P_2O_5	0.03	0.00 - 0.13	0.12	0.00 - 0.23	0.07	<0.01 - 0.17
Total Vol. Free	100.65	99.7 - 102.69	100.05	99.99 - 101.71	100.00	100.00
S	0.1	<0.01 - 0.26	NA	NA	801	<100 - 4100
Sc	3.8	1 - 14	18	10 - 21	7.1	3 - 15
Ti	1236	359-3657	1859	2 - 5216	2038	659-3297
V	24	<1.5 - 156	76	6 - 188	42	8 - 112
Cr	2.5	1 - 4	3.0	1 - 110	57	9 - 117
Co	NA	NA	NA	NA	11	<4 - 13
Ni	2.0	<1 - 5	4.6	1 - 9	17	4 - 67
Cu	15	3 - 97	15	1 - 152	19	0 - 180
Zn	44	11 - 316	162	18 - 430	41	0 - 284
As	<3	<3 - 13	8.4	6 - 26	NA	NA
Br	1.4	<1 - 1.9	NA	NA	NA	NA
Rb	150	43 - 249	197	93 - 390	197	97 - 380
Sr	92	4 - 205	230	14 - 421	118	70 - 240
Zr	131	46 - 239	210	95 - 377	204	90 - 320
Nb	15	11 - 21.8	15	11 - 23	15	3 - 29
Mo	NA	NA	<1.0	<1.0	1.1	0 - 3
Ag	NA	NA	<5.0	<5.0	NA	NA
Cd	NA	NA	NA	NA	NA	NA
Sn	2.6	<1.5 - 4.5	1.0	1.0	0.0	0 - 9
Sb	NA	NA	7.0	<3.0 - 9	NA	NA
Cs	NA	NA	NA	NA	NA	NA
Ba	1061	88 - 3152	1296	311 - 2299	925	104 - 1430
La	44	2 - 103	NA	NA	79	30 - 150
Ce	77	4 - 134	NA	NA	111	20 - 290
Nd	26	3 - 44	NA	NA	45	23 - 69
Y	14	3 - 41	31	11 - 44	43	18 - 111
W	NA	NA	NA	NA	9.5	3 - 390
Tl	NA	NA	NA	NA	NA	NA
Pb	39	2 - 196	67	3 - 293	54	6 - 435
Bi	5.9	<1.5	NA	NA	NA	NA
Th	36	13 - 45	NA	NA	38	16 - 77
U	4.7	0.9 - 11.6	NA	NA	22	2 - 27

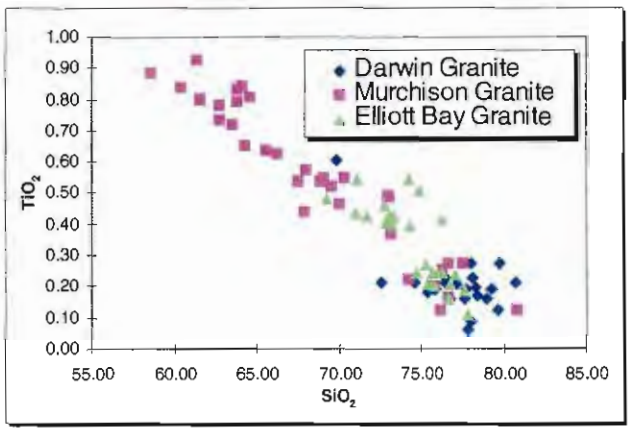

Figure 6.1. Plot of TiO_2 vs. SiO_2 for Cambrian granites. Ti is highly correlated with Zr and decreases systematically with differentation. This systematic decrease is interpreted to be a result of titaniferous magnetite fractionation (Carmichael, 1974 and Cox et al., 1980).

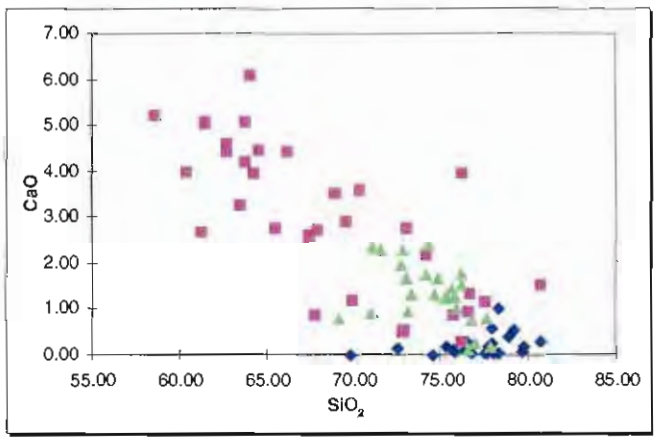

Figure 6.2. Plot of CaO vs. SiO_2 for Cambrian granites. The Darwin and Elliott Bay granites are almost lacking in calcic plagioclase as reflected by the low CaO shown. This systematic decrease is interpreted to be a result of the fractionation of calcic plagioclase (Cox et al., 1980). Legend as in Figure 6.1.

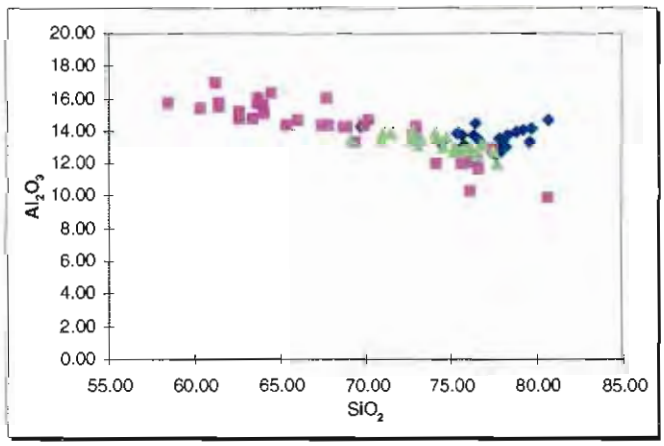

Figure 6.3. Plot of Al_2O_3 vs. SiO_2 for Cambrian granites. Lack of scatter and a pronounced linear trend support the immobile character of aluminum in the Darwin, Murchison and Elliott Bay Granites. Legend as in Figure 6.1.

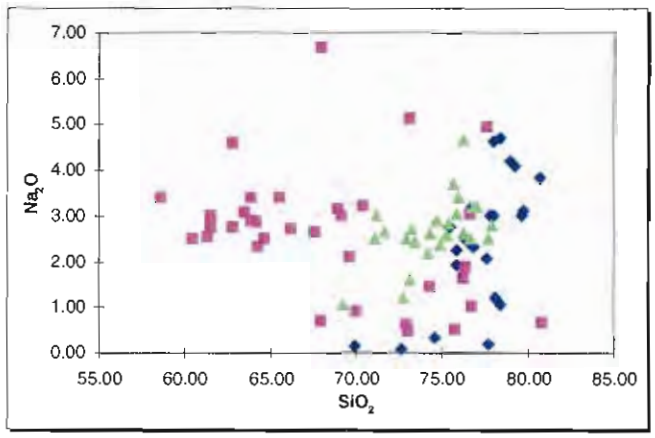

Figure 6.4. Plot of Na_2O vs. SiO_2 for the Cambrian granites. Systematically increasing sodium is poorly shown due to the wide scatter of data, and reflects the mobility of sodium during post crystallization alteration. Legend as in Figure 6.1.

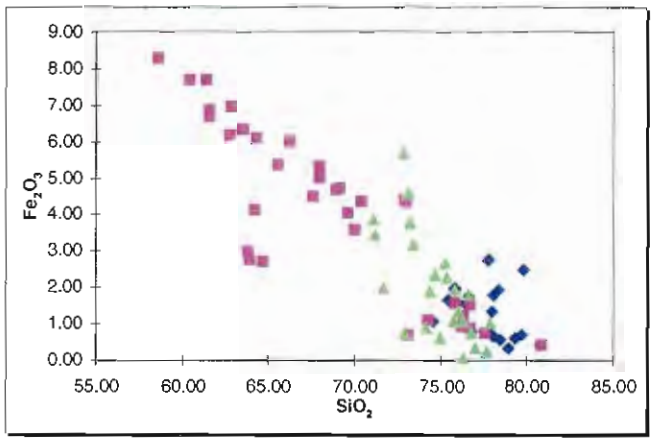

Figure 6.5. Fe_2O_3 vs. SiO_2 plot for the Cambrian granites. The decreasing trend is a typical fractionation trend from granites that have undergone fractional crystallization. This systematic decrease is interpreted to be a result of the fractionation of ferromagnesian minerals (eg. pyroxene and opaques, Cox et al., 1980). Legend as in Figure 6.1.

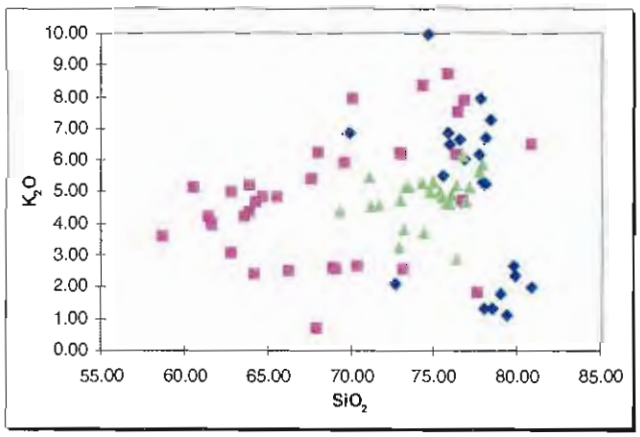

Figure 6.6. Plot of K_2O vs. SiO_2. Systematically increasing potassium is poorly shown due to the wide scatter of data and reflects the mobility of potassium during post crystallization alteration. Legend as in Figure 6.1.

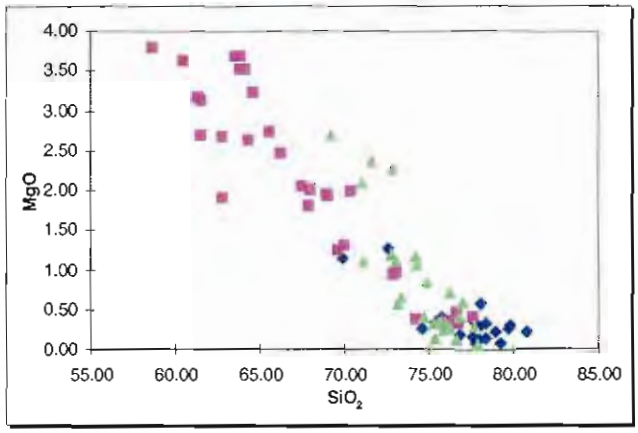

Figure 6.7. MgO vs. SiO_2 plot for the Cambrian granites. The decreasing trend is a typical fractionation trend from granites that have undergone fractional crystallization. This systematic decrease is interpreted to be a result of the fractionation of ferromagnesian minerals (eg. pyroxene and opaques, Cox et al., (1980). Legend as in Figure 6.1.

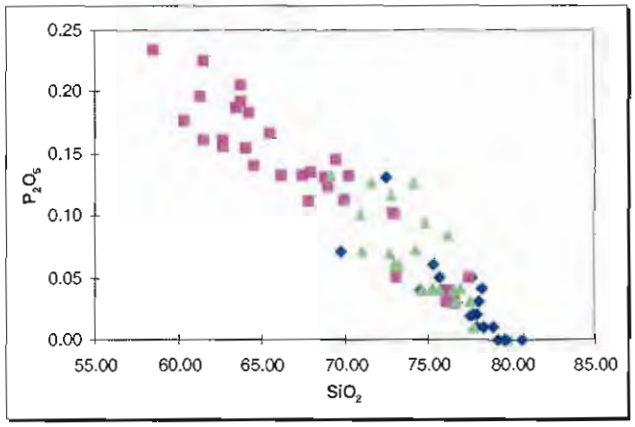

Figure 6.8. Plot of P_2O_5 vs. SiO_2. This systematic decrease is interpreted to be a result of apatite/monazite fractionation (Carmichael, 1974 and Cox et al., 1980). Legend as in Figure 6.1.

Figure 6.9 is a Ti vs. Zr plot data from Darwin, Murchison and Elliott Bay Granites. The data on Figure 6.9 is cluttered and confusing as it does not take into account that within each granite multiple intrusions are possible, each with unique Ti/Zr values. In Figures 6.10 to 6.13, Ti was plotted against Zr for each phase of granite identified from the three granites. For the Darwin Granite (Figure 6.10), there is an excellent correlation between Ti and Zr for the entire granite. When the three dominant phases of the granite are considered separately (Figure 6.11), the correlation was still strong (r values of 0.917 and 0.891 for the white and pink phases respectively). The microgranite phase has one data point and was not used in calculating the trendlines for either the white granite or pink granite phases. The data point correlates with the pink and white granites, suggesting a possible relationship to either phase.

The two phases of the Elliott Bay granite are separated on the basis of Ti vs. Zr on Figure 6.12. As previously mentioned, Elliott Bay Granite phase 1 plots in a tight cluster and is interpreted to have been weakly-altered. Elliott Bay Granite phase 2 forms a linear trend and is interpreted to have been hydrothermally altered and associated with the weak Cu-Au mineralisation.

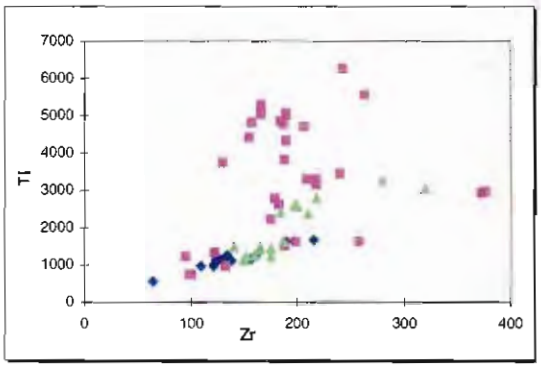

Figure 6.9. Ti vs. Zr plot of the Darwin, Murchison and Elliott Bay Granites. With respect to the Murchison granite, the figure is cluttered as it does not recognise that within each granite, multiple intrusions are possible with unique Ti/Zr ratios.

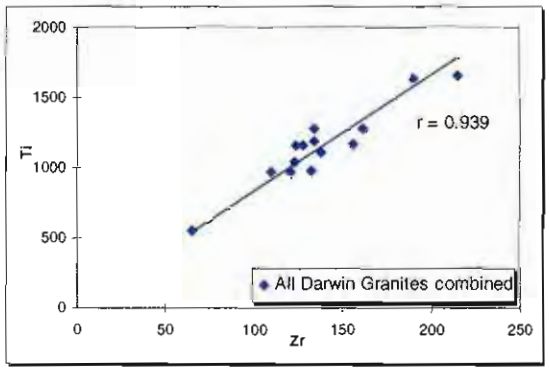

Figure 6.10. Ti vs. Zr plot for three phases of the Darwin Granite. There is a excellent correlation between Ti and Zr for the granite as a whole (r = 0.939).

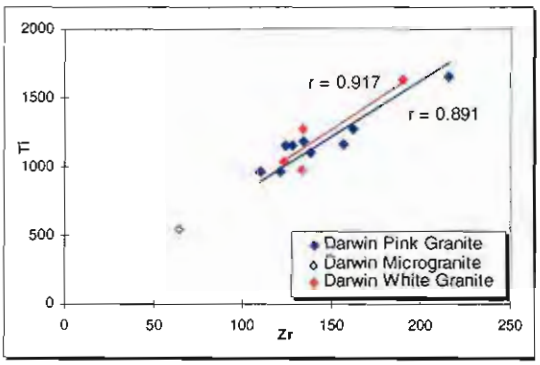

Figure 6.11. Ti vs. Zr plot for the three phases of the Darwin Granite. The correlation is strong as shown by r values of 0.917 and 0.891 for the white and pink phases respectively. The microgranite/aplite phase has only one data point and was not used in calculating the trendlines. The data point plots inline with both of the pink and white granites suggesting a relationship to one or both phases.

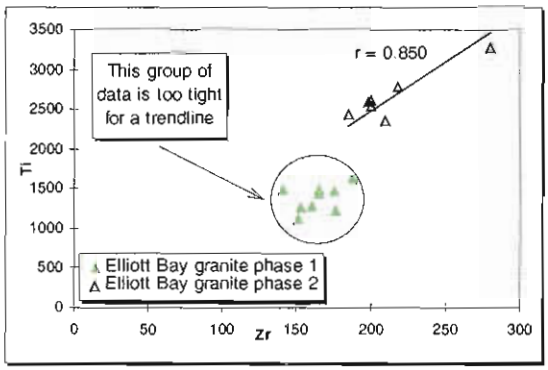

Figure 6.12. Ti vs. Zr plot for two phases of the Elliott Bay Granite. Elliott Bay Granite phase 1 plots in a cluster and is interpreted to represent an unaltered phase while Elliott Bay Granite phase 2 is unique from phase 1 and forms a linear trend. This is interpreted to represent a granite that was altered by post emplacement processes.

With respect to the Murchison Granite, the data on Figure 6.9 is scattered. Figure 6.13 is a Ti vs. Zr plot for the Murchison Granite that separates five phases of the granite. The five phases have unique SiO_2 (61-63% for phase 1, up to 72-80% for phase 5) and Fe_2O_3 contents (Figure 6.14) and occur on a well-defined fractionation trend from diorite to granite.

Evans and Hanson (1993) have considered the role of accessory minerals in granite fractionation. If the Darwin Granite melt was saturated with respect to zircon, apatite and/or sphene, then either a systematic decrease with differentiation following a trend of compatible elements, or definite flat trend following the movement of ESCs (Essential Structural Components) is expected. A systematic decrease was observed in the major element data (TiO_2 and P_2O_5, Figure 6.1 and

Figure 6.8) and is interpreted to represent sphene and apatite crystallization respectively. SiO_2 was used as an index of differentiation although Evans and Hanson (1993) used 1/Ce.

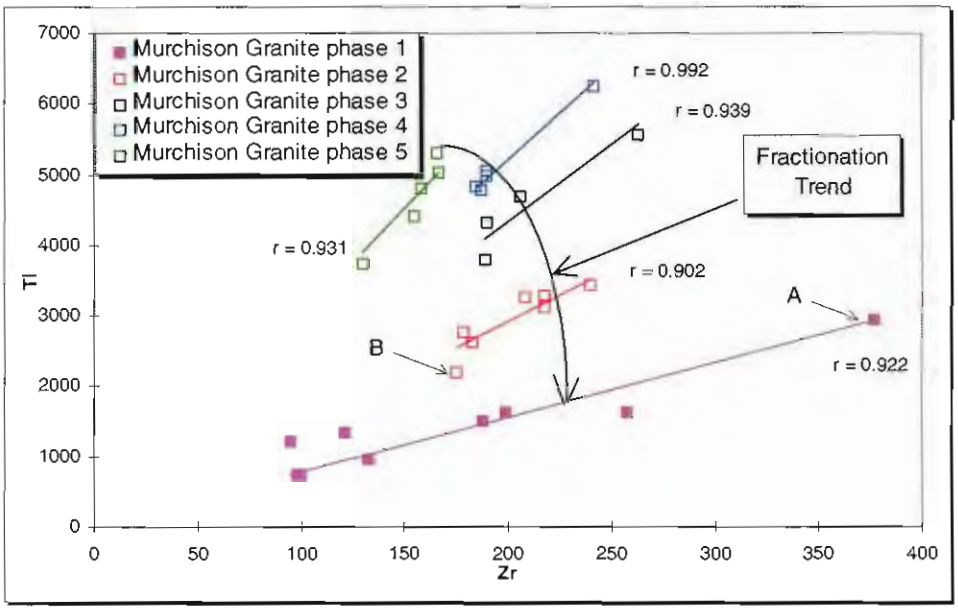

Figure 6.13. Ti vs. Zr plot for five phases of the Murchison Granite. Five unique phases of the granite are distinguished. The five phases are also supported on the basis of SiO_2 contents that range from 61-63% for phase 1, up to 72-80% for phase 5. The spread along the trendlines is interpreted to represent mass gains and mass losses due to post emplacement alteration. The five phases form a well-defined fractionation trend from diorite to granite. Points A and B correspond to A and B in Figure 6.14.

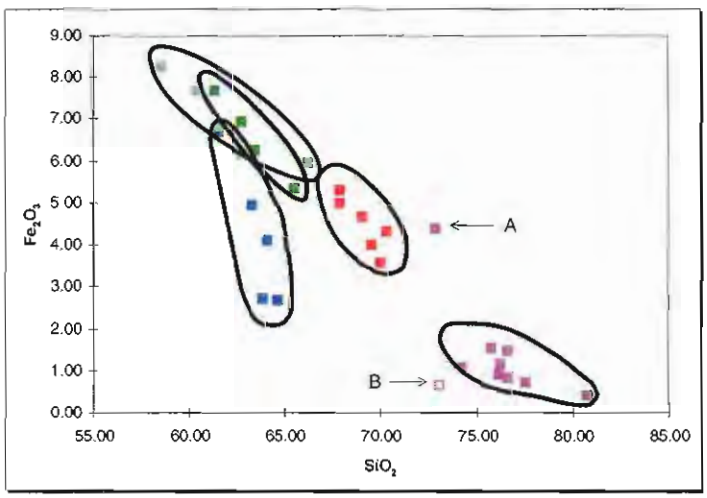

Figure 6.14. Fe_2O_3 vs. SiO_2 plot for the Murchison Granite. The two points A, and B that do not fit within their respective groups are highly altered and show extremes in iron mobility.

The minor scatter of Zr data (Figure 6.15) with respect to the Darwin Granite is interpreted to indicate inhomogeneities in the Darwin Granite itself and not to represent Zr undersaturation in the melt. Once a melt becomes saturated in Zr, Zr behaves as an ESC, not as an incompatible trace element (Evans and Hanson, 1993). Zr in the melt is buffered at the saturation level (Watson, 1979). In the case of the Darwin Granite this was about 130 ppm Zr. In a suite of related melts saturated in Zr the concentration of Zr will have less variation than incompatible or compatible trace elements (Evans and Hanson, 1993). This is consistent with the Zr distribution in the Darwin Granite suite.

Although Figure 6.1 indicates an overall decreasing trend in TiO_2 with increasing SiO_2 for the Cambrian granites as a whole, the Darwin Granite data are scattered over a narrow range in SiO_2 values. Analysis of the heavy mineral separates indicate that the main TiO_2 mineral in the Darwin Granite is rutile, and sphene occurs in trace quantities. Rutile is interpreted to be a product of alteration and the original TiO_2 bearing minerals were sphene and Ti-bearing magnetite.

A limited range of Nb values (10-23 ppm) occurs over a wide range in Zr and Ti values, regardless of granite phase (Figure 6.16 to 6.17). This narrow range indicates that the Nb content was independent of lithology and was immobile. Y has a narrow range of values (less than 22 ppm) over a limited range in Zr and Ti values for the Darwin and Murchison Granites (Figure 6.18 to 6.19). This is interpreted to represent immobility of Y in the Darwin and Murchison Granites. The Elliott Bay Granite has a broader range (up to 32 ppm) in Y values that is interpreted to represent slight mobility of Y.

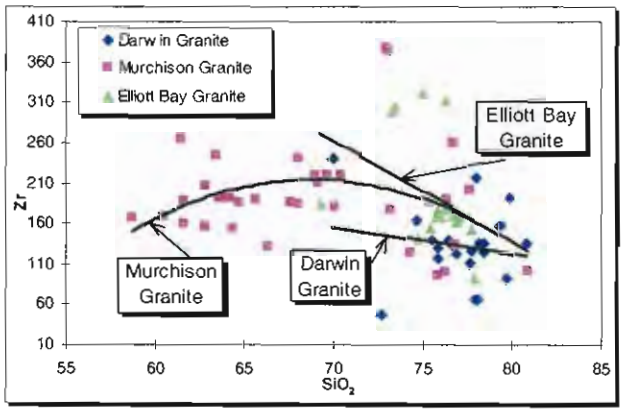

Figure 6.15. Zr vs. SiO_2 plot for the Darwin, Murchison and Elliott Bay Granites. The systematic trend for the Murchison Granite is interpreted to represent a steady increase in Zr in the melt until the melt became saturated in Zr and zircon could fractionate. Although the SiO_2 range for the Darwin and Elliott Bay Granites is higher than the Murchison Granite, the decreasing trends for both granites are interpreted to represent zircon fractionation.

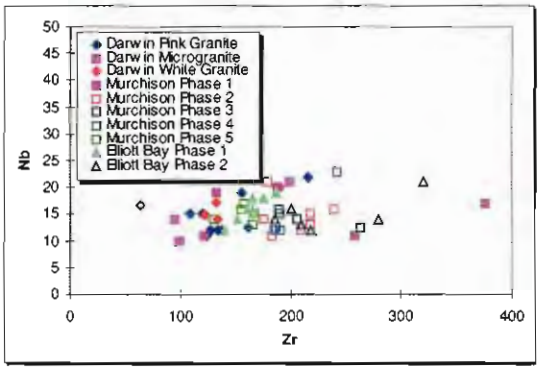

Figure 6.16. Plot of Nb vs. Zr showing that a limited range of Nb values (10-23 ppm) occurs over a wide range in Zr values. This narrow range indicates that the Nb content is independent of lithology and is immobile.

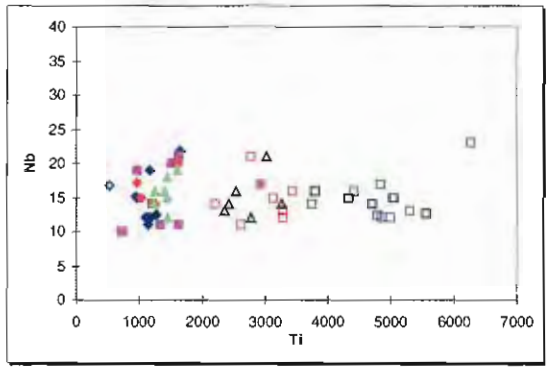

Figure 6.17. Nb vs. Ti plot showing that a limited range of Nb values (10-23 ppm) occurs over a wide range in Ti values. This narrow range indicates that the Nb content is independent of lithology and is immobile.

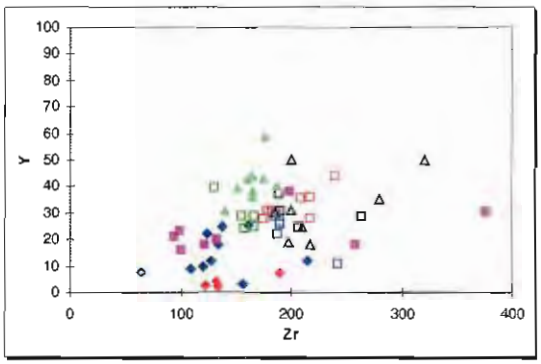

Figure 6.18. Plot of Y vs. Zr showing that Y has a range of values scattered over a wide range in Zr values. This is interpreted to represent minor mobility of Y.

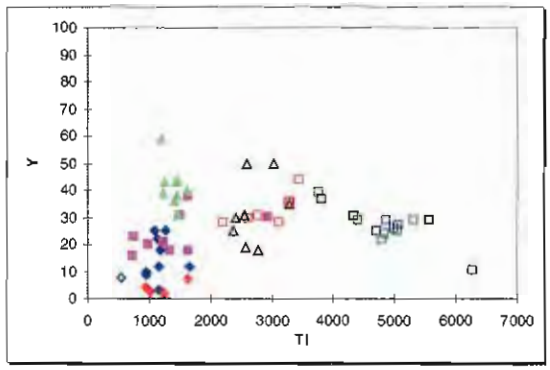

Figure 6.19. Plot of Y vs. Ti showing that Y has a range of values scattered over a wide range in Ti values. This is interpreted to represent minor mobility of Y.

Concentrations of Rb (43 to 390 ppm) and Sr (4 to 421 ppm) vary considerably (Table 6.1). Sr contents of the white granite and quartz-feldspar porphyry phases are the highest in all of the Darwin Granite samples analysed (Appendix C), consistent with partitioning into plagioclase. Conversely, the Rb content of the white granite was the lowest of all the Darwin Granite samples analysed, consistent with partitioning of Rb into K-feldspar and its earlier removal in the pink granite phase. The systematic decrease shown in Figure 6.20 is indicative of extreme crystal fractionation (Bajwah et al., 1995). Although these analyses include weakly to intensely altered rocks, well-developed fractionation trends are still evident in all but the most tourmalinised rocks at Mt. Darwin.

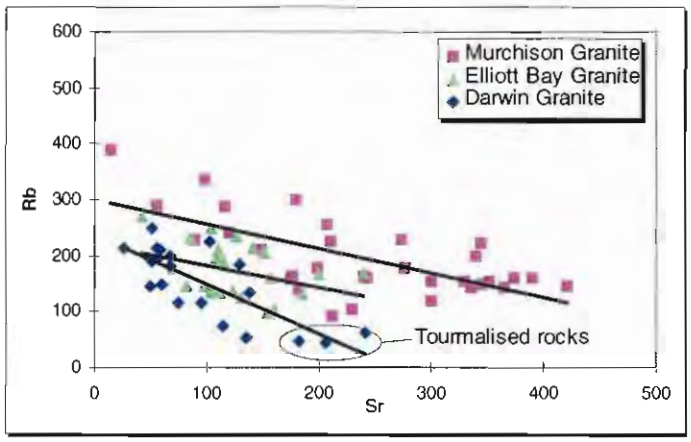

Figure 6.20 Rb vs. Sr plot for the Darwin, Murchison and Elliott Bay Granites. Although these analyses represent least-altered through highly altered rocks, well-developed fractionation trends are still evident. It is interesting to note that the Murchison Granite, on average, contains twice the amount of Rb as either the Darwin or Elliott Bay Granite.

Table 6.2 is a summary table of the epsilon Nd (εNd) and $^{87}Sr/^{86}Sr_{initial}$ data for the Murchison and Darwin Granites (Stolz, 1997, written. com., Crawford, 1997, written. com). A complete data set of Sr and Nd data is included in Appendix F. No Sr or Nd data are available for the Elliott Bay Granite. Positive εNd values imply that the magma was derived from a source with a greater Sm/Nd than CHUR (composition of chondritic meteorite), i.e. a depleted mantle source region, whereas a negative epsilon value implies a source with a lower Sm/Nd than CHUR, i.e. an enriched mantle source or crustal source Typical continental crustal rocks have lower Sm/Nd values (negative εNd values) than those derived from the mantle (Patchett and Arndt, 1986; Goldstein, 1988; Galer and Goldstein, 1991). The Murchison and Darwin Granites have negative εNd values (average -4.2) suggesting that they were derived from continental crustal rocks.

Table 6.2. Summary of Sr and Nd isotope data for the Darwin and Murchison Granites

Sample Number	Location	Rock Type	epsilon Nd (init)CHUR, 500Ma	$^{87}Sr/^{86}Sr$ (T=initial)	Nd age mod:CHUR (Ma)	Nd age mod:DEPLETED (Ma)	Reference	Comments
B2053	Darwin Granite	Pink Granite	-3.0	0.6704	716	1260	This Study	$^{87}Sr/^{86}Sr$ (T=initial) value is probably low due to alteration effects
GS-1	Darwin Granite	Pink Granite	-4.3	0.6932	833	1392	Large and Stolz, 1997 pers. com.	$^{87}Sr/^{86}Sr$ (T=initial) value is probably low due to alteration effects
GS-7	Darwin Granite	Pink Granite	-5.0	0.7008	934	1534	Stolz, 1997 pers. com.	
JD13	Darwin Granite	Pink Granite	-2.8	0.7093	694	1226	Crawford, 1997 pers. com.	
TO4137	Murchison Granite	Granite	-4.7	0.7098	964	1626	Crawford, 1997 pers. com.	
		Average	-4.2	0.7066				

6.2.2.2 Classification of Granites

Classification of Granites by Molar Ratio

A useful geochemical discrimination diagram for separating the three granites from each other is the simple ternary plot of K_2O vs. CaO vs. Na_2O (Figure 6.21). In the Murchison and Darwin Granites, the large range of data was due to potassium metasomatism. The strong shift in the Murchison Granite data toward the CaO corner reflects fundamental mineralogical differences between the exposed (and sampled) granite types compared to those of the Darwin and Elliott Bay Granites (Davidson, 1998). In the Elliott Bay Granite, alteration was weak as shown by the tighter grouping of data points.

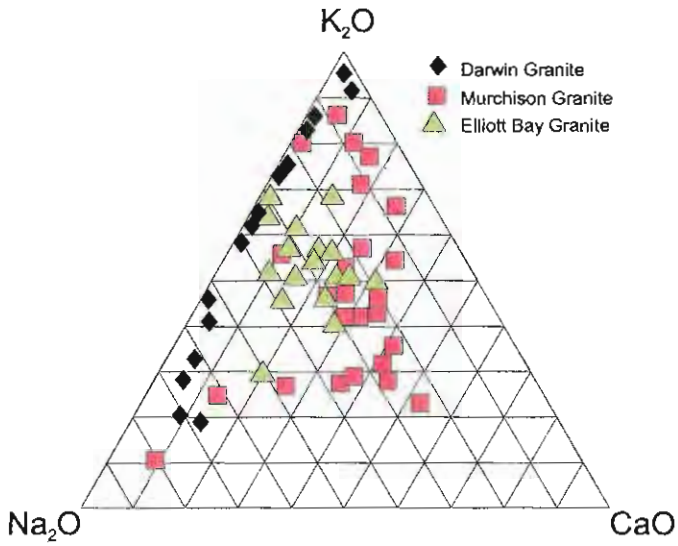

Figure 6.21. Ternary plot of K_2O, Na_2O and CaO for the Darwin, Murchison and Elliott Bay Granites. The spread of data toward the K_2O apex of the diagram is due to potassium enrichment.

Several attempts to classify the Cambrian granites of western Tasmania have made. Abbott (1992) and Jones (1993) concluded that the granites are intensely altered, high-K, magnetite-series granites following the classification of Ishihara (1981) and that the high degree of alteration renders the I & S classification of White (1983) useless. The current study has attempted to classify the Murchison, Darwin and Elliott Bay Granites using various classification schemes based on mode (Figure 3.3, Streckeisen, 1976), rock series (Lameyre and Bowden, 1982), source rock (Chappell and White, 1974; White and Chappell, 1983), oxygen fugacity (Ishihara, 1981) and tectonic setting (Pearce et al., 1984). Data used in the classifications are from the literature and this study.

Classification of granites according to their alumina saturation was developed by Shand (1947). The system uses the ratio A/CNK (molar Al_2O_3 /(Na_2O+K_2O+CaO)) which ranges from greater than one to less than one in igneous rocks. A/CNK will equal 1 in rocks with quartz and two or more feldspars, but rocks with additional minerals will shift the ratio above or below unity. For example, rocks with hornblende will shift the ratio below 1 while rocks with garnet will shift the ratio above 1. The A/CNK/SiO_2 relationship for the Darwin, Murchison and Elliott Bay Granites is shown as Figure 6.22. The I & S-type boundary of Chappell and White (1992) is shown for

reference. While the Murchison Granite overlaps the metaluminous and I-type boundary the Darwin and Elliott Bay Granites are within the peraluminous field and S-type granite field. Clark (1992) pointed out that more than one chemical type of granite can occur together; indeed a complete continuum in mineralogical and chemical compositions occurs in the granite family, so subdivisions (however useful) are arbitrary. The peraluminous-metaluminous subdivisions used here have precise chemical limits, but any process that can change the relative amounts of alumina and alkalis can cause transitions from one A/CNK group to another.

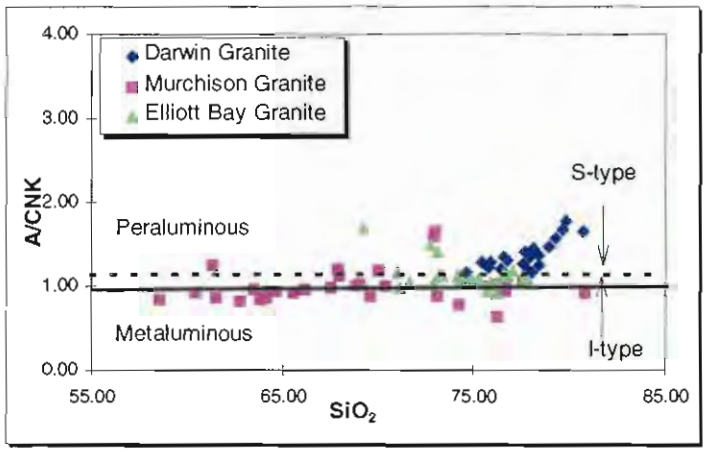

Figure 6.22 A/CNK vs. SiO_2 diagram for the Darwin, Murchison and Elliott Bay Granites. The I & S-type boundary of (Chappell, 1992) is also shown for reference. While the Murchison Granite overlaps the metaluminous and I-type boundary the Darwin and Elliott Bay Granites plot within the peraluminous field and S-type granite field. This shift, partly due to Na and Ca depletion by alteration, is also partly due to late stage aluminium oversaturation as indicated by the presence of tourmaline in the most evolved Darwin Granite phases.

Table 6.3. Tripartite chemical classification of granitic rocks. After Clark, (1992).

	The Granitoid Family QAP 60% > Quartz > 20% Alkali-feldspar/(Alkali-feldspar + Plagioclase) = 1		
	Peraluminous	Metaluminous	Peralkaline
Definition (Shand, 1947)	A > CNK (A/CNK>1)	CNK > A > NK (A/CNK<1)	A < NK
Characteristic minerals	aluminosilicates, cordierite, garnet, topaz, tourmaline, spinel, corundum	orthopyroxene, clinopyroxene, cummingtonite, hornblende, epidote	fayalitic olivine, aegirine, arfvedsonite, riebeckite
Other common minerals	biotite, muscovite	biotite, minor muscovite	minor biotite
Oxide minerals	ilmenite, tapiolite	magnetite	magnetite
Accessory minerals	apatite, zircon, monazite	apatite, zircon, titanite, allanite	apatite, zircon, titanite, allanite, fluorite cryolite, pyrochlore
Other chemical	F/Cl > 3		Low CaO, Al_2O_3, H_2O, Ba, Sr, and Eu. High SiO_2, Fe/Mg, Na + K, Zr, Nb, Ta, ΣREEs and Y. F/Cl < 3
Isotopic compositions			
$^{87}Sr/^{86}Sr_i$	0.7050-0.7200	0.7030-0.7080	0.7030-0.7120
εNd,	typically << 0	approximately 0	highly variable
Typical mineral deposits	aplite-pegmatite-greisen; polymetallic Sn-W-U-Mo-Cu and Be-B-Li-P	porphyry Cu-Mo	Sn-W-U-Mo and rare metal (Nb-Ta) greisens
General plate tectonic environment	continent-continent collision tectonics involving thickened continental crust	subduction-related continental and island arc	post-tectonic or anorogenic extension resulting in intracontinental ring complexes

A variation on Shand's theme was introduced by Clark (1992) and is reproduced in Table 6.3. Clark's classification uses Shand's terminology but adds additional mineralogical and other chemical data in support of each class. Clark (1992) added tectonic setting and mineral deposit

associations to the classification. The scheme of Clark was taken farther by Chappell and White (1992), in their discussions of I & S type granites in the Lachlan Fold Belt.

Classification of Granites by Tectonic Setting and Source Rock

The primary source materials for granitic melts are related to tectonic setting, therefor, classification schemes that give tectonic setting information should agree with the interpreted geological setting. Based on the information presented in Table 6.3, an island arc setting is consistent for the Darwin, Murchison and Elliott Bay Granites. This is in agreement with the tectonic setting proposed by Solomon (1981). However, the MRV were interpreted to be post-collisional volcanics formed after arc-continent collision (Crawford and Berry, 1992; Crawford et al., 1992).

The Chappell and White (1974) and White and Chappell (1983) classification system was developed to distinguish between granites formed from partial melting of sedimentary rocks and those formed from partial melting of igneous source rocks. Bekinsale (1979) expanded on the classification and a summary is shown in Table 6.4, together with characteristics from the Murchison, Darwin and Elliott Bay Granites. I-type criteria for the Darwin, Murchison and Elliott Bay Granites are: linear trends for P_2O_5, TiO_2 and Ti/Zr (Figures 6.1, 6.8 and 6.10-6.13); no normative diopside nor normative corundum in the Darwin Granite and traces of normative diopside in the Murchison and Elliott Bay Granites (Appendix D); abundant magnetite and little or no ilmenite; initial $^{87}Sr/^{86}Sr$ values for the Darwin Granite average 0.705, and 0.709 for the Murchison Granite; and εNd values are -2.8 to -4.9 (Table 6.2). Na_2O, K_2O and CaO (Figures 6.2, 6.4 and 6.6) were mobilised by post emplacement processes thereby affecting classifications based on abundances of these elements. As a result of alkali depletion, the molar Al_2O_3 / (Na_2O+K_2O+CaO) ratio was higher than 1.1, an S-type characteristic. In addition, whole rock $\delta^{18}O$ data for the Darwin Granite ranges from +9.3 to +12.5‰, and accessory minerals are biotite, sphene, magnetite and monazite, characteristics that are consistent with an I-type classification for the Cambrian granites. Since similarities to I-type granites are based on immobile elements, isotopes or well-documented mineral assemblages, it is concluded that the Cambrian granites are I-type granites.

The I-type and S-type granite series are considered to have resulted from the prevalence of different oxygen fugacities during evolution of the granite magmas (Ishihara, 1981). Higher oxygen fugacities (fO_2) resulted in magnetite-series granites and lower fO_2 formed ilmenite series granites. Two primary mechanisms for controlling the oxidation/reduction are the SO_2 content and dissociation of water in the hydrous magma (Takagi and Tsukimura, 1997). If the SO_2 content was >250 ppm, fO_2 was constrained by the SO_2-H_2S buffer and magnetite crystallised. If the SO_2 content was less than 250 ppm, the magma solidified as a reduced type granite (Takagi and Tsukimura, 1997). If fO_2 was buffered by H_2O-H_2, CO_2-CO, or CH_4-CO_2, no magnetite crystallised and a reduced type granite resulted (Takagi and Tsukimura, 1997). Ishihara (1981) recognised that incorporation of crustal carbon was an essential reducing agent for the ilmenite-series magmas. The magnetite-series can be correlated with I-type granitoids and the ilmenite-series with S-type and reduced I-types, although Takahashi et al. (1980) noted this correlation was not

universal. Ishihara (1981) claimed that even the presence of one grain of magnetite in a sample was enough to classify the granite as belonging to the magnetite-series. In Australia, S-types are typically ilmenite-series, but I-types are divisible into the magnetite and the ilmenite-series (Ishihara, 1981). In the western Pacific, since Jurassic time, I-type magnetite-series granites are associated with the inner marginal seacoast, and in many cases are associated with Cu sulfide mineralisation (Ishihara, 1981).

Table 6.4. Summary table of I and S-type granite characteristics and a comparison to the Darwin, Murchison and Elliott Bay Granites. Data from Chappell and White (1974), Beckinsale (1979), Jones (1993), Pitcher (1993) and Bleven and Chappell (1995). * See Appendix D, Cambrian Granite Normative Mineralogy.

I-Types	Cambrian Granites	S-Types
High sodium, Na_2O, normally >3.2% in felsic varieties, decreasing to >2.2% in more mafic types	Darwin Granite: 0.6-4.7 wt. %, average 2.9 wt.% Murchison Granite: 0.02-6.6 wt.%, average 3.1 wt.% Elliott Bay Granite: 1.05-4.64 wt.%, average 2.7 wt.%	Relatively low sodium, Na_2O normally <3.2% in rocks with approx. 5% K_2O, decreasing to <2.2% in rocks with approx. 2% K_2O
Mol $Al_2O_3/(Na_2O+K_2O+CaO)$ <1.1 and can be either peraluminous or metaluminous	Darwin Granite: 1.15-1.78, average 1.6 Murchison Granite: 0.63-1.65, average 1.0 Elliott Bay Granite: 0.92-1.7, average 1.1	Mol $Al_2O_3/(Na_2O+K_2O+CaO)$ is usually >1.1 The rocks are always peraluminous
C.I.P.W. normative diopside or <1% normative corundum	Darwin Granite: NO normative diopside or corundum* Murchison Granite: 0.29% av. normative diopside, no corundum* Elliott Bay Granite: trace normative diopside, no corundum*	>1.1% C.I.P.W. normative corundum
Tend to be the acid end of a broad compositional spectrum from basic to acid	Darwin Granite: granodiorite to granite Murchison Granite: granodiorite to granite Elliott Bay Granite: granite only	Tend to occur in restricted ranges of only acidic compositions
Regular inter-element variations within plutons; linear or near linear variation diagrams	Darwin Granite: linear or near linear variation diagrams Murchison Granite: linear or near linear variation diagrams Elliott Bay Granite: linear or near linear variation diagrams	Variation diagrams more irregular
Magmas with relatively high oxygen fugacity; Relatively high ferric/ferrous ratios; characterised by magnetite, but ilmenite is not uncommon	Darwin Granite: abundant magnetite Murchison Granite: abundant magnetite Elliott Bay Granite: abundant magnetite	Magmas with relatively low oxygen fugacity; Relatively low ferric/ferrous ratios; characterised by ilmenite
Low initial $^{87}Sr/^{86}Sr$ ratios of 0.704 to 0.712 εNd values of +3.5 to -8.9	Darwin Granite: $^{87}Sr/^{86}Sr$ =0.7008-0.709, εNd = -2.8 to -4.99 Murchison Granite: $^{87}Sr/^{86}Sr$= 0.709, εNd = -4.7 Elliott Bay Granite: $^{87}Sr/^{86}Sr$ and εNd are not available	High initial $^{87}Sr/^{86}Sr$ ratios from 0.708 to 0.720 ε Nd values of -5.8 to -9.2
Normal range of $\delta^{18}O$ values (approx. 6-10‰ , SMOH)	Darwin Granite: + 9.3 to +12.5 ‰ Murchison Granite: not available Elliott Bay Granite: not available	Enriched in ^{18}O ($\delta^{18}O$ values approx. > about 10 ‰, SMOH)
Hornblende common in mafic end members and sphene commonly present in felsic rocks	Darwin Granite: minor hornblende and sphene Murchison Granite: abundant hornblende and sphene Elliott Bay Granite: minor hornblende and sphene	Muscovite, monazite, cordierite and garnet are commonly present

Classification schemes for granites using chemical discrimination diagrams claimed to discriminate between granites from various tectonic settings (Pearce et al., 1984; Clark, 1992; Pitcher, 1993). However, caution must be used in applying these diagrams as they may reflect the composition of the source rocks of the granitic melts (Stracke and Hegner, 1998; Waight et al., 1998). With this caution in mind, the trace element and REE classification schemes of Pearce et al. (1984) were applied to the rocks of the current study since good trace element data exists. Pearce et al. (1984) distinguished between ocean ridge granites (ORG), volcanic arc granites

(VAG), within plate granites (WPG) and collisional granites (COLG). Pearce et al. assumed that Rb, Y, and Nb were less mobile in granitic rocks than in basalts by the apparent lack of alteration in granites relative to basalts. Rb-Y-Nb were plotted vs. SiO_2 in Figures 6.23-6.25 and 6.27, Nb vs. Y in Figure 6.26 and Rb vs. Y + Nb as Figure 6.28. All three granites appear to overlap the field boundaries between syn-collisional granites and volcanic arc granites (Figure 6.25). However, in Figure 6.26, the Darwin Granite occurs within the VAG + syn COLG field. It has been shown that sodium, calcium and potassium in the Darwin, Murchison and Elliott Bay Granites were mobile (Figures 6.4 and 6.6). Therefore, two possible explanations for the Rb values in Figure 6.25 are suggested: 1) Rb increases or decreases due to increased mobility of alkali elements during alteration of all three of the granites, 2) since Rb substitutes for K in potassic alteration, the effects of potassic alteration can increase the Rb content forcing the points on the diagram up toward the syn-COLG line.

Table 6.5. Magnetite vs. Ilmenite Series granite classification of Ishihara (1981).

Magnetite Series	**Ilmenite Series**
Magnetite content greater than 0.1 vol. percent	Magnetite and ilmenite content less than 0.1 vol. percent
Magnetic susceptibility higher than 1 x 10^{-4} emu/g	Magnetic susceptibility less than 1 x 10^{-4} emu/g
In calc-alkaline granites, Fe_2O_3/FeO ratio > 0.5	In calc-alkaline granites, Fe_2O_3/FeO ratio < 0.5
Positive $\delta^{34}S$ values	Negative $\delta^{34}S$ values
Low $\delta^{18}O$ values	High $\delta^{18}O$ values
Depletion in lithophile elements	Enrichment in lithophile elements
Accessory magnetite(0.1-2 vol. %), ilmenite, sphene, epidote, hematite, pyrite and chalcopyrite	Accessory ilmenite, pyrrhotite, graphite, monazite, garnet and muscovite
Biotite with high Fe_2O_3/ FeO and low refractive index	Biotite with low Fe_2O_3/ FeO and high refractive index
Intrusive sequences in which Fe/(Fe + Mg) for amphiboles and biotites decreases with increasing SiO_2 content of the host rocks	Intrusive sequences in which Fe/(Fe + Mg) for amphiboles and biotites increases with increasing SiO_2 content of the host rocks
Associated with base metal sulphides, scheelite, gold and silver, porphyry molybdenum and copper, and Kuroko-type VHMS deposits	Cassiterite, wolframite, beryl, and fluorite mineralisation

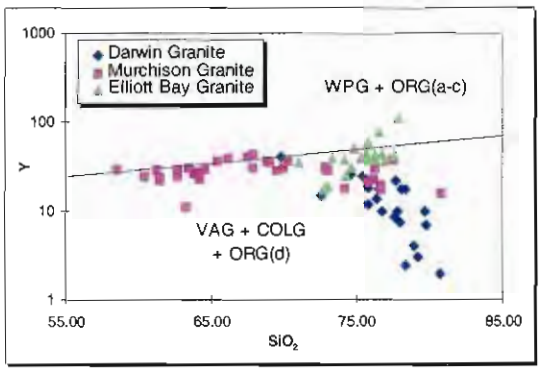

Figure 6.23. Logarithmic plot of Y vs. SiO_2 showing a linear Y relationship for the Murchison Granite parallel to the field boundary separating VAG + COLG + ORG (D) from WPG + ORG (a-c). Both the Darwin and Elliott Bay Granites show variable Y contents beginning at about 73% SiO_2. This relationship is expanded on Figure 6.24.

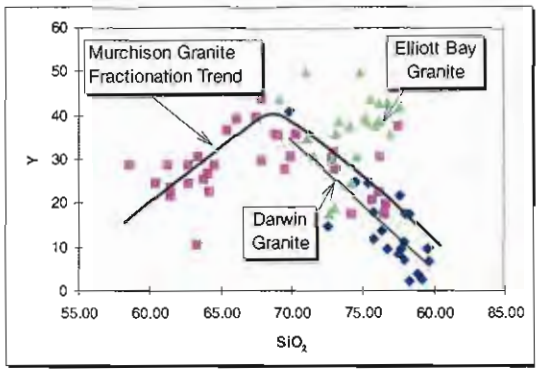

Figure 6.24. Normal binary plot Y vs. SiO_2 showing different trends for the three granites. The trend of decreasing Y for the Darwin Granite is probably due to increased fractionation of the granite and stripping out of Y by some mineral. The systematic trend for the Murchison Granite is interpreted to be a result of increased Y in the melt until the melt became saturated with a mineral that Y could partition into, probably zircon (Figure 6.15). The cause for the increasing Y in the Elliott Bay Granite is not currently known.

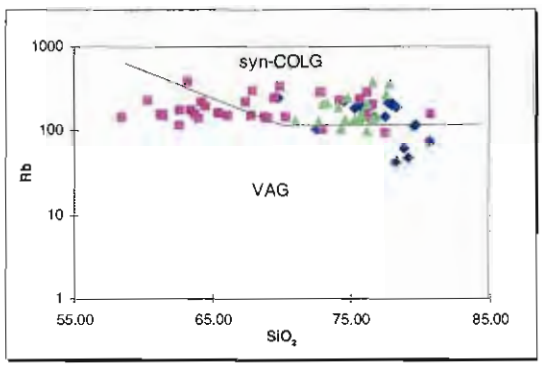

Figure 6.25. Logarithmic plot of Rb vs. SiO_2 for the Cambrian granites. Elevated Rb probably occurred due to increased mobility of alkali elements during alteration or, alternatively, due to substitution for K in potassic alteration.

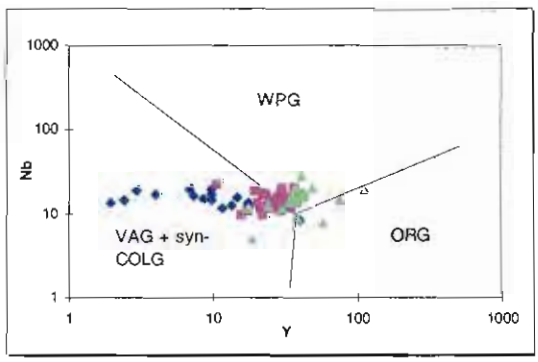

Figure 6.26. Nb vs. Y plot showing that the Darwin Granite is in the VAG + syn COLG field while the Murchison and Elliott Bay Granites overlap the VAG/WPG fields. The Nb depletion is characteristic of volcanic arc granites (Pearce et al., 1984).

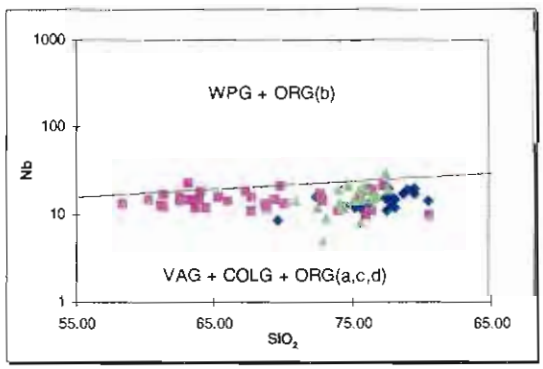

Figure 6.27. Nb vs. SiO_2 plot showing that the Nb content is not related to SiO_2.

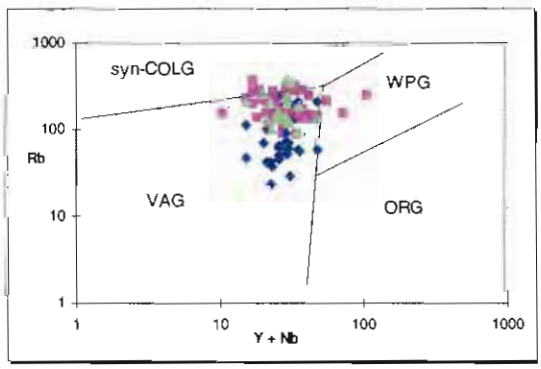

Figure 6.28. Rb vs. Y + Nb plot showing that all three granites plot in the VAG field and have Nb depletion characteristic of volcanic arc granites (Pearce et al., 1984).

In Figure 6.23 (Logarithmic plot) the Murchison Granite shows a linear Y relationship parallel to the field boundary separating VAG + COLG + ORG (D) from WPG + ORG (a-c). At SiO_2 levels less than 73%, the Y content was controlled by partitioning into calcic plagioclase or hornblende (Atherton and Tarney, 1979). Figure 6.23 is expanded as a non logarithmic plot in Figure 6.24. The Murchison Granite has a well-defined fractionation trend for SiO_2 contents between 58-78%, while the Darwin and Elliott Bay Granites have restricted ranges of SiO_2 values and granite types. The Darwin and Elliott Bay Granites have variable Y contents beginning at about 73% SiO_2. As shown on Figure 6.24 the trends for the two granites differ. The Y content of the Darwin Granite decreases with increasing SiO_2. If increasing SiO_2 was assumed to represent an increasing index of fractionation within the granite suite, as described by Evans and Hanson (1993), then Y was compatible. The common accessory mineral that will accommodate Y (high K_d) is zircon (Wark and Miller, 1993). The apparent increase in Y in the Elliott Bay Granite (Figure 6.23), is not typical of crystal fractionation and is consistent with incompatibility.

Zr data for the Darwin and Elliott Bay Granites are scattered relative to the Murchison Granite (Figure 6.15). This scatter is interpreted to indicate inhomogeneity with respect to Zr saturation, as described by Evans and Hanson (1993). The limited range of Zr values was the result of inhomogeneities within the granite itself. The data plotted in Figure 6.24 suggests that, within the Darwin Granite, Y behaved as an compatible trace element partitioning into zircon. Within the Elliott Bay Granite, Y was incompatible. All three granites have Nb depletion characteristic of volcanic arc granites and overlap the VAG/WPG fields in Figures 6.26. From Figure 6.25, it is interpreted that the Nb content in the granites was not related to SiO_2 and was controlled by partitioning into an unknown mineral.

6.2.2.3 Rare Earth Element Geochemistry

REE analyses for the Darwin, Murchison and Elliott Bay Granites are presented in Appendix E and plotted on chondrite-normalised diagrams in Figures 6.29 to Figure 6.32. The sources of the data are Crawford et al. (1992), Large et al. (1998) and this study.

Well-documented field relationships support the relative ages and states of evolution of the various phases of the Darwin Granite. The pink granite was the oldest and was intruded by microgranite dykes, white granite and quartz-feldspar porphyry. Cross-cutting relationships between the microgranite, white granite and quartz-feldspar porphyry phases were not observed in the field. However, the mineralogy and major element chemistry are similar to the pink granite, suggesting a close timing relationship. The quartz-feldspar porphyry has intruded the pink and white granite phases. Therefore the implied order of emplacement within the Darwin Granite suite was (from oldest to youngest), the pink granite, microgranite dykes, white granite and quartz-feldspar porphyry.

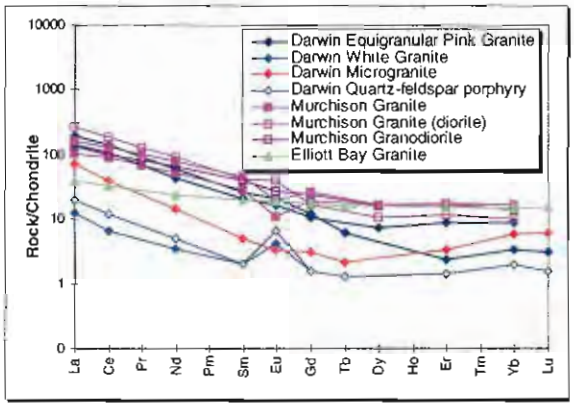

Figure 6.29. Chondrite-normalised REE diagram for the Darwin, Murchison and Elliott Bay Granites. Data from Crawford et al., (1992), Large, (1998) and the current study (Appendix F). There is strong REE enrichment and the heavy REE patterns are flat.

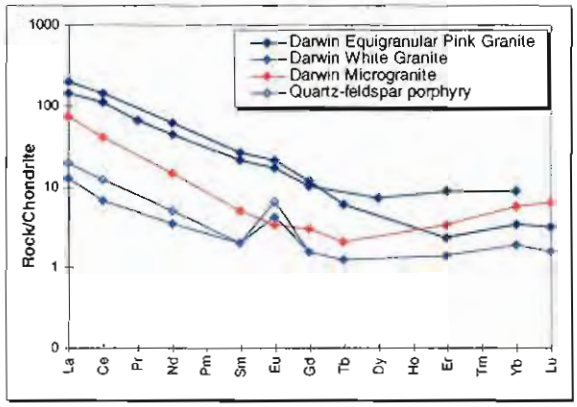

Figure 6.30. Chondrite-normalised REE diagram for the Darwin Granite. fO_2 probably controlled the flatness of the Eu anomaly. The decreasing REE content with differentiation is due to fractionation of monazite, rutile and zircon in the various phases. Data from this study.

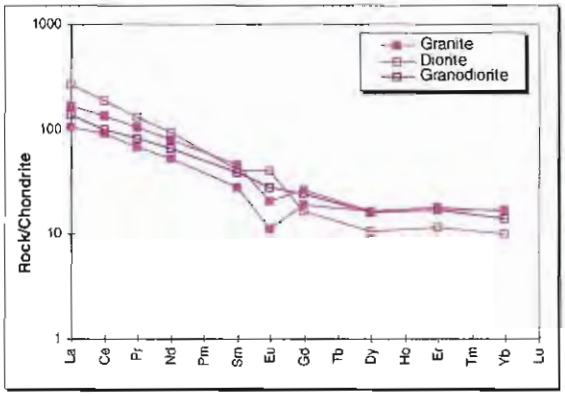

Figure 6.31. Chondrite-normalised REE diagram for the Murchison Granite. Variable oxygen fugacities probably contributed to the different Eu signatures between the granite, diorite and granodiorite phases.

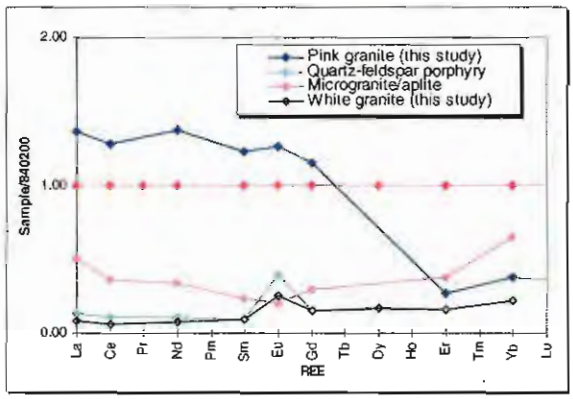

Figure 6.32. REE patterns for the Darwin Granite normalised to sample 840200 from Crawford et al. (1992). Roughly parallel patterns between the microgranite/aplite, the white granite and the quartz-feldspar porphyry suggest REE behaved compatibly. Depletion of heavy REE in the pink granite is probably due to hornblende fractionation and the large positive Eu anomalies are explained by Eu partitioning into plagioclase.

The Murchison and Darwin Granite suites are enriched in LREE elements with steep negative slopes, MREE have shallow slopes with flat Eu anomalies and HREE patterns are flat (Figures 6.29-6.31). This overall similarity in pattern shape between the Murchison and Darwin Granite samples suggests that they formed from similar magmas, but that the REE patterns for the white granite and the quartz-feldspar porphyry phases suggest that they are more highly fractionated portions of the magma. The REE pattern for the Elliott Bay Granite (green line in Figure 6.29) is depleted in LREE, relative to the Murchison and Darwin Granites. However, MREE and HREE patterns are similar. The Elliott Bay sample is from the Lower Rocky Point Pluton, a phase of the granite that was intensely hydrothermally altered to sericite, epidote and chlorite assemblages

(White, 1975; Alexander, 1981). The depletion of LREE, therefore probably occurred as a result of hydrothermal alteration or earlier-deeper fractionation and removal by minerals such as allanite (epidote mineral), with a high K_d for LREE.

Table 6.6 shows the major and trace elements that increase or decrease systematically for each of the five Darwin Granite samples analysed for REE. Interestingly, the Darwin Granite suite, shows an order of magnitude decrease in total REE with increasing granite evolution. As shown on Figure 6.30, the light REE patterns for the microgranite, white granite and quartz-feldspar porphyry are similar in shape but lower in values than the REE pattern for the pink granite phases. The evolved granites in the Darwin Granite suite, the white granite and quartz-feldspar porphyry, have a total REE content of 15 and 23 ppm respectively (Appendix E-1). This is in contrast to an average of 214 ppm for the Darwin pink granite and 253 ppm for the Murchison granite.

Intermediate to high silica (60-80 wt.% SiO_2) granitoid suites can have decreasing REE abundances with increasing indices of differentation (Nagasawa and Schnetzler, 1971; Evans and Hanson, 1993). This decreasing trend is consistent with compatibility of REE during differentiation and has been noted by several authors (Nagasawa and Schnetzler, 1971; Miller and Mittlefehldt, 1982; Evans and Hanson, 1993). Such decreasing REE abundances are difficult to accomplish through differentation involving the major rock-forming mineral assemblages (i.e. feldspar, quartz, pyroxenes, amphibole, layered silicates) although Nagasawa and Schnetzler (1971) noted that partion coefficients for the mafic minerals are considerably higher in acid magmas than mafic and intermediate ones.

Table 6.6. Elemental response to increasing fractionation within the Darwin Granite.

Increasing Fractionation	Sample Number	SiO_2	TiO_2	Fe_2O_3	MgO	CaO	Na_2O	K_2O	P_2O_5	V	Rb
↓	840200	76.58	0.22	1.74	0.38	0.28	3.15	4.66	0.03	21	135
	B2053	76.78	0.16	0.79	0.19	0.03	2.30	6.03	0.03	8	146
	B2033	78.00	0.09	0.62	0.12	0.24	3.00	5.22	0.01	2	213
	B2043	78.95	0.16	0.33	0.23	0.39	4.19	1.78	0.01	<1.5	61
	B2061	78.37	0.17	0.53	0.14	1.00	4.70	1.31	0.01	2	43

Increasing Fractionation	Sample Number	Sr	Zr	Ba	La	Ce	Nd	Y	Th	U	Total REE
↓	840200	138	132	1385	44.7	89.5	26.5	18	n/a	n/a	185
	B2053	51	121	1759	50	110	37	10	42	4	243
	B2033	26	65	88	19	33	9	8	33	8	74
	B2043	241	133	185	2	4	3	4	44	2	15
	B2061	205	123	211	5	9	3	3	36	2	23

Elements that increase with increasing fractionation.

Elements that decrease with increasing fractionation.

REE distribution coefficients (K_d's) of major rock-forming minerals are <10 and commonly <1 (Higuchi and Nagasawa, 1969; McCarthy and Kable, 1978; Henderson, 1980; Miller and Mittlefehldt, 1982; Evans and Hanson, 1993; Wark and Miller, 1993). However, K_d's for accessory minerals are several orders of magnitude higher. K_d was defined by Hanson (1980). REE are accommodated in minor accessory minerals formed from elements of high ionic potential such as Ti, Zr and P (Evans and Hanson, 1993; Wark and Miller, 1993; Bea, 1995). These minerals typically have high K_d's for REEs and include monazite, apatite, zircon, allanite, and sphene

(Watson and Capobianco, 1981; Miller and Mittlefehldt, 1982; Gromet and Silver, 1983; Sawka, 1988). The addition of high-REE-K_d accessory minerals to a modal mineral assemblage has little effect on the major- and minor element mass balance, but has an enormous effect on the REE content (Watson, 1980; Watson and Capobianco, 1981; Evans and Hanson, 1993). It has been shown that, although the K_d's for apatite and zircon are high, these minerals are refractory and in many cases the modal amount of apatite and zircon is so minor in acid rocks as to equilibrate their effect on REE abundances with that of the common rock forming minerals (Nagasawa, 1970; Nagasawa and Schnetzler, 1971; McCarthy and Kable, 1978). It has been shown that minute quantities of monazite can have an enormous effect on the total REE content of felsic rocks (Miller and Mittlefehldt, 1982; Wark and Miller, 1993) and monazite fractionation (and saturation) is reflected by a trend of decreasing LREE concentrations (Mittlefehldt and Miller, 1983). The occurrence of primary monazite grains in the pink phase of the Darwin Granite has been documented (Section 3.2.2.2). In Figure 6.33), predicted LREE compositions for the equigranular pink granite from Crawford et al. (1992), the microgranite and the white granite were modeled. The predicted LREE compositions for the microgranite and white granite assume 0.02 and 0.028 wt. % monozite in the rock respectively. From Figure 6.33, two points can be made. 1) There is a decrease in total REE with increasing fractionation. 2) The decrease in total REE with increasing fractionation is not unusual. Miller and Mittlefehldt (1982) showed the same fractionation patterns in granites from Granite Mountain and Old Woman Mountain in California. The same authors invoked a model of significant monozite fractionation to account for the decrease in LREE. Although monazites from the Darwin Granite were not analysed, Figure 6.33 shows that fraction of the LREE pattern of a monozite from the I-type Sweetwater Wash Pluton in

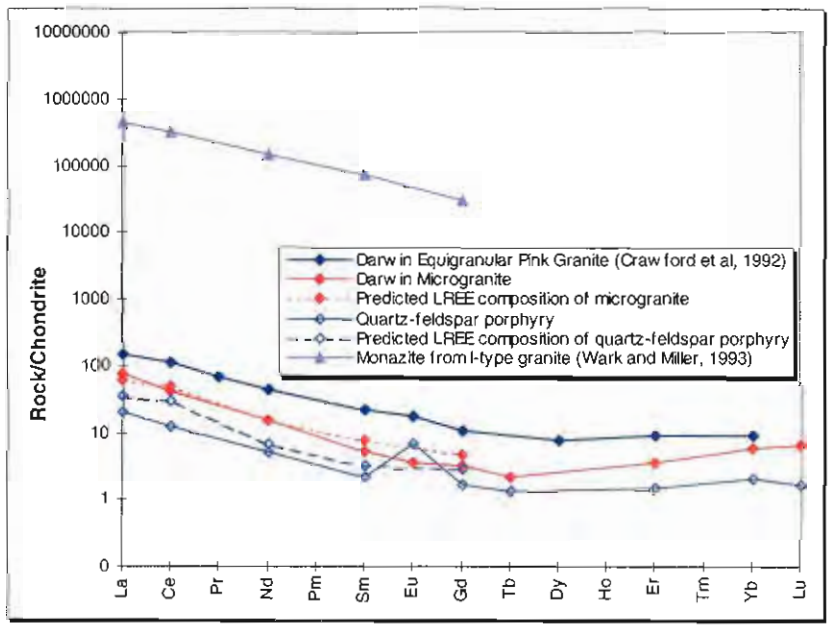

Figure 6.33. Chondrite-normalised REE diagram showing that the predicted LREE compositions for the microgranite and white granite can be achieved by assuming 0.02 and 0.028 wt. % monozite in the rock respectively.

California (Wark and Miller, 1993) can significantly control the LREE pattern in the Darwin Granite suite (except for small variations such as Ce). Therefore, the LREE patterns in Figures 6.30 and 6.33, suggest that a model of monozite fractionation as the primary control of LREE concentrations in the Darwin Granite suite is reasonable. It is therefore interpreted that the LREE patterns shown for the Darwin Granite on Figure 6.30 are a result of monazite fractionation and removal.

Another factor affecting REE concentrations is the abundance of the accessory minerals enriched in REE relative to their coexisting liquids. If REE are contained in accessory minerals during fractionation, REE concentrations correlate with the amount of those accessory minerals in each sample (Nagasawa and Schnetzler, 1971; Evans and Hanson, 1993). This results in strong correlations of accessory-mineral ESCs (such as TiO_2 for rutile and Zr for zircon) with REE abundance (Evans and Hanson, 1993). Microprobe analytical results of accessory minerals are summarised in Table 6.7, and complete results are presented in Appendix E-2.

Table 6.7. Average heavy accessory mineral microprobe analytical results and REE contents from the four phases of the Darwin Granite. In the white granite (B2043), thorite was identified qualitatively by the SEM. Similarly in the pink and white granite phases, sphene was identified qualitatively by the SEM.

	Pink granite (B2053)			Microgranite (B2033)				White granite (B2043)			Quartz-feldspar porphyry (B2061)	
Mineral	Monazite	Rutile	Zircon	Rutile	Zircon	Thorite	Magnetite	Rutile	Zircon	Magnetite	Rutile	Zircon
Si	0.50	0.13	30.96	0.00	29.63	9.84	0.21	0.04	30.24	1.39	0.12	30.13
P	28.58	0.00	0.13	0.00	0.11	5.30	0.00	0.00	0.15	0.00	0.00	0.14
Ca	0.16	0.02	0.01	0.01	0.29	0.12	0.01	0.01	0.18	0.02	0.06	0.13
Ti	0.02	94.36	0.01	91.38	0.02	2.69	0.23	94.21	0.06	0.14	94.46	0.02
Y	0.39	0.07	0.21	0.07	0.38	0.18	0.05	0.07	0.55	0.05	0.06	0.34
Zr	0.00	0.02	67.16	0.01	63.79	0.00	0.00	0.14	63.71	0.00	0.08	63.65
La	15.95	0.00	0.00	0.03	0.00	0.04	0.01	0.00	0.01	0.00	0.00	0.01
Ce	37.25	0.00	0.01	0.00	0.04	0.11	0.01	0.00	0.04	0.02	0.00	0.02
Pr	4.44	0.07	0.02	0.07	0.01	0.08	0.01	0.03	0.02	0.04	0.06	0.01
Nd	10.45	0.04	0.07	0.06	0.09	0.15	0.02	0.03	0.06	0.06	0.04	0.06
Sm	1.24	0.01	0.02	0.00	0.00	0.07	0.01	0.02	0.03	0.00	0.02	0.03
Gd	0.79	0.01	0.03	0.00	0.02	0.01	0.03	0.02	0.03	0.00	0.01	0.02
Dy	0.19	0.03	0.04	0.08	0.03	0.10	0.01	0.01	0.06	0.02	0.00	0.06
Er	0.01	0.00	0.03	0.00	0.05	0.00	0.00	0.01	0.08	0.00	0.01	0.06
Yb	0.02	0.01	0.04	0.01	0.15	0.03	0.00	0.01	0.18	0.00	0.02	0.11
Hf	0.00	0.90	1.46	0.84	2.16	0.06	0.02	0.86	1.64	0.01	0.88	1.42
Pb	0.02	0.02	0.03	0.00	0.04	0.08	0.01	0.01	0.05	0.01	0.02	0.04
Th	0.28	0.00	0.11	0.00	0.36	67.34	0.04	0.00	0.54	0.01	0.01	0.28
U	0.01	0.01	0.16	0.01	0.80	1.59	0.00	0.01	0.77	0.01	0.02	0.48
Total	100.29	95.70	100.51	92.57	97.97	87.78	0.67	95.49	98.42	1.79	95.87	97.02
Total REE in wt. %	70.34	1.07	1.72	1.09	2.57	0.65	0.12	1.00	2.15	0.15	1.04	1.81

Equation 1 was used to calculate the percent of the total REE in a rock contributed by individual accessory minerals.

Equation 1:

$$(\%\text{ of total REE in the rock}) = \frac{(\text{modal \% of mineral in rock}) \times (\text{total REE (ppm) in mineral})}{(\text{total ppm of REE in the rock})}$$

Estimated modal abundances of accessory minerals in all phases of the Darwin Granite indicate that total accessories other than biotite and hornblende, account for <0.1 wt.%. and individual accessories such as monazite are even less. Using Equation 1, it was calculated that in the pink granite (B2053), up to 96% of the total REE and 99% of the total LREE are contained in a few grains (0.0003 wt.%) of monazite. The remainder of the REE are contained in minor amounts of zircon, rutile, sphene and minor ferromagnesian minerals. Modally, the abundant REE bearing

mineral in the microgranite (B2033) and white granite (B2043) is rutile, followed by zircon, sphene and thorite. Table 6.7 shows that in the microgranite, rutile, zircon and thorite all contain less than 0.5 wt.% LREE and only zircon contains appreciable HREE at 2.5 wt.%. In the white granite (B2043) and quartz-feldspar porphyry (B2061), the REE bearing minerals are rutile and zircon, although thorite is present. Rutile contains about 1% total REE while zircon contains nearly 2%. Magnetite was analysed in the microgranite and the white granite and contains about 0.1% total REE in rock types. REE in the pink phase of the Darwin Granite are contained in the minor accessory minerals monazite, zircon and rutile. REE in the microgranite are contained in rutile, zircon, and thorite and REE in the white granite and quartz-feldspar porphyry are contained in rutile and zircon.

Published REE analyses of accessory minerals (other than monazite) shows that, although zircon does have a high K_d for the HREE, HREE and total REE are limited to around 2 wt.% of the mineral (Nagasawa, 1970; Watson, 1979; Watson, 1980; Fujimaki, 1986). This was consistent with results from this study. Similarly although sphene has a high K_d for the LREE, the total amount of REE contained in sphene is limited to several wt.% (Henderson, 1980; Gromet and Silver, 1983). Since sphene occurs in trace quantities, its effect on the total REE budget of any phase of the Darwin Granite is considered insignificant.

The range of analysed Th concentrations in the Darwin Granite was from 33 ppm for the microgranite to 44 ppm in the white granite. The Th content of monazite in the pink granite (B2053) averages 2812 ppm and although monazite is rare, it is interpreted to account for the Th in the pink granite. The restricted range of Th in the other three phases of the Darwin Granite (Appendix C) coupled with the lack of monazite suggests that Th occurs in some other mineral. The Th mineral thorite ($ThSiO_4$), occurs in the microgranite and white granite and contains 67 wt.% Th. Because of the high Th content of the mineral, trace quantities only are required to explain the Th contents of the granites.

Figure 6.32 was produced by normalising the REE patterns to Darwin Granite sample 840200 from Crawford et al. (1992). This approach, detailed in Evans and Hanson (1993), was useful for comparing REE movement in intra-pluton phases. Roughly parallel patterns were determined for the Darwin microgranite, the white granite and the quartz-feldspar porphyry. This is interpreted to indicate that REE in all three phases behaved compatibly. The exceptions are Eu in the quartz-feldspar porphyry, and HREE in the pink granite. The depletion of heavy REE in the pink granite can result from an accessory mineral with a high K_d for HREE fractionating earlier and being removed from the melt. Because Zr contents in all phases of the Darwin Granite vary from 121 to 132 ppm (Table 6.6) the fractionated mineral was not interpreted to be zircon. Partion coefficients for HREE in the mafic minerals hornblende and biotite are considerably higher in acid magmas than mafic and intermediate magmas (Nagasawa and Schnetzler, 1971; Frey et al., 1978). B2053 contained no hornblende and trace amounts of biotite suggesting that the heavy REE depletion was the result of earlier hornblende fractionation and removal.

The high plagioclase content of the white granite and the quartz-feldspar porphyry phases is consistent with increases in CaO and Na_2O and low K_2O contents. The large positive Eu anomaly

of the quartz-feldspar porphyry (Figure 6.30 and Figure 6.32) is consistent with Eu partitioning into plagioclase.

As shown on Figure 6.30, all The pink granite and microgranite granite have flat Eu anomalies. The size of typical negative Eu anomalies decrease with increased oxygen fugacity (Hanson, 1980). Plagioclase fractionation and high fO_2 values are interpreted to have contributed to the small slope of the Eu anomalies.

Immobility of REE

The movement or immobility of trace elements during water-rock interaction is dependent on where they reside: 1) as trace elements in major minerals, 2) as ESCs in accessory minerals, 3) as trace elements in accessory minerals (Bea, 1995). The decreasing abundances of total REE with decreasing TiO_2 and P_2O_5 indicate that the REE in the Darwin Granite are located as trace elements in accessory minerals. The REE in the Darwin Granite are located in the accessory minerals hornblende, monazite, zircon, rutile and thorite, except for Eu which was concentrated in plagioclase within the quartz-feldspar porphyry.

The REEs of basalts and andesites are considered to remain immobile when rocks undergo weak to moderate hydrothermal or metamorphic alteration (Ludden et al., 1982; Michard and Albarede, 1986). REEs are potentially mobile during 'vein-type' and intense hydrothermal alteration, although pervasive alteration can mobilized REE on a local scale while whole rock abundances remain unchanged (Alderton et al., 1980; Humphris, 1984). Ward et al. (1992) studied the Dartmoor Granite and concluded that during pervasive sericitisation and tourmalinisation, REE were mobilised over distances of centimetres, and the REE were redistributed into secondary alteration minerals such as sericite, chlorite, tourmaline, allanite and sphene. Ward et al. (1992) concluded that whole rock REE abundances were not affected, supporting the previous work of Alderton et al. (1980). Although the alkali elements were mobilised and the Cambrian granites were weakly metamorphosed, analysed whole rock REE concentrations are interpreted to accurately reflect the original concentrations in the rock.

Model

Within the Darwin Granite, REE partitioned into the major and accessory minerals: LREE, MREE and HREE into monazite, rutile and zircon, HREE into hornblende, and Eu into plagioclase and K-feldspar. Crystallization of these minerals is supported by the steadily and linearly decreasing trends of their ESCs, P_2O_5, TiO_2, Fe_2O_3, MgO, CaO and total REE with increasing magma evolution (Table 6.6, Figures 6.1, 6.2, 6.5, 6.7, and 6.8). Fractionation and removal of monazite in the pink granite resulted in a REE-depleted residual magma. As the Darwin Granite evolution continued, saturated trace elements such as zirconium and titanium continued to crystallise zircon and sphene. Remaining REE partitioned into zircon and sphene depleting the residual melt in REE. The microgranite is interpreted to represent an intermediate step in the final crystallization history with the final phases, the residual white granite and related quartz-feldspar porphyry phase, having an order of magnitude less total REE than the pink phase. A similar order of magnitude depletion in REE in more evolved granite phases was noted by Ward et al. (1992) in the Dartmoor Granite.

6.2.3 Partial melting and fractional crystallization

A variety of geochemical variations within the Murchison, Darwin and Elliott Bay Granites support the proposal that within-pluton fractional crystallization has taken place (Figures 6.1, 6.3, 6.5, 6.7, 6.8 and 6.21). The proposal was tested using computer-generated least-squares mixing models to determine fractionating mineral proportions for the Darwin pink granite → microgranite and pink granite → white granite. For the least-squares mixing tests, the GENMIX petrological mixing program (Le Maitre, 1980) was used. SiO_2 contents vary 1.5% for the microgranite and 2.5% for the white granite, therefore the major minerals modeled included quartz, K-feldspar, plagioclase magnetite and biotite. K-feldspar and plagioclase phenocryst compositions for the pink granite and microgranite were determined by microprobe analysis (Table 6.8). Completely fresh biotite was not observed in any of the Darwin Granite phases. Therefore, granitic biotite compositions from Gromet and Silver (1983) and Dodge et al., (1969) were used. Unaltered plagioclase was not observed in the white granite and, although the average composition of plagioclase from the microgranite provided the best fit of the data (Table 6.9), albite analyses from the pink granite provided similar results. Results for the pink granite → microgranite and pink granite → white granite are presented in Tables 6.9 and 6.10. In these two phenocryst models, the overall percentages of fractionating minerals worked well. The r^2 values of 0.3 and 0.1 for the microgranite and white granite respectively are considered good fits. In the microgranite, the largest differences are in Al_2O_3, Na_2O and K_2O. This is interpreted to be a result of minor sodium and potassium metasomatism.

It has been shown that the High Field Strength element (REE, Ti, Zr, Th and Nb) content of the Darwin Granite was controlled by fractionation and removal of monazite, zircon, apatite, sphene and hornblende. These elements can, therefore, not be used to test the GENMIX model. Large Ion Lithophile element (Cs, Rb, Sr, Ba and Eu) concentrations are controlled by the major silicate minerals, plagioclase and K-feldspar (McCarthy and R.A., 1976; McCarthy and Groves, 1979). The scatter of data on Harker diagrams of Rb vs. Sr and Rb vs. SiO_2 (Figures 6.20 and 6.25 respectively) is interpreted to represent mobility due to post emplacement processes. Since trace elements were mobile, a test of the GENMIX model was not conducted. However, the GENMIX major element modeling supports the interpretation that the microgranite and white granite were derived from fractionation from the pink granite. It cannot be interpreted that the pink granite was the source melt for the entire suite.

Table 6.8. Analytical results of microprobe analyses of feldspars and magnetite in the Darwin pink and microgranite phases.

Label	SiO_2	TiO_2	Al_2O_3	Fe_2O_3	MnO	MgO	CaO	SrO	BaO	Na_2O	K_2O	Rb_2O	Sum Ox%	Ab	An	Or
Orthoclase																
B2055-misc-09799-B-K-feld1	63.24	0.01	18.65	0.01	0.00	0.00	0.00	0.01	0.36	0.27	16.49	0.00	99.05	2.44	0.00	96.90
B2055-misc-09799-C-K-feld1	62.94	0.00	18.45	0.14	0.00	0.00	0.00	0.01	0.34	0.25	16.63	0.00	98.77	2.22	0.00	97.14
B2055-misc-09799-C-Feld1	63.12	0.01	19.09	0.50	0.02	0.02	0.00	0.08	0.37	0.81	15.22	0.00	99.24	7.39	0.00	91.71
B2055-misc-09799-E-Feld1	63.36	0.01	18.58	0.03	0.00	0.01	0.00	0.01	0.28	0.45	16.29	0.00	99.02	4.02	0.00	95.44
B2055-misc-09799-G-Feld1	62.66	0.02	19.02	0.03	0.01	0.01	0.00	0.04	0.53	0.24	16.39	0.00	98.94	2.17	0.00	96.77
B2055-misc-09799-H-Feld1	62.75	0.02	18.90	0.28	0.00	0.01	0.00	0.02	0.75	0.25	16.25	0.00	99.23	2.22	0.00	96.36
Average 2055 Orthoclase	63.01	0.01	18.78	0.17	0.01	0.01	0.00	0.03	0.44	0.38	16.21	0.00	99.04	3.41	0.00	95.72
2033-misc-09799-A-Feld1	63.83	0.00	18.38	0.06	0.00	0.00	0.03	0.07	0.00	0.39	16.58	0.00	99.35	3.41	0.14	96.26
2033-misc-09799-A-Feld4	63.64	0.01	18.57	0.08	0.00	0.00	0.02	0.01	0.05	0.27	16.65	0.00	99.30	2.36	0.10	97.43
2033-misc-09799-B-Feld4	64.22	0.01	18.50	0.09	0.00	0.02	0.00	0.02	0.01	0.54	16.43	0.00	99.83	4.75	0.00	95.19
Average 2055 Orthoclase	63.90	0.01	18.48	0.08	0.00	0.01	0.02	0.03	0.02	0.40	16.55	0.00	99.49	3.50	0.08	96.29
Albite																
B2055-misc-09799-H-Feld2	67.13	0.00	20.52	0.22	0.00	0.02	0.08	0.03	0.06	10.98	0.44	0.01	99.49	96.82	0.41	2.56
2033-misc-09799-B-Feld1	68.17	0.00	19.92	0.03	0.01	0.01	0.06	0.01	0.00	11.41	0.06	0.00	99.68	99.33	0.30	0.35
2033-misc-09799-B-Feld2	68.05	0.00	20.03	0.05	0.03	0.00	0.09	0.06	0.00	11.34	0.11	0.00	99.76	98.80	0.43	0.62
2033-misc-09799-B-Feld3	68.01	0.00	19.89	0.03	0.00	0.01	0.04	0.00	0.01	11.47	0.07	0.00	99.55	99.36	0.21	0.38
2033-misc-09799-D-Feld1	68.43	0.00	19.97	0.00	0.00	0.00	0.11	0.02	0.00	11.46	0.07	0.00	100.06	99.00	0.54	0.41
Average 2033 Albite	68.17	0.00	19.95	0.03	0.01	0.01	0.08	0.02	0.00	11.42	0.08	0.00	99.76	99.12	0.37	0.44
B2033 magnetite	0.11	0.28	0.23	99.35	0.00	0.00	0.03	0.00	0.00	0.00	0.00	0.00	100.00			

Table 6.9. Petrological mixing equation for derivation of microgranite (41372) from the pink phase of the Darwin Granite (41174). * Biotite analysis from Dodge et. al. (1969).

	% amounts	SiO_2	TiO_2	Al_2O_3	Fe_2O_3	FeO	MgO	CaO	Na_2O	K_2O	P_2O_5	Total
Reactants Used												
Pink Granite (41174)	100.00%	75.49	0.18	13.88	1.65	0.00	0.35	0.17	2.74	5.47	0.06	100.00
Products Used												
Microgranite (41372)	88.65%	77.83	0.06	12.84	0.75	0.00	0.08	0.17	2.98	5.27	0.02	100.00
Albite-B2055-Feld2	3.95%	67.54	0.00	20.65	0.22	0.00	0.02	0.08	11.05	0.44	0.00	100.00
Orthoclase-average B2055	4.02%	63.93	0.01	19.05	0.17	0.00	0.01	0.00	0.38	16.45	0.00	100.00
Biotite *	3.39%	35.60	2.90	17.09	28.30	0.00	6.10	0.00	0.42	9.59	0.00	100.00
Estimated Compositions												
Reactants		75.49	0.18	13.88	1.65	0.00	0.35	0.17	2.74	5.47	0.06	
Products		75.43	0.15	13.54	1.64	0.00	0.28	0.16	3.11	5.67	0.02	
Differences		0.06	0.03	0.34	0.02	0.00	0.07	0.02	-0.37	-0.20	0.04	
Residual Sum Squares	0.30											

Table 6.10. Petrological mixing equation for derivation of the white granite (41373) from the pink phase of the Darwin Granite (840200). ** Biotite analysis from Gromet and Silver (1983).

	% amounts	SiO_2	TiO_2	Al_2O_3	Fe_2O_3	FeO	MgO	CaO	Na_2O	K_2O	P_2O_5	Total
Reactants Used												
Pink Granite (840200)	100.00%	75.40	0.22	14.30	1.71	0.00	0.37	0.28	3.10	4.59	0.03	100.00
Products Used												
White granite (41373)	77.42%	79.74	0.12	13.42	0.70	0.00	0.27	0.08	3.01	2.66	0.00	100.00
Average 2033 Albite	5.89%	68.35	0.00	20.00	0.03	0.00	0.01	0.08	11.45	0.08	0.00	100.00
2033-misc-09799-A-Feld4	13.83%	64.13	0.01	18.71	0.08	0.00	0.00	0.02	0.27	16.78	0.00	100.00
B2033 magnetite	0.76%	0.11	0.28	0.23	99.35	0.00	0.00	0.03	0.00	0.00	0.00	100.00
Biotite **	2.10%	39.73	2.61	15.28	22.58	0.00	10.41	0.00	0.09	9.31	0.00	100.00
Estimated Compositions												
Reactants		75.40	0.22	14.30	1.71	0.00	0.37	0.28	3.10	4.59	0.03	
Products		75.46	0.15	14.48	1.78	0.00	0.43	0.07	3.04	4.58	0.00	
Differences		-0.06	0.07	-0.18	-0.07	0.00	-0.06	0.21	0.06	0.01	0.03	
Residual Sum Squares	0.10											

Linear trends on Harker diagrams such as those shown for the Murchison and Darwin Granites (Figures 6.1, 6.3, 6.7, and 6.8), have been interpreted to represent magma mixing or restite unmixing (Chappell, 1987; Wall et al., 1987; Chappell, 1996) or fractional crystallization (Cox et al., 1980; Clark, 1992). However, magma mixing takes place deep in the crust or at the interface where the melt is produced (Pitcher, 1993). If mixing occurs as suggested by some Nd-Sr-O isotope data (Cousins et al., 1998; Landenberger and Collins, 1998), then the rocks involved were not exposed at the surface. Chappell (1998) concludes that mixing must be of secondary

importance and the isotopic differences are likely due to unique source rock compositions. Chappell (1996) concluded that because mafic and intermediate members of a fractionation series would already be solid before the production of a felsic magma, that magma mixing between mafic and felsic melts to produce a fractionated I-type suite was not an issue.

Source rock compositions may be estimated from restite compositions. Model restite composition is the point where modal quartz or K-feldspar disappear as rock compositions are extrapolated to mafic values (Compston and Chappell, 1979). The more mafic members of the Darwin Granite suite are buried, eroded or non-existent. However, it has been suggested earlier (Section 6.2.2.3) that the Darwin and Murchison Granites formed from similar melts, therefore, Murchison Granite data was re-examined as a possible analogy. The Murchison Granite has wide variety of granitoid compositions illustrated on Figures 6.13-6.14. An estimate of the minimum melt composition is the composition of the most mafic granite composition (Chappell, 1984) in the Murchison suite and is given as the composition of sample AT050 from Abbott (1992). The rock is an unaltered granodiorite (Figure 3.3), although, at the location that the sample was collected, "more mafic inclusions" were observed (Abbott, 1992). This implies that the Darwin Granite and the Murchison Granite were produced by partial melts of granodiorite composition within the stability field of feldspar, i.e. continental crust.

High-grade regionally metamorphosed granulite facies terrains are the likely source for crustally derived granites (White and Chappell, 1977). Heterogeneity in these crustal sources produce scatter in Harker diagrams unless a homogeneous source was melted (Wall et al., 1987). A condition Wall et al., (1987) consider unlikely because to the large volumes of source rocks that must be melted to produce granites from partial melts. However, a large relatively homogeneous source is available in the lower crust (Chappell, 1984). Underplating of lower crustal material can produce homogeneous partial melts capable of producing I-type granites (White, 1979; Chappell, 1984).

Negative εNd values (Table 6.2) imply that the Murchison and Darwin Granites were derived from an enriched mantle source or continental crust with a lower Sm/Nd than CHUR. Nd model ages range from 694 to 964 Ma (chondritic mantle) and 1226 to 1626 Ma (depleted mantle) for the Darwin and Murchison Granites (Table 6.2). A phyllite from the Tyennan region has an Rb-Sr model age of 1100-1150 Ma and corresponds to the age of deposition (Raheim and Compston, 1977). A Pb-Pb isochron from a meta-siltstone along the Lyell Highway gives an age of 1300 ± 170 Ma (Gulson et al., 1988) and inherited zircons in the MRV were dated at up to 1600 Ma (Perkins and Walshe, 1993). These dates fall within or close to the range of depleted mantle ages.

Felsic rocks with low P_2O_5 contents (eg. <0.10 wt.%), were interpreted to have been derived from a source region with little phosphorus (Watson and Capobianco, 1981). An examination of the Proterozoic Tyennan Block geochemical database at the Tasmanian Mines Department shows an average P_2O_5 content of 0.03 wt.% with a range of 0.2 to 0.01 wt.%.

6.2.4 Comparison of the Cambrian Granites with the Devonian granites of western Tasmania

A second major granite suite in western Tasmania is of Devonian age and related to major tin and tungsten mineralisation. Because of their economic significance, the Devonian granites were the subject of numerous studies (Solomon and Griffiths, 1974; Patterson et al., 1981; Leaman and Richardson, 1989; Kitto, 1994; Bajwah, 1995; Walshe et al., 1996). The Devonian granites of western Tasmania belong to the granites of the Lachlan Fold Belt of southeastern Australia. There, studies of mainland granites (White et al., 1977; Chappell et al., 1988; Gray, 1990) formed the basis of the popular I & S classification scheme previously discussed (Chappell and White, 1974; White and Chappell, 1983; Chappell and White, 1992; Blevin and Chappell, 1995).

Table 6.11 outlines the similarities and differences between the Cambrian and Devonian granites of western Tasmania. The data for the Devonian granites was summarised from Kitto (1994) in his study of the Pine Hill Granite and was taken as representative of geochemical and morphological data for the other Devonian granites in western Tasmania. The significant differences were: the Cambrian granites are subvolcanic, I-type, oxidised, magnetite-series granites with associated Cu, Au, Pb, Zn ores; while the Devonian granites are I and S-type, reduced, ilmenite-series granites with associated Sn and W ores.

Gray (1990), has shown that Devonian granites in eastern Tasmania can be traced via islands in Bass Strait to Wilson's Promontory on the mainland and, on the basis of $^{87}Sr/^{86}Sr$ values are correlates of granites in his "central" belt (maximum initial $^{87}Sr/^{86}Sr$ values of approx. 0.720). He notes that the western Tasmanian granites may correlate to granites in his "western association (maximum initial $^{87}Sr/^{86}Sr$ values of up to 0.718)" but he lacked enough data to come to a definitive conclusion. Based solely on initial $^{87}Sr/^{86}Sr$ values as shown previously in this study, this correlation seems to fit. The Cambrian granites in Tasmania are older than the western belt mainland granites and the model for the western Tasmanian Cambrian granites involves an island arc and continental collision (Crawford et al., 1992). Subsequent to the Cambrian granites emplacement, they were uplifted and eroded in the late Cambrian to Ordovician Jukesian Orogeny (correlated with the Delamerian Orogeny on the mainland). The approximately 500 Ma granites in the Adelaide Orogenic belt (western belt) were emplaced during the peak of this metamorphic event (Gray, 1990).

6.3 ALTERATION MINERAL CHEMISTRY IN VOLCANIC ROCKS

Chlorite, sericite and carbonate were analysed using an electron microprobe in an attempt to relate the hydrothermal alteration mineral chemistry to the calculated mass gains and losses (Section 6.4). In addition, when possible, minerals have been classified on the basis of their chemical composition.

Table 6.11. Characteristics of Cambrian and Devonian Granites in western Tasmania.

CHARACTERISTIC	DEVONIAN GRANITES	CAMBRIAN GRANITES
MORPHOLOGY	Generally subrounded and batholithic in size.	Generally narrow elongate small plutons.
AGE	Late Devonian to Early Carboniferous (325-370 Ma)	Cambrian in age (approx. 500 Ma)
MINERALOGY	Hornblende Granodiorite to Biotite Granite	Diorite to Granite
PORPHYRY PHASE	Porphyritic phases common	Porphyritic phases rare
HOST ROCKS	Commonly intrude sedimentary (Carbonate) rocks	Subvolcanic in nature
I or S-type	I and S-type	I-type
OXIDISED OR REDUCED	Reduced	Oxidised
MAGNETITE OR ILLMENITE SERIES	Illmenite Series	Magnetite Series
FRACTIONATION	Highly fractionated having high SiO_2 (68-77%), K_2O (av. 4.8%), and low Na_2O (av. 2.5%).	Highly fractionated having high SiO_2 (58-78%), K_2O (av. 5%), and low Na_2O (av. 2.5%).
	CaO, TiO_2, Fe_2O_3, and MgO decrease linearly with increasing SiO_2. Rb vs Ba trend decreases with increasing fractionation (Kitto, 1994)	CaO, TiO_2, Fe_2O_3, MgO and P_2O_5 decrease linearly with increasing SiO_2. Rb vs Ba trend increases with increasing fractionation
$\delta^{18}O$ W.R.(‰)	8-11‰	9.3-12.5 ‰
DEPTH OF EMPLACEMENT	Estimated to be 4-7 km for the W bearing granites and 1-4 km for Sn bearing granites (Kitto, 1994; Jones, 1993)	Estimated to be 1-4 km (Jones, 1993).
MINERALISATION	Intimate association between granites and Sn and W mineralisation.	Primarily Cu-Au and Cu, Pb, Zn mineralisation.
MINERALISATION STYLE	Greisen and carbonate replacement.	Confined to lode style veins, the VHMS association is contentious.
ALTERATION	Zoned alteration inward goes from albitisation to sericitisation to intense tourmalinisation.	Zoned alteration inward goes from sericitisation to chloritisation to K-feldspar.
MINERALISING FLUIDS	Mineralising fluids are magmatic and derived from granites.	Mineralising fluids are contentious, may be magmatic or a mixture of magmatic and seawater.

6.3.2 Chlorite

Jukes Road exposes a cross-section through several chlorite-bearing hydrothermal alteration mineral assemblages (Section 5.5.4.2) within the feldspar-phyric dacite. This section provides an opportunity to examine variations in chlorite mineral chemistry within the observed hydrothermal alteration styles in the feldspar-phyric dacite and quartz-feldspar ± biotite porphyry dykes, and to determine the potential use of chlorite mineral chemistry as a vector toward mineralisation. A reconnaissance study was carried out on samples from the chlorite-bearing alteration styles discussed in Section 5.5.2.2. Secondary chlorite is associated with magnesium and iron enrichment (Section 6.4). Chlorites from five of the six alteration styles were probed as part of this study. The sixth alteration style, groundmass chlorite, was also sampled and analysed. However, the chlorite crystals were found to be intergrown with sericite and results were inaccurate. The five varieties of chlorite occurrences studied in this section are: 1) chlorite after biotite phenocrysts, 2) chlorite in magnetite ± sulfide veins hosted within quartz-feldspar ± biotite porphyry dykes and breccias, 3) chlorite that has replaced feldspar phenocrysts, 4) diffuse chlorite that occurs between feldspar and quartz grains in intensely altered feldspar-phyric dacites, and 5) chlorite in the matrix of mineralised hydrothermal breccias. Exact timing relationships between the 5 chlorite types are unknown but several generation are inferred based on the interpreted diagenetic, hydrothermal and metamorphic origins

Table 6.12 presents average microprobe analyses from the five chlorite varieties studied. Individual chemical analyses are included in Appendix J. Chlorite compositions are classified using a standard Hey diagram (Figure 6.34). All five chlorite varieties have iron-rich compositions,

Table 6.12. Average chlorite compositions and calculated chlorite temperatures for five chlorite hydrothermal alteration styles. Corrected Al^{IV} values and chlorite temperatures calculated using the methods of Kranidiotis and MacLean (1987).

	Feldspar-phyric dacite					Quartz-feldspar +/- biotite porphyry dykes		
Label	Biotite Phenocryst Replacement	Feldspar Phenocryst Replacement	Chlotite veins	Diffuse Chlorite	Breccia, Matrix	Biotite Phenocryst Replacement	Feldspar Phenocryst Replacement	Chlotite veins
Number of Analyses	4	2	11	4	6	17	2	9
SiO_2	25.28	24.67	24.51	23.44	23.65	23.68	23.49	23.66
TiO_2	0.05	0.05	0.04	1.13	0.04	0.08	0.03	0.03
Al_2O_3	19.55	19.16	20.42	19.56	20.39	20.14	19.20	19.87
Cr_2O_3	0.02	0.01	0.01	0.01	0.00	0.02	0.00	0.01
FeO	36.67	39.26	37.92	38.03	39.57	37.10	40.70	37.86
MnO	0.36	0.32	0.46	0.21	0.38	0.25	0.16	0.24
MgO	6.42	3.70	4.76	5.28	4.51	6.65	4.73	6.14
CaO	0.01	0.05	0.04	0.02	0.03	0.05	0.03	0.06
Na_2O	0.04	0.13	0.04	0.03	0.03	0.02	0.02	0.03
K_2O	0.22	0.30	0.34	0.31	0.09	0.04	0.12	0.06
ZnO	0.19	0.16	0.11	0.12	0.09	0.06	0.05	0.06
NiO	0.00	0.01	0.02	0.01	0.01	0.01	0.00	0.02
H_2O(c)	10.80	10.48	10.69	10.57	10.60	10.66	10.48	10.60
Sum Ox%	99.58	98.27	99.35	98.72	99.39	98.77	99.01	98.64
Cations								
Si	5.61	5.64	5.49	5.32	5.35	5.33	5.38	5.35
Ti	0.01	0.01	0.01	0.19	0.01	0.01	0.01	0.01
Al/Al^{IV}	2.39	2.36	2.51	2.68	2.65	2.67	2.62	2.65
Al^{VI}	2.73	2.81	2.89	2.56	2.79	2.67	2.55	2.65
Cr	0.00	0.00	0.00	0.00	0.00	0.00	0.00	0.00
Fe2+	6.81	7.51	7.13	7.23	7.49	6.98	7.79	7.17
Mn2+	0.07	0.06	0.09	0.04	0.07	0.05	0.03	0.05
Mg	2.12	1.26	1.59	1.78	1.52	2.23	1.61	2.07
Ca	0.00	0.01	0.01	0.01	0.01	0.01	0.01	0.01
Na	0.02	0.06	0.02	0.01	0.01	0.01	0.01	0.01
K	0.06	0.09	0.10	0.09	0.02	0.01	0.04	0.02
Zn	0.03	0.03	0.02	0.02	0.02	0.01	0.01	0.01
Ni	0.00	0.00	0.00	0.00	0.00	0.00	0.00	0.00
OH	16.00	16.00	16.00	16.00	16.00	16.00	16.00	16.00
Sum Cat#	35.86	35.84	35.86	35.92	35.94	36.00	36.05	36.00
MgO/(FeO+MgO)	0.24	0.14	0.18	0.20	0.17	0.24	0.17	0.22
FeO/(MgO+FeO)	0.76	0.86	0.82	0.80	0.83	0.76	0.83	0.78
Uncorrected Al^{IV}	2.39	2.36	2.51	2.68	2.65	2.67	2.62	2.65
Corrected Al^{IV}	2.92	2.96	3.08	3.24	3.23	3.20	3.20	3.19
Temperature Range	312-341	329-334	267-386	342-378	338-371	313-380	349-366	343-370
Chlorite Temp°C	328	331	345	362	360	357	358	356
Na+K+2Ca Range	0.15-.043	0.42-0.61	0.18-1.82	0.19-0.83	0.01-0.46	0.03-0.40	0.11-0.28	0.08-0.49
Na+K+2Ca Average	0.27	0.52	0.46	0.38	0.18	0.17	0.20	0.21

which plot mostly within the ripidolite field. Brunsvigite samples have consistently the highest Na + K + 2Ca, corrected Al^{IV}, and Si/Al values, suggesting contamination by interlayered sericite as described by Jiang et al. (1994).

To test whether chlorites were equilibrated with bulk rock compositions during regional metamorphism, Mg number ($Mg\# = 100 \times MgO_{(total)} / (FeO_{(total)} + MgO_{(total)})$) for the various chlorite alteration styles was compared to Mg# for corresponding whole rock geochemical analyses (Figure 6.35). A nonlinear relationship is apparent, which is interpreted to indicate that the iron-rich chlorites did not equilibrate with the bulk rock compositions during greenschist facies metamorphism.

On Figure 6.36, chlorite Mg# is plotted as a function of distance along Jukes Road. The five chlorite styles in the feldspar-phyric rhyolite and the quartz-feldspar ± biotite porphyry dykes are discriminated. There is a large variation in Mg# within individual samples for each alteration style. This contrasts with Mt. Lyell, where individual samples contain chlorites with homogeneous compositions, but large variations occur between samples (Hendry, 1981).

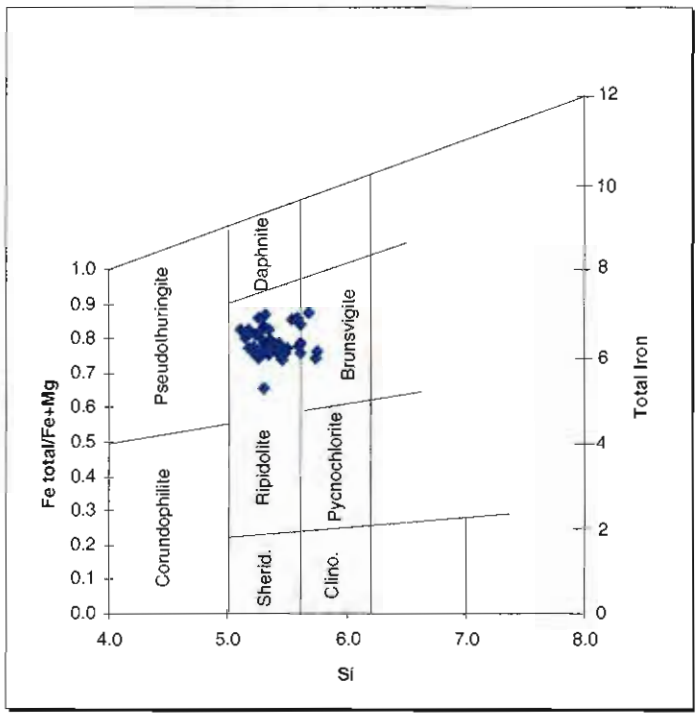

Figure 6.34. Hey diagram (Hey, 1954), Si vs. Total Iron / Fe + Mg, for classification of chlorites. Si and Fe total / Fe + Mg are calculated using cations from Appendix J.

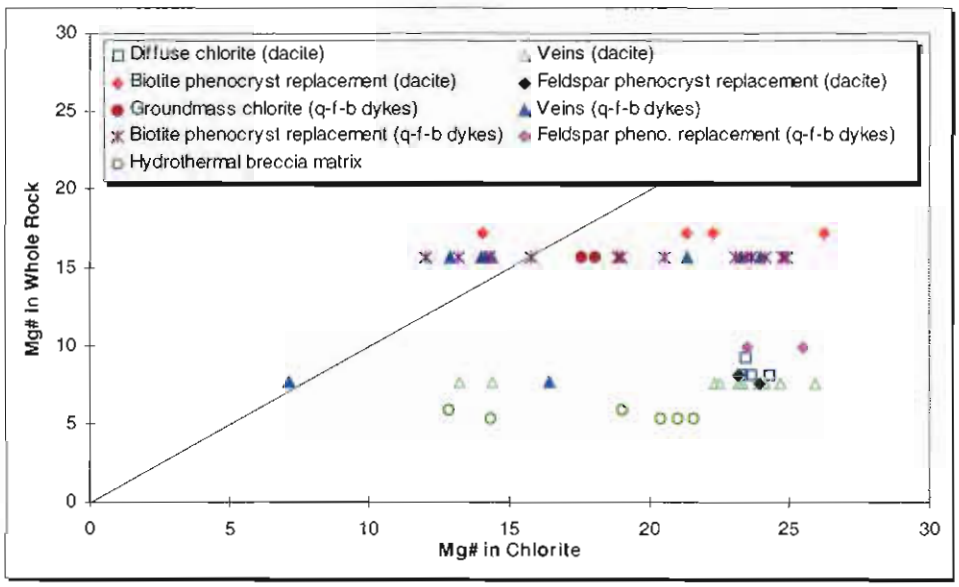

Figure 6.35. Whole rock Mg# vs. chlorite Mg# for Jukes Road samples. The higher Mg# for the chlorites suggests that the Mg in the rock is contained within chlorite and not within other minerals.

Whole rock Mg-numbers were calculated for rocks within 800 metres of the Jukes Prospect and are plotted against distance in Figure 6.37. There is a sharp decrease in whole rock Mg# within the dacites with increasing proximity to the main mineralised zone. The decrease is due to increased total iron concentration caused by the increased magnetite and pyrite abundances.

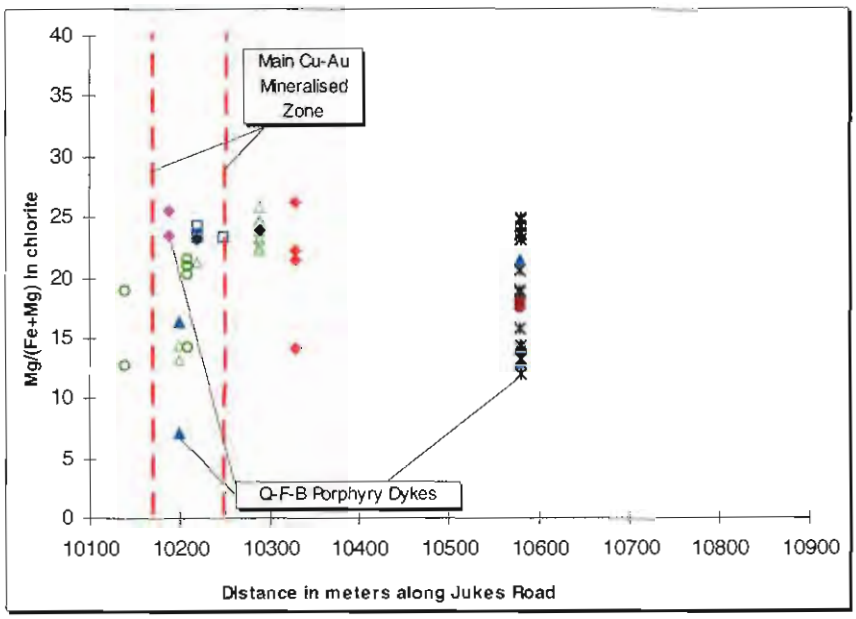

Figure 6.36. Chlorite Mg# compared to distance along Jukes Road. Variable Mg-numbers were detected for a given chlorite type within individual samples. The range of values for the replaced feldspar and biotite phenocrysts, veins and diffuse chlorite in the dacite is similar. The replaced feldspar phenocrysts in the quartz-feldspar porphyry dykes are similar to replaced feldspar phenocrysts in the dacite. The range of veins, biotite replaced phenocrysts and groundmass chlorite in the dykes overlaps the range of values of the breccia matrix chlorite. Legend as in Figure 6.35.

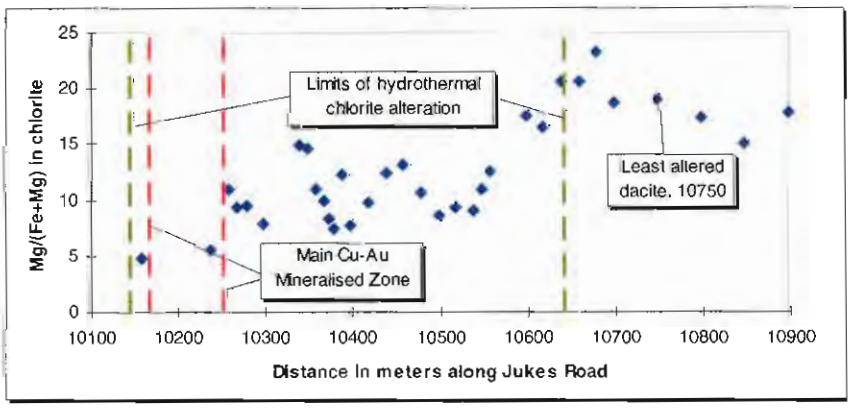

Figure 6.37. Whole rock Mg-numbers vs. distance along Jukes Road. A consistent decrease in whole rock Mg# occurs with increasing proximity to the mineralised zone due to additional iron from minerals such as magnetite and pyrite.

Hydrothermal chlorites from the MRV have been studied by Walshe and Solomon (1981), Hendry (1981), Polya et al. (1986), Doyle (1990) and Gadaloff (1996). Walshe and Solomon (1981) used chlorite microprobe data to calculate chlorite formation temperatures of 260-290^{0}C and concluded that the temperatures represented metamorphic re-equilibration. Then, using a six-component solid solution model, they calculated ore deposition temperatures of 270-310^{0}C. Polya et al. (1986) studied the Murchison River Gorge as a possible cross-section through a Cambrian massive sulfide system, which include a detailed microprobe study of chlorite mineral chemistry.

They recognised similar overall alteration mineral assemblages to those in the Jukes-Darwin area and concluded that increasing iron contents in chlorite resulted from decreasing temperature.

In addition to the six-component solid solution model (Walshe and Solomon, 1981), various other models for calculating chlorite formation temperatures have been proposed (Cathelineau and Nieva, 1985; Walshe, 1986; de Caritat et al., 1993). Kranidiotis and MacLean (1987) adapted the chlorite geothermometer of Cathelineau and Neiva (1985) and proposed the following equation for the temperature of chlorite formation, based on corrected Al^{IV} concentrations where:

Equation 6.1:

$$Al^{IV}_{correeted} = Al^{IV}_{uncorrected} + 0.7[Fe/(Fe + Mg)_{chl}]$$

Equation 6.2:

$$\text{Temperature (T)} = 106\, Al^{IV}_{corrected} + 18$$

Table 6.12 summarises the temperature ranges calculated, based on the 'corrected' Al^{IV} chlorite geothermometer, for each chlorite variety. While the range of average chlorite temperature values is narrow (328-362^{0}C), the overall range is broader (312-386^{0}C). Several groups in the temperature data were observed. First, the average calculated chlorite temperature within the quartz-feldspar ± biotite porphyry dykes (357-360^{0}C) is similar, regardless of the variety of chlorite sampled. Second, the average calculated chlorite temperatures of vein chlorite, diffuse interstitial chlorite and breccia matrix chlorite in the feldspar-phyric dacite are similar to the temperatures shown in the quartz-feldspar ± biotite porphyry dykes. Third, the calculated chlorite temperatures from the biotite and feldspar phenocrysts within the feldspar-phyric dacite are indistinguishable (328 and 331^{0}C) and are lower than chlorite temperatures calculated for the quartz-feldspar ± biotite porphyry dykes, breccia matrix and veins.

In many instances, accurate analyses of chlorites is beyond the limits of resolution of the electron microprobe (Jiang et al., 1994). Recent reviews of chlorite geothermometry (de Caritat et al., 1993; Schmidt et al., 1999), suggest that none of the geothermometers perform satisfactorily over a wide range of Al content, Fe/(Fe + Mg) values, coexisting mineral assemblages and temperatures. While major contaminations are easily detected with the microprobe, a few 1-7 nanometre (nm) mixed layers can result in subtle changes in the composition that lead to errors in interpretation (Jiang et al. 1994). Jiang et al., (1994) demonstrated a positive correlation between the amount of 1 nm layers and the Na + K + 2Ca content attributable to contamination of the chlorite by smectite or other minerals. As a result, when microprobe data is used in calculations of chlorite temperatures, lower chlorite temperatures are calculated. 'Pure chlorites' are those that have small Na + K + 2Ca contents (<0.05 per formula unit (PFU) based on cations). The chlorites probed as part of the current study contain Na + K + 2Ca contents of up to 1.82 PFU (Table 6.12, Appendix J) and are therefore interpreted to have interlayered or submicroscopic intergrowths of sericite or some other mineral. The use of chlorite geothermometry is, therefore probably not valid for chlorites analysed from the Jukes-Darwin rocks. However, since the non-linear relationship in Figure 6.35 demonstrates that minimal metamorphic re-equilibration in the Jukes Road dacites occurred, the calculated 320-360^{0}C range in chlorite temperatures is interpreted to represent minimum hydrothermal temperatures.

6.3.3 PIMA Analyses of Sericite and Chlorite.

In Chapter 5, white to light green fine-grained mica has been referred to as sericite. In order to investigate compositional variations, microprobe analyses were conducted on representative 'sericite' from the Jukes Road and short wavelength infrared spectral analyses were conducted using PIMA (Portable Infrared Mineral Analyser) on rocks from Jukes Road and Mt. Darwin.

Figure 6.38 shows microprobe data (summary in Appendix J) for micas from Jukes Road. The micas are phengites, with ΣFeO + MgO <7 Wt.%. Samples with >7 Wt.% ΣFeO + MgO lie on a linear trend toward end-member chlorite (ΣFeO + MgO >32 Wt.%). Transitional chlorite/phengite compositions are interpreted to represent analyses of mixed layers, as discussed in Section 6.3.1 and by Jiang et al. (1994) and Schmidt et al (1999). 'Pure phengites' were detected in 4 rocks from the main hydrothermal alteration system and least-altered dacites on Jukes Road. Mixed compositions and chlorites were analysed from the intensely K-feldspar and chlorite-altered portions of the Jukes Prospect. Although the spread of compositional data extend from pure phengites to pure chlorites (Appendices K and L), variations in sericite compositions do not correspond to any individual hydrothermal alteration assemblage.

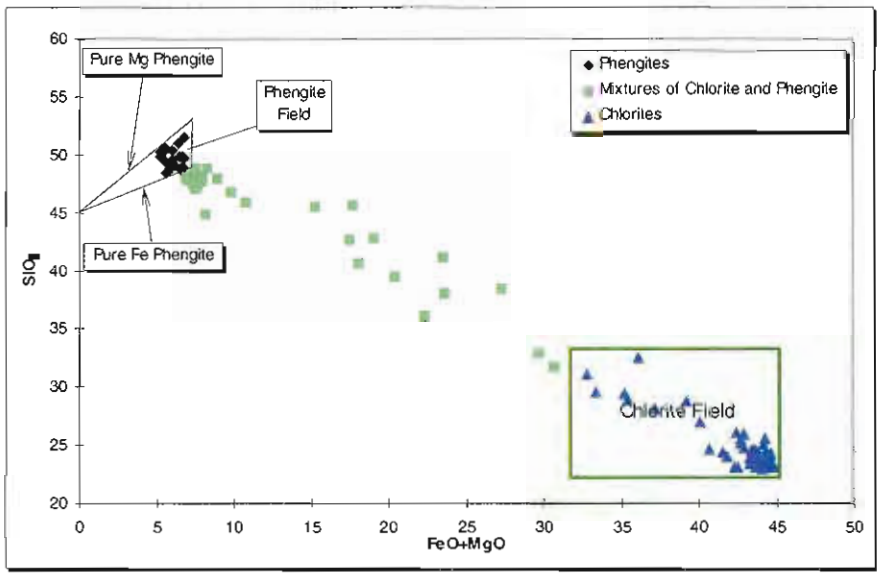

Figure 6.38. SiO_2 vs. FeO + MgO for chlorites from the Jukes Road. Mixing between chlorite and phengite is illustrated for the Jukes Road mica samples. The phengite field is bounded by the trends for a pure Mg and Fe phengite as they extend up to 7 wt.% FeO + MgO from a pure muscovite with 45% SiO_2 and zero wt.% FeO + MgO. The chlorite field is based on analyses from Kranidiotis and MacLean (1987), Cathelineau and Nieva (1985) and Hendry (1981).

The PIMA spectrometer measures reflectance in the short wavelength infrared (SWIR) range of 1300-2500 nanometres (nm). Characteristic SWIR spectra detected from unknown mineral species can be used to assist in their identification. Estimation of relative abundances of the identifiable minerals in the hydrothermal alteration assemblages along Jukes Road and at Mt.

Darwin was accomplished by examining the relative magnitudes of various spectral absorption features. The relationships between the wavelengths of certain spectral absorption features and compositional variations in some minerals (eg. white mica and chlorite) can be used for approximate estimation of mineral compositions by SWIR spectrometry (Pontual et al., 1997a; Pontual et al., 1997b). The SWIR reflectance spectrum has diagnostic absorption features in certain wavelength bands, which are attributed to particular molecular bonds (Figure 6.39). White mica spectra are characterised by sharp, deep, single absorption features in the AlOH band between 2180-2228 nm, and by moderate secondary AlOH features near 2340 and 2440 nm. The proportion of octahedral Al in the mineral structure influences the wavelength of the AlOH feature. High proportions of octahedral Al produce short AlOH wavelengths (typically less than 2195 nm), whereas low proportions relate to long AlOH wavelengths (typically >2216 nm, Post and Noble, 1993). There are a number of compositional substitutions that affect the proportion of Al^{vi}, but commonly white micas with low AlOH wavelengths (2180-2195 nm) are paragonitic in composition, and those with long AlOH wavelengths (2216-2228 nm) are phengitic (Herrmann et al., in press). Normal potassic micas (muscovite and illite) have AlOH wavelengths between 2200-2208 nm (Figure 6.39). Intermediate wavelengths relate either to intermediate compositions, or to mixtures of white mica phases. Chlorite spectra have diagnostic FeOH and MgOH absorption features in the ranges of 2235-2255 nm and 2320-2360 nm, respectively (Figure 6.39, Herrmann et al., in press). The wavelengths of these absorption features increase with increased iron contents of chlorite (Herrmann et al., in press).

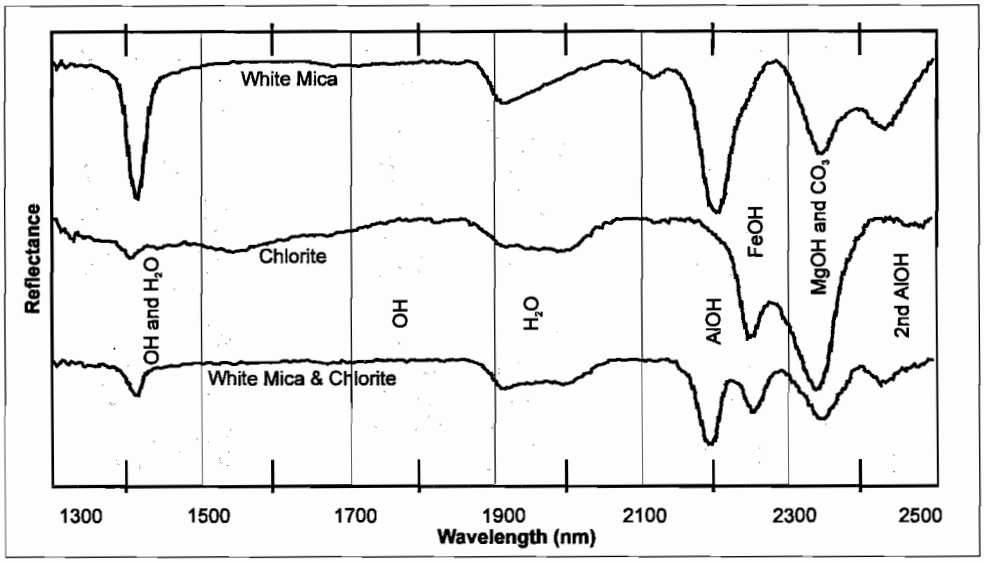

Figure 6.39. Typical white mica, chlorite and mixed white mica + chlorite SWIR spectra. The ranges of typical wavelengths for OH, H_2O, AlOH, FeOH, MgOH and CO_3 alteration features are shown. Modified from Herrmann et al. (in press).

There is little published information about the applications of spectral analysis in interpretation of hydrothermal alteration systems, particularly about VHMS-related systems. Hydrothermal alteration zones were described by Denniss et al. (1999) at the Parys Mountain deposit, UK. Huston et al. (1997) found that PIMA spectral analyses could be used to estimate sericite/chlorite

abundances, and to define local hydrothermal alteration zones associated with VHMS deposits in the Panorama district, Western Australia. Herrmann et al. (in press) interpreted SWIR spectral analyses in hydrothermal alteration zones associated with the Rosebery and Western Tharsis deposits in the MRV and the Highway-Reward deposits in the Mt. Windsor Subprovince, Queensland. The spectral characteristics of the least-altered rocks were related to bulk rock composition (as measured by Ti/Zr ratio) and phyllosilicate content. Rhyolites were found to contain abundant white mica, dacites contained mixtures of chlorite and white mica, and mafic rocks were essentially chloritic (Herrmann et al., in press).

Spectra for samples containing white mica and chlorite typically have absorption features in all three of the AlOH, FeOH and MgOH bands (Figure 6.39). Spectra from samples that contain abundant white mica and minor amounts of chlorite have a slight inflection at the FeOH band. Samples with less white mica than chlorite have a deeper FeOH feature and a weak feature or inflection at the AlOH band (Herrmann et al. in press). Consequently, the ratio of the AlOH and FeOH absorption feature depths provide an estimate of the relative proportions of white mica and chlorite in the sample. Because the white mica secondary AlOH and chlorite MgOH absorption features overlap near 2340 nm, the FeOH feature wavelength is considered to be a better indicator of chlorite composition than MgOH wavelength (Herrmann et al. in press). Low reflectance, noisy spectra without recognizable absorption features were obtained from least-altered quartzo-feldspathic volcanics, or siliceous samples with low phyllosilicate contents.

SWIR spectra for the Jukes Road and Mt. Darwin samples are provided in Appendix K. The spectral data were analysed using 'The Spectral Geologist' software (Merry and Pontual, 1998). In Figure 6.40 the relationship between AlOH and FeO + MgO for sericites is shown. Several analyses were obtained for each sample (Appendix L), and are plotted against detected AlOH wavelengths. The spread in FeO + MgO within each sample suggests no relationship between FeO + MgO and the AlOH spectra. The highest AlOH value (2215 nm) were detected from a least-altered dacite (10750) and the lower AlOH values were analysed from rocks within the Jukes hydrothermal alteration zone, suggesting a possible relationship between AlOH and intensities of hydrothermal alteration.

The detected AlOH wavelength is plotted as a function of distance (in metres) along Jukes Road (Figure 6.41). The Jukes Road dacites plot in a zone of intermediate compositions between pure phengites (2216-2228 nm) and the muscovite/illite field (2200-2208 nm) suggesting a mixture between the two. A decrease in AlOH wavelengths was detected from least-altered dacites (>10600 metres) with AlOH values around 2215, inwards towards the main mineralised zone, where lower AlOH values of 2210-2212 occur around 10200 metres. A similar relationship was observed at Western Tharsis by Huston (in press). Although, the lower AlOH values occur within the main mineralised zone, the wide range of AlOH values (2209-2215) observed is consistent with variable sericite compositions.

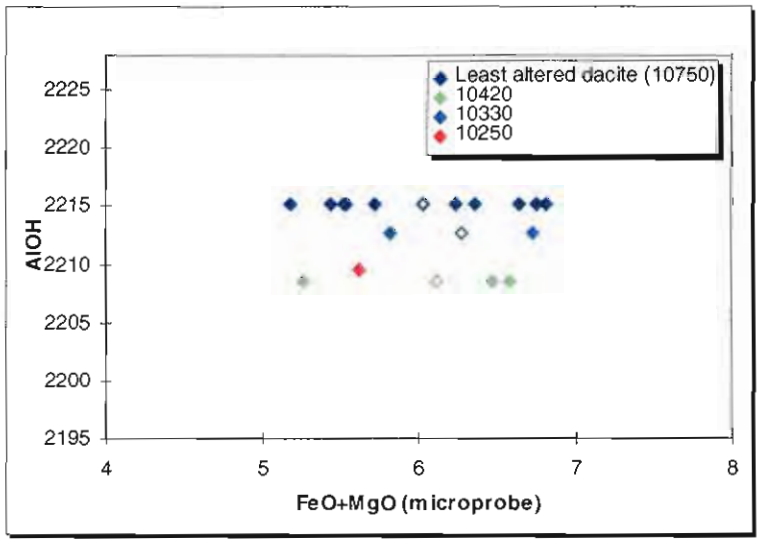

Figure 6.40. AlOH vs. average FeO + MgO values for Jukes Road dacites. The spread of data represents all analyses for the individual sample and the open symbols are the average value. The spread of data and lack of trend suggests no relationship between AlOH and FeO + MgO values.

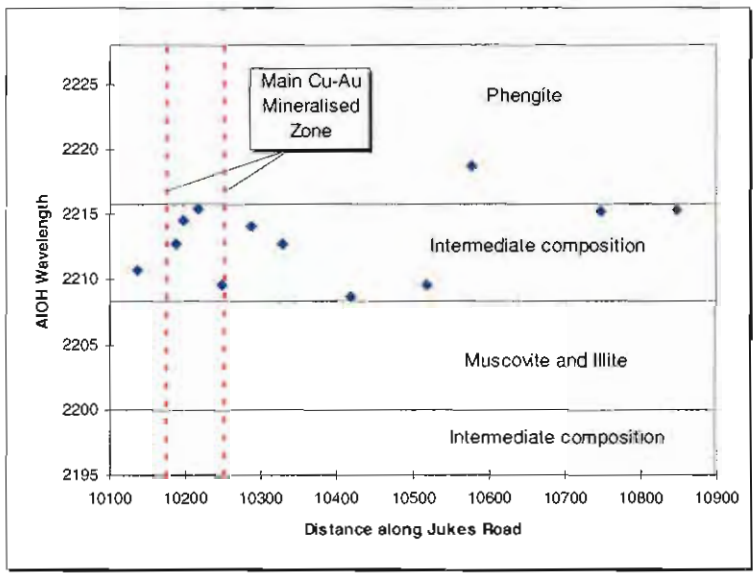

Figure 6.41. AlOH vs. distance (metres) along the Jukes Road. A weak decrease in AlOH wavelengths was detected from least-altered dacites (>10600 metres) with AlOH values around 2215, inwards towards the main mineralised zone where lower AlOH values of 2210-2212 occur. *This interpretation is based on a computer generated trend and the number of samples is limited. Additional sampling is required to further test this interpretation.*

Chlorite Mg-numbers for the Jukes Road dacites are compared to the FeOH wavelengths in Figure 6.42. Chlorites from 10290 metres have FeOH wavelengths of 2233 nm, suggesting mixing of phengite and chlorite. The other samples (10140,10190 and 10580) plot in a tight group (between 2249 and 2253 nm) at the high-iron end of the chlorite field.

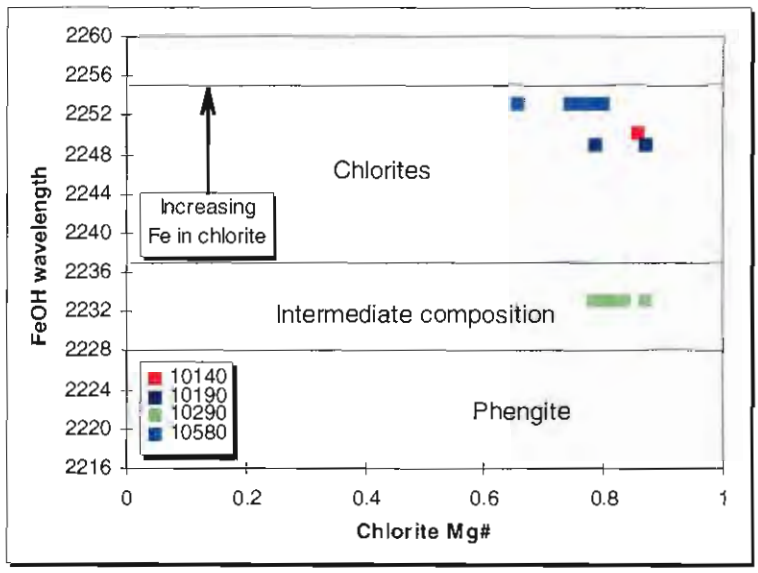

Figure 6.42. FeOH vs. chlorite Mg# for samples from Jukes Road. Chlorites plot at the high FeO end of the FeOH spectrum supporting the interpretation from Section 6.3.1 that chlorites in the Jukes-Darwin area are iron-rich chlorites. The intermediate chlorite (10290) is most likely mixed with phengite. Chlorite sample numbers are shown in the legend.

Two alteration indices have been developed that attempt to discriminate chlorite from sericite alteration intensities in VHMS systems. Ishikawa et al. (1976) created an Alteration Index (AI) and Large et al. (in press) developed the new Chlorite-Carbonate-Pyrite Index (CCPI) index. These indices and their limitations are discussed in greater detail in Section 6.8. Relationships were observed between the AI and AlOH (Figure 6.43) in altered granites and FeOH and the CCPI in altered dacites from Mt. Darwin (Figure 6.44). In Figure 6.43, AlOH correlates with AI ($r = 0.77$). A trend from illite/muscovite in the least-altered granites to more phengitic compositions in altered granites occurs. Post and Noble (1993) noted that white micas and feldspars can be converted to illite due to surface weathering. Muscovite and sericite observed from Darwin Granite samples were not weathered and the samples with lower AlOH wavelengths (<2203 nm) corresponded to the least-altered of the Darwin Granite samples. Therefore, the increasing phengite contents are interpreted to correlate with increasing hydrothermal alteration of the granite.

Four samples of feldspar-phyric dacite collected from Mt. Darwin plot on a highly correlated linear trend ($r = 0.98$) of increasing FeOH wavelength with increasing alteration as measured by the CCPI (Figure 6.11). Pontual et al., (1997a) compared chlorite Mg-numbers to FeOH wavelengths and reported chlorite Mg-numbers ranged from >1 at 2234 nm to 0.35 at 2254 nm. The wavelengths of FeOH absorption features at Mt. Darwin range from 2234 to 2254 nm, suggesting a broad range of chlorite compositions (individual chlorite analyses were not performed). The wavelengths increase systematically with increasing alteration intensity. The small number of samples (4) makes this interpretation preliminary at best.

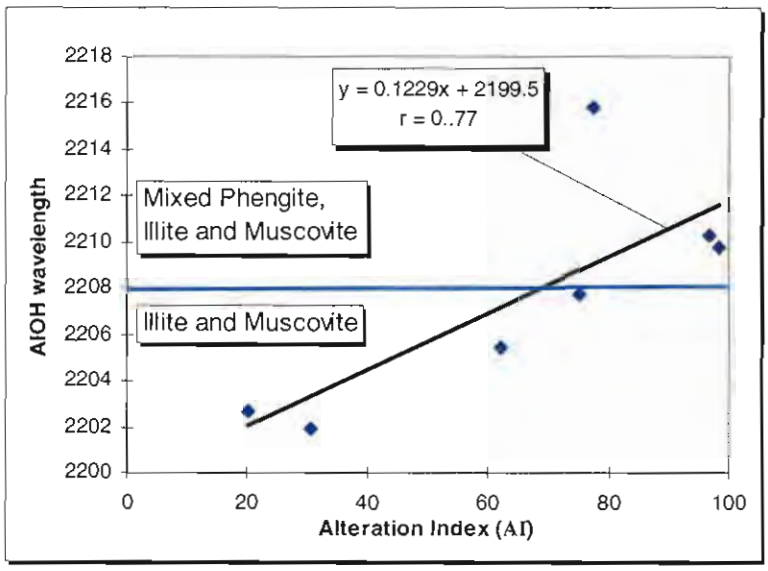

Figure 6.43. AlOH vs. Alteration Index for Darwin Granite samples. The linear relationship between alteration Index and increasing AlOH wavelength is interpreted to relate to increasing phengite contents in altered granites.

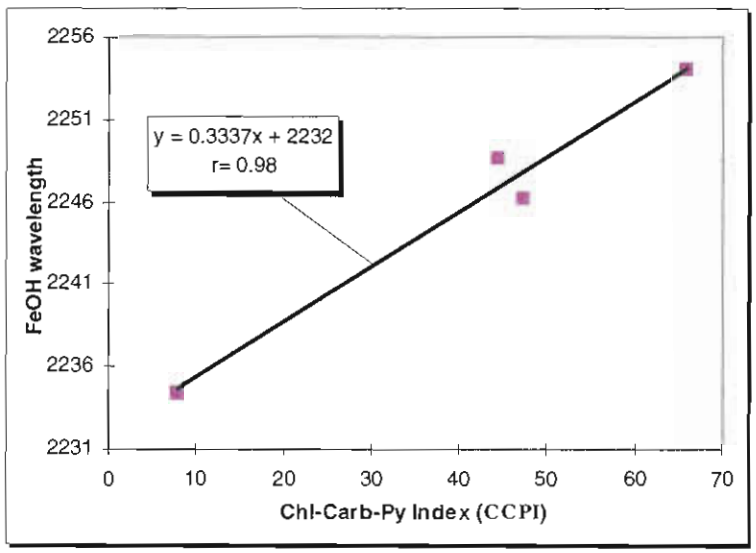

Figure 6.44. FeOH vs. Chlorite-Carbonate-Pyrite Index for Mt. Darwin Dacites. Increasing alteration intensity (CCPI) increases systematically with increasing FeOH wavelength for feldspar-phyric dacites from Mt. Darwin.

6.3.4 Apatite

The reported occurrence of apatite in magnetite veins at the Jukes Prospect (Doyle, 1990) and Lake Selina (Hunns, 1987) was one of the factors used by Large et al. (1996) to argue for a genetic link between the Cambrian Suite I granites (Crawford et al., 1992) and the Prince Lyell Cu-Au ores, while similarities between Prince Lyell and the Garfield Prospect led Halley et al. (1996) to propose a link to Suite II andesites.

Although apatite was observed at the Jukes and Lake Selina Prospects (Hunns, 1987; Doyle, 1990; Hunns, 1997), it occurs as widely scattered <0.1 mm sized grains and is rare (Doyle, 1998, pers. com., Hunns, 1998, pers. com.). Apatite was not observed in magnetite samples from the Jukes-Darwin area in this investigation. The possibility that phosphorus (as apatite), exsolved in a P_2O_5 rich volatile phase related to the Darwin Granite was investigated by analysing a variety of vein styles for P_2O_5, including magnetite, tourmaline and quartz veins (Appendix N). The highest P_2O_5 content in any vein was 0.09 wt.% P_2O_5, supporting the conclusion that significant phosphorus (as apatite) did not partition into vein assemblages around the Darwin Granite and explains the rarity of apatite at the Jukes Prospect.

Fractionation of the REE into accessory minerals such as apatite, monazite, zircon and sphene increases as igneous melts becomes silicic. Apatite and monazite tend to concentrate LREE, while zircon, sphene, hornblende and garnet concentrate HREE. Large negative Eu anomalies may indicate low fO_2 conditions at formation (Puchelt and Emmermann, 1976). However negative Eu anomalies in late-formed igneous minerals are commonly the result of earlier removal of Eu^{2+} in plagioclase. REE patterns in apatites derived from granitic and alkalic rocks commonly reflect plagioclase fractionation by the occurrence of a *pronounced* negative Eu anomaly (Freitsch and Perdahl, 1995).

REE patterns in apatite reflect REE patterns in the magma at the time of extraction. This has been shown by Freitsch and Perdahl (1995) for the Kiruna iron ores, Paster et al. (1974) for the Skaergard layered intrusive complex and Helvaci (1984) for the Avnik apatite-bearing iron ores in Turkey. Therefore, the possibility that the apatite in the Garfield and Prince Lyell systems formed from Cambrian granites was investigated by analysing Garfield apatites for REE. Two apatite samples from the Garfield Prospect were analysed for REE by Dave Huston of AGSO (Australian Geological Survey Organisation) who analysed the samples at the University of Queensland. A split from one of the same samples was analysed by solution methods at the University of Tasmania CSL. Results are tabulated in Table 6.13 and are compared to Prince Lyell apatite REE values (Raymond, 1992), Suite II andesites (Crawford et al., 1992), Garfield andesites (Halley et al., 1996; Duncan, 1997), three phases of the Darwin Granite (this study) and the diorite and granodiorite phases of the Murchison Granite in Figure 6.45. The apatites have high total REE concentrations ranging from 11,000-21,000 ppm (Table 6.13 and Raymond, 1992) and are LREE enriched. Apatite REE patterns from the Garfield Prospect and the Prince Lyell ore are tightly constrained, have negative Eu anomalies, and a significant LREE/HREE fractionation occurred.

Table 6.13. Analytical results of apatite analyses from the Garfield Prospect.

Element	B1045 (U of Queen.) ppm	B1045 (U of Tas.) ppm	B1061 (U of Queen.) ppm
Li	1.5	1.9	2.5
Be		0.2	
Sc	1.1	1.1	1.8
Ti	17.3		12.6
V	45	61	48
Cr	0.1		0.0
Ni	5.4	7.7	2.8
Cu		605	
Zn	7.0	11.4	21.1
Ga	11.3	58	16.2
Rb	0.1	0.1	0.2
Sr	821	842	604
Y	320	475	711
Zr	3.2	3.5	3.7
Nb	0.1	0.1	0.2
Mo		0.4	
Sn	0.1	1.3	0.0
Sb		0.3	
Cs	0.1	0.1	0.1
Ba	357	577	212
La	2369	2772	2980
Ce	5422	5777	7447
Pr	630	651	918
Nd	2227	2594	3411
Sm	323	386	534
Eu	58	61	62
Tb	19.6		36.9
Gd	193	235	348
Dy	86	110	169
Ho	13.9	17.5	28.4
Er	30.9	40.3	66
Yb	19.2	25.4	43.6
Lu	2.4	3.3	5.6
Hf	0.4	0.2	0.7
Ta	0.1	0.0	0.1
Pb	18.6	22.4	116
Th	90	114	192
U	7.7	9.5	16.4

If the Darwin Granite is a fractionated phase of a granitic body similar to the diorite phase of the Murchison Granite, then the possibility that a phosphorus rich volatile phase exsolved off the parental magma must be tested. To test this possibility, the diorite and granodiorite phases of the Murchison Granite were included on Figure 6.45 and the characteristics summarised on Table 6.14. The positive Eu anomaly for the diorite reflects a significant plagioclase content. Suite II hornblende-phyric andesites have values similar to Murchison diorite and granodiorite. The overall apatite REE patterns reflect significant LREE/HREE fractionation. Although the apatite LREE slopes are similar to the Murchison diorite and granodiorite and Suite II andesites, the HREE $(Gd/Yb)_N$ values) slopes are steeper (Figure 6.45). This difference may be explained by the occurrence of hornblende in the Murchison rocks, and by the occurrence of significant (up to 45%) hornblende in the Suite II andesites. It is unlikely that REEs were leached from the Suite II andesites by a seawater-dominated hydrothermal fluid and redeposited in the hydrothermal apatites. Suite II andesites in the immediate footwall rocks at Mt. Lyell would be a minor portion of the available REE reservoir available for leaching by seawater and a contribution of REE from felsic CVC Suite I rocks should be evident. Although, inconclusive, the REE patterns in the apatite

suggest that the apatite was derived from the Suite II andesites or a primitive Suite I parental magma. The location of such a melt beneath the Mt. Lyell area is currently unknown.

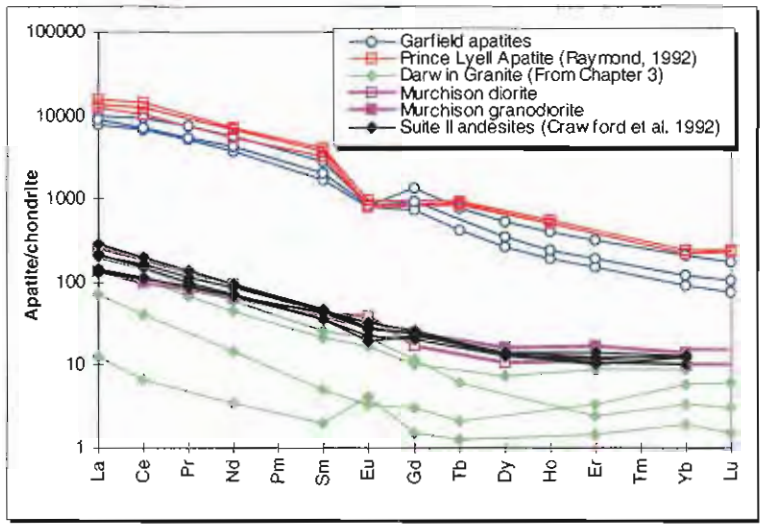

Figure 6.45. REE comparison of apatite analyses from the Garfield Prospect and Prince Lyell Deposit with Suite II andesites, Murchison diorite, and granodiorite and the Darwin Granite. Apatite REE patterns have similar LREE slopes to the Darwin Granite and Murchison diorite and granodiorite. However, apatites consistently have negative Eu anomalies and are depleted in HREE. The overall REE patterns of the Murchison diorite and granodiorite are nearly identical to the REE patterns of the Suite II andesites. The flattening of the HREE slope in the diorite and granodiorite is explained by the occurrence of hornblende. These relationships are interpreted as evidence that the apatite was derived from either the Suite II andesites or a primitive Suite I diorite or granodiorite parental magma. The similarity in the negative Eu anomaly is obscured somewhat by the lack of Gd analysis for the Prince Lyell apatites and the Garfield and Mt. Lyell andesites.

Table 6.14. Summary of REE characteristics for the Murchison diorite and granodiorite, Suite II hornblende-phyric andesites and apatite.

	Murchison diorite and granodiorite	Suite II hornblende-phyric andesite	Apatite
n =	2	4	6
$(La/Yb)_N$	10 and 26	20 to 26	65
$(La/Sm)_N$	6.4 and 3.5	3 to 6.5	3.5 to 4.5
$(Gd/Yb)_N$	1.6 and 1.7	1.6 to 2.5	6.4 to 8.1
Eu anomaly	Positive for the diorite and flat for the granodiorite	Flat or negative	Negative

$\varepsilon Nd_{(500Ma)}$ values for selected rocks and apatite from the Garfield Prospect and Prince Lyell Mine are shown on Table 6.15. Additional Rb-Sr data for selected rocks from the MRV are presented in Appendix F. The Suite I granites (Murchison and Darwin) and andesites have $\varepsilon Nd_{(500Ma)}$ values that are similar and are consistent with a crustal source (Whitford et al., 1988b; Stolz, 1995). Suite II andesites are close to the predicted bulk earth value (0), consistent with their derivation from an undepleated or enriched mantle source. The Garfield apatite $\varepsilon Nd_{(500Ma)}$ values are the same as the average Suite II andesite $\varepsilon Nd_{(500Ma)}$ value and are interpreted to have been derived from the same or a similar melt. However, the two Prince Lyell apatite $\varepsilon Nd_{(500Ma)}$ values of -3.4 and -4.1 are the same as the $\varepsilon Nd_{(500Ma)}$ values of Suite I granites and andesites. This is interpreted as strong evidence that the Prince Lyell and Garfield apatites were derived from different source rocks and

that the Prince Lyell apatite was derived from a primitive Suite I parental magma with a similar crustal source to the Darwin and Murchison Granites.

Table 6.15. $\varepsilon Nd_{(500Ma)}$ values for Cambrian granites, andesites and apatite related to Cu-Au mineralisation (summarised from Appendix F).

Sample Number	Unit/Location	Lithology	ε Nd calculated at 500 Ma.	Reference
B2053	Darwin Granite (Suite I)	Pink Granite	-3.0	This study
GS-1	Darwin Granite (Suite I)	Pink Granite	-4.3	Unpublished Data, Stolz, 1997 pers. com.
GS-7	Darwin Granite (Suite I)	Pink Granite	-5.0	Unpublished Data, Stolz, 1997 pers. com.
JD13	Darwin Granite (Suite I)	Pink Granite	-2.8	Unpublished Data, Crawford, 1997 pers. com.
TO4137	Murchison Granite (Suite I)	Granite	-4.7	Unpublished Data, Crawford, 1997 pers. com.
HR23	Halls Rivulet (Suite I)	Andesite	-5.8	Unpublished Data, Crawford, 1997 pers. com.
30039A	CVC (Suite I)	Hnbl. andesite	-4.1	Unpublished Data, Crawford, 1997 pers. com.
W93	Queenstown Reservoir (Suite II)	Andesite	0.0	Unpublished Data, Crawford, 1997 pers. com.
39233	Mt.Lyell (Suite II)	Andesite	-1.6	Unpublished Data, Crawford, 1997 pers. com.
AR6	Mt.Lyell (Suite II)	Hnbl. Andesite	-0.7	Unpublished Data, Crawford, 1997 pers. com.
Z632	Crown Hill (Suite II)	Hnbl. Andesite	-0.2	Unpublished Data, Crawford, 1997 pers. com.
M189	Crown Hill (Suite II)	Andesite	-2.2	Unpublished Data, Crawford, 1997 pers. com.
109452	Prince Lyell Apatite-Magnetite veins	Apatite	-3.5	Unpublished Data, Stolz, 1997 pers. com.
109454	Prince Lyell Apatite-Magnetite veins	Apatite	-4.1	Unpublished Data, Stolz, 1997 pers. com.
Garfield	Garfield Apatite-Magnetite veins	Apatite	-1.2	Unpublished Data, Halley, 1996 pers. com.
Garfield	Garfield Apatite-Magnetite veins	Apatite	-1.3	Unpublished Data, Halley, 1996 pers. com.

Although, similarities between hydrothermal alteration styles, pyrite-chalcopyrite and magnetite-apatite ore mineral assemblages suggest a link to Suite II andesites, apatite REE patterns and $\varepsilon Nd_{(500Ma)}$ values support the interpretation that magmatic fluids derived from a Suite I magma were directly responsible for apatite-magnetite ores at Prince Lyell. However, even if the magnetite-apatite ores were derived from a Suite I magma, the source of the copper and gold has yet to be established. The numerous Cu-Au prospects near the Cambrian Suite I granites argue strongly for a granite-related source. However, it is interesting that the Garfield apatites contain 600 ppm copper (Table 6.13), suggesting that the Suite II magmas contained significant copper.

There is an intimate association of magnetite and apatite in iron ore deposits worldwide. Two major types of magnetite-apatite ores are recognised: a) iron ores of the Kiruna type (Sweden) in volcanic rocks, and b) iron ores connected with deuteric processes and/or related to intrusive rocks. The division of the two types is, however not reflected in the REE patterns of associated apatites (Freitsch and Perdahl, 1995) and the similarity in REE compositions suggests common processes were involved in their genesis. Their genesis is, however, enigmatic. Several genetic models are argued: a) magmatic intrusive-extrusive model (Helvaci, 1984; Freitsch and Perdahl, 1995), b) a 'VHMS' exhalative-sedimentary model (Parak, 1985) and 3) hydrothermal origin (Cliff et al., 1990). Common to all of the models are alkaline to sub-alkaline, arc-related and anorogenic magmas. In a study of the Kiruna ores and ore field (Parak, 1985), chalcopyrite, pyrite and pyrrhotite exist in sufficient quantities to be mined at Tjarrojakka and copper occurs as chalcopyrite throughout the Kiruna iron ores suggesting a genetic link. Parak (1985) presents evidence suggesting that the copper ores are part of a footwall stringer zone feeding the Kiruna iron ores. The magnetite-apatite copper ores at the Garfield Prospect and the Prince Lyell mine are similar to some of the Kiruna style iron ores in their rock associations (felsic volcanics and andesites), vein style and associated copper ores. The main differences are the significant

occurrence of pyrite as the principal iron-bearing mineral, rather than magnetite, and the lack of alkaline volcanics.

6.3.5 Carbonate

Carbonates occur as accessory minerals in weak to moderate secondary sericite assemblages and in cross-cutting veins at the Jukes Prospect (Section 5.5.2). Two samples were analysed in order to quantify their compositions. Sample 10190 is carbonate from a chlorite ± pyrite + carbonate vein near the center of the Jukes hydrothermal system and 10850 is carbonate from a weakly sericite-altered rock distal to mineralisation. Analytical results are shown on Table 6.16. Carbonates from the distal sericite-altered rock (10850) were identified as calcites with elevated Mg, Fe and Mn contents. Carbonates from within the Jukes hydrothermal system (10190) were identified as siderites with elevated Mg, Mn and Ca contents. Although only limited data are available, the iron contents of carbonates is higher in the mineralised portions of the Jukes hydrothermal system. This spatial relationship between high iron carbonates (siderite) and high iron chlorite is in contrast to the lack of correlation observed between siderite and chlorite at Mt. Lyell (Hendry, 1981).

Table 6.16. Summary of carbonate microprobe analysis for selected rocks along the Jukes Road. Complete analyses are given in Appendix M.

Sample	SiO_2	$FeCO_3$	$MnCO_3$	$MgCO_3$	$CaCO_3$	$BaCO_3$	$SrCO_3$	Sum Ox%	Rhodochrosite	Magnesite	Sidérite	Calcite
10190-MJ-96-4c-carb2	0.04	82.37	0.51	15.52	1.68	0.08	0.04	100.63	0.8	20.0	77.1	1.8
10190-MJ-96-4c-carb3	0.02	82.78	0.50	13.75	1.15	0.09	0.00	99.04	0.8	18.1	79.4	1.3
10190-MJ-96-4d-carb1	0.06	82.27	4.13	9.68	0.45	0.00	0.06	97.26	6.5	12.9	79.7	0.5
10190-MJ-96-4d-carb2	0.05	82.53	3.83	9.95	0.33	0.00	0.03	97.73	6.1	13.2	79.9	0.4
10190-MJ-96-4d-carb3	0.05	81.53	4.59	10.82	0.63	0.00	0.00	98.17	7.1	14.2	77.7	0.7
10190-MJ-96-4e-carb3	0.42	80.77	3.94	10.01	0.31	0.00	0.01	98.28	6.2	13.3	77.8	0.4
10190-MJ-96-4f-carb3	0.12	81.59	4.76	9.31	1.39	0.00	0.00	98.43	7.4	12.2	78.0	1.5
10850-b carb	0.00	19.53	5.37	20.79	50.80	0.00	0.00	96.56	7.6	24.7	16.9	50.8
10850-b carb4	0.00	28.02	6.70	10.47	47.62	0.00	0.02	93.23	10.1	13.3	25.8	50.8
10850-b carb6	0.00	20.31	7.03	17.91	52.49	0.00	0.04	98.04	9.8	21.0	17.3	51.8
10850-c carb5	0.00	17.79	5.63	17.61	51.81	0.00	0.03	94.75	8.3	21.8	16.0	53.9
10850-c carb6	0.00	14.38	6.08	21.04	52.98	0.09	0.02	94.68	8.7	25.2	12.5	53.5
10850-c carb8	0.00	16.71	5.89	20.87	51.20	0.00	0.04	95.12	8.4	25.1	14.6	51.8
10850-c carb9	0.00	16.75	5.80	20.55	51.24	0.10	0.05	94.67	8.3	24.8	14.7	52.1
10850-d carb2	0.00	17.13	6.50	19.33	51.96	0.00	0.02	95.45	9.3	23.2	15.0	52.5
10850-d carb3	0.00	17.18	6.14	19.50	54.42	0.00	0.10	97.49	8.6	22.9	14.7	53.8
10850-d carb4	0.00	22.37	6.43	15.93	50.07	0.00	0.00	95.49	9.3	19.4	19.8	51.4
10850-d carb6	0.00	22.13	7.09	15.51	49.58	0.00	0.00	94.51	10.3	19.0	19.7	51.0

6.4 MASS CHANGES IN THE JUKES-DARWIN AREA

Samples used in the mass change calculations were selected on the basis of being "end members" of the alteration styles described (i.e. dominated by one or two alteration minerals). The samples did not contain veins or veinlets thereby eliminating contamination by hydrothermal channelways.

Quantifying geochemical mass changes in hydrothermally altered rocks has been discussed by numerous workers (Gresens, 1967; Grant, 1986; MacLean and Kranidiotis, 1987; Huston, 1993; MacLean and Barrett, 1993; Stanley and Madeisky, 1995). The Gresens (1967) method and its variants (Grant, 1986; Huston, 1993) make assumptions concerning volume changes or immobility of elements during alteration. In addition, the Gresens and Grant methods fail the test of scale invariance (Chayes, 1960; Rollinson, 1992; Aitchison, 1997). Scale invariance requires the composition of a rock sample to be the same regardless of the amount of sample analysed.

Secondly, scale invariance requires that the change in one variable in a sample must be independent of the other variables. Grant (1986) states:

> "Let the original composition in the original rock of say MgO be C^0_{MgO} = 10 wt.%. Assume that the rock undergoes some change in mass without gain or loss of MgO, as in simple hydration, and let this change be an increase of 25 percent. The new concentration of MgO will be C^A_{MgO} = (M^O / M^A) = (100/125)10 = 8 wt.%."

Although, Grant (1986) states that the change occurred without a gain or loss of MgO, MgO decreased from 10 wt.% to 8 wt.%. This apparent 2 wt.% depletion was caused by rescaling during calculation of percentages, and is a feature of closed compositional data and the constant sum problem.

The constant sum problem as explained by several authors (Chayes, 1960; Aitchison, 1984; Aitchison, 1997) is a result of variables summing to unity or 100%. In geochemical data, the sum of all major oxides and other trace variables (trace elements) equals 100%. Therefore, increasing or decreasing one variable affects the composition of all other variables because they are not free to take any number. As a result, closure may result in apparent increases and decreases in concentrations between altered rocks and their protoliths that are dissimilar to actual changes of mobile components in the system. Similarly, the Pearce Element Ratio approach (Stanley and Madeisky, 1995) has a common trace element denominator (Z) that forces a statistical linear correlation to the data (Rollinson and Roberts, 1986). Although results may be geologically meaningful, they can be statistically unsupportable. Alternative methods of examining geochemical data that remove the constant sum problem and allow the data to be compared in a geologically meaningful way and with statistical validity have been developed (Chayes, 1960; Chayes, 1971; Aitchison, 1984; Rollinson and Roberts, 1986; MacLean and Kranidiotis, 1987; Rollinson, 1992; MacLean and Barrett, 1993; Aitchison, 1997).

The method for calculating mass changes used in this study was developed by MacLean and Kranidiotis (1987) and refined by MacLean and Barrett (1993). In their method, volume change did not enter into the mass change calculations but can be calculated from the mass change results. Mass change is calculated for each mobile element based on the dilution of an immobile element (MacLean and Kranidiotis, 1987; MacLean and Barrett, 1993) in relation to the concentration of the same immobile element in a precursor sample. Because this method is highly reliant on the choice of the immobile element and the precursor sample, a rigorous test for immobility must be passed. The test for immobility is most effectively carried out on a single volcanic unit that can be traced laterally through the hydrothermal alteration system. The Jukes Road feldspar-phyric dacite provides an excellent opportunity to apply the MacLean and Barrett (1993) method since it is a single coherent sill or flow. For a single precursor system, immobile element pairs occur as highly correlated (r = 0.90 - 0.99) linear trends due to mass gains and mass loss of the mobile components in the hydrothermal system (MacLean and Barrett, 1993). This essentially graphical method minimizes the potential for comparing rocks with different precursors, a significant shortcoming of Grant's (1986) approach.

On Figure 6.46, Al_2O_3 is compared to Zr for the entire whole rock data set of the Jukes Road feldspar-phyric dacite. The two elements are highly correlated (r = 0.94), therefore Zr was selected as the immobile element for the mass change calculations in the Jukes Road feldspar-phyric dacite. Other potentially immobile elements such as Ti, P, Y and Nb were tested, however they were not as well correlated as Zr and are interpreted to be mobile (Table 6.17). The precursor sample (B10750) that was selected by petrographic examination as the freshest and most least-altered rock in the data set, is shown on Figures 6.46 and 6.48.

Mass changes were calculated using Equation 6.3 (MacLean and Barrett, 1993):

Equation 6.3:

$$\text{Mass change } (\Delta^*) = (Zr_{(\text{precursor})} / Zr_{(\text{Altered sample})} \times (\%\text{ component in the altered sample})) - (\%\text{ component in the precursor})$$

* Δ is in g/100g (%) and is in relation to the total initial mass of the system.

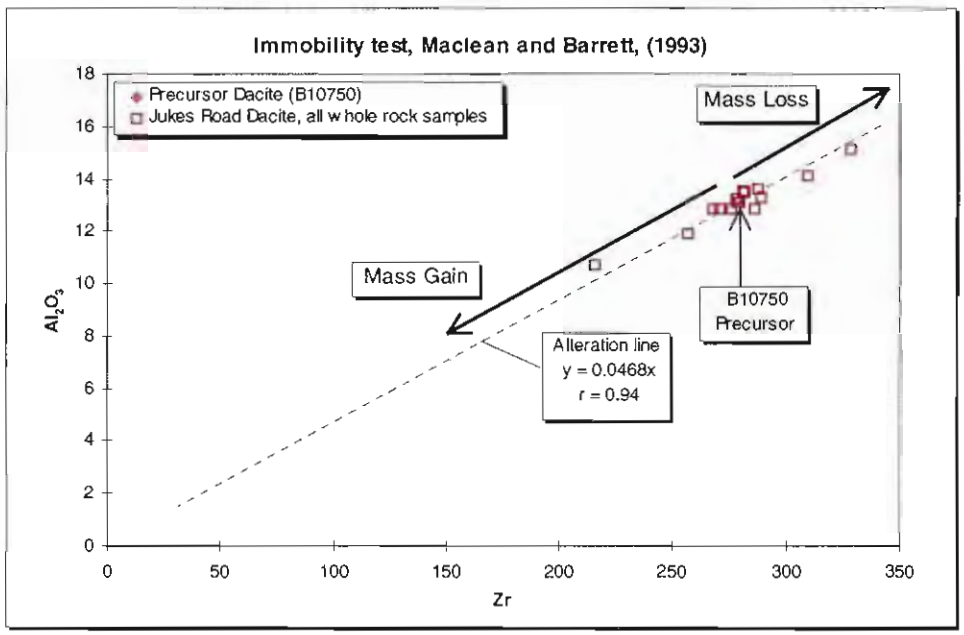

Figure 6.46. Immobility test for the Jukes Road dacite. The data points form a highly correlated linear trend (r = 0.94) or alteration line that projects through the origin. Note that the precursor sample (B10750) falls on the alteration line. Samples that plot above or below the precursor have gained or lost mass respectively. Method of MacLean and Barrett (1993).

Estimates of mass changes for the end members of the three hydrothermal alteration styles along the Jukes Road feldspar-phyric dacite are shown in Table 6.17 and summarised on a histogram in Figure 6.47.

Common to all three styles of hydrothermal alteration are major depletions in Na_2O and CaO, and insignificant MnO depletion. This is interpreted to have resulted from the breakdown of plagioclase and trace mafic minerals. Gains in K_2O, Rb, Sr, Nd and Ba were associated with secondary K-feldspar and sericite formation.

Table 6.17. Absolute mass changes for the principal ateration styles along the Jukes Road and in the King River Tunnel. Mass changes are given in g/100g for major elements and ppm for trace elements relative to the precursor composition. Method of MacLean and Barrett (1993).

Sample Number	SiO2	TiO2	Al2O3	Fe2O3	MnO	MgO	CaO	Na2O	K2O	P2O5	LOI	Total	Cu	Zn	Rb	Sr	Zr	Nb	Mo	Sn	Ba	Nd	Y	W	Pb	Th	U
Precursor Composition																											
B10750 (Jukes)	74.88	0.30	13.07	3.29	0.10	0.66	0.11	2.25	3.60	0.04	1.96	100.3	4	39	129	22	280	13	1.0	5.0	822	37	39	6.0	20	21	4.0
K-Feldspar Alteration																											
B10220 (Jukes)	0.72	-0.01	0.21	0.16	-0.08	-0.18	-0.09	-2.08	5.05	0.00	-0.8	2.8	599	6.5	71	42	0.0	0.1	1.2	-0.8	1737	1.2	12	15	-7.6	0.7	2.3
B10290 (Jukes)	4.24	-0.01	-0.08	2.63	-0.07	-0.09	-0.10	-2.11	4.55	0.00	-0.7	8.2	230	23	46	19	0.0	-0.6	3.4	5.0	1846	43.6	4.6	17	-1.5	-2.5	9.2
880381(KRT)	1.17	0.04	0.13	0.31	0.03	0.09	1.47	-2.01	5.54	0.03	1.1	7.9			55	101	0.0	1.1					-7.6				
880368 (KRT)	1.24	0.01	0.11	-0.14	-0.04	0.01	1.09	-0.32	2.15	0.01	1.3	5.4	1	6.8	32	81	0.0	0.6		-2.0	1677	2.6	-1.2		-12	-0.3	1.2
Average	1.84	0.01	0.09	0.74	-0.04	-0.05	0.59	-1.63	4.32	0.01	0.18	6.1	277	12.1	51	61	0.0	0.3	2.3	0.8	1753	16	1.8	16	-6.9	-0.7	4.2
Chlorite Alteration																											
B10350 (Jukes)	-4.81	0.05	-0.33	3.55	-0.06	0.44	-0.06	-2.10	1.27	0.01	0.2	-1.8	227	73	36	-4.3	0.0	-0.3		4.5	482	2.4	-12.4	13.7	-14	-2.3	1.6
10340 (Jukes)	-1.32	0.01	0.38	2.59	-0.06	0.37	-0.09	-2.07	2.51	0.00	0.8	3.1	1245	48	59	7.1	0.0		0.5		1057				-5.4	-0.4	3.8
880365 (KRT)	-1.38	0.00	0.09	3.68	0.00	0.49	0.75	-2.18	1.99	0.02	2.5	5.9	11	53	78	13	0.0	0.9		3.0	706	-1.7	-0.7		-17	-0.4	2.8
880411(KRT)	-8.01	-0.03	-1.89	3.11	-0.04	0.36	0.12	-1.35	1.40	0.02	-0.7	-7.0	13	-11	32	7.1	0.0	-1.5		-0.1	410	3.7	-8.7		-17	-1.7	0.3
Average	-3.88	0.01	-0.44	3.23	-0.04	0.42	0.18	-1.92	1.79	0.01	0.7	0.1	374	41	51	5.7		-0.3		2.5	664	1.5	-7.3		-13	-1.2	2.1
Sericite Alteration																											
10640 (Jukes)	-0.90	0.01	0.06	-0.12	0.03	0.17	-0.08	-1.72	2.29	0.01	0.2	-0.1	36	4.3	72	-1.9	0.0		0.5		687				8.2		16
10680 (Jukes)	-0.65	0.00	0.04	0.59	0.03	0.52	0.18	-1.69	2.12	0.01	0.5	1.6	2	8.0	60	-0.5	0.0		0.6		644				-4.7		17
B10700 (Jukes)	-0.91	-0.01	0.22	0.32	-0.08	0.32	-0.07	-1.27	1.50	0.01	0.5	0.6	0	-3.7	45	0.2	0.0	0.3	0.8	-1.6	419	10	2.3	-1.0	-17	0.2	0.8
Average	-0.82	0.00	0.11	0.26	-0.01	0.33	0.01	-1.56	1.97	0.01	0.4	0.7	13	2.9	59	-0.7			0.7		583				-4.5		11
Mixed Alteration																											
B10900 (Jukes)	-13.32	-0.01	-0.22	-1.54	-0.09	-0.17	-0.05	-0.24	1.23	0.00	-0.73	-15.1	-1	-9	23	13	0	0.7		-1.9	550	14.1	-4.1	-2	-20.0	-0.6	1.7
B10850 (Jukes)	2.56	-0.01	0.36	-0.25	0.04	0.04	0.54	-0.16	1.17	0.01	0.30	4.6	-1	5	26	12	0	0.6	0.5	-1.0	330	2.7	-1.4	-2	-12.7	0.9	0.7
B10800 (Jukes)	-0.53	-0.02	-0.02	0.55	-0.03	0.29	0.43	-0.54	0.83	0.01	0.29	1.3	5	8	22	-1	0	0.5	0.1	0.8	189	7.6	3.6	-3	-18.0	-0.7	0.7
B10420 (Jukes)	-1.98	0.00	-0.19	-1.65	-0.09	-0.25	-0.10	-2.10	3.68	-0.01	-0.42	-3.1	42	-15	55	13	0.0	0.6	0.4	-0.9	1326	8.5	-3.2	11		-2.6	0.8
B10370 (Jukes)	-3.89	0.00	0.12	-0.30	-0.08	0.14	-0.09	-2.07	3.15	-0.01	0.04	-3.0	309	14	72	12	0	0.0	0.9	-2.7	1023	12.6	4.8	15	-14.2	0.4	1.1
B10310 (Jukes)	-11.25	0.00	-0.34	1.09	-0.08	0.04	-0.09	-2.14	2.36	-0.01	0.13	-10.3	248	27	52	17	0	0.1	0.2	-0.5	943	0.0	-7.4	17	7.1	-1.1	1.7
B10300 (Jukes)	-2.85	0.01	0.33	0.37	-0.08	0.10	-0.10	-2.16	2.91	-0.01	-0.17	-1.6	943	39	63	11	0	0.5	0.9	-1.8	693	7.7	-8.2	5	0.9	-0.1	1.5
B10250 (Jukes)	-2.55	0.00	0.41	0.43	-0.09	-0.09	-0.06	-1.32	3.10	0.01	-0.67	-0.8	19	12	45	23	0	0.0	1.1	2.5	1248	16.8	-0.1	5	-15.0	-0.1	2.8
B10210 (Jukes)	5.75	0.01	0.83	20.50	-0.05	0.12	-0.07	-2.06	4.50	0.00	-0.72	28.8	1642	95	52	31	0	5.5	35.6	8.1	2061	-22.7	-6.6	34	74.6	-4.1	14.4
880344 (KRT)	-4.23	-0.01	-0.34	0.89	0.06	0.07	0.80	-0.39	3.39	0.05	0.07	0.4			27	70	0.0	1.2					-6.5				
Average	-3.23	0.00	0.09	2.01	-0.05	0.03	0.12	-1.32	2.63	0.00	-0.19	0.1	356	20	44	20	0	1.0	4.9	0.3	929	5.3	-2.9	9	0.3	-0.9	2.8

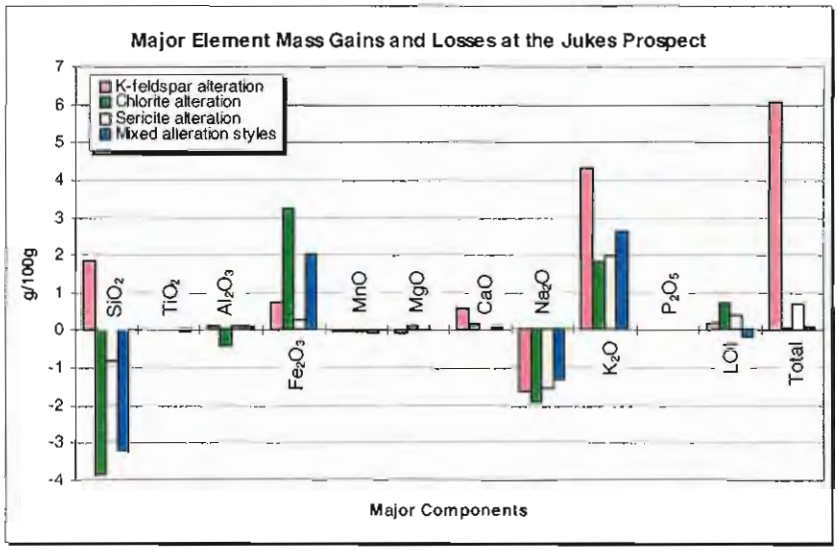

Figure 6.47. Major element mass changes at the Jukes Prospect. Significant depletions in Na_2O and gains in K_2O are evident for all three hydrothermal alteration styles. In addition, silica depletion and Fe_2O_3 gains occurred in chlorite-altered rocks. K_2O gains of >2% are characteristic of K-feldspar alteration. The K_2O gain in chlorite-altered rocks is interpreted to represent chlorite overprinting of earlier secondary sericite or K-feldspar alteration styles. Mass changes are given in g/100g.

Selected major oxides (Appendix H) for the volcanic rocks are compared to SiO_2 in Figures 6.48A-F. Hydrothermal alteration of the rocks is interpreted to have caused wide scatter in K_2O, Na_2O, CaO, Fe_2O_3 and MgO values. However, Figures 6.48A-E are excellent examples of scatter induced by the constant sum problem and forced closure (Chayes, 1960; Aitchison, 1984; Rollinson, 1992; Aitchison, 1997). Increases in K_2O and Fe_2O_3 and decreases SiO_2 and Na_2O caused larger apparent shifts in SiO_2 values than actually occurred (Table 6.17 and Figure 6.47). Even though many of the rocks were altered beyond recognition, the TiO_2 and Zr values were preserved, and in Figures 6.48F and 6.50 these elements define two populations. In Figure 6.49, the trendline for the Darwin andesites has the same slope (i.e. TiO_2/Zr ratio, 0.003) as the Suite 2 andesites from south of Queenstown (Crawford et al., 1992) and andesites from the Garfield Valley (Duncan, 1997). The 'r' value for the slope of the alteration line for the Darwin andesite is 0.94 (highly correlated). Since unaltered andesites were not observed in this study, the precursor sample (LE135) was selected from the previously published data of Crawford et al. (1992). Similarly, the Mt. Darwin feldspar-phyric dacites are compared on Figure 6.50. Since the slope of the trendline (0.001 in Figure 6.50) is the same, the two elements are positively correlated (r = 0.93). Near the Darwin Granite, unaltered feldspar-phyric rocks were not observed. Therefore, the same precursor sample (B10750) as the Jukes Road feldspar-phyric dacite was used and the mass changes calculated for the Darwin dacites were determined relative to the least-altered Jukes Road dacite. Mass gains and losses for silica and K-feldspar hydrothermal alteration styles at Mt. Darwin are summarised on Table 6.18 and shown in Figure 6.51.

Total depletions in Na_2O and CaO are typical in the andesite and feldspar-phyric dacite, and are interpreted to be a result of plagioclase feldspar destruction. In addition, Fe_2O_3, MgO and MnO were depleted in the dacitic rocks, except for samples of K-feldspar-altered feldspar-phyric dacites that have an overprint of chlorite. K-feldspar-altered feldspar-phyric dacites are

Table 6.18. Absolute mass changes for the principal hydrothermal ateration styles at Mt. Darwin. Mass changes are given in g/100g for major elements and ppm for trace elements relative to the precursor composition. Method of MacLean and Barrett (1993).

Sample Number	SiO2	TiO2	Al2O3	Fe2O3	MnO	MgO	CaO	Na2O	K2O	P2O5	LOI	Total	Cu	Zn	Rb	Sr	Zr	Nb	Sn	Ba	Nd	Y	Pb	Th	U
Feldspar-phyric Dacite																									
Precursor Composition																									
B10750 (Jukes)	74.88	0.30	13.07	3.29	0.10	0.66	0.11	2.25	3.60	0.04	1.96	100.3	4	39	129	22	280	13	5.0	822	37	39	20	21	4.0
K-Feldspar Alteration																									
B2037	42.92	0.04	6.08	-1.27	-0.08	-0.35	-0.09	-1.88	11.38	0.02	-0.6	56.2	2.0	-20	198	122	0.0	1.9	0.4	3370	-8.5	62	0.8	50	8.2
B2038	12.60	0.03	4.82	0.35	-0.09	0.47	-0.10	-1.89	7.77	0.01	0.1	24.1	5.6	73	197	78	0.0	7.6	1.5	2276	7.5	19	18	11	4.2
Average	27.76	0.04	5.45	-0.46	-0.09	0.06	-0.10	-1.88	9.58	0.02	-0.2	40.1	3.8	27	197	100	0.00	4.8	1.0	2823	-0.5	41	9.6	31	6.2
Silica Alteration																									
B1095	84.12	0.03	6.82	-0.63	-0.08	-0.09	-0.09	0.74	5.16	0.02	0.3	96.3	2.3	3.7	157	47	0.0	8.7	0.5	928	44	26	11	16	6.4
Mixed alteration																									
B2049	-11.43	0.06	-0.8	-2.6	-0.1	-0.5	-0.1	-2.0	6.5	0.0	-1.4	-12.3	0.3	-30	71	53	0.0	-0.5	-0.6	1834	-34	43	-16	-13	1.0

Sample Number	SiO2	TiO2	Al2O3	Fe2O3	MnO	MgO	CaO	Na2O	K2O	P2O5	LOI	Total	V	Cr	Ni	Rb	Sr	Zr	Nb	Ba	Y
Hornblende Andesite																					
Precursor Composition, from Crawford et al. (1992)																					
LE135	60.60	0.45	16.10	7.76	0.14	3.68	5.88	3.62	1.52	0.23	2.84	102.8	250	250	29	53	840	150	6	1500	18
K-Feldspar Alteration																					
B2051	-25.27	0.04	-7.10	-4.51	-0.13	-2.96	-5.87	-3.44	4.55	-0.20	-1.7	-46.6	-181	-249	-27	71	-785	0.0	-0.4	1049	-0.2
B2044	-16.03	0.01	-5.52	-3.40	-0.12	-2.43	-5.87	-3.47	4.84	-0.19	-1.2	-33.4	-155	-244	-23	117	-777	0.0	1.0	567	5.1
Average	-20.65	0.02	-6.31	-3.96	-0.13	-2.69	-5.87	-3.46	4.69	-0.20	-1.42	-40.0	-168	-247	-25	94	-781	0	0.3	808	2.4
Mixed Alteration styles																					
B2032	-23.81	-0.09	-8.18	-3.08	-0.12	-2.97	-5.87	-3.55	1.99	-0.19	-1.5	-47.3	-219	-248	-28	92	-812	0.0	-0.4	-192	6.7
B2047	3.0	-0.02	-8.39	-1.41	-0.13	-2.25	-5.86	-3.49	2.07	-0.19	-1.0	-17.6	-190	-245	-27	84	-822	0.0	0.7	-944	0.5
B2050	-18.73	0.01	-5.09	-2.17	-0.11	-1.93	-5.87	-3.58	2.23	-0.18	0.4	-35.0	-144	-205	-18	145	-829	0.0	-0.1	-945	2.6
Average	-13.19	-0.03	-7.22	-2.22	-0.12	-2.38	-5.87	-3.54	2.10	-0.19	-0.7	-33.3	-184	-233	-24	107	-821	0	0.1	-693	3.2

characterised by up to 43 g/100g mass increases in SiO_2, up to 11 g/100g increases in K_2O and up to 6.1 g/100g additions of Al_2O_3. Additional increases in Rb, Sr, Ba, Y, Th and U and minor additions of Cu and Nb also occurred. Silica-altered feldspar-phyric dacites are characterised by large mass gains in SiO_2 (84 g/100g) and Al_2O_3 (6.8 g/100g). Increases in K_2O, LOI, Rb, Nb, Nd, Y, Th and U are typical.

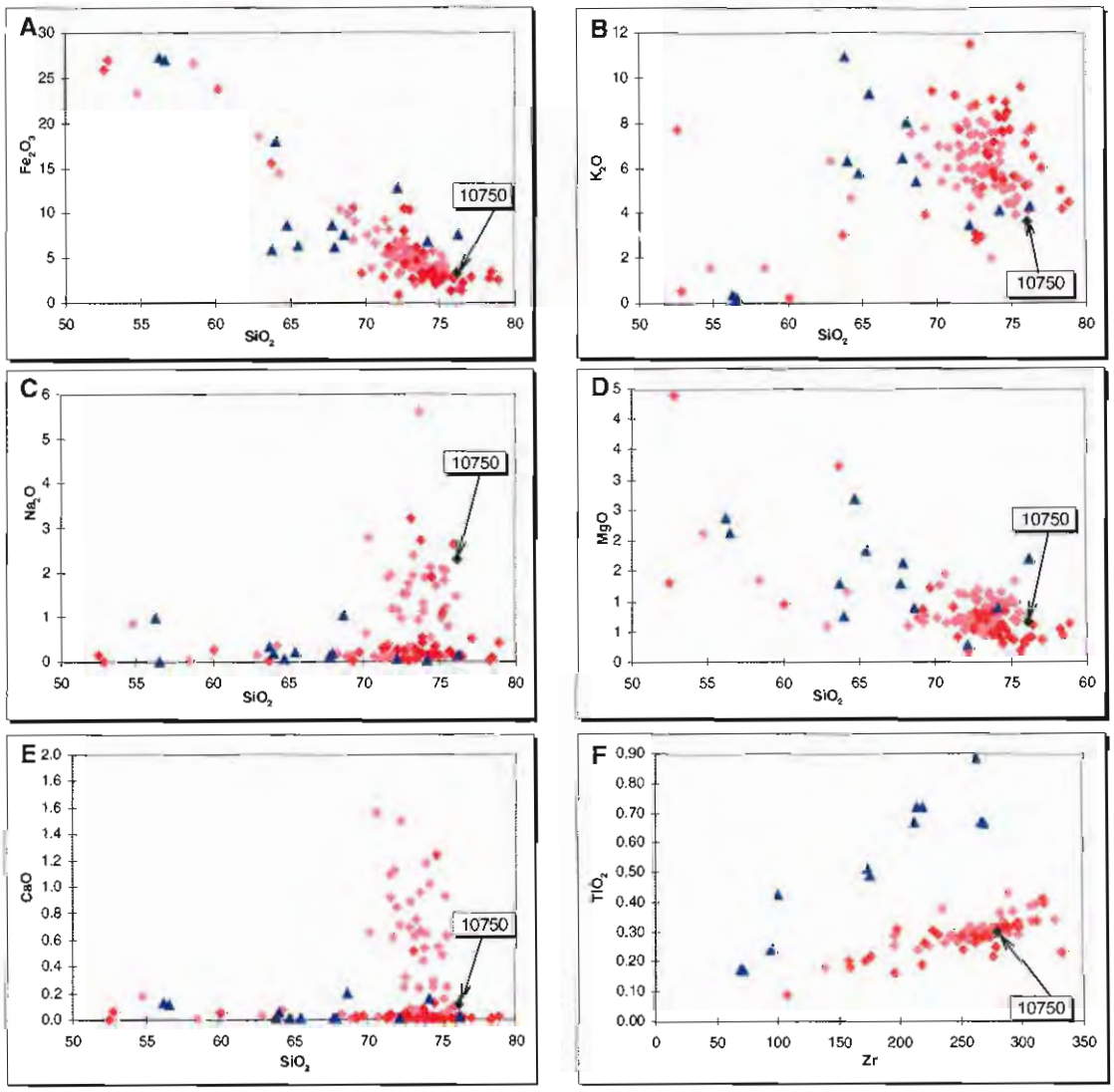

Figure 6.48. Harker diagrams for the Jukes Road feldspar-phyric dacite (Including the King River Tunnel), the Mt. Darwin and Intercolonial Spur dacites and the Darwin andesites. In some of the dacites, variable intensities of hydrothermal alteration caused increases in K_2O and Fe_2O_3 and decreases SiO_2 and Na_2O that caused larger apparent shifts in SiO_2 values than actually occurred (Table 6.17 and Figure 6.47). The Darwin andesites are separated from the dacites on the basis of TiO_2 vs. Zr (F). The least-altered dacite (B10750) is shown for reference. Data from White (1975), Doyle (1990), Gadaloff (1996) and the current study (Appendix H).

Hydrothermally altered andesites are characterised by large mass losses in major elements. Typically, andesites were overprinted and modified by several alteration styles. In K-feldspar-altered andesites, up to 25.3 g SiO_2, 7.1 g Al_2O_3 and 4.51 g Fe_2O_3 were leached per 100g rock, together with essentially all of the MnO and P_2O_5 and half of the MgO. Large depletions in V, Cr, Ni and Sr are interpreted to represent amphibole, clinopyroxene and feldspar destruction. Mass additions of K_2O, Rb, Ba and U occurred. Andesites samples that contain two or more

hydrothermal alteration styles (sericite, chlorite and K-feldspar) had similar SiO_2 losses to the K-feldspar-altered andesites (-24 g/100g), however Al_2O_3 losses were larger (-8.2 g/100g). P_2O_5, V, Cr, Ni, Sr and Ba were intensely leached. Ba losses in the mixed hydrothermal alteration styles contrast with the Ba gains in the K-feldspar-altered andesites. Mass gains of K_2O, Rb and U are probably related to the later sericite overprint.

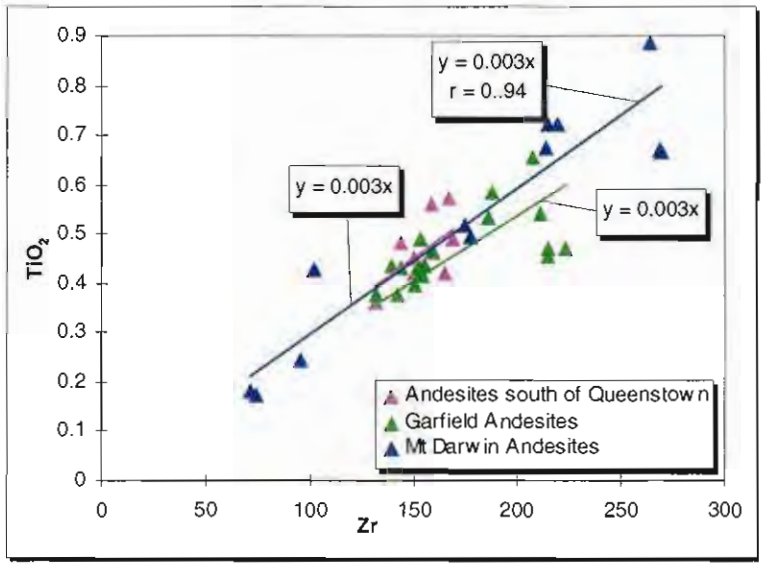

Figure 6.49. TiO_2 vs. Zr comparison for the Mt. Darwin andesites. The 'r' value of 0.94 (6 samples) for the Mt. Darwin andesites indicates the elements are highly correlated. The similar slopes of the alteration lines for the Mt. Darwin andesites, the Suite 2 andesites from South of Queenstown (Crawford et al. 1992) and the Garfield andesites (Duncan, 1997) suggests that they are equivalent. All trendlines pass through the origin.

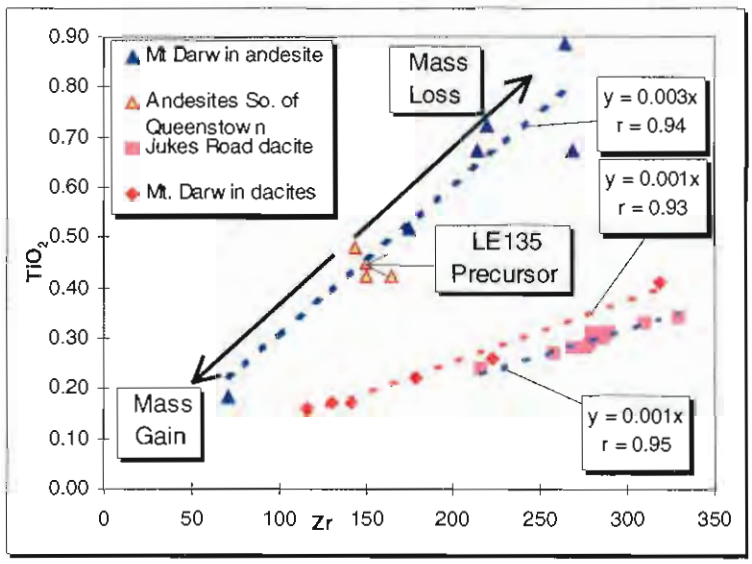

Figure 6.50. Immobility test for the Mt. Darwin dacites and andesites. The end members of the principal hydrothermal alteration styles are plotted for the Mt. Darwin andesites and feldspar-phyric dacites. The precursor sample for the andesites, LE135, plots on the trendline and was from south of Queenstown. The dacites are comparable to the Jukes Road feldspar-phyric dacite. Because the slopes of the trendlines are the same (0.001) they are interpreted to be from a similar source and the same precursor sample was used for mass gain calculations.

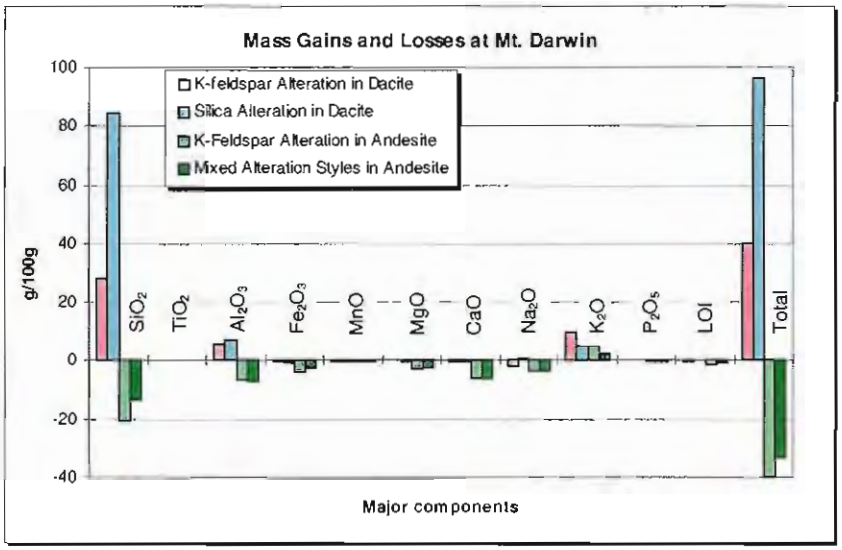

Figure 6.51. Major element mass changes at the Jukes Prospect. Average gains and losses for the principal hydrothermal alteration styles are shown. Significant gains in SiO_2, Al_2O_3 and K_2O occurred in silica and K-feldspar-altered dacites. Large losses in SiO_2, Al_2O_3 and Fe_2O_3 occurred in the altered andesites. CaO and Na_2O were totally removed during feldspar breakdown. Mass changes are given in g/100g.

6.5 MASS CHANGE TRENDS IN RELATION TO HYDROTHERMAL ALTERATION STYLES

Mass changes associated with the three principal end-member hydrothermal alteration styles from Jukes Road are compared on Figures 6.52 and 6.53. K-feldspar-altered rocks that have undergone silica addition are distinguishable from rocks that have undergone silica loss on Figure 6.52. On mass gain and mass loss plots, the origin represents zero mass change, and is where the precursor sample plots. Intensely sericite-altered rocks plot on the trendline for total sericitisation in rhyolites.

$\Delta(Fe_2O_3 + MgO)$ vs. $\Delta(CaO + Na_2O)$ for the Jukes Road data are illustrated in Figure 6.53. Sodium and calcium depletion resulting from the breakdown of plagioclase has resulted in decreasing $\Delta(CaO + Na_2O)$ with increasing alteration intensities for all three hydrothermal alteration styles. A trend of silica loss (confirmed by an average decrease of -3.9 g/100g, Table 6.17) relates to increasing intensities of hydrothermal chlorite alteration, and is associated with increasing $\Delta(Fe_2O_3 + MgO)$ as shown on Figure 6.53.

The hydrothermal alteration styles that occur in the feldspar-phyric dacite and andesites at Mt. Darwin are compared on Figure 6.54 and 6.55. On Figure 6.54, increases in K-feldspar are illustrated for all alteration styles. Silica-altered feldspar-phyric dacites had large SiO_2 and K_2O additions, and are distinguished from the K-feldspar-altered feldspar-phyric dacites that had smaller silica gains. Silica loss from the andesites is interpreted to be due to amphibole and feldspar breakdown and chlorite formation.

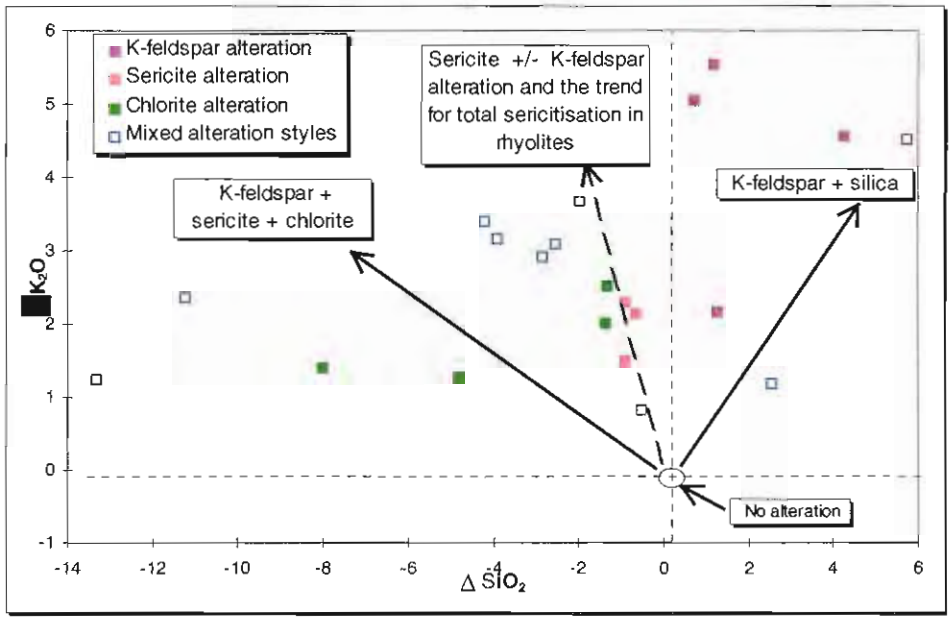

Figure 6.52. Mass changes, ΔK_2O vs. ΔSiO_2, for the Jukes Road dacite. Mass changes (Δ) for the three principal hydrothermal alteration styles in the Jukes Road Dacite (Table 6.17). All three alteration styles are associated with mass gains in K_2O. K-feldspar-altered rocks with silica addition are distinguished from those with silica loss. Chloritisation has resulted in a trend of increasing silica loss. Intense sericite-altered rocks plot on the trendline for total sericitisation in rhyolites. Mass changes are given in g/100g. Method of MacLean and Barrett, (1993).

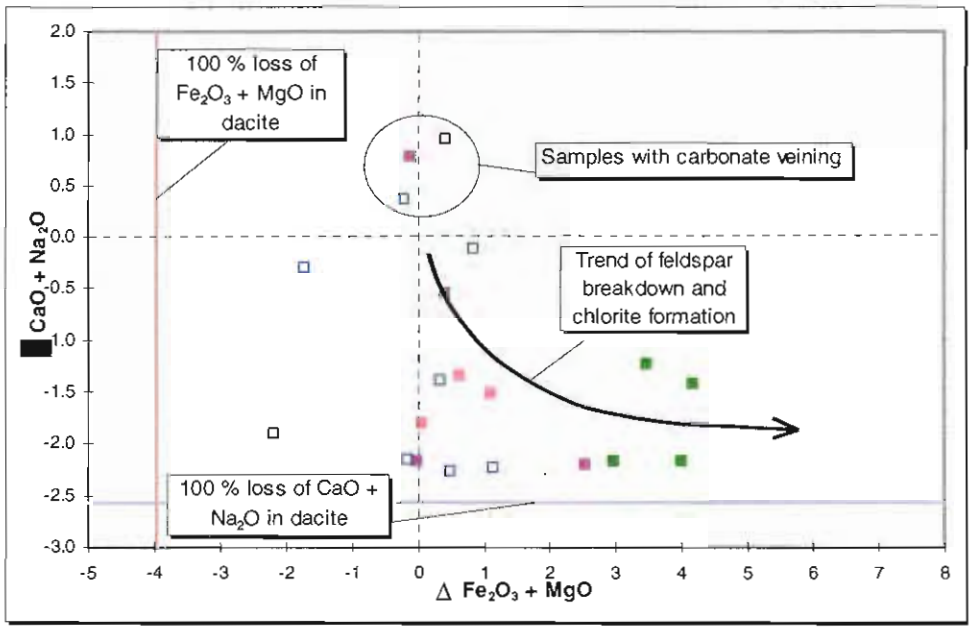

Figure 6.53. Mass changes, $\Delta CaO + Na_2O$ vs. $\Delta Fe_2O_3 + MgO$, for the Jukes Road dacite. Data for the same samples as Figure 6.19. Decreasing $\Delta CaO + Na_2O$ is associated with increasing intensities of all three hydrothermal alteration styles. Chlorite-altered rocks are characterised by an increase in $\Delta Fe_2O_3 + MgO$. Loss of $\Delta CaO + Na_2O$ occurred during breakdown of plagioclase prior to addition of ΔK_2O and $\Delta Fe_2O_3 + MgO$. A line representing the trend of plagioclase feldspar breakdown and chlorite formation is shown along with lines representing 100 % loss in $\Delta Fe_2O_3 + MgO$ and $\Delta CaO + Na_2O$. Mass changes are given in g/100g. Method of MacLean and Barrett, (1993).

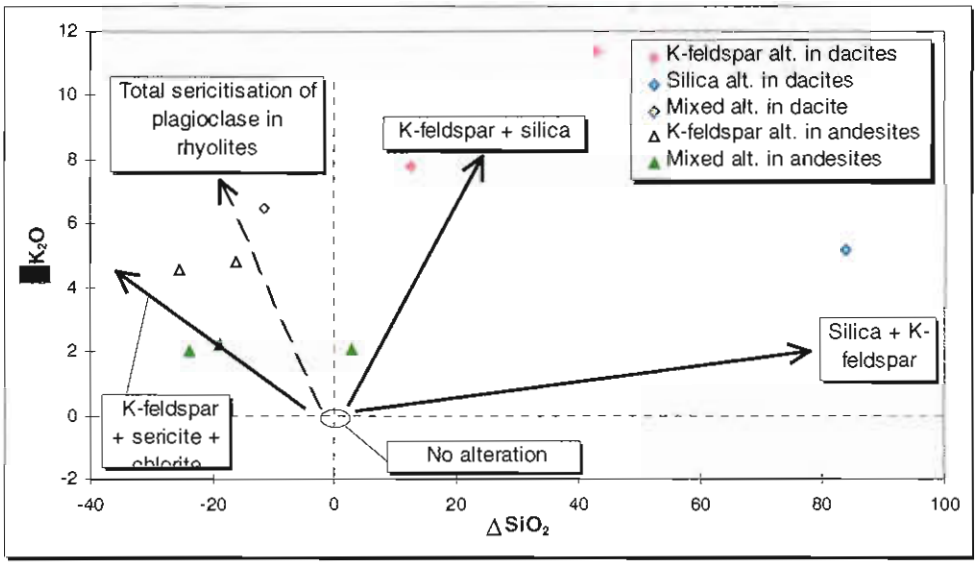

Figure 6.54. Mass changes at Mt. Darwin, ΔK_2O vs. ΔSiO_2. All of the altered rocks are characterised by mass gains in K_2O. This plot distinguishes the silica-altered rocks and silica depleted rocks from each other. Rocks with overlapping hydrothermal alteration styles plot on trends indicating silica loss and sericite and chlorite formation in addition to K-feldspar. Mass changes are given in g/100g. Method of MacLean and Barrett (1993).

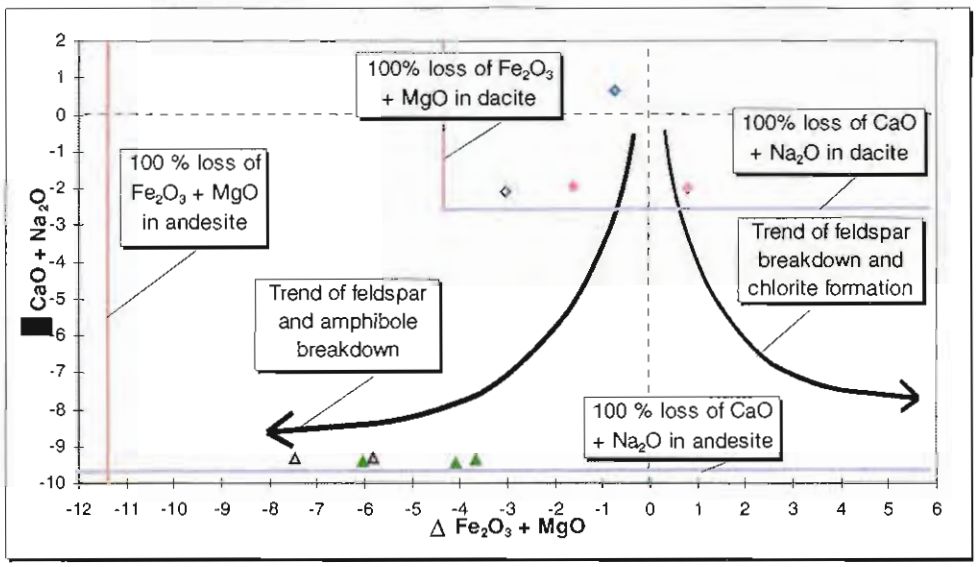

Figure 6.55. Mass changes at Mt. Darwin, $\Delta CaO + Na_2O$ vs. $\Delta Fe_2O_3 + MgO$. A line representing the trend of plagioclase feldspar breakdown and silica leaching is shown along with lines representing 100 % loss in $\Delta Fe_2O_3 + MgO$ and $\Delta CaO + Na_2O$. Note that nearly 100% of the $\Delta CaO + Na_2O$ was leached in the K-feldspar-altered dacites and altered andesites. Mass changes are given in g/100g. Method of MacLean and Barrett, (1993).

$\Delta(Fe_2O_3 + MgO)$ vs. $\Delta(CaO + Na_2O)$ for the Mt. Darwin data is illustrated in Figure 6.55. Lines indicating 100% mass loss of $\Delta(CaO + Na_2O)$ and $\Delta(Fe_2O_3 + MgO)$ in each of the rock types are shown. In the silica-altered feldspar-phyric dacite, 90% of the $\Delta(CaO + Na_2O)$ was leached due to plagioclase destruction, however Fe_2O_3 and MgO losses were variable (Table 6.18). In the silica-altered feldspar-phyric dacite, the minor gain in MgO is interpreted to represent minor chloritisation. As illustrated, in the andesite, 100% of the $\Delta(CaO + Na_2O)$, and 50% of the $\Delta(Fe_2O_3$

+ MgO) were leached during plagioclase, amphibole and clinopyroxene destruction respectively. The remainder of Fe_2O_3 and MgO remained available for conversion to chlorite.

Conventional treatment of alteration data on Harker diagrams fails the test of scale invariance and is subject to the constant sum problem because the data is constrained and recalculated to 100%. Therefore, misinterpretation of alteration intensity and significance can result. In Figures 6.48A-F, Harker diagrams of K_2O, Al_2O_3 and Ba vs. SiO_2 are compared to ΔK_2O, ΔAl_2O_3, and ΔBa vs. ΔSiO_2 for the same data set used to calculate mass changes and losses for the dacites in Section 6.4.

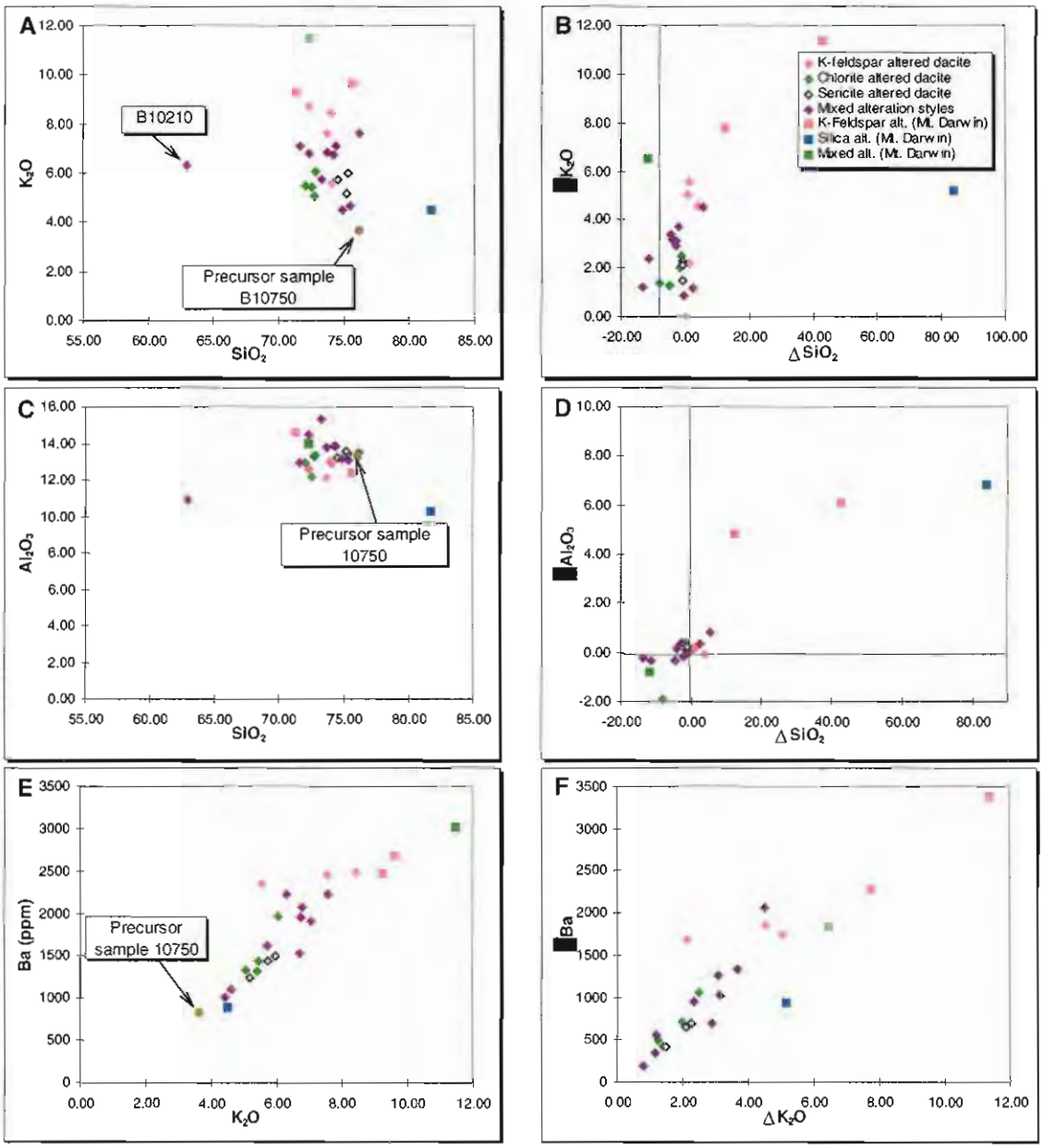

Figure 6.56. Harker diagrams of K_2O, Al_2O_3 and Ba vs. SiO_2 are compared to ΔK_2O, ΔAl_2O_3, and ΔBa vs. ΔSiO_2. The data set is the same as that used to calculate mass changes and losses for the dacites in Section 6.4. In the Harker diagrams, the least-altered dacite (B10750) was included for reference. Mass changes are given in g/100g.

In Figure 6.56A (K_2O vs. SiO_2), scatter due to 'mobility' of K_2O is the typical conclusion drawn from examining this figure. K-feldspar-altered samples have higher K_2O contents than chlorite or sericite-altered samples by about 2 wt.%. All of the samples have greater K_2O than the precursor (B10750). However, with respect to SiO_2, one sample (B10210) has 62 wt.% SiO_2 and all but two of the samples have less SiO_2 than the precursor (Figure 6.56A). In contrasting Figure 6.56A to Figure 6.56B (ΔK_2O vs. ΔSiO_2), 1-6% K_2O was added at the Jukes Prospect and SiO_2 mass changes varied from losses of 13% to gains of up to 6%. Dacite sample B10210, which had a 5.75% mass gain in SiO_2 (Table 6.17), had an analysed silica content of 62 wt.%. The low silica content relates to the addition of iron (the sample contains 20 wt.% Fe_2O_3, Appendix H).

There is a clear separation between the various alteration end members. Small K_2O gains and SiO_2 losses characterise the chlorite and sericite-altered rocks, in contrast to large changes for K-feldspar-altered dacites (Figure 6.56B). At Mt. Darwin, mass changes were larger, with 5-11% K_2O added and SiO_2 changes ranging from losses of 11% to gains of up to 84%. For the Mt. Darwin dacites, the calculated SiO_2 gains are not apparent at all from the Harker diagrams (Figures 6.48A and C).

Another example of the usefulness of the mass change information is in the comparison of Figures 6.48C and 6.56D. On Table 6.18 the mass of Al_2O_3 was shown to have increased in dacites and decreased in andesites at Mt. Darwin. On the conventional Harker diagram, Figure 6.56C, mobility is suggested by the scatter in the data, but the overall range of values is only 12-16 wt.%, and no clear separation is made on the basis of hydrothermal alteration style at either Mt Darwin or the Jukes Prospect. On Figure 6.56D, however, the intensely K-feldspar and silica-altered samples from Mt. Darwin do not plot with the other data. The weakly altered Mt. Darwin and Jukes Road samples cluster around the origin, and no clear trend is apparent. The K-feldspar and chlorite-altered rocks at the Jukes Prospect were mapped as intensely altered in terms of K-feldspar and chlorite contents, but compared to the rocks at Mt. Darwin, they are weakly altered in terms of SiO_2 and Al_2O_3 mass changes.

A comparison of Ba vs. K_2O in Figure 6.56E illustrates a linear relationship between Ba and K_2O for the altered dacites. In Figure 6.56F (ΔBa vs. ΔK_2O) a similar covariant linear relationship occurs. The difference is that actual mass gains are illustrated. For the Jukes Road chlorite and sericite-altered samples, the increase in Ba was less than 1000 ppm while K-feldspar-altered samples had increases in Ba of more than 1500 ppm. The covariant relationship of mass change is interpreted to be a result of similar behaviour by Ba and K_2O.

Figure 6.57 illustrates the relationship between ΔSr and ΔK_2O. Sr and Ba typically substitute for Ca in plagioclase or K in K-feldspar in felsic rocks (Pearce and Norry, 1979). As shown on Figure 6.57 and Tables 6.17 and 6.18, there is an increase in Sr with increasing K_2O. Chlorite and sericite-altered samples had insignificant increases in Sr (<20 ppm). At ΔK_2O values of >4 g/100g, Sr gains are typically >30 ppm in K-feldspar-altered rocks at the Jukes Prospect and in the intensely silica, chlorite and K-feldspar-altered rocks at Mt. Darwin. The linear covariant relationship of mass change for Sr and K_2O is due to Sr substitution for K in K-feldspar and may indicate a common source. On Figure 6.57, the three outliers (>70 ppm mass gain) came from

samples collected in the King River Tunnel which contained calcite veins (ΔCa from +0.8 to +1.47 g/100g, Table 6.17).

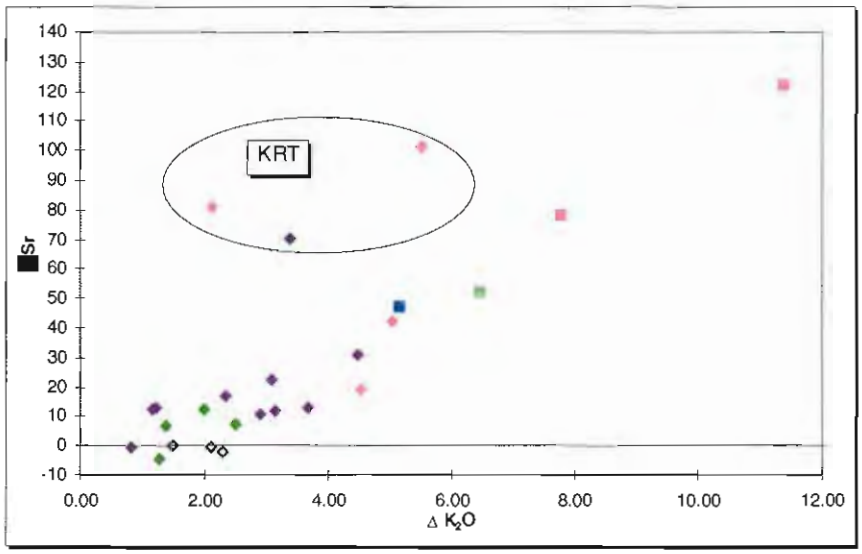

Figure 6.57. Mass changes in ΔSr vs. ΔK_2O for the Jukes Road and King River Tunnel. Mass increases in Sr are directly related to mass increases in K_2O since all of the CaO was leached from the rocks during feldspar destruction. However, the three King River Tunnel rocks (KRT) have abundant late calcite veining and increased Sr (Table 6.18). The Sr values (in ppm) double with >4% K_2O and are significant at Mt. Darwin. Legend as in Figure 6.56B. Mass changes are given in g/100g for K_2O and ppm for Sr.

If Ba and Sr are released during plagioclase dissolution, a linear correlation between Ba, Sr and CaO must exist. Figures 6.58A-B show Ba and Sr vs. CaO for the least-altered rocks along Jukes Road. The trend is interpreted to indicate that Ba and Sr contents are not related to CaO contents, but are related to the K_2O content (Figures 6.56F and 6.57).

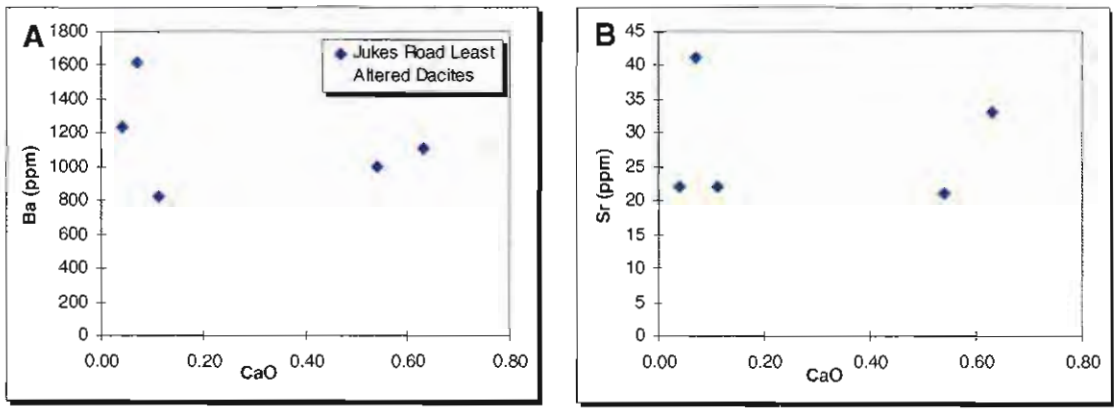

Figure 6.58. Ba and Sr vs. CaO for the least-altered rocks from Jukes Road. The flat trends demonstrate that Ba (A) and Sr (B) contents of the unaltered rocks along Jukes Road were not controlled by the CaO content of plagioclase.

6.6 ALTERATION REACTIONS

Destructive mass and chemical changes in the rocks in the Mt Darwin and Jukes Prospect areas are related to development of specific alteration assemblages. The detailed mineralogy of the least-altered feldspar-phyric dacites and hornblende-phyric andesites were discussed in Chapters 4 and alteration styles and assemblages were described in Chapter 5. The feldspar-phyric dacites were originally composed of quartz, plagioclase and K-feldspar with minor accessory minerals (Section 4.3.2.1) and were altered to various assemblages of quartz, sericite, K-feldspar and chlorite (Section 5.5.2). The original mineralogy of the andesites on Mt. Darwin has been completely replaced. It is assumed that the andesites had similar mineralogies to the Garfield andesites which consist of hornblende, plagioclase, magnetite and traces of quartz (Section 4.3.1.1).

Some areas of intense hydrothermal alteration may have been localised around faults, some of which may have been obscured by the development of breccias. However, most of the hydrothermal alteration assemblages in and around the Darwin Granite and the Jukes Prospect were pervasively developed although some was fracture controlled. It is assumed that observed differences in mass changes between lithologies (Table 6.18) were the result of different chemical reactions between the original mineralogy and hydrothermal fluids derived from the Darwin Granite. Overlapping hydrothermal alteration styles, interpreted as evidence of multiple fluid pulses, suggest that alteration assemblages evolved over time in response to changing hydrothermal fluid conditions. This section discusses possible chemical reactions to explain the observed mass changes that occurred as a result of hydrothermal conditions around the Darwin Granite.

Isotopic studies have suggested that hydrothermal fluids around the Darwin Granite and other hydrothermal systems in the MRV were seawater-dominated (Solomon, 1976; Polya et al., 1986; Solomon et al., 1988; Jones, 1993; Gemmell, 1994) and weakly acidic (represented by H^+). Seawater contains significant quantities of K^+, Mg^{2+}, Na^+, Cl^- and SO_4^{2-} and becomes modified via water-rock interaction as soon as it enters the rock column (Lofgren, 1971; Bischoff and Seyfreid, 1978; Bigger and Hansen, 1992). The reactions described in this section occur at temperatures between 100 and 350^{0}C, pressures of 0 to 3 kbars, and in acidic conditions. The various reactions are discussed in relation to their effects on the feldspar-phyric dacite and the hornblende andesite at Mt. Darwin and the feldspar-phyric dacite on the Jukes Road.

6.6.1 Replacement of Feldspars by Sericite

At Mt. Darwin and the Jukes Road, plagioclase in the feldspar-phyric dacites and andesites was replaced by secondary sericite. Two examples of H-ion metasomatic reactions that convert plagioclase to sericite by the addition of K^+ in weakly acidic evolved/modified seawater are given:

Reaction 1:

$$3NaAlSi_3O_8 + K^+ + 2H^+ + 12H_2O \Leftrightarrow KAl_3Si_3O_{10}(OH)_2 + 6H_4SiO_{4(aq)} + 3Na^+$$

albite muscovite

Reaction 2:

$$3CaAl_2Si_2O_8 + 2K^+ + 4H^+ \Leftrightarrow 2KAl_3Si_3O_{10}(OH)_2 + 3Ca^{2+}$$

anorthite muscovite

These reactions consumed acid, deposited potassium and leached silica, sodium and calcium. Both reactions could occur under hydrothermal or diagenetic conditions. Under diagenetic conditions, the mica and clay crystallinities vary as a function of temperature, with illites or smectites more likely to form. Subsequent metamorphism can recrystallise illite/smectite to muscovite. Under hydrothermal conditions, calcium liberated during H-ion metasomatism may be re-deposited nearby as epidote and/or carbonate (Beane, 1982), consistent with the occurrence of these minerals in the sericite-altered rocks along Jukes Road. Epidote forms at temperatures above 250^{o}C (Beane, 1982) and cannot be a diagenetic product. However, it may be metamorphic in origin. Sericite is interpreted to have replaced K-feldspar by the following aluminum-conserving reaction that releases potassium for use in additional sericitisation of plagioclase .

Reaction 3. (Beane, 1994):

$$3KAlSi_3O_8 + 2H^+ + 12H_2O \Leftrightarrow KAl_3Si_3O_{10}(OH)_2 + 6H_4SiO_{4(aq)} + 2K^+$$

K-feldspar sericite

At Mt. Darwin and the Jukes Prospect, reactions such as Reactions 1 released silica, and Reactions 1 and 2 released sodium and calcium from plagioclase. The mass changes in feldspar-phyric dacites caused by sericite or mixed alteration styles are illustrated in Figures 6.47-6.48, 6.51 and 6.52-6.57 and summarised on Tables 6.17 and 6.18. These reactions are dependent on temperature, pH and a_{K+} and occur at temperatures near 300^{0}C (Rose and Burt, 1979; Barrett et al., 1991; Beane, 1994). Potassium gains in sericite-altered rocks suggests high K^+ activity. Intense sericite replacement of K-feldspar (Reaction 3) accompanied chlorite alteration styles.

6.6.2 Chlorite Replacement of Feldspars and Ferromagnesian Minerals

Albite has commonly been replaced by secondary chlorite in feldspar-phyric dacites along the Jukes Road and at Mt Darwin. Chlorite has also replaced sericite, groundmass albite laths and any other phenocrysts that were not previously replaced by sericite. Reaction 4 is one possible replacement reaction for albite by iron-rich chlorite.

Reaction 4:

$$2NaAlSi_3O_8 + 2MgCl_{2(aq)} + 3FeCl_{2(aq)} + 14H_2O \Leftrightarrow$$

albite

$$Mg_2Fe_3Al_2Si_3O_{10}(OH)_8 + 2Na^+ + 8H^+ + 3H_4SiO_{4(aq)} + 10Cl^-$$

chlorite

Similar reactions occurred when anorthite or K-feldspar were the dominant feldspars. Fe addition (Tables 6.17 and 6.18) was associated with rock hydration and cation exchange (Fe for Na, Ca or K) which were both most likely associated with increasing acidity of the fluid. Similar reactions resulted in Mg-addition in solid solution with Fe-chlorite, and silica and alkali depletions.

Chlorite replacement of sericite occurred in the Mt. Darwin andesites, and moderate to intensely chlorite-altered feldspar-phyric dacites along Jukes Road and at Mt. Darwin. Assuming aluminium is conserved (such as along the Jukes Road, Table 6.17), a possible mechanism for the replacement of sericite by an iron-bearing chlorite is shown in Reaction 5. This reaction precipitates iron and magnesium from the fluid, releases potassium and increases the pH:

Reaction 5:

$$2KAl_3Si_3O_{10}(OH)_2 + 3H_4SiO_4 + 9FeCl_2 + 6MgCl_2 + 18H_2O \Leftrightarrow$$

sericite

$$3Mg_2Fe_3Al_2Si_3O_{10}(OH)_8 + 2K^+ + 28H^+ + 30Cl^-$$

chlorite

In intensely chlorite-altered rocks, K-feldspar was replaced by secondary chlorite in a reaction similar to Reaction 6 or, if prior replacement by sericite occurred, Reaction 5. Chlorite will form due to increasing pH, a_{Fe}, a_{Mg} and/or decreasing a_K and a_{Na}.(Schardt et al., in press).

Reaction 6 (Large, 1977):

$$2KAlSi_3O_8 + 3FeCl_2 + 2Mg^{2+} + 14H_2O \Leftrightarrow$$

K-feldspar

$$Mg_2Fe_3Al_2Si_3O_{10}(OH)_8 + 2K^+ + 3H_4SiO_{4(aq)} + 8H^+ + 10Cl^-$$

Mg-Fe-chlorite

Hornblende contains variable concentrations of Fe^{3+}, Fe^{2+}, Mg^{2+}, Al^{3+}, Na^{2+}, K^+ and Ca. Therefore, it is difficult to write a representative balanced equation explaining the conversion of hornblende to chlorite or other alteration products. In the andesites at Mt. Darwin, hornblende was altered to K-feldspar and chlorite. Reaction 7, an example of hornblende replacement by chlorite, occurs at 2 kbars and about 350^0C. Similar to other chlorite replacement reactions, this reaction released calcium, and consumed iron and/or magnesium. This reaction will result in chlorite deposition if acid fluids react with primary hornblende..

Reaction 7:

$$Ca_2(Fe, Mg)_4Al_2Si_7O_{22}(OH)_2 + (Fe, Mg)^{2+} + 10H_2O + 2H^+ \Leftrightarrow$$

hornblende

$$(Fe, Mg)_5Al_2Si_3O_{10}(OH)_8 + 2Ca^{2+} + 4H_4SiO_{4\,(aq)}$$

chlorite

High-T biotite is common in intrusion-related hydrothermal alteration systems (Gustafson and Hunt, 1975; Bekinsale, 1979; Beane, 1982; Titley, 1993; Battles and Barton, 1995), although it is rare in the Jukes-Darwin area. Biotite can be altered to chlorite as temperature or pH decrease (Reaction 8). The released K and Fe may then be precipitated as other secondary minerals, such as or iron oxides/sulfides.

Reaction 8 :

$$2KMgFe_2AlSi_3O_{10}(OH)_2 + 2Cl^- + 4H^+ \Leftrightarrow Mg_2Fe_3Al_2Si_3O_{10}(OH)_8 + 2K^+ + 3SiO_2 + FeCl_{2(aq)}$$

biotite chlorite quartz

Chlorite formation caused silica depletion and mass gains in magnesium and iron in the chlorite-altered rocks from Jukes Road (Table 6.17). Potassium enrichment in the chlorite-altered rocks was probably caused by sericite replacement of plagioclase. In intensely chlorite-altered rocks, chlorite has replaced hornblende (in andesites) and sericite, releasing K and Si and other elements. Excess acid and silica liberated during chloritisation (Reactions 4-7) may have been consumed by the formation of the sericite ± quartz alteration halos around the Darwin Granite.

6.6.3 Secondary K-feldspar Deposition

Some K-feldspar replacement of plagioclase in the feldspar-phyric dacites and andesites could have occurred as a simple exchange reaction, if a_{K+} was higher than a_{Na+} and/or a_{Ca+} (eg. Reaction 9). This reaction will consume potassium and release sodium to the fluid without any change in acidity. In cases where plagioclase was replaced by secondary sericite or chlorite, and pH or a_{K+} increased, then Reaction 3 is likely to produce K-feldspar by proceeding in the reverse direction. pH decrease or a_{K+} increase will produce K-feldspar at the expense of chlorite (Reaction 6) as discussed by Schardt et al. (in press). Plagioclase in the andesites was probably partially converted to chlorite (Reaction 4), and the remainder altered to K-feldspar (Reaction 6).

Reaction 9:

$$NaAlSi_3O_8 + K^+ \Leftrightarrow KAlSi_3O_8 + Na^+$$

albite K-feldspar

Sericite could have been converted into K-feldspar with aluminum conserved in a reaction such as the reverse of Reaction 3, and chlorite may have been converted to K-feldspar by the reverse of Reaction 6.

6.6.4 Secondary Quartz Deposition

The large silica gains in the feldspar-phyric dacite at Mt. Darwin (Table 6.18) are attributed to K-feldspar replacement by quartz (eg. Reaction 10). This reaction consumes acid causing a marginal increase in pH and an increase the activity of K^+ and Al^{3+} in the fluid (Large, 1977). Large mass gains in silica suggests large volume of pre-existing K-feldspar in the rocks prior to silicification. The silicified zone on Mt. Darwin overlaps the K-feldspar zone (Figures 5.2 and 5.3) and is interpreted to postdate the K-feldspar alteration event. In order to transport large quantities of silica, high acidity (as HCl) and high temperatures are typically required (Burnham, 1979). Silica sources include the granite, chlorite-altered andesites and other nearby chlorite-altered rocks.

Reaction 10:

$$2KAlSi_3O_8 + 3H_4SiO_4 + 8H^+ \Leftrightarrow 9SiO_2 + 2K^+ + 2Al^{3+} + 10H_2O$$

K-feldspar quartz

6.6.5 Replacement Reactions for Ferromagnesian Minerals

Magnetite is common in igneous rocks and in hydrothermal mineral assemblages (Beane, 1994) and has the mineral formula $Fe^{2+}(Fe^{3+})_2 O_4$. In the Jukes-Darwin system, hematite has formed at the expense of magnetite by reactions such as Reaction 11 (which could release Fe^{2+} for use in chlorite formation), or Reaction 12. Magnetite is associated with chlorite in all chlorite alteration styles observed. Magnetite pseudomorphs after pyrite were observed in and adjacent to hydrothermal veins. Reaction 13 converts pyrite to magnetite by oxidation and releases sulfate into the fluid.

Reaction 11 :

$$Fe_3O_4 + 2H^+ + 2Cl^- \Leftrightarrow Fe_2O_3 + FeCl_{2(aq)} + H_2O$$

magnetite hematite

Reaction 12 :

$$2Fe_3O_4 + 1/2O_2 \Leftrightarrow 3Fe_2O_3$$

magnetite hematite

Reaction 13 :

$$6H_2O + 3FeS_2 + 11O_2 \Leftrightarrow Fe_3O_4 + 6SO_4^{2-} + 12H^+$$

pyrite magnetite

6.6.6 Chalcopyrite Deposition

In the Jukes-Darwin area, mass gains in Cu and Fe typically accompany mass gains in K_2O in K-feldspar or chlorite-altered rocks (Tables 6.17 and 6.18). The main copper mineral observed in the Jukes-Darwin area was chalcopyrite, occurring in veins with pyrite or as small disseminated grains. Reactions 14 and 15 show how chalcopyrite can replace pyrite. In Reactions 14 to 16, Cu

and Fe occur in reduced states, as is typical in aqueous solutions at higher temperatures (Beane, 1994). Chalcopyrite can precipitate directly in veins by Reaction 16.

Reaction 14:

$$FeS_2 + CuCl_2^- + H^+ + 1/4O_2 \Leftrightarrow CuFeS_2 + 1/2H_2O + 2Cl^-$$

pyrite chalcopyrite

Reaction 15:

$$2FeS_2 + 2CuCl_2^- + H_2O \Leftrightarrow 2CuFeS_2 + 2H^+ + 1/2O_2 + 4Cl^-$$

pyrite chalcopyrite

Reaction 16:

$$4CuCl_2^- + 4FeCl_2 + 8H_2S + O_2 \Leftrightarrow 4CuFeS_2 + 12H^+ + 2H_2O + 16Cl^-$$

fluid chalcopyrite

Reactions 1-16 are examples of chemical processes that may have occurred around Mt. Darwin and the Jukes Prospect. Components released by one alteration reaction may have been added to adjacent lithologies by another alteration reaction. Similarly, localised variations in rock compositions may have contributed to localised domainal style alteration.

6.7 SUMMARY OF THE GEOCHEMICAL STUDIES AT MT. LYELL

One of the main objectives of the thesis is to compare the hydrothermal alteration in and around the Jukes-Darwin area to the Mt. Lyell mining field. Hydrothermal effects on major and trace element distribution at Mt. Lyell have been documented by Green (1971), Bryant (1975), Reid (1975), Walshe (1977), Walshe and Solomon (1981), Sheppard (1987), Manning (1990), Raymond (1992), Godsall (1997b) and Huston (in press). Table 6.19 summarises the geochemical and isotopic studies at Mt. Lyell since the late 1960s. Within the broad zone of quartz-sericite ± pyrite ± chlorite hydrothermal alteration assemblages that encloses the Mt. Lyell field, variable depletions in CaO, Na_2O, K_2O, Rb, and Sr make geochemical classification of original rock compositions difficult. SiO_2 and Zr/TiO_2 or Ti/Zr values, however were shown to be reliable indicators of original rock compositions outside the immediate orebodies (Sheppard, 1987; Crawford et al., 1992; Raymond, 1992). Results of their studies support interpretations of other workers (Cox, 1981; Corbett, 1989; Corbett et al., 1989; Corbett, 1992; Crawford et al., 1992). Sheppard (1987) studied whole rock and trace element geochemistry from several different deposits as part of his Ph.D thesis. He concluded that different hydrothermal alteration styles occur around different ore styles and the different styles are characterised by different geochemical signatures. The main geochemical patterns delineated in the footwall at Prince Lyell (disseminated pyrite-chalcopyrite) are depletions in CaO, Na_2O, Sr, Nb, Y, Sc, Ga, V and CO_2 and increases in Fe_2O_3, MnO, MgO, P_2O_5, S, Cu, Zn, Ba and Pb (Sheppard, 1987; Raymond, 1992). In the hydrothermal alteration zone around the Western Tharsis disseminated deposit, Huston (in press) noted additional depletions of Rb, Y, Be, Ga, MREE and HREE associated with

Table 6.19. Summary of geochemical and isotopic studies of hydrothermal alteration and mineralisation at Mt. Lyell.

Prospect-location	Elements or Isotopes	Interpretation	Genetic model(s)	Date/reference
Mt. Lyell, multiple deposit studies	$\delta^{34}S$, Chlorite, pyrite and chalcopyrite chemistry	Initial $\delta^{34}S$ = 7‰, Ores formed at 270-310°C	Cogenetic subsurface replacement of permeable volcananics below seafloor VHMS deposits	Solomon et al. (1969), Walshe (1971, 1977), Walshe and Solomon (1981)
Mt. Lyell, multiple deposit studies	Major and trace elements		Cogenetic subsurface replacement of permeable volcananics below seafloor VHMS deposits	Bryant (1975), Sheppard (1987)
Mt. Lyell, multiple deposit studies	Pb isotopes	Cambrian Lead		Gulson and Porritt, (1987)
Mt. Lyell, multiple deposit studies	$\delta^{34}S$	No $\delta^{34}S$ zoning in a system dominated by rock sulfur.		Solomon et al. (1988)
Mt. Lyell, multiple deposit studies	Sr in Barite	Ores involve a component of crustal contamination		Whitford et al. (1992)
Prince Lyell	Major and trace elements, $\delta^{34}S$ in sulfides and sulfates	Mixed Cambrian seawater (>10‰ and igneous rock (0‰) source	Cogenetic subsurface replacement of permeable volcananics below seafloor VHMS deposits	Reid, (1975), Walshe (1977), Walshe and Solomon (1981), Sheppard (1987)
Prince Lyell	Chlorite, phengite and siderite chemistry	Main mineralised horizon is zoned with respect to Fe, pyrite, chlorite, siderite and phengite	Seafloor exhalative VHMS combined with sub-seafloor replacement	Hendry (1981), Braithwaite (1985)
Prince Lyell	$\delta^{34}S$, Pyrite chemistry, $\delta^{18}O$ in magnetite	$\delta^{34}S$ range (3-11‰), no $\delta^{34}S$ variation between generations of pyrite, earlycobalt-rich, pyrite coeval with chalcopyrite , $\delta^{18}O$ in magnetite indicate magmatic fluid	Late replacement mineralisation focused along Great Lyell Fault, magnetite is granite related	Raymond (1992, 1996)
Prince Lyell	$\delta^{34}S$ in sulfides, $\delta^{18}O$ in magnetite	Sulfur isotope values to low to be felsic rock sulfur and must be from andesites or magmatic fluid, $\delta^{18}O$ in magnetite indicate magmatic fluid	Metals deirved from Suite II andesites, sulfur from rock sulfur and seawater	Halley (1996)
Prince Lyell	Co, Mo, Zn and magnetite in ore		Seafloor exhalative VHMS combined with sub-seafloor replacement	Sutherland (1997)
Western Tharsis	Major and Trace elements, Pyrite chemistry, $\delta^{34}S$ in sulfides, $\delta^{18}O$ in barite and/or carbonate		Convective seawater with possible magmatic input in a VHMS stringer zone. Overprinted by Devonian remobilisation	Manning (1990)
Western Tharsis	Major and trace elements	Chemical dispersions patterns are similar to porphyry copper deposits and acid-sulfate Cu-Au deposits	Hybrid acid-sulphate Cu-Au deposit with similarities to porphyry copper deposits; derived from unknown Ordovician Granite	Huston and Kamprad (in press), Huston (in press)
Royal Tharsis	Major and Trace elements		Sub-seafloor replacement	Godsell (1997)
North Lyell	$\delta^{34}S$,$\delta^{18}O$, major and trace element chemistry	$\delta^{34}S_{sulfide}$ av. -2.6‰, $\delta^{34}S_{barite}$ av. +25.3‰, $\delta^{18}O_{barite}$ = +10.6‰, Bornite precipitated from oxidised Devonian fluids	Post Cambrian (probably Devonian) ore that deposited from solutions that circulated during or after cleavage developement and reacted with Cambrian sulfide-phyllosillicate ores	Solomon et al. (1969), Solomon et al. (1987a), Solomon et al. (1988), Hart (1993)
The Blow	$\delta^{34}S$ in sulfides and sulfates	Significant magmatic (rock) contribution of metals and sulfur to sulfides but sulfates had a meteoric contribution	Seafloor exhalative VHMS	Solomon et al. (1969)
Comstock	$\delta^{34}S$ in sulfides, $\delta^{18}O$ in barite, carbonate and whole rock, C isotopes in carbonate, Pb isotopes in galena		Exhalative VHMS	MacDonald (1991)

pyrophyllite-bearing alteration assemblages while depletions in MgO, Na_2O, K_2O and Cs and increases in Sr, Ba and a positive Eu anomaly characterise the main alteration halo (Manning, 1990; Huston, in press). In the bornite-rich orebodies at Twelve West, North Lyell and Royal Tharsis, K_2O and Rb are depleted in the footwall (Sheppard, 1987; Godsall, 1997). Intensely altered rocks in the Twelve West ore horizon were totally depleted in MnO, MgO, CaO, K_2O, CO_2, and Rb and increases in SiO_2, P_2O_5, S, Cu, Zn, Sr, Ba, Pb, Y, U, Ce, Bi, Mo and Sn (Sheppard, 1987; Godsall, 1997). In addition, at Royal Tharsis, Nd, La and Ce have positive correlations with apatite in the mineralised halo (Godsall, 1997), a relationship observed at Prince Lyell by Raymond (1992) and interpreted to be a result of magmatic fluids.

Chlorite, phengite and siderite compositions at Prince Lyell were studied by Hendry (1981). In phengite, Fe contents decrease from the stratigraphic base of the zoned horizon to the top. In addition, Mg/(Mg + ΣFe) ionic ratios in chlorite (Hendry, 1981; Braithwaite, 1985) and in phengite and siderite (Hendry, 1981) increase with increasing distance from the Cu-rich deposit centre.

Hendry (1981) and Braithwaite (1985) concluded that hydrothermal alteration and mineralisation occurred close to or at the seafloor as Fe-rich waters permeated into and reacted with the top of the volcanic pile.

Studies of Co and Ni in pyrite (Loftus-Hills and Solomon, 1967; Walshe, 1977; Walshe and Solomon, 1981; Manning, 1990; Raymond, 1992; Raymond, 1996) have demonstrated a positive correlation between Co and Ni contents (>1000 ppm) and high Cu grades in disseminated pyrite-chalcopyrite deposits at Prince Lyell and Western Tharsis. Later phases of pyrite typically contain anomalous Zn and Pb, suggesting multiple fluid pulses (Manning, 1990; Raymond, 1992; Raymond, 1996). Co and Ni contents in disseminated Cu-Au deposits contrast sharply with Co and Ni contents in the Comstock, Tasman and Blow exhalative VHMS ores where average Co and Ni contents are typically less than 200 ppm each (Green, 1971; MacDonald, 1991). The high Co and Ni rich pyrite (>1000 ppm) has been used to argue for a magmatic origin to ore fluids at Prince Lyell, Western Tharsis and disseminated deposits in the Mt Lyell field (Walshe and Solomon, 1981; Manning, 1990; Raymond, 1992; Raymond, 1996).

Physicochemical conditions of disseminated pyrite-chalcopyrite formation were investigated by Walshe (1977) and Walshe and Solomon (1981) using a six-component thermodynamic solid solution model involving coexisting quartz, chlorite, pyrite and chalcopyrite. Results suggest ore forming temperatures of 270^{O}C, initial ΣS values between 5 and 30 ppm, $\delta^{34}S_{\Sigma S}$ values of about 7 and a pH of 4 to 4.25.

6.8 ALTERATION INDICES

Although no alteration index can distinguish timing and origin of alteration, a standard method of examining geochemical data in hydrothermal alteration systems is the method of Ishikawa et al. (1976). Ishikawa et al. (1976) created an Alteration Index (AI) designed to measure the intensity of sericite and chlorite hydrothermal alteration in VHMS systems. This index (Equation 6.4) is highly dependent on K_2O and Na_2O concentrations, which are taken to represent the abundances of secondary sericite and albite, respectively.

Equation 6.4:

$$AI = \frac{100(K_2O + MgO)}{(K_2O + MgO + Na_2O + CaO)}$$

Using the equation, AI values between 20-60 are typically calculated for unaltered rocks, while values between 50 and 100 represent hydrothermally or diagenetically altered rocks in VHMS systems. In the Jukes-Darwin area, calculated Ishikawa et al. (1976) AI indices are high (Appendix H, Figure 6.59), and probably relate to albite replacement by sericite and K-feldspar (Na replacement by K), a process typical of granite-related alteration systems (Lowell and Guilbert, 1970; Ishikawa et al., 1976; Beane, 1982; Titley, 1982; Thompson and Thompson, 1996). There are several problems with the Ishikawa et al. (1976) AI: 1) it cannot distinguish diagenetic albite alteration from hydrothermal albite alteration, 2) it cannot distinguish between

sericite and K-feldspar alteration and 3) it cannot discriminate sericite from chlorite alteration zones.

A new index developed in an attempt to discriminate chlorite from sericite alteration is the Chlorite-Carbonate-Pyrite Index; (CCPI, Equation 6.5; Large et al. in press). When CCPI and AI are plotted together, the resultant alteration 'Box Plot' (Large et al., in press) separates the main alteration minerals and gives a measure of alteration intensity.

Equation 6.5:

$$CCPI = \frac{100(FeO + MgO)}{(FeO + MgO + Na_2O + K_2O)}$$

AI and CCPI were calculated for volcanic rocks analysed in the current study and results are compared on the alteration 'Box Plot' (Figure 6.59). A failing of the 'Box Plot' is that it cannot be used to accurately separate rocks with large (>10 wt.%) mass gains from rocks with small (<10 wt.%) mass gains. Since the AI is sensitive to Na_2O, total leaching of Na_2O and replacement by an equivalent amount of K_2O results in a high calculated AI for rocks that have undergone relatively small mass changes. Similarly, increased FeO, in mixed alteration phases and in rocks with magnetite or pyrite, can be associated with increases in K_2O (from sericite or K-feldspar alteration), and can result in misleading shifts to the CCPI. The AI and CCPI were not specifically developed for use on granite-related hydrothermal alteration systems and do not give additional useful information. They also fail to recognise mass changes in SiO_2, often the element with the largest change in total mass. In Figures 6.43 and 6.44, AI and CCPI were compared to SWIR wavelengths (AlOH and FeOH). In these two cases, separation of alteration intensity and elemental mass movements was not the objective of the comparison and the indices provided a useful comparison. However, due to the inability of the AI and CCPI to distinguish large mass changes from small mass changes, neither was applied further to this study.

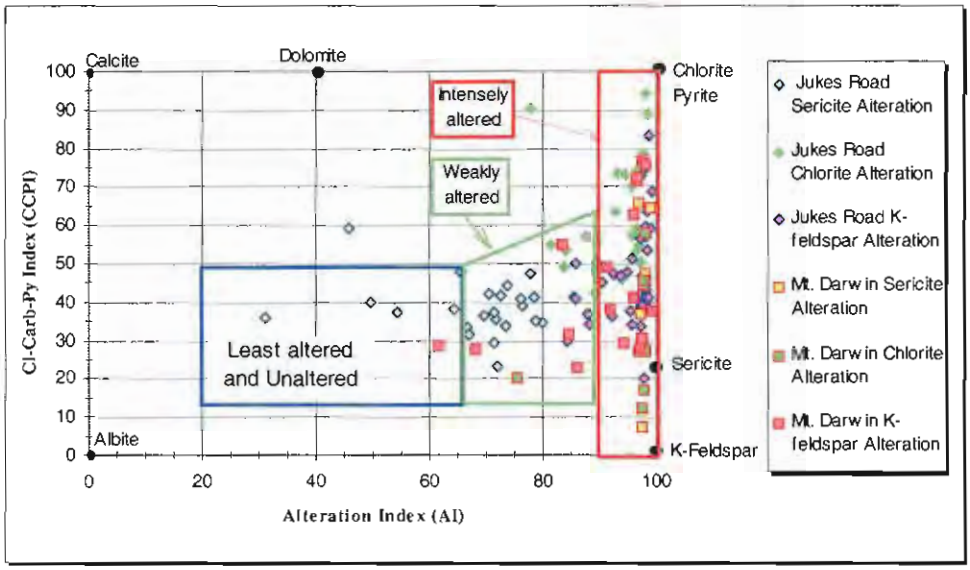

Figure 6.59. Alteration 'Box Plot'. Composition of sericite, chlorite and K-feldspar-altered dacites for the Jukes Road, King River Tunnel and Mt. Darwin as a function of AI and CCPI. The 'Box Plot' accurately separates the 'least-altered' and weakly altered dacites from the intensely altered rocks when total mass changes are small. Intensely K-feldspar and chlorite-altered rocks from Mt. Darwin are, however broadly mixed with K-feldspar-altered rocks plotting with high CCPI (due to FeO from magnetite) and chlorite-altered rock plotting with lower CCPI's. Similar trends are not as apparent for the Jukes Road and King River data due to significantly smaller overall mass changes. The location of alteration end member minerals (black dots) and the unaltered rhyolite/dacite box are shown. Method of Large et al. (in press).

6.9 SUMMARY

The Murchison and Darwin Granite series plot within the granite and granodiorite fields of Streckeisen (1976) and plot near the calc-alkaline-granodiorite trend of Lameyre and Bowden (1982, Figure 3.3). The Darwin, Murchison and Elliott Bay Granites are classified as I-type magnetite-series granites. As illustrated on the trace element diagrams of Pearce et al. (1984), the granites have characteristics consistent with emplacement in either or a collisional and volcanic arc environment (Figures 6.21-28). These classification schemes therefore support the tectonic setting proposed by Solomon, (1981), Crawford et al., (1992) and Crawford and Berry, (1992).

CaO, Na_2O and K_2O vs. SiO_2 data (Figures 6.2, 6.4 and 6.6) for all three Cambrian granites is scattered and is interpreted to be the result of post emplacement alteration events. TiO_2, Al_2O_3 and P_2O_5 vs. SiO_2 (Figures 6.1, 6.3 and 6.8) have pronounced linear trends. It was therefore concluded that these elements were immobile. REEs, Zr, Nb and Y and have behaved in an immobile fashion.

GENMIX modeling of major elements and REE data in the Darwin Granite support the model that the microgranite and white granite formed from fractionation of the pink granite phase. Negative εNd values (Table 6.2) imply that the Murchison and Darwin Granites were probably derived from continental crust with a lower Sm/Nd than CHUR. Additional support for partial melting comes

from the low P_2O_5 contents of the granites, linear variation diagrams, Nd model ages and restite in the Murchison Granite.

FeO contents of whole rocks and chlorites increase with proximity to the mineralised zone (Figures 6.36 and 6.37), suggesting a relationship to increasing temperature in contrast to the relationship observed in the Murchison Gorge by Polya et al. (1986). The 320-360^{0}C temperature range determined from chlorite geothermometry represents minimum hydrothermal temperatures. These temperatures are higher than chlorite temperatures determined by Hendry (1981) for Mt. Lyell. The 260-290^{0}C metamorphic re-equilibration temperatures and ore deposition temperatures of 270-310^{0}C of Walshe and Solomon (1981) probably represent minimums also, due to inaccuracies in the microprobe analyses (Jiang et al. 1994). Most of the magnesium within the chlorite-altered zone at the Jukes Prospect also occurs within chlorite.

The compositional range of white micas in study area samples range from muscovite/illite to phengite. Rocks with muscovite/illite have higher contents of unaltered plagioclase than phengitic rocks. Based on Figures 6.41-6.43, it is interpreted that mica compositions were controlled by bulk rock compositions and were weakly related to hydrothermal alteration intensities within specific lithologies including the Darwin Granite. The range in FeO+MgO contents analysed in dacites suggests no relationship between FeO+MgO and AlOH wavelengths.

$\varepsilon Nd_{(500Ma)}$ values and REE patterns in Prince Lyell apatites are strong evidence that magmatic fluids derived from a Suite I (Murchison-like) magma were directly responsible for apatite-magnetite ores. However, the source of the copper and gold is inferred based on similarities to other Cambrian granite-related Cu-Au prospects such as those in the Jukes-Darwin area.

The mass change method developed by MacLean and Kranidiotis (1987) and refined by MacLean and Barrett (1993) relies heavily on the correct selection of a single unaltered or 'least-altered' precursor sample from the same rock unit as the altered rocks. Calculated mass gains and losses in aluminum and phosphorus in intensely altered Mt. Darwin rocks (Table 6.18) could be due to selection of the wrong precursor. However, an examination of the Zr values for other unaltered CVC dacites (White, 1975; Gadaloff, 1996) shows that the selected value of 280 ppm Zr for the precursor sample (B10750), is within the range of Zr values for other MRV dacites in the Mt. Darwin area. Therefore, although it is possible that the dacites at Mt. Darwin had a different and unique Zr content, it is unlikely that it was significantly different from the precursor rock (B10750). Zr mobility is also unlikely since Ti/Zr values have been demonstrated to be constant in the Mt. Darwin dacites and andesites. Therefore, the calculated mass gains for Al_2O_3 and SiO_2 (and other elements) are considered to be real.

On the basis of spatial distribution, the zoned silica, K-feldspar and chlorite alteration styles and assemblages (Section 5.5 and 5.6) are assumed to be related to intrusion of the Darwin Granite. Although regional metamorphic alteration styles were recognised (Section 5.4.4), their effects on total mass changes could not be separated from hydrothermal effects. Absolute mass gains and losses differ drastically between adjacent lithologies that contain similar hydrothermal alteration assemblages in the Jukes-Darwin area (Tables 6.17 and 6.18). Total mass changes at the Jukes Prospect were minor, and typically involved replacement of one mineral with another without

significant net mass changes. K-feldspar and sericite-altered rocks had mass gains in K_2O, Fe_2O_3, Rb, Sr and Ba and depletions in Na_2O and CaO. In chlorite-altered rocks, total mass gains in K_2O, MgO and Fe_2O_3 effectively balanced depletions in Na_2O, CaO and SiO_2 (Table 6.17). In contrast to the minor mass change at the Jukes Prospect, large mass changes occurred at Mt Darwin. Massive gains in SiO_2 (+80 %) and mass gains in Al_2O_3, K_2O, Ba and Sr occurred in the dacites, while depletions of SiO_2 and Al_2O_3 occurred in the adjacent andesites. Mass changes in Si, K and Al are good indicators of hydrothermal alteration intensity at Mt. Darwin.

Large mass gains and losses of the magnitude described above are commonly associated with intense hydrothermal alteration in VHMS deposits(Kranidiotis and MacLean, 1987; MacLean and Kranidiotis, 1987; Barrett and MacLean, 1991; Barrett et al., 1991; Barrett et al., 1992; MacLean and Barrett, 1993; Barrett and MacLean, 1994) and intrusion-related ore deposits (Camus, 1975; Alderton et al., 1980; Ward et al., 1992). These hydrothermal systems are driven by heat from underlying intrusive bodies (Lowell and Guilbert, 1970; Beane, 1982; Barrett, 1992; Sillitoe, 1993; Titley, 1993; Large et al., 1996). The role of the intrusive bodies in providing elements through magmatic fluids is controversial in VHMS systems, but in intrusive-related systems it is well documented. In VHMS systems, ore forming components are, at least in part, derived from leaching of the host volcanics (Barrett et al., 1990; Barrett and MacLean, 1991; Offler and Whitford, 1992; Barrett and MacLean, 1994; Gemmell, 1994; Allen et al., 1998). In the Jukes-Darwin area, the occurrence of nearly unaltered dacites near the Jukes Prospect suggests that leaching of elements from the local host volcanics was only a minor contributor to the mass gains observed and a minor seawater contribution cannot be ruled out. Large mass changes in the Mt. Darwin area can be explained by magmatic fluids enriched in K, Fe, Ba, Sr, Cu, Mo, W, Th and U exsolving from the Darwin Granite, mixing with recycled seawater and producing K-rich and Fe-rich hydrothermal alteration assemblages (Figure 6.60). Covariant relationships between K_2O and Ba, and K_2O and Sr (Figures 6.56F and 6.57) support this model.

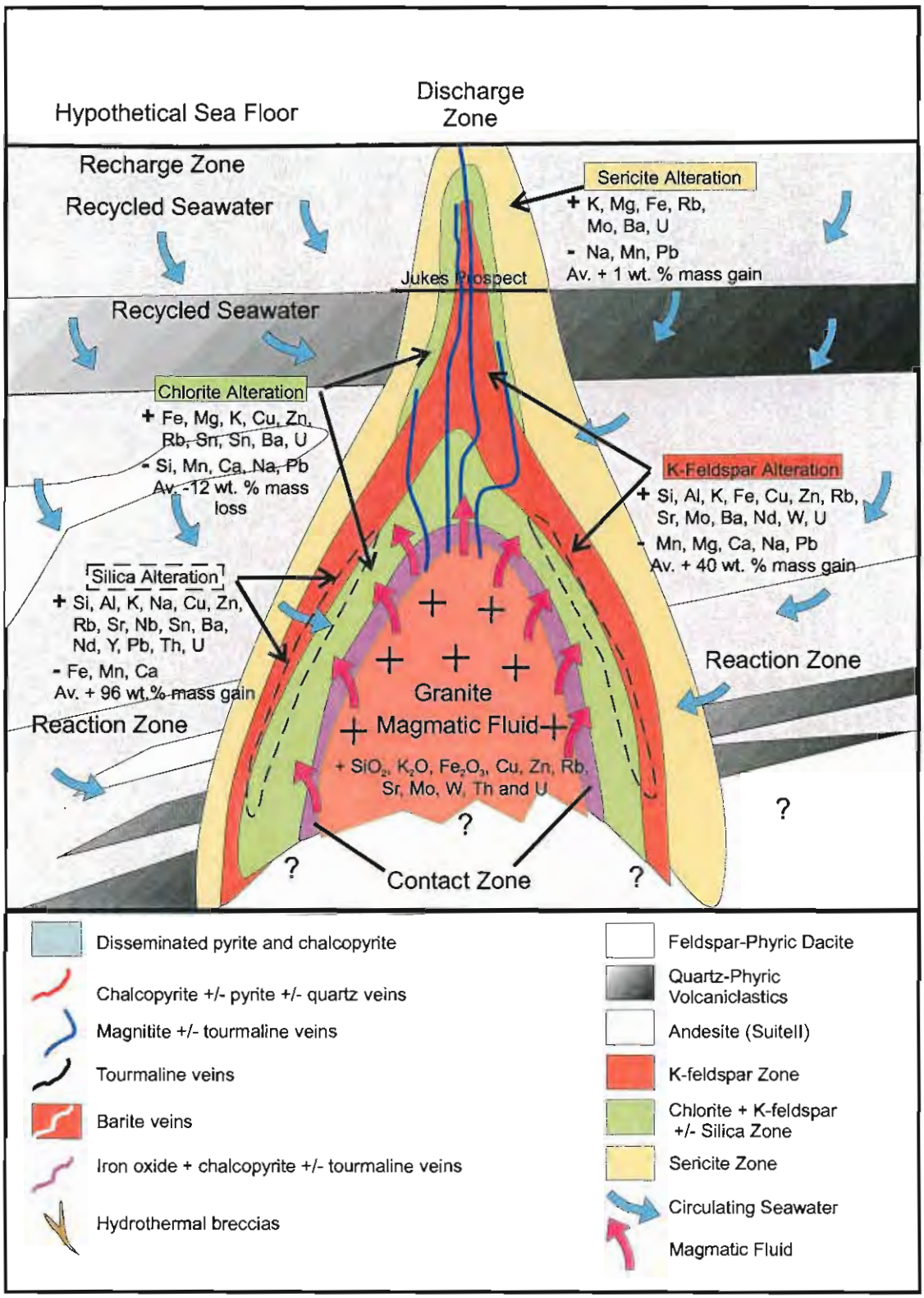

Figure 6.60. Summary diagram of mass changes for the Jukes-Darwin area. Magmatic fluids exsolved from the granite provided Si, K, Fe, Cu, Zn, Mo, Ba, U and Th. Na and Ca may have been leached from the rocks by diagenetic processes or by circulation of recycled seawater early in the development of the hydrothermal system.

CHAPTER 7

7.0 MINERALISATION IN THE JUKES-DARWIN AREA

7.1 INTRODUCTION

Copper-gold ores in the Jukes-Darwin area are confined to veins and hydrothermal breccias with minor localised disseminated zones. Five major phases of alteration and mineralisation paragenesis have been recognised and are designated; early, middle (pre-breccia), hydrothermal breccia formation, middle (post-breccia) and late. Early hydrothermal alteration and mineralisation are interpreted to be related to initial heating of the rocks and initiation of the hydrothermal circulation system. The main alteration and Cu-Au mineralisation events (middle phases) occurred during the peak of hydrothermal activity. Late stage mineralisation was related to collapse of the hydrothermal system and subsequent metamorphism.

In this chapter the various vein styles, breccias and their mineral parageneses are described in relation to the various hydrothermal alteration styles. Late syn-tectonic veins, common elsewhere in the MRV, were not involved in the mineralisation or hydrothermal alteration processes and are only discussed briefly.

7.2 VEIN STYLES AND MINERAL ASSEMBLAGES

With increasing distance from the Darwin Granite, vein styles vary from: 1) iron-oxide veins and stockworks that contain pyrite and chalcopyrite ± specular hematite ± magnetite ± tourmaline and quartz-pyrite-chalcopyrite veins, to 2) disseminated pyrite-chalcopyrite ± covellite, and 3) veins containing quartz, bornite, neodigenite, chalcopyrite and hematite. Table 7.1 and Figure 7.1 summarise the major Jukes-Darwin mineral deposits, together with their principal metals, mineralisation and hydrothermal alteration styles.

In the Mt. Darwin area, Cu-Au ores occur in iron oxide veins and stockworks at the Prince Darwin Prospect (Figures 1.2, and 7.1). The veins contain pyrite, chalcopyrite, magnetite and tourmaline and are hosted in intensely chlorite and K-feldspar-altered volcanics of the CVC. The Prince Darwin Prospect occurs within and against the contact zone of the Darwin Granite and has been interpreted as a skarn deposit (Hills, 1914; White, 1975). Elsewhere along the western margin of the granite, Cu-Au mineralisation occurs in magnetite-tourmaline-specular hematite veins. Individual veins contain disseminated chalcopyrite and pyrite, massive to semi-massive masses of chlorite with chalcopyrite, or quartz with accessory chalcopyrite and pyrite. Major stockwork zones were not observed.

Cu-Au ores in the Intercolonial Spur area occur as chalcopyrite-pyrite veins and disseminations in intense zones of secondary chlorite at East Darwin and Findons (Figures 1.2 and 7.1). This suggests that remobilisation of Cu mineralisation occurred at East Darwin during the middle-late Delamerian.

Table 7.1. Mineral deposits in the Jukes-Darwin area.

Name & Metal	Distance from Granite	Mineralisation Styles	Alteration styles	References
Jukes Prospect (Cu-Au)	>1 km	Disseminated pyrite and chalcopyrite in schistose dacitic and rhyolitic volcanics, magnetite +/- tourmaline +/- scheelite veins, chalcopyrite-pyrite-magnetite veins, and magnetite and chlorite +/- tourmaline matrix breccias.	Styles vary from intense K-feldspar altered volcanics in the mineralised zone, out to intense chlorite-sericite assemblages and peripheral sericite altered volcanics.	Hills (1914), White (1975), Doyle (1990), Gadaloff (1996)
Lake Jukes (Cu)	>1 km	Bornite, neodigenite, chalcopyrite and hematite in veins up to 1m wide.	Minor chloritic alteration styles and a lack of intense sericite altered volcanics.	Hills (1914), White (1975)
Findons (Cu)	0.5-1 km	Quartz-chalcopyrite in stringer veins, and as minor disseminations and blebs within chloritic domains.	Intense chlorite-pyrite altered volcanics and chlorite-quartz-sericite domains	Hills (1914), White (1975), Gadaloff (1996)
Taylours Reward (Ba)	0.5-1 km	Massive barite +/- pyrite +/- chalcopyrite in veins up to 1m wide and occurring in en echelon vein sets for over 1km.	Sericite and chlorite altered volcanics.	Hills (1914), White (1975), Gadaloff (1996)
Bean and Thow, Hydes (Cu)	0.5-1 km	Disseminated chalcopyrite in pyritically altered volcanics.	Sericite and chlorite altered volcanics.	Hills (1914), White (1975)
East Darwin (Cu)	0.5-1 km	Pyrite-chalcopyrite veins within the CVC, and disseminated pyrite-chalcopyrite-covellite within the EQPS. Possibly fault hosted.	Pervasive K-feldspar, chlorite and sericite alteration styles.	Hills (1914), White (1975), Gadaloff (1996)
Mt. Darwin, including Prince Darwin (Cu-Au)	0-0.5 km	Iron oxides veins and stockworks containing pyrite, chalcopyrite, magnetite and tourmaline. Quartz veins with accessory chalcopyrite and pyrite.	Pervasive K-feldspar, chlorite and sericite alteration styles.	Hills (1914), White (1975)

Table 7.2: Vein types in the study area.

Type	Subtype and Assemblage	Associated Ore Minerals	Distance from the Granite
Quartz Veins	Quartz ± chlorite veins with ladder-like structure	Carbonate, sericite, magnetite, sulfides	N/A
	White quartz veins	K-feldspar, magnetite, pyrite, chalcopyrite, galena, sphalerite and gold	0.5-1.5 km
	Quartz ± tourmaline veins	Epidote (zoisite), pyrite, chalcopyrite	Within the granite
	Fine-grained grey "drusy" quartz veins.	None	Within the granite to < 0.5 km
Tourmaline Veins	Tourmaline ± quartz veins	Magnetite, specular hematite, rock fragments	Within the granite to < 0.5 km
Magnetite Veins	Magnetite ± hematite +/- quartz veins	None	Within the granite to <1 km
	Magnetite ± iron oxides ± tourmaline ± specular hematite ± quartz veins.	Pyrite, chalcopyrite, gold	0.5-1 km
	Specular hematite ± quartz veins.	None	0-1 km
Barite Veins	Barite veins	Quartz, hematite, pyrite, chalcopyrite	Within the granite to <1 km

Orogeny, resulting in the deposition of disseminated and vein chalcopyrite in the EQPS, along the fault contact with the CVC (Gadaloff, 1996). Multiple vein-forming events occurred throughout the area producing magnetite and tourmaline veins associated with the main hydrothermal system,

late stage barite veins, and various syn-tectonic veins (Devonian ?), the most abundant of which contain quartz + chlorite.

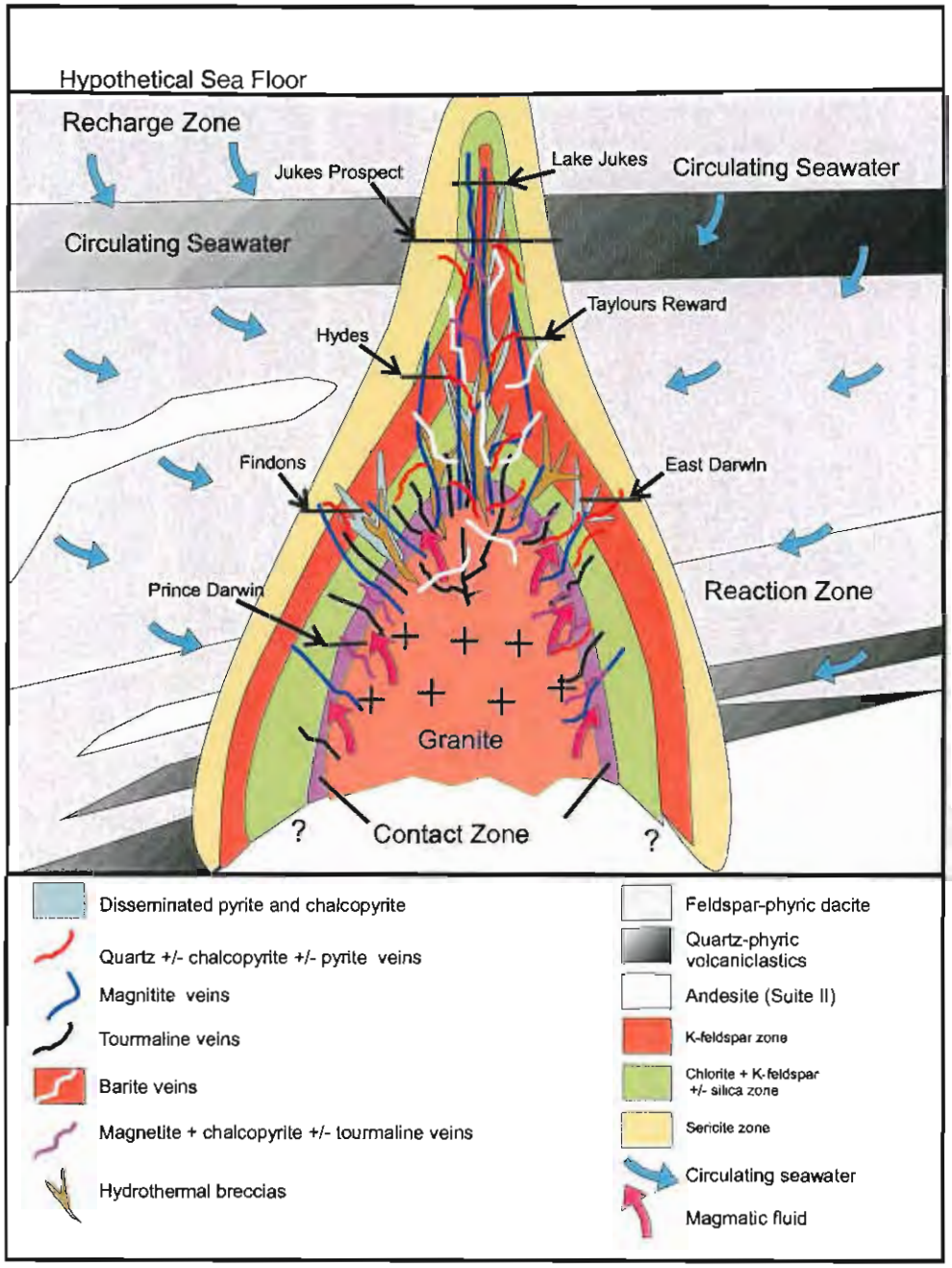

Figure 7.1. Schematic cross-section of granite-related mineralisation and mineral deposits in the Jukes-Darwin area.

At the Jukes Prospect (Figures 1.2 and 7.1), Cu-Au ores are hosted in coherent feldspar-phyric dacitic volcanics of the CVC. Mineralisation occurs as disseminated pyrite and chalcopyrite, magnetite ± pyrite ± tourmaline ± scheelite veins, magnetite ± chalcopyrite ± pyrite veins, quartz ± chalcopyrite stringers and magnetite ± chlorite + tourmaline hydrothermal breccias. Vein styles and assemblages related to mineralisation are summarised in Table 7.2. Intense chlorite alteration and accompanying copper minerals overprint the margins and bodies of the quartz-feldspar-biotite-porphyry dykes.

7.2.1.2 QUARTZ VEINS

Syn-Tectonic Quartz Veins

Syn-tectonic quartz veins occur as single veins, or as small groups (3-6) of discontinuous veins, or en echelon vein sets. All of the veins have well-developed euhedral quartz crystals perpendicular to the side of the vein, with the remaining open space filled with chlorite and light-beige carbonate (Plate 7.1A and B). Characteristic of the syn-tectonic quartz veins is their size (<1 to a few centimetres wide and <5 metres long) and discontinuity. Syn-tectonic quartz veins are closely aligned with the dominant regional northwest structural trend and are interpreted to be of Devonian age (Section 5.4.4). Veins of post-hydrothermal origin typically contain quartz, bright green or bright blue-green chlorite (in thin section) and rhombohedral carbonates. The carbonate often replaces earlier quartz and chlorite or in some cases may have been synchronous. The quartz typically occurs in ladder structures with chlorite. Chlorite occurs as fine-grained < 0.01 mm mosiacs that have filled open spaces between quartz grains.

Pre-Tectonic Quartz Veins

Four styles of pre-tectonic quartz veins were observed (Table 7.2) throughout the CVC and within the Darwin Granite. Two of the styles are white quartz veins with various accessory minerals. The others are quartz + tourmaline veins and fine-grained light-grey monomineralic 'drusy' quartz veins.

White Quartz Veins

Two styles of white quartz veins occur within and up to 1500 metres away from the Darwin Granite. The two styles are separated on the basis of size and may be related, although no transition between the two styles was observed. The larger of the two vein styles occur within and near the Darwin Granite. Veins within the granite are up to a metre wide and less than 30 metres long. They are uncommon in the pink granite, but are common in the white granite, especially near the contact between the two phases. One high angle massive white quartz vein up to 3 metres wide and over 100 metres long was observed in the CVC. Numerous veins and networks of veinlets extend outward from the larger veins into the host volcanics at high angles. Accessory minerals observed include magnetite, K-feldspar, pyrite, chalcopyrite, sphalerite and galena. The white quartz veins have been deformed and offset by faults and are therefore interpreted to be of Cambrian origin.

The smaller of the two white quartz vein styles typically occurs in association with sericite and K-feldspar alteration assemblages and accessory pyrite and chalcopyrite were observed. The quartz veins are typically less than 1 mm wide and cross-cutting relationships between veins are common (Plate 7.1C). Small quartz veins were observed cutting feldspar phenocrysts with alteration halos of chlorite within the phenocryst (Plate 7.D-E). This suggests that the quartz veins were also used as conduits for hydrothermal alteration fluids prior to sealing by quartz. Quartz veins of this style were observed in breccia fragments within the hydrothermal breccias and

Plate 7.1. Quartz veins from the Jukes Darwin area

A and B. Ladder like quartz (Q), chlorite (C) and carbonate (Carb) in a late quartz vein cutting through a K-feldspar altered feldspar-phyric dacite. The carbonate occurs along the vein margin and truncates and replaces earlier ladder-like quartz and chlorite. Sample B1006 from Jukes Road. Plane Polarized Light, and Crossed Polars. Field of view width = 3.75 mm.

C. Banded quartz vein (Q2) with pyrite(P) cross-cuts an earlier quartz vein (Q1) and is in turn cut by a later one (Q3). The groundmass is K-Feldspar altered feldspar-phyric dacite. Sample 10220 from Jukes Road (Appendix A). Plane Polarized Light. Field of view width = 1 cm.

D and E. Intense chlorite and minor sericite alteration of a feldspar phenocryst in a K-Feldspar altered feldspar-phyric dacite. Notice the increase in chlorite alteration (C) around the cross-cutting quartz vein. Sample 10220 from Jukes Road (Appendix A). Plane Polarized Light, and Crossed Polars. Field of view width = 2 mm.

F. Late quartz vein (Q) cross-cuts a quartz-tourmaline breccia. Earlier micro scale quartz veins occur within some of the breccia fragments. Sample B1008 from the Jukes Road. Plane Polarized Light. Field of view width = 1 cm.

G. Quartz and chlorite occur in a late vein (Qv). Many earlier quartz-feldspar veins have been broken by microfaults. This is typical fracture density as the alteration system is approached. Sample 10230 from Jukes Road (Appendix A). Plane Polarized Light. Field of view width = 1 cm.

A

B

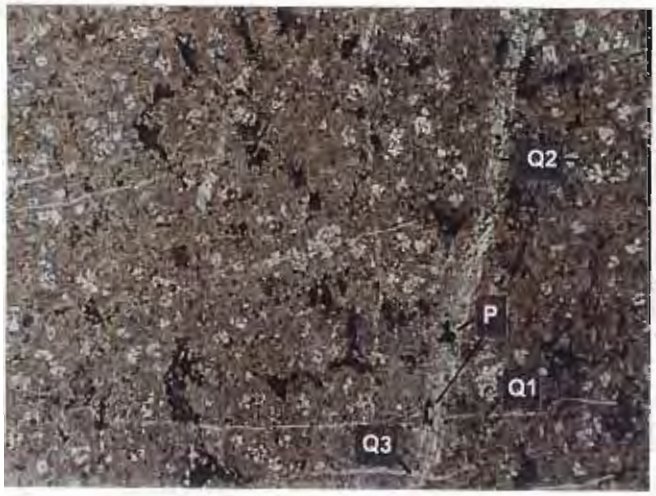

C

D

E

F

G

cross-cutting breccia matrices (Plate 7.1F) suggesting a continuum of fracturing occurred throughout the development of the hydrothermal system.

Quartz ± Tourmaline ± Epidote Veins

The quartz-feldspar porphyry has been cut by quartz + tourmaline ± epidote veins. The veins are small (up to 1 mm wide) and occur as boxwork-like networks within some outcrops. The veins contain accessory pyrite and chalcopyrite.

Fine-Grained Quartz Veins

Small (2-15 cm wide and rarely longer than 10 metres), uncommon fine-grained quartz veins occur throughout the Darwin Granite and associated volcanics. They typically occur in the granite within the first few hundred metres of the granite contact, and are spatially associated with barite veins. Accessory minerals and open space textures were not observed. Grain size is <1 mm.

7.2.1.3 TOURMALINE VEINS

Tourmaline veins (Plates 7.2A-C) occur throughout the pink granite phase of the Darwin Granite and CVC rocks, as illustrated schematically on Figure 7.1. Several varieties of tourmaline veins were recognised: 1) tourmaline + magnetite + quartz veins (Plate 7.2C), 2) tourmaline + quartz ± chlorite veins (Plate 7.2D and 7.3) and 3) tourmaline + magnetite + quartz + specular hematite veins. Tourmaline veins are typically <10 cm wide, discontinuous, and commonly contain brecciated rock fragments and rock dust derived from the host rocks (Plates 7.2B). K-feldspar-altered CVC volcanics clasts are common. Tourmaline is black and microcrystalline, and veins commonly have bleached quartz-rich alteration halos (Plate 7.2A). Tourmaline occurs as well-formed elongate hexagonal crystals up to 0.4 mm long and 0.05 mm across (Plate 7.2C). Some tourmaline-magnetite veins are zoned, with tourmaline-rich outer rims, and magnetite-hematite-rich centres. Tourmaline veins were observed within the pink granite several metres from the contact with the quartz-porphyry phase of the white granite. Tourmaline and magnetite veins cross-cut each other, suggesting multiple phases of intrusion and a close timing relationship.

At the Jukes Prospect, tourmaline-magnetite veins are typically <15 cm in width. The contacts between veins and host rocks are marked by stockwork stringers that have imparted a brecciated texture to the margins of the veins. Typically, veins contain angular to rounded clasts of country rocks up to 3.5 cm in diameter. Tourmaline veins are typically banded (Plate 7.3) suggesting multiple fluid pulses.

Table 7.3 summarises the tourmaline data from the Jukes-Darwin area. Electron microprobe analyses of tourmaline by Garrett (1989), Doyle (1990) and Gadaloff (1996), did not identify significant compositional zoning, suggesting that the tourmaline grew during a single hydrothermal event. However, color zoning was observed in the current study (Plate 7.2C). Based on FeO/(FeO+MgO) and (FeO+MgO)/(FeO+MgO+Al_2O_3) ratios (Table 7.3), the Fe-rich, Al-poor tourmalines are classified as members of the schorl-darvite solution series. They are similar to

Plate 7.2. Typical tourmaline vein characteristics from Mt. Darwin and the Jukes Road.

A. Typical tourmaline vein in the CVC volcanics west of the Darwin Granite. Notice the small angular lithic fragments (L) of altered volcanic rock incorporated into the vein. The bleached quartz-rich alteration halo (H) around the vein radiates outward from the vein and decreases in intensity with increasing distance from the vein.

B. Slabed tourmaline vein from the Mt. Darwin area. Angular rock fragments vary in size from <0.1 mm to >2 cm. Sample 128i from Large et al. (1996). Scale is in centimetres.

C. Plane polarized light photomicrograph of euhedral and subhedral tourmaline (T), magnetite (M) and quartz (Q) in the matrix of a magnetite-tourmaline breccia. Notice zoning in the hexagonal tourmaline cross-section in the centre of the photo. Clasts of feldspar-phyric dacite (D) are intensely replaced by secondary K-feldspar, quartz and chlorite. Hematite staining (H) occurs in the lower portion of the photograph. Field of view width = 1 mm. Sample B1009 from Jukes Road (Appendix A).

D. Plane polarized light photomicrograph of a chlorite-tourmaline vein cutting feldspar-phyric dacite (D). The primary vein matrix is chlorite (C) with subordinate tourmaline (T). Field of view width = 1 mm. Sample B1008 from Jukes Road (Appendix A).

A

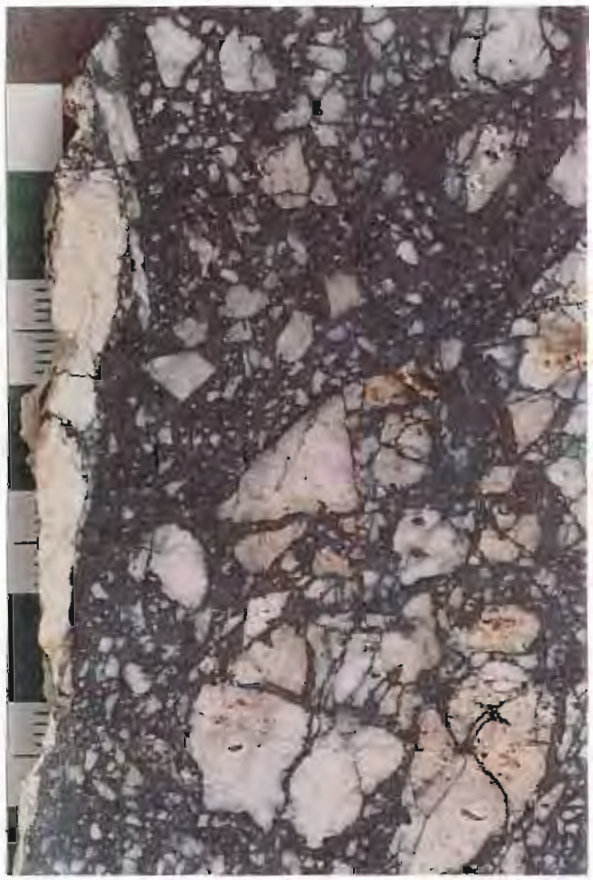

B

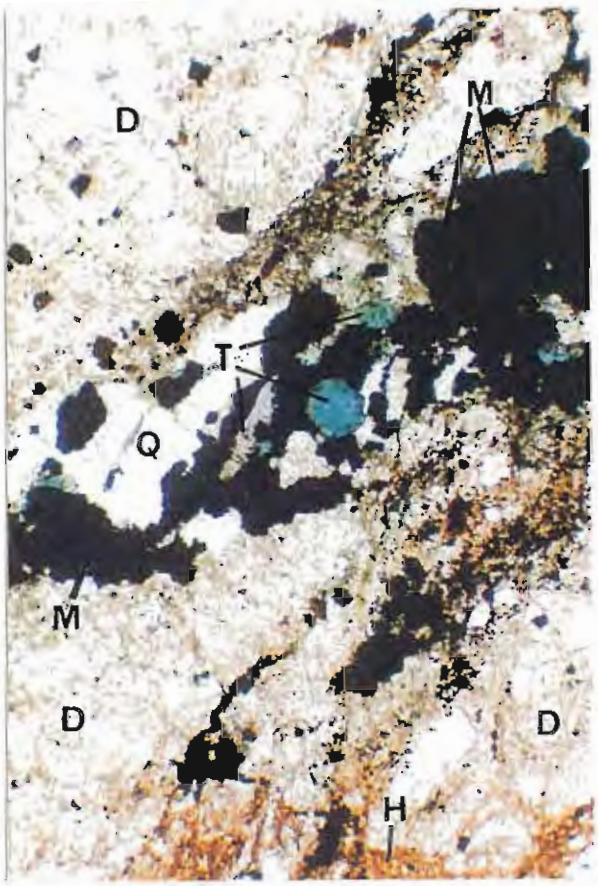

C

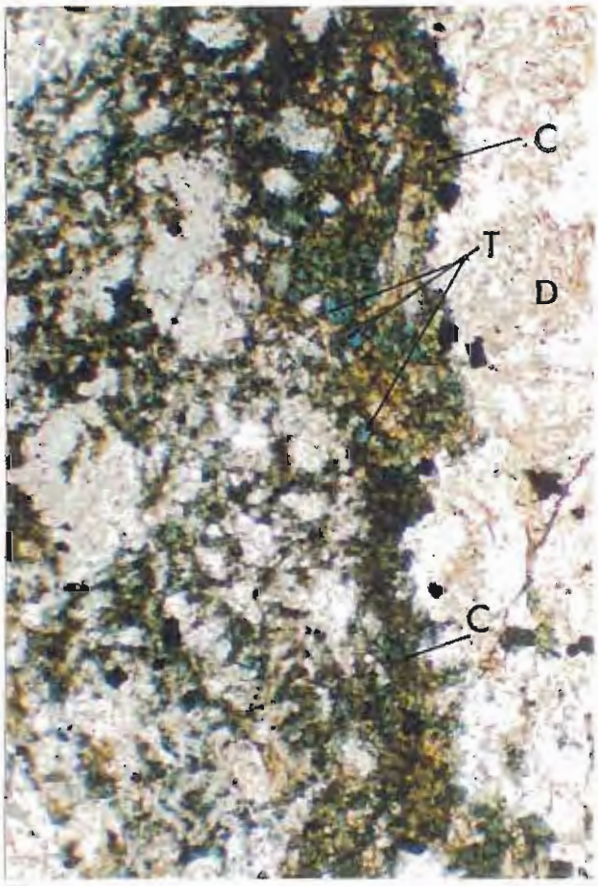

D

Plate 7.3. Complex vein relationships in a tourmaline-quartz-chlorite vein along the Jukes Road.

A. The major veining is caused by intrusion of tourmaline-quartz-chlorite breccia veins (A) into pre-existing quartz veins (B). These quartz veins (B) also cut an earlier set of micro-scale stockwork quartz veins (C). Banding (D) within the tourmaline-quartz-chlorite breccia vein suggests continued reuse of the vein by multiple fluid pulses. Sample 10390 from Jukes Road. Plane Polarized Light. Field of view is 2 cm across.


D
C
A
B
1 Cm

the more magnesian-rich granite-related tourmalines documented from Rosebery (Khin Zaw et al., 1997), and in the Meredith Granite (Plimer and Lees, 1988).

Table 7.3. FeO / (FeO+MgO) and (FeO+MgO) / (FeO+MgO+Al_2O_3) values obtained from vein tourmalines. Tourmalines throughout the Jukes-Darwin area are Fe-rich and Al-poor. Data from Eastoe et al. 1987b, Garrett 1989, Doyle 1990, Jones 1993 and Gadaloff 1996.

Location	FeO / (FeO+MgO)	(FeO+MgO) / (FeO+MgO+Al_2O_3)
Jukes Prospect	0.84	0.33
Intercolonial Spur	0.71	0.38
Darwin Granite	0.66	0.35
Prince Darwin	0.77	0.40
Elliott Bay	0.76	0.32

The Significance of Boron

H_2O, B, and F have all been shown to depress the solidus of granitic melts (Tuttle and Bowen, 1958; Wyllie and Tuttle, 1961; Chorlton and Martin, 1978; Manning, 1981; Pichavant, 1981; Pichavant, 1987; Manning and Pichavant, 1988; Anderson, 1995). The occurrence of tourmaline in veins and breccias in the Jukes-Darwin area, is consistent with high boron contents, in the Darwin Granite. B and H_2O can depress the solidus temperature of granite to less than 600^{0}C depending on the amount of B in the melt (Chorlton and Martin, 1978; Pichavant, 1981; Pichavant, 1987; Anderson, 1995). An estimate of the boron content of the original granitic melt cannot be accurately made due to the preference of boron to partition into the volatile phase (Pichavant, 1981; London, 1987; Pichavant, 1987). Boron and water probably depressed the solidus temperature of the Darwin Granite allowing the granite to intrude to a higher crustal level (2-3 km, Solomon, 1981), than would normally have been possible.

7.2.1.4 MAGNETITE VEINS

Two types of magnetite veins were observed in the study area (Table 7.2): Magnetite + hematite + quartz ± tourmaline veins and magnetite + specular hematite + quartz ± tourmaline veins. Doyle (1990) reported apatite as an accessory in magnetite veins at the Jukes Prospect. Magnetite veins occur within the pink phase of the Darwin Granite and in all facies of CVC rocks (Plates 7.4A-D), but were not observed in the white granite phase or in YRS rocks. Magnetite veins within the pink granite are small (<10 cm) and discontinuous (Plate 7.4B). Vein widths range from <1 cm to >5 m and can vary from a few centimetres, to over a metre wide, over a few metres along strike. Individual veins vary in length from 3-100 metres. Small veins (<1 cm) commonly occur as random stockworks (Plate 7.4C-D). Large veins (widths >1 metre) generally strike east-west, dip at low angle to the north and are subparallel to the current top of the Darwin Granite (Plate 7.4A). Networks of progressively thinner magnetite veins extend randomly outward from larger veins into the host volcanics; the larger the vein, the farther the network veins extend in continuously decreasing size. On the south side of Mt. Darwin, smaller networks of magnetite veins extend outward for over 50 metres from a 5 metre wide vein (Plate 7.4A). Magnetite, quartz, hematite, and specular hematite are intergrown in the veins. Hematite is commonly more abundant than magnetite due to martitisation (Solomon et al., 1988). Around the margins of larger magnetite

veins, angular blocks of altered volcanics occur that have jigsaw fit textures. The cores of the veins contain no lithic clasts, and typically have a banded appearance.

Magnetite breccia veins that contain clasts of altered volcanics, are common (Plate 7.4A). Similar styles of breccia veins occur at Mt. Darwin, Intercolonial Spur (Gadaloff, 1996) and the Jukes Prospect.

7.2.1.5 BARITE VEINS

Barite veins occur throughout the Jukes-Darwin area. At Mt Darwin, two barite veins occur in cooling related cracks within the pink phase of the Darwin Granite. The barite veins are up to 30 cm wide and have augen-like structures along strike. At Taylours Reward on Intercolonial Spur, there are a series of en echelon barite veins up to 1m wide, with the longest segment extending for approximately 20 m. The veins occur over a strike length of up to a kilometre. These veins are interpreted to be part of a 1 km long fault zone that trends east-west to northwest-southeast (Gadaloff, 1996). In these veins, barite varies in colour from milky white to red-brown, depending on the presence of fine-grained hematite. Coarse crystals of barite (averaging >1 cm) occur in a matrix of fine grained barite (0.070-0.5 mm), and subordinate quartz crystals. Fine-grained (<0.1 mm) pyrite and hematite were reported to occur as inclusions within coarse barite crystals by Gadaloff (1996). Barite was reported at the Jukes Prospect (Solomon et al., 1988) but was not observed in this study. However, at Mt Darwin, two barite veins occur in cooling related cracks within the pink phase of the Darwin Granite. Although, no relationship between barite veins and tourmaline or magnetite was observed, barite sulfur isotopes compositions from these veins are consistent with a Cambrian seawater source for sulfur (Solomon et al., 1988; Jones, 1993; Gadaloff, 1996). Therefore barite veins are interpreted to have formed late, during collapse of the magmatic hydrothermal system.

7.3 HYDROTHERMAL BRECCIAS

At the Jukes Prospect, two hydrothermal breccia pipes have been identified. They were previously described as pseudobreccias by Doyle (1990). However, the intimate intergrowths of magnetite, chlorite and tourmaline in the matrices, argues strongly for a hydrothermal origin. The breccias are predominately clast supported (60-90% clasts) although localized areas of matrix-supported breccias were observed (Plate 7.5A-D). The breccias typically occur as fine crackle breccias with jigsaw fit textures. Adjacent to the breccias, zones of crackle breccia range from one to several metres in width. Sharp contacts with unfractured wall-rocks were also observed. Within crackle zones, an increase in fracture density and rotation of clasts occurs close to the main pipe. The main breccia body is matrix supported and contains milled dacite clasts and abundant altered rock flour in the matrix (Plate 7.5C). Most of the clasts are angular to subangular blocks of intensely K-feldspar-altered feldspar-phyric dacite (Plate 7.5B). Chlorite-altered blocks and rounded clasts of quartz-feldspar porphyry dyke rocks are also present.

In the descriptions below, the breccias are separated on the basis of matrix composition: 1) magnetite + hematite + tourmaline ± chlorite; and 2) chlorite + tourmaline ± magnetite ± hematite

Plate 7.4. Typical magnetite veins from the Jukes-Darwin area.

A. Large magnetite vein (M) cutting the CVC on the ridge west of the Darwin Granite. The vein has a shallow northerly dip, and a well-developed network of smaller magnetite veins that extend outward into the host rocks. Notice the abundance of angular lithic clasts (L) scattered throughout the vein.

B. Sheeted magnetite veins within the pink phase of the Darwin Granite.

C. Magnetite-pyrite-quartz veinlets cutting K-feldspar-chlorite-altered feldspar-phyric dacite at the Jukes Prospect. The pyrite (P) is euhedral and occurs within the vein and in the dacite. All of the pyrite occurs within the veins and magnetite replacement by pyrite was not observed. Sample B1002.

D. Photomicrograph of magnetite veinlets (M) from Plate 7.4C. Notice the later sericite filled veinlet (S) with a halo of chlorite (C). Plate 7.4D is crossed polars. Field of view width = 1 cm. Sample 10140.

A

B

C

D

Plate 7.5. Typical hydrothermal breccias from Jukes Road.

A. Outcrop of matrix supported chlorite-tourmaline breccia with angular clasts of K-feldspar-altered feldspar-phyric dacite from along Jukes Road.

B. Examples of magnetite-tourmaline breccia (top, Sample B1000) and chlorite-tourmaline breccia (bottom, Sample B1011) from the Jukes Road. The clasts are K-feldspar-hematite-altered dacite. Major scale bar divisions are in centimetres.

C. Plane polarized light photomicrograph of a magnetite-tourmaline breccia. The matrix contains tourmaline, magnetite, altered milled rock flour and quartz. Some of the angular K-feldspar-altered clasts (C) have jigsaw fit textures. The large clast on the left, contains an early hydrothermal quartz vein (Q1) that was truncated at the clast margin. The clasts and the breccia are cut by a second quartz vein (Q2). Field of view width = 1 cm. Sample B1009.

D. Typical matrix of a quartz-chlorite-tourmaline breccia vein. Notice the abundant tourmaline (T), which occurs as small euhedral to subhedral crystals throughout the quartz and chlorite matrix. The breccia vein has been cut by a late sericite vein (S). Plane polarized light, field of view width = 0.5 cm. Sample 10390.

A

B

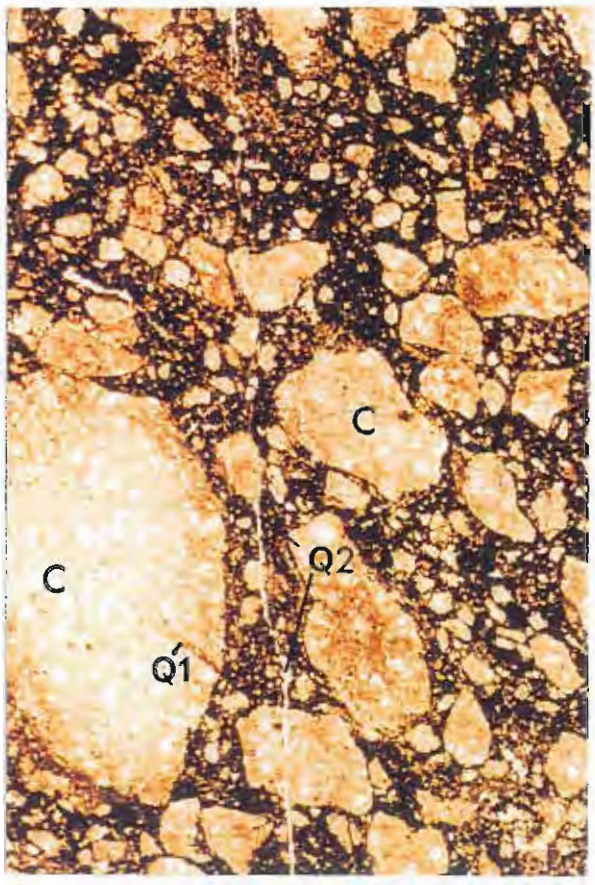

C

D

(Plate 7.5B). Clast sizes vary from <1 mm to >20 cm. Along the Jukes Road, breccias are 20-50 metres wide, however, several similar breccias up to several metres wide and 100m long occur on Intercolonial Spur (Gadaloff, 1996). Breccias were not observed in the contact zone adjacent to the Darwin Granite. Disseminated pyrite ± chalcopyrite occur irregularly throughout the breccias. Chalcopyrite is most abundant in post-breccia faults, which have presumably remobilised copper from the breccia matrix.

Chlorite ± sericite ± quartz ± tourmaline ± sulfide occurs in veins and breccias. Sulfides observed with chlorite include pyrite and chalcopyrite. Chlorite + quartz + tourmaline ± magnetite occur as the matrix in hydrothermal breccias and fractures. The breccia matrix encloses angular to subrounded, moderate to intensely K-feldspar-altered volcanic clasts and rounded to sub-rounded clasts of chlorite-altered quartz-feldspar porphyry and feldspar-phyric dacite. Chlorite ± pyrite ± carbonate occurs in veins with diffuse chlorite replaced edges.

7.3.1 Magnetite-Tourmaline Breccias

Magnetite dominates the matrix of the magnetite-tourmaline breccias, comprises up to 30% of the brecciated rock (Plate 7.5B-C), and occurs as euhedral to subhedral interlocking crystals. Tourmaline is intergrown with magnetite as euhedral to subhedral crystals up to 1 mm long. Tourmaline crystals are randomly oriented and comprise less than 5% of the matrix. The matrix also contains chlorite, milled rock flour altered to K-feldspar and fine quartz. Commonly, the clasts have undergone minimal rotation and have jigsaw fit textures (Plate 7.5B-C). Clasts are typically angular with corroded margins.

7.3.2 Chlorite-Tourmaline Breccias

Chlorite is the most abundant matrix mineral (70-100%), with lesser but variable amounts of tourmaline, magnetite and pyrite (Plate 7.5B and 7.5D). Jigsaw fit textures and a chaotic distribution of clasts were observed. Tourmaline comprises up to 30% of the matrix, and occurs as up to 0.025 mm crystals in aggregrates and masses. Magnetite occurs as evenly distributed, small (0.02-0.06 mm) euhedral crystals disseminated throughout the matrix. Carbonate occurs as rare sparsely developed anhedral crystals that postdate the brecciation event.

Fine quartz veins occur within some of the K-feldspar-altered clasts. These are interpreted to pre-date brecciation because the veins are truncated at clast margins. Other small (up to 1 mm) quartz veins and sericite veinlets have cut the clasts and breccia matrix and have a post breccia timing.

7.3.3 Discussion of Breccias

The breccias in the Jukes-Darwin area are similar to hydrothermal breccias documented from breccia pipes in North and South America (Shelnutt and Noble, 1985; Skherkenbach et al., 1985; Warnaars, 1985; Sillitoe, 1993; Titley, 1993; Streck and Dilles, 1998) but have fewer similarities to breccias in the western South Pacific (Sillitoe, 1993; Lumbis et al., 1994; Corbett and Leach, 1995). Several attempts at genetic classifications of breccias were attempted (Bryner, 1961; Kents, 1964; Bryner, 1968; Mayo, 1976). However, due to the subjective nature of many of the

descriptive parameters and a lack of support for the resulting genetic assumptions, a workable genetic classification of ore-related hydrothermal breccias has not yet been developed. Useful reviews of hydrothermal breccia characteristics are provided by Mayo (1976), Sillitoe (1985), Baker et al. (1986) and Taylor and Pollard (1993). Sillitoe (1985) described the characteristics, alteration and mineralisation of ore-related breccias in volcanoplutonic arcs and, in particular focused on granite and porphyry-related breccias. Sillitoe interpreted magmatic-hydrothermal breccias to form as a result of magmatic-hydrothermal fluids from a high-level magma chamber, regardless of the origin of the fluids (magmatic, meteoric, connate or seawater).

Ore-bearing breccias have undergone hydrothermal alteration and open-space filling that suggest alteration and mineralisation were part of the brecciation process. Sericite, chlorite, silica and K-feldspar alteration are common hydrothermal alteration styles. Tourmaline breccias are generally associated with hydrothermal sericite alteration (Shelnutt and Noble, 1985; Skherkenbach et al., 1985; Warnaars, 1985; Sillitoe, 1993; Titley, 1993; Streck and Dilles, 1998). Hydrothermal alteration of the host rocks can occur pre-, during or post-breccia emplacement and ore-grade copper and gold mineralisation typically occur in restricted zones within the breccias rather than being homogeneously distributed (Sillitoe, 1985).

In the Jukes-Darwin breccias occur as multiple pipes of variable dimension. Based on the magnetite and tourmaline compositions of their matrices, they are interpreted to have a close genetic connection to the Darwin Granite. They were emplaced at hypabyssal depths of 1-4 km, a range of depths that correspond to the inferred depth of emplacement of the Darwin Granite and mineralisation at the Jukes Prospect (Solomon, 1981). This range is consistent with depth of emplacement of other breccia pipes described by So and Shelton (1983) and Burnham (1985). Milled and rotated dacite clasts, abundant altered rock flour, jigsaw fit textures, rounded clasts of quartz-feldspar porphyry dyke rocks and sharp contacts with unfractured wall-rocks are evidence of forceful breccia emplacement. The Jukes-Darwin breccias probably formed as a result of decompression during second boiling as discussed by Burnham (1985). The violent and rapid expulsion of fluid from the magma chamber fractured the host volcanics widening pre-existing veins, created new veins and minor stockworks. Decompression, by propagating fractures to higher levels resulted in fluid mixing and milling of rock fragments (producing rock flour), hydrothermal alteration and mineralisation.

7.4 PARAGENESIS

The alteration mineral assemblages (Section 5.5) occur as alteration phases replacing primary minerals, or as infill minerals filling pore space or fractures. The alteration mineral and vein assemblages do not necessarily reflect simultaneous crystallisation, although if evidence for simultaneous deposition was observed, it was noted in Section 5.5. In the Jukes-Darwin area, the intensity of hydrothermal alteration depended upon the abundance and connectivity of fracture networks. Fracturing was probably a more-or-less continuously ongoing process throughout the hydrothermal alteration and mineralisation process. Some fractures were related, at least in part, to the development of the hydrothermal breccias observed at the Jukes Prospect and on

Intercolonial Spur. Multiple fluid pulses are suggested by multiple overprinting relationships in different parts of the Jukes-Darwin field. Therefore, at different times in the genesis of the field, different minerals could form simultaneously at different locations. For example; while K-Feldspar alteration assemblages were forming near the Darwin granite, sericite-chlorite assemblages could have been forming in more distal portions of the Jukes-Darwin area such as Intercolonial Spur or the Jukes Prospect. The actual hydrothermal alteration and mineralisation paragenetic sequence is, therefore very complex due to multiple fracturing events and multiple fluid pulses and contains numerous examples of apparent "paragenetic reversals". In order to illustrate this complexity, Tables 7.4 and 7.5 and Plates 7.6A and 7.6B were constructed to show the complexity of alteration and mineralisation events around mineralised veins. Appendix O contains a list of the field and petrographic observations and references used to construct the paragenesis discussed in this section. Appendix O contains a list of the field and petrographic observations and references used to construct the paragenesis discussed in this section. The *generalised paragenesis* in the study area can be divided into five major subdivisions including emplacement of the hydrothermal breccias. The five are: 1) early hydrothermal alteration and mineralisation, 2) middle alteration (M1, pre-breccia), 3) hydrothermal breccia formation, 4) middle alteration (M2, post-breccia) and 5) late alteration and mineralisation. The *generalised paragenesis* (Table 7.6) is based on observed overlapping relationships of hydrothermal alteration and vein mineral assemblages summarised from Appendix O.

Table 7.4. Paragenetic sequence illustrating the hydrothermal alteration and mineralisation history of Sample B1003 from the Jukes Prospect.

Event	Time
Alteration Assemblages and Infill Minerals	
Sericite alteration of "fresh" rock	
K-Feldspar alteration assemblage	
Fracturing Events	
Vein Assemblages and Infill Minerals	
Quartz	
Chlorite + tourmaline + magnetite	
Chalcopyrite	

Plate 7.6. Photographs illustrating examples of hydrothermal alteration and mineralisation paragenesis in the Jukes-Darwin area.

A. Semi-massive chalcopyrite (Cpy) in a chlorite-tourmaline breccia vein at the Jukes Prospect. Notice the K-feldspar-altered clasts (K) and the dark black chlorite-tourmaline (C). The rock is composed of pervasively K-feldspar-altered feldspar-phyric dacite. The K-feldspar alteration overprinted an earlier sericite alteration event that may or may not have been hydrothermal in origin. The K-feldspar altered rock was fractured and infilled by a quartz vein that was, intern infilled by chlorite and tourmaline (note fragments of quartz). The rock was then fractured again and filled with chalcopyrite. Sample B1003 from Jukes Road.

B. Early hydrothermal quartz + sericite veins (Q1) cut an early hydrothermal sericite alteration assemblage (A) and are both cut by a later quartz + chlorite veins (Q2). The quartz + sericite veins (Q1) extend out the other side of the larger vein but are not shown. The later quartz + chlorite vein has a halo of chlorite alteration (B), which is separated from the sericite-altered rocks by an alteration front (AF). M2 chlorite-tourmaline breccias (CT) reopened the Q2 veins as well as created new veins that have cut all early hydrothermal assemblages. Sample 10390, plane polarized light, field of view width = 1 cm.

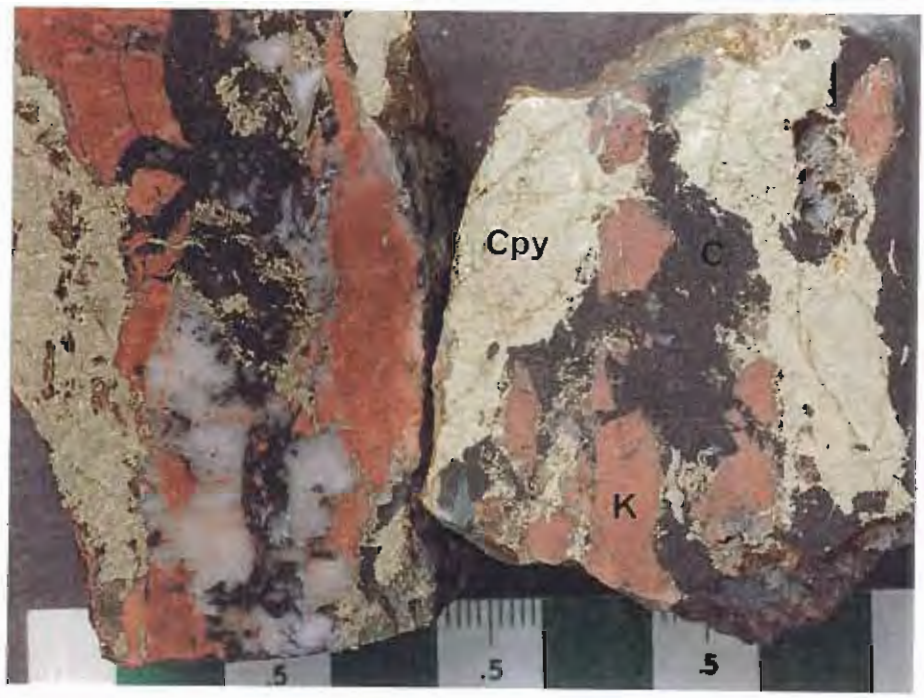

A

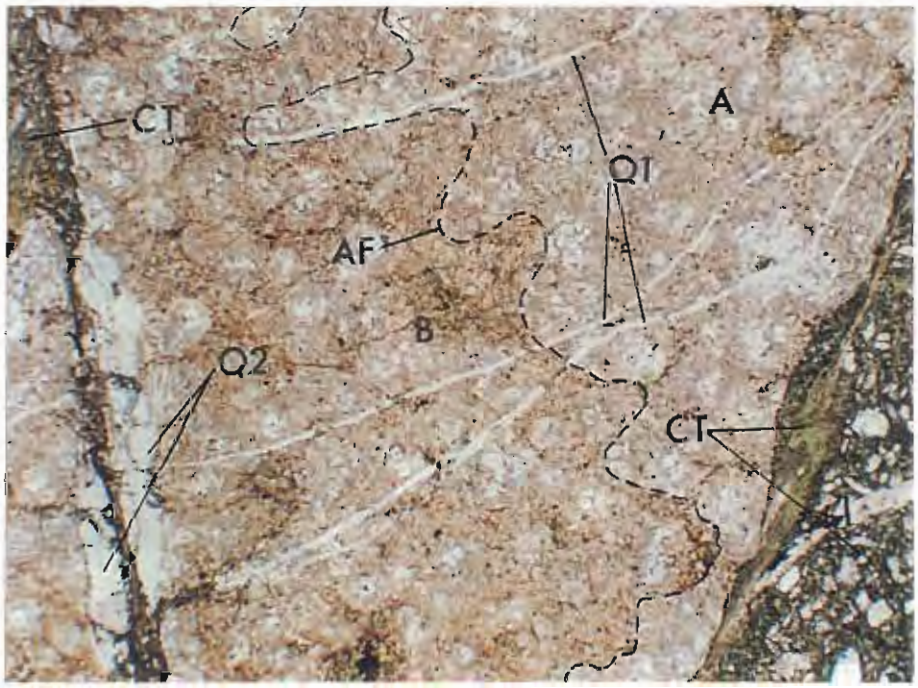

B

Table 7.5. Paragenetic sequence illustrating the hydrothermal alteration and mineralisation history of Sample 10390 from the Jukes Prospect.

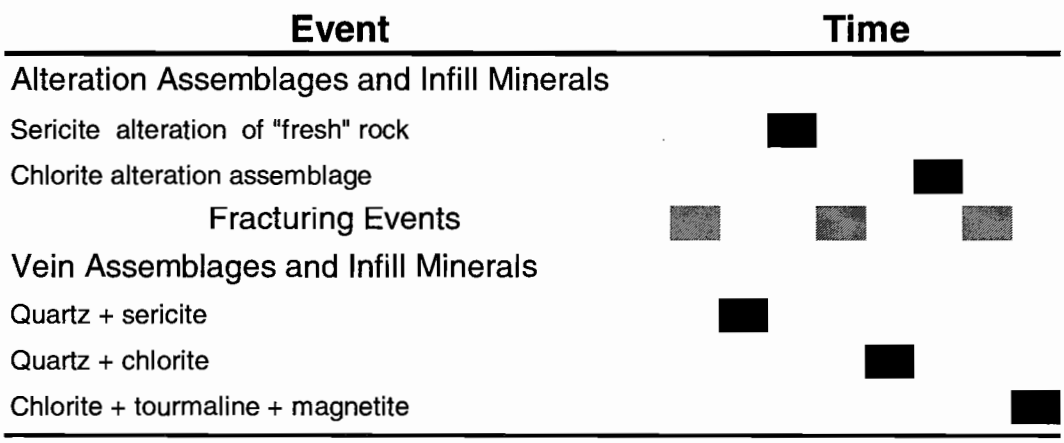

Table 7.6 Generalised paragenetic sequence of hydrothermal alteration assemblages and infill and minerals in the Jukes-Darwin area. This table is a synthesis of many observations (Appendix O) and does not represent the paragenesis for a specific sample. Fracturing was probably occurring as some location in the Jukes-Darwin field at any point in time and is therefore shown as a continuous event.

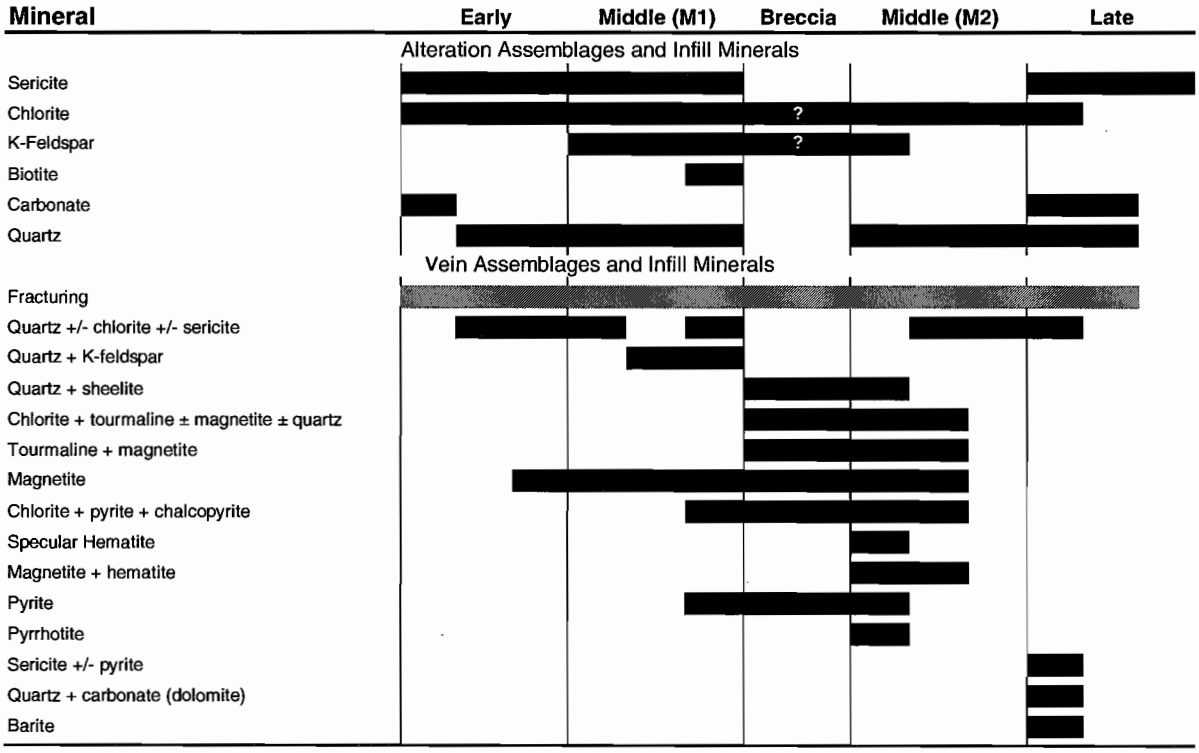

7.4.2 Early Hydrothermal Alteration and Mineralisation

The dominant process during the development of early hydrothermal alteration styles and assemblages (Table 7.4) was transfer of heat via conduction. This process resulted in initialisation of the convective hydrothermal system that circulated hydrothermal fluids around the Darwin Granite. In the distal portions of the hydrothermal system, effects of early hydrothermal alteration are subtle and characterised by increasing intensities of sericite replacement of plagioclase in the groundmass and in phenocrysts (Chapter 5, Plate 5.14E). Early hydrothermal sericite ± chlorite ± carbonate overprinted pre-hydrothermal diagenetic alteration assemblages distal to the intruding granite. Small (1-2 mm) quartz veins with chlorite halos have cross-cut the early hydrothermal sericite alteration assemblages (Plate 7.7A-B). Veins, microveinlets and stockwork domains containing quartz ± chlorite ± sericite formed at the granite contact and volcanic rocks were intensely altered to quartz + chlorite + magnetite ± K-feldspar ± pyrite and chalcopyrite. Hydrofracturing in the cupola region created larger fractures that extended up to a kilometre or more from the granite at the Jukes Prospect and Intercolonial Spur. With increasing proximity to the heat source but outside of the immediate contact zone, diffuse chlorite replaced early hydrothermal sericite along vein margins (Plate 7.7A). In intensely altered zones, feldspar phenocrysts are altered to mosiacs of sericite and chlorite. The green colour of chlorite gives the rock an overall greenish appearance although dominant alteration mineral is sericite. Feldspar phenocrysts are replaced by two distinct domains of mineralogies. One is a fine mesh of interlocking sericite (70%) and chlorite (30%, Plate 7.7C 7.7D). The second is 80% or more chlorite with minor sericite (Plate 7.7E and 7.7F). The chlorite dominant domain is common in the smaller phenocrysts and may represent selective replacement of the K-Feldspar phenocrysts in a different manner than the larger plagioclase phenocrysts. Alteration in the groundmass is dominated by sericite-chlorite.

7.4.3 Middle Alteration (M1, Pre-Breccia)

The beginning of the M1 phase (Table 7.4) is interpreted to have begun with the introduction of secondary K-feldspar and increasingly intense chlorite development. Early hydrothermal quartz-chlorite stockworks were reopened and chlorite and sericite-altered rocks were locally cut by quartz and K-feldspar stockworks. Along Jukes Road, moderate to intense diffuse chlorite replaced groundmass feldspars and feldspar phenocrysts imparting a spotted appearance to the rocks (Plate 7.A). These "spotted" rocks are cut by veins of K-feldspar that have diffuse K-feldspar replacing chlorite along the vein margins (Plate 7.8B). In intensely altered areas, increasing water to rock ratios resulted in the replacement of earlier hydrothermal alteration assemblages by K-feldspar and/or chlorite (Plates 7.8C-F). Micropoikilitic quartz was partially replaced locally. Cryptocrystalline K-feldspar occurs without other hydrothermal alteration minerals other than quartz. K-feldspar was also observed in fractures within previously chlorite-altered dacites suggesting earlier chlorite alteration or multiple K-feldspar alteration events. Secondary biotite formed with pyrite in a microgranite dyke on Mt. Darwin (Plate 5.12B). At Mt. Darwin, although silicification accompanied K-feldspar alteration, quartz veins with silicified

Plate 7.7. Examples of early hydrothermal alteration and mineralisation

A. In sericite-altered feldspar-phyric dacite, a 1-2 mm quartz vein has a halo of chlorite that has replaced groundmass feldspars (B). This zone is separated from the sericite-altered dacite (A) by an alteration front (AF). The quartz vein was later reopened allowing deposition of an M2 magnetite-tourmaline vein (T). Plane polarized light, field of view width = 1 cm. Sample 10390.

B. Similar to 7.7A, diffuse chlorite replaces groundmass and groundmass feldspar laths in FPV. Alteration front (AF) with relatively unaltered groundmass feldspars and feldspar phenocrysts on one side (A) and chlorite altered groundmass feldspars and micropoikilitic feldspars on and the other (B). The alteration front is moving from the lower left to the upper right. Plane Polarized Light, Field of view = 1 cm. Sample 10310.

C and D. This plagioclase phenocryst (F, dashed outline) is partially altered to mosiacs of sericite (S, 70%) and chlorite (Cl, 10-20%). Groundmass feldspars are completely replaced by sericite. Plane Polarized Light and Crossed Polars. Field of view = 3.75 mm. Sample 10350.

E and F. Variable amounts of chlorite (C) is replacing earlier sericite altered plagioclase phenocrysts (dashed outline) in the feldspar-phyric dacite from Jukes Road. Plane Polarized Light and Crossed Polars. Field of view = 3.75 mm. Sample 10350.

A

B

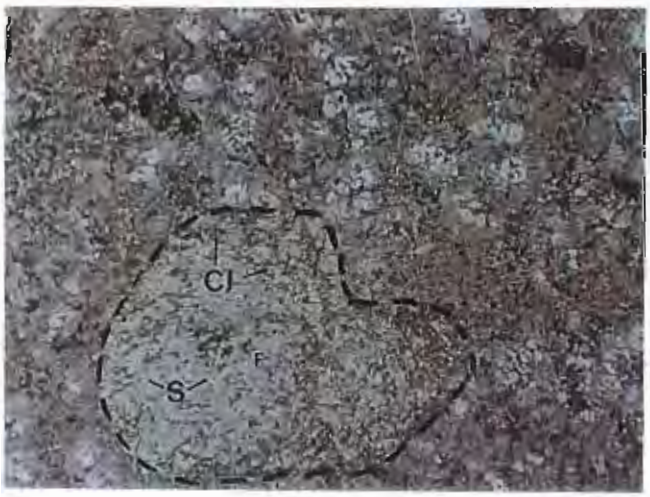

C

D

E

F

Plate 7.8. Examples of middle (M1) hydrothermal alteration and mineralisation.

A. Diffuse chlorite replaced the groundmass and feldspar phenocrysts imparting a light green "spotted" appearance to the rocks. At 10330 meters along Jukes Road. Scale is in cm.

B. M1 veins and associated K-feldspar alteration halos (K) that have replaced earlier sericite + chlorite-altered feldspar-phyric dacite (D) along fracture networks. The fractures were then reopened and filled with chlorite (C). Sample B1005 from Jukes Road.

C and D. Pinkish color in the groundmass micropoikilitic texture is due to K-Feldspar alteration of the feldspars (F), although some are unaltered to weakly sericitised. Sample 10290, plane polarized light and Crossed Polars, field of view width = 1 mm.

E. As part of a continuum of alteration from Plate 7.8C through Plate 7.8F, groundmass feldspar are K-feldspar altered and micropoikilitic feldspars (F) are weakly chlorite altered. Note the small quartz veins. Sample 10290, plane polarized light, field of view width = 1 mm.

F. As part of a continuum of alteration from Plate 7.8C, groundmass feldspar are K-feldspar altered and micropoikilitic feldspars (F) are strongly chlorite altered. Note the quartz veins. Sample 10290, plane polarized light, field of view width = 1 mm.

G and H. Pyrite (P) and chalcopyrite (Cpy) in a quartz-feldspar vein (Qv) in a K-Feldspar altered groundmass in the feldspar-phyric dacite on Jukes Road. The quartz vein cuts a previously chlorite altered feldspar phenocryst. Sample 10220, Plane Polarized Light, and Reflected Light, field of view width = 3.75 mm.

A

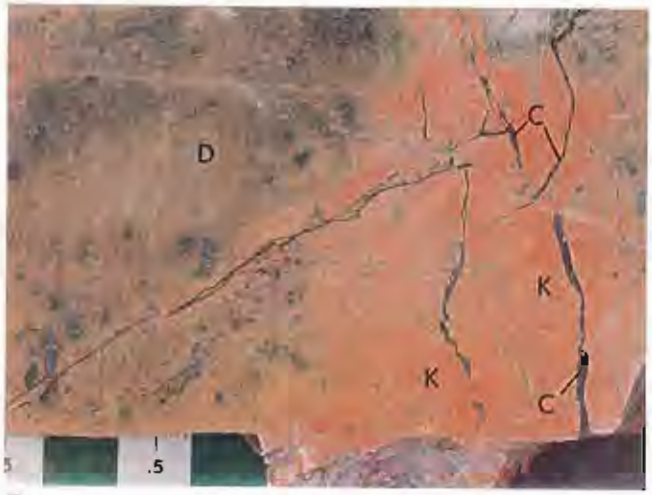

B

C

D

E

F

G

H

margins also cut the K-feldspar assemblage suggesting that silicification continued beyond M1 vein formation.

M1 mineralisation (Table 7.4) consists of chalcopyrite with accessory magnetite and pyrite. It occurs in quartz, quartz-chlorite and quartz-K-feldspar veins and disseminated domains in chlorite and K-feldspar-altered rocks (Plate 7.8G-H).

7.4.4 Hydrothermal Breccia Formation

The timing of hydrothermal breccia formation is constrained by cross-cutting relationships. Both hydrothermal breccias (Section 7.3) contain abundant clasts of K-feldspar-altered and chlorite-altered rocks and quartz vein fragments interpreted to be part of M1 (Plates 7.5B-C). The breccia clasts and matrix are cut by, and overprinted by, M2 fractures and K-feldspar alteration (Plate 7.9A).

At the Jukes Prospect and Intercolonial Spur, significant mineralisation is hosted in the matrix of hydrothermal breccias (Section 7.3). Chlorite, tourmaline and magnetite are the primary matrix filling minerals with accessory pyrite, chalcopyrite, sheelite and gold (Doyle, 1990). Breccia formation resulted in networks of magnetite-tourmaline, chlorite-magnetite-tourmaline and tourmaline veins and introduction of sulfides.

7.4.5 Middle Alteration (M2, Post-Breccia)

M2 alteration and mineralisation can be distinguished from M1 alteration by cross-cutting relationships with K-feldspar and intensely chlorite-altered rocks. Throughout the study area, M2 is characterised by vein style alteration assemblages and localised diffuse replacement zones around veins (Plate 7.10A). Intense secondary chlorite assemblages overprinted M1 K-Feldspar assemblages. Hydrothermal breccias with chlorite-tourmaline matrices were overprinted by post breccia K-feldspar alteration around veinlets (Plate 7.9A). In M1 K-feldspar-altered zones distal to the hydrothermal breccias, M1 quartz and quartz-K-feldspar stockworks were reopened and cut by M2 chlorite-sulfide veins with sericite halos (Plate 7.10B).

M2 quartz-chlorite-tourmaline, chlorite-tourmaline-magnetite and tourmaline-magnetite veins (Section 7.2) cross-cut and reopened earlier quartz and quartz-K-feldspar stockworks (Plates 7.3 and 7.7A). At the Darwin Granite, quartz-specular hematite veins were cut by magnetite veins and tourmaline veins. Some tourmaline veins have brecciated outer margins and inner zones of magnetite and hematite suggesting complex timing relationships between vein assemblages. M2 tourmaline veins observed within the pink granite were common near contacts with the white granite porphyry suggesting a relationship to its intrusion. Tourmaline veins also occur within the contact zone with the host volcanics and up to a kilometre from the granite.

At Mt. Darwin, disseminated M2 pyrite, chalcopyrite and galena (Table 7.4) occur within the contact zone (Plate 7.10C) and within magnetite-hematite stockworks at the Prince Darwin Prospect. Based on cross-cutting relationships to M1 quartz veins, pyrite veins within the pink granite have been interpreted to be M2. In the later stages of the M2 event (Table 7.4), tourmaline and magnetite-tourmaline veins were cross-cut by quartz-chlorite veins containing pyrite,

Plate 7.9. Constraint on the timing of hydrothermal breccias.

A. An M2 vein has cut a chlorite-tourmaline breccia. An alteration halo of M2 K-feldspar (K) replaced previously, M1, K-feldspar and chlorite altered dacite clasts (C) and the breccia matrix within 1-2 cm of the vein margins (dashed lines). This sample constrains breccia formation to a time between M1 and M2. Sample B1006.

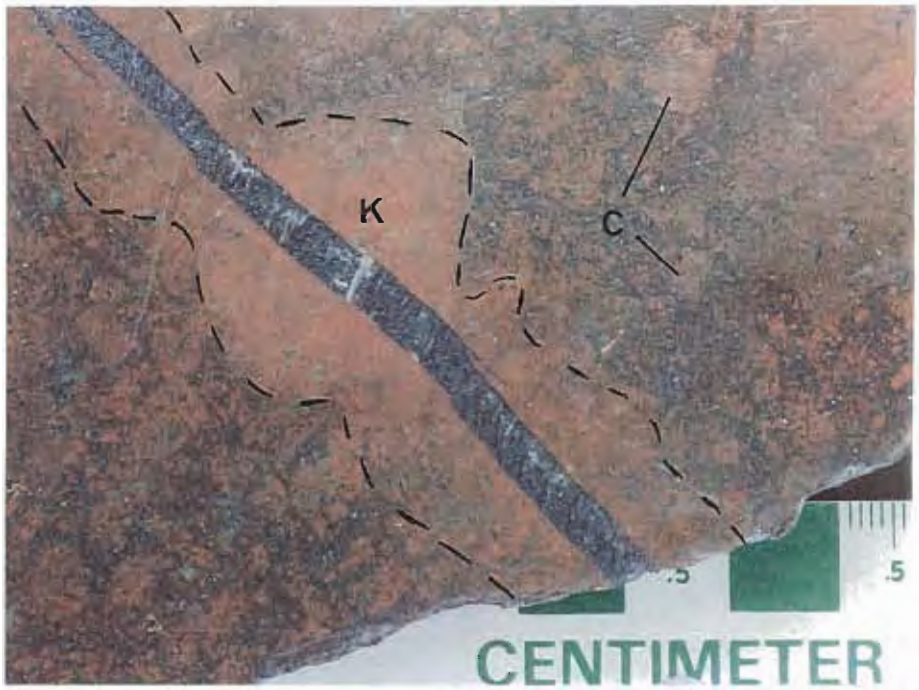
K
C
.5
.5
CENTIMETER

Plate 7.10. Examples of M2 alteration and mineralisation

A. M2 quartz-chlorite fractures with thin chlorite halos cut M1 K-feldspar altered feldspar-phyric dacite. Note the sericite + chlorite altered feldspar phenocrysts and spotted appearance to groundmass feldspars due to total replacement by M1 chlorite. Rock 10250 from Jukes Road. Scale is in cm.

B. Two M2 veins cut M1 K-feldspar + chlorite altered feldspar-phyric dacite (D) from Jukes Road. The chlorite vein (CV) with the sericite halo (S, dashed lines) was probably an M2 quartz + sericite + sulfide vein (QV) such as seen in the lower right that was later reopened and filled with chlorite. Sample 10310, plane polarized light, field of view width = 1 cm.

C. Chalcopyrite veinlets (Cpy) in chlorite-altered dacite from the contact zone of the Darwin Granite and the CVC. Sample B1004.

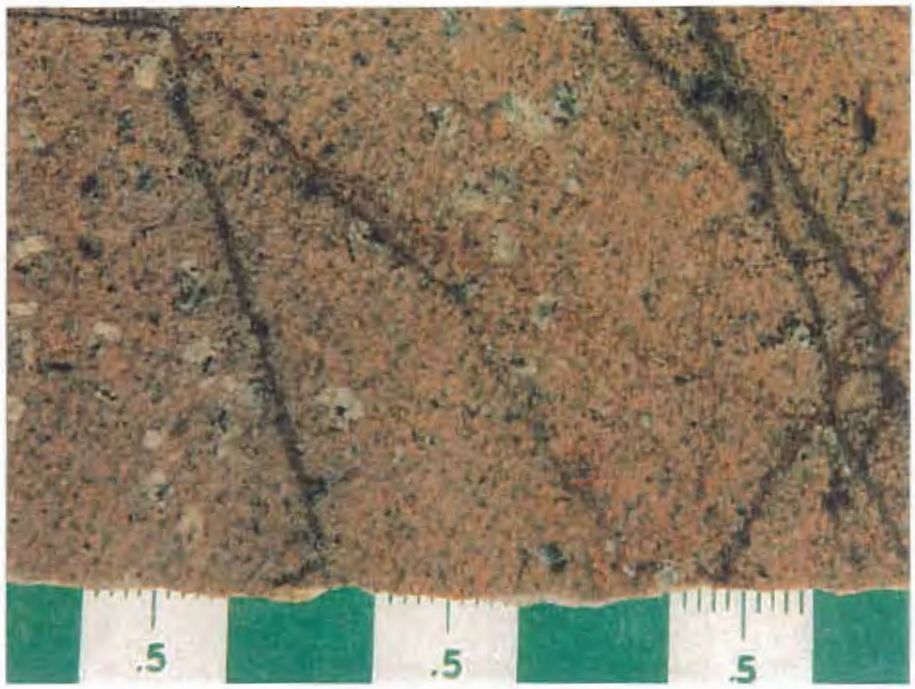

A

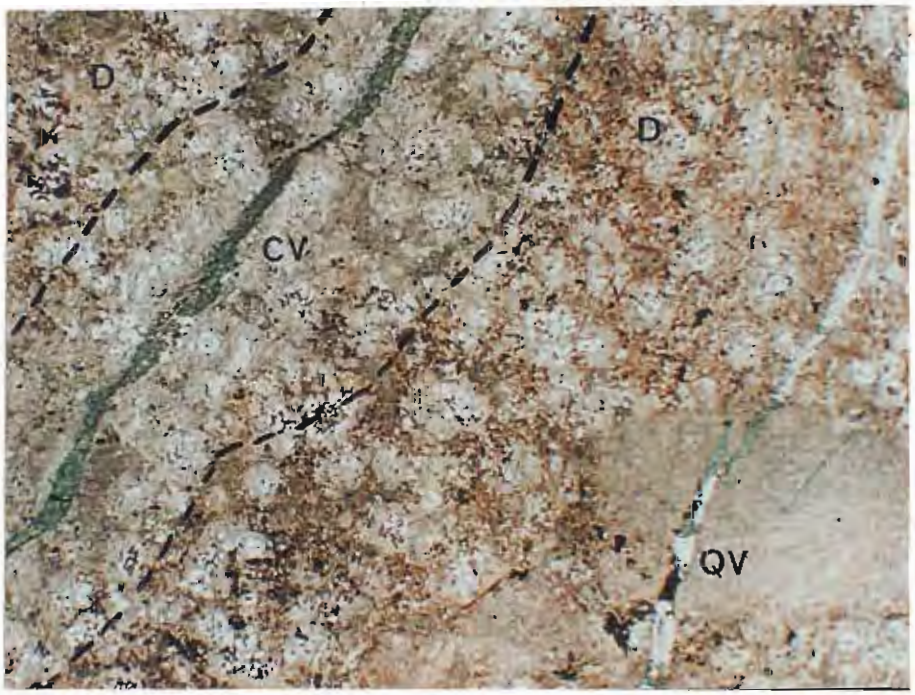

B

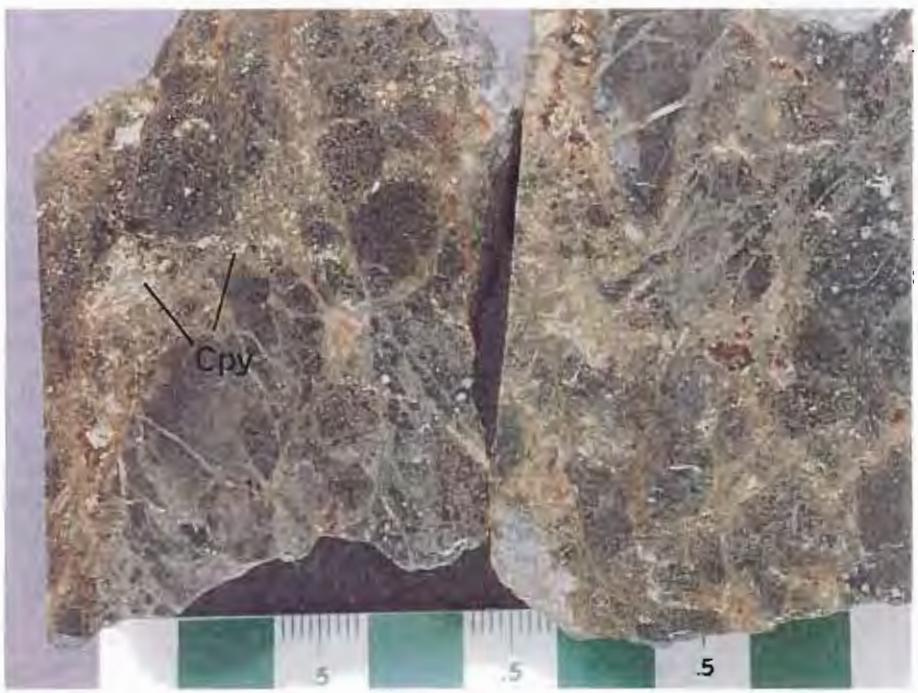

C

chalcopyrite and galena. At the Jukes Prospect and Intercolonial Spur, chalcopyrite, sheelite, galena and pyrite in magnetite-hematite veins and in intense M2 chlorite-altered zones are interpreted to be associated with the hydrothermal breccias. Magnetite contains pyrite and chalcopyrite inclusions, sheelite is intergrown with magnetite and pyrite and contains inclusions of magnetite, and galena contains inclusions of chalcopyrite (Doyle, 1990).

7.4.6 Late Alteration and Mineralisation

Collapse of the hydrothermal system is supported by sulfur isotope evidence discussed in Chapter 9. Late hydrothermal alteration phases (sericite assemblages) and barite veins are interpreted to have formed during collapse of the system, because they cross-cut or overprint early hydrothermal and middle (M1 and M2) assemblages. Quartz-sericite veins with sericite halos (Plate 7.11A) have replaced K-feldspar and chlorite-altered volcanics and magnetite-chlorite-tourmaline veins near the centre of the Jukes hydrothermal system and at Mt. Darwin. Sericite veins containing minor pyrite cut intensely chlorite-altered volcanics. In the Darwin Granite, fracture and joint controlled sericite veins altered the pink granite (Plate 5.7A). Diffuse sericite was observed to have replaced K-feldspar in K-feldspar-altered domains near the summit of Mt. Darwin.

Mineralisation associated with the collapse of the hydrothermal system is confined to barite veins that occur within the CVC at the Jukes Prospect and Intercolonial Spur and within the Darwin Granite. Late-stage sulfide mineralisation occurs as accumulations of chalcopyrite and pyrite in hydrothermal breccias, fractures, faults and shears at East Darwin, Findons (Gadaloff, 1996) and the Jukes Prospect (Doyle, 1990 and this study). Chalcopyrite typically occurs with chlorite in these late occurrences. Minor amounts of remobilised chalcopyrite were reported within the basal Tyndall Group east of the Darwin Plateau (Jones, 1993) but were not observed in this study. Sulfides in post mineral structures were interpreted to have been remobilised and concentrated during the Late Cambrian Delamerian Orogeny that resulted in the uplift and erosion of the Darwin Granite prior to Tyndall group deposition. The occurrence of remobilised sulfides in the Tyndall Group rocks suggests that further remobilisation occurred in subsequent tectonic events (Gadaloff, 1996).

7.5 DISCUSSION

Fluids responsible for the hydrothermal alteration and mineralisation styles observed in the Jukes-Darwin area gained access to the host rocks via breccias, fractures and associated stockworks that formed during several episodes of hydrothermal activity (Figure 7.2). Lateral hydrothermal alteration assemblages around vein systems and multiple fluid pulses resulted in mixed alteration domains. Mineralisation styles include magnetite veins and networks of smaller magnetite, magnetite + tourmaline, tourmaline and quartz veins. Although veins contain pyrite, chalcopyrite gold and secondary (supergene) copper minerals, stockwork zones of copper mineralisation were not observed. In addition to vein assemblages, Cu-Au ores occur as disseminated pyrite and chalcopyrite in zones of chlorite and/or K-feldspar alteration.

Plate 7.11. Examples of late alteration and mineralisation

A. Late sericite (S), related to the collapse of the hydrothermal system, has replaced the M1 K-feldspar-altered matrix (K) in one of the quartz-feldspar ± biotite porphyry dykes along Jukes Road. Crossed-polarized light, field of view width = 3.75 mm. Sample 10580.

B. Chalcopyrite in a late chlorite vein. The late chlorite veins cut M1 and M2 K-feldspar altered dacite. From 10300 along Jukes Road.

A

B

Second boiling probably fractured the host rocks at depths of 4-5 km, consistent with estimated depths of emplacement of the Darwin Granite. The resultant fractures provided conduits for the alteration fluids and hydrothermal breccias. The hydrothermal breccias underwent multiple phases of hydrothermal alteration and open-space filling suggesting alteration and mineralisation were part of the brecciation process.

The granite-related mineralisation styles differ significantly from VHMS styles in hydrothermal alteration assemblages and ore minerals. Pb and Zn sulfides are conspicuously insignificant.

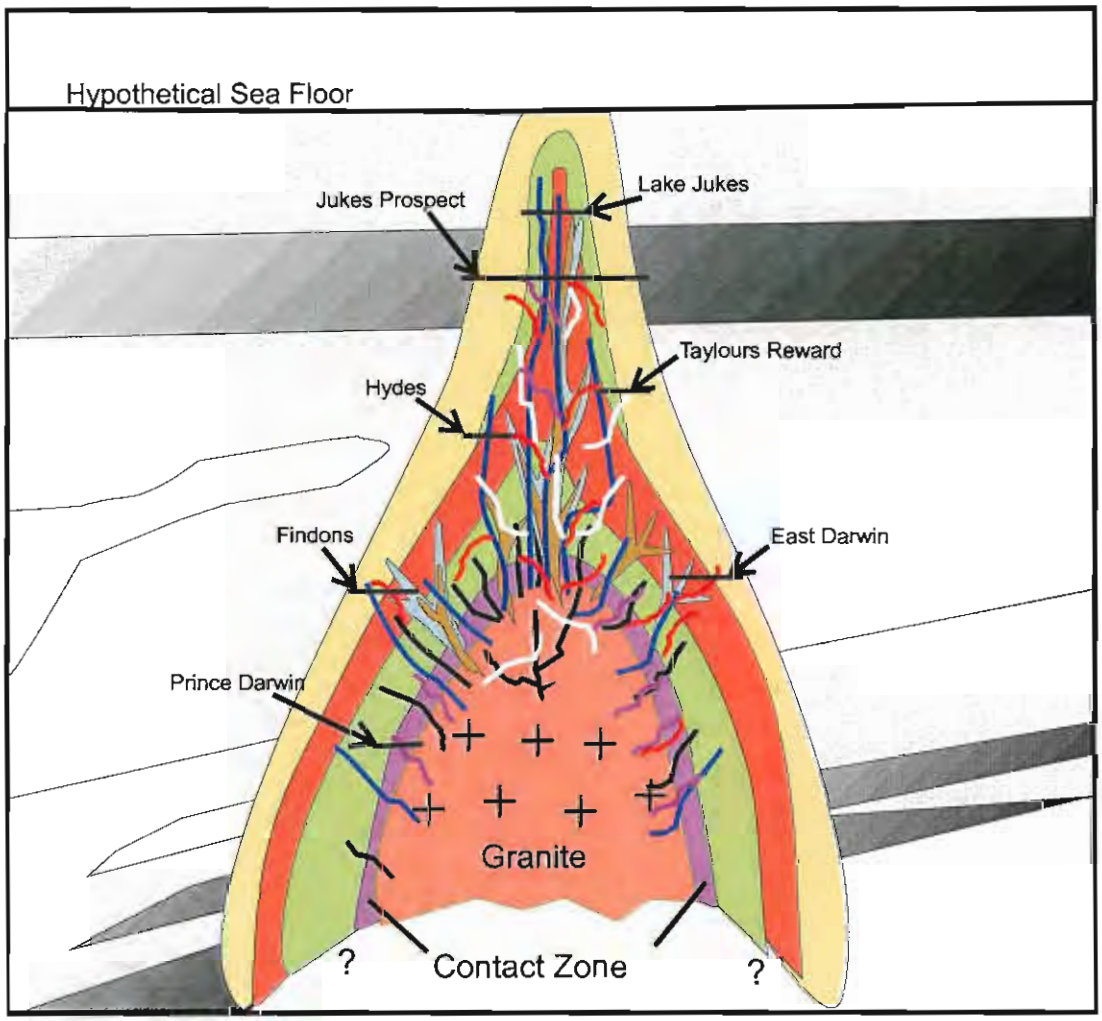

Figure 7.2 Cross-section of Cambrian granite-related hydrothermal alteration and mineralisation in the Jukes-Darwin area. Magnetite ± tourmaline veins, tourmaline veins, hydrothermal breccias and related Cu-Au mineralisation exsolved from a B-rich granite that intruded to a high level in the crust. Hydrothermal breccias, fractures and associated stockworks formed as a result of second boiling. Legend on Figure 7.1.

CHAPTER 8

8.0 OXYGEN-DEUTERIUM ISOTOPE GEOCHEMISTRY

8.1 INTRODUCTION

Oxygen and deuterium (D/H) isotopes can be used to yield information critical to the development of ore deposit models (Sheppard et al., 1971; Ohmoto and Rye, 1974; Taylor, 1974; Taylor, 1979; Sheppard, 1981; Green et al., 1983). Apart from a few oxygen isotope analyses on magnetite and chlorite from the Jukes Prospect (Doyle, 1990) and Mt. Darwin (Jones, 1993; Large, 1995, pers. comm.) no other oxygen or hydrogen isotope data existed for the southern MRV, south of Mt. Lyell, subsequent to this study. Therefore, the aims of this study were: 1) to provide evidence on the temperature, source and water to rock ratios (W/R) of ore forming hydrothermal fluids derived from of the Darwin Granite, and 2) to quantify whole rock magmatic $\delta^{18}O$ values of the freshest Darwin Granite samples observed.

Representative samples of hydrothermal chlorite, magnetite, quartz and K-feldspar were selected from a cross-section through the alteration zones along Jukes Road. Chlorite samples were selected from several different chlorite-bearing hydrothermal alteration styles at variable distances from the center of the ore zone. In addition, K-feldspar and quartz were taken from an intensely K-feldspar-altered zone. One magnetite sample was selected from a large magnetite-pyrite vein previously sampled by Doyle (1990). The sample was collected in order to confirm questionable $\delta^{18}O$ results from his study. The Darwin Granite was also sampled in order to establish magmatic $\delta^{18}O$ values of unaltered granite, from which equilibrium fluid values could be calculated.

The $\delta^{18}O$ value of ore-forming fluids can be measured or estimated by direct or indirect methods. Direct methodology involves the determination of the $\delta^{18}O$ value of fluids extracted from fluid inclusions. Fluid inclusions were not examined as part of this study, therefore the $\delta^{18}O$ values of mineral separates were used with the estimated temperature of mineralisation and an equation for the isotopic fractionation factor between the mineral and water, to calculate $\delta^{18}O$ values of ore-forming fluids. W/R values for altered rocks along Jukes Road were determined using the equations of Taylor (1977) and Taylor (1974).

8.2 MINERAL SEPARATION AND ANALYTICAL METHODS

D/H and oxygen isotope samples were prepared by the author in the Geology Department, University of Tasmania. Samples were crushed by hand in an agate mortar and pestle. Oxidised portions of the rock, sulfides and carbonates were then hand-picked and disposed. The remaining sample was then crushed in a tungsten-carbide disc mill to 50 microns (300 mesh sieve). For oxygen and deuterium analysis on chlorite and magnetite, mineral grains were separated according to specific gravity using sodium polytungstate. After separation, samples were washed, dried and examined under a binocular microscope to verify purity. If the samples were not visually pure, the specific gravity separation was repeated. Final separation of magnetite was

accomplished magnetically. Grains of quartz and K-feldspar were hand picked under a binocular microscope. The clean samples were then analysed by XRD and results are reported in Appendix G. The powder fraction was used for isotopic analyses.

Oxygen and hydrogen isotope analyses were performed at the Centre for Mineral Resources, University of Arizona by Dr. Mark Barton. Analyses were performed using a conventional fluorination line under vacuum and a laser line (hydrogen line). Accuracy is ± 2 per mil (‰) for D/H and ± 0.3‰ for $\delta^{18}O$ (M. Barton, 1997, pers. comm.). Standards (NCSU Qz and UWG Gt) were analysed along with the samples and results were corrected to published values for these standards. NCSU Qz was used to correct quartz numbers (typically on the order of 1‰) while UGG Gt was used to correct other phases requiring a correction (typically on the order of 0.5‰). The results are expressed in the standard δ notation relative to Vienna Standard Mean Ocean Water (V-SMOW).

8.3 RESULTS

Hydrothermal alteration assemblages within the Darwin Granite are mostly fracture controlled, and previous workers have shown that infiltration by seawater-dominated fluids occurred (Solomon et al., 1988; Jones, 1993). Nonetheless, zones of unaltered or weakly altered granite were observed during the current study. Fresh granite samples contain scattered unaltered primary muscovite (to 1 mm), biotite and feldspar crystals. Sericite alteration of the feldspars was limited to weak replacement of <10% of the feldspar crystal rims. In Table 8.1, $\delta^{18}O$ values are shown for the freshest equigranular coarse-grained pink and white granite samples that were observed. In the pink granite, $\delta^{18}O$ values range from 9.3‰ to 12.5‰ ± 0.3‰ and in the white granite from 9.9‰ to 10.6‰ ± 0.3‰.

To determine the oxygen isotope values of the hydrothermal fluids at the Jukes Prospect, samples of magnetite, quartz and K-feldspar were analysed for oxygen and/or deuterium. Sample 10250 consists of euhedral magnetite taken from a magnetite-quartz-pyrite vein that cuts K-feldspar-altered dacite. The K-feldspar sample (10290, Plate 8.1) is stage M1 secondary K-feldspar from an intensely K-feldspar-altered dacite and presumably formed in equilibrium with the M1 fluid. The lack of an alteration halo suggests that the fluid and rock were un-reactive or in equilibrium. Rapid fluid flow may have limited the time necessary for a reaction to occur. The small stockwork quartz veins were only observed in early K-feldspar altered rocks (sometimes later replaced by sericite) and sometimes contained K-feldspar crystals. Sample (B10510) is a composite sample of hand picked vein quartz from M1 stage quartz veinlets (Plate 8.1A) in a sample similar to 10290. The quartz veinlets lack alteration halos, suggesting that fluids in the veinlets were either in equilibrium with, or were flowing rapidly through the impermeable K-feldspar-altered host rock. In this case, the quartz is assumed to have crystallised in equilibrium with the M1 fluids and the quartz veinlets are interpreted to be related to the K-feldspar alteration. The quartz veinlets typically contain magnetite (Plate 8.1A). Although the quartz, K-feldspar and magnetite samples analysed are from different samples, they occur in rocks with the same hydrothermal alteration styles, assemblages and vein paragenesis and are, therefore, assumed to have formed from the same hydrothermal fluid.

Several chlorite types have been analysed, including chlorite-altered feldspar phenocrysts and chlorite veins. Oxygen and deuterium results are tabulated in Table 8.2.

Table 8.1. Whole rock $\delta^{18}O$ values for the Darwin Granite. V-SMOW = 1.048., Analysed by Oxygen Isotope Lab, Univ. of Arizona, by Dr. Mark Barton.

Sample Number	Type	$\delta^{18}O$ (V-SMOW)
B2040	Pink Granite	10.2 +/- 0.3‰
B2043	White Granite	9.9 +/- 0.3‰
B2053	Pink Granite	9.3 +/- 0.3‰
B2054	Pink Granite	12.5 +/- 0.3‰
B2061	White Granite	10.6 +/- 0.3‰

Table 8.2. $\delta^{18}O$ and δD values for mineral separates from the Jukes Road. V-SMOW = 1.048., Analysed by Oxygen Isotope Lab, Univ. of Arizona, by Dr. Mark Barton. Precision is ± 0.2 per mil for $\delta^{18}O$ (accuracy is ± 0.3) and ± 2 per mil for δD

Sample Number	Type	$\delta^{18}O$ (V-SMOW)	δD (V-SMOW)	Description
10250	Magnetite	-0.5 +/- 0.3‰		Magnetite from quartz-magnetite-pyrite veins that cut massive K-feldspar altered feldspar-phyric dacite
10270	Chlorite	5.2 +/- 0.3‰	-104.8 +/- 2‰	Chlorite from chlorite veins in massive K-feldspar altered feldspar-phyric dacite
10350	Chlorite	4.6 +/- 0.3‰	-95.0 +/- 2‰	Chlorite from intense chlorite altered feldspar-phyric dacite
B1006	Chlorite	2.6 +/- 0.3‰	-84.2 +/- 2‰	Chlorite from chlorite vein that cut K-feldspar + chorite altered breccia
B1010	Chlorite	3.8 +/- 0.3‰	-79.0 +/- 2‰	Chlorite from K-feldspar altered feldspar-phyric dacite with chlorite replaced feldspar phenocrysts
10290	K-feldspar	8.2 +/- 0.3‰		K-feldspar from K-feldspar altered feldspar-phyric dacite cut by quartz + magnetite + tourmaline + chlorite + pyrite veins
10510	Quartz	10.0 +/- 0.3‰		Quartz from K-feldspar altered feldspar-phyric dacite cut by numerous quartz and quartz-magnetite veins

8.4 DISCUSSION

The temperature dependence of oxygen isotope fractionation between two minerals, or a mineral and water, can be expressed as Equation 8.1.

Equation 8.1 (Javoy et al., 1970).

$$1000 \ln \alpha_{x\text{-}y} = A*10^6/T^2 + B$$

Where: $\alpha_{X\text{-}Y}$ is the ratio $(^{18}O/^{16}O)_X / (^{18}O/^{16}O)_Y$, A and B are constants determined experimentally and vary with species. Temperature T is in ^{O}K.

Plate 8.1. Typical examples of M1 quartz and quartz-magnetite veinlets in K-feldspar-altered feldspar-phyric dacite from Jukes Road.

A. M1 stockwork style quartz veinlets (Q) within intensely K-feldspar-altered micropoikilitic feldspar-phyric dacite (K) from the Jukes Road. Polarized light, field of view = 8 mm. Sample 10370.

B. M1, stockwork style quartz veinlets similar to Plate 8.1A. The larger quartz vein (Q) contains magnetite (M) that is interpreted to be in equilibrium with the quartz. The rock also contains finely disseminated chlorite (C). Polarized light, field of view = 8 mm. Sample 10220.

A

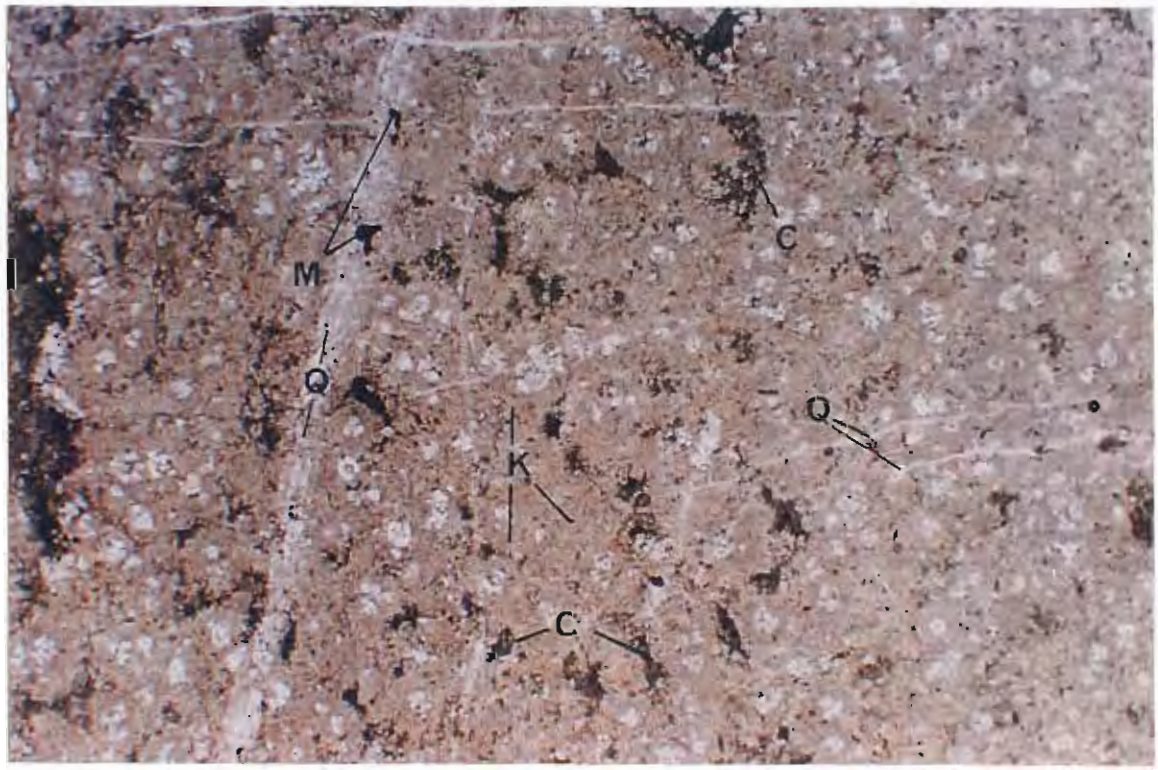

B

Because fractionation factors are usually close to unity (Campbell and Larson, 1998):

$$1000 \ln \alpha_{X\text{-}Y} \cong \Delta_{X\text{-}Y} = \delta^{18}O_X - \delta^{18}O_Y$$

Where $\Delta_{x\text{-}y}$ is >0 other expressions are used.

Using Equation 8.1, if the $\delta^{18}O$ values of mineral (X) and fluid (Y) are in equilibrium, the temperature of formation can be calculated. Conversely, if the temperature was independently determined by other means (eg., fluid inclusions), the $\Delta^{18}O$ value of the $\Delta_{mineral\text{-}water}$ can be calculated.

$\Delta_{mineral\text{-}water}$ values are determined experimentally. Table 8.3 lists the experimentally derived equations used in temperature and $\delta^{18}O$ calculations in this chapter, based upon recent literature revisions.

Table 8.3. Experimentally derived oxygen isotope mineral-water fractionation equations used in calculating temperature and $\delta^{18}O$ values.

	Fractionation Equation	Error	Reference
$\Delta_{Calcite\text{-}water}$	$2.78(10^6/T^2) - 2.89$	+/- 0.12‰	O'Neil et al. (1969)
$\Delta_{Albite\text{-}calcite}$	$-0.57(10^6/T^2)$	+/- 0.1‰	Clayton et al. (1989)
$\Delta_{Anorthite\text{-}calcite}$	$-1.59(10^6/T^2)$	+/- 0.1‰	Clayton et al. (1989)
$\Delta_{Quartz\text{-}water}$	$3.65(10^6/T^2) - 2.9$	+/- 0.14‰	Sharp and Kirschner (1994)
$\Delta_{K\text{-}feldspar\text{-}water}$	$2.39(10^6/T^2) - 2.51$	+/- 0.1‰	Matsuhisa et al. (1979)
$\Delta_{Albite\text{-}water}$	$2.21(10^6/T^2) - 2.9$	+/- 0.22‰	O'Neil et al. (1969) + Clayton et al. (1989)
$\Delta_{Anorthite\text{-}water}$	$1.19(10^6/T^2) - 2.9$	+/- 0.22‰	O'Neil et al. (1969) + Clayton et al. (1989)
$\Delta_{Chlorite\text{-}water}$	$2.693(10^9/T^3) - 6.342(10^6/T^2) + 2.969(10^3/T)$	+/- 0.5‰	Cole and Ripley (1999)
$\Delta_{Quartz\text{-}magnetite}$	$1.60(10^6/T^2) + 6.59(10^3/T) - 2.81$	+/- 0.1‰	Zheng (1995)
$\Delta_{Calcite\text{-}magnetite}$	$1.13(10^6/T^2) + 6.7(10^3/T) - 2.83$	+/- 0.1‰	Zheng (1995)
$\Delta_{Magnetite\text{-}water}$	$2.88(10^6/T^2) - 11.36(10^3/T) + 2.89$	+/- 0.1‰	Zheng (1995)

In the Jukes-Darwin area, mixing of Cambrian meteoric and magmatic water seems unlikely, given the well-documented submarine setting of the MRV (Corbett et al., 1974; Solomon, 1976; Corbett, 1981; Corbett, 1992; Large, 1992). The two most likely sources of primary fluids were magmatic water and circulating seawater or modified seawater, although Devonian metamorphic water is also possible. To test this hypothesis and to assess the possibility of metamorphic water involvement, oxygen and hydrogen isotopes were used. The $\delta^{18}O$ value of seawater in the hydrothermal system was unlikely to have remained at 0‰ as it is expected to have increased during diagenetic alteration and subsequent reaction with rocks during descent into the volcanic pile (Sheppard et al., 1971; Taylor, 1979; Ohmoto, 1986). A metamorphic water component was possible due to the greenschist metamorphic grade. However, as shown by the non-linear relationship between Mg# in chlorite and Mg# in whole rocks (Section 6.3.1), metamorphic equilibration of Fe and Mg did not occur. Meteoric waters may have been introduced during subsequent uplift and erosion.

Magmatic fluids typically have restricted δD and $\delta^{18}O$ values of -40‰ to -80‰ and +5‰ to +9.0‰ respectively (Sheppard et al., 1971; Taylor, 1979; Taylor, 1986), but high $\delta^{18}O$ granites can have $\delta^{18}O$ values up to +13‰ (O'Neil et al., 1977; Sheppard, 1977; Sheppard, 1986; Harris et al., 1997). Modern day seawater (VSMOW) by definition has δD and $\delta^{18}O$ values of 0‰ (Taylor, 1974), and ancient seawater is expected to have had similar values (Muehlenbachs, 1986; Gregory, 1991).

8.4.2 Oxygen Isotopes in the Darwin Granite

In Table 8.1, $\delta^{18}O$ values are shown for the freshest equigranular coarse-grained pink and white granite samples collected from the Darwin Granite. Using the normative mineralogy for the Darwin Granite (Appendix D), and mineral-water fractionation equations from Table 8.3, an equation for $\Delta_{\text{whole rock - water}}$ was calculated for each of the analysed granite samples.

The $\Delta_{\text{whole rock - water}}$ equations were calculated as follows. From Appendix D, the normative percentages of quartz, orthoclase, albite, anorthite and magnetite were selected and the percentages of each of these minerals from Appendix D were recalculated to total 100%, eliminating phases that were not analysed by the whole rock oxygen method such as carbonate. The mineral-water fractionation equation for each mineral-water species was then multiplied by the percentage of each mineral and new $A_{\text{quartz-water}}$ and $B_{\text{quartz-water}}$, $A_{\text{orthoclase-water}}$ and $B_{\text{orthoclase-water}}$, $A_{\text{albite-water}}$ and $B_{\text{albite-water}}$ etc. were calculated. The new $A_{\text{whole rock-water}}$ and $B_{\text{whole rock-water}}$ numbers are equal to the sum of all of the new individual calculated mineral A's and B's as shown, effectively producing a fractionation expression for that particular rock:

$$A_{\text{whole rock-water}} = \Sigma\ (A_{\text{quartz-water}} + A_{\text{orthoclase-water}} + A_{\text{albite-water}} + A_{\text{anorthite-water}} + A_{\text{magnetite-water}})$$

$$B_{\text{whole rock-water}} = \Sigma\ (B_{\text{quartz-water}} + B_{\text{orthoclase-water}} + B_{\text{albite-water}} + B_{\text{anorthite-water}} + B_{\text{magnetite-water}})$$

Analytical error and error in the experimentally derived fractionation equations are cumulative and total 1.1‰. The following example is provided to illustrate the method of calculating the $\Delta_{\text{whole rock - water}}$ equations.

Table 8.4. Example of calculating $\Delta_{\text{whole rock - water}}$ equations.

Sample Number	Qz	Or	Ab	An	Mt	Sum
Normative values of sample B204C (Appendix D) recalculated to equal 100%	36.90	38.40	16.14	8.26	0.31	100
Recalculating as proportions gives	0.369	0.38	0.16	0.08	0.00	1

Multiplying the A and B in the appropriate $\Delta_{\text{mineral-water}}$ equations in Table 8.3 by the appropriate percentage and summing them gives new $A_{\text{whole rock-water}}$ and $B_{\text{whole rock-water}}$.

	$A_{\text{Quartz-Water}}$	$A_{\text{Orthoclase-Water}}$	$A_{\text{Albite-Water}}$	$A_{\text{Anorthite-Water}}$	$A_{\text{Magnetite-Water}}$	New $A_{\text{whole rock-water}}$
$A_{\text{Mineral-Water}}$	1.35	0.92	0.36	0.10	0.01	2.73
	$B_{\text{Quartz-Water}}$	$B_{\text{Orthoclase-Water}}$	$B_{\text{Albite-Water}}$	$B_{\text{Anorthite-Water}}$	$B_{\text{Magnetite-Water}}$	New $B_{\text{whole rock-water}}$
$B_{\text{Mineral-Water}}$	-1.07	-0.96	-0.47	-0.24	-0.05	-2.79
New whole rock-water equation	$\Delta_{\text{whole rock - water}} = 2.73(10^6/T^2) - 1.72$					

Granite crystallisation temperatures are dependent upon lithostatic pressure, composition and water contents but felsic granites typically crystallise at in the 600°C to ~800°C range (Tuttle and Bowen, 1958; Taylor, 1977; Wyllie, 1977; Huang and Wyllie, 1986; Wall et al., 1987). Therefore, a range of granitic crystallisation temperatures from 550°C to 800°C was assumed for the Darwin Granite and $\delta^{18}O$ values for magmatic water in equilibrium at various temperatures were calculated (Table 8.5). The highest $\delta^{18}O$ fluid value corresponds to highest measured $\delta^{18}O$ rock value (12.5 ‰) from the pink granite (sample No. B2054, Table 8.1). This high rock $\delta^{18}O$ value is interpreted to be the result of reaction of granite with cooler hydrothermal fluids during collapse of

the hydrothermal system, and the calculated equilibrium fluid $\delta^{18}O$ values (11.2 to 12.9 ± 1.1‰) are not interpreted to be magmatic equilibrium fluid values.

Table 8.5. Calculated $\delta^{18}O$ values for waters in equilibrium with the Darwin Granite at assumed crystallisation temperatures of 550, 600, 650, 700 and 800°C. *Average calculated without B2054, which is interpreted to have reacted with cooler hydrothermal fluid. Values in ‰. Error ± 1.1‰.

Sample Number	550°C	600°C	650°C	700°C	800°C
B2040	9.0	9.4	9.8	10.1	10.6
B2043	8.8	9.1	9.5	9.8	10.4
B2053	8.1	8.5	8.9	9.2	9.7
B2054	11.2	11.7	12.1	12.4	12.9
B2061	9.5	9.8	10.2	10.5	11.0
Average*	8.8	9.2	9.6	9.9	10.4

Due to the minimal amount of hydrothermal alteration and the narrow range of measured $\delta^{18}O$ values (average 10 ± 0.6‰), the Darwin Granite is interpreted to have crystallised from a magma having $\delta^{18}O$ values between 9 and 10.5 ‰. Over the range of possible crystallisation temperatures outlined above, fluids in equilibrium with the granite would have $\delta^{18}O$ values ranging from 8.8‰ to 10.4‰ ± 1.1‰. This range is consistent with other high $\delta^{18}O$ granites such as the Cornubian batholith in SW England (Sheppard, 1977) and I-Type granites from the New England Batholith in south eastern Australia (O'Neil et al., 1977) and the Cape Granite suite in South Africa (Harris et al., 1997). Other high $\delta^{18}O$ granites are described by Sheppard (1986) to occur as volumetrically significant components associated with collisional settings, and in orogenic zones.

Although the exact crystallisation temperature of the Darwin Granite is unknown, the discussion of boron in Section 7.2.1.3 suggests that the solidus temperature of the granite could have veen 600°C or lower. The average $\delta^{18}O$ value of 9 ± 1‰ calculated for a magmatic fluid at 600°C is, therefore considered to be the starting magmatic $\delta^{18}O$ value for fluids derived from the Darwin Granite.

Since the two possible fluids involved in the Jukes-Darwin hydrothermal system were seawater and magmatic fluid, it is possible to predict mixing paths for potential mineralising fluids in the hydrothermal system. The predicted paths form a zone shown on Figure 8.1 along with the magmatic water boxes of Taylor (1974) and Sheppard (1977). In predicting the mixing paths, it is assumed that δD values for the Darwin Granite would be consistent with other magmatic δD values as discussed by Taylor (1974). The Darwin Granite water box is based on calculated equilibrium fluid values from Table 8.5.

The predicted hydrothermal water zone represents a zone of mixing between seawater or modified seawater and the Darwin Granite magmatic fluid. Any combination of these fluids should lie within the predicted hydrothermal water zone. Fields shown are from Epstein (1965), Taylor (1974) and Sheppard (1981).

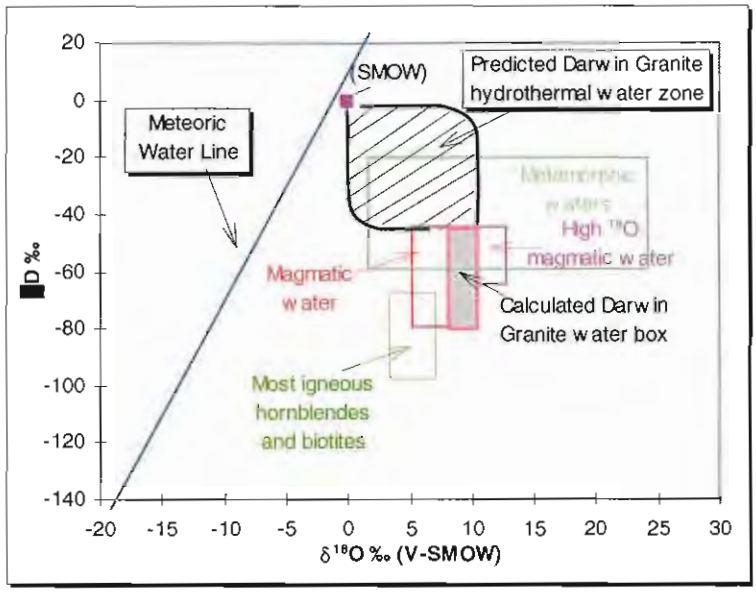

Figure 8.1. δD vs. $\delta^{18}O$ diagram showing the predicted range in hydrothermal water compositions for the Darwin Granite.

8.4.3 Temperature and Isotopic Composition of the Hydrothermal Fluids

In the case of the Jukes-Darwin area, no mineral pairs were sampled, and oxygen isotope geothermometry could not be carried out. Therefore, the interpretations in this section rely on alternative temperature estimates. The 320-360^{0}C range in chlorite temperatures (Section 6.3.1) was interpreted to represent minimal greenschist facies metamorphic temperatures due to contamination by interlayered smectite or other minerals and therefore cannot be used reliably. An alternative approach is to use the $\Delta_{mineral\text{-}water}$ equations for chlorite, K-feldspar and quartz to solve for fluid temperature using estimated water $\delta^{18}O$ values. Since the two possible end member fluids involved in primary hydrothermal alteration and mineralisation were seawater and magmatic fluid, values of 0‰ and 9.2‰ respectively were chosen and a range of minimum and maximum temperatures was calculated for each mineral species (Table 8.6). A major factor to take into consideration is that the $\delta^{18}O$ of the fluid involved in the water-rock interaction cannot have maintained its original value, and cannot be used as an indicator for the origin of the fluid (Green et al., 1983). Therefore, the actual mineralising fluid temperatures are expected to have been somewhere in between the two calculated fluid temperature extremes as determined from seawater and magmatic fluid (Table 8.6).

Table 8.6. Minimum and maximum fluid temperature ranges calculated from mineral species using seawater and magmatic fluid.

Mineral	Minimum temperature with 0‰ seawater	Maximum temperature with, 9.2‰ magmatic water	Equation Reference
Quartz	258 +/- 10°C	716 +/- 10°C	Sharp and Kirschner (1994)
K-feldspar	199 +/- 10°C	985 +/- 10°C	Matsuhisa et al. (1979)
Chlorite	215 +/- 10°C	Indeterminable	Cole and Ripley (1999)

8.4.3.2 DISCUSSION OF FLUID TEMPERATURES AND COMPOSITIONS

Quartz and K-feldspar Evidence

The calculated fluid temperatures for quartz and K-feldspar range from minimums of 200 to 260°C (Table 8.6), based on a pure 0‰ seawater value, to maximums of 700-980°C based on a pure 9.2‰ magmatic water value. Since only one sample each of hydrothermal quartz and K-feldspar were analysed for $\delta^{18}O$, ranges of temperatures and fluid compositions based on quartz and K-feldspar were not calculated. Although the quartz and K-feldspar come from separate samples, geological evidence (Section 8.2 and Plate 8.1) suggests that they may have formed from similar fluids. Therefore, quartz and K-feldspar were selected as the most reliable temperature indicators in the Jukes hydrothermal system. Using the fractionation equations for quartz and K-feldspar vs. water (Table 8.3), the $\delta^{18}O$ equilibrium fluid values can be calculated for any temperature. The single analysis of vein quartz has an analysed $\delta^{18}O$ value of 10 ± 0.3‰ which may potentially be in equilibrium with fluids with $\delta^{18}O$ values of -7.5 to +7.5 ± 0.4‰ over a temperature range of 150-550°C (+90°C/-60°C). Likewise, K-feldspar has an analysed $\delta^{18}O$ value of 8.2‰, potentially in equilibrium with fluid $\delta^{18}O$ values of -2.6 to +7.2 ± 0.4‰ over the same temperature range.

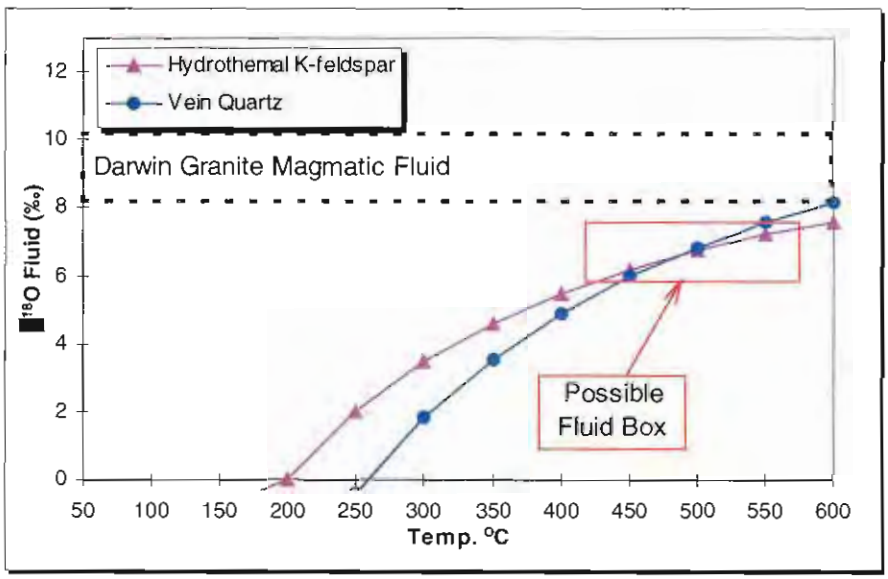

Figure 8.2. $\delta^{18}O$ fluid vs. temperature diagram for quartz and K-feldspar at temperatures from 150-600°C. The quartz and K-feldspar lines cross at about 485 +90°C/-60°C and an equilibrium fluid value of about 6.35 ± 1‰. The Darwin Granite possible fluid box (dashes) is shown for reference.

If the hydrothermal alteration minerals observed formed from a magmatic fluid with a $\delta^{18}O$ value of ~9 ±1‰, then calculated equilibrium fluid compositions for each mineral at a range of temperatures will converge on the magmatic fluid $\delta^{18}O$ value of 9 ± 1‰ at 600°C (Figure 8.2). At locations where mineral paths cross, hydrothermal fluids would be in equilibrium with both minerals at that temperature. Assuming that the single quartz and K-feldspar samples formed from the same generation of hydrothermal water, the intersection of the quartz and K-feldspar equilibrium curves provide a single *estimate* of the temperature range (445-510°C) and an

estimated equilibrium fluid $\delta^{18}O$ values (6 ± 1‰) for the hydrothermal system. The estimated range of values is outlined on Figure 8.2. The temperature range is within the calculated range for quartz and K-feldspar as shown on Table 8.5 and is considered geologically reasonable. Although the W/R component of the hydrothermal fluids is unknown, it must have been between a pure magmatic fluid (est. 9.2‰) and pure seawater (0‰) due to mixing with a modified seawater component. A fluid value of 6‰ requires a 3 to 2 mixture magmatic fluid (9.2‰) with seawater. Since the $\delta^{18}O$ value of seawater in the hydrothermal system was unlikely to have remained near 0‰, due to increases during diagenetic alteration and subsequent reaction with rocks during descent into the volcanic pile, the ratio was also calculated using a modified seawater value of 3‰. Using a value of 3‰, the ratio of mixed waters becomes close to 1 to 1. Therefore, the estimated equilibrium fluid $\delta^{18}O$ value of 6 ± 1‰ supports the interpretation that mineralising fluid was a mixture of magmatic water and modified seawater in roughly equal amounts. *It must be stressed that these calculations are based on a single quartz and K-feldspar sample and are indicative only. Many additional samples that formed at the same time and from the same fluid are required to test this result.*

Chlorite Evidence

Measured chlorite $\delta^{18}O$ and δD values vary from 2.6 to 8.0 ± 0.3‰ and -79 to -104 ±2‰ respectively (Table 8.2; Doyle, 1990). This wide variability in $\delta^{18}O$ values is reflected in the plots of chlorite equilibrium fluid values at temperatures from 150-600°C (Figure 8.3). The spread in $\delta^{18}O$ data is interpreted to result from re-equilibration of the chlorite $\delta^{18}O$ values with later fluids. The question is, what fluids?

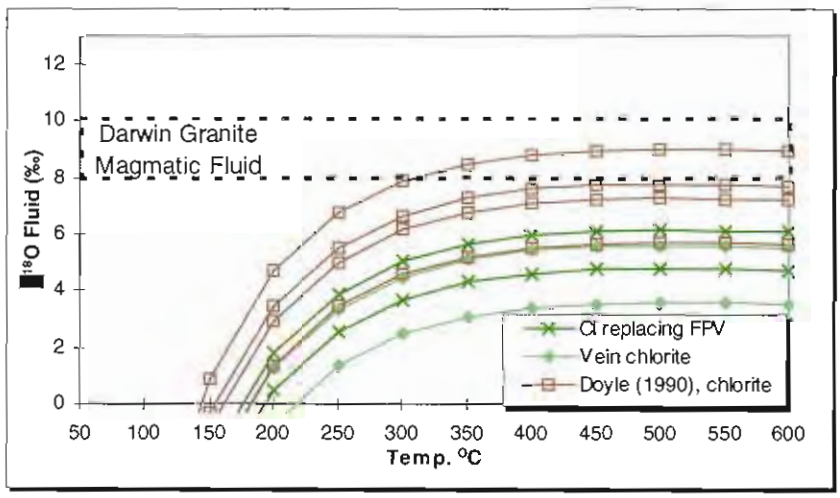

Figure 8.3. $\delta^{18}O$ fluid vs. temperature diagram of Jukes Road chlorites for temperatures from 150-600°C. Chlorite fluid values plot over a wide range of values at 600°C suggesting disequilibrium or later resetting.

Graham et al. (1987) studied deuterium-hydrogen isotopic exchange between chlorite and water in the temperature range 200-700°C. In their experiments, $\Delta_{chlorite\text{-}water}$ values consistently fell in the range -30‰ to -40‰ over the temperature range 200-500°C and at temperatures between 500°C and 700°C, $\Delta_{chlorite\text{-}water}$ values were not sensitive to temperature. This temperature-

independent behavior was also observed at lower temperatures by Marumo et al. (1980). Therefore, fluid compositions in equilibrium with chlorite in the Jukes-Darwin area were calculated using a $\Delta_{chlorite\text{-}water}$ value of -30‰. δD was determined for four chlorite samples, 10270, 10350, B1006 and B1010 (Table 8.2). Calculated equilibrium fluid δD values were -75‰, -65‰, -54‰ and -49‰ respectively. These values were assumed to be consistent over all temperatures in the Jukes hydrothermal system.

The calculated $\delta^{18}O$ values of fluid in equilibrium with chlorite range from -4.5‰ to 0.9 ± 0.4‰ at 150°C to 3.5 to 9.0 ± 0.4‰ at 550°C. The $\delta^{18}O$ and δD values for fluids in equilibrium with chlorite and the measured values of the minerals were compared on the $\delta^{18}O$ and δD diagram in Figure 8.4. The chlorite mineral values are highly depleted in D and recalculated equilibrium fluid values plot between the calculated Darwin Granite magmatic water box and the meteoric water line regardless of temperature. Three possible explanations are: 1) hydrothermal chlorite $\delta^{18}O$ values were lowered by reaction with seawater during collapse of the hydrothermal system; 2) hydrothermal chlorite $\delta^{18}O$ values were lowered by reaction with ^{18}O depleted low temperature meteoric fluid infiltrating during uplift either in the Late Cambrian to early Ordovician Jukesian or Devonian Tabberabberan orogenies; or 3) meteoric water was a component of the hydrothermal fluid during chlorite formation.

Although some modification of the $\delta^{18}O$ values is expected to have occurred during collapse of the hydrothermal system, it would have occurred at cooler temperatures than the 300-400°C required by reactions with seawater. The unconformity of Tyndall Group conglomerates on the Darwin Granite is evidence for uplift and erosion during the Late Cambrian, prior to Tyndall Group deposition (Jones, 1993). A similar unconformity between Tyndall Group volcanics and the Owen Conglomerate is evidence for another uplift and erosion event in the early Ordovician (Corbett and Cuffley, 1970; Corbett et al., 1974; Corbett and Lees, 1987; Corbett, 1992). During the Devonian Tabberabberan Orogeny, the entire MRV were recrystallised and regional cleavage developed (Corbett and Cuffley, 1970; Corbett, 1981; Corbett et al., 1989; Corbett, 1992; Corbett et al., 1993). Although, all of these uplift events exposed the Jukes-Darwin area to meteoric waters, the pre-Tyndall unroofing of the Darwin Granite is considered likely to have provided the meteoric inflow of water necessary to alter the newly formed chlorite $\delta^{18}O$ and δD values. The subsequent events may have partially recrystallised chlorites and further altered $\delta^{18}O$ and δD values, therefore, their effect cannot be completely ruled out.

Magnetite Evidence

Magnetite commonly preserves its $\delta^{18}O$ value during cooling, at least at temperatures below 600°C (Taylor, 1968), and retrograde exchange is not expected to take place at lower temperatures (Wenner and Taylor, 1971). In addition, magnetite is inherently one of the minerals that is resistant to $\delta^{18}O$ exchange (Wenner and Taylor, 1971). However, deuteric recrystallisation can change $\delta^{18}O$ values (Taylor and Noble, 1969). Except for one magnetite sample from the Darwin Granite, the range of magnetite $\delta^{18}O$ values from the Darwin Granite and the Jukes Prospect is narrow: -0.5‰ to +1.6‰ and +0.2‰ to +1.9‰ respectively.

Using the $\Delta_{Magnetite\text{-}water}$ equilibrium equation of Zheng (1995), $\delta^{18}O$ values for fluids in equilibrium with magnetite were calculated for samples from this study and other magnetite samples collected by Doyle (1990) and Large (1995, pers. com.). The temperature range of 100-600^{O}C reflects the range of possible hydrothermal temperatures in the Jukes-Darwin system as previously discussed. Results for Jukes Road and Mt. Darwin samples are compared on Figure 8.5. The majority of the calculated fluid values cross the quartz and K-feldspar lines in the temperature range 460-550^{O}C and in a range of $\delta^{18}O$ fluid values from 6‰ to 7.5‰.

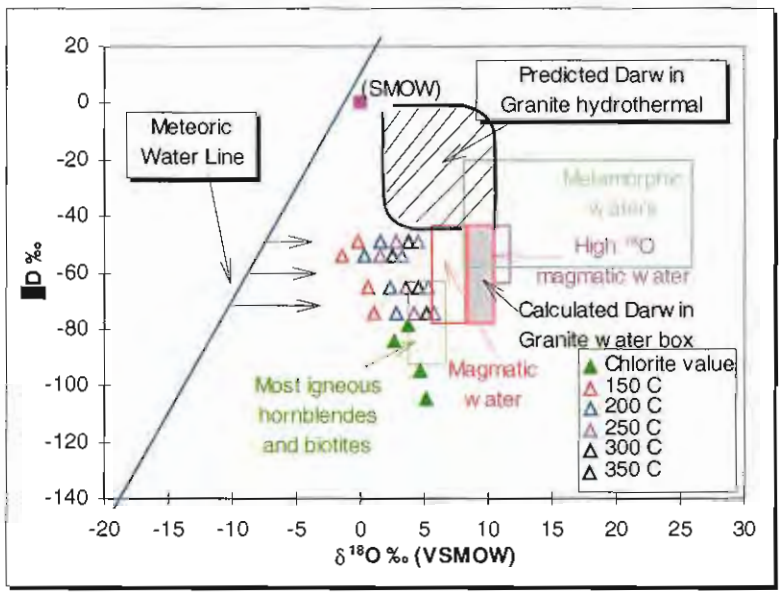

Figure 8.4. δD vs. $\delta^{18}O$ diagram showing fluids in equilibrium with chlorite at various temperatures. Equilibrium fluid values do not plot within the magmatic fluid box calculated for the Darwin Granite nor within the predicted Darwin Granite hydrothermal water zone for mixing with seawater. The plotted location suggests that fluids mixed with meteoric water of similar δD values but a depleted $\delta^{18}O$ value or later re-equilibrated with such a fluid.

Magnetite occurs in some quartz veins in the Jukes-Darwin area. Although only the single quartz $\delta^{18}O$ value was determined (Sample 10510, Table 8.2), an attempt to calculate a range of fluid temperatures was made using the $\Delta_{quartz\text{-}magnetite}$ equation (Zheng, 1995). Calculated fluid temperatures averaged 717 ± 25^{O}C. Given the assumption that the Darwin Granite crystallised at 600^{O}C or less, these results are considered to be unreasonably high for fluids derived from the Darwin Granite. Therefore, the sampled quartz vein and magnetite samples are probably not in isotopic equilibrium.

Since K-feldspar and magnetite commonly occur together in the same hydrothermal alteration zones and assemblages, a similar attempt was made to calculate a range of fluid temperatures using the K-feldspar $\delta^{18}O$ value (Sample 10290, Table 8.2). The $\delta^{18}O$ value of anorthite is assumed to be representative of the $\delta^{18}O$ value of alkali feldspars (O'Neil and Taylor, 1967). Using the $\Delta_{Anorthite\text{-}calcite}$ equation of Clayton et al. (1989) and the $\Delta_{Calcite\text{-}magnalite}$ equation of Zheng (1995), a $\Delta_{Anorthite\text{-}magnetite}$ equation was calculated. Calculated fluid temperatures ranged from 373-522 ± 25^{O}C and averaged 448 ± 25^{O}C. Calculated $\Delta_{Anorthite\text{-}calcite}$ values range from 6-9‰ and average 7.5‰ ± 0.5‰. These results agree with the $\delta^{18}O$ range in Figure 8.5 and are geologically

reasonable for the Jukes-Darwin system. Therefore, K-feldspar and magnetite may be in isotopic equilibrium. The *estimated* equilibrium fluid $\delta^{18}O$ value of 7.5‰ ± 0.5‰ supports the interpretation that mineralising fluids were dominated by a magmatic component derived from the Darwin Granite. *It must be stressed again, that these calculations are based on a single K-feldspar sample and that many additional K-feldspar-magnetite mineral pairs are required to test this result.*

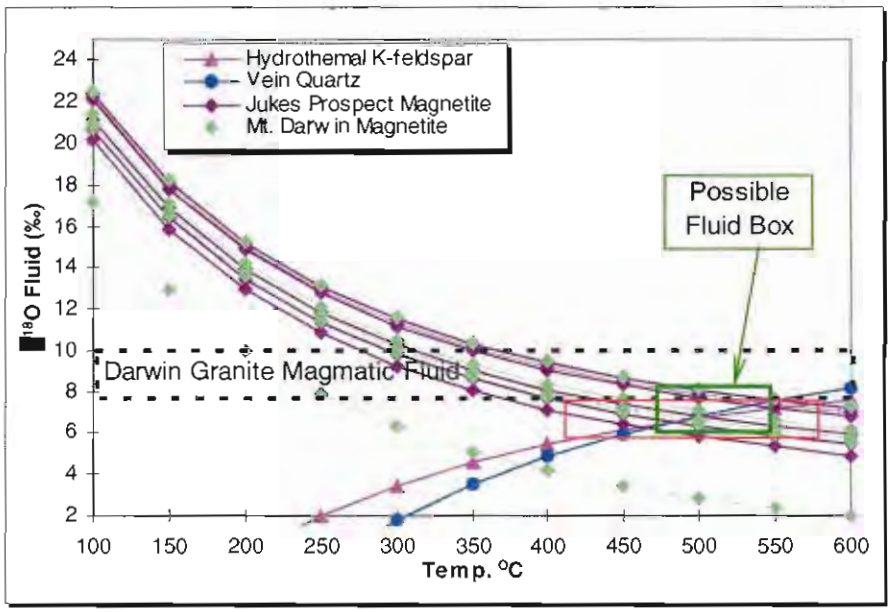

Figure 8.5. $\delta^{18}O$ equilibrium fluids vs. temperature diagram for Jukes Road and Mt Darwin magnetites for temperatures from 100-600°C. The majority of magnetite equilibrium fluid values intersect the quartz and K-feldspar lines in the temperature range 460-550°C and $\delta^{18}O$ fluid values 6‰ to 7.5‰. These data are outlined by a possible magnetite fluid box (Green Box) that overlaps the quartz and K-feldspar fluid box (Red Box) from Figure 8.2. The Darwin Granite possible fluid box (dashed) is shown for reference.

8.4.4 Water to Rock Values

The calculated or estimated water to rock ratio (W/R) refers to the atom percent of oxygen exchanged during hydrothermal alteration (Sheppard et al., 1971). Taylor (1977) argued that the typical range of W/R values averaged over an entire hydrothermal system is seldom >1.

The magnitude of the change in the $\delta^{18}O$ values of water by isotopic exchange reactions with volcanics depends upon a number of factors (Ohmoto and Rye, 1974):

- the initial isotopic composition of the water;
- the initial isotopic composition of the volcanics involved in the isotopic exchange reactions;
- the ratio of exchangeable oxygen atoms in the water to those in the rock (W/R);
- temperature, which determines the equilibrium isotopic fractionation between the rock and the water;
- the degree of isotopic equilibration.

The isotopic data was modeled for closed and open systems (Equations 8.4 and 8.5 respectively) derived from the W/R equation (Equation 8.3) of Taylor (1974; 1977). Equation 8.4 gives the W/R values integrated over the lifetime of the hydrothermal system, assuming continuous recirculation and re-equilibration of the fluid. Nevertheless, some of the hydrothermal fluid will be lost, eg. by escape to the surface. In the extreme open system case where the water passes through the rocks once, the integrated W/R is given by Equation 8.5 (Taylor, 1977).

Equation 8.3 (Taylor, 1974).

$$W/R = \delta^{18}O_{\text{final rock}} - \delta^{18}O_{\text{initial rock}} / \delta^{18}O_{\text{initial fluid}} - \delta^{18}O_{\text{final fluid}}$$

Equation 8.4 for closed system (Taylor, 1974, 1979).

$$W/R_{\text{closed}} = \delta^{18}O_{\text{final rock}} - \delta^{18}O_{\text{initial rock}} / \delta^{18}O_{\text{initial fluid}} - (\delta^{18}O_{\text{final rock}} - \Delta)$$

Equation 8.5 for open system (Taylor, 1977; Nabelek, 1987).

$$W/R_{\text{open}} = \ln(W/R_{\text{closed}} + 1)$$

Where:

Δ is $\delta^{18}O_{\text{final rock}} - \delta^{18}O_{\text{final water}}$

W/R is the water to rock ratio;

$\delta^{18}O_{\text{initial rock}}$ is the estimated or measured isotopic composition of the initial unaltered rock;

$\delta^{18}O_{\text{final rock}}$ is the calculated isotopic composition of the final rock;

$\delta^{18}O_{\text{final fluid}}$ is the estimated isotopic composition of the altering fluid;

$\delta^{18}O_{\text{final rock}}$ values are typically measured and $\delta^{18}O_{\text{initial rock}}$ values are typically estimated. The problem is the selection of appropriate fractionation curves, because rocks are composed of multiple minerals and the mineral-water fractionation factors can either undergo equilibrium or kinetic isotopic fractionation (O'Neil and Taylor, 1967; Taylor, 1974; Taylor, 1979; Sheppard, 1981). In previous studies where the $\delta^{18}O_{\text{final rock}}$ values were unknown, rock-water fractionation was approximated by the $\delta^{18}O_{\text{anorthite-water}}$ fractionation curve (Taylor, 1974, 1979). In the Jukes-Darwin area, $\delta^{18}O_{\text{final rock}}$ values were not measured and must be estimated. The $\delta^{18}O_{\text{final rock}}$ values were estimated using a fractionation equation for the $\Delta_{\text{water-rock}}$ of an average MRV dacite ($\Delta_{\text{water-rock}} = (2.76*10^6 / T^2) - 3.31$, Herrmann, 2000, pers. comm.) compiled using individual mineral fractionation equations of Matsuhisa et al. (1979) and average MRV dacite normative compositions.

Rearranging Equations 8.4 and 8.5, to solve for $\Delta_{\text{final rock}}$ as a function of temperature and W/R yields Equations 8.6 and 8.7. The changes in the estimated $\delta^{18}O$ values of the feldspar-phyric dacites from the Jukes-Darwin area were calculated as a function of temperature and W/R under two conditions: 0‰ for seawater and 9.2‰ for a magmatic fluid from the Darwin Granite. Results are shown on Figures 8.6 -8.9.

Equation 8.6 for closed system.

$$\delta_{\text{final rock}} = (\delta_{\text{initial rock}} + W/R * (\delta_{\text{initial water}} + \Delta_{MRV})) / (1 + W/R)$$

Equation 8.7 for open system.

$$\delta_{final\ rock} = \delta_{initial\ water} + \Delta_{MRV} - ((\delta_{initial\ water} + \Delta_{MRV} - \delta_{initial\ rock}) / e^{W/R})$$

Where: Δ_{MRV} is the average MRV dacite equation as a function of temperature.

As shown in Figures 8.6 and 8.7, in an unmodified (0‰) seawater system, quartz and K-feldspar require large W/R values (>0.1) and relatively cool temperatures (<200°C), unreasonable conditions in the M1 stage of the Jukes-Darwin system. In contrast, in a magmatic water-dominated system (9.2‰) shown in Figures 8.8 and 8.9, temperatures (>200°C) and W/R values (>0.1) are easily met with reasonable hydrothermal conditions. This evidence is interpreted as support for a magmatic origin for the Jukes-Darwin system. As with previous interpretations based on *single quartz and K-feldspar samples, many additional samples are required to adequately test this speculation.*

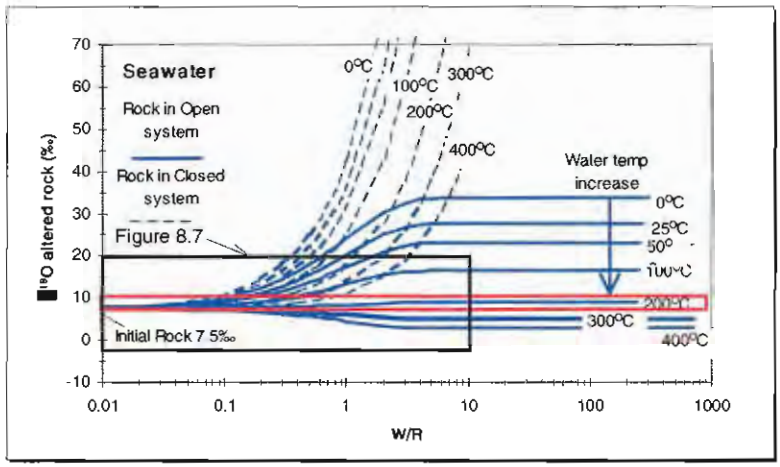

Figure 8.6. $\delta^{18}O$ altered rock vs. W/R for feldspar-phyric rocks from the Jukes Road calculated with 0‰ seawater. W/R values and $\delta^{18}O$ compositions for altered rocks are shown at temperatures from 25-400°C. The assumed $\delta_{initial\ rock}$ $\delta^{18}O$ value is 7.5‰. Enlarged details are discussed on Figure 8.7.

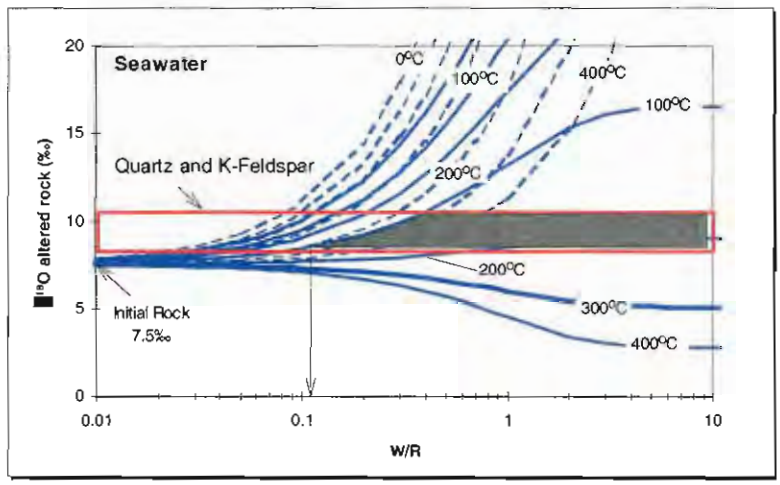

Figure 8.7. $\delta^{18}O$ altered rock vs. W/R for feldspar-phyric rocks from the Jukes Road calculated with 0‰ seawater (enlarged). Quartz and K-feldspar require W/R values from >0.1(shaded area) and cool seawater (<200°C). Conditions that are geologically unreasonable in the Jukes-Darwin system.

A major factor to take into consideration is that the $\delta^{18}O$ of the fluid involved in water rock interaction cannot have maintained its original isotopic composition, and cannot be used as an indicator for the origin of the fluid (Green *et al.*, 1983). Any fluid, regardless of its origin, can end with the same $\delta^{18}O$ value if the W/R value was <1, i.e. rock-dominated. Only when the W/R value of the hydrothermal system is water-dominated i.e. >1 can the $\delta^{18}O$ value estimated from Figures 8.6-8.9 be used to identify the isotopic composition of the final rock.

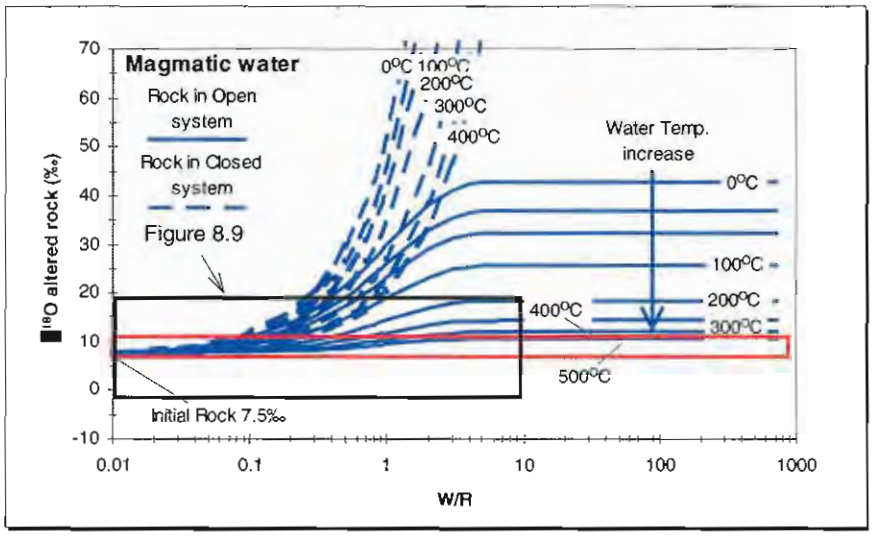

Figure 8.8. $\delta^{18}O$ altered rock vs. W/R for feldspar-phyric rocks from the Jukes Road calculated with 9.2‰ magmatic water. Conditions similar to Figure 8.6 but values to 500°C were calculated. Enlarged details are discussed on Figure 8.9.

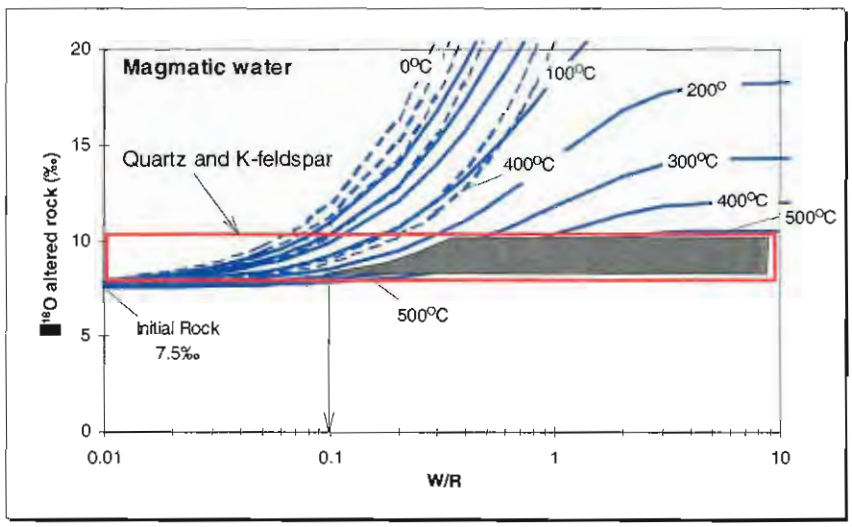

Figure 8.9. $\delta^{18}O$ altered rock vs. W/R for feldspar-phyric rocks from the Jukes Road calculated with 9.2‰ magmatic water (enlarged). Quartz and K-feldspar can form at temperatures >200°C and W/R values >0.1 (shaded area). These temperatures and conditions are geologically reasonable for the Jukes-Darwin system and support the interpretation that hydrothermal alteration and mineralisation fluids were dominated by magmatic fluids.

8.5 SUMMARY

Based on a limited data set the following preliminary conclusions and speculations were made:

1) The whole rock $\delta^{18}O$ data for the Darwin Granite is consistent with the interpretation that the Darwin Granite crystallised from a magma with $\delta^{18}O$ values between 9‰ and 10.5‰. This range is consistent with other high $\delta^{18}O$ granites associated with collision zones and orogenic areas. Magmatic fluids in equilibrium with the granite had $\delta^{18}O$ values around 9 ± 1‰.

2) Although the Fe and Mg in chlorite do not appear to have re-equilibrated during later metamorphic events, $\delta^{18}O$ exchange with meteoric fluids occurred at some point and influenced the $\delta^{18}O$ chlorite compositions. The timing of this infiltration is uncertain, with potential events possible being a) uplift of the pluton and associated altered volcanics into the meteoric water regime late in the intrusion's history; in this case the isotopic history is recording a part of the evolution of the primary hydrothermal system; or b) recrystallisation during the Ordovician or Devonian cleavage forming event.

3) Quartz and K-feldspar data from separate but related sites, selected on the assumption that they formed from the same fluid, are indicative of equilibrium at 485 $+90^{O}C/-60^{O}C$ and $\delta^{18}O_{fluid}$ value of 6.35 ± 1‰. Similarly, magnetite precipitated from fluids with $\delta^{18}O$ values of 6 to 7.5 ± 1‰ at temperatures of 460-550^{O}C. With the assumptions of these methods, the quartz, K-feldspar and magnetite formed from nearly pure magmatic fluids, the likely source of which was the Darwin Granite.

4) Seawater-dominated fluids produce unlikely W/R values at unreasonable temperatures compared to magmatic fluids for the Jukes-Darwin hydrothermal system (Figures 8.6 and 8.7). Although W/R values were not determined for chlorite, values of >0.1 were determined based on quartz and K-feldspar samples. This range is consistent with other granite-related hydrothermal systems (Taylor, 1974; Taylor, 1977).

CHAPTER 9

9.0 SULFUR ISOTOPES IN THE JUKES-DARWIN AREA

9.1 INTRODUCTION

For volcanic terrains such as the MRV, Sangster (1968) noted a parallel variation between the $\delta^{34}S$ compositions of stratabound sulfide deposits and that of corresponding ancient seas throughout geologic time. Large (1992) and other authors, argued that this parallelism implicates seawater as the major contributing source of sulfur for these types of deposits. However, numerous authors (Shanks et al., 1981; Ohmoto et al., 1983; Alt et al., 1989; Alt, 1994; Ohmoto, 1996; Ohmoto and Goldhaber, 1997; Herzig et al., 1998) and others, have shown that the seawater $\delta^{34}S$ component ranges from 10% to 50%, the remaining sulfur being derived from magmatic or rock sulfur, and changes substantially during the duration of the hydrothermal system. Shanks et al. (1981) and Ohmoto et al. (1983) have shown that the largest control on the percentage of reduced seawater sulfate is the W/R value, which is complicated by a number of factors in natural systems. However, typically, the smaller the W/R value, the smaller the seawater contribution. In VHMS deposits, variation in $\delta^{34}S$ values between different mineralised phases has been used to provide an understanding of the evolution of a hydrothermal system, not only through time but with regards as to the source of sulfur (Ohmoto and Rye, 1979; Green et al., 1981; Alt et al., 1989; Herzig et al., 1998) and others. These authors agree that variation in $\delta^{34}S$ sulfate values can be caused predominantly by mixing between an ascending hydrothermal fluid (± evolved seawater sulfate, ± igneous sulfur) and near-surface circulating seawater.

In hydrothermal mineral deposits, Fe, Cu, Pb and Zn are typically bound as sulfides, but the sulfur need not be sourced from the same environment as other components in the ore-forming fluids. Sulfur isotope data (expressed as $\delta^{34}S$ values) can be used to gain information on the chemical and thermal environment of mineral deposition, fluid mixing processes and W/R values. Typically, they are used to determine sulfur sources and temperatures of sulfide deposition (Large, 1995). Although different sulfur sources (eg. igneous, biogenic and seawater) have distinctive $\delta^{34}S$ values and patterns (Sangster, 1968; Shanks et al., 1981), in many cases sulfur sources cannot be unambiguously resolved due to mixing of reservoirs and redox reactions (Ohmoto, 1986).

Although there is a significant body of sulfur isotope data for the Jukes-Darwin area, no systematic study has been conducted to establish the existence of isotopic zoning related to the hydrothermal alteration or mineralisation. The aim of the current sulfur isotope study is to examine the possibility and significance of sulfur isotope zoning from the centre of the Cu-Au system at the Jukes Prospect outward to the least-altered volcanics. This was accomplished by analysing a set of samples collected along the Jukes Road and King River Tunnel cross-sections. This data was combined with data from other studies to also assess possible sulfur sources, and to compare the sulfur isotope signature of the Jukes-Darwin area to other mineralised areas within the MRV.

Sulfur isotope geothermometry was not attempted, because of the lack of appropriate mineral pairs.

9.2 MINERAL SEPARATION AND ANALYTICAL METHODS

In total, 27 sulfur isotope analyses were performed on pyrite samples from the Jukes Road, King River Tunnel and Mt. Darwin areas. Pyrite was selected for the current study because it occurs in multiple mineralisation styles throughout the paragenetic sequence. Optically homogeneous pyrite was selected for each of the M1 and M2 paragenetic stages (Section 7.4) to simplify interpretations and to isolate the $\delta^{34}S$ values of each paragenetic stage. Prior to sample selection, a polished thin section of each potential sample was examined in order to determine if impurities or obvious intergrain zoning was present. Two hundred micron thick laser ablation polished sections were then prepared for each selected sample. Individual sulfide grains were analysed using laser ablation facilities at the Central Science Laboratory, University of Tasmania. An 18 watt Quantronix model 117 Nd:YAG laser was used to ablate a 150-200 micron wide by 150 micron deep ablation pit in each sample. SO_2 gas released by the ablation was collected, cryogenically cleaned and analysed in a VG Sira Series II mass spectrometer. Samples were then calibrated against galena standards from Broken Hill ($\delta^{34}S$ = +3.4‰) and Rosebery ($\delta^{34}S$ = +12.4‰). A fractionation factor of 6.75‰ results in one sigma precision of ± 0.15‰ for pyrite. The detailed analytical method is outlined in (Huston et al., 1995).

In addition to the Jukes Prospect samples, an attempt was made to analyse five samples of the Darwin Granite for whole rock sulfur in order to determine a primary magmatic $\delta^{34}S$ value. However, due to a lack of sulfide in four of the samples, only one analysis was successful. The Darwin Granite samples were prepared by the author at the Geology Department at the University of Tasmania. Samples were crushed by hand in an agate mortar and pestle. Oxidised portions of the rocks were hand-picked and disposed. The remaining samples were then crushed in a tungsten-carbide disc mill to 50 microns (300 mesh sieve). The clean samples were then analysed by Nilar Hlaing using the method described in Alt (1994), and the resulting Ag_2S separate was analysed following cuprous oxide extraction of SO_2 on the above mass spectrometer.

9.3 RESULTS

Alteration and mineralisation near the Darwin Granite are primarily fracture controlled, although localised disseminated occurrences were observed. Vein mineralisation characterises most of the various prospects within the Jukes-Darwin field. In order to determine if sulfur isotope zoning occurred within the fracture-dominated hydrothermal system at the Jukes Prospect, samples were collected at 10-60 metre intervals along the Jukes Road from the centre of the mineralised system outward for over 400 metres. Within the King River Tunnel, a similar suite of samples was collected at similar intervals. The King River Tunnel suite passes entirely across the width of the mineralised zone. Sulfides were not observed within the least-altered rocks along the Jukes Road or King River Tunnel. In addition, several samples were collected from the Darwin Granite area

from veins that were distal to but related to the granite intrusion. Sulfur isotope results are tabulated in Table 9.1.

Table 9.1. $\delta^{34}S$ results for the Jukes Prospect, King River Tunnel and Darwin Granite.

Sample Number	Location and description	$\delta^{34}S$ ‰
10140	Jukes, chlorite + K-feldspar altered quartz-feldspar phyric dyke, disseminated pyrite, M1 phase	13.1
10160	Jukes, chlorite + K-feldspar altered feldspar-phyric dacite, disseminated pyrite, M2 phase	15.7
10180	Jukes, chlorite + K-feldspar altered quartz-feldspar phyric dyke, M2 phase	19.0
10200	Jukes, chlorite veins in chlorite altered quartz-feldspar phyric dyke, M1 phase	11.3
10210	Jukes, chlorite + magnetite breccia matrix, M1 phase	13.3
10220	Jukes, K-feldspar altered feldspar-phyric dacite, chlorite + pyrite vein, M2 phase	12.4
10290	Jukes, chlorite altered feldspar-phyric dacite, pyrite in chlorite vein, M2 phase	15.4
10350	Jukes, sericite + chlorite altered feldspar-phyric dacite, pyrite in quartz vein, Late alteration phase	23.6
10390	Jukes, chlorite + magnetite breccia matrix, M2 phase	17.4
10520	Jukes, chlorite altered quartz-feldspar phyric dyke, disseminated pyrite, M1 phase	13.2
10550	Jukes, chlorite altered quartz-feldspar phyric dyke, disseminated pyrite, M1 phase	14.7
10580	Jukes, chlorite altered quartz-feldspar phyric dyke, disseminated pyrite, M2 phase	16.5
10650	Jukes, sericite + chlorite altered feldspar-phyric dacite, disseminated pyrite, M2 phase	14.4
400503	KRT, chlorite veined K-feldspar altered quartz-feldspar-phyric volcaniclastic, disseminated pyrite, M1 phase	12.9
400512	KRT, K-feldspar altered feldspar-phyric dacite, pyrite in chlorite vein, M2 phase	15.7
400520	KRT, sericite + chlorite altered feldspar-phyric dacite, pyrite in K-feldspar vein, M2 phase	17.4
400532	KRT, K-feldspar altered clasts in magnetite breccia, pyrite in magnetite vein, M1 phase	13.8
400543	KRT, K-feldspar altered feldspar-phyric dacite, pyrite in chlorite vein, M2 phase	15.2
400552	KRT, sericite + chlorite altered feldspar-phyric dacite, pyrite in chlorite + magnetite vein, M1 phase	13.7
400556	KRT, sericite altered feldspar-phyric dacite, pyrite in chlorite vein, M2 phase	14.9
400563	KRT, K-feldspar altered feldspar-phyric dacite, pyrite in magnetite + chlorite vein, M1 phase	12.7
400575	KRT, K-feldspar altered feldspar-phyric dacite breccia, pyrite in magnetite + chlorite vein, M2 phase	14.8
B2020	Mt Darwin, sericite + chlorite altered quartz-phyric volcaniclastic, disseminated pyrite	8.0
B2028	Mt Darwin, sericite + chlorite altered feldspar-phyric dacite, disseminated pyrite	15.1
B2035	Mt Darwin, sericite + chlorite altered quartz-phyric volcaniclastic, disseminated pyrite	13.0
B2047	Mt Darwin, chlorite altered quartz-phyric volcaniclastic, disseminated pyrite in quartz vein, M2 phase	17.0
B2051	Mt Darwin, K-feldspar altered feldspar-phyric dacite, disseminated pyrite, M2 phase	16.5
B2054	Darwin Granite, pink granite, whole rock	12.7

The $\delta^{34}S$ results listed in Table 9.1 are plotted together with the geology and hydrothermal alteration at the Jukes Prospect and King River Tunnel on Figure 9.1. There is no obvious systematic prospect scale $\delta^{34}S_{sulfide}$ zoning. When the data in Table 9.1 is combined with data from other previously published studies (Table 9.2), the data for the Jukes Prospect falls in the range of 10.0-23.6‰. Within this range, two groups of $\delta^{34}S$ values occur. Population 1 has $\delta^{34}S_{sulfide}$ values between 10.5‰ and 14.5‰, and Population 2 has values between 15.0‰ and 19.0‰ (Figure 9.2). Population 1, 10.5‰ to 14.5‰, occur in mineralised pyrite-chalcopyrite-bearing M1 veins (Section 7.4.2) irrespective of width, and characterise the Jukes Prospect ores. M1 veins are surrounded by localised disseminated pyrite halos, and these have similar $\delta^{34}S_{sulfide}$ values. Population 2, 15.0-19.0‰, is typically confined to M2 veins and disseminated mineralisation (Section 7.4.4). Because M2 veins cut earlier M1 veins; overlapping $\delta^{34}S_{sulfide}$ values of the two vein types masks systematic large scale zoning patterns. The highest $\delta^{34}S_{sulfide}$ value at the Jukes Prospect is 23.6‰ and occurs in a late quartz vein.

When $\delta^{34}S_{sulfide}$ data for the entire Jukes-Darwin area is evaluated in Table 9.2, three groups of values are recognised: Group A, 5-9‰; Group B, 10-19‰; and Group C, 22-26‰ (Figure 9.3). Average $\delta^{34}S_{sulfide}$ values (Table 9.2) range from 5.3-9.0‰ at Taylours Reward, Prince Darwin and the Darwin Granite contact zone, to 21.9‰ at East Darwin. Sulfate (barite) $\delta^{34}S$ values occur in a single population ranging from 28-30‰. Within individual prospects, $\delta^{34}S_{sulfide}$ populations commonly overlap.

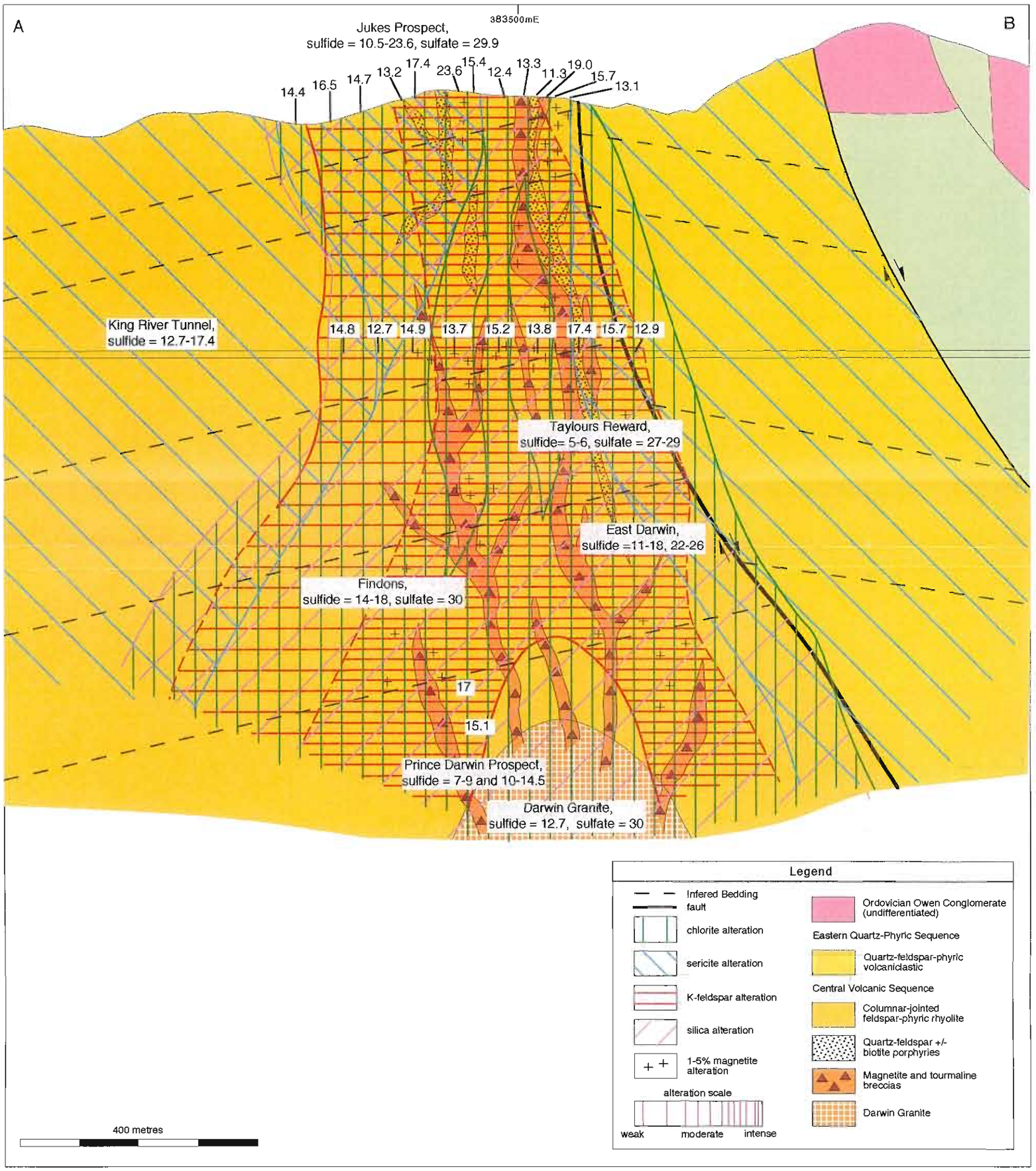

Figure 9.1. Cross-section along the King River Tunnel and Jukes Road showing sulfur isotopes distribution in the Jukes-Darwin area. The location of the cross-section is shown on Figure 5.5 and an explanation of the geology accompanies Figure 5.6. The locations of Findons, East Darwin, Taylours Reward and the Prince Darwin Prospects are extrapolated onto the section in order to emphasise sulfur isotope patterns. Sulfur isotope values are in per mil. (figure is modified from Large et al. 1996)

Table 9.2. Summary of $\delta^{34}S$ results for the Jukes-Darwin area. Data summarised from Polya et al. (1986), Eastoe et al. (1987), Solomon et al. (1988), Doyle (1990), Jones (1993), Gadaloff (1996) and this study.

Location	No. of Samples	Range of $\delta^{34}S_{sulfide}$ (‰)	Average $\delta^{34}S_{sulfide}$ (‰)	No. of Samples	$\delta^{34}S_{sulfate}$ (‰) ave.
Lake Jukes	1	17			
Jukes Prospect					
Adits	13	10.5-13.5	12.8		
Altered feldspar-phyric dacite	13	10.8-15.7 (23.6)	12.9	1	29.9
Altered quartz-phyric dykes	7	11.3-19.0	15		
King River Tunnel	10	12.7-17.4	14.6		
East Darwin Prospect					
Population 1	6	22.2-26.1	21.9		
Population 2	23	10.2-17.5	14.1		
Findons	13	13.6-17.5	15.6	1	30
Taylours Reward	2	4.9-5.6	5.3	10	27.6
Granite contact area and the Prince Darwin Prospect					
Population 1	5	7.1-9.3	8.3		
Population 2	13	10.3-17.0	12.9	2	29
Darwin Granite (Whole Rock)	1	12.7			

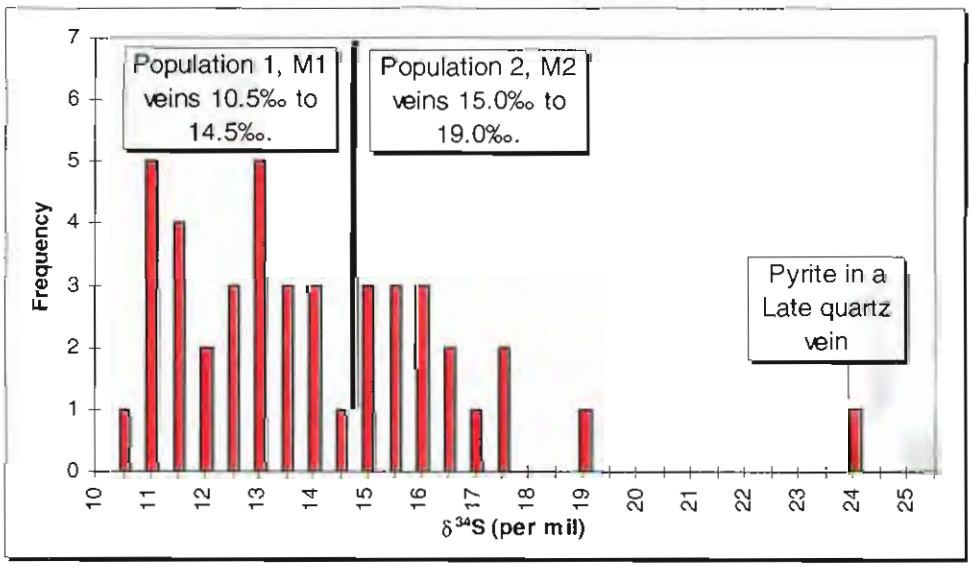

Figure 9.2. Frequency distribution vs. $\delta^{34}S$ results for the Jukes Prospect and King River Tunnel. Two populations are shown. Population 1 has $\delta^{34}S_{sulfide}$ values between 10.5‰ and 14.5‰ and is related to M1 veins (Section 7.4.2). Population 2 has $\delta^{34}S_{sulfide}$ values between 15.0‰ and 19.0‰ and is related to the M2 phase of alteration and mineralisation (Section 7.4.4).

9.4 DISCUSSION

$\delta^{34}S$ values of minerals deposited entirely from magmatic sources range from -30‰ to +8‰ (Ohmoto and Rye, 1979; Banks, 1982; Herzig et al., 1998; Streck and Dilles, 1998). Those in the Jukes-Darwin hydrothermal system are typically heavier than typical magmatic $\delta^{34}S$ values suggesting an alternative source. Within the contact zone of the Darwin Granite, $\delta^{34}S$ values in pyrite range from 7-9‰, and are the same as $\delta^{34}S$ values in pyrite (7-9‰) from the contact zone

of the Murchison Granite (Solomon et al., 1969; Solomon and Walshe, 1979; Solomon et al., 1988; Abbott, 1992; Large, pers. com.). One explanation for these contact zone values is that they represent $\delta^{34}S$ values produced as a result of mixing between variable proportions of magmatic sulfur, volcanic rock sulfur and interstitial trapped seawater.

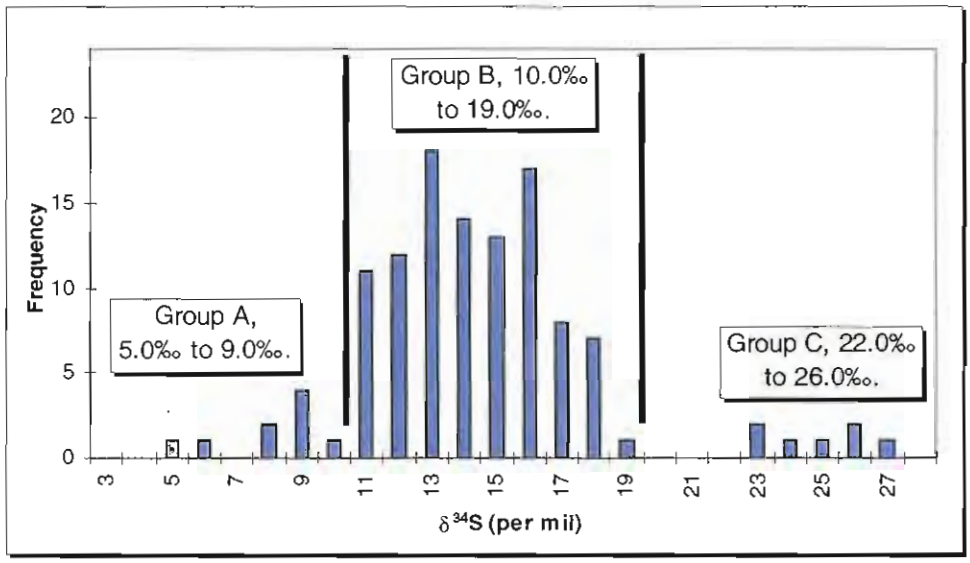

Figure 9.3. Frequency distribution vs. $\delta^{34}S$ results for the Jukes-Darwin area. Group A is a contact zone related population with $\delta^{34}S_{sulfide}$ values between 5‰ and 9‰. Group B is related to the main hydrothermal alteration and mineralisation and has values between 10‰ and 19‰ and Group C is related to Late stage alteration (Section 7.4.5) with values 22‰ to 26‰.

9.4.2 Magmatic Sulfur

What was the initial $\delta^{34}S$ value of Darwin Granite magmatic sulfur and, similarly, what was the magmatic value of sulfur in the host felsic volcanics? The $\delta^{34}S$ value of primary igneous sulfide minerals is essentially the same as that of sulfur in the melt or parent rock because high temperature fractionation is negligible (Ohmoto and Rye, 1979), therefore, isotopically, rock sulfur derived from felsic volcanics is indistinguishable from magmatic sulfur derived from their parent granite (Solomon et al., 1988). In the study area, this means that the initial $\delta^{34}S$ values of the CVC volcanics were the same as the $\delta^{34}S$ values of their parent magma, a Murchison Granite-like melt (Chapter 4). An attempt, in this study, to directly determine the primary magmatic $\delta^{34}S$ values in the Darwin Granite failed. Of five Darwin Granite samples analysed, four had non-detectable sulfur (as sulfide) and a fifth sample (B2053) had a $\delta^{34}S$ value of 12.7‰ (Table 9.1), a value interpreted to be a result of mixing magmatic sulfur with reduced Cambrian seawater sulfate (about 30‰, Claypool et al., 1980). $\delta^{34}S$ values from the Murchison Granite area have an average value of 12‰, and a range from 4.1‰ to 22.6‰ (n = 26), and similar genetic interpretations have been made (Solomon et al., 1969; Solomon and Walshe, 1979; Solomon et al., 1988; Abbott, 1992; Large et al. 1996.). Least-altered CVC volcanics have highly variable $\delta^{34}S$ values that range from negative too positive and are interpreted to represent variable proportions of mixing between reduced Cambrian seawater, leached host-rock sulfur, oxidised secondary sulfur, sulfur derived from or reduction by biogenic and metamorphic fluid processes (G. Davidson, 1999, pers. com.).

Typically, sulfur isotope data in the MRV is interpreted to indicate a strong influence of reduced Cambrian seawater, and does not support a definitive magmatic source for the various mineralisation styles.

Historically, $\delta^{34}S$ values of igneous rocks were believed to be within a range of 0‰ ± 5‰. This belief was based partly on the fact that many igneous rocks in the western United States, from which the earlier data was collected, have $\delta^{34}S$ values around 0‰. However, newer studies from other areas have shown that igneous rocks with $\delta^{34}S$ values outside the 0‰ ± 5‰ range are common, and that regional variations exist in the $\delta^{34}S$ values of igneous rocks (Ohmoto and Rye, 1979). Granitic rocks worldwide have a range in $\delta^{34}S$ values of -10 to +30‰, although typically maximums are about +10‰ (Holser and Kaplan, 1966; Coleman, 1977; Ohmoto and Rye, 1979; Sasaki and Ishihara, 1979). I-type magnetite-series granites typically have values that fall between 5-7‰ (Ohmoto and Rye, 1979), although variations from +1 to +9‰ have been documented in Japanese examples (Sasaki and Ishihara, 1979). Island arc related andesites and rhyolites have values between +0‰ and +10‰ (Taylor, 1986), but are typically between +5 and +7‰ (avg. +4 to 5‰, Ueda and Sakai, 1984; Woodhead et al., 1987).

Studies on the source of sulfur in granitoids suggest that sulfur can be acquired from the wallrocks during emplacement (Kibilus, 1983; Wesolowski, 1984; Ishihara et al., 1985; Ohmoto, 1986) and that I-type granites have a greater potential for assimilation because of higher initial magmatic temperatures (Burnham, 1979). However, it is difficult for a magma to achieve a higher sulfur content than the country rocks into which it intrudes by bulk rock assimilation (Ohmoto, 1986). Other studies suggest that the source region for the granitic melt has the strongest influence on the sulfur content (Ueda and Sakai, 1984; Hawkins and Melchior, 1985). Felsic rocks that are produced during early stages of back-arc development reflect the influence of the subducting slab on the melting region and have $\delta^{34}S$ values similar to island-arcs (Alt et al., 1993; Herzig et al., 1998). Consequently, hydrothermal fluids circulating through felsic back-arc volcanics can have sulfur isotope ratios that reflect the influence of heavy crustal sulfur (Herzig et al., 1998). Three different isotopic reservoirs of sulfur exist: 1) mantle-derived sulfur with $\delta^{34}S$ values in the range of 0.0 ±3‰ (Chaussidon and Lorand, 1990); 2) sedimentary sulfur with $\delta^{34}S$ values in the range of -70 to +70‰, but which are typically depleted in the heavier isotope (Ohmoto and Rye, 1979); and 3) crustal sulfur with an average value of +7‰ for the continental crust (Chaussidon et al., 1989). Nd model ages and low P_2O_5 contents of the Darwin and Murchison Granites are consistent with the interpretation that the Cambrian granitic melts in the eastern MRV were derived from partial melts of granodiorite composition generated in the lower crust of the Proterozoic Tyennan Block (Section 6.2.3), although a mantle component to the granites cannot be entirely ruled out.

Unambiguous magmatic $\delta^{34}S$ value for the Cambrian granites and CVC volcanics were not obtained analytically. Because crustal source rocks (estimated $\delta^{34}S$ value of 7‰) and host rocks for granitic melts have the strongest influences on sulfur isotope compositions, a value of 6‰ will be assumed for the Darwin Granite based on averages for I-type magnetite-series granites and

associated intermediate and felsic rocks elsewhere (Ohmoto and Rye, 1979; Sasaki and Ishihara, 1979).

If the magmatic $\delta^{34}S$ value is ~6‰, what quantity of sulfur of this value was available for use in production of sulfides? Burnham (1979) suggests that sulfur in hydrous silicate melts dissolves mostly as HS^-. However studies by Banks (1982), Ueda and Sakai (1984) and Ishihara et al. (1985) have shown that oxidised forms of sulfur (SO_4^{2-} and SO_3^{2-}) are more important than sulfide-sulfur in magmas with high fO_2, such as I-type magmas. These studies suggest that sulfur solubility at P_f<2 Kbar ranges from 500-2000 ppm in basaltic magmas, and from 10-200 ppm in granodiorite and granite magmas. In a study of sulfur concentrations in various minerals in I-type granites, Banks (1982) showed total sulfur to be typically <50 ppm, occurring in trace hydrous mafic minerals (eg., biotite and hornblende) and apatite. Less than 5 ppm occurred as sulfide. Ohmoto (1986) noted that the actual content of sulfide-sulfur in many granitoids, excluding hydrothermal sulfur, exceeded the solubility values, a factor particularly important in intrusives associated with sulfide mineralisation. However, Mutschler (1981) studied porphyry molybdenite systems and concluded that mineralised intrusions contained at least 2000 ppm sulfur while barren intrusions contained <500 ppm.

In granitic magmas, sulfur will partition into to the aqueous fluids during second boiling and the granite will be depleted in sulfur unless it acquires additional sulfur through assimilation of rock sulfur (Burnham, 1979). For example, in calculating the concentration of sulfur in aqueous fluids in equilibrium with sulfide minerals, Ohmoto (1986) concluded that for every 1 wt.% H_2O exsolved from a melt, 1,000 to 10,000 ppm of sulfur is removed from the granite magma. Thus, ore-bearing granites, and particularly porphyry copper-molybdenite deposits, must have high initial sulfur contents. For granites with sulfur contents of 2,000 ppm (porphyry copper type values), the association with mineralisation implies an initial sulfur content of >5,000 ppm before second boiling (Ohmoto and Goldhaber, 1997). The Darwin and Murchison Granites contained an average of 1.5 and 2.5 wt.% LOI respectively but the proportion of water is unknown. However, a review of water contents in I-type Lachlan Fold Beld granites (Chappell, 1984; Chappell and White, 1992) and other granites (Taylor, 1977; Manning and Pichavant, 1988; Clark, 1992) shows that the average water contents of granites is ~1.3 wt.%. In addition, Darwin Granite whole rock samples observed in the current study have low sulfur contents (averaging below the detection limits of 100 ppm; Appendix C) implying that the granites had low initial sulfur contents before second boiling or that sulfur was leached from the rocks by heated indrawn metamorphic waters. The Darwin Granites then, may fit the description of barren intrusions as described by Mutschler (1981), although the same can not be unambiguously said for the Murchison Granite because no whole rock sulfur data are available

9.4.3 Seawater Sulfur

What is the influence of Cambrian seawater on the sulfur isotope values? Claypool et al. (1980) demonstrated that, although modern day seawater sulfur has a value of +20‰, this value has varied through geological time from a low of about 10‰ in the Permian to a high of 35‰ in the

Cambrian. The spread of Cambrian seawater $\delta^{34}S$ values is 26‰ to 36‰ (Claypool et al., 1980) with an average around +30‰. This is consistent with the value quoted for Cambrian seawater (Solomon et al., 1988). Experimental data and theoretical models for seafloor hydrothermal systems indicate that the circulation of seawater through the upper crust results in anhydrite precipitation at temperatures between 150 and 200°C (Shanks et al., 1981). Part of the seawater sulfate precipitates as anhydrite, but a remnant fraction of seawater sulfate enters the hotter portions of the hydrothermal system (Shanks et al., 1981; Herzig et al., 1998). Leaching additional Ca from the host volcanics increases anhydrite precipitation, but even if Ca-rich basalts are leached, some excess sulfate remains in the hydrothermal seawater (Bischoff and Dickson, 1975). In the study area, precipitation of significant additional sulfate as anhydrite was precluded by the low Ca content (average 0.46 wt.%, Table 4.1) of the host volcanics, a conclusion similar to that of Polya et al. (1986) for the Murchison Granite.

9.4.4 Formation Mechanism for 5‰ to 9‰ Sulfide Population

There are several possible explanations for $\delta^{34}S$ values between 5‰ and 9‰: 1) they were in isotopic equilibrium with reduced seawater, 2) they represent leached igneous sulfur derived from the host volcanics, or 3) they represent a mixture of primary magmatic sulfur and reduced seawater sulfate. $\delta^{34}S$ values of hydrothermal barite cluster around 30‰, the Cambrian seawater value. Values lower than 30‰ require contributions from lighter sulfate sources such as local oxidation of isotopically lighter H_2S or sulfide minerals, lighter magmatic sulfate (in high sulfidation systems) whereas values >30‰ indicate local partial hydrothermal reduction of seawater sulfate by the isotopic enrichment of *residual* sulfate (Shanks et al., 1981). Typically, residual sulfate becomes dramatically heavier as a significant fraction of H_2S is produced by reduction. The H_2S isotopic value is always less than the sulfate value by the equilibrium fractionation value (Δ), a temperature dependent function. At Taylours Reward, two chalcopyrite samples with $\delta^{34}S$ values near 5‰ occur in barite ($\delta^{34}S$ = +30‰) veins (Solomon et al., 1988; Gadaloff, 1996). Solomon et al. (1988) have calculated that the barite was in isotopic equilibrium with the chalcopyrite and probably precipitated from reduced seawater sulfate at temperatures 250°-300°C. However, this explanation for $\delta^{34}S$ values between 5‰ and 9‰ near the granite contact is considered unlikely due to the lack of appreciable barite, the hypothesised low W/R values and the higher temperatures near the granite contact. Although, $\delta^{34}S$ values between 5‰ and 9‰ are consistent with leached igneous sulfur derived from the host volcanics (~6‰) mixing with a minor amount of reduced seawater sulfate, several problems with this model exist; 1) oxygen isotope systematics are consistent with a magmatic hydrothermal fluid (~6‰), and 2) the low W/R values preclude significant leaching.

Mixing of isotopically heavy seawater sulfur with sulfur of magmatic origin could readily explain the isotopic variations observed in the Jukes-Darwin area. With magmatic $\delta^{34}S$ values near 6‰, and low W/R values, the contribution of sulfur from seawater sulfate reduction or modified rock sulfur was minimal for $\delta^{34}S$ values in the 5‰ to 9‰ range. However, with an increase in W/R values as the hydrothermal system developed, sulfate was retained in solution to higher

temperatures as larger water volumes passed through previously altered rock that had already been depleted in Ca, such as the Jukes feldspar-phyric dacites. In the contact zone of the Darwin Granite, mixing of isotopically heavier seawater sulfur with variable proportions of magmatic and rock sulfur (6‰) resulted in increasingly heavier sulfur values (10-19‰) occurring in the same rocks as lighter 5‰ to 9‰ values. In this zone, two populations of $\delta^{34}S$ values (10‰ to 12‰, and 15‰ to 17‰) occur within a distance of <30 metres from the granite contact in the same rocks as 5‰ to 9‰ values. Although zoning was not recognised, the simultaneous occurrence of three sulfide populations over a 30 meter distance is interpreted to relate to increasing W/R values and increasing reduced Cambrian seawater components outward from the centre of the alteration system. A similar explanation is interpreted to explain zoning in vein assemblages observed at the Jukes Prospect.

9.4.5 Sulfate Compositions

MRV dacites and the Darwin Granite have Ba concentrations that are typically >1000 ppm (Appendices D and J) and significant Ba probably existed in all of the hydrothermal fluids exsolving from the Darwin Granite. Within the Darwin Granite $\delta^{34}S_{barite}$ value in veins is +29‰ (Jones, 1993) and the range throughout the Jukes-Darwin area is 28-30‰ (Table 9.4). Solomon et al. (1988) argued that in felsic rocks, the reducing agents (normally Fe^{2+}) can be totally reacted throughout the hydrothermal system and sulfate reduction cannot proceed to completion. The reduction of seawater sulfate at high temperatures (>250-400^{O}C) and low W/R values is rapid and quantitative and does not lead to isotopic fractionation (Shanks et al., 1981; Ohmoto and Lasaga, 1982; Shanks and Seyfreid, 1987; Alt, 1994). In other words, the initial Cambrian seawater value of around 30‰ should have remained unchanged in this instance. The increased content of seawater sulfate in late stage oxidised fluids can account for most of the barite precipitation in the Jukes-Darwin system. However, some of the barite precipitated directly from seawater in isotopic equilibrium with coexisting sulfides and has $\delta^{34}S$ values higher than the coeval fluid (Shanks et al., 1981), the case observed at Taylours Reward (Solomon et al., 1988). Cambrian seawater sulfate values were maintained in solution to high temperatures by high water volumes (high WR) rapidly passing through previously altered rock previously depleted in Ca, such as the Jukes feldspar-phyric dacites. Precipitation of barite in the early and main stages of hydrothermal activity was probably precluded due to temperatures >400^{O}C and occurred only in later stages when the hydrothermal system cooled to <300^{O}C.

9.4.6 Heavy Sulfide Populations

The highest $\delta^{34}S_{sulfide}$ values, 22-26‰ (Table 9.3, Figure 9.3) were observed in chalcopyrite from a magnetite-hematite-quartz vein and a barite vein at East Darwin (Gadaloff, 1996) and from pyrite in a late stage quartz vein at the Jukes Prospect (this study). All heavy $\delta^{34}S$ values in sulfide and sulfates are confined to wide (>1 cm) veins, of either late stage hydrothermal or metamorphic origin. The late hydrothermal veins are interpreted to have acted as conduits for seawater during late stage pulsing or collapse of the hydrothermal system. Carbonate was observed in the late hydrothermal veins at the Jukes Prospect (this study) and barite was observed in similar veins in a study by Doyle (1990). If pyrite and chalcopyrite replaced barite, replacement must have

occurred after barite deposition late in the hydrothermal systems cycle or during later metamorphism. Based on sulfur isotope data, Gadaloff (1996) concluded that chalcopyrite, remobilised during Delamerian metamorphism, replaced barite in veins on Intercolonial Spur. Therefore, the high $\delta^{34}S_{sulfide}$ values (22-26‰), represent late stage precipitation during late hydrothermal or a subsequent metamorphic event.

The range of $\delta^{34}S$ values observed at the Jukes Prospect and in the King River Tunnel is similar to the range of values that occur at East Darwin, Intercolonial Spur and the contact zone of the Darwin Granite (Figure 9.4). Throughout the Jukes-Darwin area, sub-group values in the range of 10‰ to 14‰ consistently occur within and surrounding M1 veins. As demonstrated by Ohmoto and Lasaga (1982), $\delta^{34}S_{sulfide}$ values decrease with increasing temperatures (Figure 9.4). Although sulfide pairs were not sampled, and direct temperatures of precipitation have not been determined, the data supports the interpretation that higher temperatures controlled the $\delta^{34}S_{sulfide}$ values within the cores of the M1 vein systems at and or near the Darwin Granite contact.

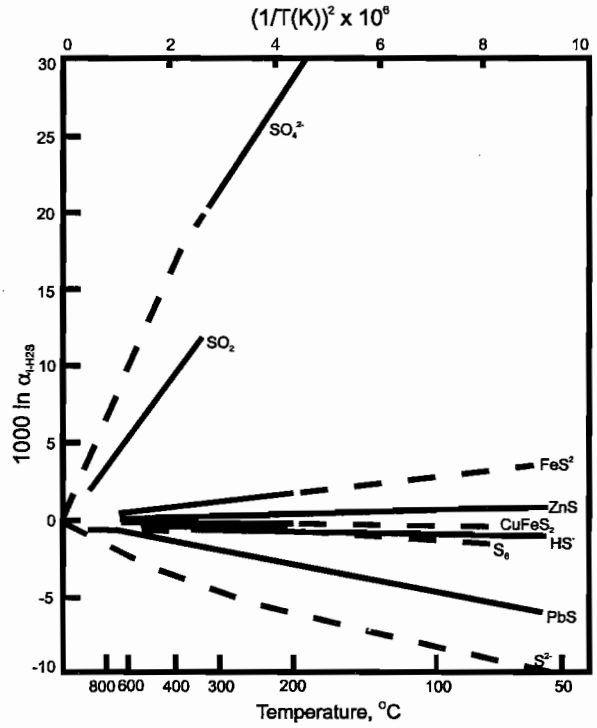

Figure 9.4. Equilibrium isotopic fractionation factors among sulfur compounds relative to H_2S. Solid lines are experimentally determined. Dashed lines are extrapolated or theoretically calculated. Figure modified from Ohmoto and Lasaga (1982) and Ohmoto and Goldhaber (1996).

9.5 A REVIEW OF PREVIOUS SULFUR ISOTOPE STUDIES IN THE JUKES-DARWIN AREA AND COMPARISONS TO THE CURRENT STUDY

Previous sulfur isotope studies within the Jukes-Darwin area were carried out by Polya et al. (1986), Eastoe et al. (1987), Solomon et al. (1988), Doyle (1990), Jones (1993) and Gadaloff (1996). Their $\delta^{34}S$ results for sulfide and sulfate minerals are summarised and compared to results for other mineral deposits in the MRV in Tables 9.3 and 9.4.

Table 9.3. A comparison of $\delta^{34}S_{sulfide}$ data for mineral deposits in the MRV. $\delta^{34}S_{sulfide}$ values >10‰ are interpreted to represent variable proportions of mixing with Cambrian seawater (30‰). However, $\delta^{34}S_{sulfide}$ values <10‰ are interpreted to be magmatic values as discussed in the text. The entire range of values is shown and the mode for the population is indicated by the peak. Data summarised from Solomon et al. (1969, 1988), Polya et al. (1986), Eastoe et al. (1987), Doyle (1990), Raymond (1992), Jones (1993), Large (1995, pers. com.), Gadaloff (1996), Duncan (1997) and this study. $\delta^{34}S_{sulfide}$ values in per mil.

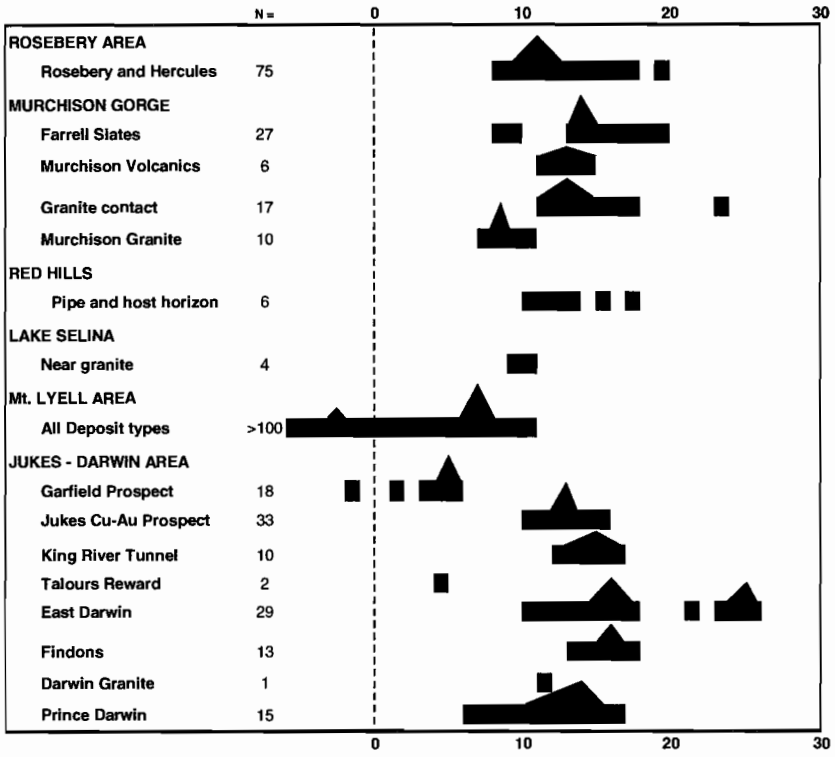

Table 9.4. A comparison of $\delta^{34}S_{sulfate}$ data for mineral deposits in the MRV. The Cambrian seawater $\delta^{34}S_{sulfate}$ value is about 30‰ (Claypool et al., 1980). $\delta^{34}S_{sulfate}$ values near 30‰ precipitated directly from seawater without significant fraction, values appreciably higher than 30‰ represent values produced by partial reduction but in isotopic equilibrium with coexisting sulfides, and values lower than 30‰ indicate contributions from local oxidation of isotopically lighter H_2S or sulfide minerals (Green et al., 1981; Solomon et al., 1988). The entire range of values is shown and the mode for the population is indicated by the peak. Data summarised from Solomon et al. (1969, 1988), Doyle (1990), Abbott (1992), Jones (1993), Gadaloff (1996) and this study. $\delta^{34}S_{sulfate}$ values in per mil.

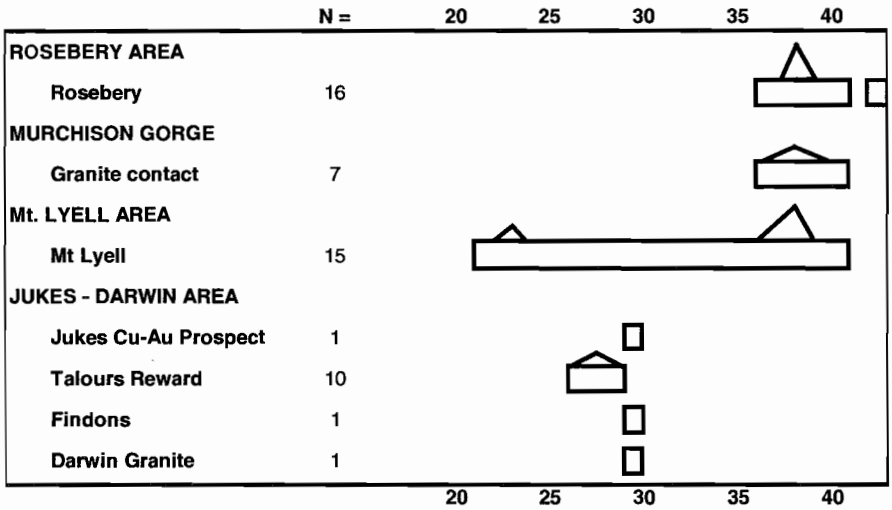

In the hydrothermal systems associated with the Darwin and Murchison Granites, hydrothermal sulfur has been interpreted to be a mixture derived from the host volcanics, granites, and sulfate derived from reduced Cambrian seawater (Polya et al., 1986; Solomon et al., 1988; Jones, 1993). Solomon et al (1988) interpreted the $\delta^{34}S$ values for many of the VHMS deposits in the MRV (7-15‰) to be the result of similar mixing.

Jones (1993) suggested that a spatial relationship existed between distance from the Darwin Granite and heavier sulfur isotope values, and showed that the average $\delta^{34}S$ values for sulfides at the East Darwin, Findons and Lake Jukes prospects increased with distance from the surface exposure of the granite. Table 9.2 shows that the ranges of $\delta^{34}S_{sulfide}$ values for all of the deposits overlap and a detailed examination of the sulfide-bearing mineral parageneses suggests that zoning does not occur on the scale Jones (1993) suggested. Results of the current study and that of Solomon et al. (1988) indicate that $\delta^{34}S_{sulfide}$ values ranging from 7‰ to 9‰ are confined to a zone within several metres (<10) of granite contacts and do not occur outside that zone (except for the two samples from Taylours Reward). At the Darwin Granite, $\delta^{34}S_{sulfide}$ values in the range of 10.3‰ to 17.0‰ overprinted lower $\delta^{34}S_{sulfide}$ values as a result of increasing W/R values and the increasing influence of reduced Cambrian seawater, consistent with the model of Solomon et al. (1988). The narrow zone of increasing $\delta^{34}S$ values with increased distance from the Darwin Granite is similar to the relationship observed by Polya et al. (1986) in the Murchison Gorge.

Solomon et al. (1988) proposed an explanation for the spatial distribution observed at the Darwin Granite. In the early hydrothermal stages of the system, sulfur saturation was confined to the granite and its close contacts (where mixing with magmatic sulfur was significant). In the later stages, seawater sulfur saturation took place throughout the whole hydrothermal system, reducing the effect of magmatic sulfur input. Based on sulfur isotopic evidence, Solomon et al. (1988) concluded that the Jukes Prospect was a late epigenetic vein system related to Late Cambrian fluid circulation and sulfide dissolution. This interpretation was based on a geological interpretation that placed the Jukes Prospect in Tyndall Group rocks that post-dated Darwin Granite emplacement (Chapter 4). Subsequent work by Doyle (1990) and the current study have demonstrated that the Jukes Prospect is hosted in CVC and EQPS rocks that pre-date the Darwin Granite intrusion. Similarities in mineralisation styles throughout the Jukes-Darwin field, combined with CVC host rocks, support the interpretation that most alteration and mineralisation was related to the Middle Cambrian intrusion of the Darwin Granite and not to a Late Cambrian event. However, minor remobilisation during Delamerian metamorphism or a subsequent metamorphic event as proposed by Gadaloff (1996) for the East Darwin prospect cannot be ruled out.

The heavier $\delta^{34}S$ values for sulfate in the Jukes-Darwin area (28-30‰) compared to other mineralised fields in the MRV (Table 9.3) was discussed by Solomon et al., (1988). They concluded that for the northern mineral fields (eg. Rosebery), the nature of the hydrothermal solutions and the hangingwall sequence inhibited oxidation and subsequent modification of the Cambrian sulfur isotope values. Whereas, in the Jukes-Darwin area, the circulation of weakly acid, oxidised fluids (evidenced in the study area by the common presence of magnetite-hematite veins), caused partial reduction of the Middle Cambrian seawater sulfur resulting in a mixture of

$\delta^{34}S$ values. At Mt. Lyell, barite precipitated when weakly acid, reduced sulfide-rich fluids transitioned into highly oxidised conditions and lower temperatures at the contact of the Owen Conglomerate and the underlying volcanics (Hart, 1993).

At the Garfield Prospect, $\delta^{34}S$ values in pyrite and chalcopyrite range from -2‰ to +6.1‰ (n = 17, Halley et al., 1996; Duncan, 1997). Fifteen samples fall within the range of 4.7‰ to 6.1‰ (ave. 5.0‰); the other two values are -2‰ and +1.5‰. The sulfur isotope values at the Garfield Prospect are among the lowest within the MRV, and are shown in relation to other mineralised areas in Table 9.3. All of the values fall within the same range as the Prince Lyell ores at Mt. Lyell, although the average $\delta^{34}S$ value (5‰) is lower than the Mt. Lyell average (7‰). Halley et al. (1996) and Duncan (1997) interpreted the $\delta^{34}S$ values from the Garfield andesites as magmatic values. Light REE and P_2O_5 enrichment and high-K affinities of the Suite II andesites are similar to island arc andesites (Crawford et al., 1992) that typically have $\delta^{34}S$ values between +5 and +7‰ (avg. +4 to 5‰, Ueda and Sakai, 1984; Woodhead et al., 1987). This supports to the interpretation of Halley et al. (1996) and Duncan (1997) that the average $\delta^{34}S$ values (5‰) for the Garfield andesites are primary magmatic values.

9.6 A SUMMARY OF SULFUR AND LEAD ISOTOPES IN THE MT. LYELL FIELD

Sulfur and oxygen isotope analyses of sulfides and sulfates (barite) from the Blow, West Lyell, Tasman, Crown Lyell Extended, North Lyell, Crown Lyell and King Lyell were obtained by Solomon et al., (1969). Although there is a continuum of $\delta^{34}S_{sulfide}$ values from -6‰ to +11‰, two separate peaks in the population occur, a lighter group with values averaging -2.7‰ and a heavier group averaging 7‰ (Figure 9.1). Solomon et al. (1969) favored a model for the lighter group (-2.7‰) involving mobilisation of lighter sulfur during Devonian metamorphism or late volcanic activity. In addition, based on $\delta^{18}O$ values in barite, a possible meteoric water contribution was recognised. The heavier group of $\delta^{34}S_{sulfide}$ values (7‰) represent either; 1) sulfide produced as a result of mixing between magmatic (or rock sulfur, $\delta^{34}S$ value 0 to 8‰) and seawater modified felsic volcanic rock sulfur (10-15‰); or 2) primary magmatic sulfur. Sulfur and oxygen isotope signatures at Western Tharsis support a model involving convective Cambrian seawater with a component of magmatic input (Manning, 1990) and the Comstock deposit was interpreted to be a typical VHMS deposit (Walshe, 1977; MacDonald, 1991).

Walshe (1977), concluded, based on $\delta^{34}S$ from sulfides and sulfates, that 1) Cambrian seawater had mixed with igneous rock sulfur in forming ores at Prince Lyell and 2) that sulfur isotopic zoning did not occur. Later studies (Walshe and Solomon, 1981; Solomon et al., 1988; Raymond, 1996) on Prince Lyell supported Walshe's interpretation. Solomon et al. (1988) recognised that the $\delta^{34}S$ values (range 5-11‰, av. 7‰) were too low for a seawater-dominated hydrothermal system and were rock-dominated, probably by leached basement basaltic rocks with $\delta^{34}S$ values near 0‰. Halley et al. (1996),argued that the average sulfur isotope values for Prince Lyell are too low to be derived by leaching modified rock sulfur from felsic rocks, and that the likely sulfur source was either the nearby Suite II andesites, or from direct magmatic input. This argument is

supported by modified rock $\delta^{34}S$ values of 10-15‰ from least-altered felsic volcanics in the CVC south of the Henty Fault that have equilibrated with Cambrian seawater sulfate during burial (Davidson and Kitto, 1997).

Solomon et al. (1988) estimated that a 400 km^3 convection cell would yield 5 x 10^{12} grams (g, 0.5 Mt) of sulfur by leaching one third of the available sulfur from a volcanic pile that was composed primarily of felsic rocks. Within the mine stratigraphy at Mt. Lyell a zone of quartz sericite-chlorite-pyrite hydrothermal alteration styles 10 km long by 0.5 km wide by 3 km deep contains >5% pyrite (Wills, 1995) and hosts 19 of the 22 known Mt. Lyell ore deposits. The amount of sulfur in the >5% pyrite alteration envelope (excluding the sulfur in the ore deposits) is calculated to be more than 7 x 10^{14} g (70 Mt). When the sulfur in the ore deposits and associated hydrothermal alteration zones (with >1% and <5% pyrite) is included, the amount of sulfur at Mt. Lyell is >12 x 10^{14} g (120 Mt). By comparison, the Rosebery VHMS deposit contains 10^{13} g (10 Mt) of sulfur (Solomon et al., 1988). Using similar calculations for Fe yields 2 x 10^{15} g (2000 Mt) Fe. Since a 400 km^3 convection cell yields 5 x 10^{12} g (0.5 Mt) sulfur, a *significant* additional component of sulfur (ie. 94%) from other sources such as reduced seawater sulfate or magmatic sulfur is required. Solomon et al. (1988) used similar calculation to those above for other metals and concluded that there must be a significant magmatic contribution of metals to the ores.

Convection cell models for the formation of VHMS deposits have been proposed by several authors (Cathles, 1978; Cann and Strens, 1982; Cathles, 1983; Cann et al., 1985; Strens and Cann, 1986) but struggle with explanations for deposits with >3 million tons. Cathles (1978; 1983) calculated that even if ore fluids contained 100 ppm Cu, metal availability from magmatic sources alone was several orders of magnitude to low to form the Kuroko VHMS deposits. Similarly, Cann and Strens (1982) and Strens and Cann (1986) used a fracture model for hydrothermal convection at mid-oceanic ridges and showed that sustained discharge of hydrothermal fluid at temperatures >300^{O}C could not be maintained for more than 100 years. Cann et al. (1985) calculated that if the heat were extracted from a 30 km^3 convecting basaltic magma chamber, a 350^{O}C ore fluid would only deposit 3 million tons of iron in 4000 years, assuming 70% accumulation at the seafloor and 115 ppm Fe. Therefore, it is apparent from the convection models that enormous volumes of magma are required to form deposits with >100 million tons and $\delta^{34}S$ values must reflect a modified rock and modified seawater signature. In the stratal aquifer model (Hodgson and Lydon, 1977; Lydon, 1988), ore fluids originate as pore waters in a porous rock unit (aquifer) which have been prevented from migrating during burial and compaction due to overlying impermeable cap rocks. This model allows large volumes of fluid to accumulate at relatively shallow depths (<1 km) at ore forming temperatures (>300^{O}C) in volcanically active areas. When released, these fluids can reach an ore horizon in a short period of time and deposit large tonnage VHMS ores. However, as with the convection cell models, $\delta^{34}S$ values must reflect a modified rock and modified seawater signature. In magmatic hydrothermal models (Solomon, 1976; Urabe and Sato, 1978; Sawkins and Kowalik, 1981), higher concentrations of metal and magmatic sulfur can be contained in late stage ore forming volatiles resulting from magmatic fractionation. These fluids will reflect magmatic $\delta^{34}S$ values and as demonstrated with porphyry-copper systems, large tonnages can be achieved. Although none of

the models presented can be simply applied to the Mt. Lyell deposits, $\delta^{34}S$ values strongly suggest a magmatic input with a minor contribution from modified rock sulfur.

If the Mt. Lyell disseminated Cu-Au deposits formed as a result of granite intrusion, as suggested by Large et al. (1996), well-constrained $\delta^{34}S$ values (7‰) would suggest mixing with substantial modified rock sulfur or modified seawater did not occur. In the Jukes-Darwin hydrothermal system, higher W/R values around the granites resulted in $\delta^{34}S$ values increasing to 10‰ to 14‰, and 15‰ to 19‰ in the M1 and M2 phases respectively. This is interpreted then, as evidence that seawater-dominated fluids did not overprint the Mt. Lyell disseminated pyrite-chalcopyrite orebodies, in contrast to the Jukes Darwin mineral deposits.

9.7 A SULFUR ISOTOPE MODEL FOR THE Cu-Au ORES IN THE JUKES-DARWIN AREA

The $\delta^{34}S$ value of a hydrothermal fluid cannot be directly estimated from the $\delta^{34}S$ value of the sulfide mineral unless variables such as fO_2 and pH are known (Ohmoto and Rye, 1979). In addition, the $\delta^{34}S$ value of a sulfide mineral cannot be used to directly determine the source of the sulfur since, in addition to fO_2 and pH, it is a function temperature. However, given limited sources for sulfur, a knowledge of the geologic setting, hydrothermal alteration and mineralisation paragenesis, a four stage model for sulfur isotope evolution is proposed and is summarised on Figure 9.6. The model corresponds to the four phases of alteration and mineralisation (excluding the hydrothermal breccia emplacement) discussed in Section 7.4.

A) Early sulfide formation: During intrusion of the Darwin Granite, magmatic sulfur (6‰) mixed with rock sulfur (10-15‰) that had previously equilibrated with Cambrian seawater. Due to low W/R values, the effects of magmatic sulfur-dominated the sulfur budget near the granite contact, resulting in $\delta^{34}S$ values in the contact zone of 7‰ to 9‰. The low $\delta^{34}S$ values near the Darwin Granite do not occur higher in the section. This distribution suggests that in the early hydrothermal stages of alteration and mineralisation, sulfide saturation was confined to the granite and its contacts (Solomon et al., 1988) where mixing between magmatic sulfur and rock sulfur were significant. Seawater infiltration into the deeper volcanic pile had not begun, and the seawater contribution was negligible.

B) Middle alteration (M1): W/R values increased after initial hydrofracturing and formation of M1 vein systems (Section 7.4.2). Heated Cambrian seawater began to circulate to deeper levels of the hydrothermal cell. The limited magmatic sulfur content of the magmatic fluids (<100 ppm) was overwhelmed by seawater sulfur and resultant $\delta^{34}S$ values in M1 veins increased to 10‰ to 14‰. Variability in $\delta^{34}S$ values was enhanced by variations in fO_2, temperature and seawater sulfur contents.

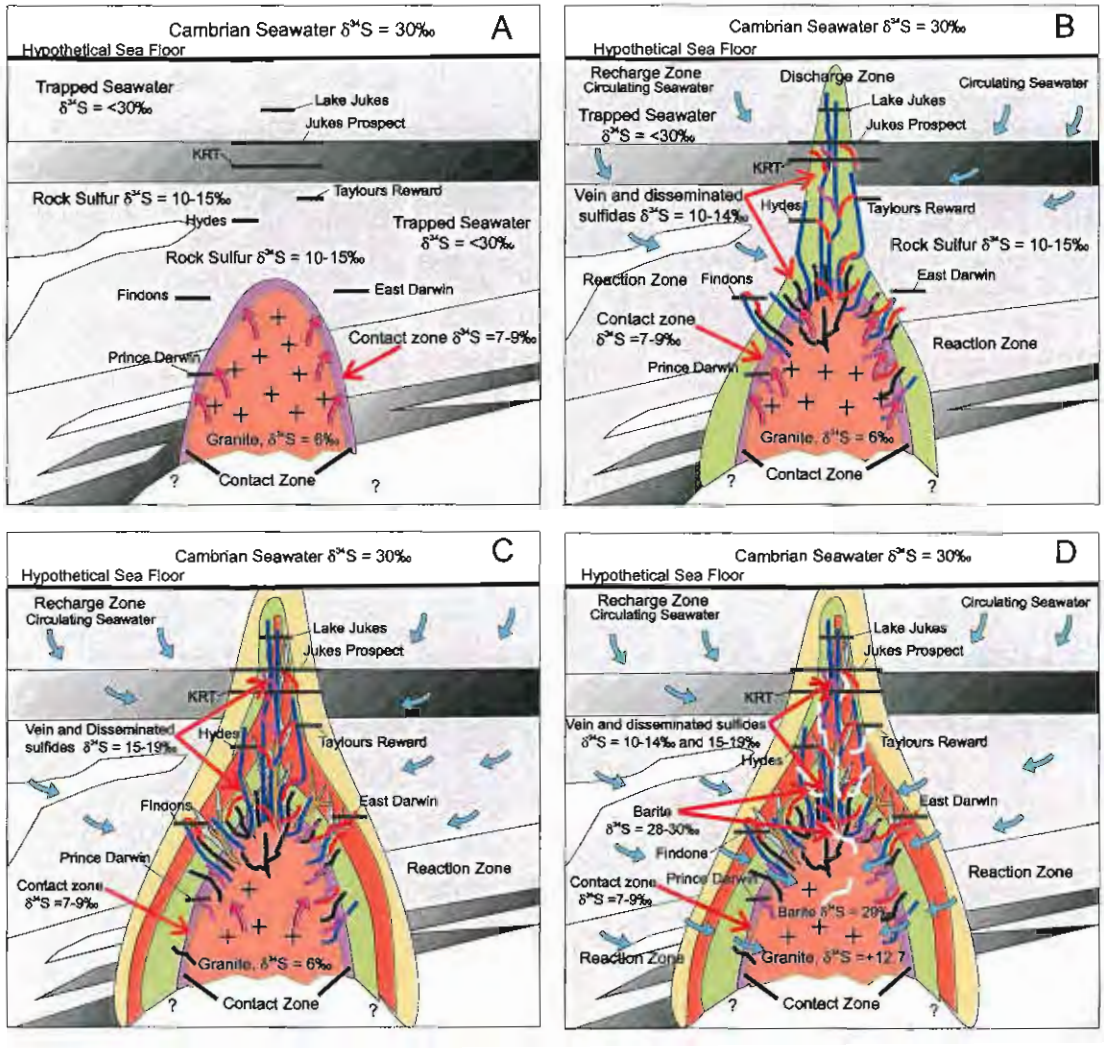

Figure 9.5. Cross-section illustrating the interpreted paragenetic sequence of sulfur isotopes in the Jukes-Darwin system. A) During intrusion of the Darwin Granite, magmatic sulfur (6‰) mixed with rock sulfur (10-15‰) that had previously equilibrated with seawater, resulting $\delta^{34}S$ values in the contact zone from 7-9‰. Initial seawater infiltration into the deeper volcanic pile had not yet begun. B) Initial hydrofracturing and M1 vein formation resulted in higher W/R values. Resultant $\delta^{34}S$ values in the veins are 10-14‰ and variable due to variations in fO_2, temperature and associated fluid $\delta^{34}S$ values. C) During and after breccia intrusion, the circulation system became better established. M2 veins disseminated mineralisation formed with higher $\delta^{34}S$ values (15-19‰) due to interaction with descending seawater. D) As the hydrothermal system collapsed due to loss of heat, unreacted seawater swamped the remaining hydraulic conduits and precipitated barite. Barite veins (around 30‰) within the Darwin Granite and Darwin Granite whole rock value of 12.7‰ support this interpretation.

C) Middle alteration (M2): After breccia formation, the hydrothermal circulation system became well-established and M2 veins formed (Section 7.4.4). Although significant anhydrite was likely to precipitate at shallower levels in the crust, seawater sulfate values were probably maintained in solution to high temperatures by high water volumes (high W/R) passing through previously altered rock that had been depleted in Ca, such as the Jukes feldspar-phyric dacites. The excess seawater sulfur saturated the hydrothermal system, resulting in $\delta^{34}S$ values ranging from 15-19‰ in M2 veins and disseminated mineralisation.

D) Late stage sulfide and sulfate formation: As the granite began to cool, and the hydrothermal system began to collapse, finally, seawater penetrated into the Darwin Granite itself. Multiple

pulses of fluid with variable chemistry resulted in variable $\delta^{34}S$ compositions forming in close proximity. The $\delta^{34}S_{sulfate}$ value of barite (29‰) within the Darwin Granite, the range of $\delta^{34}S_{sulfate}$ values throughout the Jukes-Darwin area (28-30‰) and Darwin Granite whole rock value of 12.7‰ support this interpretation. High Ba is a characteristic of the Darwin Granite therefore high concentrations of Ba in granitic fluids are assumed. Precipitation of barite occurred when the hydrothermal system cooled sufficiently to allow free sulfate to be available (<300^{o}C), was rapid and did not lead to isotopic fractionation, i.e., the initial Cambrian seawater value of around 30‰ remained unchanged.

9.8 SUMMARY

In previous sulfur isotope studies of granite-related Cu-Au mineralisation in the MRV (eg., Solomon et al., 1969; Walshe, 1977; Green et al., 1981; Polya, 1981; Polya et al., 1986; Eastoe et al., 1987; Solomon et al., 1988; Doyle, 1990; Manning, 1990; Jones, 1993; Gadaloff, 1996), no attempt was made to quantify the magmatic $\delta^{34}S$ value. The magmatic value was simply assumed to be near 0‰, and as a result, magmatic contributions to the sulfur budget were probably underestimated and seawater contributions overestimated. For example, if the magmatic $\delta^{34}S$ value was near 0‰, the seawater contribution to a $\delta^{34}S$ value of 7‰ is >75% (assuming $\delta^{34}S_{seawater}$ = 30‰). In contrast, if the magmatic $\delta^{34}S$ value was nearer 6‰, the resultant seawater contribution is <25% of the total sulfur. This mixture assumes that the seawater sulfate value was unchanged by other fractionation processes. Although direct analyses of whole rock sulfur isotope compositions of the Darwin Granite failed, the Cambrian granites are crustal melts (Chapter 3). Therefore, it is reasonable to assume that the magmatic $\delta^{34}S$ value was nearer to 6‰ than 0‰, consistent with other I-type magnetite series granites worldwide (Ohmoto and Rye, 1979; Sasaki and Ishihara, 1979). A more realistic assumption for initial mixing is magmatic water and modified volcanic rock sulfur ($\delta^{34}S$ values of 10-15‰). With this combination of sulfur sources, the magmatic contribution is probably between 65 and 75% of the total sulfur budget. The model presented for the Jukes-Darwin hydrothermal system suggests that the initial sulfur budget was dominated by magmatic and volcanic rock sulfur (>75%), and the seawater contribution was minor (<25%). In the main circulation stages of the Jukes-Darwin field (M1 and M2), $\delta^{34}S$ values are interpreted to be a decreasing combination of rock sulfur and magmatic sulfur and an increasing volume of reduced seawater sulfate, consistent with the arguments of Solomon et al. (1988). A similar relationship occurs at Lake Selina (Solomon et al., 1988; Hunns, 1997) and the Murchison Granite (Polya et al., 1986) and a similar origin is proposed. Although, as Solomon et al. (1988) point out, the processes are not necessarily coeval.

Based on sulfur isotopic evidence, Solomon et al. (1988) concluded that the Jukes Prospect was a late epigenetic vein system related to Late Cambrian fluid circulation and sulfide dissolution. This interpretation was based on a geological interpretation that placed the Jukes Prospect in Tyndall Group rocks and therefore, post-dated Darwin Granite emplacement (Chapter 4). Subsequent work by Doyle (1990) and the current study have demonstrated that the Jukes Prospect is hosted in CVC and EQPS rocks that predate the Darwin Granite intrusion. Similarities in mineralisation styles throughout the Jukes-Darwin field, combined with CVC/EQPS host rocks,

support the interpretation that major alteration and mineralisation was related to the Middle Cambrian intrusion of the Darwin Granite and was not a Late Cambrian event. However, minor remobilisation by subsequent metamorphic events was possible (Gadaloff, 1996).

Prince Lyell $\delta^{34}S$ values are similar to $\delta^{34}S$ values from the andesite hosted Que River and Hellyer VHMS deposits (+5‰ to +11‰, McGoldrick and Large, 1992), the Garfield Prospect (+5‰), and the Cambrian granites (6‰). As demonstrated near the Darwin Granite, $\delta^{34}S$ values increase with increasing distance from the granite contact due to increasing seawater contributions. Therefore, unless the sulfur source was deep beneath the Prince Lyell deposit, it would be unlikely that the $\delta^{34}S$ values would be maintained throughout the Mt. Lyell orebodies without recognizable contributions from the host volcanics, Cambrian seawater or the effects of hydrothermal system collapse. The Prince Lyell $\delta^{34}S$ values are interpreted to be magmatic values, but are not uniquely definitive of a genetic source of sulfur. Therefore, based on $\delta^{34}S$ values, either the Suite II andesitic magmas or Cambrian granites could have provided the magmatic sulfur in the Mt. Lyell pyrite-chalcopyrite ores.

CHAPTER 10

10.0 SUMMARIES, CONCLUSIONS AND GENETIC MODEL FOR THE JUKES-DARWIN HYDROTHERMAL SYSTEM

10.1 INTRODUCTION

The relationship, if any, between Cambrian granite-related Cu-Au mineralisation and Cu-Au mineralisation at Mt Lyell is one of the more interesting dilemmas in the geology of the MRV. Due to its proximity to Mt. Lyell, comparisons with the Darwin Granite and related Cu-Au mineralisation in the Jukes-Darwin field are inevitable.

A magmatic contribution to the ore fluids at Mt Lyell is not a new concept (Gregory, 1905; Loftus-Hills, 1927; Nye et al., 1934; Wade and Solomon, 1958). However, with the development of VHMS models (Markam, 1968; Solomon et al., 1969; Green, 1971; Bryant, 1975; Reid, 1975; Hendry, 1981; Walshe and Solomon, 1981; Braithwaite, 1985; Sheppard, 1987), the magmatic model has received little recent attention in recent times. Large et al. (1996) revived the model by suggesting that Mt. Lyell is part of a large, Cambrian granite-related hydrothermal system.

This chapter compares the Lyell and Jukes-Darwin mineral fields and proposes a genetic model for the formation of Cambrian granite-related Cu-Au mineralisation in the Jukes-Darwin area. The genetic model is subdivided into three sections: 1) background tectonic setting in which the Cambrian granites evolved, 2) an overall model for the formation of Cambrian granites and their relationship to associated Cu-Au deposits, and 3) a detailed genetic model for the Jukes-Darwin hydrothermal system.

10.2 A COMPARISON OF THE JUKES-DARWIN HYDROTHERMAL SYSTEM TO MT. LYELL

A total of 22 ore bodies are known to occur in the Mt. Lyell field, whereas none have been found in the Jukes-Darwin area. Since their hydrothermal alteration zones are of similar size, the question is, why the lack of minable size ore bodies in the Jukes-Darwin area? A review of the geology, alteration and mineralisation styles of the Mt. Lyell field is presented in Section 2.4. This section compares the findings of this study and others in the Jukes-Darwin area to the Mt. Lyell data and speculates on reasons for the differences.

10.2.1 Alteration Assemblages and Mass Changes

In the Jukes-Darwin system, hydrothermal sericite, chlorite and K-feldspar alteration assemblages occur throughout a 15 km long x 3 km wide zone that directly overlies the Darwin Granite and its subsurface northward extension. Vertically and laterally, pervasive hydrothermal alteration occurs at distances of at least 1.5 km from the granite margin, as observed in the Clark Valley, Intercolonial Spur and the Jukes Road area. Weak to moderate secondary sericite-chlorite

alteration assemblages are assumed to represent a transition from diagenetically altered and regionally metamorphosed volcanics inward to the peripheral hydrothermal alteration zones. Copper-gold bearing veins occur in moderate to intense chlorite, K-feldspar and silica altered rocks that contain <1% pyrite. Hydrothermal alteration assemblages and mineralised veins formed as a result of hydrofracturing of the cupola region above the granite. Fluid access was enhanced by hydrothermal brecciation that resulted in a series of barren alteration-related fracture networks and veins of magnetite and tourmaline.

At Mt. Lyell, a zone of pervasive sericite-chlorite-pyrite alteration assemblages similar in size to the Jukes-Darwin hydrothermal system encompasses much of the Mine Sequence. Throughout the Lyell Schist member, pyrite is abundant, averaging >5% (Wills, 1995). In the remaining Mine Sequence, pyrite averages >1%. The widespread sericite-chlorite-pyrite alteration assemblages suggest that hydrothermal fluids moved freely throughout the volcaniclastics. At Mt. Lyell, there is no evidence of hydrothermal brecciation and the larger Cu-Au deposits are typically disseminated.

Mt. Lyell Cu-Au deposits appear to distal from the source magma when compared to the Cu-Au prospects in the Jukes-Darwin area. Evidence in support of this argument includes:

- Hydrothermal alteration assemblages in the Jukes-Darwin area are typically enriched in K_2O (as secondary K-feldspar) compared to consistent depletions in K_2O at Mt. Lyell. At Mt. Lyell, hydrothermal K-feldspar does not occur and K_2O typically occurs in sericite.
- Significant mobility of SiO_2 and Al_2O_3 have been identified at Mt. Darwin proximal to the Darwin Granite. SiO_2 and Al_2O_3 remain immobile at Mt. Lyell (Manning, 1990; Huston, in press) except in silicified rocks in feeder zones at Twelve West and Western Tharsis.
- At Mt Darwin, due to proximity of the granite, K-feldspar and silica alteration assemblages are characterised by large mass gains in SiO_2 with smaller gains in Al_2O_3, K_2O, Cu and Ba (Table 6.7).
- At the Jukes Prospect, due to increased distance from the granite, K-feldspar, chlorite and sericite alteration assemblages are characterised by small mass gains in Fe_2O_3, MgO, K_2O and Cu as well as other trace elements (Table 6.6). Similar small mass gains in Fe_2O_3, MnO, MgO, P_2O_5, S, Cu, Zn, Ba, and Pb were noted at Prince Lyell and Western Tharsis (Sheppard, 1987; Raymond, 1992; Huston, in press).

10.2.2 Geochemistry

In the Mt. Lyell system, and particularly at Prince Lyell and Royal Tharsis, magnetite occurs in veins and disseminated domains associated with abundant apatite. Apatite REE patterns for the Prince Lyell and Garfield apatites are similar to the Suite I Murchison Granite and Suite II andesites (Figure 6.12), but are not similar to the Darwin Granite. $\varepsilon Nd_{(500Ma)}$ values for Garfield apatite closely match the $\varepsilon Nd_{(500Ma)}$ values of Suite II andesites (Table 6.4). However, $\varepsilon Nd_{(500Ma)}$ values for Prince Lyell apatites are identical to, and are interpreted to have been derived from, Suite I granites (Table 6.4).

$\delta^{18}O$ values in magnetite are interpreted to be indicative of magmatic waters in both the Jukes-Darwin and Mt. Lyell areas (Doyle, 1990; Raymond, 1992; Jones, 1993, and this study). This hypothesis is consistent with the observed $\delta^{34}S$ values. At Jukes-Darwin, $\delta^{34}S$ values from 5-9‰ overlap a similar range of values at Mt Lyell (6-11‰) and are interpreted to have formed as a result of mixing between early stage magmatic sulfur, volcanic rock sulfur and interstitial trapped seawater. However, at the Darwin Granite, sulfides with $\delta^{34}S_{sulfide}$ values in the range of 10-17‰ are spatially associated with 5-9‰ sulfides, suggesting increasing W/R values and overprinting by later Cambrian seawater sulfate-dominated fluids during collapse of the hydrothermal system. Increasing water to rock ratios and overprinting by later Cambrian seawater sulfate-dominated fluids during collapse of the hydrothermal system, such as observed in the Jukes-Darwin field, apparently did not occur at Mt. Lyell.

10.2.3 Summary and Speculation

The previous comparisons do not point to a definitive reason for the lack of orebodies in the Jukes-Darwin area and the abundance in the Mt. Lyell field. However, as a result of the comparisons between the Jukes-Darwin area and the Mt. Lyell field, the following speculations can be made:

- The Mt. Lyell orebodies occur at the intersection of a major northerly trending Cambrian graben fault and E-W transfer fault (Berry and Keele, 1997). The resultant deep crustal fractures could have tapped a deep magma body and provided abundant channelways and structural traps for rising magmatic fluids (Sections 2.3 and 10.5.1). Similar structures have not been identified in the Jukes-Darwin area.

- Better traps for mineralisation probably existed at Mt. Lyell. The host rocks for the Mt. Lyell field are primarily quartz-phyric volcaniclastics that have been intruded by andesitic sills and coherent rhyolitic and dacitic sills. Ore fluids could have migrated through the volcaniclastics and mixed with seawater beneath an appropriate aquiclude, such as a fault or impermeable sill, resulting in the precipitation of disseminated ores such as at Prince Lyell. In areas that lacked an appropriate aquiclude, widespread diffusion of magmatic fluids could occur resulting in formation of the large sericite-pyrite alteration halo.

- It is possible that there were different fluid compositions and/or different physicochemical conditions of ore mineral precipitation in the two fields, although the available data does not indicate any dramatic differences. Precipitation of the abundant ores at Mt. Lyell may have been a result of differences in metal contents, pH or sulfur content of the fluid.

The Darwin Granite has been deeply eroded at least twice, once in the Late Cambrian, prior to Tyndall Group deposition, and currently. It is possible that large orebodies related to the Darwin Granite, have been eroded away. The Mt. Lyell field has also been eroded, but the occurrence of typical seafloor VHMS deposits such as the Comstock and the Blow, suggest that the erosion level is not as deep, allowing preservation of near-seafloor ore deposits.

Whatever the reason for the differences between the Mt. Lyell and Jukes-Darwin area, further research focused on the genesis of Mt. Lyell is warranted.

10.3 DISCUSSION OF THE CAMBRIAN GRANITE-RELATED GENETIC MODEL OF LARGE ET AL. (1996)

There is little doubt, that the Cu-Au mineralisation styles in the Jukes-Darwin field, Murchison Gorge and numerous other smaller prospects are related to intrusion of Cambrian granites. However, the link between granites and mineralisation are less obvious at the Mt. Lyell mining field. Historically, the missing piece of the Mt. Lyell genetic story has been the lack of an appropriately sized heat engine capable of driving a world-class VHMS hydrothermal cell. The occurrence of an elongate belt of plug-like granites along the eastern margin of the MRV (Leaman, 1986; Leaman and Richardson, 1989), several kilometres east of Mt. Lyell, led Large, et al. (1996) to propose a model that assumes that the hydrothermal systems in the MRV are granite-related, and that the granites may contribute metals to the ore fluids. Similarities in hydrothermal alteration and mineralisation styles between the granite-related systems, pervasive replacement ore styles such as Prince Lyell and discrete focused exhalative VHMS centres such as the Blow and Comstock can all be accommodated in a genetic model involving Cambrian granites as the source of heat. However, the Prince Lyell deposit differs from the MRV granite-related alteration systems by its distinctive sulfur isotope values, sulfide veinlet stockworks, association of apatite with magnetite and lack of K-feldspar alteration assemblages.

One of the most significant factors that supports the granite model for Mt. Lyell is the geophysical evidence, which relies heavily of interpretation of aeromagnetic data (Large et al., 1996). Detrital magnetite in Tyndall Group volcanic rocks forces the magnetic susceptibility of Tyndall Group rocks to fall within the same range as the Cambrian granites, therefore, it is not possible to distinguish between buried Tyndall Group rocks and buried granite (Large et al., 1996). The Mt. Lyell Cu-Au deposits are located near a bulge in the postulated Cambrian granite ridge (Figure 3.1). Jukes-Darwin style hydrothermal alteration at the Lake Burbury prospect (Jaeger, 1996) is strong evidence of a granite at depth in that area, but the Mt. Lyell deposits are offset by 2-3 km to the west of the postulated Cambrian granite ridge, and no evidence for thrusting to the west exists (Berry, 1990; Berry, 1992b; Berry, 1992a; Berry and Keele, 1993b). Therefore, either the source granite for the Mt. Lyell magnetite-apatite mineralisation is too deep to be geophysically detectable or the fluids migrated from the east, consistent with the arguments of Raymond (1992, 1996).

On Figure 10.1, a modified version of the genetic model proposed by Large et al. (1996) shows a zone of granite style hydrothermal alteration underlying the zone of alteration and ore styles observed at Mt. Lyell. Between the two alteration zones, a transition zone of overlapping hydrothermal assemblages should be expected. It was suggested by Large et al. (1996) that the apatite-magnetite assemblage in the Prince Lyell deposit represented part of this link between the two mineralisation styles (Figure 10.1).

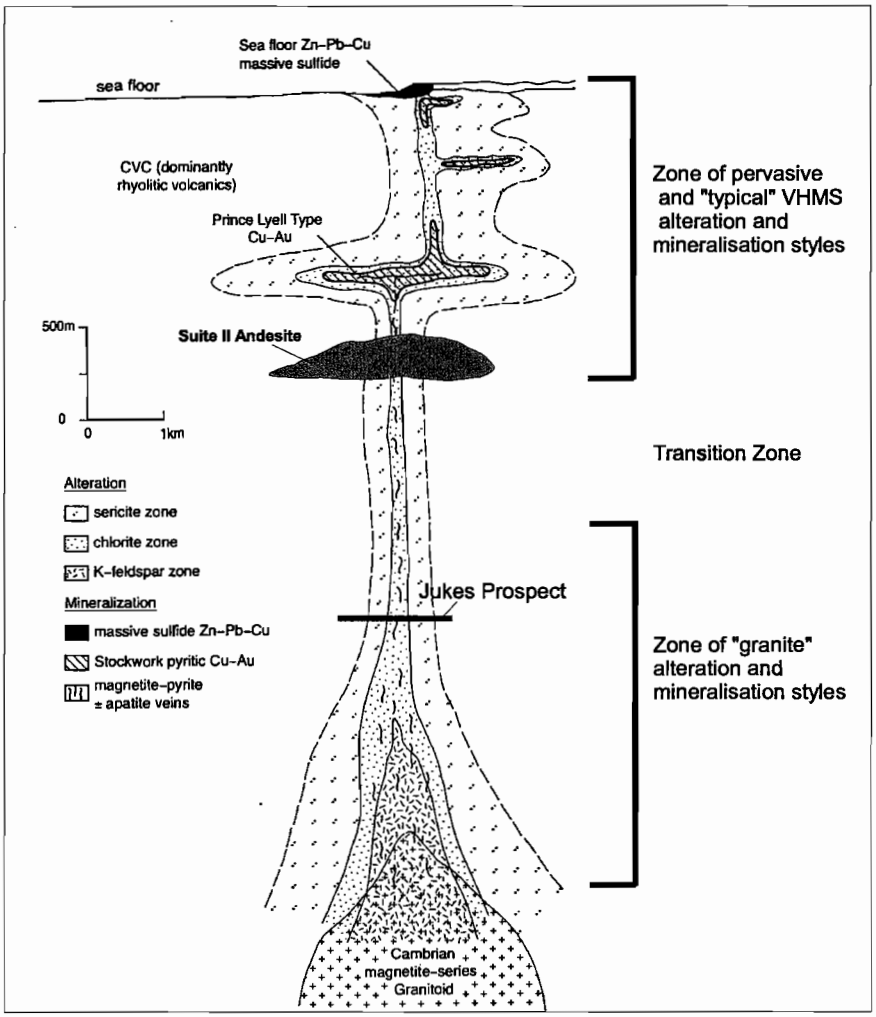

Figure 10.1. Alternative geology-alteration model for the hydrothermal system related to the Mt. Lyell VHMS deposits. In this model, the Suite II andesite occurs beneath the Prince Lyell deposit, rather than above it as proposed by Large et al. (1996). The andesite would be leached of phosphorus by rising magmatic fluids derived from a buried Suite I granite. Figure modified after Large et al. (1996).

Suite II andesites below the Prince Lyell deposit could, theoretically, be leached of phosphorus and REE by fluids from an underlying Cambrian granite (Figure 10.1). However, either intense focused hydrothermal fluids or fluids of an appropriate composition are required (Barrett et al., 1990; MacLean and Barrett, 1993). The amount of apatite in the Prince Lyell deposit implies that a large volume of phosphorus-rich rocks had to be leached nearby or that there was direct magmatic input. Suite II andesites occur throughout the Mine Sequence and are not depleted in P_2O_5 (MRV Suite II andesites average 0.23 wt.% P_2O_5, Crawford et al., 1992) but are enriched, averaging 0.3 wt.% (Raymond, 1992). REE support for apatite precipitation from either Suite II andesites or Suite I granites is inconclusive. However, $\varepsilon Nd_{(500Ma)}$ values in Prince Lyell apatites support the interpretation that the magmatic fluids were derived from a Suite I parental magma. A genetic model involving leaching also falls short of providing the required metal and sulfur budget required. Therefore, a model involving a direct magmatic contribution is favored, consistent with the arguments of Large et al. (1996). It is therefore concluded that the parental magma is probably too deep to be geophysically detectable (>8 km, Leaman, 1986), as first proposed by Large et al. (1996).

10.4 CONCLUSIONS

This research project had four major goals: 1) evaluate the evidence for a genetic link between the Cambrian granites and their host volcanic rocks within the CVC in the southern MRV; 2) document the regional extent of hydrothermal alteration associated with the Cambrian granites and evaluate the genetic link between the hydrothermal alteration in and around the granites and the hydrothermal alteration around the Prince Lyell VHMS deposit at Mt. Lyell; 3) evaluate the relationship of hornblende-phyric andesites to the VHMS deposits and the hydrothermal alteration within the CVC; 4) establish the source of ore-forming fluids involved in the generation of Cambrian Cu-Au mineralisation in western Tasmania and determine the extent of mixing between various fluid types. This research has led to the following conclusions and interpretations.

1) The Darwin, Murchison and Elliott Bay Granites are I-type magnetite-series granites and have characteristics consistent with emplacement in a collisional or volcanic arc environment (Figures 3.26-31). This interpretation is consistent with the post-collisional tectonic setting proposed by Crawford et al. (1992) and Crawford and Berry (1992).

2) GENMIX modeling of major elements and REE data in the Darwin Granite support the model that the microgranite and white granite formed from fractionation of the pink granite phase. Negative $\varepsilon Nd_{(500Ma)}$ values (Table 3.2), low P_2O_5 contents, linear variation diagrams, Nd model ages and restite in the Murchison Granite support the interpretation that the Murchison and Darwin Granites were derived from continental crust.

3) REE patterns and abundances in YRS rhyolites, EQPS dacites and CVC dacites are similar, supporting the interpretation that they are time-equivalent parts of the same volcanic centre. All three units are characterised by enriched LREE, small negative Eu anomalies, flat HREE patterns and similar ranges in $(La/Yb)_N$ values. REE characteristics of the YRS, EQPS and CVC match Suite I characteristics of Crawford et al. (1992). Based on REE patterns and Nb, Y, TiO_2 and Ti/Zr values (Figures 4.11-4.14), the YRS, EQPS and CVC are interpreted to be comagmatic with a parental magma with geochemical characteristics similar to the Murchison Granite. Such a granite is postulated to exist beneath the Jukes-Darwin area. In addition, based on REE patterns, Nb/Y, Ti/Zr and P_2O_5/TiO_2 values, the Type 1 and Type 2 quartz-feldspar-phyric dykes are also interpreted to be comagmatic with the same magma. The Darwin Granite does not appear to be comagmatic with any of the volcanic rocks in the study area.

4) Hydrothermal alteration styles occur in zones around the Darwin Granite and at the Jukes Prospect. Around the Darwin Granite five alteration zones (Zones 1-5) were described (Figure 5.4): 1) Zone 1 consists of overlapping moderate to intense secondary chlorite, moderate K-feldspar, weak to moderate secondary silica and weak to moderate sericite alteration assemblages. 2) Zone 2 is characterised by moderate to intense chlorite, weak K-feldspar and moderate silica alteration assemblages. Magnetite and magnetite + tourmaline veins occur throughout the zone. 3) Zone 3 is characterised by intense silicification and weak to moderate chlorite alteration assemblages. 4) Intense secondary K-feldspar and moderate to intense secondary silica alteration assemblages occur from approximately 800 to over 1000 metres

above the granite contact in Zone 4. 5) In Zone 5, hydrothermal alteration intensities decrease rapidly into regional diagenetic and metamorphic alteration styles.

Along Jukes Road, alteration styles are zoned around a hydrothermal vein system that developed in the cupola region above the Darwin Granite. An inner zone of intense K-feldspar alteration assemblages is cut by magnetite ± tourmaline ± sulfide veins and hydrothermal breccias. The K-feldspar zone grades outward into middle and outer zones of chlorite and sericite alteration assemblages. The vertical extent of the hydrothermal system remains unknown, but the hydrothermal alteration zones at Mt. Darwin and the Jukes Prospect are interpreted to represent different parts of the same hydrothermal system (Figure 5.1).

5) Near the Darwin Granite, hydrothermal alteration assemblages are characterised by large mass changes. SiO_2 mass gains up to 80 gms/100gms accompanied significant mass gains in Al_2O_3, K_2O, Ba and Sr. Depletions of SiO_2 and Al_2O_3 occurred in adjacent andesites. In contrast to the large mass changes near the Darwin Granite, total mass changes at the Jukes Prospect were minor. In K-feldspar and sericite-altered rocks, mass gains in K_2O ranged from 1 to 5 gms/100gms, while silica mass changes ranged from -8 to 4 gms/100gms in chlorite and K-feldspar-altered rocks respectively. In sericite-altered rocks, K_2O gains effectively balanced $\Delta(Na_2O + CaO)$ depletions, and total mass changes were insignificant (average 0.7 gms/100gms). Similarly, total mass changes in chlorite-altered rocks effectively balance $\Delta(K_2O + MgO + Fe_2O_3)$ gains with $\Delta(Na_2O + CaO + SiO_2)$ losses, for overall insignificant mass gains averaging 0.7 gms/100gms.

6) The Darwin Granite crystallised from a magma with $\delta^{18}O$ values between 9‰ and 10.5‰, consistent with other high $\delta^{18}O$ granites associated with collision zones and orogenic areas. Magmatic fluids in equilibrium with the granite had $\delta^{18}O$ values around 9 ± 1‰. At the Jukes Prospect (based on limited quartz and K-feldspar data), equilibrium fluid temperatures were 485 ± 25°C and $\delta^{18}O_{fluid}$ values around 6 ± 1‰. These ranges are supported by magnetite temperatures of 460-550°C and $\delta^{18}O$ values of 6 to 7.5 ± 1‰. These temperatures, combined with minimum temperatures of 320-360°C as determined by chlorite geothermometry, suggest a wide range of hydrothermal temperatures in the Jukes-Darwin system. Based on $\delta^{18}O$ data, quartz, K-feldspar are interpreted to have formed from nearly equal mixture of magmatic fluids and modified seawater. Uplift of the Darwin Granite prior to Tyndall Group deposition exposed the granite to meteoric water as documented by $\delta^{18}O$ values in chlorite. Further research on quartz, k-feldspar and magnetite mineral pairs is recommended.

7) $\varepsilon Nd_{(500Ma)}$ values in Prince Lyell apatites are strong evidence that magmatic fluids derived from a Suite I parental magma were directly responsible for apatite-magnetite ores, as proposed by Large et al. (1996). The Prince Lyell values contrasts sharply with $\varepsilon Nd_{(500Ma)}$ values for the Garfield apatites that closely match the $\varepsilon Nd_{(500Ma)}$ values of Suite II andesites. Interestingly, the two Cu-Au occurrences with similar hydrothermal alteration and mineralisation styles occur in the same mining district and appear to have different fluid sources. Therefore, although this model proposes a granite as the magmatic fluid source for the Prince Lyell ores, further research on apatite and magnetite at both locations is suggested.

8) The initial sulfur budget in the Jukes-Darwin hydrothermal system was dominated by magmatic sulfur ($\delta^{34}S$ = 6‰) with minor contributions of modified volcanic rock sulfur ($\delta^{34}S$ = 10-15‰). The modified reduced seawater contribution was small (<25%). As the hydrothermal system developed, the contribution of rock sulfur and magmatic sulfur decreased and the contribution of reduced seawater sulfate increased resulting in sulfur isotope zonation. At Prince Lyell, $\delta^{34}S$ values (average 7‰) represent magmatic values but are not uniquely definitive of a genetic source and could have been derived from either Suite II andesites (Crawford et al., 1992) or Cambrian granites. However, because of the definitive $\varepsilon Nd_{(500Ma)}$ link with apatite, the most probable sulfur source was a mixture of magmatic sulfur derived from a Suite I magma ($\delta^{34}S$ value 7-9‰) and a minor component of modified felsic volcanic rock sulfur (10-15‰).

10.5 GENETIC MODEL FOR THE DARWIN GRANITE AND ASSOCIATED Cu-Au DEPOSITS

10.5.1 Background Tectonic Setting

The Cambrian granites in western Tasmania are comagmatic with, the post-collisional MRV. The Late Proterozoic and Early Palaeozoic history of the MRV has been summarised by Crawford and Berry (1992; Figure 2.3). Crawford et al. (1992) added geochemical support to the model and described one tholeiitic and three calc-alkaline volcanic suites in the MRV (Section 4.4.2). During the Middle to Upper Cambrian, a N-S graben was produced with a complex series of E-W transfer zones (Berry and Keele, 1997). Many of the VHMS deposits are located near intersections of E-W transfer faults and N-S graben faults (Figure 10.2). The Cambrian granites and CVC volcanic rocks belong to Suite I (Crawford et al., 1992) and $\varepsilon Nd_{(500Ma)}$ values indicate a crustal component to the parental magmas. These magmas formed during the Middle to Upper Cambrian (phase 'd' on Figure 2.3) and intrusion continued on into the Cambro-Ordovician boundary (early phase 'e'). The significance to the Darwin Granite evolution is the post-collisional extensional environment that dominated the structural setting. Large et al. (1987) and Large (1988) proposed a rift model for VHMS formation in the CVC (Figure 10.3). Although this model did not recognise the post-collisional nature of the MRV, it can be accommodated into the Crawford and Berry (1992) model if updated. The genetic model proposed here suggests that the rift model can be modified to fit into the relaxation rift of Crawford and Berry (1992) phase 'd.' In addition, the Large et al. (1987) and Large (1988) rift model attempts to lump all of the mineral deposits in the MRV into one all encompassing model. The modifications presented below deal only with mineral deposits in the Mt. Lyell to Mt. Darwin area, essentially the right-hand side of Figure 10.3.

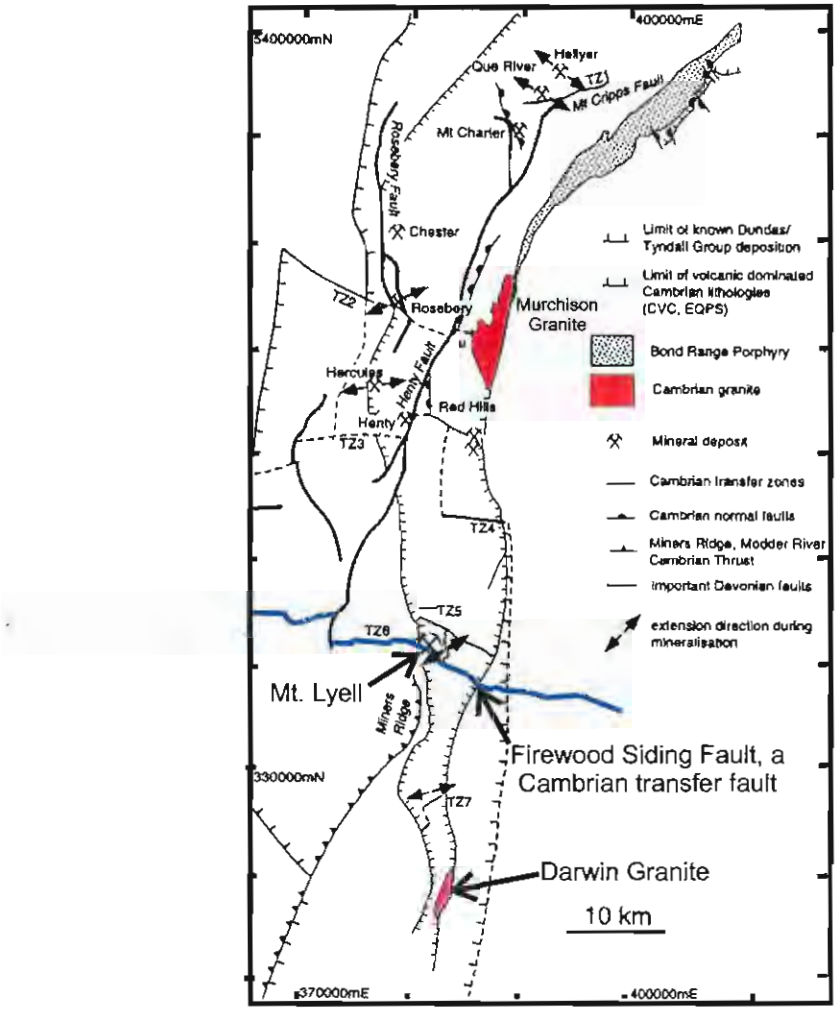

Figure 10.2. Cambrian fault patterns in the Dundas Trough. Mt. Lyell occurs beneath the intersection of the major Firewood Siding transfer fault and the N-S extensional rift. The Darwin Granite occurs along the margins of the rift and probably intruded along a rift margin fault. The figure illustrates interpretations of Berry and Keele (1997), and is modified from Crawford and Berry (1992).

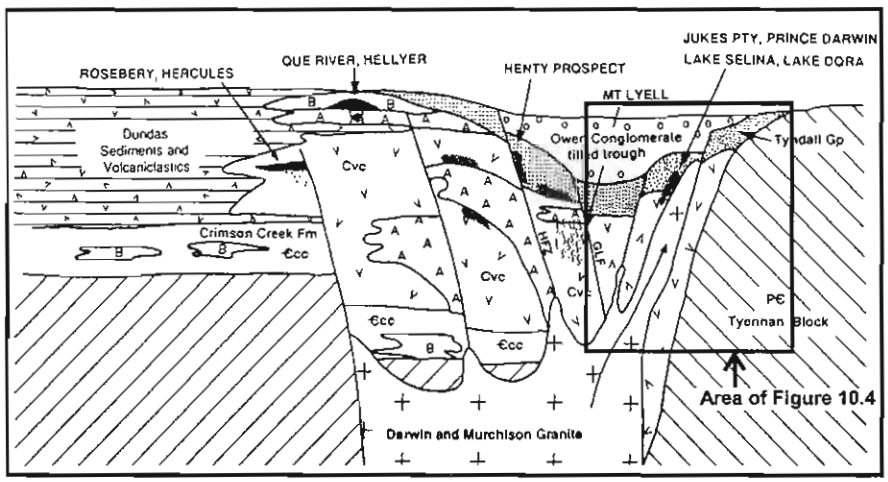

Figure 10.3. Diagrammatic rift model for formation of the MRV showing the interpreted setting of major mineral deposits. Modified from Large et al. (1987) and Large (1988).

10.5.2 Formation of Cambrian Granites and their Relationship to Associated Cu-Au Deposits: the Big Picture

The overall model for the formation of Cambrian granites in western Tasmania has four major parts: 1) compression and melting, 2) extension, magma emplacement and initiation of volcanism, 3) additional extension and subvolcanic intrusion, and 4) final emplacement and crystallisation. The four are described in more detail below.

1) Compression during arc-continent collision depressed the base of the Precambrian crust and initiated partial melting of the lower crust. Initial Suite I and Suite II parental magmas formed. Geochemical characteristics of the granites support a crustal source ($\varepsilon Nd_{(500Ma)}$ values), and I-type, magnetite series compositions are consistent with a collisional environment.

2) Extension and relaxation rifting (Crawford, 1992; Crawford and Berry, 1992) commenced. Parental Suite I magmas rose along the eastern, west-dipping rift-margin faults. Some magmas reached shallow crustal levels and erupted forming Suite I rocks of the MRV. In the Jukes-Darwin area, a low phosphorus Murchison-like parental magma erupted and formed the thick CVC + EQPS + YRS volcanic and volcaniclastic pile with similar geochemical characteristics throughout.

Although the Darwin Granite parental magma had similar geochemical characteristics to the Murchison Granite, it is unlikely to have been the same magma. Geological relationships suggest that the Darwin Granite is slightly older than the granite at Mt. Lyell or the Murchison Granite. The Darwin Granite was uplifted and eroded prior to Tyndall Group deposition. At the Lake Burbury prospect, Jukes-Darwin style granite-related hydrothermal alteration assemblages are related to a granite younger than the Tyndall Group (Jaeger, 1996). In addition, the Murchison Granite intrudes EQPS rocks and granite-related hydrothermal alteration and mineralisation styles occur in EQPS and Tyndall Group rocks at Lake Selina and Lake Dora (Polya et al., 1986; Eastoe et al., 1987; Hunns, 1987; Corbett, 1992; Hunns, 1997). Therefore, the geochemical similarities between the granites are most likely a result of similarities in source rocks and partial melting conditions in the lower crust.

3) As extension continued, additional deep-seated east and west-dipping rift related growth faults provided further channelways for Suite I and Suite II magmas. Most of the parental magmas probably remained in the Precambrian crust at depths >8 km (Leaman, 1986; eg. Mt. Lyell). Fractionated magmas rose along these structural channelways and intruded earlier deposited volcanics as sills and plugs. A major N-S striking west-dipping backtrust fault, or series of N-S striking west-dipping rift margin faults, along the eastern margin of the MRV provided a significant structural control on Cambrian granite emplacement and explain the linear N-S Cambrian granite ridge in Figure 3.1. However, granite intrusion was not necessarily coeval.

4) Fractionation of a low phosphorus Murchison-like parental magma, and intrusion to high crustal levels (4-5 km) along a N-S striking rift margin fault, resulted in emplacement of the elongate Darwin Granite and its various phases. Continued fractionation of the pink granite and removal of monazite, zircon and sphene resulted in REE-depleted residual magma. Microgranite dykes intruded the host volcanics near the granite margins. Residual white granite and the related

quartz-feldspar porphyry phase, were last to crystallise with an order of magnitude less total REE than the pink phase.

In the Mt. Lyell area, a different parental magma, probably of diorite-granodiorite composition, intruded beneath the central portions of the MRV near or along the intersection of a major E-W striking Cambrian transfer fault and a N-S striking backtrust fault or rift margin growth fault (such as the Great Lyell Fault). This magma exsolved the hydrothermal fluid rich in phosphorus, sulfur, iron and copper that formed the Prince Lyell and Western Tharsis Cu-Au deposits via replacement of favorable porous volcaniclastic horizons. Further intrusion of fractionated portions of this magma into the west-dipping zone of weakness created by the intersection of the two structures, resulted in granite emplacement, and related hydrothermal alteration and mineralisation at the Lake Burbury prospect.

10.5.3 Detailed Genetic Model for the Jukes-Darwin System

The rift margin setting for the Darwin Granite and its hydrothermal alteration system is illustrated schematically on Figure 10.4. Hydrothermal alteration and mineralisation in the Jukes-Darwin area can be summarised in five stages (Figure 10.5A-E): 1) magmatic fluid and volatile formation, alteration of the contact zone, 2) initial hydrofracturing and initiation of the hydrothermal system, 3) hydrothermal breccia intrusion and main stage alteration, 4) outer zone development and cooling, and 5) collapse and seawater overprint. These five stages are discussed below.

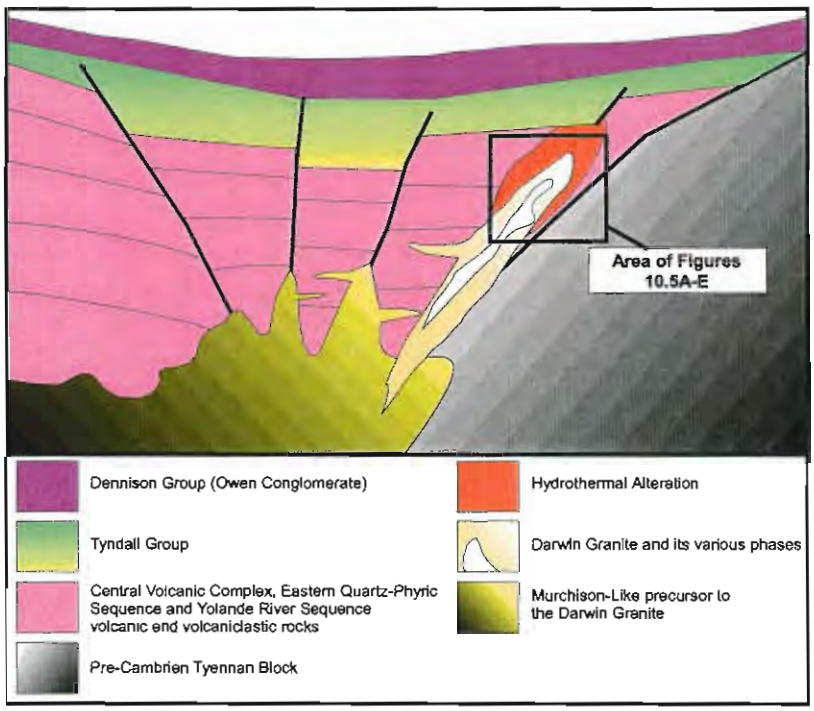

Figure 10.4. Schematic cross-section illustrating the geologic setting for the Jukes-Darwin system.

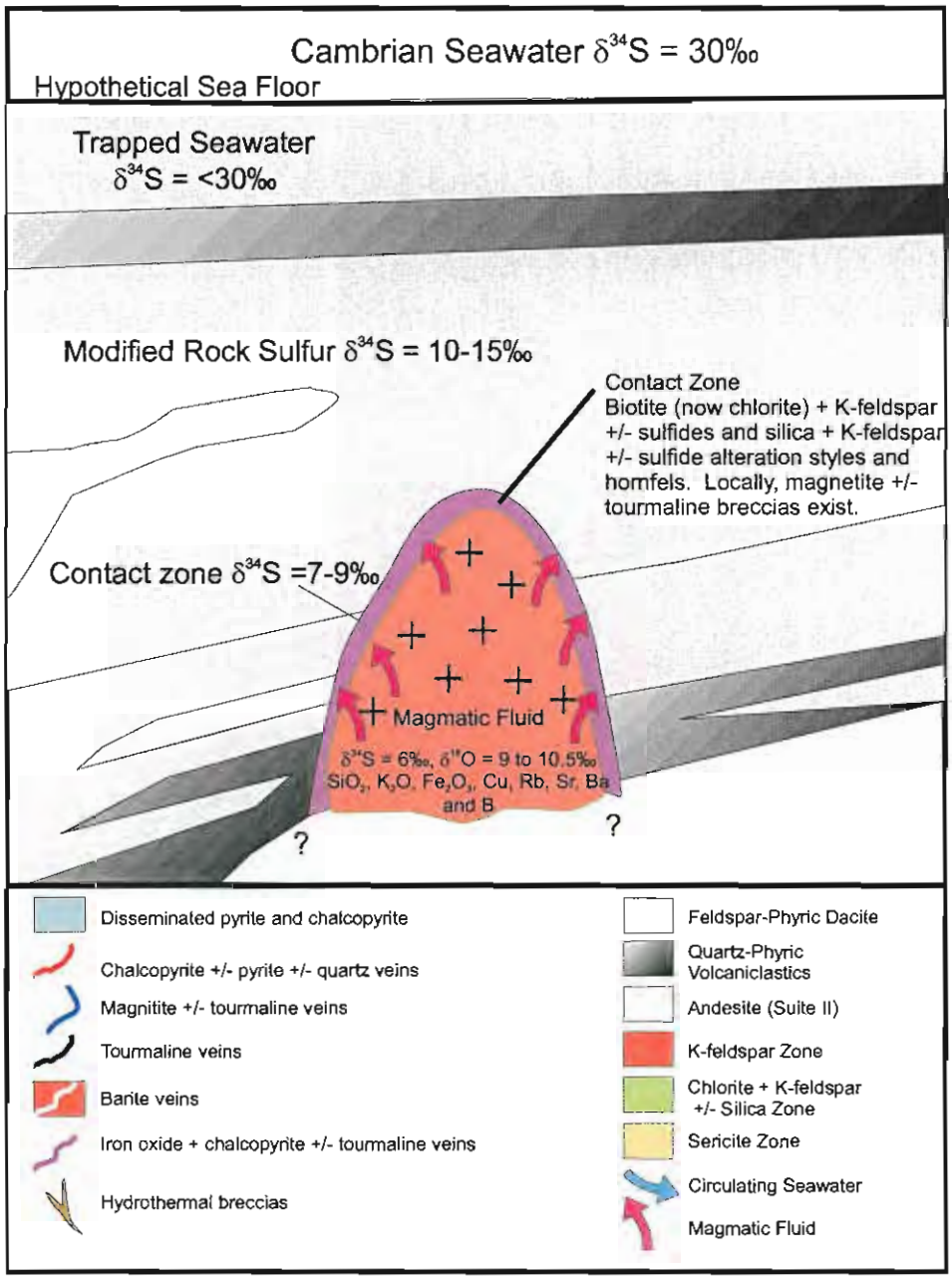

Figure 10.5A. Stage 1, detailed genetic model for the Jukes-Darwin hydrothermal system.

Stage 1: After intrusion of the Darwin Granite magma to a depth of 4-5 km, crystallisation initiated formation of a SiO_2, Fe_2O_3, K_2O and B-rich magmatic fluid with $\delta^{34}S$ ~8‰ and $\delta^{18}O$ ~9‰ to 10.5‰. As solidification of the granite continued, magmatic fluid exsolved from the granite in the immediate contact zone, resulting in biotite (now chlorite) + K-feldspar ± sulfides and quartz + K-feldspar ± sulfide alteration assemblages and hornfels (Figure 10.5A). Locally, magnetite and tourmaline veins cross-cut coarse magnetite ± tourmaline breccias. Magmatic sulfur initially mixed with minor modified rock sulfur ($\delta^{34}S$ ~ 10-15‰) resulting $\delta^{34}S$ values in the contact zone of 7-9‰. Initial seawater infiltration into the deeper volcanic pile had not yet begun.

Stage 2: Fluid over-pressure caused initial hydrofracturing and M1 vein formation (Figure 10.5B). Near the Darwin Granite, magmatic fluids dominated the hotter portions of the upflow zones and intense secondary chlorite, moderate K-feldspar and moderate silica alteration assemblages

(Zone 1) were developed. Due to the dominance of magmatic fluids rich in a SiO_2, K_2O, and Fe_2O_3, mass changes were large. Fracturing caused W/R values to increase and minor amounts of modified seawater reacted with magmatic fluids. Resultant $\delta^{34}S$ values in the veins are 10-14‰ and are variable due to fluctuations in fO_2, temperature and associated fluid $\delta^{34}S$ values. Higher in the system, at Intercolonial Spur and the Jukes Prospect, initial quartz, K-feldspar and magnetite-bearing assemblages formed from a nearly pure magmatic fluid. Fluid temperatures were hot, 460-550^{O}C with $\delta^{18}O$ values of 6 to 7.5 ± 1‰.

Stage 3: Hydrothermal breccia intrusion resulted in development of a fully established circulation system (Figure 10.5C). Magmatic fluids mixed with modified seawater in hotter portions of the upflow zones and K_2O, and Fe_2O_3 rich alteration assemblages resulted. Around the Darwin Granite, magmatic fluids formed intense chlorite, K-feldspar and silica alteration assemblages (Zones 2, 3 and 4) in addition to large (up to 5m wide) magnetite ± tourmaline veins. M2 veins and disseminated mineralisation have higher $\delta^{34}S$ values (10-15‰) due to interaction with descending seawater. At the Jukes Prospect, hydrothermal breccias formed a related fracture system filled with chlorite, magnetite and tourmaline. A zone of intense chlorite replaced some earlier K-feldspar domains during multiple alteration episodes. The modified seawater component of the hybrid fluids increased. Overall mass changes were small.

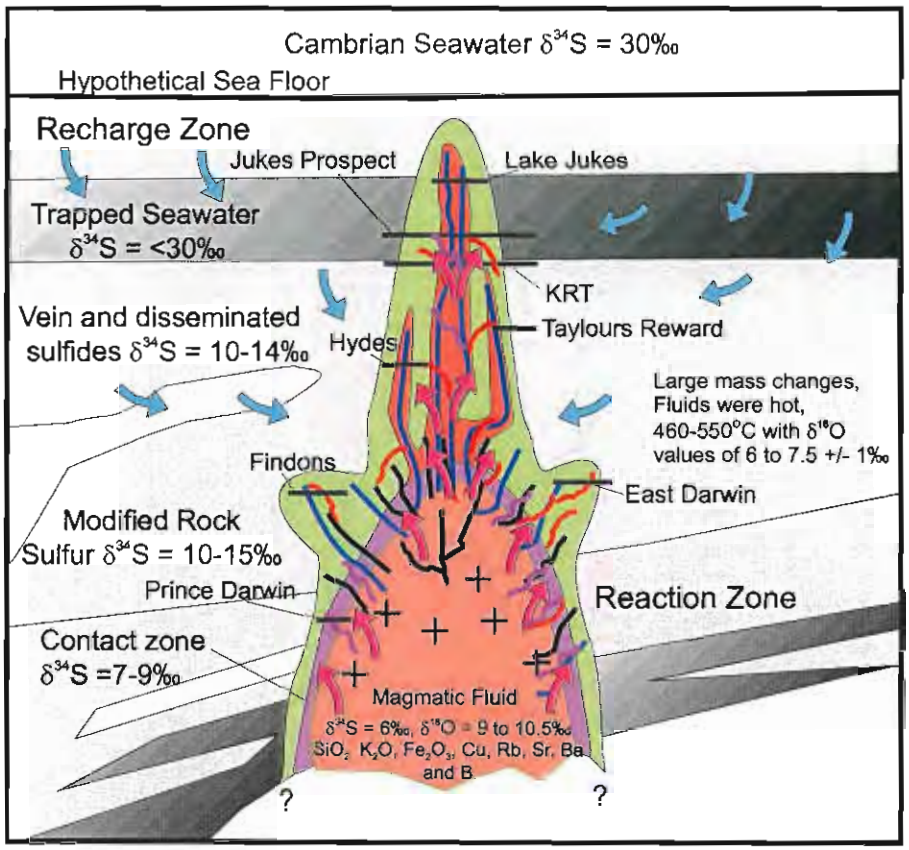

Figure 10.5B. Stage 2, detailed genetic model for the Jukes-Darwin hydrothermal system. Legend as Figure 10.5A.

Stage 4: The outer alteration zone (Zone 5) grades, with decreasing intensities, from sericite ± chlorite alteration assemblages into least-altered volcanics in the Darwin Granite region (Figure 10.5D). At the Jukes Prospect, an outer weak sericite zone of moderate to intense secondary sericite ± chlorite ± carbonate and sericite + quartz ± carbonate alteration assemblages, form a transition zone from hydrothermal alteration styles into diagenetic and metamorphic alteration styles. $\delta^{34}S$ values increased to 15‰ to 19‰ as a result of the increasing dominance of modified Cambrian seawater. Multiple fluid pulses with variable chemistry, resulted in close association of mutually overlapping $\delta^{34}S$ values in close proximity.

Stage 5: Hydrothermal system collapse and loss of heat (Figure 10.5E). Fluids were dominated by unreacted seawater that swamped hydraulic conduits and precipitated barite ($\delta^{34}S$ = 29‰). Within some pervasively altered zones, granite $\delta^{34}S$ values increased to 12.7‰ while sulfide values range from 22‰ to 26‰. Weak sericite-chlorite alteration assemblages overprinted earlier intensely developed K-feldspar alteration assemblages.

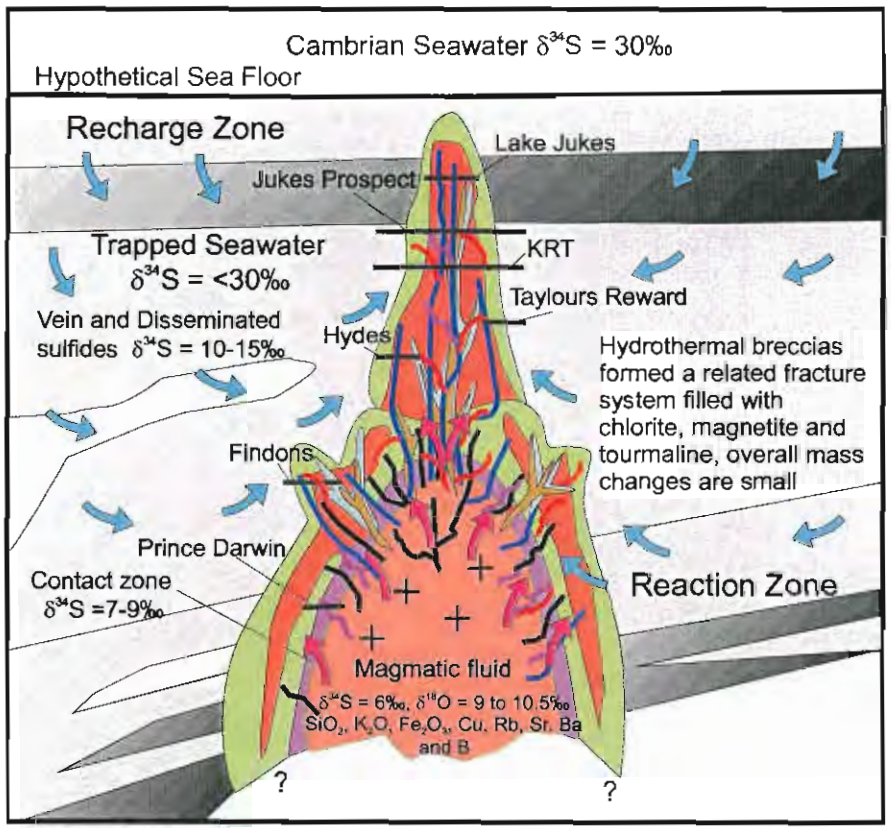

Figure 10.5C. Stage 3, detailed genetic model for the Jukes-Darwin hydrothermal system. Legend as Figure 10.5A.

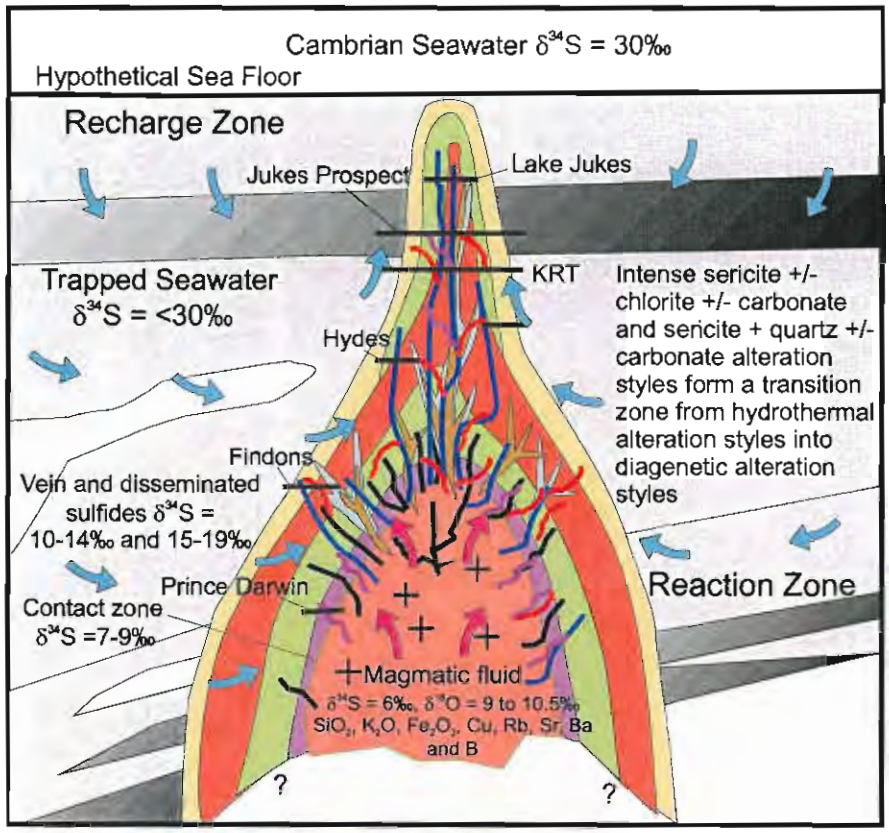

Figure 10.5D. Stage 4, detailed genetic model for the Jukes-Darwin hydrothermal system. Legend as Figure 10.5A.

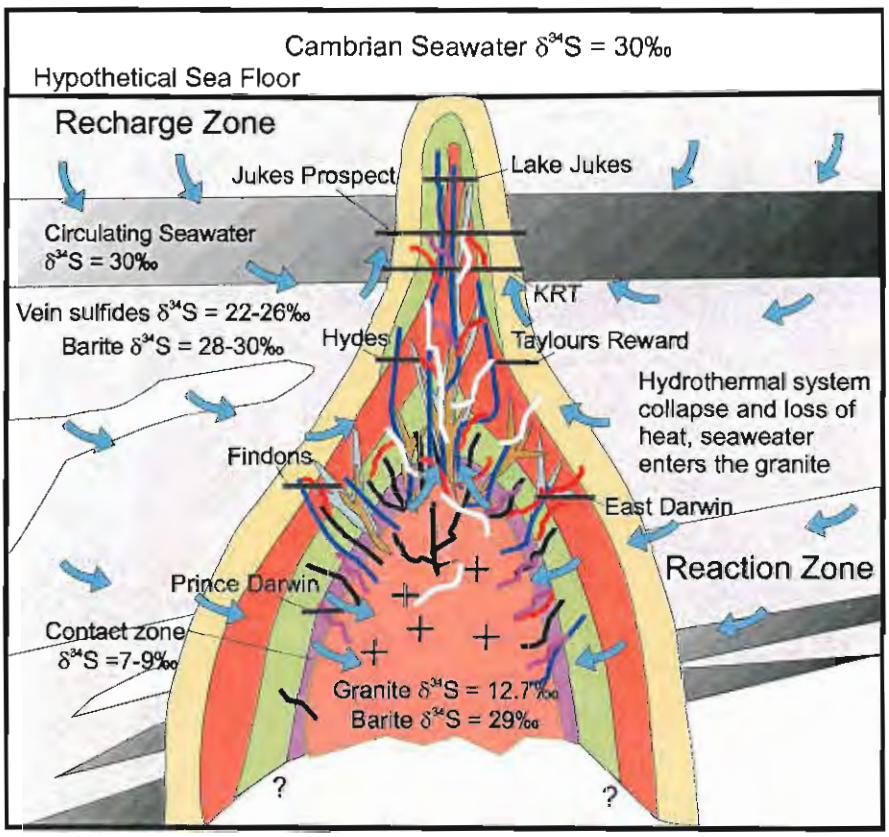

Figure 10.5E. Stage 5, detailed genetic model for the Jukes-Darwin hydrothermal system. Legend as Figure 10.5A.

10.6 RECOMMENDATIONS FOR FURTHER WORK

- One of the primary aims of this study was to establish the source of ore forming fluids involved in the generation of Cambrian Cu-Au mineralisation. The conclusion that a Cambrian granite was involved in the Mt. Lyell mineralisation relies heavily on two apatite εNd values of Stolz (pers. comm. 1997). Although the data (Appendix F) appears to be conclusive, it is minimal, and additional εNd values from systematically gathered apatite samples from Prince Lyell and Western Tharsis and whole rock εNd values from the Cambrian granites and Suite II andesites would be useful in supporting this conclusion.

- Hydrothermal fluid compositions and temperatures at the Jukes Prospect and the Prince Lyell deposit have not been studied in detail and the results of this study are preliminary. A focused fluid inclusion study combined with an oxygen and deuterium isotope study of K-feldspar-quartz, K-feldspar-magnetite and quartz-magnetite mineral pairs would significantly improve the understanding of the nature of the mineralising fluids.